Universidade Federal do Rio De Janeiro

Programa de Engenharia Ambiental

Rodrigo Moulin Ribeiro Pierott

ADVANCING STRUCTURAL DESIGN: INTEGRATION OF FINITE DATA AND MACHINE LEARNING FOR OPTIMIZING REINFORCED CONCRETE STRUCTURES

RIO DE JANEIRO

2024

UFRJ

Rodrigo Moulin Ribeiro Pierott

ADVANCING STRUCTURAL DESIGN: INTEGRATION OF FINITE DATA AND MACHINE LEARNING FOR OPTIMIZING REINFORCED CONCRETE STRUCTURES

Doctoral thesis presented to the Environmental Engineering Program, Escola Politécnica & Escola de Química, from Universidade Federal do Rio de Janeiro, as part of the requirements for obtaining a Doctor of Science degree in Environmental Engineering.

Advisors:
Prof. Dr. Assed Naked Haddad
Prof. Dr. Vivian WY Tam

RIO DE JANEIRO
2024

Rodrigo Moulin Ribeiro Pierott
Advancing Structural Design: Integration of Finite Data and Machine Learning for Optimizing Reinforced Concrete Structures / Rodrigo Moulin Ribeiro Pierott – 2024.
388 f.: il.; 30 cm.

Tese (doutorado) - Universidade Federal do Rio de Janeiro, Escola Politécnica, Escola de Química, Programa de Pós-Graduação em Engenharia Ambiental, 2024.

1. Predictive Modeling 2. Concrete Structures 3. Discrete Optimization 4. Machine Learning 5. Finite Data I. Haddad, Assed Naked, orient. II. Tam, Vivian WY.

ADVANCING STRUCTURAL DESIGN: INTEGRATION OF FINITE DATA AND MACHINE LEARNING FOR OPTIMIZING REINFORCED CONCRETE STRUCTURES

Rodrigo Moulin Ribeiro Pierott

Advisors: Prof. Dr. Assed N. Haddad and Prof. Dr. Vivian WY Tam.

Doctoral thesis presented to the Environmental Engineering Program, Escola Politécnica & Escola de Química, from Universidade Federal do Rio de Janeiro, as part of the requirements for obtaining a Doctor of Science degree in Environmental Engineering.

Approved by the board of examiners:

President, Prof. Assed Naked Haddad, PhD, UFRJ.

Prof. Vivian WY Tam, PhD, Western Sydney University.

mohammad najjar

Prof. Mohammad Najjar, PhD, UFRJ.

Prof. Bruno Barzellay Ferreira da Costa, PhD, UFRJ.

Prof. Sergio Luis González Garcia, PhD, UENF.

Prof. Christine Kowal Chinelli, PhD, UFF.

Prof. Nélida Gladys Maquera Sosa, PhD, Universidad Peruana Unión.

RIO DE JANEIRO

2024

To my mother, Monica Moulin, who has always supported and believed in me.

"I don't not know what I may appear to the world, but to myself I seem to be only like a boy playing on the sea-shore, and diverting myself in now and then finding a smoother pebble or a prettier shell than ordinary, whilst the great ocean of truth lay all undiscovered before me."

Sir. Isaac Newton.

ACKNOWLEDGMENT

With immense gratitude and a deep sense of fulfillment, I begin these acknowledgments, reflecting on the journey that has brought me to this moment. This thesis is the culmination of perseverance, and countless moments of reflection and growth. However, this achievement would not have been possible without the unwavering support of so many special individuals who have stood by my side throughout this journey.

First and foremost, I wish to thank **God**, for without His guidance and the help of His messengers, I would not have had the strength or clarity to complete this thesis. My faith has been a strong base, and I am deeply grateful for the divine support that has carried me through the challenges of this journey.

I extend my deepest gratitude to my mother, **Monica Moulin**, who has always been my pillar of strength. Her unwavering belief in me and her endless support have been my greatest inspiration. She is my role model, my guiding light, and her unconditional love has provided me with the courage to pursue my dreams. I also want to thank my grandmother, **Cely Moulin**, who, as she often reminds me, has been my mother twice over. Her lessons in kindness, love, and generosity have shaped who I am today. Though he is no longer with us, I also wish to honor my grandfather, **Geraldo Netto**. His teachings of courage, integrity, and the importance of service have left an indelible mark on my life. As he used to say, "Tá tudo bom pra carambotanca!". I would like to express my deepest gratitude to my late father, **Fajardo Pierott Júnior**, whose unwavering support and inspiration continue to remind me of the profound importance of education and dedication. His presence remains with me, guiding my every step.

I am deeply grateful to my girlfriend, **Caroline Brum**, whose wisdom, despite her youth, has been a source of strength and encouragement for me at the end of this journey. Her belief in my abilities and her constant support have pushed me to strive to be better each day.

I also want to thank my cousin, **Juam Pierott**, who has been like the brother I never had. Our mutual exchange of knowledge and experiences has enriched my life in countless ways. To my business partner, **Pedro Rocha**, I extend my sincere thanks for taking care of our shared responsibilities while I was in Australia, allowing me to focus on completing this work and without him I would not be able to fulfill this duty. I also would not forget the support and help that both **Cristiane Brum** and **Gustavo Brum** provided me during this period.

I would also like to extend my heartfelt thanks to my family members—**Maíra Maria Moulin, Marcos Moulin, José Manoel Moulin, Cristiane Moulin, Saly Pierott, Fajardo Pierott, Marcos Pierott, Shirley Pierott, Dayse Pierott, Carlos Luiz Clark, Luciano**

Pierott, Sheila Sampaio, Cristina Pierott, Darcileu Amaral—and all their descendants, for their constant support and encouragement throughout my journey.

A special thank you goes to **Professor Vivian Tam**, who graciously accepted me as her student at Western Sydney University. The lessons I learned from her extend far beyond research, as her example has taught me much about life and professionalism.

I am also profoundly thankful to my colleagues from the PhD program, especially **Mohammad Najjar**, whose generosity and sincerity have been a guiding light throughout this journey. His genuine desire for my happiness and growth has enriched my experience in ways words cannot fully capture. I am also grateful to **Karoline Figueiredo**, who has been a true inspiration, embodying the essence of dedicated research. Her unwavering support and friendship, despite her own busy schedule, have meant so much to me. During my time at Western Sydney University, I was fortunate to meet incredible individuals who became an important part of my life. Among them, **Lei Liu** and **Yijun Zhou** stand out as not just members of Professor Vivian's team, but also dear friends who provided invaluable support throughout my journey. I also want to thank **Mary Wang** for her friendship and kindness.

I would also like to extend my heartfelt thanks to **Professor Sergio González** for his unwavering friendship, goodwill, and support. His guidance has been a constant source of inspiration, starting from my undergraduate days and continuing throughout my academic journey and my life.

A special acknowledgment goes to my supervisor and friend, **Professor Assed Haddad**. Without his belief in me, his patience, and his unwavering support, I would not have been able to complete my studies. His dedication to guiding me and his genuine investment in my success have been invaluable. I hope to continue working with him to repay, in some way, the mentorship he has so generously shared with me.

Finally, I want to express my gratitude to **UFRJ**, especially **PEA**, for providing me with the opportunity to grow as a researcher. To all the staff at **PEA** who assisted me throughout my Ph.D., I extend my heartfelt thanks.

Thank you all.

ABSTRACT

PIEROTT, R. M. R. **Advancing Structural Design: Integration of Finite Data and Machine Learning for Optimizing Reinforced Concrete Structures**. DSc. Thesis (Doctorate in Environmental Engineering), Environmental Engineering Program, Escola Politécnica & Escola de Química, Federal University of Rio de Janeiro, 2024. Advisors: Assed Haddad.

This thesis presents a novel approach to enhancing the structural design and performance of reinforced and prestressed concrete structures through the integration of finite data sets and advanced machine learning techniques. The research addresses a gap in traditional structural engineering methods, which often rely on static assumptions and deterministic models that inadequately account for the dynamic factors influencing long-term structural performance. The cornerstone of this work is the development of a discrete optimization model that shifts from the conventional continuous methods, enabling the practical optimization of real-world reinforced concrete structures. This model, which utilizes genetic algorithms, not only optimizes material usage but also establishes a robust foundation for incorporating predictive tools, particularly random forest machine learning models, into the structural design process. The thesis further explores the application of these methodologies in various contexts, including the analysis of stress corrosion cracking in prestressed concrete, the predictive modeling of corrosion dynamics in chloride-rich environments, and the evaluation of innovative reinforcement techniques using welded steel mesh stirrups. Additionally, the research investigates the potential of recycled aggregate concrete (RAC) in structural applications, supported by a predictive model tailored for RAC in bridge dry joints, and examines the shear strength of sand-lightweight concrete deep beams reinforced with steel fibers. The integration of finite data with machine learning prediction methods has led to the proposal of new equations that enhance the design process across several fields related to concrete structures. This innovative methodology not only addresses existing challenges but also opens new ways for future research and application. By providing a reliable and adaptable framework, this thesis contributes to the field of engineering, paving the way for the development of more resilient, efficient, and sustainable concrete structures.

Keywords: Predictive Modeling, Machine Learning, Discrete Optimization, Finite Data, Concrete Structures.

RESUMO

PIEROTT, R. M. R. **Advancing Structural Design: Integration of Finite Data and Machine Learning for Optimizing Reinforced Concrete Structures**. Tese (Doutorado em Engenharia Ambiental), Programa de Engenharia Ambiental, Escola Politécnica & Escola de Química, Universidade Federal do Rio de Janeiro, 2024. Orientadores: Assed Haddad, Vivian WY Tam.

Esta tese apresenta uma abordagem inovadora para aprimorar o projeto estrutural e o desempenho de estruturas de concreto armado e protendido por meio da integração de conjuntos de dados finitos e técnicas avançadas de aprendizado de máquina. A pesquisa aborda uma lacuna nos métodos tradicionais de engenharia estrutural, que frequentemente se baseiam em suposições estáticas e modelos determinísticos que não levam adequadamente em conta os fatores dinâmicos que influenciam o desempenho estrutural a longo prazo. O ponto central deste trabalho é o desenvolvimento de um modelo de otimização discreta que se afasta dos métodos contínuos convencionais, permitindo a otimização prática de estruturas reais de concreto armado. Este modelo, que utiliza algoritmos genéticos, não apenas otimiza o uso de materiais, mas também estabelece uma base sólida para a incorporação de ferramentas preditivas, particularmente modelos de aprendizado de máquina baseados em floresta aleatória (random forest), no processo de design estrutural. A tese explora ainda a aplicação dessas metodologias em diversos contextos, incluindo a análise da corrosão sob tensão em concreto protendido, a modelagem preditiva da dinâmica de corrosão em ambientes ricos em cloretos e a avaliação de técnicas inovadoras de reforço utilizando estribos de malha de aço soldada. Além disso, a pesquisa investiga o potencial do concreto com agregados reciclados (CAR) em aplicações estruturais, apoiada por um modelo preditivo adaptado para CAR em juntas secas de pontes, e examina a resistência ao cisalhamento de vigas profundas de concreto leve com areia reforçadas com fibras de aço. A integração de dados finitos com métodos de previsão por aprendizado de máquina resultou na proposta de novas equações que aprimoram o processo de design em diversos campos relacionados às estruturas de concreto. Essa metodologia inovadora não só resolve os desafios existentes, como também abre novas possibilidades para futuras pesquisas e aplicações. Ao fornecer uma estrutura confiável e adaptável, esta tese contribui para o campo da engenharia, pavimentando o caminho para o desenvolvimento de estruturas de concreto mais resilientes, eficientes e sustentáveis.

Keywords: Modelagem de Previsão, Aprendizado de Máquina, Otimização Discreta, Conjunto Finito de Dados, Estruturas de Concreto.

FIGURE LIST

TABLE LIST

ABBREVIATIONS

AI - Artificial Intelligence

BIM - Building Information Modeling

CI - Confidence Interval

DT - Digital Twin

FEA - Finite Element Analysis

FEM - Finite Element Method

GWP - Global Warming Potential

LCA - Life Cycle Assessment

LCC - Life Cycle Costing

LCI - Life Cycle Inventory

LCIA - Life Cycle Impact Assessment

MCDM - Multi-Criteria Decision-Making

ML - Machine Learning

RAC - Recycled Aggregate Concrete

RF - Random Forest

RMSE - Root Mean Square Error

SCC - Stress Corrosion Cracking

SVM - Support Vector Machine

INDEX

1 INTRODUCTION

1.1 BACKGROUND AND MOTIVATION

Structural engineering has long relied on established empirical methods and standardized codes to guide the design and construction of reinforced and prestressed concrete structures. These methods, while robust, are often constrained by their inability to fully anticipate the long-term performance of structures, especially when exposed to complex and evolving environmental conditions. The need for more advanced, predictive approaches in structural design has become increasingly evident as the construction industry faces growing demands for sustainability, resilience, and efficiency.

Predictive modeling offers a promising solution to these challenges, providing a means to simulate the behavior of structural elements under a wide range of conditions. By integrating empirical data into these models, engineers can enhance the reliability and accuracy of their predictions, leading to better-informed design decisions. This approach aligns with the broader goal of sustainable construction, where the long-term performance of structures is a critical consideration. Predictive models can address various structural concerns, from material degradation and corrosion to load-bearing capacity and failure mechanisms, all of which significantly impact the longevity and safety of concrete structures.

The importance of integrating predictive modeling into the structural design process is underscored by the growing complexity of modern infrastructure. Traditional design methods, which often focus on immediate performance and compliance with static code requirements, may not adequately account for the dynamic factors that influence a structure's lifespan. These factors include environmental stressors, material aging, and unforeseen operational loads, all of which can degrade structural integrity over time. By contrast, predictive models can incorporate these variables into the design process, offering a more comprehensive assessment of a structure's long-term behavior.

Moreover, the integration of predictive modeling techniques is not merely a technical challenge but also a strategic one. The adoption of these models requires a shift in how structural design is approached, moving from a reactive to a proactive mindset. This shift involves not only the development of sophisticated models but also the establishment of frameworks that allow these models to be seamlessly integrated into the design and construction workflow. Such integration is crucial for ensuring that predictive models are not just theoretical tools but practical solutions that enhance the durability, safety, and sustainability of concrete structures.

1.2 MOTIVATION OF THE STUDY

The motivation for this study stems from the limitations of current structural design practices in addressing the long-term performance of reinforced and prestressed concrete structures. Traditional methods often rely on empirical data and static analysis, which, while useful, do not fully capture the complexities of real-world conditions. The dynamic nature of environmental stressors, material degradation, and operational loads requires a more nuanced approach, one that predictive modeling is uniquely positioned to provide.

Predictive modeling techniques, supported by empirical data, offer a pathway to overcoming these limitations. These models can simulate the effects of various stressors on concrete structures over time, providing engineers with the tools to design structures that are not only compliant with current codes but also resilient to future challenges. The integration of these models into the structural design process represents a significant advancement in the field, allowing for more accurate predictions of structural performance and, consequently, more reliable and sustainable designs.

However, the practical implementation of predictive modeling in structural design is fraught with challenges. One of the key issues is the lack of standardized methodologies for integrating these models into the existing design frameworks. While predictive models are widely used in other fields, their application in structural engineering is still emerging. This gap presents an opportunity to develop new approaches that bridge the divide between predictive modeling and traditional structural design practices.

Another critical challenge is the validation of predictive models. While these models can generate valuable insights, their accuracy depends on the quality of the empirical data used to support them. Ensuring that predictive models are based on reliable and relevant data is essential for their successful integration into the design process. This study aims to address these challenges by exploring how predictive modeling techniques, underpinned by robust empirical data, can be effectively integrated into the structural design of reinforced and prestressed concrete structures to enhance their long-term performance.

The research presented in this thesis is motivated by the need to push the boundaries of structural design beyond the limitations of traditional methods. By integrating predictive models into the design process, this study seeks to contribute to the development of more resilient and sustainable concrete structures, capable of withstanding the challenges of a changing environment and evolving operational demands.

1.3 RESEARCH QUESTION AND OBJECTIVES

1.3.1 Research Question

The central research question of this thesis is: *How can predictive modeling techniques, supported by empirical data, be integrated into the structural design process to enhance the long-term performance of reinforced concrete structures?*

This question addresses a gap in the field of structural engineering, where traditional design methods often fall short in considering the complex, dynamic factors that influence the long-term performance of reinforced concrete structures. These methods typically rely on static assumptions and deterministic models, which may not fully capture the variability and uncertainties present in real-world conditions. As a result, there is a risk of underestimating vulnerabilities that could affect the safety and durability of concrete structures over time.

By incorporating predictive modeling techniques into the structural design process, this research aims to develop a more resilient and adaptable approach to design. Predictive models, informed by empirical data from specimen testing and performance evaluations, can simulate a wide range of scenarios, including environmental stressors, material degradation, and varying load conditions. This allows for better anticipation of future challenges and the strengthening of structural designs to address them.

Integrating these models into the design process ensures that structures are designed not only to meet current standards but also to optimize long-term performance. This approach enhances the reliability and safety of concrete structures, equipping engineers with tools to design buildings and infrastructure that can endure over time, even as conditions change.

This research question is significant because it addresses key aspects of modern engineering: the need for sustainability in construction, the importance of long-term structural integrity, and the role of advanced technologies in the design and analysis of complex systems. By exploring how predictive models can be applied in structural design, this thesis aims to contribute to the development of more durable and sustainable concrete structures.

1.3.2 Research Objectives

The objectives of this research are threefold, each aimed at addressing different aspects of the central research question:

Objective 1: Development of Predictive Models

The first objective is to develop predictive models that can accurately simulate the behavior of reinforced and prestressed concrete structures under a variety of conditions. These models will be based on empirical data, ensuring that they reflect real-world performance. The goal is to create models that are theoretically and practically applicable, capable of predicting stressors, material degradation, and operational loads on structural integrity.

Objective 2: Comparative Performance Evaluation

Analyze the collected data to evaluate the performance of different materials and structural configurations under stress. This comparative evaluation will highlight the strengths and weaknesses of each approach, informing the development of more robust design practices.

Objective 3: Integration of Machine Learning Models and Equation Development

Utilize the empirical data to develop machine learning models that refine or create new structural equations with high reliability. These models will be integrated into the design process, providing engineers with advanced tools to predict structural performance accurately and enhance standard codes.

1.4 INITIAL RESEARCH

Chapter 4, titled "A Mathematical Optimization Model for the Design and Detailing of Reinforced Concrete," marks the beginning of the research journey that led to this thesis. This chapter, which was the second published paper in this series of research efforts, provided critical insights into the optimization of reinforced concrete design. The work done in this chapter laid the groundwork for the development of more advanced predictive models, aiming finite quantity of data, setting the stage for the broader exploration of predictive modeling techniques in structural engineering.

The optimization model developed in this chapter introduced key concepts and methodologies that were later expanded upon in the subsequent research. It provided a practical framework for improving the efficiency and accuracy of reinforced concrete design, considering standard codes restrictions. The optimization model developed in this chapter is a crucial tool for the subsequent work on predictive modelling by defining the reinforcement layouts as matrixes. It offers a method for determining optimal design variables, which can then be used to enhance the accuracy and reliability of predictive models.

However, the scope of the thesis has since expanded to address a broader and more complex set of challenges. While Chapter 4 remains an important part of the research, the main focus of the thesis is now on the integration of predictive modeling techniques into the structural design process. This shift reflects the evolving nature of the research, as it moved from a specific focus on optimization to a more comprehensive exploration of predictive modeling in structural engineering. Specifically, the thesis explores how predictive modeling can be integrated into the structural design process to improve the long-term performance of reinforced and prestressed concrete structures.

This evolution of the research focus reflects the growing recognition of the importance of predictive modeling in structural engineering. As the field continues to advance, the ability to anticipate and mitigate potential issues before they arise is becoming increasingly important. By building on the work done in Chapter 4, this thesis seeks to contribute to the development of more resilient and sustainable concrete structures, ultimately enhancing the safety and reliability of the built environment.

1.5 THESIS STRUCTURE

1.5.1 Overview of the Thesis

This thesis is structured to systematically address the research question and objectives outlined above. Each chapter builds on the findings of the previous ones, creating a cohesive narrative that leads to a comprehensive understanding of the integration of predictive modeling techniques into structural design.

Chapter 2: Literature Review and Theoretical Framework

This chapter provides a detailed review of the existing literature on predictive modeling, structural design, and sustainability in concrete structures. It sets the theoretical foundation for the thesis, identifying key concepts, methodologies, and gaps in the current research that this study aims to address.

Chapter 3: Mathematical Optimization Model

This chapter details the development of a mathematical optimization model for reinforced concrete. While this chapter serves as the starting point for the research, it also provides essential insights and data that inform the development of predictive models in subsequent chapters.

Chapter 4: Predictive Modeling Techniques

This chapter explores the development and validation of predictive models, focusing on their application in structural engineering. It discusses the methodologies used to create these models and how they are validated using empirical data.

Chapter 5: Integration into Design Process

This chapter examines how predictive models can be integrated into the structural design process. It discusses the challenges of integration, the methodologies developed to address these challenges, and the potential benefits of using predictive models in design practice.

Chapter 6: Case Studies and Experimental Validation

This chapter presents case studies and experimental results that validate the effectiveness of the integrated predictive models. It provides practical examples of how these models can be applied in real-world scenarios and assesses their performance in terms of structural integrity and durability.

Chapter 7: Discussion and Synthesis

This chapter synthesizes the findings from the previous chapters, discussing their implications for the field of structural engineering. It explores the broader impact of the research and suggests potential directions for future studies.

Chapter 8: Conclusion

The thesis concludes by summarizing the key findings, addressing the research question, and proposing recommendations for further research. This chapter also reflects on the limitations of the study and discusses how the research could be expanded in future work.

1.5.2 Interconnectedness of Chapters

The chapters of this thesis are interconnected, each contributing to the overall narrative and research objectives. Chapter 3 serves as the foundation, introducing key concepts and methodologies that are further developed in Chapters 4 and 5. Chapter 6 provides empirical validation of the predictive models discussed in Chapters 4 and 5, while Chapter 7 synthesizes the findings to offer a broader perspective on the research question. The final chapter, Chapter 8, ties everything together, providing a comprehensive conclusion to the thesis.

This interconnectedness ensures that the thesis is cohesive, with each chapter building on the work of the previous ones. The progression from optimization to predictive modeling and integration reflects the natural evolution of the research, culminating in a comprehensive understanding of how predictive modeling techniques can enhance the long-term performance of reinforced and prestressed concrete structures.

1.6 CONCLUSION

This introductory chapter has established the foundation for the research presented in this thesis. It has provided a general background on the challenges of structural design and the potential of predictive modeling techniques to address these challenges. The chapter has also identified the scientific gap that this research aims to fill, articulated the research question, and outlined the objectives of the study.

In addition, this chapter has explained the role of Chapter 4 in the broader context of the thesis, demonstrating how the initial work on mathematical optimization models informed the development of more advanced predictive models. Finally, the chapter has provided an overview of the thesis structure, highlighting the interconnectedness of the chapters and the progression of the research.

The next chapter, Chapter 2, will build on the concepts introduced here by providing a comprehensive review of the existing literature. This literature review will identify key theories, methodologies, and gaps in the current research, setting the stage for the development of the predictive models and integration frameworks discussed in the subsequent chapters.

2 LITERATURE REVIEW AND THEORETICAL FRAMEWORK

2.1 INTRODUCTION

The field of structural engineering has witnessed significant advancements over the past few decades, particularly in the areas of predictive modeling and the application of standard codes and empirical data. These developments have enhanced the ability of engineers to design structures that not only meet current performance standards but also anticipate and mitigate potential long-term issues. However, the integration of these advancements into a cohesive framework for structural design remains a challenge. This chapter provides a comprehensive review of the existing literature on predictive modeling techniques, the use of standard codes and empirical data in structural design, and the theoretical frameworks that support the integration of these approaches.

The purpose of this literature review is twofold. First, it aims to establish a theoretical foundation for the research by summarizing key contributions in the fields of predictive modeling and structural engineering. Second, it seeks to identify gaps in the current literature that this research will address, particularly in the context of enhancing the long-term performance of reinforced and prestressed concrete structures through the integration of predictive models.

The scope of this review includes an examination of used predictive modeling techniques in structural engineering, with a focus on their application to concrete structures. It also covers the role of standard codes in guiding design practices and the ways in which empirical data is utilized to refine these models. The chapter concludes with the presentation of a theoretical framework that integrates these elements, setting the stage for the research presented in subsequent chapters.

2.2 PREDICTIVE MODELING IN STRUCTURAL ENGINEERING

2.2.1 Overview of Predictive Modeling Techniques

Predictive modeling has become an essential tool in structural engineering, providing a means to simulate the behavior of structural elements under a wide range of conditions. These models and equations are particularly valuable in the design of reinforced and prestressed concrete structures, where the complexity of material behavior under stress and environmental conditions can be difficult to predict using traditional methods, especially when dealing with the nuances of different materials, such as Recycled Aggregates Concrete (RAC). The inherent variability and uncertainty in the properties of RAC, for instance, pose significant challenges to conventional design approaches, making predictive modeling an indispensable asset in ensuring accurate and reliable structural performance assessments for new material variations.

The development and adaptation of predictive models in structural engineering have been driven by advances in computational methods, such as finite element analysis (FEA) and machine learning, which allow for the detailed simulation of structural behavior. Finite element analysis (FEA) has long been an important tool for predictive modeling in structural engineering. FEA divides a complex structure into smaller, more manageable elements, each of which is analyzed individually. The results are then synthesized to provide an overall prediction of the structure's behavior under various loads and conditions. FEA has been particularly useful in modeling the behavior of concrete structures, allowing engineers to predict how these structures will respond to factors such as load distribution, thermal expansion, and material degradation over time [1].

In recent years, the application of machine learning techniques in structural engineering has gained traction. Machine learning models can analyze large datasets to identify patterns and correlations that may not be immediately apparent through traditional analysis methods. These models are particularly well-suited to predicting the long-term performance of structures, as they can incorporate data from a wide range of sources, including environmental monitoring, material testing, and historical performance data. By training machine learning models on empirical data, engineers can develop predictive tools that are not only accurate but also adaptable to a variety of conditions [2].

Other computational methods, such as neural networks and genetic algorithms, have also been explored for their potential to enhance predictive modeling in structural engineering.

Neural networks, for instance, are capable of processing complex, nonlinear relationships within data, making them particularly useful for modeling the behavior of materials like concrete, which can exhibit highly variable properties under different conditions. Genetic algorithms, on the other hand, are optimization techniques that mimic the process of natural selection, allowing engineers to identify the most effective design solutions from a range of possibilities [3].

As predictive modeling techniques continue to evolve, they offer increasingly sophisticated tools for structural engineers. However, the integration of these models into the design process presents several challenges, particularly when it comes to ensuring that the models are both accurate and practical for use in real-world applications. The following sections will explore how these models have been applied in structural engineering and the challenges associated with their use.

2.2.2 Applications of Predictive Models

The application of predictive models in structural engineering has expanded significantly, particularly in the design and analysis of reinforced and prestressed concrete structures. These models are employed across various stages of the structural design process, from initial concept development to detailed analysis and optimization. One of the primary advantages of predictive modeling is its ability to simulate complex interactions within a structure, enabling engineers to anticipate potential issues before they manifest in the physical world.

In the context of reinforced concrete structures, predictive models have been instrumental in assessing the performance of materials under various loading conditions. For instance, finite element models are frequently used to simulate the behavior of concrete under compression, tension, and shear, providing insights into how these materials will perform when subjected to different stressors. These models are particularly valuable in identifying areas of potential weakness within a structure, allowing for targeted reinforcement and optimization efforts [4].

For prestressed concrete, predictive models play a crucial role in understanding the long-term effects of prestressing forces on structural integrity. By simulating the distribution and evolution of these forces over time, engineers can predict how a prestressed structure will behave under service conditions, including the effects of creep, shrinkage, and relaxation of the prestressing tendons [5]. This predictive capability is essential for ensuring that prestressed structures maintain their desired performance characteristics throughout their intended lifespan.

The use of predictive models is not limited to traditional materials like standard reinforced concrete. As mentioned earlier, the integration of Recycled Aggregates Concrete (RAC) into structural design introduces additional complexities that can be effectively managed through predictive modeling. The variability in the properties of recycled aggregates, such as differences in particle size distribution, strength, and durability, can significantly impact the performance of RAC. Predictive models enable engineers to simulate these variations and their effects on the overall structural behavior, thereby facilitating the development of more reliable RAC-based designs [6].

Machine learning models have also found increasing application in structural engineering, particularly in the prediction of material properties and structural performance. By analyzing large datasets, these models can identify trends and correlations that may not be immediately apparent through conventional analysis methods. For example, machine learning algorithms have been used to predict the compressive strength of concrete based on a range of input variables, such as mix proportions, curing conditions, and aggregate types. These predictions can then be used to optimize the concrete mix design, ensuring that the final product meets the required performance criteria [7].

In addition to material properties, predictive models are also applied to assess the overall structural response to external factors, such as environmental conditions and load variations. For instance, models that simulate the impact of temperature fluctuations, humidity, and chemical exposure on concrete structures are essential for predicting long-term durability and service life. These models help engineers design structures that are resilient to the environmental conditions they will face over time, thereby reducing the likelihood of premature failure and the associated maintenance costs [8].

The application of predictive models extends beyond individual structures to larger systems, such as infrastructure networks and buildings subjected to seismic activity. In such cases, predictive models are used to assess the vulnerability of these systems to natural disasters, enabling engineers to design structures that are better equipped to withstand seismic forces. By incorporating data from past earthquakes and advanced simulations, these models can provide valuable insights into the behavior of structures during seismic events, informing design decisions that enhance safety and resilience [9].

2.2.3 Challenges and Limitations

Despite the advancements in predictive modeling, several challenges and limitations remain in their application to structural engineering. One of the primary challenges is the inherent complexity of accurately modeling the behavior of concrete, particularly when dealing with non-homogeneous materials like Recycled Aggregates Concrete (RAC). The variability in material properties, coupled with the complex interactions between different components within a structure, makes it difficult to develop models that are both accurate and generalizable across different scenarios [10].

Another significant challenge is the integration of predictive models into the design process. While these models offer valuable insights, their practical application in real-world engineering projects can be limited by factors such as computational complexity, the availability of accurate input data, and the need for specialized knowledge to interpret the results. Engineers must balance the need for detailed, accurate models with the constraints of time, budget, and available resources, which can lead to compromises in the level of detail or the scope of the models used [11].

Moreover, the accuracy of predictive models is heavily dependent on the quality of the input data. In many cases, the data required to develop and validate these models may be incomplete, outdated, or subject to significant uncertainty. This is particularly true for models that rely on empirical data from past projects, where variations in construction practices, environmental conditions, and material properties can introduce significant variability into the data. Ensuring the reliability and relevance of the data used in predictive modeling is therefore a critical concern for engineers [12].

The use of machine learning and other advanced computational techniques in predictive modeling also presents challenges related to transparency and interpretability. While these models can provide highly accurate predictions, they are often treated as "black boxes," with limited insight into how specific input variables influence the output results. This lack of transparency can make it difficult for engineers to trust the results of these models, particularly when they deviate from traditional engineering intuition or established design practices [13].

Finally, there is the challenge of validating predictive models against real-world performance. While simulations and laboratory tests can provide valuable data for model validation, the true test of a model's accuracy lies in its ability to predict the behavior of structures over time in real-world conditions. This requires long-term monitoring and data collection, which can be resource-intensive and logistically challenging. Without adequate validation, the predictive power of these models may be limited, reducing their utility in practical engineering applications [14].

3 METHODOLOGY

3.1 INTRODUCTION

This chapter outlines the research methodology employed in this study, which integrates empirical testing, data collection, and machine learning techniques to develop and refine predictive models for the structural design of reinforced and prestressed concrete structures. The methodology is designed to systematically address the research question posed in Chapter 1, focusing on enhancing the long-term performance of these structures through a combination of experimental data and advanced computational models.

This study employs a methodology that integrates empirical testing, data collection, and machine learning to enhance the structural design of reinforced and prestressed concrete. The research begins with the selection of materials, including traditional concrete and recycled aggregate concrete (RAC), and the preparation of test specimens, such as beams and bridge consoles, subjected to confining stresses and various loading conditions. Real-time data collection during testing captured critical stress-strain responses, which were validated and analyzed to generate stress-strain curves, assess failure modes, and compare the performance of RAC with traditional concrete. These insights informed the refinement of structural designs, particularly for sustainable construction.

Machine learning models, particularly Random Forest, were employed to predict structural behavior using the collected data. After training and validation, the models demonstrated strong predictive accuracy, outperforming traditional models in predicting stress-strain behavior and failure modes. New predictive equations were developed from these models and validated against empirical data, then integrated into the structural design process. Comparative analysis with existing design codes and real-world validation confirmed the reliability of these models, leading to recommendations for their adoption in industry practices and potential updates to design standards.

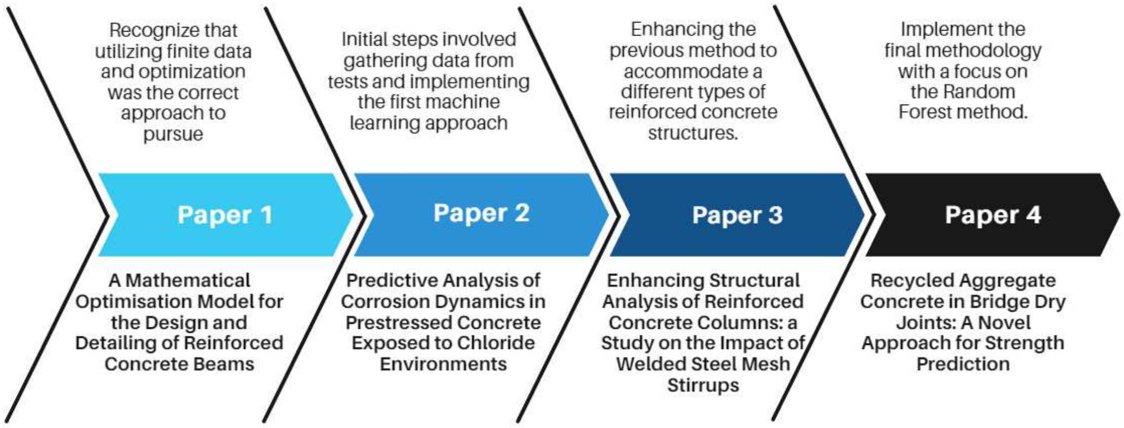

Figure 3.1 – Sequence of methodology publications highlighting their key contributions to the thesis.

3.2 SPECIMEN TESTING

3.2.1 Material Selection

Reinforced and Prestressed Concrete: The study focuses on reinforced and prestressed concrete structures, with an emphasis on understanding how different structural approaches, behave under various stress conditions.

Recycled Aggregates Concrete (RAC): Particular attention is given to RAC due to its increasing use in sustainable construction practices. The variability in RAC properties necessitates thorough testing to understand its structural performance.

3.2.2 Test Specimen Preparation

Specimen Types: The specimens used in this study includes structural bridges consoles, such as flat, single-keyed, and three-keyed RAC dry joint specimens, and also traditional reinforced and prestressed concrete beams.

Dimensions and Configurations: The dimensions and configurations of the specimens were chosen based on standard testing protocols and tailored to investigate specific structural behaviors under stress.

Curing and Conditioning: All specimens underwent standard curing processes, with additional conditioning applied to simulate various environmental exposure conditions relevant to real-world applications.

3.2.3 Testing Procedure

Confining Stresses: Specimens were subjected to confining stresses ranging from 1.0 to 3.0 MPa to simulate the conditions that occur in actual reinforced concrete structures.

Loading Conditions: The specimens were tested under different loading conditions, including compression, tension, and shear, to evaluate their structural behavior comprehensively.

Instrumentation and Data Acquisition: Advanced instrumentation, including strain gauges and load cells, was employed to capture real-time data on the stress-strain response of the specimens. The data acquisition system was calibrated to ensure accuracy and reliability in capturing the critical parameters.

3.3 DATA COLLECTION AND ANALYSIS

3.3.1 Data Collection

Real-Time Monitoring: During the testing phase, data was continuously monitored and recorded to capture the stress-strain behavior of the specimens under various loading conditions.

Environmental Factors: Additional data was collected on environmental factors such as temperature and humidity, which can influence the performance of concrete materials.

Data Validation: The collected data was subjected to rigorous validation procedures to ensure its accuracy and relevance for subsequent analysis.

3.3.2 Analysis of Structural Behavior

Stress-Strain Curves: The primary analysis involved generating stress-strain curves for each specimen to understand their mechanical behavior under different stress conditions.

Failure Modes: The failure modes of the specimens were analyzed to identify critical weaknesses in the material or structural configuration.

Comparative Analysis: A comparative analysis was conducted between RAC and traditional concrete specimens to evaluate differences in performance and identify areas where RAC may require additional reinforcement or design adjustments.

3.4 INTEGRATION OF MACHINE LEARNING MODELS

3.4.1 Model Development

Model Selection: Several machine learning models were initially considered, including linear regression, neural networks, and support vector machines. After evaluating their performance, the Random Forest model was selected due to its superior ability to accurately predict structural behavior using the collected data. The Random Forest model's robustness in handling complex interactions and its capability to provide reliable predictions made it the most suitable choice for this research.

Training and Testing Data: The dataset was split into training and testing sets to evaluate the performance of the models. The training data was used to develop the models, while the testing data was used to assess their predictive accuracy.

Feature Engineering: Key features were extracted from the raw data, such as material properties, stress levels, and environmental factors, to improve the models' predictive capabilities.

3.4.2 Model Training and Validation

Hyperparameter Tuning: The models were fine-tuned using hyperparameter optimization techniques to enhance their performance.

Cross-Validation: Cross-validation was employed to assess the generalizability of the models and prevent overfitting.

Model Evaluation: The models were evaluated based on metrics such as mean squared error (MSE), R-squared, and predictive accuracy to determine their effectiveness in predicting the structural behavior of the specimens.

3.5 PREDICTIVE ACCURACY AND FEATURE IMPORTANCE ANALYSIS

3.5.1 Predictive Accuracy

Performance Metrics: The predictive accuracy of each model was assessed using standard performance metrics, with a focus on how well the models predicted the stress-strain behavior and failure modes observed in the empirical tests.

Comparison with Traditional Models: The performance of the machine learning models was compared with traditional predictive models to evaluate any improvements in accuracy and reliability.

3.5.2 Feature Importance

Identification of Key Features: The models were analyzed to identify which features (e.g., material properties, environmental factors) had the most significant impact on the predictive accuracy.

Interpretability of Results: Efforts were made to enhance the interpretability of the machine learning models, ensuring that the key features identified align with engineering intuition and established knowledge.

3.6 MODEL EVALUATION AND COMPARATIVE ANALYSIS

3.6.1 Model Evaluation

Real-World Validation: The predictive models were validated against real-world performance data where available, ensuring their applicability in practical engineering scenarios.

Sensitivity Analysis: Sensitivity analysis was conducted to understand the robustness of the models under different conditions and to identify any limitations.

3.6.2 Comparative Analysis

Comparison with Standard Codes: The newly developed or refined predictive equations were compared with existing standard codes to assess their reliability and potential for adoption in the industry.

Case Studies: Specific case studies were analyzed to demonstrate the practical application of the models in real-world structural design.

3.7 EQUATION DEVELOPMENT

3.7.1 New Equation Formulation

Equation Derivation: Based on the insights gained from the machine learning models and empirical data, new equations were derived to predict structural behavior more accurately.

Validation Against Empirical Data: The new equations were validated against the empirical data to ensure their accuracy and reliability.

3.7.2 Integration into Design Practice

Application to Structural Design: The newly developed equations were integrated into the structural design process, offering a more precise tool for engineers in designing reinforced and prestressed concrete structures.

Recommendations for Industry Adoption: Recommendations were provided for how these equations could be adopted by the industry, including potential updates to existing design codes.

3.8 METHODOLOGY SCHEMA

To provide a clear and concise overview of the methodology employed in this study, the following schema illustrates the key steps and processes involved in the research. This visual representation encapsulates the integration of empirical testing, data collection, machine learning model development, and the derivation of new predictive equations within the structural design process.

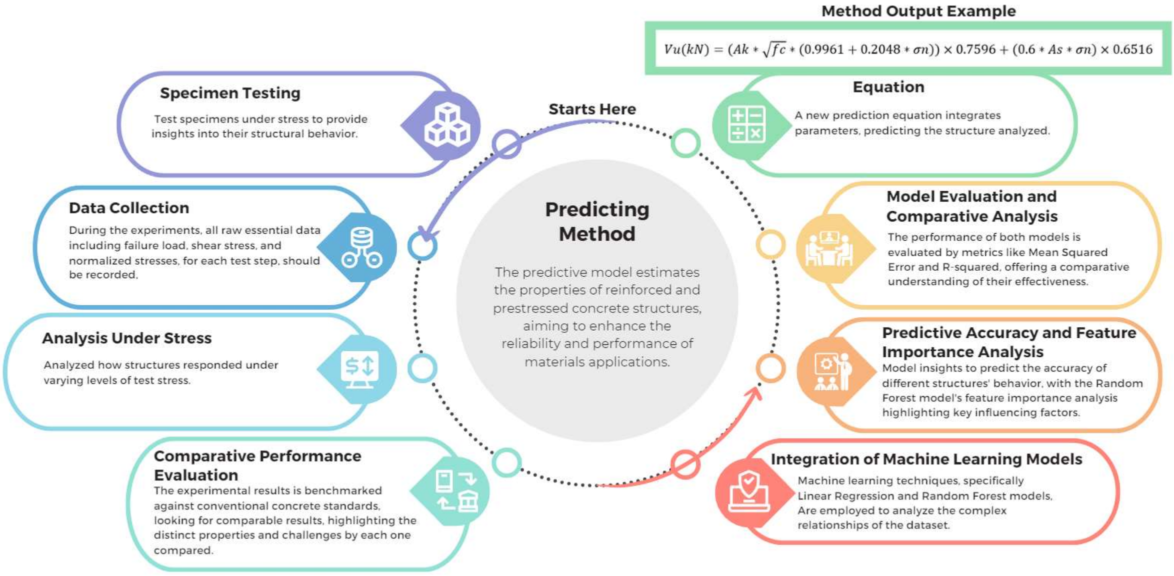

Figure 3.2 - Overview of the research methodology employed in this study, highlighting the sequential steps from specimen testing through to equation development and integration into design practice.

Chapter 4 delves into this foundational shift by introducing a mathematical optimization model specifically designed for the efficient detailing of reinforced concrete. This model represents a departure from traditional continuous optimization techniques, instead utilizing discrete optimization to accurately address the complexities of real-world structures. The chapter explores the development and application of this model, setting the stage for its influence on subsequent research presented in this thesis.

4 A MATHEMATICAL OPTIMISATION MODEL FOR THE DESIGN AND DETAILING OF REINFORCED CONCRETE BEAMS

This chapter is published as an original research article in Engineering Structures. *https://doi.org/10.1016/j.engstruct.2021.112861*

PIEROTT, Rodrigo *et al.*. A mathematical optimisation model for the design and detailing of reinforced concrete beams. **Energy Reports**, v. 7, p. 8162–8175, 2021.

ABSTRACT

An evolutionary metaheuristic optimization model for sizing reinforced concrete beams is presented. The proposed optimization model transcends ones in the literature as it is able to consider characteristic concrete strength (fck), cross-section area and reinforcement bars' diameters as discrete design variables, thus representing a more realistic model. The goal is to minimize construction costs via configuring cross-sectional dimensions, determining reinforcement layouts, and defining fck. The design constraints formulated in the mathematical model proposed are related to structural integrity, considering ultimate limit state, serviceability limit state, and good construction practices. A finite element method program was developed to obtain the stresses and strains of beams, geometries, and load forces. Additionally, a longitudinal reinforcement database generator was developed, ensuring that the reinforcement layouts generated are within codes of practice. A Genetic Algorithm was adopted to solve the resulting optimisation problem. Results of case studies demonstrate that the cost variance implications are directly related to the reinforcement detailing arrangements, with 3.63% to 17.07% improvements in costs that are achieved when compared with other studies in the literature.

Keywords:
Continuous beams; Structural optimization; Reinforced concrete; Genetic algorithm.

4.1 INTRODUCTION

In building and infrastructure construction, rational use of the mechanical characteristics of materials enables the development of more efficient and economical structures. Concrete usage worldwide is very significnat in the existing building stock. Its usage level is estimated to be three tonnes per year for every person around the world [41]. Given that concrete is relatively an expensive material, with many environmental impacts, it is wise to ensure optimized section areas of structural concrete components.

In recent years, the multi-story building construction market has required lighter and more mechanically efficient reinforced concrete structures [20]. Beams are linear structural elements widely adopted in multi-story buildings to resist load applied axially to the structure [2]. Structural beams can be classified mainly as simply supported or continuous beams. Simply supported beams have exactly one span. Continuous beams extend beyond one span, with several supports that may vary. Continuous beams may contain primary and secondary reinforcement aimed at counteracting positive and negative bending moments in critical cross-sections. A simplified example of a continuous beam is illustrated in Fig. 4.1.

In Fig. 4.1, Li is the distance between supports, Si denotes support identification, wi support width, h beam height, bw beam width, and t_{slab} height.

The design of continuous beams contains several critical sections that must be dimensioned considering their respective particularities [19]. For a one-span clamped beam on supports, there is a critical section on the left, mid and right spans, where negative bending moments at the supports are dominant. Thus, it is important to define the cross-section dimensions, the number of bars and layers (reinforcement template), and the best characteristic strength of concrete (fck) for each critical section to counteract the bending moments that result [5].

Rules of thumb adopted by structural designers, such as beam height being 10% of the span length of simply supported beams, or the biggest span length divided by 12 for continuous beams, along with pre-design techniques that are commonly practiced by structural designers worldwide, have not kept pace with the evolution of modern computational tools. Such pre-design techniques are outdated and inefficient, as they generally do not consider structural costs [14].

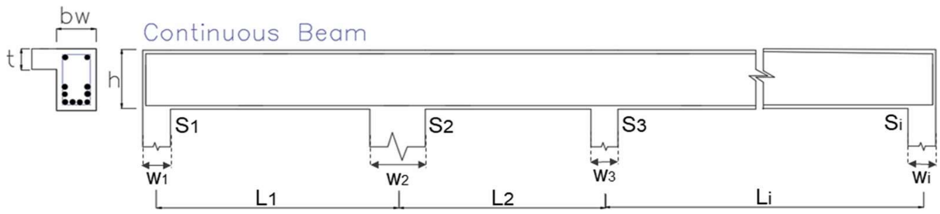

Figure 4.1 - Representation of heat flow in a building and with its energy system

for a given structural problem, where the design constraints imposed are fully satisfied. In the literature, common approaches include the use of optimization to structural purposes. For instance, [27] outlined an application of genetic algorithm based strategies to a class of optimization tasks associated with the design of steel reinforced concrete structures, though the authors did not consider layer limitations and doubly reinforced solutions. [31] developed a methodology to optimize building frames based on minimum embedded CO2 emissions; the design involved optimization via a simulated annealing (SA) algorithm, and the calculation method were simplified, without optimizing steel bar allocation. [40] developed a methodology based on a multi-objective optimization technique that incorporates the performance-based seismic design methodology of concrete building structures, though the authors did not consider serviceability limits in the optimization process and did not optimize reinforcement selection layouts. [39] employed GA with constraints on the mechanical properties of reinforced concrete beams under different load combinations and limited by code restrictions, but did not optimize concrete strength nor reinforcement selection layout. These limitations are addressed in this study.

The optimization model presented herein aims to minimize the fabrication cost of beams following [2] construction guidelines for ultimate limit state analysis and [1] for serviceability limit state analysis. To generate realistic models, discrete design variables are used, such as commercial diameters and the number of longitudinal steel reinforcement bars. Additionally, the height and width of beams and the characteristic strength of concrete (fck) are considered as discrete design variables. The inclusion of fck as a discrete design variable rather than a known amount is one of the highlights of the developed methodology since optimal concrete resistance may lead to more efficient mechanical designs.

The design constraints considered in the optimization model are those proposed by the standard code of practice [2] and [1]. Thus, resistance and ductility constraints that satisfy the ultimate limit state (ULS) and restrictions related to deflection and durability required by the serviceability limit state (SLS) are considered.

4.1.1 Literature review

The literature contains several studies on the optimization of reinforced concrete beams, mostly related to simply supported beams, with few that focus on continuous beams. [22] developed a methodology for reinforced concrete optimization in continuous beams, comparing their results with those obtained by [23]. The optimization model considers cross-section height as a design variable. The authors used reinforcement tables for each beam cross-section. Thus, reinforcement was not considered as a design variable but was determined from the smallest steel area available from the database related to the current cross- section. The design constraints were the ULS conditions, and GA was used as the optimization algorithm.

[26] developed an optimization methodology for a reinforced concrete system of columns and beams. They constructed a database containing the cross-sections of pre-established beams and columns. Dynamic programming was used to find the most economical section within the pre-defined database in the optimization process. The objective was to find a preliminary design of RC frame structures, yet the method goal was not to find global optimal solutions, but rather improved solutions.

[7] presented a method for the structural optimization of reinforced concrete beams on a minimal cost problem. The design variables were neutral axis (x) height and reinforcement area (As), both defined as continuous variables. The authors used a classical mathematical programming algorithm based on the Kuhn-Tucker (KKT) optimality condition. Singly and doubly reinforced sections were analyzed separately.

[3] proposed a methodology using GA to find the optimal cost of RC prestressed simply supported beams, according to the ACI 318-05. The design variables considered were width, depth, number of flexural bars, diameters of flexural bars, number and diameters of tendons of the beam, and the eccentricity of the tendons. No SLS or reinforcement detailing was performed.

[17] developed a methodology to optimize cross-sections of columns submitted to bending, considering the materials' non-linearity. The technique sought an optimal solution within a predetermined database of possibilities, aided by genetic algorithms. The author used the finite element method (FEM) to obtain the displacements of the elements analyzed.

[15] studied RC structures' design, such as beams and columns, considering the Indian Standards and using the enhanced Particle Swarm Optimization (PSO) algorithm. The study's objective was to get the optimal cost of these structures. RC beams had been designed assuming that the independent design variables were the beam width and depth; other design parameters were calculated accordingly. No doubly reinforced sections were analyzed in the study.

[38] Presented an optimum design of reinforced concrete beams using metaheuristic methods. The optimization method utilised the harmony search algorithm (HS) and proved to be effective in solving the problem via several random stages. The proposed method was tested for two-story, two-span RC frames. The results show that metaheuristic- based methodology is feasible but presented no mentioning of SLS and ULS.

According to [35], the complexity of the RC beams design optimization problem had led to many oversimplified models in the literature, as current metaheuristic search algorithms cannot deal with the design problem efficiently. The authors instead proposed new design variables, such as cutoff steel and percent of positive and negative bending cutoff steel, along with a new parameter-setting-free harmony search algorithm. The optimization objectives were to minimize the total cost, total weight, and the cost/weight simultaneously for designing concrete beams. The final results came up with optimal reinforcement detailing.

[24] analyzed a sustainable design of reinforced concrete frames with non-prismatic beams. The relation between optimal cost and optimal carbon dioxide emission was analyzed. The objective functions minimized the CO2 emissions and construction cost, and the design variables were defined as the cross-section geometry and reinforcing bars of beams and columns. The performance of five optimization algorithms was compared for the proposed methodology. No realistic detailing was proposed, nor SLS constraints were implemented.

[25] presented a standardized formulation procedure for the cost- safety optimization of the steel–concrete composite beam (SCCB). A sensitivity analysis was performed to investigate the influence of design parameters of the steel profile. The results obtained indicated that the standardized formulation has the appropriate capability to yield significant savings on cost and improve the safety of SCCB regarding steel beams.

Some works present the relations of doubly reinforcement as part of the optimization process, including [8] and [18] who developed methodologies considering doubly reinforcement predefined cases. [9] developed the previous methodology, and [36] followed a similar methodology but applied Particle Swarm Algorithm. In these works, all reinforcement (single and doubly) needed were calculated after the optimization process of choosing the beam cross-section. In this way, the optimization process tries only different cross-sections and not different reinforcement layouts. The approach thus does not have the freedom to try doubly reinforcements as the top reinforcement are not independent design variables. This limitation fails to find solutions in which doubly reinforcement are enforced, as determined by the standard calculation code design proposed by [2] and demonstrated in Fig. 4.2.

Three studies were taken into account when the proposed methodology was developed for this study, namely [5], [30] and [38]. The main idea behind these three works is that they proposed an adaptation of real structures to fit an optimization model. [5] and [38] presented a feasible way to approach optimization in High-rise buildings structures while [30] came up with different load geometry applied over beams. None of the previous studies however presented a realistic reinforcement detailing solution nor SLS constraints.

The presented literature handled the problem of designing reinforced concrete members by simplifying and ignoring the complexity of strucutral design, such as doubly reinforcement solution verifications, as well as calculating required steel reinforcement after cross-section definition. This approach disallows the optimization process to try uncommon or unexpected layouts, losing some possible optimal solutions and never finding doubly reinforcement solutions.

4.1.2 RESEARCH SIGNIFICANCE

The design of reinforced concrete structures using optimization methods represents a major challenge [29]. This is because concrete structures are composite materials with many calculation factors presented in standard codes. This is not the case when steel or masonry is adopted as the main structural material in the building. Another degree of difficulty is providing optimal designs that are detailed enough to be easily adopted and applicable to reality, and in accordance with international codes, manuals and recommendations [12,10].

For reinforced concrete structures, simplification must be wisely applied since missing parameters, such as deformation domains of concrete structures, can result in non-optimal solution, along with disregarding solutions that could have been optimal. For instance, disallowing double reinforcement in the calculation process because of its recursive calculation nature would be easier to implement but would not represent real projects. In general, doubly reinforced concrete sections drag the neutral axis of beams near the centre of the beam and grant better overall resistance to beams. Depending on the region’s steel cost, the optimization considering the reinforcement bars as design variables can reach cheaper results with double reinforcement compared to a single reinforcement section. In this situation, an algorithm that does not consider the reinforcement bars as a design variable will not find optimal solutions.

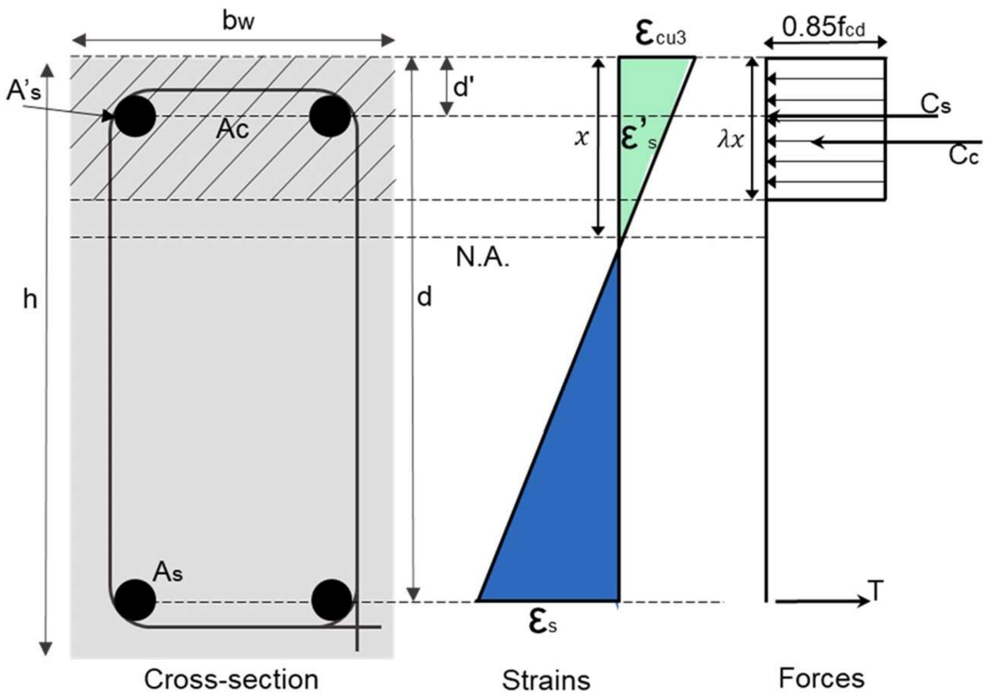

Figure 4.2 - Doubly reinforcement with top reinforcement collaboration [2].

Till date, the most widespread design software used for reinforced concrete structures does not include an improved optimization technique to establish characteristics such as reinforcement layout, crosssection length, or properties, such as concrete strength of structural elements. It is possible that such an important improvement is not implemented because the structural optimization methods available are not usable in realistic projects.

The base parameters and assumptions related to optimization reinforced concrete beams, such as ACI requirements (steel and concrete limit ratio, deflection limit, crack opening limit, neutral axis depth limits, clear spacing limits between stirrups and others), and a wider diversity of design variables limitations, such as maximum number and usage of different diameters of steel bars, width, and height limits of beams, were not well implemented in previous studies.

In the present study, a new computational methodology is proposed for the optimization of the geometrical sizing of reinforced concrete continuous beam sections, accounting for commercial diameters for reinforcing steel bars and different concrete strengths, while complying with the latest American Concrete Institute code requirements for both resistance and serviceability conditions. Discrete variables were used to better represent realistic structures since the output of the structural design process is usually determined not as steel area and not as continuous widths and heights, but as discrete numbers of bars in discrete stepped sizes (15 cm, 20 cm, 25 cm instead of 17.48 cm for instance). A wide range of reinforcement possibilities are defined for the critical sections of beams in this study. A reinforcement database is generated within a computational module developed based on codes requirements, which defines and stores hundreds of realistic steel reinforcement possibilities that satisfy geometric restrictions, according to [2]; this database is automatically generated in the initial steps of the optimization process. A FEM program is also designed to obtain the stress and strains on critical sections of continuous beams, with different geometries and load forces applied; here, load combinations as described in [2] and [1] are considered. The FEM was implemented following the CALFEM [6] program. The bending moment redistribution is performed as recommended in [2] and [1]. Second, a GA method is developed, generating various populations with realistic solution candidates that utilize as input the boundary conditions, commercial material properties, and structural information as spans sizes and applied loads. According to [4], optimization using GA exhibits satisfactory computational performance and robustness; it has high capability in determining the global minima, along with dealing with discrete, continuous, and mixed design variables, as [21] subsequently confirmed. Third, the solutions are generated and analyzed iteratively, which leads to better candidates, that converge to optimal solutions.

The analyses that are described in the next sections are well implemented in the proposed method, enabling the consideration of several reinforced concrete verifications, without core modifications to real-life scenarios. This enables realistic reinforcement design to be generated.

4.1.3 Reinforced concrete optimization framework

Computational codes were developed to carry out the optimization process and all verifications needed for concrete beam structures. Fig. 4.3 displays a flowchart of the entire optimization process.

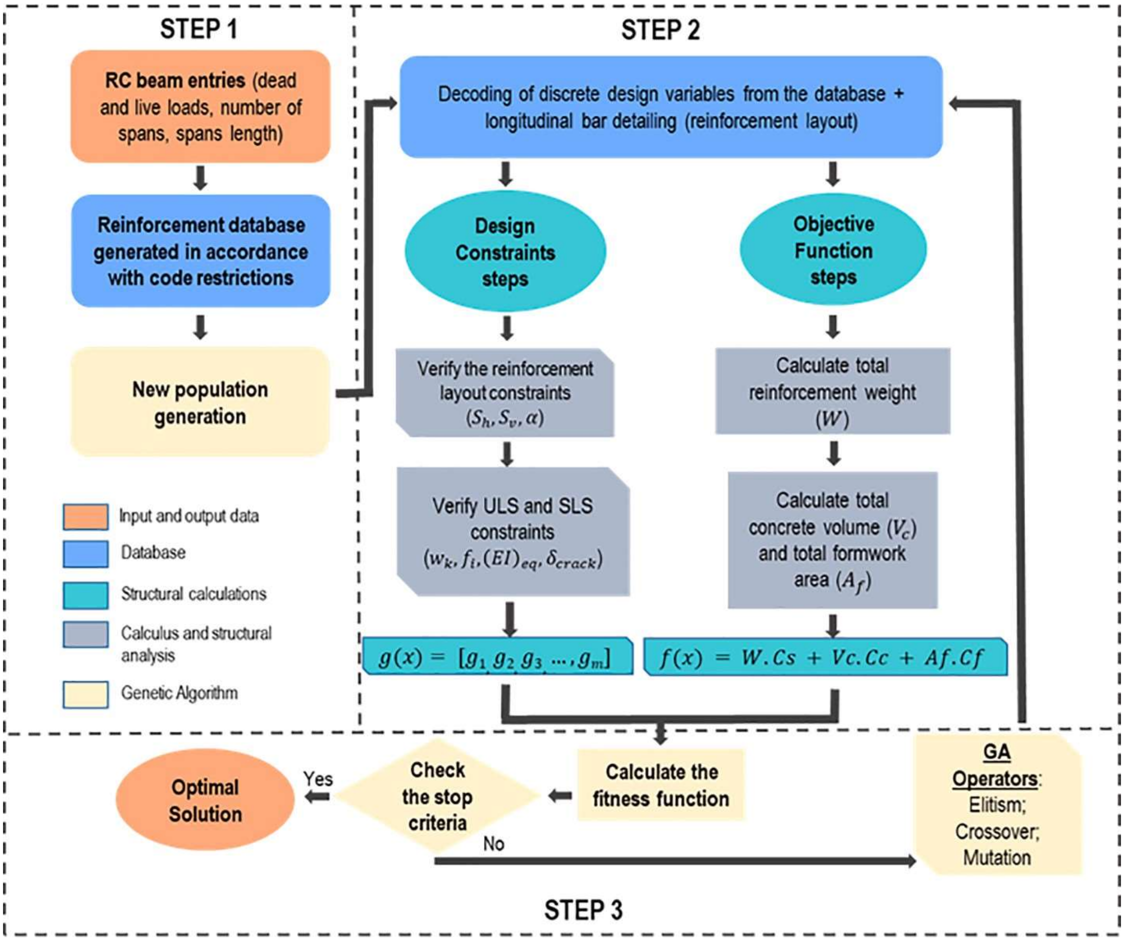

Figure 4.3 - Flowchart of the computational method developed.

4.2 REINFORCEMENT MODEL DETAILING WITHIN THE DATABASE GENERATOR

The optimization model proposed here considers RC beams' particular characteristics, such as geometry, steel reinforcement, concrete strength, loading, and support conditions as presented in RC beam entries step in Fig. 4.3.

Initially, a general optimization method that is similar to the existing literature may present issues when many constraints are assigned. The usage of correlated constraints can limit the systematic optimization search, slows the optimization algorithm, and limits the range of possible solutions. As such, a different approach was adopted in this study. Specifically, an algorithm was created separate from the constraints, in order to generate reinforcement detailing solutions that comply with requirements and boundary conditions [2]. These detailing solutions were then stored in a structured database. The algorithm is easily updated for different standard code requirements. Table 4.1 is presented to summarise all the notation adopted throughout the study. It is important to note that the usage of the created database generator algorithm for every chromosome is not recommended, since it may complicate the selection of the needed reinforcement layout and may mislead the fitness function. The algorithm generates a comprehensive database based on the most common possibilities of reinforcement templates in a beam structure, considering the maximum dimensions for setting the highest number of reinforcement possibilities. As a result, any reinforcement template requested by the optimization process is contained in the database. After that, the database is sorted by the total steel area (in Database Generation within the Setup Stage of Fig. 4.3). The optimization process may use all the possibilities for the design pre-set, allowing the GA to penalize solutions that do not follow the reinforcement allocation constraints. The reinforcement allocation requirements were implemented with three constraints, being Sh, Sv, and α (as presented in Decoding of discrete design variable from database & Longitudinal bar detailing in Step 2 of Fig. 4.3). Furthermore, depending on the designer region (standard code limitations), the designer may set up the database generator algorithm to only use one reinforcement diameter or one diameter for each layer or even let the optimization process completely mix reinforcement diameters in all layers.

For continuous beams, the database generator defines the reinforcement in critical sections by generating possible reinforcement layouts in these sections. The critical sections are important since they represent maximum bending moments at different regions of the beam. The reinforcement in critical sections defines the longitudinal reinforcement template for continuous beams. Critical sections' locations for a simply supported beam are shown in Fig. 4.4, and the number of commercial steel bars and reinforcement layers with their corresponding positions, can be seen in Fig. 4.5.

The main terms defined in the algorithm are represented in Figs. 6 and 7.

Reinforcements in critical sections are restricted by code rules, such as [2], and may contain:

- Maximum number of reinforcement layers;
- Maximum number of bars per layer (for the present study, the maximum number that can be used in each layer, if it complies with Sv, Sh, and α;
- Each layer must contain bars with the same commercial diameter (gauge);
- Minimum and maximum clear horizontal and vertical spacing between bars;
- Clear side cover

In accordance with steel bars commercialized in Brazil and Australia, the following commercial gauges for longitudinal reinforcements were considered: 6.3, 8, 10, 12.5, 16, 20, 22.5, 26, 32mm.

Fig. 4.6 presents a simplified reinforcement layout creation that is developed automatically, independent of the RC cross-section beam, by the database generator that will be discussed later in this section.

Looking at Fig. 4.6, the database generator algorithm works as follows: To create reinforcement templates, each reinforcement possibility is created with the addition of a new reinforcement bar. The algorithm starts by creating the first template with two of the minimal reinforcement diameters and keeps adding reinforcement bars until all the possibilities constrained by codes are created. This addition of bars continues to the next layer if the distance Sh allows it, and if the total steel area of the previous layer is greater than or equal to the total steel area of the next layer, as limited by code and the alpha (α) limits imposed. The database generation demonstrated in Fig. 4.6 is showing the generation of a reinforcement template, starting with bars of 12.5 mm. For example, the following information would be required before continuing to generate the reinforcement database proposed in Fig. 4.6.

Table 4.1 - Notations and symbols used in the proposed optimization model.

Notation	Description	Notation	Description	Notation	Description
bw	Beam width (cm)	Csc	Concrete section cover (cm)	βx	Ductility parameter
h	Beam height (cm)	CG	Center of gravity (cm)	x	Neutral axis (cm)
As_i	Steel area (cm^2)	$Smax$	Maximum horizontal clear spacing (mm)	d	Effective height of the beam (cm)
fck	Characteristic strength of concrete (MPa)	fi	Initial deflection (mm)	fcd	Design strength of concrete (MPa)
t	Slab height (cm)	αf	Deflection factor	fi	Initial deflection (mm)
L_i	Distance between supports (cm)	$(EI)eq$	Equivalent resistance of the beam (GPa)	Msd	Design bending moment (kN.m)
CC	Concrete cost (depending on resistance) ($/m3)	Mr	Concrete cracking bending moment (kN.m)	Mu	Ultimate bending moment (kN.m)
CS	Steel cost ($/kg)	Ic	Moment of inertia of the gross concrete section (kN.m)	w_k	Crack opening (mm)
Cf	Formwork cost ($/m^2)	σs	Tensile stress at the center of gravity of the considered bar gauge (MPa)	Sh	Horizontal clear spacing (mm)
w	Support width (cm)	pr	Passive reinforcement ratio (%)	Sv	Vertical clear spacing (mm)
τwd	Shear design stress (Mpa)	Asc	Compressed steel area (cm^2)	n_{stir}	Number of stirrups
$\tau wd2$	Shear resistance stress (MPa)	Def_{inf}	Deflection at an infinite time (mm)	α	Distance between total steel area and first layer steel area (cm)
$Sstir$	Clear spacing between stirrups (mm)	wk_{allow}	Crack opening limit (mm)	dk	Stirrup gauge size (mm)
η_1	Reinforcement type	Wt	Transverse steel weight (kg)	Vc	Volume of concrete (m^3)
η_{ij}	Number of stirrups in shear region i of span j	Ws	Longitudinal and transverse steel weight (kg)	d'	Effective depth from the top of a reinforced concrete beam to the centroid of the compression steel (cm)
ρr	Steel reduction factor	Af	Formwork area (m^2)	$f_{t=\infty}$	Final deflection (mm)
ϕ_i	Longitudinal bar gauge in	L	Span Length (cm)	Ma	Concrete bending moment of most requested

	the first layer (mm)				serviceability (kN.m)
ρs	Specific steel weight (kg/cm^3)	Ecs	Concrete secant modulus of elasticity (GPa)	I_{II}	Part's moment of inertia in stage II (kN.m)
Es	Modulus of elasticity of the steel bar (GPa)	$\delta cracking$	Cracking limit (mm)	Ast	Tractive steel area (cm^2)
$Deflimit$	Maximum deflection allowed (mm)	$x23$	Neutral axis position of domain 2-3 (cm)	$x34$	Neutral axis position of domain 3-4 (cm)
Fd	Ultimate combination case load (kN)	γq	Coeficient for variable loads	Fgk	Permanent direct load (kN)
γg	Coeficient for permanent loads	$\psi 0\varepsilon$	Unstable variable indirect loads factor	$F\varepsilon gk$	Retraction action load (kN)
$\gamma \varepsilon g$	Coeficient for constructive loads	$F\varepsilon qk$	Temperature action load (kN)	$Fq1k$	Variable loads (kN)
$Fqjk$	Permanent indirect load (kN)	$\psi 0j$	Unstable variable direct loads factor		

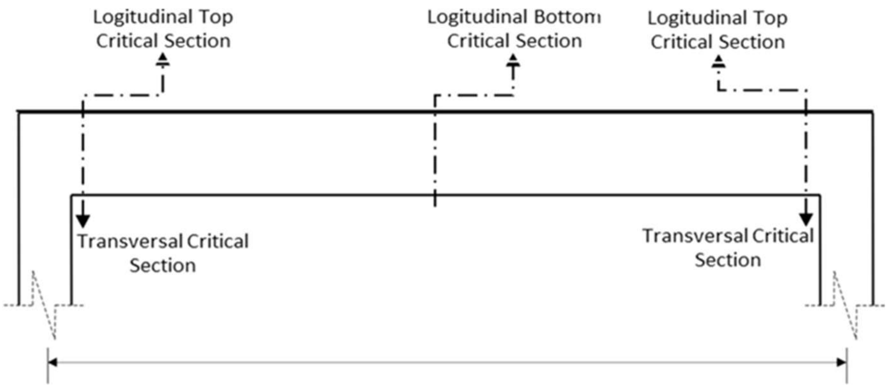

Figure 4.4 - Representation of critical sections positions in an RC beam.

- Clear side cover (Csc): 30 mm;
- Maximum number of reinforcement layers: as many as parameter α allows;
- Minimum clear spacing required between bars, Sh and Sv: based on code provisions;
- Maximum number of bars allowed in each layer: as many as Sh allows;
- Possibilities for bar gauges in each layer: personal designer choice considering region commercial bars and workability with reinforcement bars.

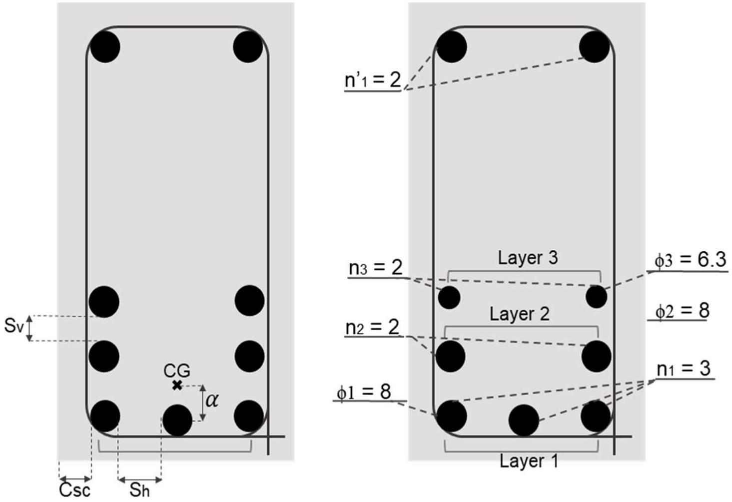

Figure 4.5 - Schematic representation of terms, layers, number of bars, and gauges in a standard reinforced concrete beam used in the proposed approach.

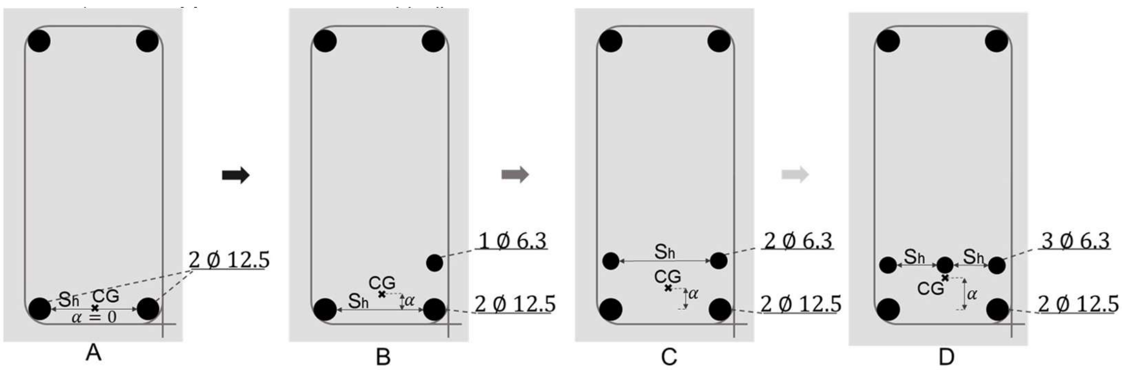

Figure 4.6 - Sample of the database generator process.

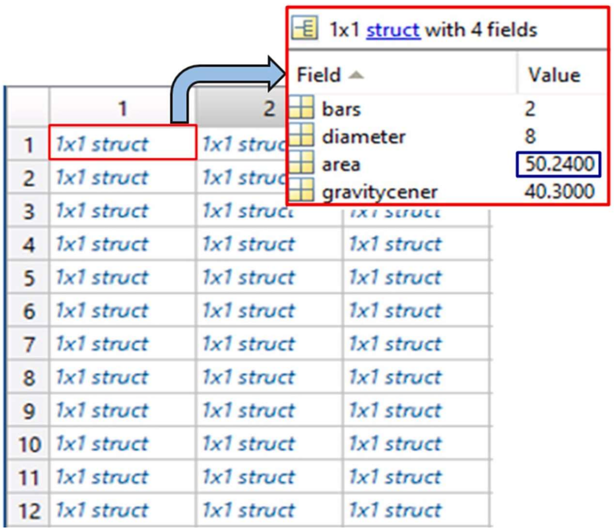

Figure 4.7 - Example of reinforcement template possibilities database (MATLAB, 2016).

To demonstrate how the Database Generator works, an example is given in Fig. 4.6. Fig. 4.6A indicates the initial reinforcement template (two 12.5 mm bars in the first layer for this example). In Fig. 4.6B, there is a geometrical impossibility of adding another 12.5 mm bar to layer 1, since Sh would be less than the minimum allowed by code. Then, the creation of a new layer starting with a 6.3 mm bar (since 6.3 mm bar is the smallest in the list of commercial gauges given by the user) and respecting the α limit is required. Then, in Fig. 4.6C, an addition of the second 6.3 mm bar in layer 2 creates a new reinforcement layout. In Fig. 4.6D, addition of the third 6.3 mm bar to layer 2, respects the condition: $Asn \leq Asn+1$ and another reinforcement layout is created and stored in the database generated.

Thus, respecting α limit, the spacing and steel area limits, the templates are generated according to current codes.

According to international standard codes and best practices, the following constraints are applied [32,2]:

- In the previous layer, the total steel area shall be greater than or equal to the next layer total steel area.
- The number of bars for the bottom and top steel layer shall be greater than or equal to 2, for stirrup allocation purposes.
- The distance between the centre of gravity (CG) of the first layer and CG of all layers (this distance is called α) shall be equal or less than 10% of the beam height (h).

- Total steel area (bottom plus top plus lateral bars) shall be less than or equal to 4% of the concrete cross-section (bw*h).
- The steel area (bottom or top) shall be less than or equal to 50% of the secondary steel area for doubly reinforced limits.

Considering the total number of longitudinal reinforcement possibilities generated in the database, the overall number of possible configurations for the longitudinal reinforcement template depends directly on the boundary conditions of the analysis. Each database position has different numbers and gauges in each layer. An example of the database generated by the proposed algorithm is presented in Fig. 4.7. As shown, the database is generated and stored as a three-dimensional matrix. Each line contains a complete reinforcement layout, and each cell represents information about its respective layer, such as the number of bars, bar gauge, total steel layer area, and the layer's CG etc. The database is sorted by the total steel area.

For instance, all the cells of the first line represent an entire reinforcement layout. The first line and first column cell contain the information of layer 1 of the first reinforcement layout. These cells are organized as a structure of 4 fields as shown in Fig. 4.7. The entire line has information on all the layers of a respective reinforcement layout. All this data comprises the reinforcement layout database. The selection of the reinforcement layout is performed in the new population generation, shown in Fig. 4.3.

4.2.1 Selection of the reinforcement templates

The reinforcement template is selected from a database spreadsheet for each critical section. Each reinforcement is typically located on the left, mid, and right spans. The reinforcement bar layout for all critical sections generates a continuous beam model. The process of selecting reinforcement layouts is repeated for every span, creating the entire RC bream's reinforcement detailing.

4.2.2 Shear reinforcement

In the form of vertical stirrups, shear reinforcements are determined by dividing the shear force envelope into three regions. An example of a shear envelope region is presented in Fig. 4.8. For each region, different spacing and gauges are tested.

The optimized shear reinforcement module considers 5, 6.3, 8, 10, and 12.5 mm as commercial gauges. For each shear envelope region, the module starts from the first gauge (5 mm) and proceeds to the verification code with 90-degree stirrups. The computer module finds the maximum and minimum spacing. The validation of the reinforcement for 90-degree stirrups is given by verifying if the shear force applied (Vsd) is greater than or equal to the shear force resistance of the section (Vrd), as can be obtained by Eq. (4.1).

$$\mathrm{Vrd} = 0,27.\left(1 - \frac{\mathrm{fck}}{250}\right).\mathrm{fcd.bw.d} \qquad (1)$$

If the spacing exceeds the maximum allowed by code, the spacing is set as the maximum (same as spacing 2 from Fig. 4.8), and the region is considered reinforced. If the spacing is between the maximum and minimum allowed by the code (same as spacing 1 and 3 from Fig. 8), the region is considered as reinforced. If the spacing is smaller than the minimum allowed by code, the computer module recursively tries the next gauge until it finds the optimal solution. If the horizontal spacing is smaller than the minimum and the gauge is set at 12.5 mm, the module returns a message indicating the configuration is impossible to design. Fig. 4.8 presents an example of three reinforcements at their shear regions, using the method described above. After the detailing of vertical reinforcement, the proposed method calculates the total vertical reinforcement weight, as shown in Fig. 4.3 in the Objective Function steps.

The optimization model considers the maximum and minimum spacing limits in the constraints function, along with the stirrup weight. Eq. (4.2) is used to calculate the vertical stirrup weight. Reinforcement layouts is repeated for every span, creating the entire RC bream's reinforcement detailing.

$$Wt = \sum_{i=1}^{n} \sum_{j=1}^{3} \pi \times \frac{dk^2}{4} \times n_{ij} \times L_i \qquad (2)$$

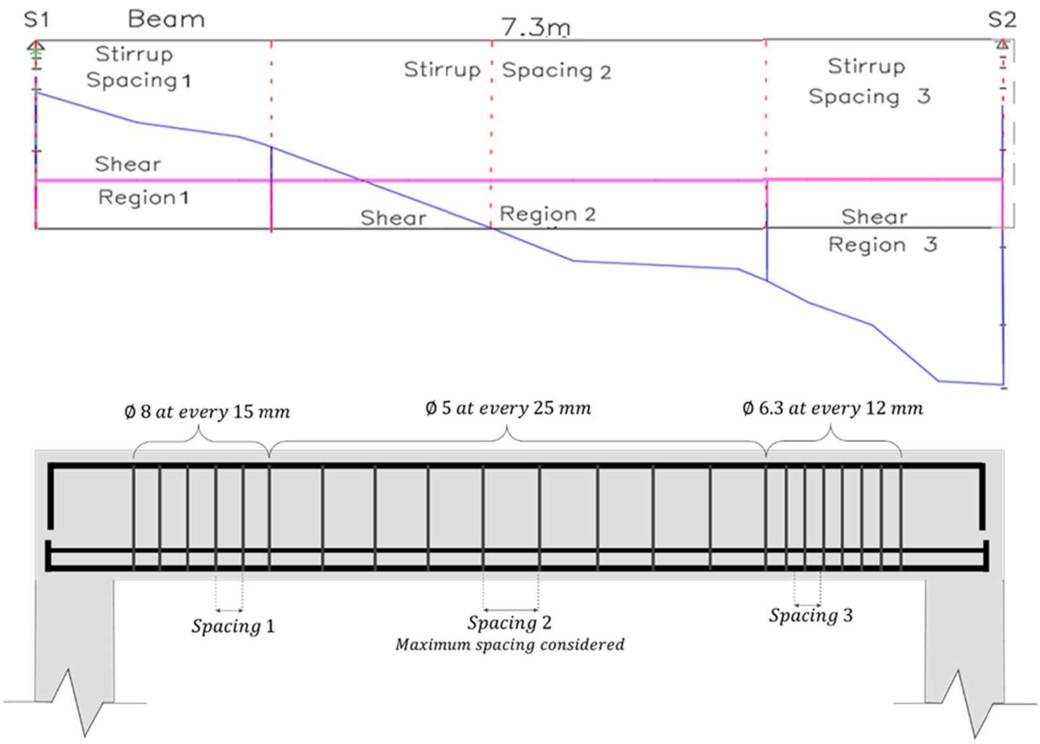

Figure 4.8 - Example of a beam with reinforcements of three shear regions, left, middle, and right.

4.3 OPTIMIZATION MODEL

Formulating the optimal strctural design problem consists of identifying the design variables, the objective function (fobj), and constraints to be satisfied (gi(X) and hi(X)). The fobj shall be optimised, subject to satisfying the equality and inequality constraints gi(X) hj(X) respectively, and within the lower (Xl) and upper boundaries (Xu) of the problem, as can be seen in Eqs. (4.3)–(4.5).

$$f_{obj} = f(X) \tag{3}$$

Subject to:
$g_i(X) = 0$, i = 1, 2,…, m
$h_j(X) \leq 0$, j = 1, 2,…, p.(4)Where:

$$X^l < X^n < X^u \tag{5}$$

Where m and p are the number of equality and inequality design constraints, respectively; l and u the lower and upper bounds of design variables, and n is the current design variable.

The structural optimization problem formulated in this study aims to minimize beam fabrication cost, while obtaining realistic designs. The constraints are formulated based on serviceability and ultimate limit strength constraints, along with structural designers' preferences, following standard codes' prescriptions. The solution optimizes the reinforced concrete steel bars layouts, with relatively low computational cost.

4.3.1 Finite element method

Finite Element Method (FEM) is a numerical procedure widely used in engineering research and other study fields [33]. In the present study, FEM supplies the optimization model information regarding the stress and strain of continuous beams generated by the optimization model. The CALFEM program libraries, a software procedure library based on the FEM technique, was implemented inside the optimization process, allowing the optimization algorithm to request loads for different optimal candidates and calculate the stress and strain of reinforced concrete beams. FEM was carried out in a batch-oriented fashion. The sequence of functions is written in a separate file for the entire population of chromosomes of the GA. Four main functions were used to implement FEM within the optimization method developed, namely Material function, Element function, System function, and Matrix function. The Material function contains methods for constitutive models to treat linear elastic and isotropic hardening von Mises materials. The Element function contains methods to create an element and forces for a beam elements matrix. The System function comprises the systems of equations related to FEM, containing static functions (eigenvalue analysis, static condensation, element displacements, and coordinates) and dynamic functions (modal analysis and frequency domain analysis). The Matrix function comprises matrix operations methods and sparse matrix handling since sparse matrices are not created automatically, but once initiated, sparsity propagates.

Operation on sparse matrices usually produces other sparse matrices, and operations mixing sparse and full matrices also usually produce sparse matrices [6].

4.3.2 Genetic algorithm

Metaheuristic methods emerged in the last quarter of the 20th century. They are stochastic optimization methods inspired by biological and natural observations . The number of metaheuristic algorithms is continuously increasing with new analogies imitating various phenomena. One of the first metaheuristic techniques used is GA. Using GA makes it possible to reach successful results in structural engineering problems without necessitating complex mathematical programming approaches. Constraints in GA can be handled easily if compared to classical optimization techniques [37].

The GA technique coded herein is based on improving a bunch of candidate solutions. This algorithm is easy to implement, does not depend on other heuristics, and may be used independently to solve parts of a problem using discrete and continuous variables with external algorithms (for the present work, the database generator algorithm is used as an external algorithm to GA). The Matlab Global Optimization Toolbox provides several algorithms to find optimal configurations in engineering problems, including the GA module used in the present study.

GA begins with the input parameters, being an objective function (OF), constraints functions (CF), lower boundary (lb), upper boundary (ub), population size (n), maximum generations number (g_{max}), tolerance function (t_f), fitness value (χ), and mutation rate (μ). After the algorithm gathers the input parameters, it starts generating a random initial population, consisting of a set of elements denominated chromosomes, which are the solution candidates. Each chromosome of the population is evaluated iteratively through a measure of its suitability as a good solution candidate. The algorithm performs characteristic exchanges between two chromosomes to generate new populations, creating new individuals, following the recursive optimization operation, as shown in Fig. 4.9.

For each iteration of the optimization process, the fitness function makes it possible to identify candidates with better characteristics. Thus, some of the best chromosomes are selected during the crossover steps. Several techniques can be used to choose the chromosomes that will undergo the crossover process, including roulette, Boltzmann, championship, classification, and steady-state selection, among others [34].

The stochastic uniform selection was used in the present study.

Briefly, the algorithm begins generating an initial population, and on each GA iteration, the solution candidates are submitted to three evolution stages (selection, crossover, and mutation). Applying these operations makes it possible to define new populations, which are closer to the optimal result. The GA is recursively repeated for several generations until it reaches a predetermined tolerance, and the optimal solution for the proposed problem is given [28]. Table 4.2 presents the principal GA configurations used in the present study.

Maximum stall generations and function tolerance are related since one of the algorithms stopping criteria happens if the average relative change in the best fitness function value in the range of the maximum stall generations is less than or equal to the function tolerance, and the constraint tolerance is used to determine if a linear or nonlinear constraint is feasible.

4.3.3 Design variables

In realistic design processes, reinforcement templates are defined by the commercial gauges and the number of bars used in each reinforcement layer. Thus, discrete variables better represent a realistic structural design process than continuous variables. This step is performed to decode discrete Design Variables step presented in Fig. 4.3, when the database and reinforcement detailing of beams are created.

Using the concrete fck property as a design variable raises the possibility of finding better results even in more complex problems since defining smaller cross-sections and optimizing material costs usually makes the structure lighter, achieving lower bending moments and smaller cross-sections. Using high strength concrete increases the overall cost of the concrete, however. As such, it is important to ensure that fck is assigned as a design variable as this can greatly improve the optimization cost of structures. The use of fck as a design variable is one of the major highlights of the present study. Thus, all design variables (h, bw, As and fck) used in the proposed method are discrete design variables.

// **Algorithm output**:
Solution value;
Objective function value at the solution;
Exit flag code related to the reason the algorithm stopped;
Number of generations computed;
Number of evaluations of the fitness function;
Final scores related to the penalty fitness values of the population members;
// **Database generator based on boundaries conditions**
Generation of the database with the aid of CF;
// **Initialise generation 0**:
$k := 0$;
$P :=$ *a population of n randomly generated beams individuals within lb and up*;
// **Evaluate** P_k:
Compute fitness(i) *for each* $i \in P_k$;
do
{ // *Create generation* $k + 1$:
// **1. Selection**:
Select $(\chi) \times n$ *members of* P_k *and insert into* $P_k + 1$ *based on fitness*
and roulette wheel selection rank (χ);
// **2. Crossover**:

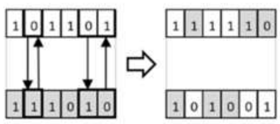

Select $\chi \times n$ *members of* P_k *within roulette*; *pair them up*
// *produce offspring*; *insert the offspring into* $P_k + 1$;
// **3. Mutation**:

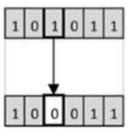

Select $\mu \times n$ *members of* $P_k + 1$; *invert a randomly − selected bit in each*;
// **Evaluate** $P_k + 1$:
Compute fitness(i) *for each* $i \in P_k$ *based on OF and penalized by CF*;
// **Increment**:
$k := k + 1$;
}
while *fitness of fittest individual in* P_k *is not high enough* (t_f) **NOR** n_{max};
return *the fittest individual from* P_k;

Figure 4.9 - Genetic Algorithm optimization pseudocode based on the presented methodology usage.

Table 4.2 – Fine tunning.

Genetic Algorithm Configurations	
Population Size	100
Generation	75
Elite Count	70
Mutation	$12*10^{-4}$
Crossover Fraction	0.85
Maximum Stall Generations	20
Initial Penalty	8
Penalty Factor	85
Function Tolerance	10^{-4}
Constraint Tolerance	10^{-4}

4.3.4 Objective functions

The convergence phenomenon present in evolutionary algorithms is treated in the present study by diversifying the initial population. The algorithm developed creates a regular average distance between individuals of the population by prior tuning the initial population range function. Two of the stopping criteria consider optimization convergence directly. The stopping criteria used are maximum stall generations (when the average relative change in fitness function is less the pre-set tolerance) and maximum stall time (when there is no improvement in the objective function during a pre-set interval of time).The Objective Function steps can be seen in Fig. 4.3. The objective function considers the costs associated with the construction of continuous beams, namely formwork, concrete (volume and changes for each fck available), and reinforcement costs (considering longitudinal primary and secondary, lateral, and transverse reinforcements). Material costs depend on each study and generally includes labor cost. The simplified cost expression is presented by Eq. (4.6).

$$F = Vc.Cc + Ws.Cs + Af.Cf \tag{6}$$

The volume of concrete is calculated as shown in Eq. (7), by finding the total beam volume.

$$Vc = \left(\sum_{i=1}^{n} bw.(h-t).L_i\right) + bw.(h-t).\left(\frac{w_1 + w_{n+1}}{2}\right) \tag{7}$$

The formwork area, Af is calculated as shown in Eq. (8) by finding the perimeter areas without the beam's top face.

$$Af = \sum_{i=1}^{n} (bw + 2.h).L_i + 2.\left(\left\{\sum_{i=1}^{n+1} h.w_i\right\} + bw.h\right) \tag{8}$$

The steel weight is calculated as shown in Eq. (9) by finding the total steel volume (Asi .Li plus stirrup volume) and multiplying by the steel specific weight (ρs).

$$Ws = \left\{ \sum_{i=1}^{2.n+1} (As_i .L_i) + \left(\frac{\pi.dstir^2}{4} .2.(bw + h - 4.Cs + 10) \right) nstir \right\} \rho s \quad (9)$$

Fig. 4.10 presents some parameters adopted in the present RC beam model. The following parameters must be specified before the optimization process in order to determine the variables: loading conditions, support conditions, unit costs of different materials, and spacing/cover detailing requirements.

Since the slab is not part of the optimization process, to obtain the beam's concrete volume, the beam and slab are assumed not to be cast monolithically. As such, thickness (t) is considered a constant parameter and is disregarded in the total concrete volume by subtracting it from the beam height (h).

4.3.5 Fitness function

The GA function that is responsible for the whole computational GA optimization steps can handle linear and nonlinear constraints, with each handled differently. For the linear constraints, all the bounds are satisfied throughout the optimization process since the use of the crossover function only generates feasible points. But since the GA function is not able to meet all nonlinear constraints at every generation, the penalty algorithm is requested. The GA function used in this method attempts to minimize a penalty function, not the fitness function. In cases that the individual chromosome is feasible, the penalty function is the fitness function. Otherwise, in cases that the individual chromosome is infeasible, the penalty function is the maximum fitness function among feasible chromosomes from that population plus the constraint violations of the infeasible chromosome. This penalty function is combined with the binary tournament selection algorithm to apply values for selecting individuals for the next generations.

In order to see the progress of the optimization process throughout the process, two plot functions can be used. For each generation, the best and mean population penalty value is plotted. As seen in Fig. 4.11, this resource is directly related to the fitness score of the population, and the closer these two values are, the closer the algorithm reaches a stopping criterion. A second progress verification may be used to plot the maximum constraint violation of a nonlinear constraint at every generation.

4.3.6 Model constraints

The model constraints presented in this study form part of the Design Constraints steps presented in Fig. 4.3, and are summarised as follows.

4.3.7 Design constraints

The constraints are based on ULS and SLS conditions, according to NBR 6118 [1]. The constraints were normalized to reduce numerical errors that could occur during the iterative optimization process, since normalizing the constraints makes it easy for the user to compare constraints. Normalizing also avoids issues with the optimization algorithm in terms of executing the fitness function properly without size category influences.

4.3.8 Flexural constraints

As presented in Fig. 4.3, ULS is developed in the present study, and the most important constraint is Msd shall be less than or equal to Mu, considering the geometry, supports, and loads of continuous beams. Additionally, the following requirements were considered to calculate ductility and neutral axis (x) limits demonstrated in Eq. (10).

$$\beta x = x/d \tag{10}$$

A simplified diagram of strain domains is illustrated in Fig. 4.12. Given the strain domains for reinforced concrete sections, the neutral axis (x) must obey the limits of domains 2 and 3, and domains 3 and 4 for ductility purposes as proposed by [1]. Thus, the reinforcement would result in the correct neutral axis position.

In the present study, the neutral axis (x) position may vary as a unction of the effective beam height (d). The reinforcement used depends on the width of the beam (bw). For the cases of boundary limits 2, 3, or 4, Eqs. (4.10), (4.11), (4.12), and (4.13) below are applied.

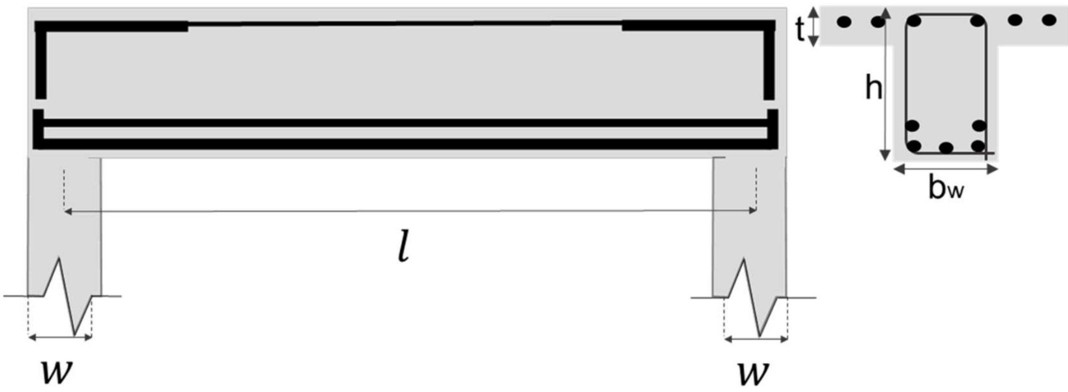

Figure 4.10 - Beam parameters representations.

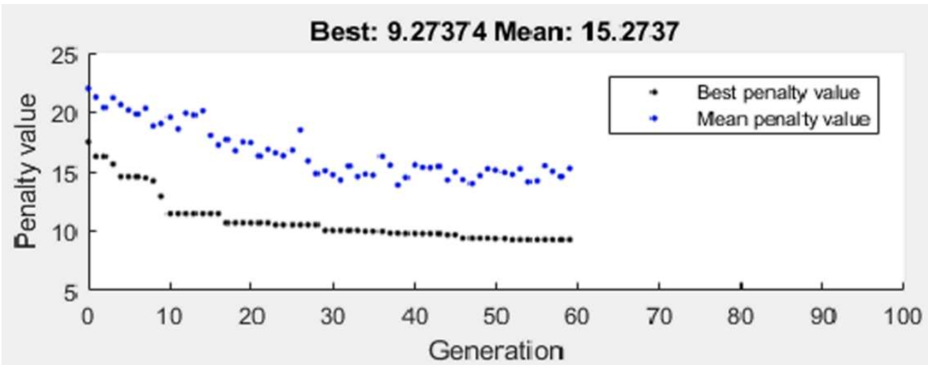

Figure 4.11 - Output example of the developed methodology showing the optimization process fitness function comparing penalty values for the best candidate and mean population penalty (blue dots).

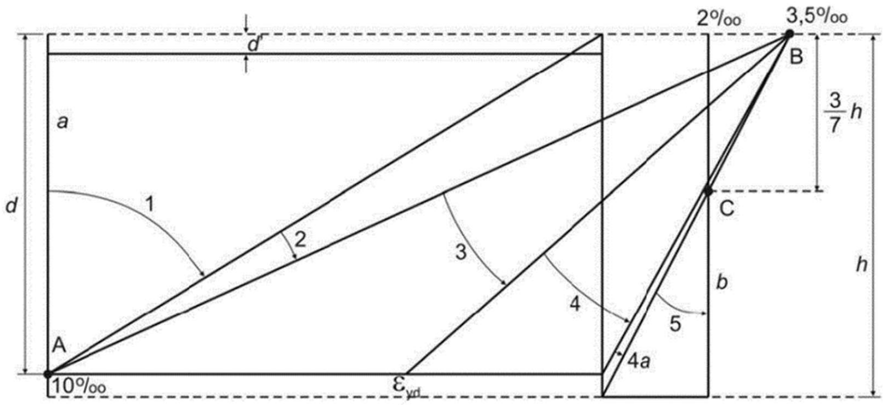

Figure 4.12 - Strain domains for reinforced concrete sections.

4.3.9 Shear stress constraints

Following the Ritter-Morch ̈ truss model, which is commonly adopted in standards, and in line with the [19], the truss model adopted was formulated as the ultimate bending moment. Eqs. (11)–(14) are coded.

$$\tau wd \leq \tau wd_2 \tag{11}$$

$$\tau wd_2 = 0.27.\left(1 - \frac{fck}{250}\right) \text{fcd}.bw.(h - d^{'}) \tag{12}$$

Eq. (12) require that the design stress (τwd) does not exceed the stress resistance (τwd2) and Eq. (13) defines the maximum spacing between stirrups (Smax).

$$\begin{cases} if\ \dfrac{\tau wd}{\tau wd_2} \leq 0.67 \rightarrow S_{max} = 0.6(h - d^{'}) \leq 300mm \\ if\ \dfrac{\tau wd}{\tau wd_2} > 0.67 \rightarrow S_{max} = 0.3(h - d^{'}) \leq 200mm \end{cases} \tag{13}$$

4.3.10 Deflection constraints

In this section, the serviceability limit state (SLS) constraints of deflection considered in the proposed method are presented. The immediate deflection is calculated based on the equivalent stiffness, according to [11].

Eq. (14) presents the calculation process to estimate the deflection of continuous beams.

$$f_i = \frac{p_i.l^4}{384(EI)_{eq}} K \tag{14}$$

$$(EI)_{eq} = Ecs\left\{\left(\frac{Mr}{Ma}\right)^3.Ic + \left[1 - \left(\frac{Mr}{Ma}\right)^3\right] I_{II}\right\} \leq Ecs.Ic \tag{15}$$

$$f_{t=\infty} = f_i(1 + \alpha f) \leq \frac{L}{250} \tag{16}$$

The final deflection at an infinite time (ft=∞), obtained via Eq. (16), needs to be less than or equal to the maximum deflection allowed, which considers the effect type. For visual comfort, and to avoid a state of alert in users, the deflection limit is set as L/250.

4.3.11 Cracking constraints

A constraint needs to be imposed to ensure that cracking be limited according to the code limits. As is known, shear stresses result in a cracks in RC structures. Most codes of practice set the crack opening limit considering an aggressive environment. Knowing the limit state of cracking, the crack opening limit is computed via Eq. (17).

$$wk = \frac{\phi_i}{12.5\eta_1}.\frac{\sigma s}{Es}.\left(\frac{4}{\rho r} + 45\right) \leq \delta_{cracking} \quad (17)$$

The limit state of cracking in structural concrete design codes usually considers environmental aggression. The limit used here (δcracking) is 0.3 mm.

4.3.12 Load combinations

The standard codes used to verify the reinforcement concrete load combinations are shown in Eq. (18)[1] as load combination for ULS within the depletion of resistance capacity.

$$Fd = \gamma g.Fgk + \gamma \varepsilon g.F\varepsilon gk + \gamma q\left(Fq1k + \sum \psi 0j.Fqjk\right) + \gamma \varepsilon g.\psi 0\varepsilon.F\varepsilon qk \quad (18)$$

Design constraints consider code limitations concerning the ULS and SLS, as well as several constructive constraints. In summary, all constraints used in the present study are shown below, and parameter gi represents each design constraint, as can be seen in Fig. 4.3, Design Constraints steps.

The compressed steel area (Asc) must be less than or equal to half the tractive steel area (Ast), as demonstrated in Eq. (19).

$$g_1 = \frac{Asc}{0.5Ast} - 1 \quad (19)$$

The steel area must be less than 4% of the concrete cross-section area, as illustrated in Eq. (20).

$$g_2 = \frac{As}{0.04bw.h} - 1 \quad (20)$$

Deflection at an infinite time (Def∞) must be less than the maximum permissible (Deflimit), as shown in Eq. (21).

$$g_3 = \frac{Def_\infty}{Def_{limit}} - 1 \quad (21)$$

Crack opening (wkexis) must be less than the limit allowed by the code (wkallow), as per Eq. (22).

$$g_3 = \frac{Def_\infty}{Def_{limit}} - 1 \tag{21}$$

The α factor must be limited by beam height (h), according to Eq. (23).

$$g_5 = \frac{\alpha}{0.10{*}h} - 1 \tag{23}$$

Neutral axis depth (x) must be between domains 2 (lower limit x23) and 4 (upper limit x34), as per Eq. (24).

$$g_6 = \frac{x_{23}}{x} - 1 g_7 = \frac{x}{x_{34}} - 1 \tag{24}$$

Flange height (t) must be lower than the effective height of the beam (d) and less than 80% of the neutral axis (x) (and vice-versa in this case), as demonstrated in Eqs. (25).

$$g_8 = \frac{t}{d} - 1 g_9 = \frac{t}{0.8.x} - 1 \tag{25}$$

The clear spacing between stirrups (Sstir) must be between the maximum (Sstirmax) and minimum (Sstirmin) allowed by the code, as per Eqs. (26).

$$g_{10} = \frac{Sstir}{Sstir_{max}} - 1 g_{11} = \frac{Sstir_{min}}{Sstir} - 1 \tag{26}$$

Clear spacing restrictions for longitudinal reinforcements must be within the pre-established limits, according to the following equation.

$$g_{12} = \frac{Sh}{Sh_{max}} - 1 g_{13} = \frac{Sv}{Sv_{max}} - 1 g_{14} = \frac{Sh_{min}}{Sh} - 1 g_{15} = \frac{Sv_{min}}{Sv} - 1 \tag{27}$$

The ultimate bending moment (Mu) must be less than or equal to the design bending moment (Msd), as per Eq. (28).

$$g_{16} = \frac{Msd}{Mu} - 1 \tag{28}$$

Concerning the side constraints, since the optimization model uses discrete design variables, the upper and lower boundaries are vector positions instead of geometries or material limits. The lower boundaries always has a value of one, the first position on the possibilities vector.

4.4 NUMERICAL APPLICATION AND RESULTS

Two case studies are presented and compared with the results available in the literature. Since the present study considers the characteristic strength of concrete (fck) as a design variable, fck values were adapted in all study cases, considering the average percentage increase/decrease for each fck cost studied, based on average market variations at the time of the research. These comparisons were made to verify if when discrete variables instead of continuous ones (number of bars instead of area of steel) are used, the optimization process would still reach equivalent results.

4.4.1 Applications considering simply supported beams

A simply supported beam was analyzed. For the sake of simplicity of this first analysis, the study by [16] was used for result comparison to check if, even with a realistic approach, the proposed methodology

would provide competitive solutions. As previously mentioned, these researchers also used a genetic algorithm (GA) to study reinforced concrete beam optimization. Additionally, a second comparison was made with the results presented by [13], who used another optimization method for the same case study. The simplified scheme for the proposed problem is illustrated in Fig. 4.13.

The costs of the materials and the applied loads used in this first case study are presented in Table 4.3.

The results obtained in the present study (PS), [16] and [13] are depicted in Table 4.4. Table 4.4 shows that the optimal configuration obtained here is less costly than the references. An optimal result cost 13.5% less than [13], and 17.07% less than [16] was obtained, even representing a more realistic reinforcement layout solution.

4.4.2 Second study case considering simply supported beams

For the second comparison of simply supported beams case, the study by [22] was used. The authors had also used GA for reinforced concrete beam optimization. A second comparison was made with the results presented by [23] since they used another optimization method

Table 4.3 - Material costs and applied load for the simply supported case study.

Material	Specifications	Value
Concrete	15 MPa	50.38 $/m^3
Concrete	20 MPa	55.15 $/m^3
Concrete	25 MPa	59.28 $/m^3
Concrete	30 MPa	64.50 $/m^3
Concrete	40 MPa	69.60 $/m^3
Steel	300 MPa	0.72 $/kg
Formwork	–	2.155 $/m^2
–	Structural load	15 kNm and 20 kNm

Table 4.4 - Comparison between the results of the present study (PS), [16], and [13]. The column of values referenced was proposed by [13] in February 1992.

Properties Research	Height (cm)	Width (cm)	Steel area (cm^2)	f_{ck}(MPa)	Total Cost ($)	PS Cost Relation (%)
Chakrabarty (1992)	95.47	30	37.69	30	37.25	113.50
Coello et al. [16]	87.70	20.68	31.16	30	38.85	117.07
Present Study	70	35	28.49	35	32.22	100

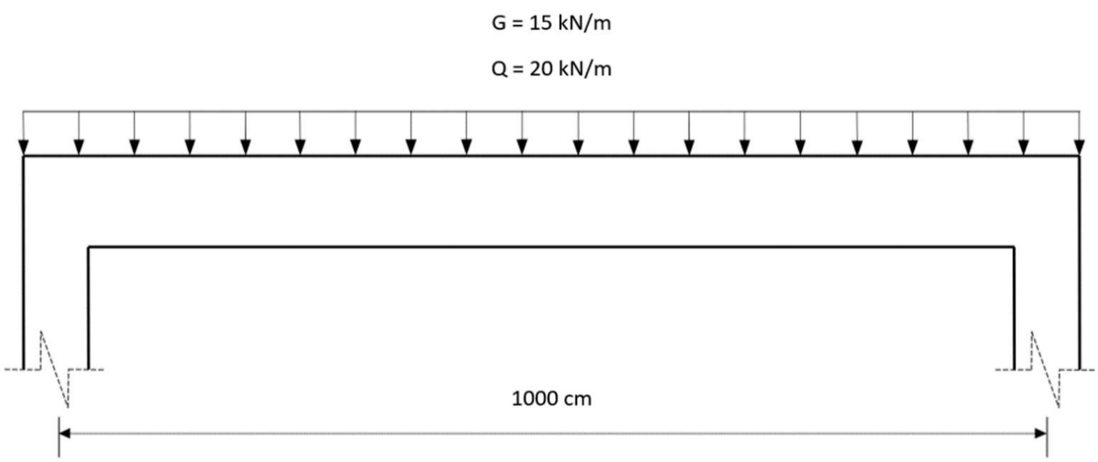

Figure 4.13 - Strain domains for reinforced concrete sections.

Table 4.5 - Material costs and applied load for the simply supported case study, proposed by [22] and adapted by the present study.

Material	Specifications	Value
Concrete	15 MPa	0.862 $/m^3
Concrete	20 MPa	0.936 $/m^3
Concrete	25 MPa	1.000 $/m^3
Concrete	30 MPa	1.081 $/m^3
Concrete	40 MPa	1.160 $/m^3
Steel	400 MPa	0.01515 $/kg
Formwork	–	0.42 $/m^2

for the same case study. Another computational experiment was conducted, considering the fck as a parameter rather than a variable, using the same concrete strength and cost used in [23] and [22] (fck equals to 25 MPa), but keeping the discrete reinforced bars in order to verify the impact of the having fck as a variable. The fck found by the present study here was 30 MPa. For the case studies from the literature, the simplified structural disposal and loads can be seen in Fig. 4.14.

The costs of the materials and applied loads used in the second case study are presented in Table 4.5.

The results obtained in the present study (PS), [22] and [13] are illustrated in Table 4.6.

Table 4.6 shows that the optimal configuration obtained in the present study was less costly than the references. The optimal result cost obtained by [23] was 14.98% higher than the present work, and results obtained by [22] was 8.14% higher than the present work, even the proposed method achieving a more realistic reinforcement layout solution.

The present study without fck as a design variable achieved results 8.89% more expensive then [22]. This may be due to the adoption of the steel bars as a discrete variable, and this tends to obtain worst results if compared with solutions that use continuous variables.

The adoption of a discrete variable tends to obtain worst results in relation to the use of continuous variable and the use of fck as design variable tends to enhance the optimization results pattern.

4.4.3 Applications considering continuous beams

For continuous beam applications, the studies from the literature were also used for comparison with the present investigation. The case study considered a continuous beam with three spans (7 m, 5 m, and 4 m) and 28, 56, 28, and 28 cm supports, respectively. The loads considered were rectangular uniformly distributed loads of 18 kN/m as dead load and 20 kN/m as live load, as shown in Fig. 4.15. [22] also used discrete design variables and fck equal to 25 MPa. The fck found by this methodology were 30 MPa for this study case and doubly reinforcement for some critical sections, as presented in Fig. 4.16.

The materials costs were the same as shown in Table 4.5. A flange height of 12 cm was considered, and labor is included in the material costs.

The references stated that beam width (bw) was fixed at 24 cm and, as such, was not deemed a design variable. This geometrical condition was not inputted in the present study.

The height (h) was considered constant in all spans. Table 4.7 presents the results obtained by the three optimization models.

Table 4.7 shows that the optimal total cost configuration obtained here is lower than the references. The optimal result obtained by [23] costs 12.09% more than the present study, and [22] costs 3.63% more than the present study. Same as for the second study case, the optimization without using fck as a design variable was performed, reaching results 10.03% more expensive than the present study proposed method considering fck as a design variable.

The present study considers beams and their reinforcements as a complete model, which includes longitudinal reinforcement along with the design variables previously mentioned, thereby achieving similar or better results than those of less encompassing methodologies.

The design constraint values obtained by the optimal configuration of the present study, compared with [22], are shown in Fig. 4.16. The values presented in Fig. 4.16 are organized by critical section constraints, span constraints, and those of the entire beam model.

The design constraint values of the optimal configuration for both [16] and [22] are shown in Fig. 4.16. Values lower than 0 mean that the constraint is feasible and meets the standard code requirements. Values near 0 indicate that the constraints limit the cost reduction and are considered active.

Table 4.6 - Comparison between the results of the present study, [22] and [13].

Quantities				Material Costs ($)			Total Cost	PS Cost Relation
Research	Concrete (m^3)	Formwork (m^2)	Steel (kg)	Concrete	Formwork	Steel	(u)	(%)
Kanagasundram and Karihaloo (1991)	0.35	3.878	26.589	0.35	1.629	0.4028	2.3818	114.98
Govanindaraj and Ramasamy (2005)	0.224	2.829	46.251	0.224	1.188	0.701	2.1131	108.14
Present Study without f_{ck} as design variable	0.297	3.289	41.103	0.297	1.478	0.6227	2.3011	111.73
Present Study	0.478	3.037	30.811	0.412	1.211	0.437	2.0596	100

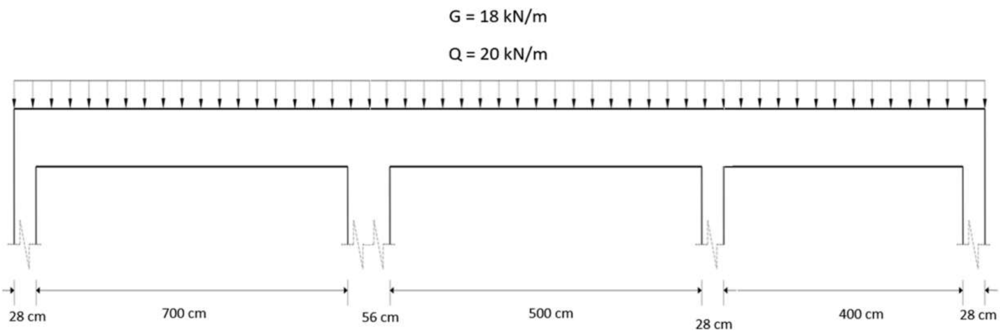

Figure 4.14 - Case study proposed by [23] and compared with that of [22].

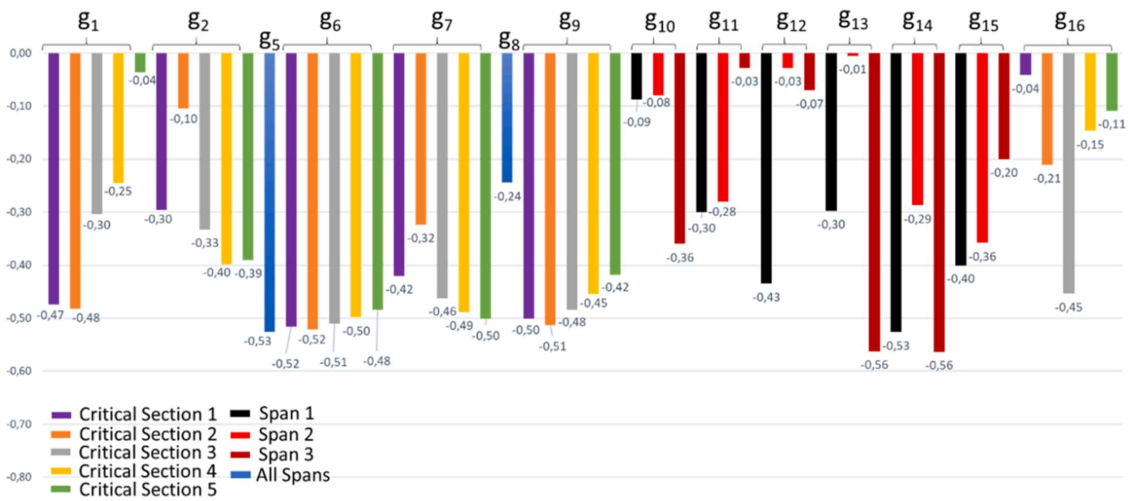

Figure 4.15 - Design constraints obtained by comparing the present study with that of [22].

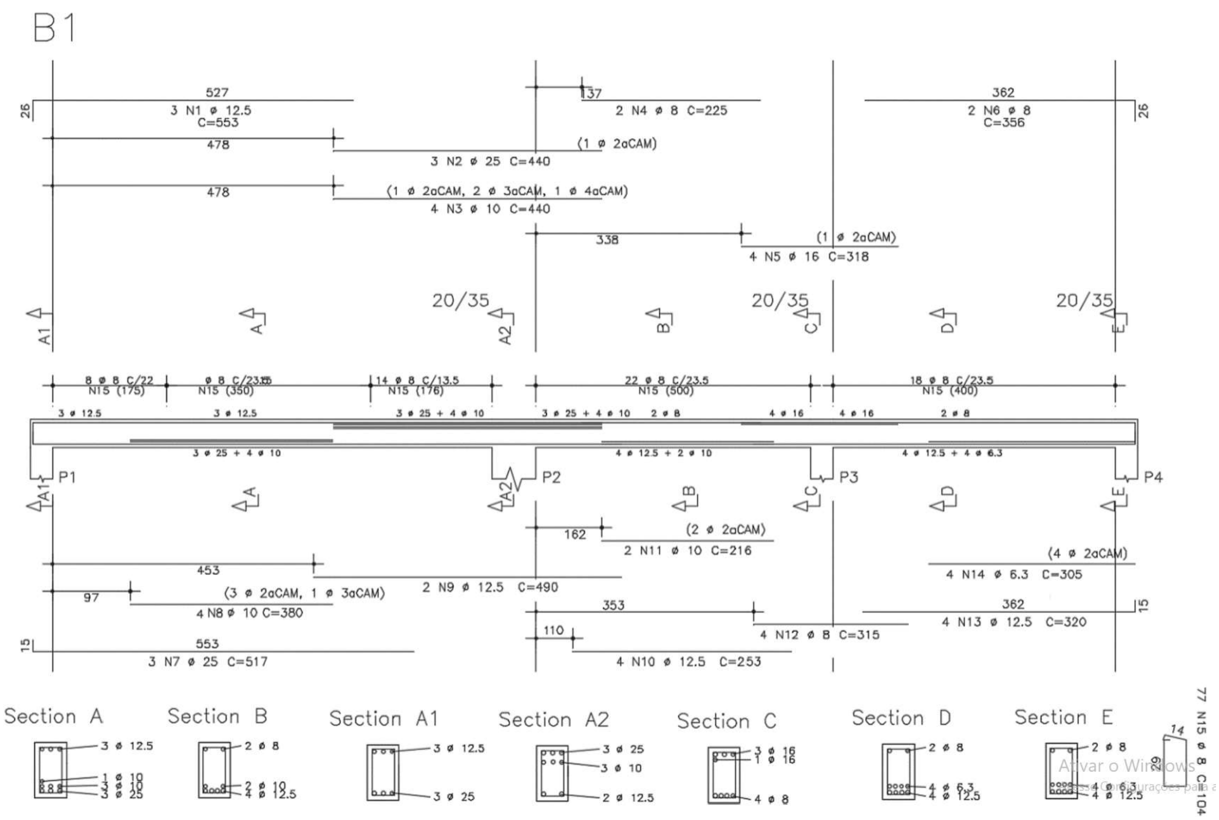

Figure 4.16 - Optimal design detailing obtained by the present methodology for the continuous beam case study.

Table 4.7 - Comparison of results obtained in the present study (PS), present study without using fck as a design variable, [22] and [23].

Amount				Material Costs ($)		Total Cost		PS Cost Relation
Research	Concrete (m^3)	Formwork (m^2)	Steel (kg)	Concrete	Formwork	Steel	(u)	(%)
Kanagasundram and Karihaloo (1991)	2.1395	19.064	174.5	2.1395	8.01	2.64	12.79	112.09
Govanindaraj and Ramasamy (2005)	1.462	14.544	281.60	1.462	6.11	4.27	11.84	103.63
Present Study without f_{ck} as design variable	1.892	17.840	209.10	1.892	7.49	3.17	12.55	110.03
Present Study	1.3781	12.96	288.45	1.5986	5.44	4.37	11.41	100

For both comparisons, the neutral axis (x) limits the region and the ultimate bending moment, design constraints being g7, and g16, respectively, both being active constraints. For the comparison with [16], flange height (t) was less than 80% of the neutral axis, considered constraint g9, also active.

It can be observed that g1 in critical section 5, g10 in span 1 and 2, g11 in span 3, g12 in span 2 and 3, g13 in span 2 and g16 in critical section 1 are cost reduction limits, and, as such, considered active design constraints.

Thus, although the present study used discrete variables and gave a more realistic output, it obtained significantly lower values than the results presented by [16] and [13]. It also showed better results when compared with [22] and [13]. Thus, these results demonstrate that the use of different characteristic strength of concrete as a design variable (considering the respective cost for each fck) had a significant impact on the final results.

In the present study, the bending moment diagrams obtained by FEM show the regions that need longitudinal reinforcement. Sequentially, the possible reinforcement layouts are considered in the optimization process. Thus, the algorithm has the freedom to select different reinforcement layouts for each critical section of the beam.

The advantage of considering the fck, top and bottom reinforcements as discrete design variables is that, depending on the material costs, there may be cases where doubly reinforcements and smaller cross-sections achieve better results. The use of the database generator presented in Fig. 4.3 allows the proposed method to achieve code verified and more realistic solutions and doubly reinforcements.

The optimal design detailing obtained by the present methodology is shown in Fig. 4.16.

4.5 CONCLUSIONS

A computational method was presented for the optimal design of reinforced concrete continuous beams using a new database system to define steel reinforcement and solved using genetic algorithms.

The developed computational tool provides rational and realistic optimization solutions for any reinforced concrete continuous beam problem. The optimization model exhibits low mathematical, numerical, and computational complexity, allowing future upgrade. It can also be included in commercial structural design software because of its low computational cost.

Besides, optimal design results can be controlled in a user-friendly manner by specifying the design variable boundaries, modifying material characteristics, changing material costs to suit the time and geographic region, and updating business sales patterns, among others.

The results obtained in comparison with those generated in [16] and [13] for simply supported beams were 17.07% and 13.50% cheaper, respectively. The findings of the comparison between [22] and [23] with this study on simply supported beams were 8.14% and 14.98% cheaper, respectively. Results obtained when contrasting [22] and [23] with the present study for continuous beams were 3.63% and 12.09% cheaper, respectively. As the optimization method optimizes chromosomes by each reinforcement bar, and each bar may have different costs due to the reinforcement database used to aid the database generator, the reflected prices may include labour for better precision and accuracy, representing real structural projects.

The comparison with other studies was made in order to verify if the proposed method granted near of even better results, when discrete variables were utilised in the optimization. Better results were obtained, indicating that fck usage as a design variable may be an important improvement for optimizing reinforced concrete beams. Using the reinforcement database generator proposed, considering top and bottom reinforcements as design variables, allows the optimization algorithm to test doubly reinforcement solutions in the optimal search that was not used in previews case studies. Another degree of freedom added to the method proposed is the use of fck as a design variable, allowing the optimization algorithm the freedom to try several cross-section solutions that would otherwise not be tested. As such, the method was able to find better solutions for the case studies presented and would be a better fit for industry software adaptation.

One limitation of the methodology is the lack of consideration of slab design as part of the optimization process. Future studies suggest a broader optimization method, including slabs and columns, encompassing an entire building.

4.6 DISCUSSION OF CHAPTER 4

4.6.1 Key Findings

The discrete optimization model introduced in this chapter represents a significant advancement over previous continuous optimization methods. By working with a finite set of data, the model successfully optimizes reinforcement layouts in reinforced concrete structures, offering both material efficiency and structural integrity. This approach was groundbreaking at the time of its publication, as it allowed for the practical application of optimization techniques to real-world structures for the first time. The shift from continuous to discrete optimization was not only more aligned with the realities of engineering practice but also set the stage for the integration of machine learning techniques in later stages of this research.

4.6.2 Implications

The implications of this work are profound. The discrete optimization model has the potential to transform standard practices in the design and detailing of reinforced concrete structures. By enabling more accurate and efficient material usage, this approach supports both economic and environmental goals. Additionally, the success of this model demonstrates the viability of using finite datasets in engineering optimization, which directly contributes to the broader field of machine learning in structural engineering. This chapter’s findings have influenced subsequent research, leading to the development of new predictive models and optimization techniques that are more practical and applicable to real-world scenarios.

4.6.3 Limitations

While the discrete optimization model offers significant advantages, its effectiveness is still contingent on the quality and accuracy of the input data. Inaccurate material properties or loading conditions could result in suboptimal design outcomes. Additionally, the computational demands of the optimization process, while reduced compared to continuous models, may still pose challenges in very large or complex structures, particularly when computational resources are limited.

4.6.4 Future Work

Building on this foundational work, future research could explore the integration of machine learning techniques to further enhance the optimization process. By training models on the finite dataset used in this chapter, it may be possible to develop even more efficient and accurate predictive tools. Additionally, applying this discrete optimization model to a wider range of structural types and conditions, including dynamic loading scenarios, could expand its applicability. Real-world testing and validation of the model's outcomes would also be valuable in solidifying its role in structural design practice.

4.7 CONCLUSION FOR CHAPTER 4

This chapter laid the foundation for the entire research presented in this thesis. The development of a mathematical optimization model using discrete optimization techniques marked a significant breakthrough in the field of reinforced concrete design. Prior to this work, continuous optimization models were the norm, but they often fell short in addressing the practical challenges of optimizing real-world reinforced concrete structures. By introducing a discrete optimization model, this research made it possible to accurately and efficiently optimize reinforcement layouts for actual structures for the first time.

The use of a finite set of data, rather than relying on continuous models, opened up new possibilities for further research and application. This approach not only improved the optimization process itself but also paved the way for integrating machine learning techniques, which could leverage this finite dataset to train predictive models. This chapter is therefore crucial, as it represents the starting point from which the broader thesis developed, leading to innovative methodologies that build upon this foundational work.

This model not only optimizes material usage but also lays the groundwork for integrating more advanced techniques in structural analysis. With the establishment of this optimization model, the focus now shifts to addressing specific challenges in concrete structures, such as durability under environmental stressors.

4.8 REFERENCES FOR CHAPTER 4

Aditya, L., Mahlia, T.M.I., Rismanchi, B., Ng, H.M., Hasan, M.H., Metselaar, H.S.C.,Muraza, O., Aditiya, H.B., 2017. A review on insulation materials for energy conservation in buildings. Renew. Sustain. Energy Rev. 73, 1352–1365. http://dx.doi.org/10.1016/j.rser.2017.02.034.

[1] ABNT, N. (2014). 6118:2014 Projeto de estruturas de concreto - Procedimento. Associaçao ˜ Brasileira de Normas T´ecnicas, 256. [2] ACI Committee 318. (2019). Building Code Requirements Available for Public Review (ACI 318-19). ACI Materials Journal.

[3] Alqedra Mamoun, Arafa Mohammed, Ismail Mohammed. Optimum Cost of Prestressed and Reinforced Concrete Beams using Genetic Algorithms. J Artific Intell 2010;4(1):76–88.

[4] Andrei P, Iulian-Valentin C. Nonlinear Design Optimization of Reinforced Concrete Structures Using Genetic Algorithms. Cham: Springer; 2018. p. 405–19.

[5] Kulkarni Ashwini R, Bhusare Vijaykumar. Structural optimization of reinforced concrete structures. Int J Eng Res 2016;V5(07):07.

[6] Austrell PE, Dahlblom O, Lindemann J, Olsson A, Olsson KG, Petersson K, Ristinmaa M, Sandberg G, Wernberg PA. CALFEM: A finite element toolbox

(Version 3.4); 2004.

[7] Barros AFM, Barros MHFM, Ferreira CC. Optimal design of rectangular RC sections for ultimate bending strength. Struct Multidisc Optim, Springer, 2012;45(6): 845–60.

[8] Bekdas G, Nigdeli SM. Cost Optimization of T-shaped Reinforced Concrete Beams under Flexural Effect According to ACI 318. In: Proceedings of the 3rd European Conference of Civil Engineering; 2012. p. 122–6.

[9] Bekdas G, Nigdeli SM, Yang XS. In: Proceedings of the 5th European Conference of Civil Engineering; 2014. p. 184–8.

[10] Bhatt P, MacGinley TJ, Choo BS. Reinforced concrete design to eurocode design theory and examples. Springer Tracts in Civil Engineering; 2017.

[11] Bischoff PH. Comparison of existing approaches for computing deflection of reinforced concrete. ACI Struct J 2020;117(1):231–40.

[12] Calavera. Manual for Detailing Reinforced Concrete Structures to EC2. Manual for Detailing Reinforced Concrete Structures to EC2. 2014.

[13] Chakrabarty BK. Models for optimal design of reinforced concrete beams. Comput Struct, Pergamon 1992;42(3):447–51.

[14] Christensen PW, Klarbring A. An introduction to structural optimization. Solid Mech Appl, Springer Verlag 2009;153:1–220.

[15] Chutani Sonia, Singh Jagbir. Design Optimization of Reinforced Concrete Beams. J Inst Eng (India): Ser A, Springer India 2017;98(4):429–35.

[16] Coello Carlos Coello, Hernandez ´ Filiberto Santos, Farrera Francisco Alonso. Optimal design of reinforced concrete beams using genetic algorithms. Expert Syst Appl, Elsevier Ltd 1997;12(1):101–8.

[17] De S, Pires L. OTIMIZAÇAO ˜ POR ALGORITMOS GENETICOS ´ DE PILARES ESBELTOS DE CONCRETO ARMADO SUBMETIDOS A ` FLEXAO ˜ OBL´IQUA CAMPINAS 2014. [s.n.]; 2014.

[18] Dole MR, Ronghe GN, Gupta LM. Optimum design of reinforced concrete beams using Polynomial optimization technique. Adv Struct Eng. 2000;3(1):67–79.

[19] Eurocode 1992-1-1. (2011). Eurocode 2: Design of Concrete Structures - Part 1-1 : General Rules and Rules for Buildings. British Standards Institution.

[20] Ferdous W, Bai Y, Ngo TD, Manalo A, Mendis P. New advancements, challenges and opportunities of multi-storey modular buildings – A state-of-the-art review. Eng Struct, Elsevier Ltd; 2019.

[21] Gan Vincent JL, Wong CL, Tse KT, Cheng Jack CP, Lo Irene MC, Chan CM. Parametric modelling and evolutionary optimization for cost-optimal and lowcarbon design of high-rise reinforced concrete buildings. Adv Eng Inf, Elsevier Ltd 2019;42:100962. https://doi.org/10.1016/j.aei.2019.100962.

[22] Govindaraj V, Ramasamy JV. Optimum detailed design of reinforced concrete continuous beams using Genetic Algorithms. Comput Struct 2005;84(1-2):34–48.

[23] Kanagasundaram S, Karihaloo BL. Minimum-cost design of reinforced concrete structures. Comput Struct, Pergamon 1991;41(6):1357–64.

[24] Kaveh A, Mottaghi L, Izadifard RA. Sustainable design of reinforced concrete frames with non-prismatic beams. London: Engineering with Computers, Springer; 2020. p. 0123456789.

[25] Korouzhdeh Tahereh, Eskandari-Naddaf Hamid. Cost-safety optimization of steelconcrete composite beams using standardized formulation. Eng Sci Technol, Int J, Elsevier BV 2019;22(2):523–32.

[26] Kwak Hyo-Gyoung, Kim Jieun. Optimum design of reinforced concrete plane frames based on predetermined section database. CAD Comput Aided Des, Elsevier 2008;40(3):396–408.

[27] Lepˇs Matˇej, Sejnoha ˇ Michal. New approach to optimization of reinforced concrete beams. Comput Struct 2003;81(18-19):1957–66.

[28] Mirjalili S, Song Dong J, Sadiq AS, Faris H. Genetic algorithm: Theory, literature review, and application in image reconstruction. Stud Comput Intell, Springer Verlag 2020:69–85.

[29] Nigdeli Sinan Melih, Bekdas¸ Gebrail. Optimum design of RC continuous beams considering unfavourable live-load distributions. KSCE J Civ Eng 2017;21(4): 1410–6.

[30] Nigdeli SM, Bekdas¸ G. Live/dead load factor on optimum design of reinforced concrete continuous beams: AIP Conference Proceedings. 260004: American Institute of Physics Inc.; 2018.

[31] Paya-Zaforteza Ignacio, Yepes Víctor, Hospitaler Antonio, Gonzalez- ´ Vidosa Fernando. CO2-optimization of reinforced concrete frames by simulated annealing. Eng Struct 2009;31(7):1501–8.

[32] Prakash Rao DS. DETAILING OF REINFORCEMENT IN CONCRETE STRUCTURES - 3. Indian Concrete Journal 2012;59(3):74–6.

[33] Rao JS. Finite Element Methods. John Wiley & Sons Ltd, Chichester, UK 2017: 141–83.

[34] Saini N. Review of Selection Methods in Genetic Algorithms. Int J Eng Comput Sci 2017;6(12):23261–3.

[35] Shaqfa Mahmoud, Orban ´ Zolt´ an. Modified parameter-setting-free harmony search (PSFHS) algorithm for optimizing the design of reinforced concrete beams. Struct Multidiscip Optim, Springer Verlag 2019;60(3):999–1019.

[36] Shenbagam NK, Arunachalam N. Least cost design of axially loaded compression member using particle swarm optimization. In: IEEE International Conference on Innovative Mechanisms for Industry Applications, ICIMIA 2017 - Proceedings. Institute of Electrical and Electronics Engineers Inc; 2017. p. 138–44.

[37] Toklu YC. Metaheuristics and engineering. AIP Conf Proc 2013:421–4.

[38] Ulusoy Serdar, Ece Kayabekir Aylin, Bekdas¸ Gebrail, Melih Nigdeli Sinan. Optimum Designof Reinforced Concrete Multi-Story Multi-Span Frame Structures under Static Loads. Int J Eng Technol 2018;10(5):403–7.

[39] Zhu E, Najem RM, Dinh-Cong D, Shao Z, Wakil K, Ho LS, et al. Optimizing reinforced concrete beams under different load cases and material mechanical properties using genetic algorithms. Steel Compos Struct, Techno Press 2020;34(4): 467–85.

[40] Zou XK, Chan CM, Li G, Wang Q. Multiobjective optimization for performancebased design of reinforced concrete frames. J Struct Eng. 2007;133(10):1462–74.

[41] Gagg Colin R. Cement and concrete as an engineering material: An historic appraisal and case study analysis. Eng. Fail. Anal. 2014;40:114–40. https://doi.org/10.1016/j.engfailanal.2014.02.004. ISSN 1350-6307.

5 STRESS CORROSION CRACKING IN PRESTRESSED CONCRETE: A STUDY OF SCC IN PRESTRESSED CONCRETE APPLICATIONS

This chapter is being published as an original research article in International Conference on Construction Project Management 2024.

PIEROTT, Rodrigo *et al*. Stress corrosion cracking in prestressed concrete: a study of SCC in prestressed concrete applications. In: **International Conference on Construction Project Management 2024**.

Chapter 5 builds on the optimization framework by examining one of the critical durability challenges in prestressed concrete: stress corrosion cracking (SCC). This chapter investigates the conditions under which SCC occurs and its impact on structural integrity, providing essential insights that complement the optimization strategies introduced earlier.

ABSTRACT

This paper delves into the prevalent issue of pathological problems in concrete structures, with a specific focus on corrosion in steel reinforcement. It details an experimental investigation into the effects of chloride environments on prestressed concrete structures. Central to this study is the analysis of stress corrosion cracking (SCC) in 5 mm prestressing strands. The findings reveal that SCC predominantly manifests as pitting corrosion, which in turn initiates micro cracking on the wire surface. Intriguingly, the stress applied to the wires appears not to alter the composition of the corrosion products. This research offers comprehensive insights into the behavior of high-carbon steel wires under SCC conditions. A critical discovery is the significant influence of stress level on SCC progression, which markedly diminishes the ultimate strength of the corroded wires. This is particularly evident in the 48% reduction in ductility of wires at 95% of the tensile strength (fptk), a consequence of the formation of localized microcracks. These findings underscore the need for a deeper understanding of SCC in prestressed concrete structures, which is vital for enhancing their durability and longevity..

Keywords:

Chloride Attacks, Stress Corrosion Cracking, Steel Wire Degradation, Civil Infrastructure Durability, Prestressed Concrete.

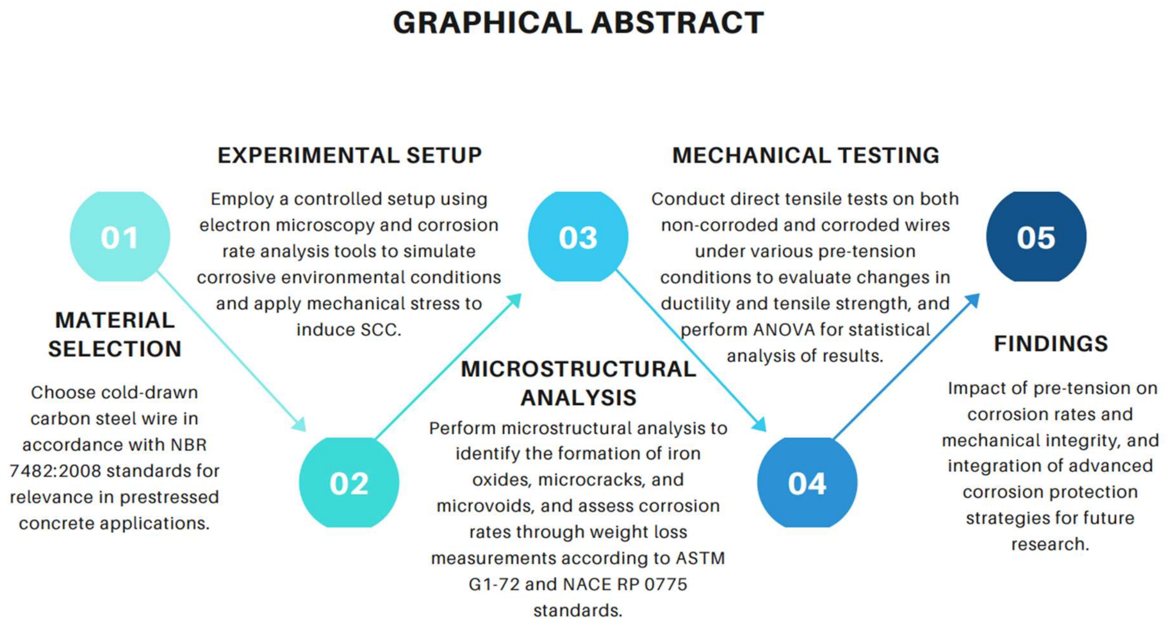

5.1 INTRODUCTION

Prestressed concrete, a cornerstone in modern construction, benefits from the pre-application of stress to enhance its strength and durability under service loads. This engineering marvel utilizes high-performance concrete coupled with high-strength steel, enabling structures to withstand significant stress levels before external loads are applied [1]. Despite its widespread adoption for its superior performance, prestressed concrete is not immune to the insidious threat of stress corrosion cracking (SCC). SCC represents a critical failure mode, where the synergistic effects of mechanical stress and corrosive environments precipitate the formation of microcracks on steel surfaces [2,3,4]. These microcracks can expand rapidly under continued stress, leading to sudden and often unpredictable failures in structural elements, significantly reducing their yield strength and, ultimately, their service life.

The phenomenon of SCC is particularly alarming due to its ability to compromise the integrity of structures without prior deformation or visible signs of distress, making early detection and intervention challenging [5]. SCC is influenced by a trinity of factors: the material's inherent susceptibility, the level of applied stress, and the presence of a corrosive environment [6,7,8]. This complexity is further compounded by the diverse nature of these elements, including variations in stress types (residual or externally applied) [9], material properties, and environmental conditions such as temperature, aeration, and the presence of specific corrosive agents. For instance, the susceptibility of different alloys to SCC can vary dramatically in the presence of certain chemicals, highlighting the intricate interplay between material science and environmental chemistry in the context of SCC [5].

The pressing need to understand and mitigate SCC in prestressed concrete is underscored by its prevalence in critical infrastructure, including nuclear power plants, where the long-term performance and safety of such structures are of paramount importance [10]. Despite the durability of prestressed concrete, the advent of chloride-induced steel corrosion emerges as a dominant factor undermining the structural integrity of these constructions [11]. Recent studies have illuminated the detrimental impact of corrosion on the residual strength of prestressed tendons, indicating significant reductions in ultimate strength and ductility, which in turn affect the failure modes of the structures [12-27].

Amidst this backdrop, our study endeavors to bridge a crucial knowledge gap by examining the behavior of prestressing strands, particularly those with diameters less than 8 mm, a domain less explored in contemporary research. Given the heightened risk of cross-sectional loss and subsequent deterioration in smaller diameter strands, our investigation seeks to shed light on the nuanced impacts of different prestressing levels on SCC, employing an experimental approach that encompasses a comprehensive analysis of material behavior under simulated environmental conditions [28]. Through this research, we aim to contribute to the broader understanding of SCC mechanisms, offering insights that could inform more resilient design and maintenance strategies for prestressed concrete structures.

5.2 BACKGROUND

The phenomenon of stress corrosion cracking (SCC) has emerged as a significant concern for the longevity and reliability of prestressed concrete structures. SCC involves the initiation and propagation of cracks in a material subjected to tensile stress in a corrosive environment, leading to premature failure of structural components. In prestressed concrete, this manifests as a critical threat, particularly due to the high levels of stress applied to the steel reinforcement to achieve desired prestress levels.

Recent advancements in monitoring technologies have allowed for a more nuanced understanding of corrosion-induced degradation within these structures. (Jiang et al., 2017) developed a piezoceramic-based sensing approach to monitor the progression of corrosion within prestressed concrete beams, highlighting the potential for early detection of corrosion-induced damage before visual signs become apparent.

The susceptibility of prestressed steel to SCC is further complicated by the presence of local concrete cracks. (Sun et al., 2014) investigated the impact of such cracks on the stress corrosion sensitivity of prestressed steel, uncovering that local concrete defects significantly increase the material's vulnerability to SCC.

Despite the recognition of these risks, the behavior of corrosion cracks in pretensioned prestressed concrete members remains less explored. (Agus et al., 2013) provided insights into the mechanisms of corrosion crack in such members, emphasizing the need for further research in this area.

Understanding the bond loss between the prestressed steel and concrete due to corrosion is crucial for assessing structural integrity. (Ortega et al., 2018) reviewed the mechanical effects of reinforcement corrosion on the bond strength in prestressed concrete beams, shedding light on the factors that reduce service life and load-bearing capacity.

Furthermore, the propagation of corrosion in prestressing steel strands embedded in concrete exposed to chlorides has been identified as a significant risk factor for structural failure. (Li et al., 2011) conducted a long-term experimental program to examine this phenomenon, finding that stress levels and the type of steel significantly affect corrosion rates, with pitting corrosion being the predominant form of damage in such environments.

Understanding the impact of corrosion on the structural performance of prestressed concrete beams, especially under transverse loads, is crucial for assessing their long-term reliability. (Recupero & Spinella, 2019) undertook experimental tests on corroded prestressed concrete beams to evaluate how tendon corrosion influences their response behavior. Their work highlights the detrimental effects of corrosion on the load-bearing capacity of beams, thus emphasizing the importance of timely corrosion detection and intervention strategies.

Moreover, the initiation of SCC in prestressing steel within hardened cement mortar, particularly under chloride exposure, remains a complex issue warranting further investigation. (Joseline et al., 2021) shed light on this matter by exploring the passive to active transition indicative of SCC onset. Their study underscores the critical role of environmental conditions, such as chloride concentration, in facilitating this transition, thereby contributing to our understanding of SCC initiation mechanisms and the pivotal factors that influence them.

By situating our study within this context, we aim to address the gaps identified in the current understanding of SCC in prestressed concrete, particularly focusing on the behavior of smaller diameter prestressing strands under various corrosive conditions. Our research seeks to contribute to the development of more durable and resilient prestressed concrete structures capable of withstanding the challenges posed by corrosive environments.

5.3 EXPERIMENTAL RESEARCH

5.3.1 Selection and Characterization of Materials

This study focuses on cold-drawn carbon steel wire, a material extensively used in prestressed concrete applications. Its selection was guided by its compliance with NBR 7482:2008 standards, ensuring that our findings are directly applicable to the construction industry. The chemical and mechanical properties of the specimen were meticulously analyzed to understand their influence on the steel's performance, especially its susceptibility to stress corrosion cracking (SCC).

Table 5.1 - Chemical composition of the specimen (Weight Percent, wt.%).

Elements	Carbon	Manganese	Silicon	Phosphor	Sulfur
(%)	0.79	0.65	0.21	0.013	0.010

The chemical composition, as detailed in Table 5.1, highlights a high carbon content which is known to significantly affect the steel's mechanical properties, including its strength and ductility. The controlled amounts of manganese, silicon, phosphorus, and sulfur contribute to the wire's overall performance in harsh environments.

Table 5.2 - Mechanical Properties of the Specimen.

Maximum load	Elongation	Creep load	Modulus of elasticity	Ultimate Tensile Strength	Average Hardness
37.5 kN	4.6%	32.20kN	202.5 GPa	1860 MPa	509 HV10

Table 5.2 presents the mechanical properties of the steel wire, including its ultimate tensile strength and modulus of elasticity, which are critical in determining its behavior under stress. The wire's high hardness level further underscores its potential for high performance in prestressed concrete applications, albeit with considerations for its brittleness.

5.3.2 Microstructural Analysis

The wire's microstructure was extensively examined to provide deeper insights into its characteristics that might influence its susceptibility to SCC. The analysis revealed a predominantly pearlitic structure with fine lamellar spacing, indicative of the wire's high strength and hardness. The presence of pearlite, along with trace amounts of cementite, suggests that the wire, while high in strength, may also exhibit a level of brittleness — a factor that could influence its behavior in corrosive environments typically encountered in prestressed concrete applications.

The detailed examination of the wire's microstructure is crucial for understanding how its inherent properties affect its durability and performance, particularly its resistance to stress corrosion cracking. The high carbon content, responsible for the wire's strength, also necessitates careful consideration of its application in environments where corrosion could precipitate brittle failure.

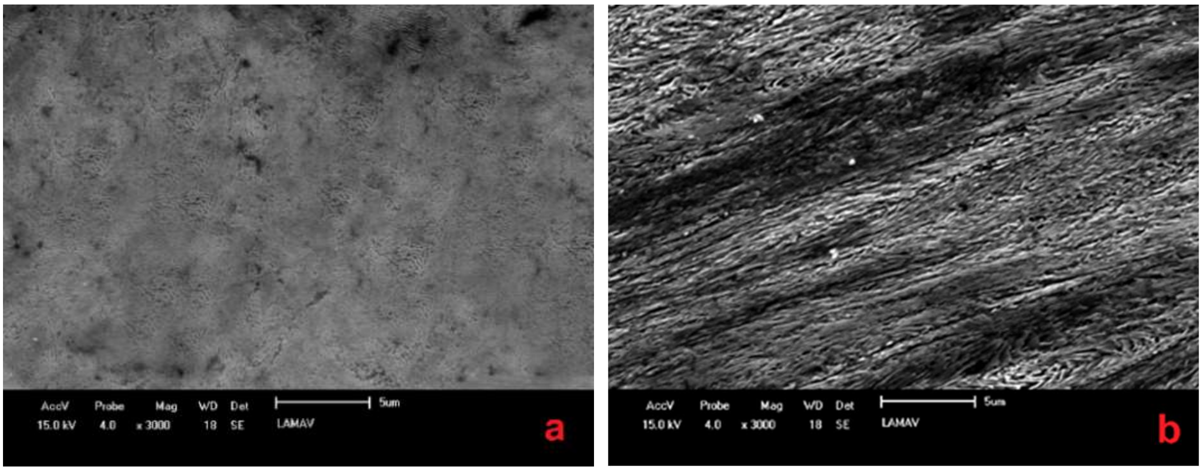

Figure 5.1 - Microstructure of the wire, a: Transverse view, and b: Longitudinal view.

The microstructure of the cold-drawn carbon steel wire was meticulously analyzed to uncover characteristics that potentially influence its susceptibility to stress corrosion cracking (SCC). Understanding the microstructural features is paramount, as they directly impact the mechanical behavior and corrosion resistance of the material.

2.1b (Longitudinal View): The longitudinal view further elucidates the wire's microstructure, emphasizing the orientation of pearlite and the presence of cementite lines. This arrangement not only contributes to the wire's notable strength and hardness but also to its brittleness, a factor that could enhance its vulnerability to SCC in corrosive environments.

The analysis of the wire's microstructure reveals a dual nature: while its strength and hardness are desirable for prestressed concrete applications, the brittleness—stemming from its high carbon content and microstructural features—necessitates a cautious approach to its use in environments prone to corrosion.

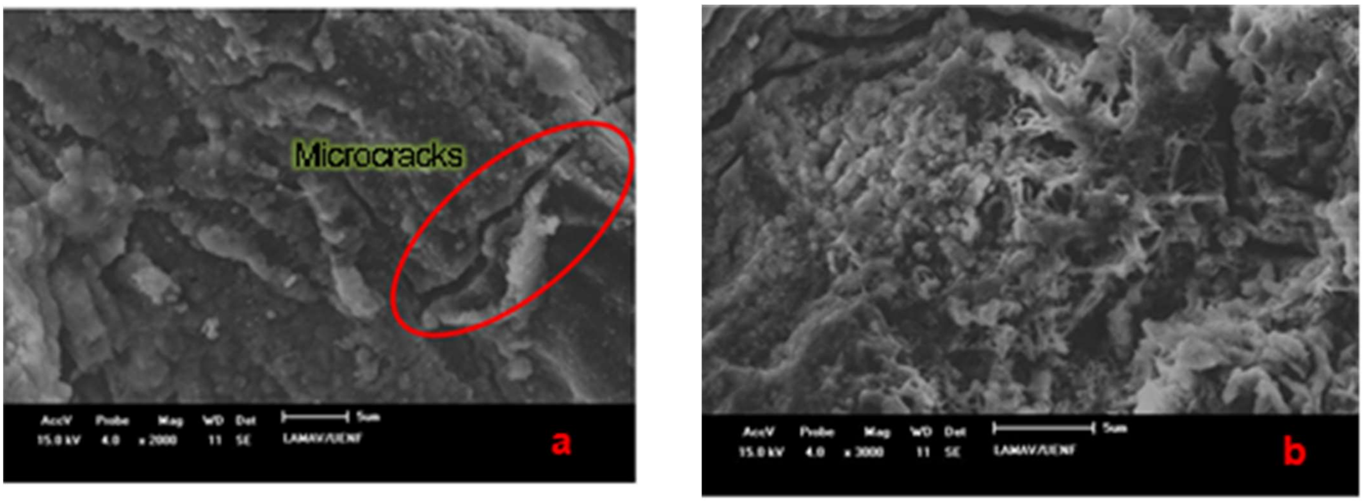

Figure 5.2 - Microscopy details of the 95%fptk wire: (a) microcracking on the wire surface (2000x magnification); (b) presence of microvoids (3000x magnification).

Figure 5.2 presents microscopy evidence of the microstructural degradation in 95% fptk prestressed steel wires under corrosive stress. Part (a) of the figure, captured at 2000x magnification, reveals the presence of microcracks on the wire surface. These microcracks are critical indicators of the onset of stress corrosion cracking (SCC), a significant concern for the longevity and safety of prestressed concrete structures. The high magnification allows for a clear visualization of the damage, emphasizing the severity of the microcracking phenomenon.

This figure provides visual confirmation of the microcracking and underscores the intricate details of the corrosion process that can lead to structural failure. The presence of microcracks is a testament to the vulnerability of the material when exposed to simultaneous mechanical stress and corrosive environments. The detailed visualization offered by this figure is essential for understanding the micro-mechanisms contributing to SCC and serves as a powerful tool for elucidating the material's behavior under conditions that mimic real-world applications.

The analysis of such microstructural damage is vital for advancing the field's understanding of SCC and for developing more effective corrosion-resistant materials and protective measures. It is through such detailed studies that engineers and researchers can improve the design and durability of prestressed concrete structures, ensuring their performance and reliability over time.

The anchoring system plays an important role in the application of pre-tension to the steel wires, simulating the operational stresses encountered in real-world prestressed concrete scenarios. This system ensures that the wires are subjected to a uniform pre-tension, crucial for the study of stress corrosion cracking under controlled conditions.

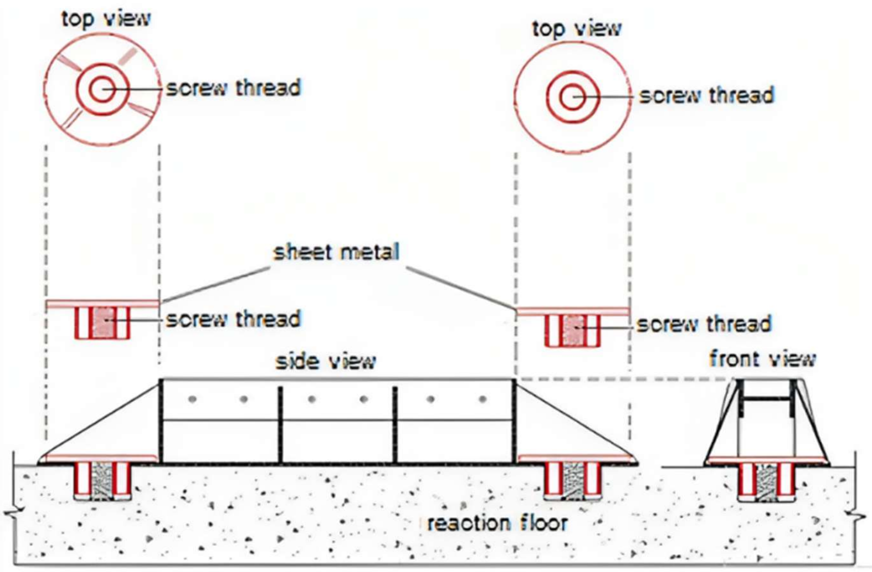

Figure 5.3 - Schematic of the anchoring system showing the devices used to fix the profile to the reaction slab.

Figure 5.3 provides a detailed schematic view of the anchoring system, illustrating the components and their arrangement for securing the wire to the reaction slab. The design of this system is instrumental in applying a precise and consistent pre-tension to the steel wire, mimicking the conditions under which prestressed concrete is utilized in construction projects.

Layout of the Prestressing System. Succeeding Figure 5.4, this layout offers an overview, to understanding of the experimental setup for prestress application.

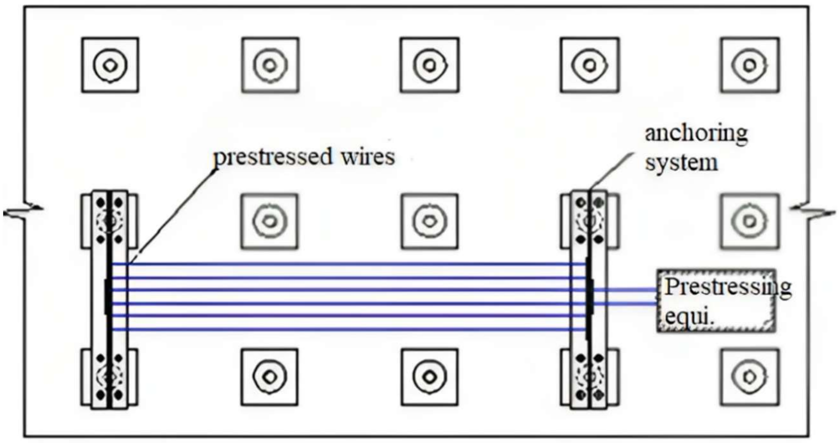

Figure 5.4 - Layout of the prestressing system.

The development and implementation of a robust anchoring system are essential for accurately replicating the stress conditions that prestressed steel wires undergo in service. By ensuring the uniform application of pre-tension, the anchoring system facilitates a controlled investigation into the effects of mechanical stress on the corrosion behavior of the steel wire.

Following the schematic, this layout offers an expansive view of the entire prestressing setup, including the anchoring system and the mechanism for applying pre-tension. This overview is crucial for understanding the experimental framework within which the SCC analysis is conducted.

The prestressing process is a crucial aspect of our study, designed to closely replicate the stress conditions that are inherent to prestressed concrete structures in real-world scenarios. A sophisticated hydraulic system was employed to apply and precisely control the tension across the steel wires. This methodology ensures that the applied pre-tension closely mimics the operational stresses experienced by prestressed concrete components, thereby enhancing the relevance of our findings to practical applications.

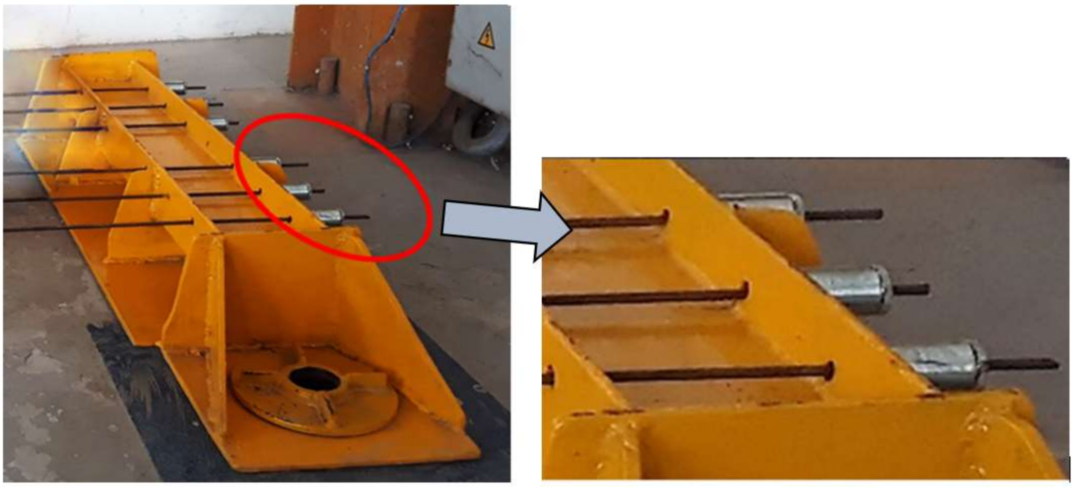

Figure 5.5 - Anchoring system of the prestressed strands.

Figure 5.5 illustrate the sophisticated arrangement designed to maintain consistent wire tension throughout the experiment. The visual provided in Figure 5.5 is essential for understanding the mechanical setup that enables the precise application of pre-tension, a critical factor in exploring the relationship between stress levels and their influence on corrosion behavior. The figure showcases the hydraulic system and its components, highlighting the meticulous design that underpins the replication of prestress conditions.

To investigate the synergistic effects of mechanical stress and corrosive environments on SCC, we established a controlled experimental setup. This setup was meticulously designed to simulate the environmental conditions known to precipitate SCC, thereby allowing for a comprehensive analysis of how such conditions affect the susceptibility of steel wires to corrosion when under stress.

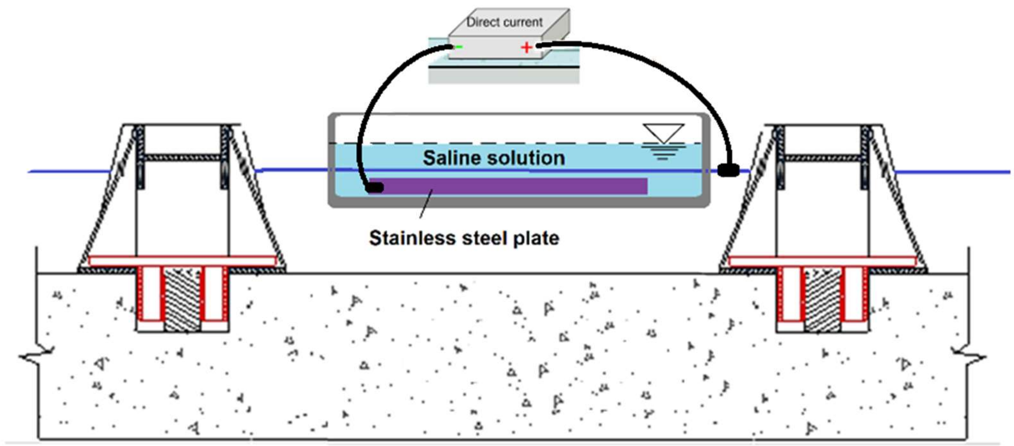

Figure 5.6 - Experimental setup.

Figure 5.6 provides a vivid illustration of the laboratory setup tailored for this purpose. This figure serves as a visual guide to the experimental arrangement, elucidating the methods employed to create a corrosive environment that simulates real-world conditions. The setup depicted in Figure 5.6 includes the corrosion-inducing elements and the system for applying tension, facilitating a controlled study of SCC under conditions that reflect the challenges faced in the field.

To accurately simulate the aggressive conditions that lead to stress corrosion cracking (SCC), a meticulous corrosion acceleration test was conducted. This involved the application of a direct current to the steel wire samples, a method proven to expedite the corrosion process and thereby mimic the accelerated deterioration observed in real-world scenarios.

Figure 5.7 - Corrosion Acceleration Test.

Figure 5.7 captures the setup used to apply electrical current to the steel wires. The image demonstrates how multimeters are employed to monitor the current flow, ensuring that the desired conditions for accelerated corrosion are achieved. This visual aid is pivotal in conveying the practical steps taken to induce corrosion, offering readers a clear window into the experimental procedures that underpin our findings.

Understanding the impact of varying stress levels and environmental exposures on corrosion behavior necessitated a systematic classification of steel wire samples. This organization allows for a nuanced analysis of how different pre-tension levels and exposure durations influence the development of corrosion patterns, providing insights into the complex interplay between mechanical stress and corrosive environments.

Table 5.3 - Stress levels.

Sample	Diameter (ϕ)	Quantity	Stress (MPa)	Time (hours)
0% f_{ptk}	5.0	3	0.0	3
50% f_{ptk}	5.0	3	930	3
70% f_{ptk}	5.0	3	1302	3
95% f_{ptk}	5.0	3	1767	3
0% f_{ptk} - 6	5.0	3	0.0	6
50% f_{ptk} - 6	5.0	3	930	6
70% f_{ptk} - 6	5.0	3	1302	6
95% f_{ptk} - 6	5.0	3	1767	6

In Table 5.3, samples are grouped according to their pre-tension levels and assigned exposure times. This classification forms the basis of our experimental design, facilitating a targeted investigation into the specific effects of prestress conditions on corrosion susceptibility. The table serves as an essential reference for interpreting the experimental setup and understanding the rationale behind the grouping strategy.

A comprehensive assessment of corrosion rates was carried out, leveraging both quantitative weight measurements and qualitative microstructural analyses. This dual approach enables a thorough understanding of SCC effects, merging numerical data with microscopic observations to paint a complete picture of the corrosion process.

The evaluation of corrosion rates involved precise measurements of weight loss before and after exposure to corrosive conditions, adhering to established standards for accuracy. Concurrently, advanced microscopy techniques were employed to examine the microstructural changes in the wires, identifying the presence of corrosion products, pit formation, and any indications of crack initiation and propagation. This meticulous analysis sheds light on the material's degradation mechanisms, offering valuable insights into the factors that contribute to the susceptibility of prestressed steel wires to stress corrosion cracking.

Table 5..4 - Analysis of variance of the weight loss results obtained

Analysis of Variance						
Source of variation	QS	DOF	RMS	F	P-value	Critical F value
Attack Period	34.56	4	8.64	11.62	0.00043	3.25
Pre-applied tension	62.73	3	20.91	28.12	1.03E-05	3.49

where:
QS = the sum of between-sample and within-sample variation
DOF = degree of freedom
RMS = QS/DOF
F = the ratio of between-sample to within-sample variation

Table 5.4 presents a comprehensive analysis of variance (ANOVA) for the weight loss results, a critical metric in evaluating the severity of corrosion in steel wires subjected to different conditions. This statistical examination meticulously quantifies the impact of two major experimental variables: the attack period and the pre-applied tension on the corrosion process. By delineating the sum of squares (QS), which aggregates both between-sample and within-sample variations, and the degrees of freedom (DOF) associated with each factor, the table offers a nuanced insight into the experimental data's variability. The mean square (RMS), calculated as QS divided by DOF, alongside the F-ratio, which contrasts between-sample variation to within-sample variation, highlights the statistical significance of each variable in influencing corrosion rates. The remarkably low P-values associated with both the attack period and pre-applied tension underscore their substantial impact on corrosion, further validated by F-values surpassing the critical F-value thresholds. This analysis not only reinforces the precision of the experimental setup but also elucidates the complex dynamics governing corrosion in prestressed steel wires, providing a solid foundation for the subsequent discussion on material behavior and corrosion mitigation strategies.

The integration of detailed visual aids, such as Figure 5.7, with methodical classification strategies and rigorous analytical techniques enriches the manuscript significantly. By providing a comprehensive overview of the experimental framework and analytical methodologies, this enhanced content ensures a deep and well-rounded understanding of the study's foundations. Such a detailed exposition supports the subsequent discussion of findings, laying a solid groundwork for addressing the challenges of stress corrosion cracking in prestressed concrete applications and contributing to the development of more durable infrastructure solutions.

5.4 EXPERIMENTAL RESULTS AND DISCUSSION

The initial stages of corrosion were observed just one hour after exposure, with the formation of black and red rust at the solution-air interface of the wire, indicating the onset of corrosion. As the exposure continued, corrosion products progressively covered the portions of the wire submerged in the corrosive solution. This phenomenon highlights the rapid development of corrosion under experimental conditions designed to simulate stress corrosion cracking (SCC) environments.

Figure 5.8 presents the findings from the energy dispersive spectroscopy (EDS) analysis conducted using a scanning electron microscope (SEM). Figure 5.8 captures the elemental composition of both the reference (unexposed) and corroded (exposed for 3 hours) samples, providing a visual representation of the corrosion products that formed on the wire's surface. The EDS analysis offers insights into the nature and composition of the corrosion products, revealing that the development of these compounds is largely independent of the mechanical stress levels applied to the steel, as indicated by the absence of significant variation in chemical composition across different stress levels [6][8].

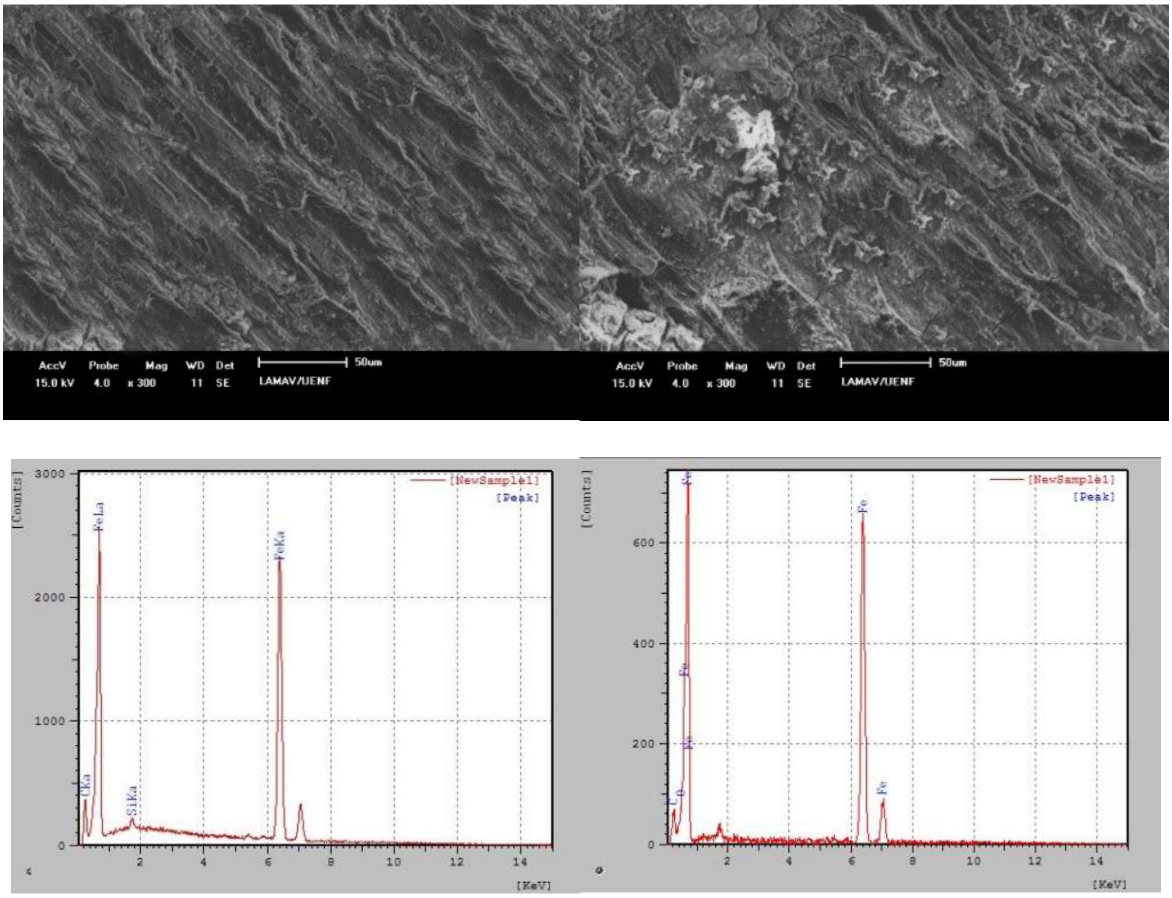

Figure 5.8 - Testing the 0% fptk wire: SEM of the wire as received (300x magnification).

The electron and optical microscopy analyses shed light on the microstructural changes occurring at the onset of corrosion, offering a detailed look at the corrosion process's dynamics. The emergence of rust and subsequent coverage by corrosion products underscore the aggressive nature of the simulated SCC environment. Notably, the radiographic corrosion analysis performed alongside EDS revealed that the chemical makeup of the corrosion products remains consistent, regardless of the stress conditions applied to the steel. This observation suggests that the susceptibility of the steel to corrosion in the given environment is not directly influenced by the applied stress, at least in the context of the chemical composition of the resulting corrosion products.

The utilization of advanced microscopy techniques, such as SEM and EDS, in this study provides a comprehensive understanding of the corrosion mechanisms at play. By analyzing the corrosion products at a microscopic level, we gain invaluable insights into the early stages of corrosion development and its progression over time. These findings are crucial for developing strategies to mitigate SCC in steel wires used in prestressed concrete applications, emphasizing the importance of material composition and environmental factors in influencing corrosion behavior.

5.4.1 Microscopic Analysis of Corrosion Products

The microscopic examination of the steel wire samples post-exposure revealed the formation of corrosion products characterized by continuous, irregular, and porous layers, indicative of iron oxide and its derivatives. This signals the onset of corrosion on the steel's surface. Utilizing Energy Dispersive Spectroscopy (EDS) analysis, we identified the primary chemical constituents of these corrosion products as Iron (Fe), Carbon (C), and Oxygen (O)[citation needed]. It's crucial to note that EDS provides insight into the elemental composition on a microscopically small area, highlighting the presence or absence of elements within the corrosion products.

5.4.2 Corrosion Rate Analysis

The assessment of corrosion rate, particularly in relation to tensile strength under stress corrosion conditions, involved measuring weight loss due to corrosion[citation needed]. Adhering to standards set by ASTM G1-72 and NACE RP 0775[citation needed], we calculated the corrosion rates (T) for our samples. The findings reveal minimal discrepancies between the average corrosion rates determined by the two methodologies, underscoring the comparability of these techniques. Notably, the uniform corrosion rate for wires with no applied pre-tension (0% fptk) was classified as strong, ranging from 0.13 to 0.25 mm/year. In contrast, wires under different pre-tension conditions exhibited more severe corrosion rates, suggesting that mechanical stress plays a significant role in accelerating corrosion.

An Analysis of Variance (ANOVA) was conducted to evaluate the impact of varying pre-tension levels and exposure durations on weight loss due to corrosion. The ANOVA results highlight significant differences across conditions, suggesting that both the duration of exposure to corrosive environments and the level of applied pre-tension are critical factors influencing corrosion susceptibility.

5.4.3 Mechanical Strength Assessment

The decline in mechanical strength due to corrosion was assessed through direct tensile tests on samples exposed to the aggressive solution for three hours. The resulting stress-strain curves show a substantial reduction in the ultimate capacity of the wires, with decreases in both the elastic limit and ultimate strain observed in the prestressed, corroded wires. This reduction not only demonstrates the negative effects of corrosion on material integrity but also underscores the necessity for protective measures in prestressed concrete applications to mitigate corrosion over time.

The assessment of ductility, which represents the wire's capacity to undergo significant deformation before rupture, reveals critical insights into the effects of corrosion on mechanical properties. For the unstressed corroded wire (0% fptk), a notable reduction in ductility was observed, affirming findings from other research in the field [6,27,36]. Comparative analysis showed that ductility in the 50, 70, and 95% fptk wires declined by 30, 45, and 48%, respectively. Interestingly, the corroded 0% fptk wire exhibited a 25% reduction in ductility, underscoring the detrimental impact of corrosion on material flexibility and resilience.

Direct tensile tests further elucidated the influence of tension levels on the mechanical behavior of the wires. A decrease in yield stress, modulus of elasticity, and ultimate tensile strain was noted, particularly in wires subjected to stress and corrosive environments. This reduction in mechanical integrity highlights the critical interplay between prestressing levels and corrosion in determining the wire's overall structural performance.

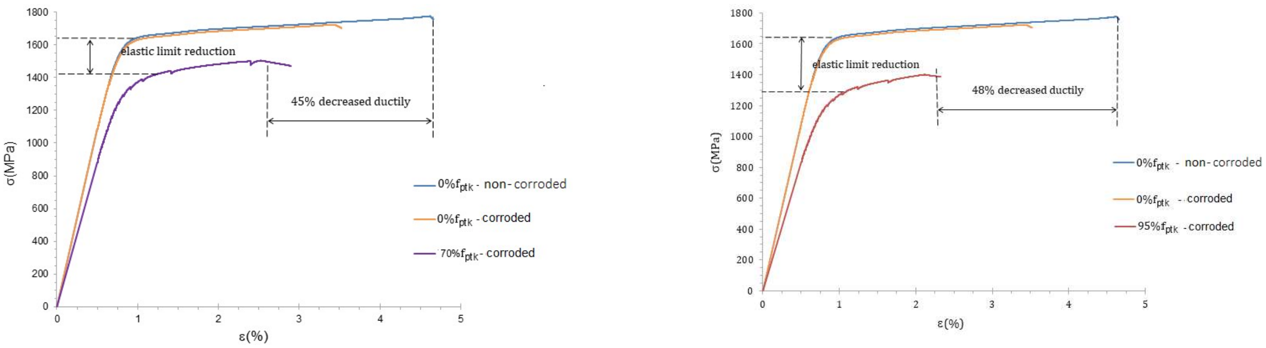

(a) **(b)**

Figure 5.9 - Comparison between the behavior unstressed (a) non-corroded and (b) corroded wire and corroded 70% fptk-stressed wire.

Figure 5.9 presents a comparative analysis between (a) unstressed non-corroded and (b) corroded wires, as well as corroded wires under 70% fptk stress. The visual comparison starkly illustrates the impact of corrosion and stress on wire ductility and strength, providing a clear depiction of the material's degradation under varying conditions. It also Showcase the effect of prestressing and corrosion on the ultimate strength of the wires. The findings from this comparison reveal the localized nature of pitting corrosion and its influence on the wire's mechanical properties, including reductions in ultimate load and stress due to decreased cross-sectional area [6,35,36,37]. The localized stress increase, resulting from the diminished cross-section, does not significantly alter the average stress distribution along the wire's length but critically impacts its load-bearing capacity and ductility.

This analysis highlights the presence of micro voids and microcracks in the corroded wires, factors contributing to potential failure due to stress concentration near cracked regions. The aggregation of micro voids near microcracks, indicative of significant material damage, underscores the loss of elastic modulus and elastic limit observed in corroded wires [32]. This phenomenon, more pronounced in corroded strands, accelerates the growth rate of surface microcracks compared to non-corroded strands, emphasizing the exacerbated vulnerability of corroded materials to mechanical failure [7,38,39].

5.5 CONCLUSIONS

The comprehensive study presented in this research provides insights into the effects of stress corrosion cracking (SCC) on prestressed concrete wires, emphasizing the critical interplay between mechanical stress and corrosive environments. Through experimental design, including electron and optical microscopy analysis, corrosion rate evaluation, and mechanical strength assessment, it was delineated the nuanced impact of corrosion on the structural integrity and mechanical properties of cold-drawn carbon steel wires. The findings underscore the importance of considering both the chemical composition and the microstructural characteristics of materials in the context of their susceptibility to SCC. The observed decline in ductility and mechanical strength, particularly in wires subjected to pre-tension and corrosive environments, highlights the urgent need for robust protective strategies in prestressed concrete applications to mitigate the deleterious effects of corrosion.

The study's experimental results, notably the localized nature of pitting corrosion and its influence on material properties, offer valuable contributions to the field of materials science and engineering. By demonstrating that the corrosion-induced damage does not uniformly affect the wire's stress distribution but significantly reduces its ultimate load-bearing capacity, it was provided a basis for reevaluating existing design and maintenance practices for prestressed concrete structures. Furthermore, the analysis of variance in corrosion rates across different pre-tension levels and exposure times presents a compelling argument for the inclusion of comprehensive corrosion assessment protocols in the standard testing regimen for prestressed concrete components.

In conclusion, this research advances the understanding of SCC in prestressed concrete structures and sets the stage for the development of more durable materials and innovative protective measures. The insights gained from this study contribute to enhancing the longevity and safety of existing structures and inform the design and construction of future infrastructure projects. As the field continues to evolve, ongoing investigations into the mechanisms of corrosion and the development of advanced mitigation techniques will be essential in addressing the complex challenges posed by SCC, ensuring the resilience and reliability of prestressed concrete structures in diverse environmental conditions.

5.6 DISCUSSION FOR CHAPTER 3

5.6.1 Key Findings

The experimental results revealed that SCC is a significant threat to the longevity and safety of prestressed concrete structures, particularly in environments where exposure to corrosive agents, such as chloride ions, is prevalent. The study showed that SCC can severely compromise the load-bearing capacity of prestressed concrete, leading to premature failure. The identification of specific conditions that exacerbate SCC, such as the presence of tensile stress combined with corrosive environments, provides engineers with critical information for designing more resilient structures.

5.6.2 Implications

The implications of these findings are far-reaching, particularly for the design and maintenance of infrastructure exposed to harsh environmental conditions. Engineers must account for the risk of SCC in their designs, incorporating protective measures such as corrosion-resistant materials, coatings, or cathodic protection systems. Additionally, the findings suggest that regular monitoring and maintenance are essential to detect early signs of SCC and prevent catastrophic failures. This research contributes to the broader understanding of corrosion-related failures in concrete structures and emphasizes the need for ongoing vigilance in managing these risks.

5.6.3 Limitations

The study's focus on specific environmental conditions, such as chloride exposure, may limit the generalizability of the findings to other corrosive environments or stress conditions. Additionally, while the experimental setup provided valuable insights into the mechanisms of SCC, real-world structures may experience a more complex interplay of factors that could influence the occurrence and progression of SCC. Further research is needed to explore these additional variables and their impact on the overall risk of SCC in prestressed concrete.

5.6.4 Future Work

Future research should aim to expand the scope of this study by investigating SCC under a broader range of environmental conditions and stress scenarios. Exploring the effectiveness of various preventive measures, such as the use of corrosion inhibitors or alternative materials, could provide practical solutions for mitigating the risks associated with SCC. Additionally, long-term field studies on existing structures could offer valuable data to validate the laboratory findings and refine predictive models for SCC in prestressed concrete.

5.7 CONCLUSION FOR CHAPTER 2

This chapter focused on the critical issue of stress corrosion cracking (SCC) in prestressed concrete, a phenomenon that poses significant risks to the durability and integrity of concrete structures. The experimental investigation conducted in this chapter provided valuable insights into the conditions under which SCC occurs and its effects on the structural performance of prestressed concrete. The findings highlight the importance of considering environmental factors, particularly in corrosive environments, when designing and maintaining prestressed concrete structures. This research underscores the need for robust design strategies and preventive measures to mitigate the risks associated with SCC, ensuring the long-term safety and reliability of these structures.

Understanding the mechanisms and risks associated with SCC is crucial for developing durable and resilient concrete structures. However, predicting and mitigating such risks requires more than just understanding; it necessitates advanced analytical tools.

5.8 REFERENCES FOR CHAPTER 2

1. Carvalho, R.C. Prestressed Concrete Structures - Prestressing, Post-tensioning, Calculation and Detailing. São Paulo, Ed. Pini, 2012, 431p.
2. Böhni, H. (Ed.) Corrosion In Reinforced Concrete Structures. Cambride: Woodhead, 2005, 248p
3. P. Andresen, R. Jones, Stress Corrosion Cracking-Material Performance and Evaluation, ASM International, Materials Park, OH, 1992, pp. 181–210.

4. J. Kovac, C. Alaux, T.J. Marrow, E. Govekar, A. Legat, Correlations of electrochemical noise, acoustic emission and complementary monitoring techniques during intergranular stress-corrosion cracking of austenitic stainless steel, Corros. Sci. 52 (2010) 2015–2025.
5. ASTM - Internacional Handbook Committee. Asm Handbook: Corrosion: undamentals, Testing, And Protection. V. 13a. Usa. 2013.
6. N.A. Vu, A. Castel, R. François, Effect of stress corrosion cracking on stress–strain response of steel wires used in prestressed concrete beams, Corros. Sci. 51 (2009) 1453–1459.
7. J. Woodtli, R. Kieselbach, Damage due to hydrogen embrittlement and stress corrosion cracking, Eng. Fail. Anal. 7 (2000) 427–450.
8. S. Wu, H. Chen, H. L. Ramandia,, P. C. Hagan, A. Crosky, S. Saydama, Effects of environmental factors on stress corrosion cracking of cold-drawn high-carbon steel wires, Corros. Sci. 132 (2018) 234-243.
9. Schön, C. G. Mechanics of Materials. 1ª Ed. Rio De Janeiro: Ed Elsevier. 2013.
10. Cascudo, O. The Control of Reinforcement Corrosion in Concrete: Inspection and Electrochemical Techniques. São Paulo: Pini; Goiania: Ed Ufmg, 1997.
11. Andrade, C. Et Al. Determination Of The Corrosion Rate Of Steel Embedded In Concrete By The Polarization Resistance And A.C. Impedance Methods. 1986.
12. H. Liu, Stress-corrosion cracking and the interaction between crack-tip stress field and solute atoms, J. Basic Eng. 92 (1970) 633–638.
13. R. Parkins, Environment sensitive fracture and its prevention, Br. Corros. J. 14 (1979) 5–14.
14. H.L. Logan, Film-rupture mechanism of stress corrosion, J. Res. Nat. Bur. Stand. 48 (1952) 99–105.
15. M. Perrin, L. Gaillet, C. Tessier, H. Idrissi, Hydrogen embrittlement of prestressing cables, Corros. Sci. 52 (2010) 1915–1926.
16. E. Gamboa, A. Atrens, Stress corrosion cracking fracture mechanisms in rock bolts, J. Mater. Sci. 38 (2003) 3813–3829.
17. A. Turnbull, Modelling of environment assisted cracking, Corros. Sci. 34 (1993) 921–960.
18. K.R. Trethewey, Some observations on the current status in the understanding of stress-corrosion cracking of stainless steels, Mater. Design 29 (2008) 501–507.
19. K. Bhargava , Y. Mori , AK Ghosh, Time-dependent reliability of corrosion-affected RC beams - Part 1: estimation of time-dependent strengths anda associated variability. Nucl. Eng. Des. 241 (2011) , pp. 1371 – 1384

20. L. Wang , X. Zhang , J. Zhang , Y. Ma , Y. Xiang , Y. Liu, Effect of insuficiente grouting and strand corrosion on flexural behavior of PC beams. Constr. Build. Mater. 53 (2014) , pp. 213 – 22

21. C. Naito , R. Sause , I. Hodgson , S. Pessiki , T. Macioce, Forensic examination of a noncomposite adjacente precast pretressed concrete box beam bridge. J. Bridge Eng. , 15 (2010) , pp. 408 - 418

22. H. Minh , H. Mutsuyoshi , H. Taniguchi , K. Niitani, Chloride-induced corrosion in insufficiently grouted posttensioned concrete beams. J. Mater. Civ. Eng. , 20 (2008) , pp. 85 - 91

23. M. Kiviste , J. Miljan Evaluation of the residual flexural capacity of existing precast precast concrete panels - a case study Eng. Struct. , 32 (2010) , pp. 3377 - 3383

24. Z. Rinaldi , S. Imperatore , C. Valente, Experimental evolution of the flexural behavior of corrored P/C beams. Constr. Biuld. Mater. 24 (2010) , pp. 2267 - 2278

25. D. Coronelli , A. Castel , NA Vu , R. François, Corred post-tensioned beams with bonded tendons and wire failure. Eng. Struct. , 31 (2009) , pp. 1687 - 1697

26. F. Li , Y. Yuan, Experimental study on bending property os prestressed concrete beams with corrored steel strands. J. Build. Struct. , 32 (2010) , pp. 78 – 84

27. F. Li , Y. Yuan , C. Li. Corrosion propagation of prestressing steel strands in concrete subject to chloride attack. Constr. Build Mater, 25 (2011), pp. 3878 - 3885

28. R. W. K. Honeycomb , Steels Microstructure and Properties. 3ed. Elsevier. Oxford. (2006), pp344.

29. NF A 05 - 302, Pre-control reinforcement - distillate corrosion tests, December de 1981.

30. NF A 05 - 303, Pre-control reinforcement - ammonium thiocyanate corrosion tests, December de 1981.

31. ISO – International Organization for Standardization, 1987)

32. Eurocódigo 2 - NF EN 1992-1-1Calculate concrete structures - Part 1-1: General rules and company rules, October de 2005

33. Nace – National Association Of Corrosion Engineers. Nace Rp0775-2013

34. ASTM G1-90 Standard Practice for Preparing, Cleaning, and Evaluating Corrosion Test Specimens,1999.

35. Cairns J. , Plizzari Ga, Y. Du , Dw Law , C. Franzoni - Mechanical Properties of Corrosion Damage Reinforcement – Aci. 2005.

36. Castel A., François R., Arliguie G.- Mechanical Behavior of Corroded Reinforced Concrete Beams - Part 1: Experimental Study of Corroded Beams. Pp. 539 – 544. 2000.

37. A. Castel, R. François, G. Arliguie, Model of mechanical behavior of corroded reinforced concrete, Comptes Rendus of the Academy of Sciences - Series IIb / Mechanics, Editions Elsevier, Amsterdam, vol. 330, 2002, pp. 45–50.

38. L. Coudreuse, Fragilization par I’hydrogéne et corrosion sous contrainte, Corrosion sous contrainte – Phénoménologie et mécanisme: Bombannes, Edition de Physique 1992, pp. 397-424. (1990).

39. L. Vehovar , V. Kuhar , A. Vehovar Hydrogen-assisted stress-corrosion of pretressing wires in a motorway viaduct, Eng Fail 5 (1), p. 21 – 27. (1998).

6 PREDICTIVE ANALYSIS OF CORROSION DYNAMICS IN PRESTRESSED CONCRETE EXPOSED TO CHLORIDE ENVIRONMENTS

This chapter is published as an original research article in the Infrastructures Journal.
https://doi.org/10.3390/infrastructures9080133

PIEROTT, Rodrigo et al. Predictive Analysis of Corrosion Dynamics in Prestressed Concrete Exposed to Chloride Environments. **Infrastructures Journal**.

Chapter 6 introduces predictive modeling as a powerful tool to analyze corrosion dynamics in prestressed concrete, particularly in chloride-rich environments. Building on the findings from the previous chapter, this chapter explores how these models can forecast the progression of corrosion, enabling more proactive and informed decisions in the design and maintenance of concrete structures.

ABSTRACT

This study investigates the corrosion behavior of 5 mm diameter prestressed wires in concrete beams under chloride attack, a prevalent issue for coastal infrastructure. The study simulated aggressive chloride environments to understand their impact on structural integrity and service life. Utilizing a combination of advanced digital image correlation (DIC) techniques and a novel machine learning-based predictive model, the research provides a nuanced analysis of the interplay between stress levels, corrosion rates, and concrete strength. Empirical findings reveal a significant correlation between increased prestress levels and accelerated corrosion, indicating a crucial consideration for the design and maintenance of prestressed concrete structures. Notably, this study found that beams with a 95% prestress level exhibited a corrosion rate of 0.64 mm/year, significantly higher than the 0.37 mm/year for non-prestressed beams. The predictive model's accuracy was validated with a mean squared error of 0.517 and an R^2 value of 0.905, offering a valuable tool for quantifying the impact of corrosion. Therefore, the predictive model is a valuable tool for quantifying the impact of corrosion, enhancing the ability to assess and improve the durability of such infrastructure. This study's insights highlight the necessity for a balanced approach to design and regular monitoring, especially in chloride-rich

environments. By helping to develop more resilient construction practices and contributing to sustainable development goals, this study can significantly impact the safety and service life of coastal bridges and structures, aligning with global efforts to create more sustainable and durable infrastructure.

Keywords:
Prestressed Concrete; Corrosion Dynamics; Structural Integrity; Predictive Modeling.

6.1 INTRODUCTION

The deterioration of prestressed concrete structures in chloride-rich environments due to corrosion is a significant concern, affecting both the service life and safety of such infrastructure. This issue is crucial for civil and environmental engineering, where the degradation of infrastructure due to corrosion represents not only a safety hazard but also a substantial environmental and economic burden [1,2]. Recent studies have highlighted the use of advanced materials and coatings to mitigate corrosion, improving the durability of these structures in aggressive environments [3]. This issue is crucial for civil and environmental engineering, where the degradation of infra-structure due to corrosion represents not only a safety hazard but also a substantial environmental and economic burden. The corrosion of steel reinforcement in concrete structures significantly impacts their serviceability, safety, and service life, necessitating a comprehensive understanding of corrosion mechanisms and their impacts on developing sustainable civil engineering practices.

Previous studies highlighted the severe consequences of corrosion in concrete structures. Ref. [4] noted that corrosion leads to cracking, bond strength reduction, and structural integrity loss, emphasizing the necessity of understanding corrosion rates to predict serviceability loss. Similarly, Ref. [5] explored steel corrosion mechanisms, particularly carbonation and chloride penetration, and discussed approaches for designing durable structures to extend their service life in aggressive environments. Additionally, the effectiveness of electrochemical repair methods and the performance of corrosion inhibitors were extensively studied, providing insights into the long-term protection of concrete structures against corrosion stimulation [6,7]. Recent advances in mechanical–transport–chemical modeling further enhanced our ability to evaluate the effectiveness of electrochemical repair methods for corrosion-induced cracking in concrete structures, providing a robust framework for optimizing repair techniques and improving durability [1]. Moreover, the broader environmental implications associated with resource utilization, energy consumption, and emissions from manufacturing and construction activities further underscore the importance of addressing this issue [8].

The necessity of developing sustainable practices in civil engineering is evident, as discussed by [3], highlighting the importance of corrosion protection in sustainable energy systems and infrastructure. Another study reviewed the use of ionic liquids as sustainable corrosion inhibitors, emphasizing their potential to reduce environmental impacts and enhance material service life [9]. Furthermore, the application of artificial neural networks (ANNs) in predicting chloride diffusivity in concrete has shown promising results, enhancing the accuracy and robustness of corrosion modeling under various environmental conditions [2].

While many documented cases of corrosion pertain to post-tensioned members, pre-tensioned members are also susceptible to corrosion, especially in chloride-rich environments. The literature includes instances of failures due to corrosion in pre-tensioned members, highlighting the need for focused research in this area.

Research shows that prestressed concrete structures, particularly those containing 5 mm diameter wires, are highly susceptible to accelerated corrosion in chloride-laden environments, increasing the risk of structural collapse compared to reinforced con-crete [10]. Besides, models predicting the flexural strength of partially prestressed concrete structures emphasize the critical nature of corrosion in such environments [11]. In this context, methodologies for predicting the corrosion-free service life of concrete structures exposed to chlorides underscore the importance of regular maintenance and evaluation to prevent corrosion-related failures [12].

Despite this growing discussion, there remains a critical gap in understanding the specific corrosion dynamics in prestressed concrete [13], especially for small-er-diameter wires. Addressing this gap is essential for developing effective prevention and mitigation strategies that enhance structural service life and safety [14].

Therefore, this study explicitly simulates the aggressive chloride environments to replicate the corrosive conditions faced by coastal infrastructure closely. By focusing on the corrosion behaviors of prestressed concrete beams used in bridges and other coastal structures, this study aims to provide direct implications for such infrastructure's maintenance, design, and service life.

To achieve this goal, this study investigates the corrosion behavior of 5 mm diameter prestressed wires in chloride environments through a combination of empirical analysis and predictive modeling. This study uses advanced digital image correlation (DIC) techniques and a novel machine learning-based predictive model to analyze the interplay between stress levels, corrosion rates, and concrete strength.

To complement the experimental investigation of corrosion in prestressed concrete beams, we employed statistical and machine learning techniques to analyze the relationship between key variables and predict the structural integrity of the beams. These techniques provide a robust framework for understanding interactions and enhancing predictive accuracy.

Ultimately, the novelty of this research is its direct contribution to developing more durable and environmentally sustainable construction materials and methods, enhancing the safety and integrity of concrete structures, and supporting the global movement towards environmentally responsible civil engineering practices.

6.2 BACKGROUND

Corrosion in prestressed concrete primarily results from chloride ion penetration, which is prevalent in corrosive environments. When chloride ions breach the concrete cover and reach the steel reinforcement, it leads to the formation of rust. This process expands the volume of the steel, causing cracking and spalling of the concrete cover and reducing the effective cross-sectional area of the reinforcement. Notably, [15] demonstrated that the loss of beam section and the breakage of prestressed steel strands due to corrosion significantly reduce beam stiffness and structural integrity.

Recent advancements in digital image correlation (DIC) technology and machine learning havesignificantly enhanced the ability to analyze and predict corrosion be-havior in concrete structures. DIC technology provides high-resolution and non-contact measurement of surface deformation, enabling detailed monitoring of crack formation and propagation. Meanwhile, machine learning algorithms offer powerful tools for predictive modeling, capable of identifying complex patterns and relationships within large datasets to forecast corrosion impact with high accuracy.

In addition, experimental studies have provided insights into how corrosion affects the mechanical performance of prestressed concrete beams. For example, two different studies investigated the flexural performance of post-tensioned beams under different corrosion and grouting conditions. These studies found that corrosion de-creased the flexural capacity and altered the crack patterns and load-deflection responses [16,17]. Additionally, [18] conducted experiments to evaluate the bending characteristics and bearing capacities of corroded beams, highlighting the critical role of corrosion rates in determining the extent of structural degradation. In a similar manner, [19] provided an overview of modeling corrosion in steel and reinforced concrete and highlighted the role of environmental factors. Finally, [20] developed a finite element framework to evaluate the effects of various exposure conditions on corrosion, demonstrating the significance of integrating environmental stressors in predicting structural durability.

Over time, several empirical models have been developed to predict the residual flexural capacity of corroded prestressed concrete beams. These models typically con-sider factors such as sectional area loss, mechanical property degradation, grouting defects, and bond deterioration due to corrosion. For instance, [17] proposed models that incorporate the reduction in the cross-sectional area of the steel reinforcement and the degradation of mechanical properties due to corrosion. Likewise, [21] pro-posed a method using machine learning to predict the service life of reinforced concrete structures. Additionally, [18] developed a model that evaluates the cooperative behavior between corroded steel and concrete, providing a comprehensive under-standing of how corrosion impacts the structural integrity of prestressed concrete beams. However, these models exhibit varying degrees of accuracy and often require calibration against experimental data to ensure reliability.

In this context, the development of non-destructive testing techniques advanced the ability to detect and monitor corrosion in prestressed concrete structures. For ex-ample, a study published in 2013 explored the use of acoustic emission (AE) techniques for early-stage corrosion detection and crack classification [22], while [23] presented a review of the advances in the use of sensors for reinforcement corrosion monitoring. Their research demonstrated the effectiveness of AE in identifying corrosion, macrocracks, and crack propagation, providing a valuable tool for structural health monitoring and proactive maintenance.

Nonetheless, the recent literature underscores the complexity of corrosion dynamics in corrosive environments for prestressed concrete structures. While our understanding of the mechanisms and impacts of corrosion and developing predictive models have come a long way, challenges remain in ensuring the accuracy and applicability of these models across diverse environmental conditions. The integration of advanced monitoring techniques, such as AE, offers promising avenues for enhancing the detection and mitigation of corrosion-related damage, ultimately contributing to the durability and safety of coastal infrastructure.

6.3 PROPOSED METHODS

The computational methodology component complements the experimental re-search by providing detailed analysis through computer-based modeling and simulations. This includes the EDA process, visual insights, model validation, and mathematical equations, as presented in Figure 6.1. Therefore, this study proposes processing the experimental data using statistical and computational techniques to identify patterns and correlations between stress levels, corrosion rates, and concrete strength. Based on the findings, a machine learning-based predictive model is developed to quantify the impact of corrosion. This model should be trained on the empirical data obtained from the experiments and validated through cross-validation techniques to ensure accuracy and reliability.

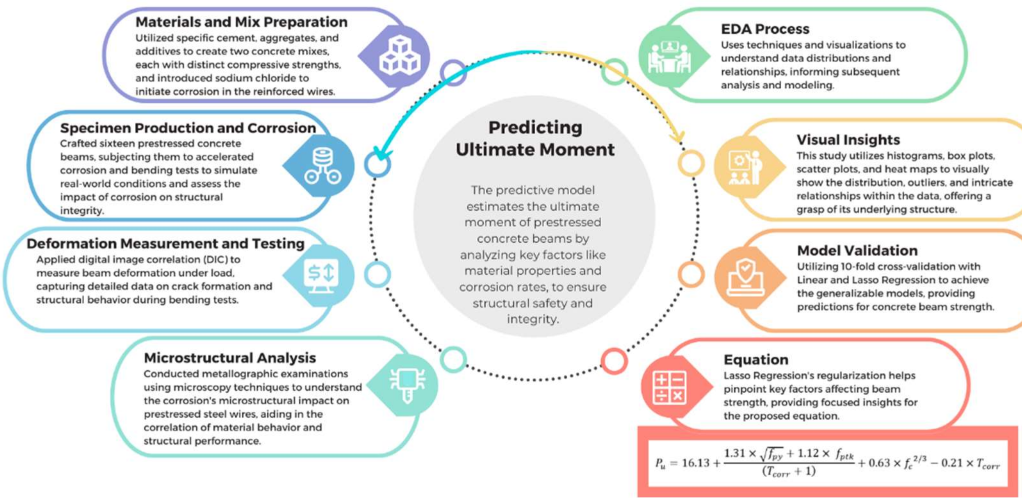

Figure 6.1 - Proposed methodology of the study.

The proposed methodology for this study is divided into two main components: experimental research and computational methodology. In the experimental research component, this study proposes a series of practical experiments focusing on the behavior of prestressed concrete beams under chloride attack. This involves several steps, as follows: (i) material and mix preparation, (ii) specimen production and corrosion, (iii) microstructural analysis, and (iv) deformation measurement and testing [24,25]. Thus, a thorough understanding of corrosion mechanisms [26] and their impact on concrete structures is crucial for advancing sustainable civil engineering practices aimed at reducing both the environmental footprint and ensuring structural safety [27].

This study focuses on the corrosion of prestressed concrete structures, particularly on the behavior of 5 mm diameter prestressed wires in chloride environments. While there is extensive research on corrosion in reinforced concrete, studies specifically ad-dressing prestressed concrete are limited. Prestressed structures, due to their unique design and material properties, often exhibit different, sometimes more severe, corrosion responses compared to reinforced structures [22]. The collapse of the Ynys-y-Gwas bridge in the UK and the recent and notable example of the catastrophic impact of corrosion on prestressed concrete structures, the collapse of the Morandi Bridge in Italy in 2018, underscore the critical need to understand the specific corrosion dynamics in prestressed concrete, particularly in smaller diameter wires. The utility of guided ultrasonic waves in inspecting embedded tendons in post-tensioned bridges, a method driven by the necessity to prevent incidents like the Ynys-y-Gwas bridge collapse, was emphasized by [28]. These studies collectively stress the urgency of developing effective corrosion prevention strategies for prestressed concrete structures to avoid catastrophic failures.

From an environmental standpoint, the significance of this research is twofold. Extending the lifespan of concrete structures through better understanding and prevention of corrosion formation can significantly reduce the need for frequent repairs and reconstructions [29], thereby minimizing the related environmental impacts. This approach is aligned with sustainable civil engineering principles, which emphasize durable and low-impact construction practices. Moreover, our study contributes to the critical knowledge base needed for the shift towards more sustainable construction practices. It underscores the possibilities for innovative designs and material choices that not only improve structural durability but also contribute to environmental conservation.

In exploring the corrosion behavior of prestressed wires in chloride environments, this study aims to offer insights that could lead to advancements in both material science and construction methodologies. These advancements are expected to profoundly impact the field of civil engineering, contributing to the development of infrastructure that is more resilient and more in harmony with our environmental responsibilities.

6.4 MATERIALS

This study utilized high-early-strength Portland cement (CPV ARI) with a density of 3100 kg/m³ and Blaine fineness of 470 kg/m². Basalt-type coarse aggregate (unit weight of 2.73

g/cm³ and bulk density of 1.58 g/cm³) and natural quartz sand (unit weight of 2.63 g/cm³ and bulk density of 1.54 g/cm³) were chosen for their compatibility and performance. Silica fume (density of 2.20 g/cm³) and a superplasticizer based on modified carboxylic ether (density of 1.070 g/cm³, pH 6) were also incorporated. The superplasticizer facilitated high water removal rates, ensuring workability without altering the setting time. The reinforcement used in the prestressed beams comprised notched ribbed CP-175 RB 5 wire, with a diameter of 5.0 mm and a tensile strength of 1860 MPa, as established through preliminary tensile tests and highlighted in Figure 6.2.

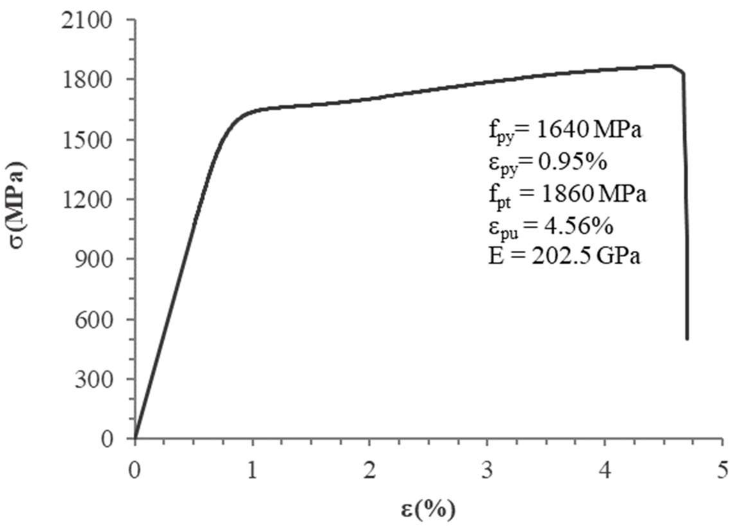

Figure 6.2 - Stress versus strain of the prestressed reinforcement.

6.4.1 Concrete Proportions

Two concrete mixes were prepared with target compressive strengths of 32 MPa and 68 MPa, with subsequent testing to measure the actual compressive strengths for use in structural analyses. The 32 MPa mix had a 1:2.25:3.25 cement/sand/coarse aggregate ratio, 0.58 w/c ratio, and an 80 mm slump. The 68 MPa mix was denser with a 1:0.94:1.89 ratio, 0.34 w/c ratio, 0.25 water/cementitious material factor, plus 0.5% superplasticizer and 10% silica fume, achieving a 90 mm slump. Both mixes included 2% sodium chloride (NaCl) by cement weight to initiate corrosion, as per Mancini et al. (2014). Material volumes are presented in Table 6.1.

Table 6.1 - Amount of material used per m3 of concrete in the beams tested.

Materials	32 MPa (kg/m^3)	68 MPa (kg/m^3)
Portland cement	329	550
Sand	740	520
Gravel	1069	1043
Water	191	154
Silica fume	-	55
Superplasticizer	-	2.78
NaCl	6.58	11

6.4.2 Specimen Details and Casting

Sixteen prestressed concrete beams (150 × 300 × 1500 mm) underwent three-point bending tests, as illustrated in Table 2. Classified as VX-Y-Z (X = concrete strength, Y = wire stress, Z = corrosion status), they varied in prestress and strength levels. Half had non-corroded (NCB), and half had corroded pre-cracked wires (CB). Beams were cast in a 3 m formwork, producing six at a time, using a hydraulic system for prestressing. After a 24 h demolding period, they were wet-cured for 28 days. The anchoring system of the prestressed wire and the metal formwork for concreting the prestressed beams are presented in Figure 6.3 and Figure 6.4, respectively.

Figure 6.3 - Anchoring system of the prestressed wire.

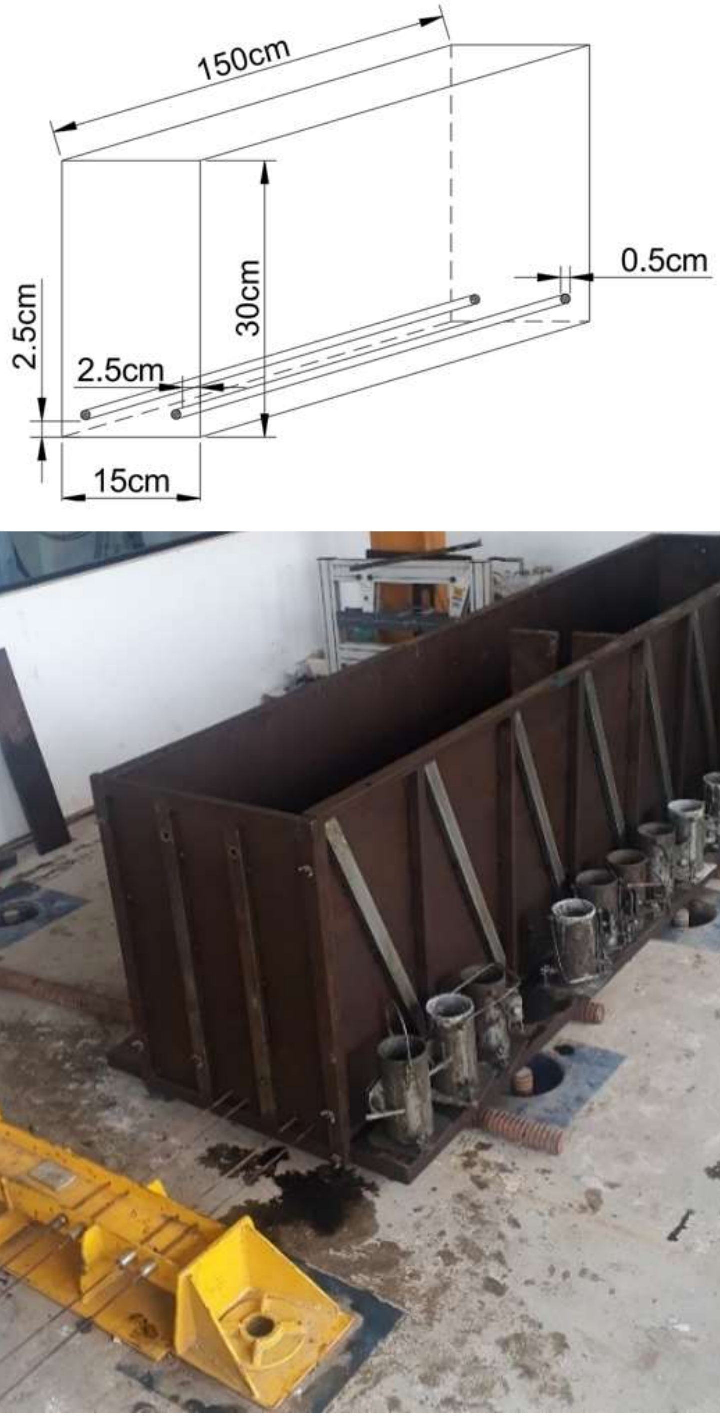

Figure 6.4 - Cross section of the beam, measuring 30 cm in height, 15 cm in width, 150 cm in length, and containing two reinforcements with a diameter of 0.5 cm. The metal formwork for casting multiple prestressed beams each time is also shown.

The cross section of the beam models included four prestressed steel wires, positioned symmetrically around the neutral axis, with two wires in the upper layer and two in the lower layer, ensuring the uniform distribution of prestressing forces.

We acknowledge that the a/d ratio used in the tests is below 5, indicating significant shear in addition to bending. Future studies in this area will need to adjust the beam model proportions to ensure a/d ratios above 5 and span-to-height ratios over 20 to better isolate bending effects.

Table 7.2 - Specimen details.

Samples	Compressive Strength (MPa)	Stress Level	Cl-Concentration	Pre-Tension (MPa)	Replica
V32-0-Z.	32	0% f_{ptk}	2	0	2
V32-0.5-Z		50% f_{ptk}	2	930	2
V32-0.7-Z		70% f_{ptk}	2	1302	2
V32-0.95-Z		95% f_{ptk}	2	1767	2
V68-0-Z	68	0% f_{ptk}	2	0	2
V68-0.5-Z		50% f_{ptk}	2	930	2
V68-0.7-Z		70% f_{ptk}	2	1302	2
V68-0.95-Z		95% f_{ptk}	2	1767	2

In Table 2, the chloride concentration in the concrete was controlled by adding a specified amount of sodium chloride (NaCl) to the mix during the preparation phase, ensuring consistent chloride content across samples.

The experimental setup expedited the corrosion of prestressed steel wires in concrete beams, beginning after a 28-day wet curing period. The purpose of this acceleration was to replicate natural corrosion rapidly and under controlled laboratory conditions, facilitating an in-depth study of its effects.

Corrosion was induced using a sophisticated electrochemical setup comprising four direct current (DC) power supplies connected in series. This system provided a range of 12 to 30 volts, enabling a current of up to 1 ampere and a maximum voltage of 66 volts. Beams with a higher compressive strength of 68 MPa required this increased voltage to achieve significant current levels for corrosion, compared to their 32 MPa counterparts.

In this setup, the prestressed steel wire within each beam was the anode, connected to the positive terminal of the power supply. This connection caused the wire to undergo accelerated oxidation, simulating the natural rusting process at a much faster rate. A less electronegative plate, introduced during casting and connected to the negative terminal, acted as the cathode, where reduction reactions typically occurred.

This controlled electrochemical environment within each beam led to an accelerated onset and progression of corrosion on the steel wires. To monitor this process, corrosion potential (Ecorr) readings were systematically taken. Using two multimeters, the current for each beam and Ecorr were recorded at 15 strategic points along the wire's length, providing a detailed map of corrosion progression.

Over 168 h, Ecorr readings were continuously recorded every 24 h. These readings showed significant potential differences, with −730 mV for 32 MPa beams and −510 mV for 68 MPa beams at 95% fptk pre-tension of the wires, indicating varying corrosion rates and initiation points across different beam types. Figures 6.5, 6.6, and 6.7 show the beams connected to the power supplies and the corresponding Ecorr readings, illustrating the comprehensive monitoring and analysis carried out in this study.

Figure 6.5 - Current applied to the beams being recorded by multimeters.

Precise monitoring and control of the accelerated corrosion process were im-portant to accurately mimic real-world scenarios in prestressed concrete beams. This method provided insight into how concrete strength and prestressing levels affect steel wire corrosion.

6.4.3 Instrumentation

This study measured beam deformation during bending tests using digital image correlation (DIC), a non-contact optical metrology technique providing detailed de-formation and strain measurements. Beam surfaces were prepared with a high-contrast speckle pattern for effective DIC tracking, as shown in Figure 6. Cameras captured images before and after load application, and the DIC software analyzed the displacement and strain by tracking speckle movements, creating a detailed deformation map (Figure 6). This precise method offered a comprehensive understanding of the beam's behavior under stress, enhancing the study's insights into beam response under bending loads.

6.4.4 Digital Image Correlation (DIC)

The experimental phase included measuring beam deformation during bending tests using digital image correlation (DIC), a non-contact optical method that extensively measures and visualizes material deformation and strain. The beams were pre-pared with a white base layer and black speckles to enhance the DIC system's tracking accuracy. This preparation allowed the DIC software to precisely correlate changes before and after load application, providing crucial data on beam displacement and deformation (Figure 6).

The models were tested to the point of failure. The observed failure modes included significant flexural cracking followed by concrete crushing in the compression zone and bond failure between the prestressed steel and concrete due to corrosion.

Figure 6.6 - Area selected for displacement analysis.

After preparing the beams, two cameras captured images from different angles for digital image correlation (DIC) analysis. The DIC system compared pre- and post-load images to track speckle movements and calculate beam displacement and strain. This process produced a detailed strain distribution pattern for the loaded beam (Figure 6.6).

6.4.5 Bending Test Procedure

The bending tests involved 1500 mm long beams with a 1400 mm span between supports. Subjected to a three-point loading configuration to assess flexural strength and behavior, these tests formed a critical part of the experimental research (Figure 6.7).

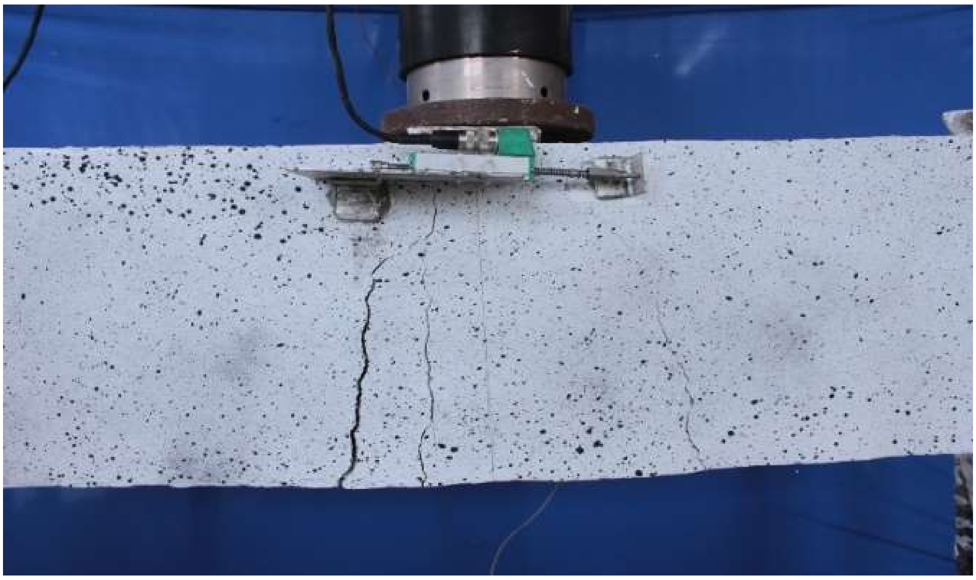

Figure 6.7 - Cracks in beam V32-0.5-NCB.

The bending tests were performed at the UENF Civil Engineering Laboratory using a robust testing setup. This setup included a metal frame and a high-capacity hydraulic actuator, specifically an MTS® 244.41 model. The hydraulic actuator, coupled with a 500 kN capacity load cell, applied the load to the beams. The load was applied monotonically at a controlled rate of 0.1 mm/min. This slow and steady rate of loading was important for accurately observing the progression of cracks and other failure modes in the beams.

The cross section of the beam models included four prestressed steel wires, positioned symmetrically around the neutral axis, with two wires in the upper layer and two in the lower layer, ensuring a uniform distribution of prestressing forces. The de-formation along the cross-section at mid-span in the 32 MPa beams is illustrated in Figure 6.8, while the bending crack pattern of the specimens is presented in Figure 6.9.

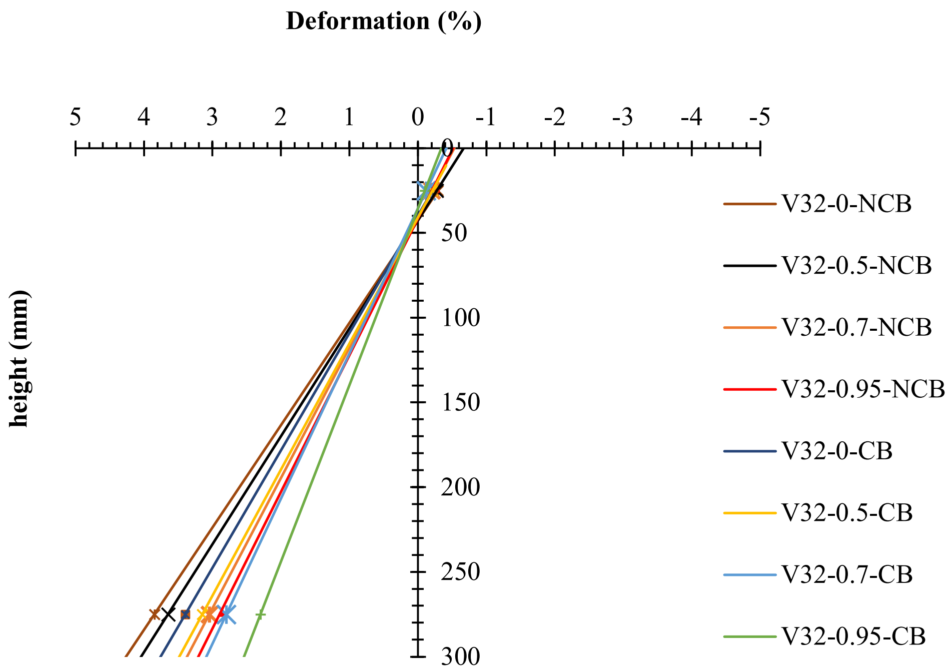

Figure 6.8 - Deformation along the cross-section at mid-span in the 32 MPa beams.

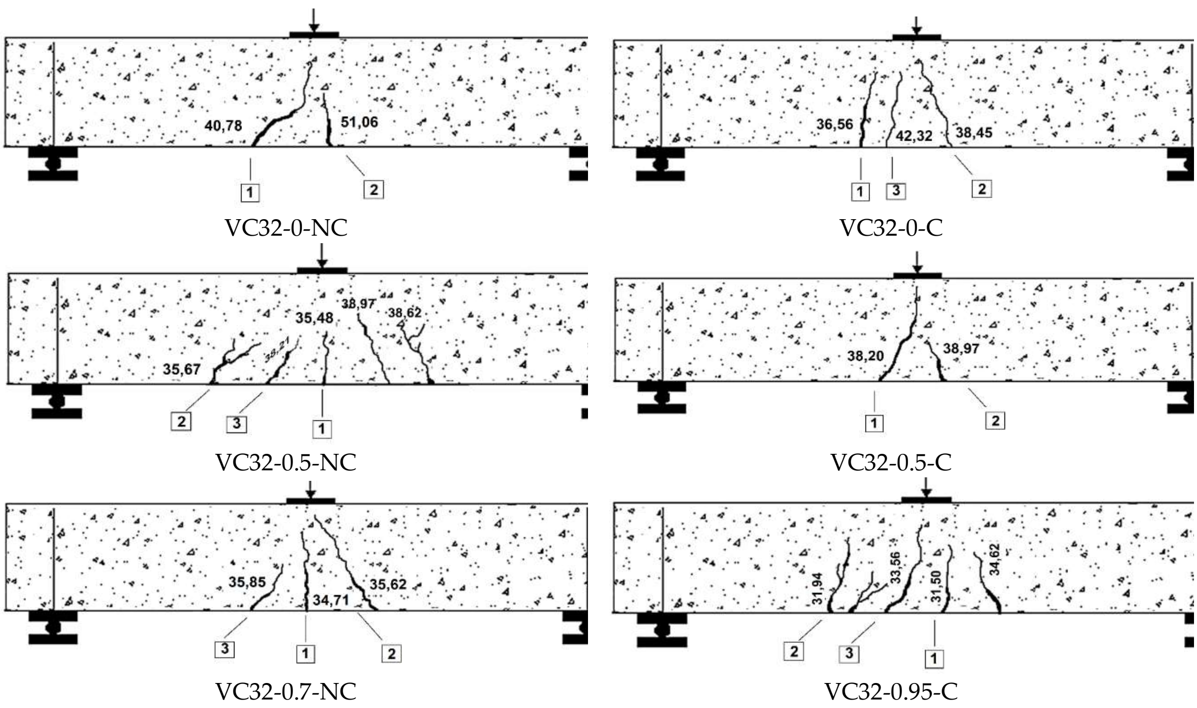

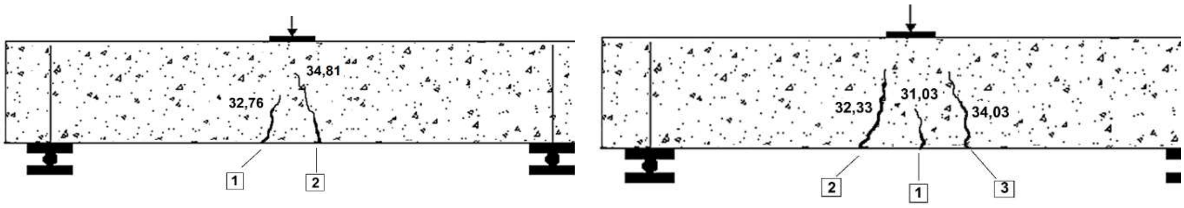

Figure 6.9 - Proposed methodology of the study.

In Figure 6.9, the numbers on the beam indicate the measured fracture widths in millimeters, highlighting areas of significant stress concentration where the most severe cracks developed.

All of the beams failed due to excessive deformation of the prestressed longitudinal reinforcement, demonstrating structural ductility.

As the load was applied, the beams were closely monitored for any signs of cracking, deformation, or ultimate failure. The DIC system played a pivotal role in this phase, providing real-time data on the deformation patterns of the beams. This data was essential for understanding how the corrosion of the prestressed wires affected the structural behavior of the beams, particularly in terms of crack formation, propagation, and the overall flexural performance. The corrosion rate versus rupture deformation is simulated in Figure 10.

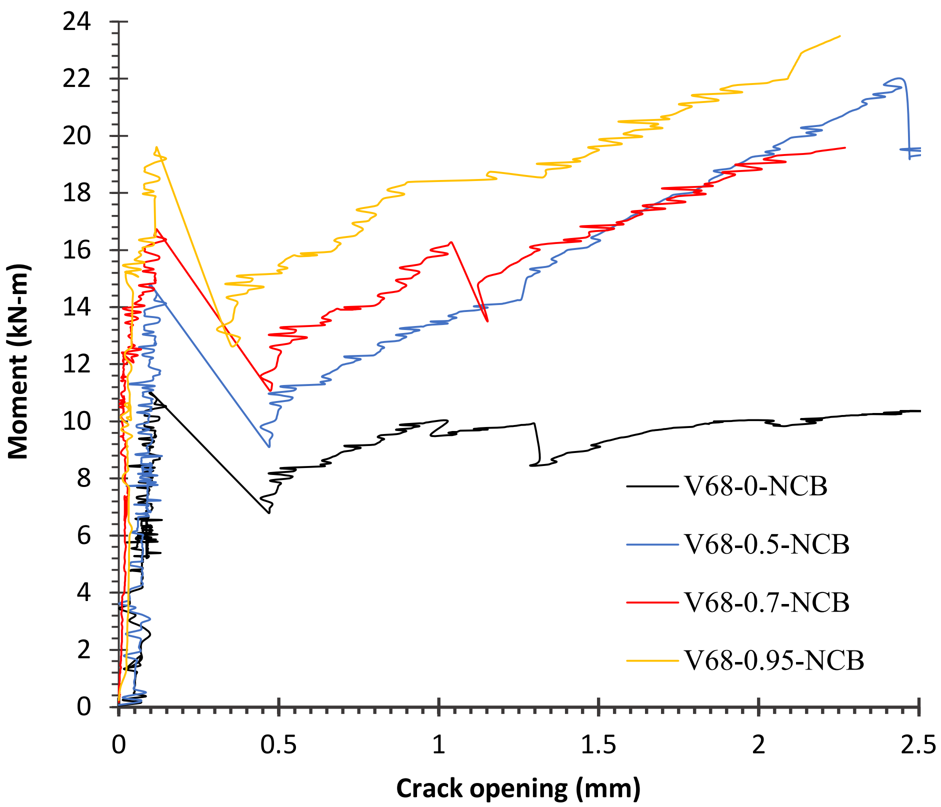

Figure 6.10 - Corrosion rate versus rupture deformation.

Figure 6.10 presents the corrosion rate versus rupture deformation. The data illustrate the relationship between measured corrosion rates and the deformation at rupture of the beams, indicating how increased corrosion accelerates the reduction in de-formation capacity.

The combination of the DIC instrumentation and the controlled bending test setup allowed for a comprehensive analysis of the impact of corrosion on the prestressed concrete beams. The data gathered provided insights into the changes in mechanical properties due to corrosion, contributing significantly to the study's findings on the durability and resilience of prestressed concrete structures in corrosive environments.

6.4.6 Metallographic Characterization of the Wires

The metallographic characterization of the prestressed steel wires was part of the experimental research, as it provided critical insights into the microscopic changes and damage mechanisms caused by corrosion [30]. This characterization involved a series of analyses using optical microscopy, confocal microscopy, and scanning electron microscopy (SEM). These techniques were instrumental in identifying and understanding the microstructural alterations in the wires due to corrosion processes. Figure 6.10 illustrate the significant differences in corrosion morphology and potential for both 32 MPa and 68 MPa beams.

Before the microscopic examination, the prestressed wires were carefully extract-ed from the concrete beams to preserve the integrity of the corrosion layer. This extraction was carried out meticulously to avoid any additional mechanical damage that could interfere with the accuracy of the metallographic observations.

6.4.7 Optical Microscopy Analysis

The initial examination was conducted using optical microscopy. This phase in-volved observing the cross-section of the corroded wires from the 32 MPa and 68 MPa beams. In the optical microscopy images (Figure 6.11), a distinction was evident between the dark and light regions, representing the embedding product of the sample and the intact wire, respectively. A key observation was the identification of areas with corrosive characteristics between the embedding product and the wire, indicating the extent and nature of the corrosion [32]. The full perimeter of the wire was analyzed to assess the uniformity of corrosion and identify any surface layer loss, characterized by protrusions and indentations. The corrosion potential is illustrated in Figure 6.12

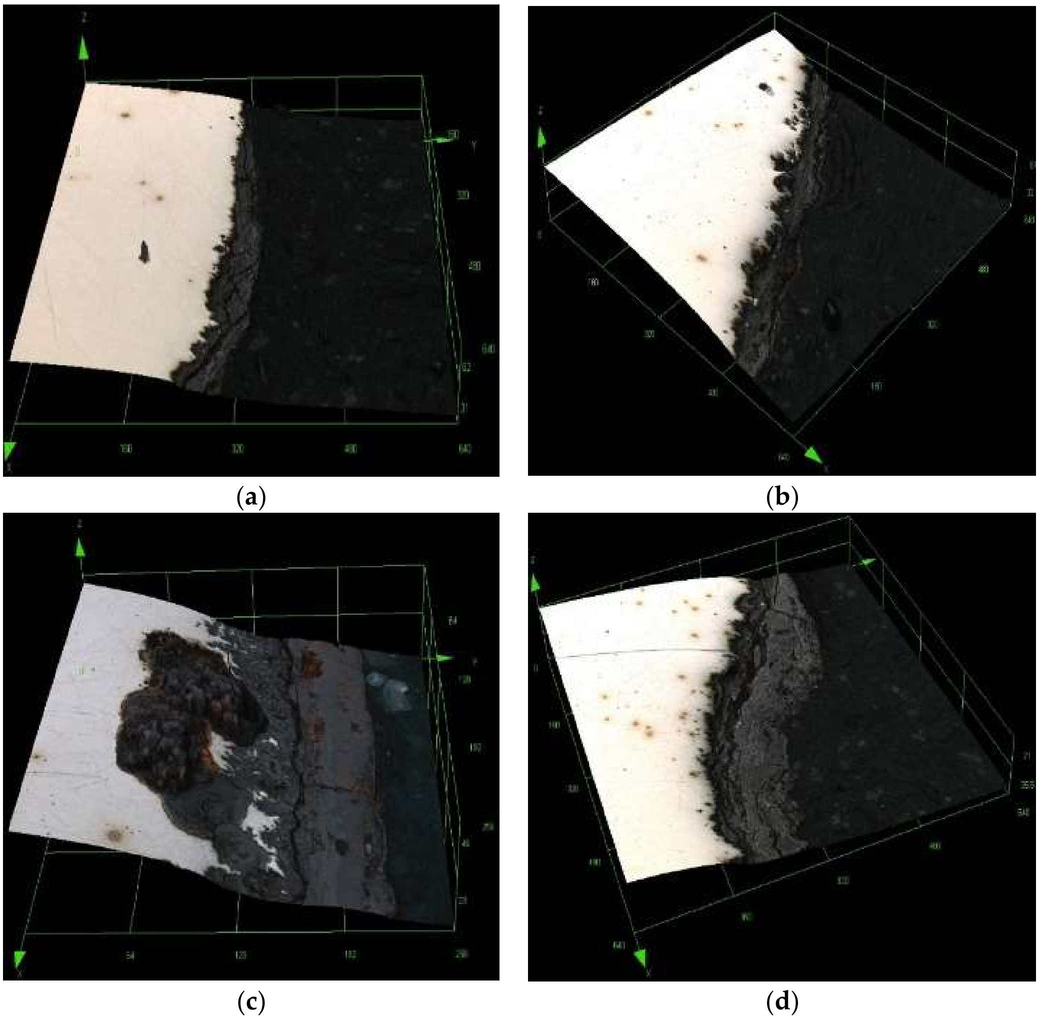

Figure 6.11 - Optical microscopy images of corrosion from the environment of 32 MPa beams at different stress levels: (a) V32-0-CB; (b) V32-0.5-CB; (c) V32-0.7-CB; (d) V32-0.95-CB.

Figure 6.11 shows the optical microscopy images for the 32 MPa beams, revealing distinct corrosion characteristics at different stress levels. The dark regions represent the corrosion products, while the light regions indicate the intact wire material. The extent of corrosion increases with higher stress levels, as indicated by the larger dark regions in the higher-stressed samples.

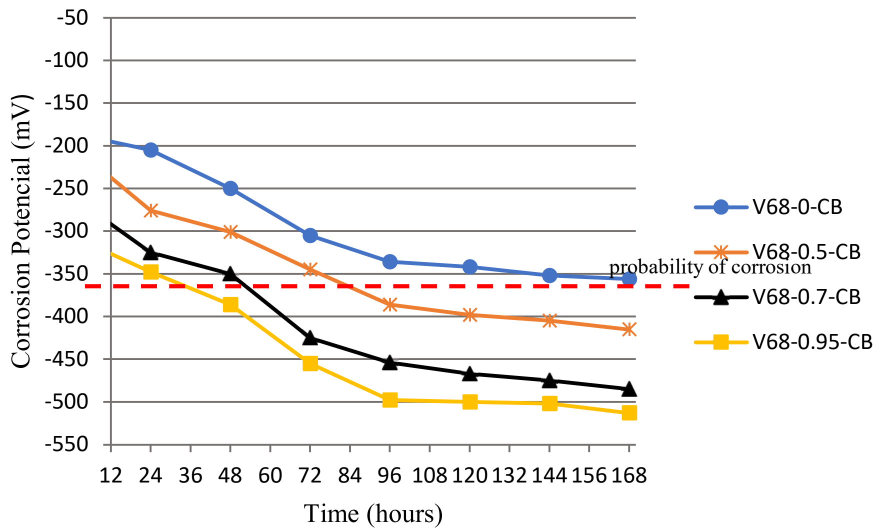

(a)

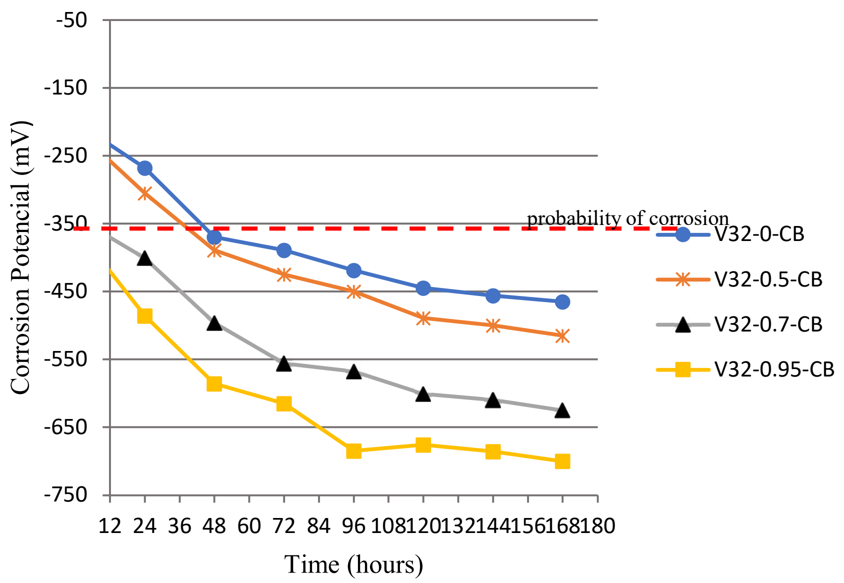

(b)

Figure 7.12 - Corrosion potential (Ecorr) measurements for 68 MPa beams at various stress levels.

In contrast, Figure 6.12 shows the corrosion potential (Ecorr) for both 32 MPa and 68 MPa beams at various stress levels. For the 32 MPa beams, the corrosion potential readings indicate a higher susceptibility to corrosion compared to the 68 MPa beams. The Ecorr values for 32 MPa beams at 95% fptk pre-tension are significantly lower, indicating a more advanced corrosion state.

After an optical analysis, confocal microscopy offered a clearer view of corrosion morphology, detailing oxide layer thickness variations across different wire stress levels, especially between 70 and 95% fptk in 32 MPa beams (Table 3).

Table 7.3 - Oxide layer measurement.

Samples	Oxide Layer on the Surface of the Corroded Wire (μm)
V32-0-CB	67.169
V32-0.5-CB	104.402
V32-0.7-CB	119.115
V32-0.95-CB	154.919

The final characterization phase used SEM analyses for a detailed, magnified view of wire surfaces, focusing on beams with pronounced corrosion (Figure 6.13). SEM revealed microstructural changes, corrosion patterns, and variations in porosity and corrosion product concentration, particularly in highly corroded beams like V32-0.5-CB, highlighting the advanced corrosion stage and stress-related surface cracks.

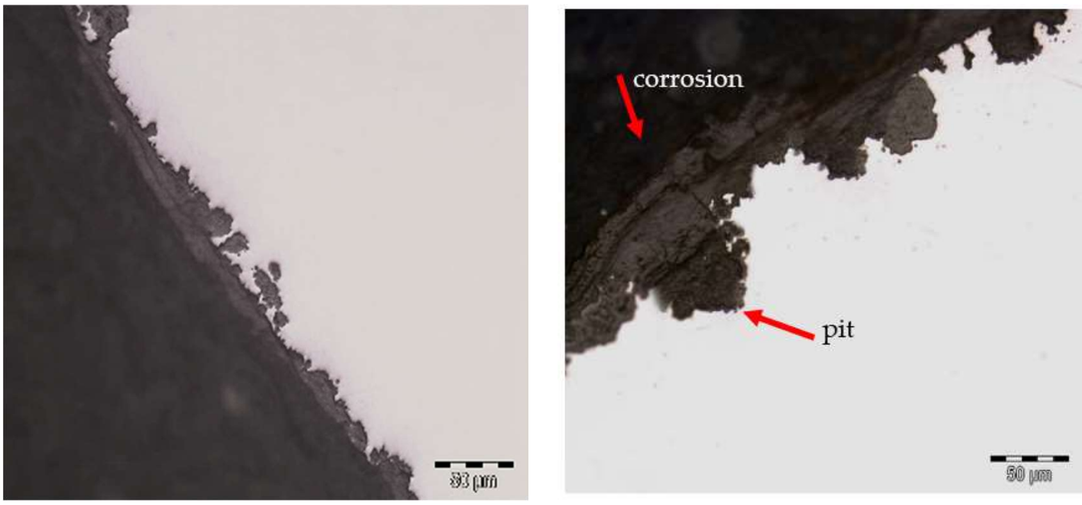

(a) (b)

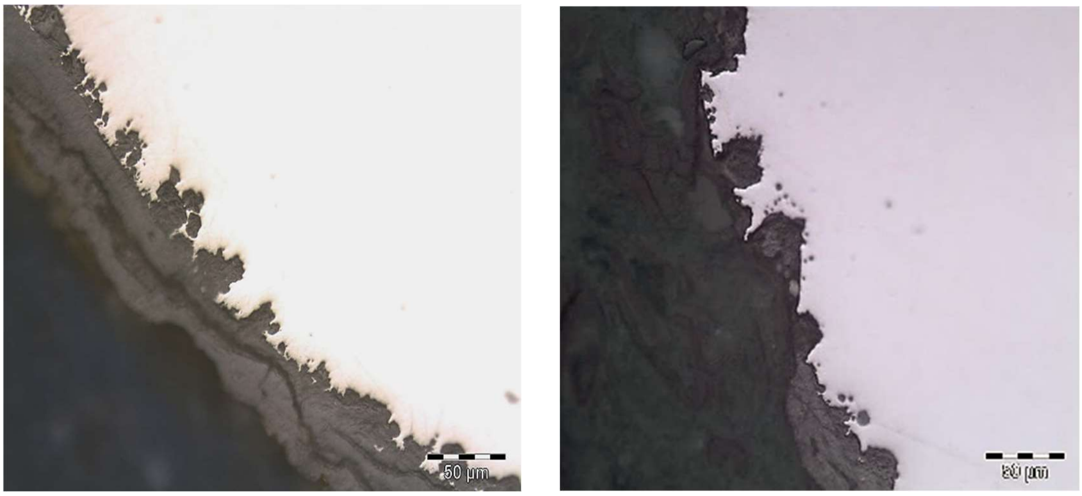

(c) (d)

Figure 6.13 - Appearance of the corroded wire cross-section: (a) V32-0-CB; (b) V32-0.5-CB; (c) V32-0.7-CB and (d) V32-0.95-CB, 400× magnification.

These metallographic analyses collectively provided a comprehensive under-standing of the corrosion mechanisms at play [33]. They revealed how different stress levels and environmental conditions influenced the corrosion behavior of the pre-stressed wires. This detailed examination was crucial for correlating the macroscopic behavior observed in the bending tests with the microscopic changes occurring in the material, thereby contributing significantly to the overall findings of the study (Figure 6.14).

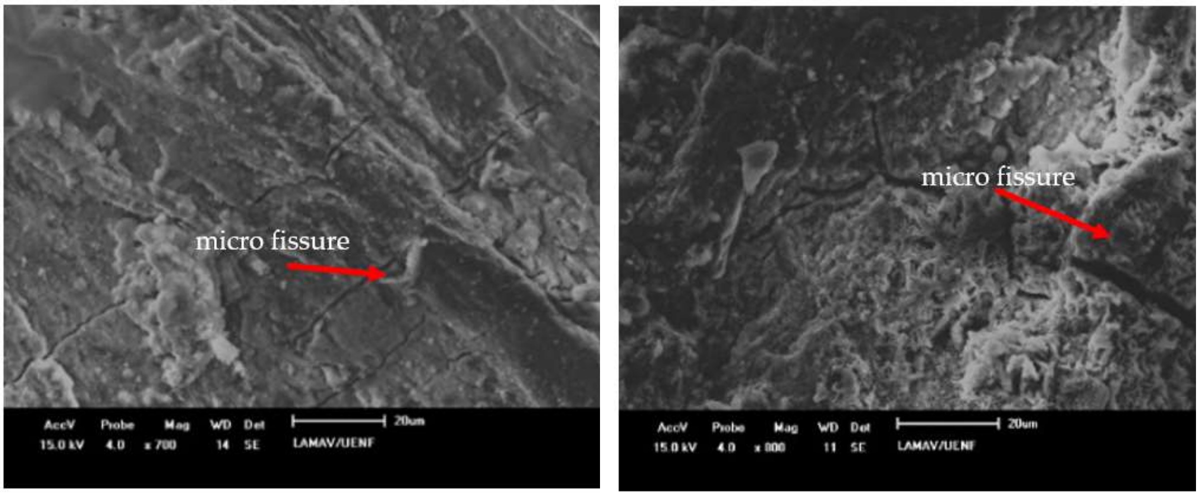

(a) (b)

Figure 6.14 - Details of the wires extracted from the fck 32 MPa beams, after cleaning.

6.4.8 Statistical and Machine Learning Analysis

This study employed advanced statistical and machine learning techniques to develop predictive models for the ultimate bending moment of prestressed concrete beams. The primary focus was on understanding the impact of concrete strength, reinforcement strength, and corrosion on the structural integrity of these beams.

A statistical analysis methodology was designed for thorough interpretation and validation of data from both experimental and computational phases of the research. Initially, the analysis involves an extensive data collection process, gathering data from various sources, including material property measurements, corrosion rate assessments, beam deformation metrics, and computational model outputs. After data collection, data preparation focused on accuracy and completeness. This involved identifying and correcting any errors or inconsistencies in the data, converting the data into a format suitable for analysis through normalization or categorization, and identifying and understanding data points that significantly differ from the rest of the data set.

Descriptive statistics provided a preliminary overview of the data, which was critical for establishing a baseline understanding [33]. This includes calculating the average, median, and mode to identify the central value in the data, as well as assessing the spread or dispersion of the data through standard deviation and variance. The distribution of the data was analyzed using histograms and box plots to under-stand its shape and spread.

The inferential statistics stage applied statistical methods to infer properties about a population based on sampled data. This includes conducting tests like t-tests, chi-square tests, or ANOVA, depending on the type of data type, to assess statistical significance. Regression analysis, both linear and nonlinear, was employed to under-stand relationships between variables such as concrete strength, corrosion rate, and the material's properties. The correlation analysis measured the strength and direction of relationships between important variables.

For the complex data (increasing corrosion rate), advanced statistical techniques were used, including multivariate analysis methods like principal component analysis or factor analysis, to understand the structure of complex data sets, while time-series analysis methods like ARIMA models were used to understand temporal trends and patterns. Python's statistical libraries were used for these analyses, offering functionalities for complex calculations, graphical data representation, and model building.

In the final phase, the outcomes of the statistical analyses were interpreted in relation to the research objectives. This includes contextualizing the results within the broader context of the study's goals, identifying key patterns, trends, and anomalies, and discussing the implications of the statistical results for understanding corrosion in prestressed concrete structures.

Throughout the process, measures were taken to ensure the rigor and reliability of the statistical analysis. This includes verifying the validity of the assumptions under-lying each statistical method, identifying and reporting potential errors or uncertain-ties in the analysis, and maintaining a transparent approach to ensure the replicability of the analysis by other researchers. This detailed and methodical approach aims to provide a deep and accurate interpretation of the data, supporting the research findings with robust statistical evidence.

6.4.9 Statistical Exploratory Data Analysis of Concrete Beam Data

To complement the experimental investigation of corrosion in prestressed concrete beams, we employed statistical and machine learning techniques to analyze the relationship between key variables and predict the structural integrity of the beams. These techniques provide a robust framework for understanding complex interactions and enhancing predictive accuracy.

Exploratory data analysis (EDA) is an indispensable phase in the data analysis process, laying the groundwork for subsequent statistical analysis. It involves a range of techniques aimed at understanding the distributions of variables, detecting outliers, uncovering patterns, and identifying relationships between variables within a dataset.

Through graphical representations such as histograms, box plots, scatter plots, and more sophisticated visualizations (as used in this methodology), EDA provides a visual insight into the data, offering an intuitive understanding of its main characteristics. Summary statistics further complement this by quantifying central tendencies, dispersion, and other key attributes.

EDA is a continuous process, guiding and informing the modeling choices, hypothesis formulation, and data preprocessing decisions. Its iterative nature helps in refining research questions, validating assumptions, and ensuring that the conclusions drawn are based on a comprehensive and nuanced understanding of the data's under-lying structure.

Exploratory data analysis (EDA) is an indispensable phase in the data analysis process, setting the stage for subsequent statistical analysis. It employs a range of techniques aimed at understanding variable distributions, detecting outliers, uncovering patterns, and identifying relationships within a dataset. Through graphical representations such as histograms, box plots, scatter plots, and sophisticated visualizations, as implemented in the current analysis, EDA offers visual insight into the data, providing an intuitive grasp of its main characteristics. Summary statistics complement these visual insights by quantifying central tendencies, dispersion, and other key attributes.

EDA is not just a preliminary step but a continuous process that guides and in-forms modeling choices, hypothesis formulation, and data preprocessing decisions. Its iterative nature aids in refining research questions, validating assumptions, and ensuring that conclusions are drawn from a comprehensive and nuanced understanding of the data's underlying structure.

Transitioning from theory to practice, the code for our EDA follows a structured approach. It begins by setting up a DataFrame with sample data on concrete beams, detailing attributes like concrete strength, reinforcement strength, corrosion rate, and bending moment. This DataFrame, named merged_df, serves as the basis for all subsequent analyses. Initially, the code calculates basic statistics such as the mean and standard deviation for all numerical columns in the DataFrame, providing an initial quantitative understanding of each variable.

The code then presents the frequency of different values through histograms for each numerical variable, helping visualize data distribution. It assesses the relation-ships between variables using a correlation matrix visualized as a heatmap, making it easier to see any strong relationships or patterns. To identify outliers or unusual values, the code generates boxplots for each numerical variable. These boxplots effectively dis-play the median, quartiles, and potential outliers, offering a visual means to identify data points that stand out.

Further, the code extracts additional information from the 'Beam_ID' column, specifically the prestress level and corrosion status, adding these as new columns to the DataFrame. For a deeper analysis, it runs two statistical tests: an independent t-test and a Mann-Whitney U test. These tests determine if the differences in bending moments between corroded and non-corroded beams are statistically significant. The code calculates the average bending moments for both groups and presents them along with the test results, indicating the significance of the differences.

Finally, the algorithm visualizes the data by creating boxplots to compare bending moments between corroded and non-corroded beams, as well as a scatter plot to ex-amine the relationship between prestress level and the ultimate bending moment while considering the corrosion status. This approach combines statistical calculations and visualizations to thoroughly explore and understand the dataset, paving the way for informed modeling and analysis.

The pseudocode that presents the EDA developed using this methodology can be seen in Figure 6.15.

Algorithm 1 Statistical Analysis of Concrete Beam Data

```
Import pandas numpy seaborn matplotlib.pyplot
# Create a DataFrame with sample data
Initialize data with Beam ID, Concrete strength, etc.
Create DataFrame merged_df from data
# Descriptive Statistics
Print descriptive statistics of merged_df
# Distribution Analysis
Define numerical columns
Plot histograms for each numerical column in merged_df
# Correlation Analysis
Select numerical columns from merged_df
Calculate correlation matrix
Print correlation matrix
Plot heatmap of correlation matrix
# Outlier Detection
Plot boxplots for each numerical column
# Extract prestress level and corrosion status
Extract Prestress_Level from Beam_ID
Extract Corrosion_Status from Beam_ID
Print updated DataFrame
# Statistical Tests
Import ttest_ind, mannwhitneyu from scipy.stats
Separate ultimate moments based on corrosion status
Print mean values for non-corroded and corroded moments
Perform t-test and Mann-Whitney U test
Print p-values of the tests
# Data Visualization
Plot boxplots for bending moments based on corrosion status
Plot scatter plot for relationship between prestress level and ultimate bend-
    ing moment
```

Figure 6.15 - Pseudo algorithm exploratory data analysis.

The process to develop a predictive model of concrete beam strength begins with creating a DataFrame using CSV files containing detailed attributes of concrete beams. These attributes include concrete strength, reinforcement strength, corrosion rate, and the ultimate bending moment, which is the primary variable of interest, indicating the structural integrity and safety of the beams. The initial step involves merging data from different sources based on a common ‘Beam_ID’, ensuring a comprehensive dataset for analysis (Figure 6.16).

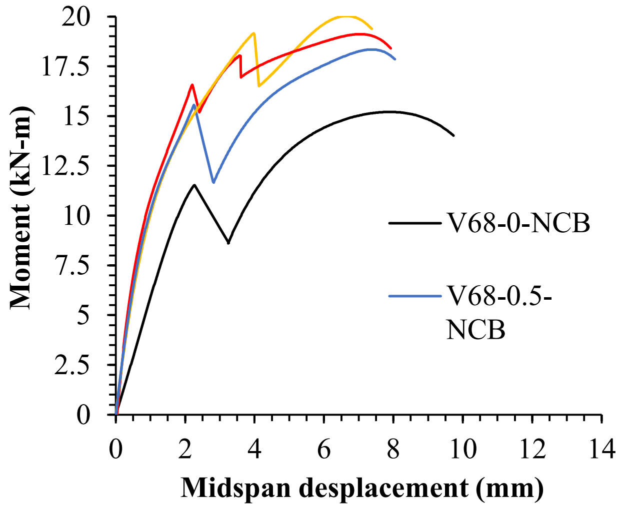

Figure 6.16 - Vertical displacement at the center of the span of the non-corroded 68 MPa beams.

To capture the complex relationships and physical characteristics influencing beam strength, new features 'A', 'B', 'C', and 'D' are engineered and are written as,

$$Q = T_{corr} + 1$$

$$A = {f_c}^{2/3}$$

$$B = {f_{py}}/{Q}$$

$$C = {f_{ptk}}/{Q}$$

$$D = -\,T_{corr}$$

where

T_{corr} represents the adjusted corrosion rate, being the average corrosion rate measured in mm/year from the dataset;

f_c is the concrete strength at 28 days;

f_{py} is the yield steel resistance from the prestressed reinforcement;

f_{ptk} is the prestressed applied in the reinforcement;

These features are derived using domain-specific transformations that reflect how various factors, like concrete strength, reinforcement tension, and corrosion rates, interact to affect the beam's bending moment. Standardizing these features is crucial for effective modeling, especially given the wide range of data. Therefore, the Standard-Scaler is employed to normalize the features, removing the mean and scaling them to unit variance.

The core of the predictive analysis is built on two regression techniques: linear regression and lasso regression. Linear regression is implemented to model the linear relationship between the engineered features and the ultimate bending moment. To assess the model's robustness and its ability to generalize to unseen data, 10-fold cross-validation is performed using cross_val_score, providing a reliable estimate of the model's predictive performance.

Evaluating the model's accuracy and fit is essential. The mean squared error (MSE) and R^2 were calculated for the linear regression model. The MSE provides a measure of the average squared difference between the observed actual outcomes and the model's predictions, with a lower value indicating a better fit. On the other hand, R^2 indicates the proportion of variance in the ultimate bending moment that is predictable from the features, with a higher value suggesting a better explanatory model.

To enhance the model and potentially reduce overfitting, a lasso regression was also used. Lasso introduces regularization to the model, adding a penalty equivalent to the absolute value of the magnitude of the coefficients. This not only helps prevent overfitting but also performs feature selection by shrinking some coefficients to zero. A range of alpha values (regularization strengths) was considered, and GridSearchCV was employed to find the optimal alpha that balances model complexity and accuracy. The best Lasso model is then evaluated, calculating its MSE and R^2 to understand its performance.

The equations representing the predicted ultimate bending moment for both the linear and lasso regression models were developed. These equations highlight the in-fluence of each feature on the predicted outcome, offering insights into the underlying physical phenomena. The performance metrics and regression equations are presented, providing a comprehensive overview of the models' predictive capabilities and the relative importance of each feature in determining the ultimate bending moment of concrete beams.

$$\begin{aligned}
&Average\ MSE\text{: } 2.426\\
&Standard\ deviation\ of\ MSE\text{: } 2.580\\
&Best\ alpha\text{: } 0.013\\
&Best\ MSE\text{: } 1.505\\
&Lasso\ regression\ MSE\text{: } 0.517\\
&Lasso\ regression\ R2\text{: } 0.905
\end{aligned}$$

$$Predicted\ ultimate\ bending\ moment\text{: } = 16.13 + (0.63 \times A) + (1.31 \times$$

Through this methodical approach, this study predicted the structural behavior of concrete beams under corrosion condition as can be seen below.

$$P_u = 16.13 + \frac{1.31 \times \sqrt{f_{py}} + 1.12 \times f_{ptk}}{(T_{corr} + 1)} 0.63 \times {f_c}^{2/3} - 0.21 \times T_{corr}$$

The pseudocode for the ultimate bending moment prediction is presented in Figure 6.17.

Algorithm 2 Pseudocode for Ultimate Bending Moment Prediction with Linear and Lasso Regression

```
IMPORT libraries
LOAD the CSV files into properties_df and ultimate_df
MERGE the dataframes on 'Beam_ID' into merged_df
DEFINE new feature Q in merged_df
CALCULATE new features A, B, C, and D in merged_df
PREPARE the dataset for the model with features ['A', 'B', 'C', 'D'] and
target 'actual_ultimate_bending_moment(kN.m)'
SCALE the features using StandardScaler
procedure TrainLinearRegression(X, y)
    Initialize LinearRegression model
    Calculate cross-validation scores
    Fit the model on X and y
    Predict and calculate MSE and R2
    Verify Linear Regression MSE, R2, and the equation
    Verify Average MSE and Standard Deviation of MSE from cross-
validation
end procedure
procedure TrainLassoRegression(X, y)
    Initialize Lasso model with a range of alphas
    Perform GridSearchCV to find the best alpha
    Fit the model with the best alpha on X and y
    Predict and calculate MSE and R2
    Verify Lasso Regression MSE, R2, and the equation
end procedure
MAIN
X ← scaled features, y ← target values
TrainLinearRegression(X, y)
TrainLassoRegression(X, y)
END
```

Figure 6.17 - Pseudo algorithm to obtain the ultimate bending moment based on the methodology developed in this study.

Experimental results served as the training data for the machine learning models. For example, the corrosion rates measured during the experiments were used to train the models to predict the ultimate bending moment. This integration ensures that the models are grounded in empirical evidence.

6.5 RESULTS

This study investigated the effects of corrosion on prestressed concrete beams with 5 mm diameter wires, revealing key insights. Detailed in Tables 4 and 5, the results indicate the complex interplay between corrosion, concrete strength, and prestressing levels, significantly impacting structural integrity.

Our findings, as shown in Table 4, demonstrate considerable corrosion rates across all sample groups, with a greater impact in beams under higher pre-tension. An ANOVA with a 5% significance level confirmed the substantial influence of stress on wire weight loss, suggesting that corrosion accelerated under conditions of increased stress. This phenomenon is partly due to decreased capillary porosity in stronger beams, which impedes oxygen flow and exacerbates the corrosion process.

Deflection versus load-like curves (Figures 6.8, 6.10, and 6.15) offered critical insights into the beams' structural behavior under load. Intriguingly, both corroded and non-corroded prestressed beams displayed similar displacement patterns pre-flexural cracking, implying that initial stiffness is largely unaffected by corrosion. However, a marked decline in post-cracking stiffness and load-bearing capacity was observed with increased corrosion, as higher corrosion rates significantly reduced post-cracking stiff-ness, highlighting the detrimental impact of corrosion on structural performance.

The bond strength between steel wires and concrete, crucial for structural integrity, deteriorated with corrosion. This was evidenced by the kinematics of critical flexural crack openings (Figures 6.7 and 6.9), where corroded beams reached ultimate tensile stress quicker than non-corroded ones, resulting in premature cracking. The compromised bond strength and loss of prestressing due to corrosion culminated in more ex-tensive crack openings and reduced overall structural integrity, with cracking patterns (Figure 6.10) showing more extensive propagation in corroded beams.

Table 6.4 - Corrosion rate results.

Samples	Attack Time (hours)	Mass Loss (%)	Corrosion Rate (mm/year)
V32-0-CB	168	4.63	0.37
V32-0.5-CB		5.75	0.46
V32-0.7-CB		6.98	0.55
V32-0.95-CB		8.01	0.64
V68-0-CB		2.56	0.20
V68-0.5-CB		3.15	0.25
V68-0.7-CB		4.32	0.35
V68-0.95-CB		5.32	0.42

Table 6.5 presents a discernible decrease in the load-bearing capacity of corroded beams. Corroded V32 beams exhibited a 23% to 34% reduction in ultimate load com-pared to non-corroded ones, while V68 beams showed a 9.5% to 16% decline. This significant reduction

is an important factor in the design and assessment of prestressed concrete structures, underscoring the urgency for effective corrosion mitigation strategies.

Table 6.5 - Experimental Pfiss and Pult values of the tested beams.

Beam	Corroded		Non-Corroded	
	P_{fiss} (kN)	P_{ult} (kN)	P_{fiss} (kN)	P_{ult} (kN)
V32-0	32.76	42.99	31.03	34.86
V32-0.5	36.56	50.16	34.71	38.21
V32-0.7	38.20	51.59	35.48	39.08
V32-0.95	40.78	54.21	31.50	35.76
V68-0	33.87	-	32.53	-
V68-0.5	41.00	52.29	40.50	43.83
V68-0.7	45.26	52.96	44.06	47.91
V68-0.95	54.86	-	51.36	-

The observed deformation patterns (Figure 6.15) and specific strain values at breaking load (Table 6.5) corroborate the loss of tensile strength in wires due to corrosion. This reduction in deformation capacity has profound implications for the durability and service life of prestressed concrete structures, emphasizing the need for designs that account for long-term corrosion impacts. Table 6.6 presents the specific strain of the reinforcement for each beam's ultimate load capacity.

Table 6.6 - Specific strain of the reinforcement for ultimate load.

Beam	Deformation (ε) (‰)
V32-0-NCB	3.75
V32-0.5-NCB	3.5
V32-0.7-NCB	3.2
V32-0.95-NCB	2.9
V32-0-CB	3.4
V32-0.5-CB	3.15
V32-0.7-CB	2.8
V32-0.95-CB	2.3

Our findings underscore the critical importance of corrosion resistance in sustainable civil engineering practices. By enhancing our understanding of corrosion dynamics in prestressed structures, engineers can develop more resilient and durable de-signs, reducing the need for frequent repairs and replacements and, consequently, minimizing the environmental footprint of construction activities.

Incorporating statistical and machine learning analyses, we've identified a consistent decrease in load-bearing capacity and tensile strength in corroded beams. This predictive insight, derived from a rigorous data-driven approach, not only validates our experimental observations but also provides a quantitative framework for assessing and mitigating corrosion impact in prestressed concrete structures.

Correlation analyses revealed strong links between corrosion rates and ultimate bending moments. Higher corrosion rates were associated with lower bending moments, indicating a detrimental effect of corrosion on structural integrity.

The linear regression model achieved an R^2 of 0.86, indicating a strong linear relationship between the input features and the predicted bending moment. The lasso regression model further improved accuracy, with an R^2 of 0.905 and reduced MSE.

These results not only highlight the need for effective corrosion mitigation strategies but also pave the way for future research and development in corrosion-resistant materials and design practices. Our study contributes to a more sustainable and resilient built environment, aligning with global efforts to enhance infrastructure service life and performance.

6.6 DISCUSSION

This study developed a novel predictive model to quantify the impact of corrosion on prestressed concrete beams, focusing on the relationship between stress levels, corrosion rates, and concrete strength. Through rigorous empirical analysis and advanced machine learning algorithms, the model provides a robust numerical equation to assess structural integrity and service life of prestressed concrete beams, marking a significant advancement in civil engineering.

The simulation conducted in the laboratory focused primarily on chloride-induced corrosion. Factors such as Mg, K, Ca, SO4 ions, dissolved oxygen, marine organisms, temperature, hydrostatic pressure, and tidal action were not included. These addition-al variables significantly impact corrosion and should be considered in future studies for a more comprehensive simulation. The model accurately integrates variables such as concrete strength (fc), yield strength of prestressed reinforcement (fpy), prestress applied (fpt), and average corrosion rate ($Tcorr$) to predict the ultimate bending moment (Pu).

The empirical analysis revealed that higher stress levels and concrete strengths significantly influence corrosion rates and structural integrity. Beams with 95% pre-stress level exhibited a corrosion rate of 0.64 mm/year, compared to 0.37 mm/year for non-prestressed beams, indicating that higher prestress levels exacerbate the corrosion process. These findings are consistent with previous studies that highlight the vulnerability of prestressed concrete in chloride environments.

Digital image correlation (DIC) provided insights into deformation and crack patterns, showing significant reductions in post-cracking stiffness and load-bearing capacity in corroded beams. For instance, the ultimate load capacity of 32 MPa beams decreased by 23% to 34% due to corrosion, while 68 MPa beams showed a reduction of 9.5% to 16%. These results underscore the critical importance of monitoring and maintaining prestressed concrete structures in corrosive environments.

The machine learning-based predictive model achieved a mean squared error of 0.517 and an $R2$ value of 0.905, indicating high accuracy in predicting the ultimate bending moment of corroded beams. This capability can significantly enhance corrosion risk assessment and management in coastal infrastructure. The model’s practical application lies in its ability to inform maintenance schedules and assess the remaining service life of existing structures.

The statistical and machine learning analysis confirms the significant impact of corrosion on the structural integrity of prestressed concrete beams. The predictive models developed provide a valuable tool for assessing the potential degradation of such structures over time, enabling more proactive maintenance strategies.

Our findings highlight the need for regular maintenance and inspection of pre-stressed concrete structures in corrosive environments. The predictive models developed can serve as a basis for creating maintenance schedules and assessing the remaining service life of existing structures.

Future research should refine the model by incorporating additional environmental factors like temperature and humidity. Exploring advanced materials and coatings to mitigate corrosion in prestressed concrete structures would also be beneficial. Inte-grating real-time monitoring systems with predictive analytics could further enhance the durability and safety of coastal infrastructure.

By enhancing our understanding of corrosion dynamics and developing predictive tools, this research contributes to more resilient and durable construction practices, ultimately supporting the goal of sustainable infrastructure development.

6.7 CONCLUSIONS

This study introduced a novel predictive model to quantify the impact of corrosion on prestressed concrete beams, emphasizing the intricate relationship between stress levels, corrosion rates, and concrete strength. Developed through rigorous empirical analysis combined with advanced machine learning algorithms, the model pro-vides a robust numerical equation to assess structural integrity and service life, representing a significant analytical advancement in civil engineering. By enhancing our understanding of corrosion dynamics and developing predictive tools, this research contributes to more resilient and durable construction practices, ultimately supporting the goal of sustainable infrastructure development. The model's technical accuracy and precision are its core strengths, effectively integrating complex variable relation-ships into a practical tool for industry professionals. This development marks a step forward in predictive analytics for assessing the degradation of prestressed concrete structures. The formula used to predict the ultimate bending moment (Pu) is given by

$$Pu = 16.13 + Tcorr + 11.31 \times fpy + 1.12 \times fptk + 0.63 \times fc2/3 - 0.21 \times Tcorr$$

The empirical analysis revealed that higher stress levels and concrete strengths significantly influence corrosion rates and the structural integrity of the beams. The ultimate load capacity of beams with higher prestress levels exhibited significant reductions due to corrosion, highlighting the importance of regular maintenance and proactive measures. For instance, Figure 6.11 shows the optical microscopy images for the 32 MPa beams, revealing distinct corrosion characteristics at different stress levels. In Figure 6.12, the corrosion potential (Ecorr) readings for both 32 MPa and 68 MPa beams indicate varying susceptibility to corrosion, with 32 MPa beams showing higher corrosion rates at 95% fptk pre-tension.

These findings underscore the need for effective corrosion mitigation strategies and provide a quantitative framework for assessing and managing the risk of corrosion in prestressed concrete structures. Future research should focus on refining the model and exploring innovative materials and monitoring techniques to enhance the durability and sustainability of coastal infrastructure. The findings also demonstrated pronounced corrosion rates across all sample groups, with an accentuated effect in beams under higher pre-tension, as detailed in Tables 6.4 and 6.5. The de-tailed analysis of deflection versus load-like curves (Figures 6.8, 6.10, and 6.15) offered critical insights into the beams' structural behavior under load, highlighting the accelerated corrosion in higher stressed beams and the corresponding reduction in structural integrity.

The machine learning analysis demonstrates the effectiveness of integrating statistical and machine learning techniques with experimental data to predict the impact of corrosion on structural integrity. Future research should explore additional environmental factors and advanced modeling techniques to further enhance predictive accuracy.

The bond strength between steel wires and concrete, crucial for structural integrity, deteriorated with corrosion. The kinematics of critical flexural crack opening (Figures 6.7 and 6.9) showed that corroded beams reached ultimate tensile stress quicker than non-corroded ones, resulting in premature cracking. The compromised bond strength and loss of prestressing due to corrosion culminated in more extensive crack openings and reduced overall structural integrity.

Future research should focus on refining these predictive models and investigating novel approaches to addressing the pervasive challenge of corrosion in corrosive environments. By continuing to improve the model's precision and applicability, the field can progress toward more durable and sustainable construction practices, ultimately enhancing the service life and safety of coastal infrastructure.

6.8 DISCUSSION OF CHAPTER 6

6.8.1 Key Findings

The predictive models developed and applied in this chapter successfully simulated the behavior of prestressed concrete when exposed to chloride environments, offering accurate forecasts of corrosion rates and their impact on structural performance. The models identified key factors influencing corrosion dynamics, such as chloride concentration, concrete permeability, and environmental conditions, enabling more precise predictions of when and where corrosion-related damage is likely to occur. The accuracy of these predictions was validated against empirical data, confirming the models' reliability as tools for assessing the long-term durability of prestressed concrete structures.

6.8.2 Implications

The implications of this research are significant for the design and maintenance of infrastructure in chloride-rich environments. By integrating these predictive models into the design process, engineers can better anticipate the effects of chloride-induced corrosion and implement design strategies that mitigate these risks. For instance, the models can inform decisions on material selection, concrete mix design, and the application of protective measures such as sealants or corrosion inhibitors. Furthermore, the ability to predict the timing and extent of corrosion damage allows for more effective maintenance planning, potentially extending the service life of structures and reducing overall lifecycle costs.

6.8.3 Limitations

While the predictive models offer robust insights, their accuracy is dependent on the quality and comprehensiveness of the input data, such as chloride concentration levels and environmental conditions. In real-world applications, variations in these parameters could affect the models' predictions. Additionally, the models are based on assumptions that may not fully capture the complexities of actual corrosion processes in situ, particularly in heterogeneous or dynamically changing environments. Future research should aim to refine these models to account for such complexities, enhancing their applicability across a wider range of scenarios.

6.8.4 Future Work

Future research could focus on enhancing the predictive models by incorporating additional environmental factors, such as temperature fluctuations, humidity, and the presence of other corrosive agents. Additionally, expanding the models to include dynamic simulations that account for changes in environmental conditions over time could improve their accuracy and reliability. Long-term field studies that monitor corrosion progression in real structures would also provide valuable data for validating and refining these models. Finally, exploring the integration of these predictive tools into comprehensive asset management systems could optimize maintenance schedules and resource allocation, further extending the service life of prestressed concrete structures.

6.9 CONCLUSION FOR CHAPTER 6

This chapter presented a detailed predictive analysis of corrosion dynamics in prestressed concrete exposed to chloride-rich environments. Using predictive models, the study provided a more nuanced understanding of how chloride ions penetrate concrete, accelerate corrosion, and ultimately affect the structural integrity of prestressed concrete. The findings demonstrate the effectiveness of these predictive models in forecasting corrosion rates and the progression of damage, offering engineers valuable tools for proactive maintenance and design. This research underscores the critical importance of considering chloride-induced corrosion in the lifecycle management of prestressed concrete structures, particularly in coastal or industrial environments where chloride exposure is prevalent.

The predictive models developed in this chapter offer valuable tools for anticipating and mitigating corrosion-related damage. As we continue to explore innovations in concrete design, attention now turns to enhancing structural performance through improved reinforcement strategies.

6.10 FUNDING

This research was funded by Coordenação de Aperfeiçoamento de Pessoal de Nível Superior grant number 88881.846502/2023-01.

The authors would like to acknowledge the support of Conselho Nacional de Desenvolvimento Científico e Tecnológico (CNPq 304726/2021-4) and Fundação Carlos Chagas Filho de Amparo à Pesquisa do Estado do Rio de Janeiro (FAPERJ E-26400.205.206/2022(284891)) and (FAPERJ E-26/210.950/2024 (295973)), and CAPES Finance Code 01, which helped in the development of this research.

6.11 REFERENCES FOR CHAPTER 7

1. Meng, Z.; Liu, Q.F.; Xia, J.; Cai, Y.; Zhu, X.; Zhou, Y.; Pel, L. Mechanical–Transport–Chemical Modeling of Electrochemical Repair Methods for Corrosion-Induced Cracking in Marine Concrete. Comput. Aided Civ. Infrastruct. Eng. 2022, 37, 1854–1874. https://doi.org/10.1111/MICE.12827.

2. Liu, Q.F.; Iqbal, M.F.; Yang, J.; Lu, X.Y.; Zhang, P.; Rauf, M. Prediction of Chloride Diffusivity in Concrete Using Artificial Neural Network: Modelling and Performance Evaluation. Constr. Build. Mater. 2021, 268, 121082. https://doi.org/10.1016/J.CONBUILDMAT.2020.121082.

3. Aljibori, H.S.; Alamiery, A.; Kadhum, A.A.H. Advances in Corrosion Protection Coatings: A Comprehensive Review. Int. J. Corros. Scale Inhib. 2023, 12, 1476–1520. https://doi.org/10.17675/2305-6894-2023-12-4-6.

4. Cabrera, J. Deterioration of Concrete Due to Reinforcement Steel Corrosion. Cem. Concr. Compos. 1996, 18, 47–59. https://doi.org/10.1016/0958-9465(95)00043-7.

5. Bertolini, L . Steel Corrosion and Service Life of Reinforced Concrete Structures. Struct. Infrastruct. Eng. 2008, 4, 123–137. https://doi.org/10.1080/15732470601155490.

6. Jiang, T.; Kong, Q.; Peng, Z.; Wang, L.; Dai, L.; Feng, Q.; Huo, L.; Song, G. Monitoring of Corrosion-Induced Degradation in Prestressed Concrete Structure Using Embedded Piezoceramic-Based Transducers. IEEE Sens. J 2017, 17, 5823–5830. https://doi.org/10.1109/JSEN.2017.2728807.

7. McDonald, D.B. Corrosion Protection for Concrete Structures in Marine Environments. Coastal Engineering Practice. In Proceedings of the 2011 Conference on Coastal Engineering Practice, San Diego, CA, USA, 21–24 August 2011; pp. 78–88. https://doi.org/10.1061/41190(422)8.

8. Bender, R.; Féron, D.; Mills, D.; Ritter, S. Corrosion Challenges towards a Sustainable Society. Mater. Corros. 2022, 73, 1730–1751. https://doi.org/10.1002/maco.202213140.

9. Verma, C.; Ebenso, E.; Quraishi, M. Ionic Liquids as Green and Sustainable Corrosion Inhibitors for Metals and Alloys: An Overview. J. Mol. Liq. 2017, 233, 403–414. https://doi.org/10.1016/J.MOLLIQ.2017.02.111.

10. Li, F.; Yuan, Y.; Li, C. Corrosion Propagation of Prestressing Steel Strands in Concrete Subject to Chloride Attack. Constr. Build. Mater. 2011, 25, 3878–3885. https://doi.org/10.1016/J.CONBUILDMAT.2011.04.011.

11. Darmawan, M.S. Pitting Corrosion Model for Partial Prestressed Concrete (Pc) Structures in a Chloride Environment. IPTEK J. Technol. Sci. 2009, 20, 78-88. https://doi.org/10.12962/J20882033.V20I3.109.

12. Funahashi, M. Predicting Corrosion-Free Service Life of a Concrete Structure in a Chloride Environment. Materials 1990, 87, 581–587. https://doi.org/10.14359/2533.

13. Nguyen, T.H.Y.; Tran, V.M.; Pansuk, W.; Cao, N.T.; Bui, V.H.L. Electrochemical Chloride Extraction on Reinforced Concrete Contaminated External Chloride: Efficiencies of Intermittent Applications and Impacts on Hydration Products. Cem. Concr. Compos. 2021, 121, 104076. https://doi.org/10.1016/J.CEMCONCOMP.2021.104076.

14. Kanagaraj, B.; Priyanka, R.; Anand, N.; Kiran, T.; Andrushia, A.D.; Lubloy, E. A Sustainable Solution for Mitigating Environmental Corrosion in the Construction Sector and Its Socio-Economic Concern. Case Stud. Constr. Mater. 2024, 20, e03089. https://doi.org/10.1016/J.CSCM.2024.E03089.

15. Lu, Z.H.; Zhou, Q.H.; Li, H.; Zhao, Y.G. A New Empirical Model for Residual Flexural Capacity of Corroded Post-Tensioned Prestressed Concrete Beams. Structures 2021, 34, 4308–4321. https://doi.org/10.1016/J.ISTRUC.2021.10.005.

16. Minh, H.; Mutsuyoshi, H.; Niitani, K. Influence of Grouting Condition on Crack and Load-Carrying Capacity of Post-Tensioned Concrete Beam Due to Chloride-Induced Corrosion. Constr. Build. Mater. 2007, 21, 1568–1575. https://doi.org/10.1016/J.CONBUILDMAT.2005.10.004.

17. Coronelli, D.; Castel, A.; Vu, N.A.; François, R. Corroded Post-Tensioned Beams with Bonded Tendons and Wire Failure. Eng. Struct. 2009, 31, 1687–1697. https://doi.org/10.1016/J.ENGSTRUCT.2009.02.043.

18. Zhang, X.; Wang, L.; Zhang, J.; Ma, Y.; Liu, Y. Flexural Behavior of Bonded Post-Tensioned Concrete Beams under Strand Corrosion. Nucl. Eng. Des. 2017, 313, 414–424. https://doi.org/10.1016/J.NUCENGDES.2017.01.004.

19. Hussain, R. Modeling of Corrosion; Steel, Concrete and Environment. J. Civ. Environ. Eng. 2014, 4, 1–5. https://doi.org/10.4172/2165-784X.1000E114.

20. Shafei, B.; Alipour, A.; Shinozuka, M. Prediction of Corrosion Initiation in Reinforced Concrete Members Subjected to Environmental Stressors: A Finite-element Framework. Cem. Concr. Res. 2012, 42, 365–376. https://doi.org/10.1016/J.CEMCONRES.2011.11.001.

21. Taffese, W.Z.; Sistonen, E. Machine Learning for Durability and Service-Life Assessment of Reinforced Concrete Structures: Recent Advances and Future Directions. Autom. Constr. 2017, 77, 1–14. https://doi.org/10.1016/J.AUTCON.2017.01.016.

22. Elfergani, H.A.; Pullin, R.; Holford, K.M. Damage Assessment of Corrosion in Prestressed Concrete by Acoustic Emission. Constr. Build. Mater. 2013, 40, 925–933. https://doi.org/10.1016/J.CONBUILDMAT.2012.11.071.

23. Shevtsov, D.; Cao, N.L.; Nguyen, V.C.; Nong, Q.Q.; Le, H.Q.; Nguyen, D.A.; Zartsyn, I.; Kozaderov, O. Progress in Sensors for Monitoring Reinforcement Corrosion in Reinforced Concrete Structures—A Review. Sensors 2022, 22, 3421. https://doi.org/10.3390/S22093421.

24. Wang, Y.; Pan, Z.; Zhao, C.; Zeng, B. Long-Term Behavior of Prestressed Concrete Industrial Buildings in Chloride-Based Industrial Environments. J. Build. Eng. 2023, 76, 107344. https://doi.org/10.1016/J.JOBE.2023.107344.

25. Robles, K.P.V.; Gucunski, N.; Kee, S.H. Evaluation of Steel Corrosion-Induced Concrete Damage Using Electrical Resistivity Measurements. Constr. Build. Mater. 2024, 411, 134512. https://doi.org/10.1016/J.CONBUILDMAT.2023.134512.

26. Angst, U. Challenges and Opportunities in Corrosion of Steel in Concrete. Mater. Struct. 2018, 51, 4. https://doi.org/10.1617/S11527-017-1131-6.

27. Apostolopoulos, C. The Consequences of Chloride-Induced Corrosion on Steel Bar and Reinforced Concrete Structures. 2012, 1, 1000e109. https://doi.org/10.4172/2168-9873.1000e109.

28. Pavlakovic, B.; Lowe, M.; Cawley, P. Guided Ultrasonic Waves for the Inspection of Post-Tensioned Bridges. In Review of Progress in Quantitative Nondestructive Evaluation; Springer: New York, NY, USA, 1998; pp. 1557–1564. https://doi.org/10.1007/978-1-4615-5339-7_202.

29. Dai, L.; Wang, L.; Zhang, J.; Zhang, X. A Global Model for Corrosion-Induced Cracking in Prestressed Concrete Structures. Eng. Fail Anal. 2016, 62, 263–275. https://doi.org/10.1016/J.ENGFAILANAL.2016.01.013.

30. Lee, B.; Koh, K.-T.; Ismail, M.; Ryu, H.-S.; Kwon, S.-J. Corrosion and Strength Behaviors in Prestressed Tendon under Various Tensile Stress and Impressed Current Conditions. Adv. Mater. Sci. Eng. 2017, 2017, 1–7. https://doi.org/10.1155/2017/8575816.

31. Lu, Z.-H.; Wang, H.; Qu, F.; Zhao, Y.-G.; Li, P.; Li, W. Novel Empirical Model for Predicting Residual Flexural Capacity of Corroded Steel Reinforced Concrete Beam. Front. Struct. Civ. Eng. 2020, 888–906. https://doi.org/10.1007/s11709-020-0637-0.

32. Jia, H.; Qiao, G.; Han, P. Machine Learning Algorithms in the Environmental Corrosion Evaluation of Reinforced Concrete Structures—A Review. Cem. Concr. Compos. 2022, 133, 104725. https://doi.org/10.1016/J.CEMCONCOMP.2022.104725.

7 ENHANCING STRUCTURAL ANALYSIS OF REINFORCED CONCRETE COLUMNS: A STUDY ON THE IMPACT OF WELDED STEEL MESH STIRRUPS

This chapter is being published as an original research article in Engineering Sustainability.

PIEROTT, Rodrigo *et al*. Enhancing Structural Analysis of Reinforced Concrete Columns: A Study on the Impact of Welded Steel Mesh Stirrups. In: **Engineering Sustainability**.

Chapter 5 focuses on one such reinforcement strategy: the use of welded steel mesh stirrups in reinforced concrete columns. This chapter examines how this approach can significantly enhance the load-bearing capacity and ductility of concrete columns, offering a practical solution to the challenges of designing resilient structures.

ABSTRACT

This study formulates an empirical equation to predict the Confinement Effect of Welded Steel Mesh Stirrups (Cwsm) in reinforced concrete columns, leveraging a substantial dataset and examining relationships between experimental ultimate loads, concrete strength, theoretical predictions, and stirrup volume ratios. Advanced statistical and machine learning methods, including Polynomial Features and Linear/Nonlinear Regression, address data normality and enhance model accuracy. Rigorous validation via normality tests and residual analysis ensures the model's reliability. A crucial element is a comparative analysis with existing studies, proving the equation's efficacy and adaptability in real-world scenarios. An experimental program further validates the model, testing manufactured concrete columns against established data. This comprehensive approach demonstrates the equation's robustness and its potential to optimize column design for improved sustainability and efficiency in structural engineering.

Keywords:

Reinforced Concrete Columns; Welded Steel Mesh Stirrups; Structural Behavior Analysis; Empirical Equation Development; Confinement Effect; Machine Learning in Structural Engineering.

7.1 INTRODUCTION

The evolution of concrete technology has led to an increased utilization of high-strength concretes in modern construction, driven by the demand for enhanced compressive strength (Mwafy et al., 2014). This shift emphasizes not only inherent strength but also long-term durability and multifunctionality of reinforced concrete structures (Wangler et al., 2019). These structures are expected to support larger clear spans and endure higher load capacities, presenting new challenges and opportunities in architectural and structural design (Cheng et al., 2023).

Table 7.1 - Dimensions and criteria to be considered in the analysis

Cement type	Theoretical Resistance	w/c	Material consumption kg/m³				Superplasticizer (%)	f_{cm} (MPa)
			Water	Cement	Sand	Crushed Stone		
CPV	30	0.45	205.0	456.0	682.0	1005.0	-	36.2
	60	0.34	164.4	478.0	905.3	860.0	0.83	51.1

In this context, building columns, which are fundamental in resisting compressive forces, have received considerable attention. These columns typically employ longitudinal reinforcements to facilitate load absorption, while transverse reinforcements are used for positioning and improving ductility through confinement. The mechanical properties of concrete, particularly its strength and deformability, play a critical role in determining the behavior of columns (Hou et al., 2019). The mechanical properties of concrete, particularly its strength and deformability, is important in determining the behavior of building columns, which are fundamental in resisting compressive forces (Benzaid et al., 2010). Longitudinal reinforcements are employed to facilitate load absorption, while transverse reinforcements are used for positioning and improving ductility through confinement (Zhang et al., 2019). However, the reduced ductility of high-strength concrete columns compared to other reinforced concrete elements often leads to brittle concrete rupture, especially under high stress or load conditions.

The role of transverse reinforcement in mitigating these challenges is of paramount importance.

The spacing of stirrups, a key component of transverse reinforcement, can lead to unconfined concrete areas, which may become vulnerable to detachment and high internal stress gradients under load, compromising the column's structural integrity (Qu & Chang, 2019). The spacing of stirrups can result in unconfined concrete areas, which can compromise the structural integrity of the column (Agustiar et al., 2017). But also, enhanced rates of transverse reinforcement not only significantly increase the lateral pressure within the concrete core, but improve the overall axial resistance of the column (Ali et al., 2021). The provision of sufficient transverse reinforcement is crucial for confining the compressed concrete, preventing buckling of the longitudinal bars, and averting shear failure if well employed (Shin et al., 2010).

The use of Welded Reinforcement Grids (WRG) presents a promising alternative to traditional stirrup configurations in addressing the challenges of reinforced concrete columns. WRG not only enhances structural performance but also offers practical and economic advantages (Thomason, 2010). The impacts of the volumetric rate of transverse reinforcement, stirrup spacing, and concrete compressive strength on the behavior of short square concrete pillars improves the overall resistance of reinforced concrete structures (Kytinou et al., 2020). It is also an alternative for optimize reinforced concrete column design, particularly in high-strength concrete applications (Smarslik & Mark, 2019). The provision of sufficient transverse reinforcement is crucial for confining the compressed concrete, preventing buckling of the longitudinal bars, and averting shear failure (Rajeev & Krishnamoorthy, 1998).

Existing literature tends to focus on conventional reinforcement methods, with limited exploration into the potential of WSM stirrups. Furthermore, while the qualitative benefits of WSM stirrups in reinforcing concrete columns have been documented, quantitative models that integrate the complex interactions between material properties, stirrup design, and confinement effects are yet to be fully developed and validated against empirical data.

This study aims to deepen the understanding of Welded Reinforcement Grids (WRG) in reinforced concrete columns, focusing on the development of an empirical equation that highlights the structural benefits of Welded Steel Mesh (WSM) stirrups while embracing sustainable construction practices. Leveraging a comprehensive dataset and detailed statistical analysis, the research evaluates the effects of transverse reinforcement rate, stirrup spacing, and concrete compressive strength on the performance of short square concrete pillars with dimensions of 150x150mm. The goal is to expand current knowledge and provide insights into optimizing column design, especially for high-strength concrete applications. This effort offers a practical and innovative approach for engineers and designers to effectively use WSM in reinforced concrete columns as stirrups, filling an important research gap in sustainable structural engineering.

7.1.1 Welded Steel Mesh Stirrups in Concrete Reinforcement

The incorporation of welded steel mesh (WSM) stirrups in reinforced concrete columns has been shown to be a significant advancement in contemporary construction methodologies, offering implications for structural performance, but also improve the economic efficiency, and sustainability (Holz & Curbach, 2023). Research has indicated that the use of WSM as shear reinforcement in reinforced concrete beams can provide marginally higher strength and cracking resistance when combined with conventional stirrups (Seshu et al., 2020). Furthermore, the combination of stirrups and steel fibers has demonstrated a positive hybrid effect on the mechanical behavior of reinforced concrete beams (You et al., 2010). It has also been emphasized that the provision of sufficient transverse reinforcement is crucial for confining the compressed concrete, preventing buckling of the longitudinal bars, and averting shear failure (M. Zhao et al., 2023).

The use of WSM stirrups in concrete columns enhances ductility and load-bearing strength, crucial for seismic-prone areas and high-stress structures (Dilger, 2000). These stirrups facilitate uniform stress distribution, mitigating crack formation and improving structural durability (J. Zhao et al., 2018). Additionally, the superior confinement provided by WSM stirrups enhances the column's resistance to buckling under high-pressure scenarios (Li et al., 2018). Studies have shown that increasing the yield strength of stirrups effectively improves the ductility, energy dissipation, and shear deformation of concrete joints (Wang, 2019). Furthermore, the confinement offered by stirrups has been found to enhance the resistance of reinforced concrete columns to seismic forces (Zhang et al., 2019).

The prefabricated nature of WSM stirrups allows for rapid customization and installation, leading to significant reductions in construction time and labor costs, particularly beneficial for large-scale or time-sensitive projects (Hong et al., 2018). The consistency in quality and dimensions of these factory-made stirrups ensures uniformity in reinforcement and structural integrity across construction projects. Prefabrication has been shown to offer various benefits, including safe construction, waste minimization, quality improvement, and productivity enhancement, making it an increasingly important construction mode, especially for buildings requiring a short construction time (Heidbach et al., 2019).

The precise fabrication of WSM stirrups can lead to minimal material wastage, aligning with the sustainability goals of modern construction practices. Additionally, depending on the type of steel and coating used, these stirrups can offer enhanced corrosion resistance, an important consideration in harsh environmental conditions (Singh et al., 2022).

The use of high-strength stirrups has been found to be an effective measure to ensure good ductility of high-strength concrete columns under high axial compression ratios, enhancing their seismic performance (Yang et al., 2021). Additionally, the confinement provided by stirrups has been shown to enhance the resistance of reinforced concrete columns to seismic forces.

7.2 METHODOLOGY

The research's primary objective was to systematically investigate the behavior of short reinforced concrete columns with transverse reinforcement in wrapped round bars made of Glass Fiber Reinforced Polymer (GFRP). This analysis was crucial in understanding the structural performance and durability of these novel reinforcement systems.

Here, “Section 2 – Methodology”, is divided into two subsections for clarity and depth. Section 2.1 Experimental Program: Reinforcement and Load Capacity Assessment", presents the direct outcomes of our experimental research, detailing the procedures and observations from the tests conducted on concrete columns. Following this, “Section 2.2 Statistical Analysis and Empirical Equation Development", delves into the analytical interpretation of these experimental results, employing statistical methods to extract deeper insights and formulate empirical equations. This structured approach ensures a comprehensive understanding, starting from practical experimentation to analytical generalization.

7.2.1 Experimental Program: Reinforcement and Load Capacity Assessment

Thirty-six concrete columns (150x150x450mm) were constructed and divided into three groups: Reference Columns (RC), and those with Model I (CI) and Model II (CII) stirrups, differing in stirrup geometry and reinforcement ratios. RC comprised four columns without reinforcement for baseline comparison, two each at 36.2MPa and 51.1MPa compressive strengths. CI and CII, with 16 columns each, varied in longitudinal and transverse reinforcement specifics, illustrating different structural configurations.

7.2.2 Testing Procedures

The columns underwent axial loading tests to evaluate their structural performance under stress. Each column was subjected to progressive axial loading using a specific testing machine until failure. Details of the rate of load application and control mechanisms were documented to ensure replicability and accuracy. The setup was equipped with instruments designed to measure longitudinal and transverse displacements, as well as deformations in the reinforcements. This setup included, but was not limited to, strain gauges and displacement transducers, providing precise and reliable data.

7.2.3 Data Collection and Analysis

The research team collected data on load versus displacement curves (both longitudinal and transverse), deformations at the midpoint of the longitudinal reinforcement, and deformations at the central stirrup of the transverse reinforcement. The failure pattern of each column was also recorded.

The analysis involved an examination of the relationships between the observed behaviors and the various reinforcement configurations and concrete strengths. This process utilized advanced software or statistical methods to discern patterns, identify trends, and draw informed conclusions from the collected data.

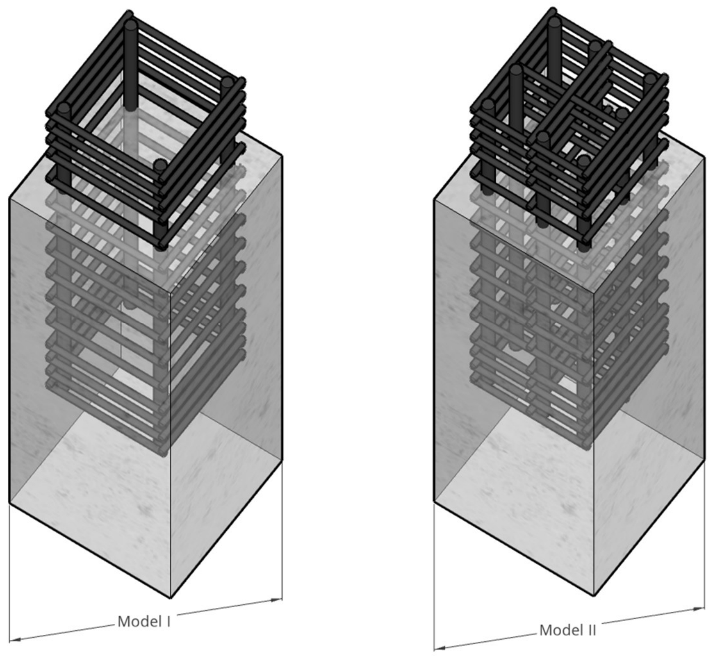

Figure 7.1 - Stirrup Models presenting: Model I and Model II.

7.2.4 Columns Materials

The materials used in the construction of the concrete columns were selected to ensure quality, consistency, and relevance to the study's objectives. This section details the specifications of the aggregates, concrete mix, and steel reinforcement bars used in the experiments.

The study employed natural quartz sand from the Paraíba do Sul River as the fine aggregate. This sand was characterized by a fineness modulus of 2.47 and a specific mass of 2609.0 kg/m³. The choice of fine aggregate significantly impacts the workability and strength characteristics of the concrete.

The concrete mix used in the study was designed to meet specific strength and durability criteria:

Table 7.2 - Concrete Mix Design.

Cement type	Theoretical Resistance	w/c	Material consumption kg/m³				Superplasticizer (%)	f_{cm} (MPa)
			Water	Cement	Sand	Crushed Stone		
CPV	30	0.45	205.0	456.0	682.0	1005.0	-	36.2
	60	0.34	164.4	478.0	905.3	860.0	0.83	51.1

Table 7.2 provides detailed information on the material consumption for each cubic meter of concrete. It includes data on the type of cement used, the theoretical resistance, water-to-cement ratio (w/c), and quantities of water, cement, sand, and crushed stone in kg/m³. Additionally, it records the percentage of superplasticizer added and the average compressive strength (fcm) in MPa.

Understanding the properties of the steel bars used for reinforcement is vital for analyzing the structural behavior of the columns. Table 7.2 presents details about the steel bars used in the experiments. It includes information on the diameter, yield strength (fyk), yield stress (fy), ultimate tensile strength (fu), strain at yield stress (εsy), strain at yield stress in percentage (εsy*), and ultimate strain (εu).

Table 7.2 - Characteristics of the steel bars used.

Table 7.2 - Characteristics of the steel bars used.

Diameter (mm)	f_{yk} (MPa)	f_y (MPa)	f_u (MPa)	ε_{sy}(‰)	ε_{sy}^*(‰)	ε_u(‰)
10.0	500	609.0	658.9	2.17	2.17	10.0
4.2	600	840.0	844.0	4.06	2.12	5.37
5.0	600	735.0	747.0	4.00	2.00	5.87

Where:

Steel properties include characteristic yield stress (fyk), yield stress (fy), ultimate stress (fu), yield strain (εsy*) and specific yield strain (εsy), and strain at failure (εu).

7.2.5 Reinforcement Configuration and Instrumentation

To understand experimental results, reinforcement configuration and measurement methods are crucial. Reinforcement details are depicted in Figures 7.2 and 7.3, showing longitudinal and transverse layouts. A nomenclature system (PX-Y-Ø-W) clarifies column types and features. Accurate measurements using LVDTs and strain gauges on reinforcements are vital for recording displacements, strains, and evaluating column performance under load.

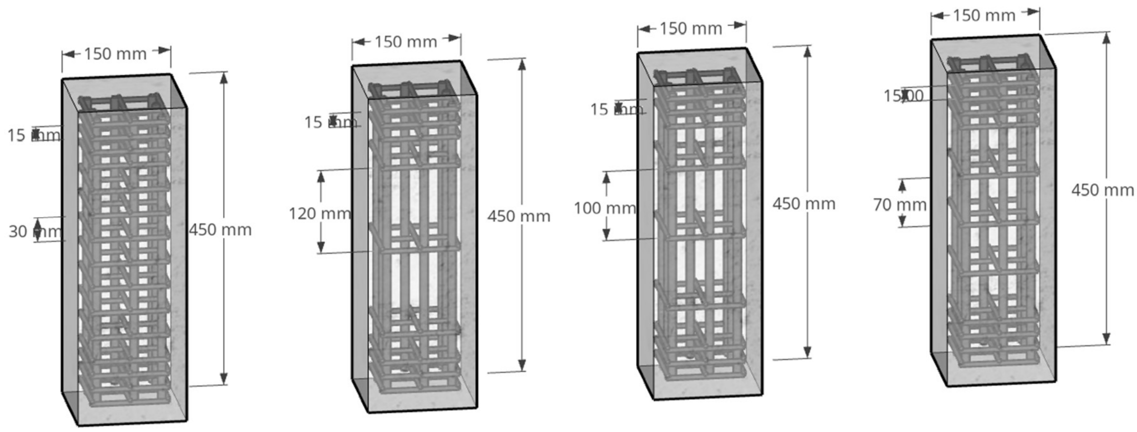

Figure 7.2 - Columns measure details.

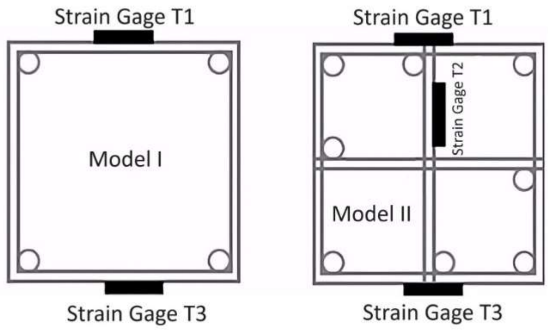

Figure 7.3 - Positioning of strain gauges on reinforcement bars.

The design of the stub columns, as presented in Figure 7.2, was meticulously planned to ensure they accurately represent the conditions and challenges encountered in real-world reinforced concrete (RC) column applications. The dimensions and configurations of these columns were chosen based on a comprehensive review of relevant literature and industry standards, aiming to capture the essential aspects of structural behavior and confinement effects in RC columns. Each specimen's size and reinforcement layout were specifically tailored to explore the impact of welded steel mesh (WSM) stirrups on the columns' load-bearing capacity and ductility. The dimensions were selected to facilitate a controlled and observable study of the confinement effects while ensuring the specimens' manageability and the practical feasibility of the testing procedures. The design process involved extensive consultations with structural engineering experts and was guided by established principles in civil engineering research to simulate typical loading conditions and failure modes in RC columns. This approach ensured that the experimental setup provided a reliable and relevant basis for assessing the performance of WSM stirrups in enhancing the structural integrity of concrete columns.

Table 7.3 compiles other pertinent characteristics of the columns. It includes data on reinforcement ratios, concrete mix properties, and other relevant information.

Table 7.3 - Geometric properties of columns.

Column	Longitudinal reinforcement		Transverse reinforcement			Concrete Strength
	ρ (%)	ϕ(mm)	ϕ(mm)	ρ_w(‰)	s(mm)	(MPa)
PI-30-4.2-30	1.4	10	4.2	0.362	30	36.2
PI-30-4.2-70				0.207	70	
PI-30-4.2-100				0.145	100	
PI-30-4.2-120				0.121	120	
PI-30-5.0-30			5	0.689	30	
PI-30-5.0-70				0.295	70	
PI-30-5.0-100				0.207	100	
PI-30-5.0-120				0.172	120	
PII-30-4.2-30	2.8		4.2	0.723	30	
PII-30-4.2-70				0.31	70	
PII-30-4.2-100				0.217	100	
PII-30-4.2-120				0.181	120	
PII-30-5.0-30			5	1.033	30	
PII-30-5.0-70				0.443	70	
PII-30-5.0-100				0.31	100	
PII-30-5.0-120				0.258	120	

This table provides the diameter of the steel bars in millimeters, along with their respective mechanical properties, such as yield strength, yield stress, ultimate tensile strength, and strains at various stress levels, all crucial for assessing the reinforcement's performance under load.

7.2.6 Manufacturing of the Columns

The manufacturing process of columns, crucial for their structural integrity and testing suitability, involves several key steps. Initially, the reinforcement for each column is prepared and instrumented, a critical phase for determining the columns' structural response under load. The reinforcements are placed horizontally in plywood formworks designed to preserve the columns' shape and integrity during concrete pouring and setting. Two concrete mixes aiming for compressive strengths of 36.2 MPa and 51.1 MPa are prepared in a 200-liter mixer, with careful control over mixing time for consistency. Following mixing, the concrete is manually placed into formworks and compacted on a vibrating table to eliminate air pockets and ensure uniform distribution. The columns are demolded after 24 hours and cured in lime-saturated water for 28 days to optimize hydration, thereby improving strength and durability. After curing, the columns are stored under controlled laboratory conditions until testing, to maintain stable properties.

7.2.7 Execution of Tests

The following section details the procedures and methodologies employed in evaluating the compressive behavior of the columns.

Axial Compression Tests: Centered axial compression tests were conducted using a DL 300 Universal Testing Machine (capacity of 2000 kN) by EMIC. The load was applied at a constant speed of 0.006 m/s, ensuring uniform stress distribution.

Load Application and Monitoring: The load was continuously monitored and applied until a significant decrease, indicative of strength loss and structural failure, was observed. This point provided insights into the columns' load-bearing capacity.

The use of a metal collar for the confinement of column ends and support for the installation of LVDTs is crucial for maintaining column alignment and stability during testing (Abdulhussein & Al-Sherrawi, 2021). A metal collar was employed to serve dual purposes: confinement of the column ends and support for the installation of LVDTs. This collar was integral in maintaining column alignment and stability during testing.

The assessment of compressive behavior in reinforced concrete columns can be thoroughly evaluated through experimental testing, providing essential data for analyzing their structural integrity and performance characteristics (Lei et al., 2020). Experimental investigations on the behavior of reinforced concrete columns under axial compression loads have been conducted to study their compressive behavior and structural performance (Lei et al., 2020). Additionally, the influence of concrete compressive strength on the overall behavior of reinforced concrete columns subjected to eccentric loads has been studied, emphasizing the significance of concrete properties in column behavior (Fareed et al., 2022).

This testing approach allowed for a thorough evaluation of the columns' behavior under compression, providing data for analyzing their structural integrity and performance characteristics.

7.2.8 Experimental Program: Results and Behavioral Analysis

The behavior of reinforced concrete columns under axial compression loads has been extensively studied, emphasizing the significance of confinement in enhancing the structural performance of the columns (Mahgub et al., 2017). The consistent pattern of behavior observed across the majority of the columns during testing, including the displacement of the concrete cover and the achievement of ultimate loads higher than the maximum loads, underscores the importance of stirrups in providing effective confinement and creating a robust confined core within the columns (Mahgub et al., 2017). Furthermore, research has investigated the influence of non-uniform corrosion on the cracking pattern of concrete and the stress distribution in concrete due to non-uniform radial pressure, providing insights into the behavior of reinforced concrete elements under various loading conditions (Abdelatif et al., 2020).

To provide a visual representation of these failure modes, Figure 7.4 has been included in the study. This figure illustrates the specific ways in which the columns failed under the applied loads, offering insights into the structural limits and the efficacy of the strategies used.

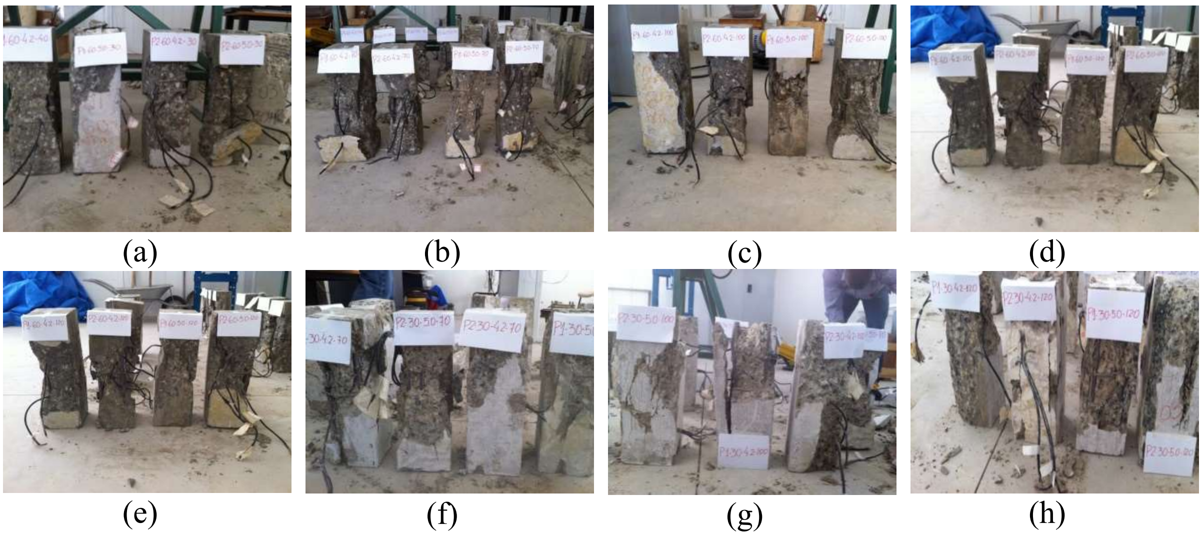

Figure 7.4 - Failure pattern of the tested pillars for (a), (b), (c), (d) for 38 MPa and (e), (f), (g), (h), for 62 MPa specimens.

In Figure 7.4, the failure modes of the tested columns are categorized based on the concrete strengths employed in the study. Images (a) through (d) illustrate the failure patterns for columns with concrete strength of 38 MPa, while images (e) through (h) correspond to columns with a higher strength of 62 MPa. For the columns with 38 MPa concrete strength, images (a) to (d) show typical failure modes such as crushing at the column ends, longitudinal cracking, and buckling of internal reinforcement. These phenomena are indicative of the stress distribution and the confinement effectiveness of WSM stirrups at this strength level. In contrast, for the 62 MPa strength columns, depicted in images (e) to (h), the failure patterns demonstrate more pronounced confinement effects, with failures characterized by more distributed cracking and less pronounced buckling of the reinforcement, reflecting the higher confinement provided by WSM stirrups at increased concrete strengths.

This elaboration ensures that the readers can clearly discern how the confinement effect of WSM stirrups influences the failure patterns at different concrete strengths, providing a deeper understanding of the structural behavior under varied loading conditions.

Figure 7.5 in the study illustrates the impact of transverse reinforcement ratio on the strength and ductility of tested columns, categorized into subgroups. The results show that an increase in the transverse reinforcement ratio significantly enhances the columns' strength, aligning with previous research that suggests closer stirrup spacing improves confinement, thus boosting ductility and strength. Initially, all columns responded linearly until the first strength peak, with columns having a 70 mm stirrup spacing showing superior capacities. Interestingly, columns with a 30 mm spacing did not reach the highest strength, indicating an optimal transverse reinforcement range exists, beyond which reinforcement might not effectively improve confinement. The study also found that columns with a strength of 51.1 MPa generally had higher capacities than those with 36.2 MPa, with Model I and II columns showing significant ultimate capacity increases of over 34% and 53%, respectively. This underscores the importance of confinement in concrete structures and suggests an optimal reinforcement range for maximizing column strength and ductility.

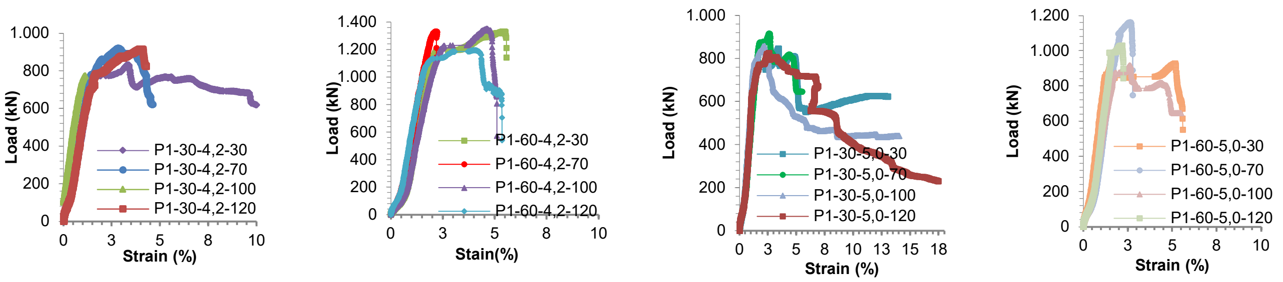

(a) (b) (c) (d)

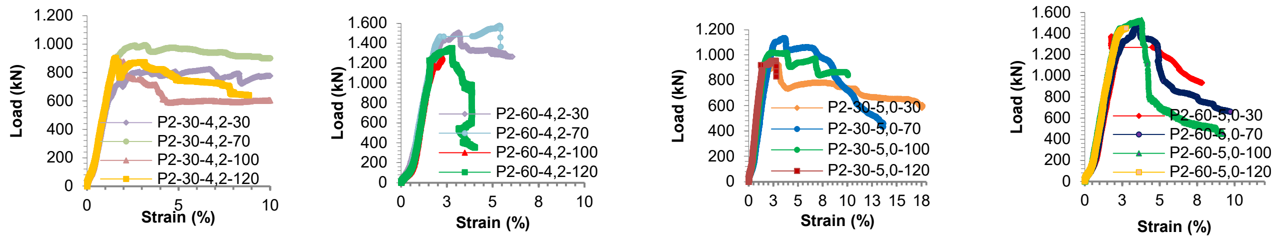

(e) (f) (g) (h)

Figure 7.5 – Load vs Strain plots for all specimens, where (a) refers to the column-1, 30MPa and reinforcement 4.2mm. (b) refers to the column-1, 60MPa and reinforcement 4.2mm. (c) refers to the column-1, 30MPa and reinforcement 5.0mm. (d) refers to the column-1, 30MPa and reinforcement 5.0mm. (e) refers to the column-2, 30MPa and reinforcement 4.2mm. (f) refers to the column-2, 60MPa and reinforcement 4.2mm. (g) refers to the column-2, 30MPa and reinforcement 5.0mm. (h) refers to the column-2, 60MPa and reinforcement 5.0mm.

Figure 7.5 illustrates the distinct behavioral patterns under axial loading for each subgroup of reinforced concrete columns. Subgroup A, represented by the first curve, shows a rapid decline in load-bearing capacity post-peak, indicative of brittle failure. Subgroup B, depicted in the second curve, demonstrates a more gradual decline and increased ductility, suggesting better energy dissipation before failure. Subgroup C, corresponding to the third curve, exhibits the highest peak load and sustained ductility, indicating superior confinement effects provided by the WSM stirrups. Each curve's shape and peak point provide insights into the varying degrees of strength and ductility enhancement achieved through different configurations and spacings of WSM stirrups in the tested column specimens.

7.2.9 Influence of the Model or Configuration of Stirrups.

In our study, Figure 7.6 illustrate the relationship between load and the volumetric ratio of transverse reinforcement (ρw) for the two stirrup models, I and II, considering the concrete strengths under investigation. A notable observation from this comparison is the superior efficacy of Model II over Model I in terms of confining the concrete core. This increased effectiveness can be attributed to the larger area of confined concrete provided by the distinct geometry of Model II.

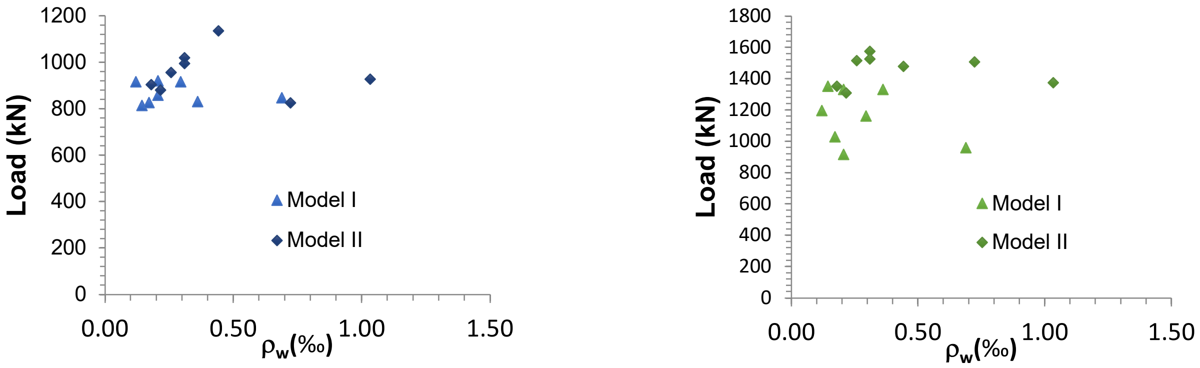

a) b)

Figure 7.6 – Load vs ρw values for different strengths: a) fcm = 36.2 MPa and b) fcm = 51.1 MPa.

This specific finding aligns with the research conducted by (Tavio & Kusuma, 2015), who explored similar configurations and reported comparable outcomes. A key feature of Model II is the presence of four cells within its design, which appears to enhance confinement markedly. This enhanced confinement translates into a noticeable improvement in both the strength and ductility of the columns. The geometry of Model II, therefore, plays an important role in determining the overall structural performance, underscoring the importance of stirrup design in reinforced concrete applications.

7.3 MACHINE LEARNING ANALYSIS AND EMPIRICAL EQUATION DEVELOPMENT

This section presents an analysis of the experimental outcomes, juxtaposed with theoretical predictions, focusing particularly on the ultimate load capacity of the tested columns.

The study employs a regression algorithm with polynomial features to accurately predict the enhanced strength due to the confinement of Welded Steel Mesh (WSM) stirrups. The model's evaluation centered on quantitative metrics such as RMSE and R^2, which facilitated a nuanced assessment of its predictive accuracy and explanatory power. Validation procedures, including statistical tests for normality and homoscedasticity of residuals, were employed to verify the model's assumptions and reliability. Furthermore, the model's coefficients were interpreted within the context of civil engineering, offering insights into the impact of WSM stirrups on the structural performance of RC columns. This comprehensive analysis not only underscored the empirical relevance of our machine learning approach but also aligned with the stringent criteria of scholarly rigor, reinforcing the study's contribution to the domain of structural engineering.

Table 7.4 provides a comparison between the theoretical and experimental results concerning the ultimate load capacity of the columns, specifically focusing on the intact concrete section. For that, the theoretical ultimate loads, designated as Pteo,cp and Pteo,pr, were calculated using the following equation:

$$Pteo,cp \ or \ Pteo,pr = 0.85 \times (fcm \ or \ fc,pr) \times (Ac - As) + fy \times As \quad (1)$$

Here, Ac represents the cross-sectional area of the columns, As denotes the area of the longitudinal reinforcement, and fy is the experimentally obtained yield stress as outlined in Table 7.2.

Strength Discrepancy: A notable observation from the analysis is that the experimental strengths consistently surpassed the theoretical values. This discrepancy suggests that additional factors, beyond the resisting capacities of the longitudinal reinforcement and the concrete’s cross-sectional area, significantly influence the column's strength.

Influence of Confined Concrete Core: This behavior is attributed to the presence of a confined concrete core, created by the transverse reinforcement under stress, resulting from the transverse deformation of the concrete.

Post-Peak Behavior Analysis: According to (ACI-441.R1, 2018), the concrete cover is lost once the column reaches the peak of its stress-strain curve, indicating that post-peak behavior is predominantly governed by confinement. Notably, high-strength concrete exhibits distinct behavior from regular-strength concrete, particularly after reaching peak stress.

7.3.1 Theoretical Ultimate Capacity Considering Concrete Core

The theoretical ultimate capacity was also calculated considering the concrete core defined either by the stirrup's perimeter or the area of concrete between the stirrups (Acn).

Table 7.4 illustrates the comparison and relationship between this revised theoretical capacity and the experimentally obtained ultimate capacity.

7.3.2 Explanation of Key Variables and Parameters

This subsection clarifies the fundamental variables and parameters employed in our analysis, which are essential for understanding the results and their implications.

The terms 'fcm' and 'fc,pr': 'fcm' refers to the mean compressive strength of the concrete used in constructing the columns. Conversely, 'fc,pr' indicates the compressive strength measured in the reference column, which serves as a benchmark for comparison. These values are critical in assessing the structural integrity and capacity of the columns.

The terms 'Pteo,cp' and 'Pteo,pr': The theoretical ultimate loads for the columns with different reinforcement patterns (CPs) and the reference column are denoted by 'Pteo,cp' and 'Pteo,pr', respectively. These theoretical calculations provide an essential basis for evaluating the expected performance of the columns under axial loads.

The term 'Pexp' represents the experimental ultimate load, which is the actual load capacity observed during the testing. This empirical measurement is crucial for understanding the real-world performance of the columns and for validating the theoretical predictions.

In this context, 'Average' refers to the average ratio of the experimental ultimate load to the theoretical ultimate load for the CPs (Pexp/Pteo,cp). This average ratio is key in summarizing the relationship between experimental outcomes and theoretical expectations. It highlights the effectiveness of the design and the influence of different reinforcement approaches on the columns' performance.

The theoretical ultimate load was also calculated using a modified approach:

$$Pteo,cp \ or \ Pteo,pr = (fcm \ or \ fc,pr) \times Acn + fy \times As \qquad (2)$$

Here, Acn represents the area of the concrete core defined by the stirrup's perimeter or the area of concrete between the stirrups, and As denotes the area of the longitudinal reinforcement. This equation provides a more refined theoretical estimate by considering the specific area of the confined concrete core.

Table 7.4 - Theoretical and experimental ultimate capacities of the columns considering the concrete data.

Columns	f_{cm} (MPa)	$f_{c,pr.}$(MPa)	$P_{teo,cp}$(kN)	$P_{teo,pr}$(kN)	$P_{exp.}$ (kN)	$P_{exp.}/P_{teo,cp}$	$P_{exp.}/P_{teo,pr}$	Average
PI-30-4,2-30	36,2	32,3	451,89	423,37	830	1,84	1,96	1,91
PI-30-4,2-70			466,68	436,57	919	1,97	2,11	
PI-30-4,2-100			451,43	422,96	813	1,80	1,92	
PI-30-4,2-120			469,68	439,25	916	1,95	2,09	
PI-30-5,0-30			455,83	426,88	846	1,86	1,98	
PI-30-5,0-70			421,83	396,52	916	2,17	2,31	
PI-30-5,0-100			437,75	410,74	858	1,96	2,09	
PI-30-5,0-120			467,69	437,47	826	1,77	1,89	
PII-30-4,2-30			642,37	613,30	824	1,28	1,34	1,51
PII-30-4,2-70			642,37	613,30	994	1,55	1,62	
PII-30-4,2-100			618,94	592,37	879	1,42	1,48	
PII-30-4,2-120			616,09	589,83	902	1,47	1,53	
PII-30-5,0-30			619,91	593,24	926	1,49	1,56	
PII-30-5,0-70			622,86	595,87	1134	1,82	1,90	
PII-30-5,0-100			634,63	606,38	1018	1,61	1,68	
PII-30-5,0-120			658,76	627,93	955,11	1,45	1,52	
PI-60-4,2-30	51,1	37,3	586,59	478,13	1330	2,27	2,78	1,96
PI-60-4,2-70			595,25	484,45	1330	2,24	2,75	
PI-60-4,2-100			603,91	490,77	1351	2,24	2,75	
PI-60-4,2-120			612,62	497,12	1196	1,95	2,41	
PI-60-5,0-30			554,96	455,05	959	1,73	2,11	
PI-60-5,0-70			614,37	498,40	1161	1,89	2,33	
PI-60-5,0-100			562,25	460,37	916	1,63	1,99	
PI-60-5,0-120			597,01	485,73	1028	1,72	2,12	
PII-60-4,2-30			753,98	650,37	1506	2,00	2,32	1,91
PII-60-4,2-70			749,35	646,99	1574	2,10	2,43	
PII-60-4,2-100			740,60	640,61	1307	1,77	2,04	
PII-60-4,2-120			762,73	656,76	1350	1,77	2,06	
PII-60-5,0-30			751,55	648,60	1373	1,83	2,12	
PII-60-5,0-70			735,06	636,57	1477	2,01	2,32	
PII-60-5,0-100			735,06	636,57	1525	2,08	2,40	
PII-60-5,0-120			773,03	664,27	1513	1,96	2,28	

"Column" specifies each tested type and configuration. "fcm (MPa)" and "fc,pr(MPa)" indicate actual and predicted compressive strengths. "Pteo,cp" and "Pteo,pr" represent theoretical ultimate loads for intact and predicted sections. "Pexp" is the observed experimental load. Ratios "Pexp/Pteo,cp" and "Pexp/Pteo,pr" compare experimental and theoretical loads. "Average" is the mean across configurations.

The research presented in our study elucidates insights into the ultimate load capacity of reinforced concrete columns, particularly those reinforced with Welded Steel Mesh (WSM) stirrups. Our findings demonstrate a close alignment with the (Pexp/Pteo) ratios observed in Lima's 1997 study. When considering the intact concrete section, these ratios hover around 1, indicating a harmony between experimental and theoretical values. Yet, a deviation emerges when focusing on the concrete core, where the (Pexp/Pteo) ratio surpasses 1, suggesting that the concrete core exhibits greater resistance than theoretical models predict.

This phenomenon echoes the research of Agostini (1992), Cusson and Paultre (1993), and Paiva (1994), all highlighting the concrete core's importance in determining column strength and resistance. Our study contributes to this established knowledge, reaffirming the concrete core's significance in the structural integrity of reinforced concrete columns.

Our research culminates in the formulation of a comprehensive equation integrating concrete and steel reinforcement contributions, alongside the advantageous effects of WSM stirrup confinement. The equation is:

$$Pult = 0.85 \times fcm \times (Ac - As) + fy \times As + Cwsm \qquad (3)$$

The base equation representing the ultimate load capacity of reinforced concrete columns is given by Equation 2. This equation considers the compressive strength of concrete, the cross-sectional area of concrete and steel reinforcement, and the yield strength of the steel (Dilger, 2000). Additionally, research has shown that factors such as axial compression ratio and shear-span ratio significantly affect the load capacity and deformation capacity of reinforced concrete columns (Jin et al., 2017). Furthermore, the addition of steel fibers has been found to affect the load-deflection behavior, ultimate strength capacity, ductility, and confinement of eccentrically loaded high-strength reinforced concrete columns (Alkufi & Al-Sherrawi, 2018).

The equation includes concrete's load capacity $0.85 \times fcm \times (Ac - As)$ steel's tensile strength $fy \times As$, and a confinement term C for WSM stirrups' strength and ductility enhancement.

This equation bridges theoretical analysis with practical civil engineering adjustments, especially where WSM stirrups are utilized. It offers a nuanced perspective on reinforced concrete columns under load, enhancing the precision of structural design and analysis. Research has shown that factors such as axial compression ratio significantly affect the load capacity and deformation capacity of reinforced concrete columns (Hasan et al., 2019).

Furthermore, our study addresses slenderness in column design, a crucial aspect affecting stability under compressive forces. While our experimental setup did not focus on extremely slender columns, it provided data on the interplay between column dimensions, material properties, and buckling risk. The presence of WSM stirrups potentially alters buckling behavior, a key consideration in reinforced concrete column design. By comparing theoretical predictions with empirical data, our study enhances understanding of WSM stirrups' role in column resistance and confinement. This knowledge significantly informs design practices, balancing strength, and stability for safer, more efficient, and reliable concrete structures.

Our study culminates in the derivation of a novel empirical equation designed to predict the ultimate load capacity of reinforced concrete columns, particularly those employing Welded Steel Mesh (WSM) stirrups for reinforcement. This equation, formulated from our comprehensive regression analysis, is a significant advancement in understanding the intricate dynamics of reinforced concrete behavior.

7.3.3 Statistical Analysis Implementation

A Polynomial Regression is utilized, which extends linear regression by considering polynomial features of the input variables. This approach is selected due to its capacity to capture the nonlinear impact of WSM stirrup confinement on the column's load-bearing capability.

The statistical analysis conducted in this study was comprehensive and methodical, aiming to derive an empirical equation for predicting the ultimate load capacity of reinforced concrete columns reinforced with Welded Steel Mesh (WSM) stirrups. The following steps presented by the pseudo-algorithm outline algorithm implementation.

Algorithm 1 Machine Learning Model for Predicting Ultimate Load Capacity

```
procedure PredictUltimateLoad
    Import libraries (Pandas, NumPy, Seaborn, Matplotlib, scikit-learn, SciPy)
    Load dataset from 'dataorigin.csv'
    Select independent (X) and dependent (Y) variables
    Apply polynomial features to X
    Split dataset into training and testing sets
    Create a Linear Regression model
    Train the model on training data
    Predict on testing data
    Calculate RMSE and R-squared
    Plot residuals versus predicted values
    Perform Shapiro-Wilk test on residuals
    if data is not Gaussian then
        Apply transformations (log, square root, etc.)
    end if
    Update Y using the log transformation
    Re-split dataset
    Re-train model on transformed data
    Predict and evaluate on transformed data
    Calculate and print new RMSE and R-squared
    return Model coefficients and intercept
end procedure
```

Data Collection and Preparation: We compiled a dataset from experiments focusing on variables such as concrete strength, stirrup volume ratio, theoretical resistance, and other relevant parameters. This dataset was formatted into a CSV file, ensuring accuracy and consistency across all data points.

An initial Exploratory Data Analysis (EDA) involves examining data distributions, identifying potential outliers, and understanding underlying patterns and correlations between variables (Organisciak et al., 2021). For this work, the EDA of the dataset was performed using various statistical tools. This phase involved examining data distributions, identifying potential outliers, and understanding underlying patterns and correlations between variables.

Based on EDA, independent variables believed to significantly impact the dependent variable (ultimate load capacity) were selected. These included the compressive strength of concrete, theoretical predictions, stirrup volume ratio, and spacing, among others.

We employed regression analysis, specifically linear regression, as our primary statistical method. This choice was due to its effectiveness in understanding relationships between multiple independent variables and a dependent variable.

Data is split in an 80/20 ratio for training and testing to ensure ample data for both constructing and validating the model. A 5-fold cross-validation method is employed to verify the model's generalizability and to refine the hyperparameters.

Features including concrete strength, stirrup spacing, and the volume ratio of WSM stirrups are selected based on their correlation with ultimate load capacity. Feature importance analysis indicates that the stirrup volume ratio and concrete strength are paramount in influencing the model's predictions, underscoring their significance in the confinement effect.

Incorporation of Polynomial and Interaction Terms: To capture the non-linear relationships and the interaction effects among variables, polynomial and interaction terms were generated and included in the regression model. This approach allowed for a more nuanced representation of the complex behaviors of materials and structural elements under stress.

Based on the initial model outputs and performance metrics, the model should be undergone through several iterations of refinement, involving adjustments, variable additions or removals, and testing different combinations of polynomial and interaction terms to achieve the best fit (Rácz et al., 2019). For this study, the regression model was trained on a subset of the data (training set), and its performance was evaluated using another subset (testing set). Performance metrics such as Root Mean Squared Error (RMSE) and R-squared (R^2) score were used to assess the model's accuracy and predictive power.

The polynomial degree is determined to be 2, based on a preliminary analysis that identifies this level as offering an optimal trade-off between model complexity and predictive accuracy. To prevent overfitting, Ridge regularization is applied with a coefficient (λ) of 0.1, following the model's performance evaluation on the validation set.

Model Refinement: Based on the initial model outputs and performance metrics, the model underwent several iterations of refinement. This process involved adjusting the model, adding or removing variables, and testing different combinations of polynomial and interaction terms to achieve the best fit.

Final Equation Formulation: The final step was to consolidate the findings from the regression analysis into a coherent empirical equation. This equation incorporated the identified significant predictors, their coefficients, and the model intercept, providing a tool for predicting the ultimate load capacity of WSM-reinforced concrete columns.

Validation and Interpretation: The final equation was then interpreted within the context of civil engineering principles. Further validation was conducted by applying the equation to external datasets and comparing the predicted results with actual outcomes, ensuring the model's practical applicability and reliability.

This statistical analysis has been pivotal in achieving an empirical understanding of the behavior of reinforced concrete columns. It bridges the gap between theoretical knowledge and practical application, offering a tool for engineers in the field.

The empirical equation, derived to encapsulate the complex relationships influencing ultimate load capacity, is as follows:

$$Pult = 0.85 \times fcm \times (Ac - As) + fy \times As + Cwsm \qquad (4)$$

$$Cwsm = C0 + C1 \times log(fcm) + C2 \times rw + C3 \times (fcm \times Pteo.pr) + C4 \times As \qquad (5)$$

In the development of Equation (5), the terms were the result of initial analyses that aimed to identify the key factors influencing the enhanced strength of reinforced concrete (RC) columns with welded steel mesh (WSM) stirrups. These analyses comprised a combination of theoretical study, empirical data examination, and preliminary statistical modeling. Through a detailed review of existing literature and theoretical models on RC column behavior, the presented variables were hypothesized to have significant impacts on the columns' strength. Subsequent empirical data analysis, which included correlation studies and sensitivity analysis on the dataset of 36 short column tests, helped in validating these hypotheses and refining the selection of variables. Preliminary regression models were then constructed to quantitatively assess the influence of each variable. The terms included in Equation (5) were those that consistently showed a strong correlation with the columns' load-bearing capacity and had a statistically significant impact in the regression models.

The methodology adopted in this study transcends traditional regression analysis, incorporating machine learning techniques to advance the predictive modeling of the strength of reinforced concrete (RC) columns. This innovative approach is characterized by the integration of feature engineering, polynomial transformations, and rigorous model validation processes, all hallmarks of machine learning. Specifically, in developing Equations (4) and (5), we applied machine learning strategies such as optimizing polynomial degrees based on model performance metrics and employing cross-validation to mitigate overfitting risks. This fusion of regression analysis with machine learning principles has enabled a more complex and detailed exploration of the structural behavior of RC columns reinforced with welded steel mesh (WSM) stirrups. The novelty of our research stems from this systematic application of machine learning techniques to construct a comprehensive model that precisely predicts the confinement effects of WSM stirrups, representing a notable advance in structural engineering analysis.

From the statistical analysis, the following analysis were presented:
Transformed scores: $R2 = 0.79$, $RMSE = 0.11$. Intercept $C0 = 0.71$, $C1 = 3.88$, $C2 = 30.52$, $C3 = 1.41$.

Substituting the coefficients obtained from our regression model, the equation translates to:

$$Cwsm = 0.71 + 3.88 \times log(fcm) + 30.52 \times rw + 1.41 \times As \qquad (6)$$

Here, Pexp denotes the experimental ultimate load capacity, fcm represents the concrete's compressive strength, Pteo.pr signifies the theoretical ultimate load capacity predicted for the concrete section, rw indicates the volume ratio of stirrups, and the Longitudinal Reinforcement (As) term captures the influence of the column's steel reinforcement.

The equation reflects the collective impact of the concrete's compressive strength (both linearly and logarithmically), theoretical ultimate load capacity, stirrup volume ratio, and an interaction between concrete strength and theoretical capacity, along with the effect of longitudinal reinforcement. The incorporation of both linear and logarithmic terms for the compressive strength captures the non-linear behavior of concrete under stress, offering a nuanced representation of structural dynamics.

This equation, integral to our research, provides a practical method for estimating the load-bearing capacity of concrete columns reinforced with WSM stirrups. It offers a bridge between statistical rigor and engineering principles, enhancing the precision of structural design and analysis in the field of civil engineering.

7.4 RESULTS AND DISCUSSION

Our study makes significant strides in understanding reinforced concrete columns, particularly highlighting the benefits of using Welded Steel Mesh (WSM) stirrups. We found that WSM stirrups notably enhance both the load-bearing capacity and ductility of these columns, supporting our theoretical predictions about their effectiveness.

Shifting from conventional stirrups, our research underscores the economic and structural advantages of WSM stirrups, relevant in the context of sustainable construction practices. Despite these advancements, we acknowledge challenges in accurately predicting load capacity for slender columns, indicating an area for future research.

A major achievement of our study is the creation of an empirical equation that predicts the ultimate load capacity of columns reinforced with WSM stirrups. This equation considers key factors like concrete strength and stirrup volume ratio.

Our findings offer new insights into the role of WSM stirrups in reinforcing concrete columns and suggest a reevaluation of the contribution of concrete core strength. This research provides practical guidance for the use of WSM stirrups, paving the way for future explorations in this field.

7.4.1 Comparative Validation of Empirical Equation Case Study

To validate the empirical equation developed in this study, we compared its predicted ultimate load capacities with those obtained by (Guerrante, 2006), (Collins et al., 1993), (Lima et al., 2003), and (Queiroga & Giongo, 2003). Selected columns from these studies, chosen for their similarity in stirrup design, concrete strength, and reinforcement details, allowed for a rigorous benchmarking of our model against established methodologies.

Table 7.5: Comparative Analysis of Ultimate Load Capacities (kN) for Reinforced Concrete Columns Across Different Studies.

Table 7.5 - Comparative Analysis of Ultimate Load Capacities (kN) for Reinforced Concrete Columns Across Different Studies.

Column nomenclature	Present Work (kN)	I. F. Guerrante, 2006	Present Work/I. F. Guerrante, 2006	Collins et al., 1993	Present Work Pu/Collins et al., 1993	LIMA (kN)	QUEIROGA (kN)
P1/1	2680.49	2681.6	0.9995879	2899.73	0.924394684	2630	-
P1/2	2680.49	2681.6	0.9995879	2899.73	0.924394684	2701	-
P1/3	2680.49	2681.6	0.9995879	2899.73	0.924394684	2834	-
P1/r2	2711.55	2713.02	0.9994587	2928.61	0.925883384	3063	-
P1/r3	2711.55	2713.02	0.9994587	2928.61	0.925883384	2820	-
P2/2	2746.88	2726.45	1.0074927	2913.26	0.942888211	2950	-
P2/3	2856.72	2837.63	1.0067263	3015.47	0.947353689	3210	-
P1-series 1	2040.07	1946.81	1.0479043	2219	0.919364859	-	2278
P2-series 1	2153.89	2061.77	1.0446801	2325	0.926404318	-	2292
P3-series 2	1897.88	1818.18	1.0438341	2101	0.903321424	-	1835
P4-series 2	1897.88	1818.18	1.0438341	2101	0.903321424	-	1864
P5-series 3	1977.48	1953.16	1.0124533	2225	0.888756529	-	2158
P6-series 3	1977.48	1953.16	1.0124533	2225	0.888756529	-	2312

The findings illustrate a high degree of concordance between our equation's predictions and the results from (Guerrante, 2006), with all compared cases showing a ratio of 1.00, highlighting the precision of our model in capturing the confinement effects in high-strength concrete columns. In comparison to (Collins et al., 1993), our model tends to be slightly more conservative, with ratios ranging from 0.888 to 0.947. This suggests that while our equation is in reasonable agreement, it may incorporate a more cautious approach to confinement modeling, which could be further explored for refinement.

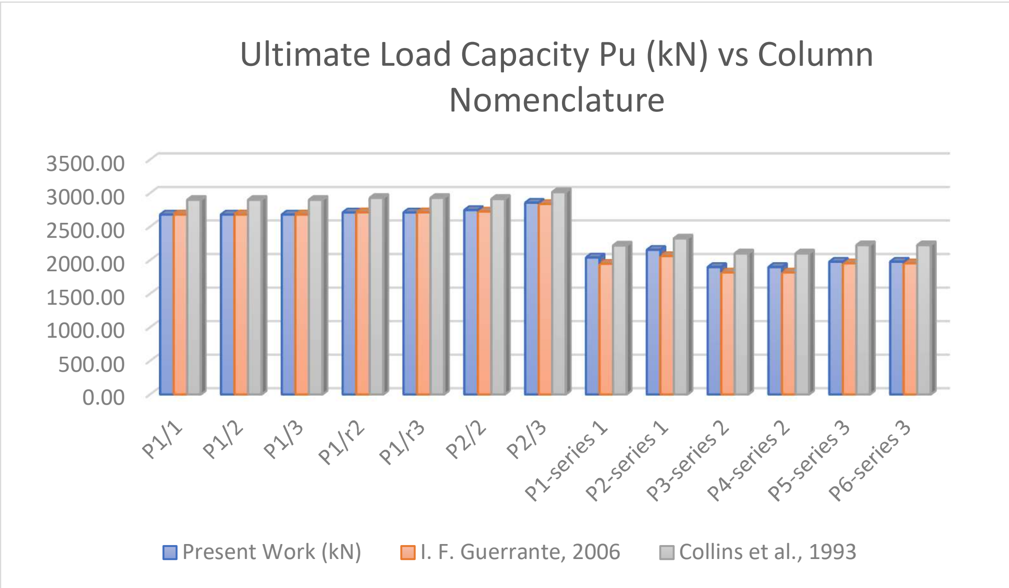

Figure 7.7 – Comparative Analysis of Ultimate Load Capacities for Reinforced Concrete Columns Across Different Studies.

The model exhibits a robust correlation with the empirical data, affirming the quantitative predictability of the confinement effect provided by WSM stirrups. The consistency between the model's predictions and the theoretical understanding of confinement in reinforced concrete columns substantiates the WSM stirrups' role in enhancing column strength.

The comparison underlines the robustness of our empirical equation across varied structural scenarios and reinforces its reliability as a tool for structural engineering design, particularly when employing WSM stirrups. The close alignment with established research accentuates the potential of our model to contribute meaningfully to the design and analysis of reinforced concrete structures.

7.5 CONCLUSION

Our investigation has revealed the structural advantages of utilizing welded steel mesh (WSM) stirrups in reinforced concrete (RC) columns, showcasing their ability to augment strength and ductility. Drawing from the experimental data and the derived analytical models, we propose specific structural solutions for practical implementation. The column models presented in Figures 7.1 and 7.2 demonstrate the ideal configurations and dimensions of WSM stirrups that markedly enhance the load-bearing capabilities and seismic resilience of RC columns. These configurations are recommended for engineers and designers in the conceptualization and execution of new construction projects or the retrofitting of existing structures, with the goal of achieving superior performance and safety standards.

This study presents an advancement in the structural analysis of concrete columns reinforced with Welded Steel Mesh (WSM) stirrups. It was demonstrated that WSM stirrups substantially enhance both the load-bearing capacity and ductility of concrete columns, supporting the hypothesis that they can play a crucial role in modern construction practices. This improvement in structural performance not only contributes to engineering efficiency but also aligns with sustainable construction goals by potentially reducing material usage and minimizing environmental impact.

This research contributes to this area by offering a novel empirical equation that effectively bridges theoretical concepts with practical applications. This equation, grounded in rigorous statistical analysis, incorporates both linear and non-linear relationships to estimate the load-bearing capacity of WSM-reinforced concrete columns reliably.

One limitation of this study is that the empirical equation requires validation across broader variables and long-term performance metrics to account for the full spectrum of influences on reinforced concrete column behavior. Future research should include a diverse range of environmental conditions, load dynamics, and column geometries to enhance predictive accuracy. Additionally, investigations into the sustainability and life cycle impacts of WSM stirrups will aid in their integration into sustainable construction practices.

7.6 DISCUSSION FOR CHAPTER 7

7.6.1 Key Findings

The experimental investigation revealed that reinforced concrete columns with welded steel mesh stirrups exhibit superior performance compared to those with traditional reinforcement methods. The welded steel mesh not only enhances the columns' ability to withstand higher loads but also improves their ductility, allowing for better energy absorption and distribution under stress. This improvement is particularly significant in seismic zones, where structures are required to endure dynamic loading without catastrophic failure. The findings suggest that welded steel mesh could be a key component in the next generation of reinforced concrete structures, offering a balance between strength, ductility, and cost-effectiveness.

7.6.2 Implications

The implications of these findings are substantial for structural engineering, particularly in the design and construction of buildings and infrastructure in regions prone to seismic activity. The enhanced performance of reinforced concrete columns with welded steel mesh stirrups could lead to revisions in design codes, promoting their use as a standard practice. Additionally, the economic benefits of using welded steel mesh, which allows for material savings without compromising safety, align with industry goals for cost reduction and sustainability. These advantages make welded steel mesh an attractive option for both new construction projects and the retrofitting of existing structures to meet higher safety standards.

7.6.3 Limitations

While the study provides strong evidence for the benefits of welded steel mesh stirrups, it is important to acknowledge certain limitations. The experimental setup was based on specific column configurations and loading conditions, which may not cover the full range of scenarios encountered in real-world construction. Additionally, the long-term durability of welded steel mesh in various environmental conditions, such as high humidity or corrosive atmospheres, was not addressed in this study. Further research is needed to evaluate the performance of welded steel mesh under different conditions and to explore its application in a broader range of structural elements.

7.6.4 Future Work

Future research should focus on extending the application of welded steel mesh stirrups to other structural elements, such as beams and slabs, to assess their potential for broader use in reinforced concrete construction. Additionally, long-term studies that monitor the performance of welded steel mesh in different environmental conditions would provide valuable insights into its durability and maintenance needs. Exploring the integration of welded steel mesh with other advanced reinforcement materials, such as fiber-reinforced polymers, could also open new avenues for innovation in structural design. Finally, field testing in seismic zones could offer practical validation of the findings and support the adoption of welded steel mesh stirrups in seismic design codes.

7.7 CONCLUSION FOR CHAPTER 7

This chapter focused on enhancing the structural analysis of reinforced concrete columns, particularly through the use of welded steel mesh stirrups. The study demonstrated that incorporating welded steel mesh significantly improves the load-bearing capacity, ductility, and overall structural performance of reinforced concrete columns. These findings provide a solid basis for revising current reinforcement practices, offering a more effective and economical approach to designing concrete columns that are both resilient and durable. The research underscores the potential of welded steel mesh stirrups as a valuable reinforcement strategy, contributing to safer and more cost-efficient construction practices.

The use of welded steel mesh has demonstrated substantial improvements in structural performance, particularly in reinforced concrete columns. Moving forward, the thesis explores the potential of sustainable materials in structural applications, starting with recycled coarse aggregates concrete.

7.8 REFERENCES FOR CHAPTER 3

[1] R. Islam, T.H. Nazifa, A. Yuniarto, A.S.M. Shanawaz Uddin, S. Salmiati, S. Shahid, An empirical study of construction and demolition waste generation and implication of recycling, Waste Management. 95 (2019) 10–21. https://doi.org/10.1016/j.wasman.2019.05.049.

Abdelatif, A. O., Ožbolt, J., & Omara, A. (2020). Stress Distribution in Thick-walled Cylinder Due to Non-uniform Radial Pressure on the Example of Reinforcement Corrosion in Concrete. In Materials and Corrosion. https://doi.org/10.1002/maco.202011661

Abdulhussein, A. A., & Al-Sherrawi, M. H. (2021). Experimental and Numerical Analysis of the Punching Shear Resistance Strengthening of Concrete Flat Plates by Steel Collars. In Engineering Technology & Applied Science Research. https://doi.org/10.48084/etasr.4497

Agustiar, A., Tavio, T., & Raka, I. G. P. (2017). Study of Confinement Index of High-Strength Concrete Columns Reinforced With High-Strength Steel Bars. Iptek Journal of Proceedings Series. https://doi.org/10.12962/j23546026.y2017i6.3311

Ali, M., Abbas, S., Salah, B., Akhter, J. I., Saleem, W., Haruna, S., Room, S., & Abdulkadir, I. (2021). Investigating Optimal Confinement Behaviour of Low-Strength Concrete Through Quantitative and Analytical Approaches. Materials. https://doi.org/10.3390/ma14164675

Alkufi, H. A., & Al-Sherrawi, M. H. (2018). Efficiency of Steel Fiber on Carrying Capacity of Short Square Columns. In Civil Engineering Journal. https://doi.org/10.28991/cej-0309197

Benzaid, R., Mesbah, H. A., & Chikh, N. (2010). FRP-confined Concrete Cylinders: Axial Compression Experiments and Strength Model. In Journal of Reinforced Plastics and Composites. https://doi.org/10.1177/0731684409355199

Cheng, Z., Zhao, H., Long, G., Yang, K., Chen, M., & Wu, Z. (2023). The Mechanical Characteristics of High-Strength Self-Compacting Concrete With Toughening Materials Based on Digital Image Correlation Technology. Materials. https://doi.org/10.3390/ma16041695

Collins, M. P., Macgregor, J. G., & Mitchell, D. (1993). Structural Design Considerations for High-Strength Concrete. Concrete International, 15(5).

Dilger, W. H. (2000). Reinforced Concrete: Mechanics and Design. Canadian Journal of Civil Engineering. https://doi.org/10.1139/cjce-27-6-1316

Fareed, S., Ayub, L., & Khan, A.-R. (2022). Parametric Investigation on Behaviour of Carbon Fiber Reinforced Polymers Wrapped Reinforced Concrete Columns Under Eccentric Loads. In Materialwissenschaft Und Werkstofftechnik. https://doi.org/10.1002/mawe.202200024

Foster, S. J., & Attard, M. M. (2001). Strength and Ductility of Fiber-Reinforced High-Strength Concrete Columns. In Journal of Structural Engineering. https://doi.org/10.1061/(asce)0733-9445(2001)127:1(28)

Guerrante, I. F. (2006). Hight performance Columns enhanced by transversal reinforcements.

Gylltoft, C. C. and K. (n.d.). Slender Concrete Columns Subjected to Sustained and Short-Term Eccentric Loading. ACI Structural Journal, 97(1). https://doi.org/10.14359/832

Hasan, H. A., Sheikh, M. N., & Hadi, M. N. S. (2019). Maximum Axial Load Carrying Capacity of Fibre Reinforced-Polymer (FRP) Bar Reinforced Concrete Columns Under Axial Compression. In Structures. https://doi.org/10.1016/j.istruc.2018.12.012

Heidbach, O., Rajabi, M., Reiter, K., & Ziegler, M. (2019). World Stress Map. https://doi.org/10.1007/978-3-319-02330-4_195-1

Holz, K., & Curbach, M. (2023). Carbon Reinforced Concrete Exposed to High Temperatures. Structural Concrete. https://doi.org/10.1002/suco.202200343

Hong, J., Shen, G. Q., Li, Z., Zhang, B., & Wan-qiu, Z. (2018). Barriers to Promoting Prefabricated Construction in China: A Cost–benefit Analysis. Journal of Cleaner Production. https://doi.org/10.1016/j.jclepro.2017.10.171

Hou, Y., Cao, S., Ni, X., & Li, Y. (2019). Research on Concrete Columns Reinforced With New Developed High-Strength Steel Under Eccentric Loading. Materials. https://doi.org/10.3390/ma12132139

Institute, A. C. (2018). Report on Equivalent Rectangular Concrete Stress Block and Transverse Reinforcement for High-Strength Concrete Columns.

Jin, L., Zhang, S., Li, D., Du, X., & Li, Z. (2017). A Combined Experimental and Numerical Analysis on the Seismic Behavior of Short Reinforced Concrete Columns With Different Structural Sizes and Axial Compression Ratios. In International Journal of Damage Mechanics. https://doi.org/10.1177/1056789517735679

Kytinou, V. K., Chalioris, C. E., Karayannis, C. G., & Elenas, A. (2020). Effect of Steel Fibers on the Hysteretic Performance of Concrete Beams With Steel Reinforcement—Tests and Analysis. Materials. https://doi.org/10.3390/ma13132923

Lei, M., Wang, Z., Li, P., Zeng, L., Liu, H., Zhang, Z., & Su, H. (2020). Experimental Investigation on Short Concrete Columns Reinforced by Bamboo Scrimber Under Axial Compression Loads. In Advances in Civil Engineering. https://doi.org/10.1155/2020/8886384

Li, W., Sun, L., Zhao, J., Lu, P., & Yang, F. (2018). Seismic Performance of Reinforced Concrete Columns Confined With Two Layers of Stirrups. The Structural Design of Tall and Special Buildings. https://doi.org/10.1002/tal.1484

Lima, F. B., Giongo, J. S., & Takeya, T. (2003). Experimental analysis of high-performance concrete columns. Caderno de Engenharia de Estruturas, 21, 1–26.

Mahgub, M., Ashour, A., Lam, D., & Dai, X. (2017). Tests of Self-Compacting Concrete Filled Elliptical Steel Tube Columns. In Thin-Walled Structures. https://doi.org/10.1016/j.tws.2016.10.015

Mwafy, A., Nadeem, H., & Khaled, E.-S. (2014). Seismic Performance and Cost-effectiveness of High-rise Buildings With Increasing Concrete Strength. The Structural Design of Tall and Special Buildings. https://doi.org/10.1002/tal.1165

Organisciak, P., Schmidt, B. M., & Downie, J. S. (2021). Giving Shape to Large Digital Libraries Through Exploratory Data Analysis. In Journal of the Association for Information Science and Technology. https://doi.org/10.1002/asi.24547

Qu, D., & Chang, W. (2019). Design Methods for Spiral Stirrups Confined Concrete Columns by Evaluating the Lateral Performance of Transverse Reinforcements. Sn Applied Sciences. https://doi.org/10.1007/s42452-019-1772-x

Queiroga, M. V. M., & Giongo, J. S. (2003). Experimental analysis of high-performance concrete columns subjected to simple compression. Cadernos de Engenharia de Estruturas, 21, 107–130.

Rácz, A., Bajusz, D., & Héberger, K. (2019). Multi-Level Comparison of Machine Learning Classifiers and Their Performance Metrics. In Molecules. https://doi.org/10.3390/molecules24152811

Rajeev, S., & Krishnamoorthy, C. S. (1998). Genetic Algorithm–Based Methodology for Design Optimization of Reinforced Concrete Frames. Computer-Aided Civil and Infrastructure Engineering. https://doi.org/10.1111/0885-9507.00086

Seshu, D. R., Manjula, Ch., Rao, T. D. G., & Rao, C. B. R. (2020). A New Way of Using Welded Wire Mesh [WWM] for Enhancing the Shear Strength in Reinforced Concrete Beams. Cement Wapno Beton. https://doi.org/10.32047/cwb.2020.25.3.3

Shin, S. J., Kim, J. K., & Ahn, J.-M. (2010). Transverse Reinforcement of RC Columns Considering Effective Lateral Confining Reduction Factor. Journal of Asian Architecture and Building Engineering. https://doi.org/10.3130/jaabe.9.501

Singh, A., Kumar, V., Verma, P., & Ramtiyal, B. (2022). Can Suppliers Be Sustainable In construction Supply Chains? Evidence From a Construction Company Using Best Worst Approach. Management of Environmental Quality an International Journal. https://doi.org/10.1108/meq-03-2022-0057

Smarslik, M., & Mark, P. (2019). Hybrid Reinforcement Design of Longitudinal Joints for Segmental Concrete Linings. Structural Concrete. https://doi.org/10.1002/suco.201900081

Tavio, T., & Kusuma, B. (2015). Analytical model for axial stress-strain behavior of welded reinforcement grid confined concrete columns. Journal of Asian Concrete Federation, 1, 1. https://doi.org/10.18702/acf.2015.09.1.1

Thomason, J. (2010). Dependence of Interfacial Strength on the Anisotropic Fiber Properties of Jute Reinforced Composites. Polymer Composites. https://doi.org/10.1002/pc.20939

Wang, J. (2019). Mechanical Properties of Concrete Frame Joints With High-Strength Stirrups Under Axial and Cyclic Lateral Loads. RDLC. https://doi.org/10.7764/rdlc.18.2.334

Wangler, T., Roussel, N., Bos, F., Salet, T. A., & Flatt, R. J. (2019). Digital Concrete: A Review. Cement and Concrete Research. https://doi.org/10.1016/j.cemconres.2019.105780

Yang, K., Shi, Q., & Qi, L. (2021). Seismic Performance and Confinement Reinforcement Design of High-Strength Concrete Columns Confined With High-Strength Stirrups. Advances in Structural Engineering. https://doi.org/10.1177/1369433221992491

You, Z., Ding, Y., & Niederegger, C. (2010). Replacing Stirrups of Self-Compacting Concrete Beams With Steel Fibers. Transactions of Tianjin University. https://doi.org/10.1007/s12209-010-1416-0

Zhang, R., Jin, L., YiShui, T., Dou, G., & Du, X. (2019). Static and Dynamic Mechanical Properties of Eco-friendly Polyvinyl Alcohol Fiber-reinforced Ultra-high-strength Concrete. Structural Concrete. https://doi.org/10.1002/suco.201800247

Zhang, S., Zhang, X., Xu, S., & Li, X. (2019). Seismic Behavior of Normal-Strength Concrete-Filled Precast High-Strength Concrete Centrifugal Tube Columns. Advances in Structural Engineering. https://doi.org/10.1177/1369433219878855

Zhao, J., Liang, J., Chu, L., & Shen, F. (2018). Experimental Study on Shear Behavior of Steel Fiber Reinforced Concrete Beams With High-Strength Reinforcement. Materials. https://doi.org/10.3390/ma11091682

Zhao, M., Ding, M., & Chiew, S.-P. (2023). Bar Continuity and Strain Compatibility for High-Strength Steel Reinforcement in Reinforced Concrete Structures. Advances in Structural Engineering. https://doi.org/10.1177/13694332231184321.

8 DEVELOPMENT OF THE MAIN METHODOLOGY

This chapter presents two published articles. Section 8.1 focuses on the laboratory phase of the research, detailing the data collection process and emphasizing the critical lab procedures that were essential to ensuring the accuracy and volume of data required. These meticulous efforts were fundamental to achieving the high reliability of the results, which is further demonstrated by the method proposed in Section 8.2.

8.1 SHEAR BEHAVIOR OF RECYCLED COARSE AGGREGATES CONCRETE DRY JOINTS KEYS USING DIGITAL IMAGE CORRELATION TECHNIQUE

This chapter is published as a Paper at Infrastructures.
https://doi.org/10.3390/infrastructures8030060

SOUSA, Jedson Batista; GARCIA, Sergio Luis Gonzalez; **PIEROTT, Rodrigo** Shear Behavior of Recycled Coarse Aggregates Concrete Dry Joints Keys Using Digital Image Correlation Technique. In: **Infrastructures**: doi.org/10.3390/infrastructures8030060.

Section 8.1 investigates the shear behavior of recycled coarse aggregates concrete (RAC) dry joints keys. As sustainability becomes an increasingly important consideration in construction, this chapter evaluates how RAC can be effectively utilized in structural applications, ensuring that performance is maintained without compromising on environmental responsibility.

ABSTRACT

In this work, twenty-seven dry joint specimens of prestressed segmental bridges produced using recycled coarse aggregate concrete (RAC) were subjected to push-off tests. The substitution rate of coarse aggregate for recycled aggregate was 100%. The variables observed were the number of keys, including flat, single-keyed, and three-keyed, and the magnitude of the confining stress, varying at 1.0, 2.0, and 3.0 MPa. The slippage between both parts of the joint and the cracking of the specimens were analyzed using the digital image correlation technique (DIC). Equations from the literature were used to predict the shear strength of dry joints with recycled coarse aggregate concrete. The experimental results obtained from the present research

were compared to those of other conventional concrete researchers. The results showed that the dry joints produced with recycled coarse aggregate concrete presented a crack formation in conventional concrete joints following a similar mechanism of failure; however, they presented lower strength. Some equations in the literature predicted the strength of dry joints with recycled coarse aggregate concrete. Based on the analysis performed, adopting a reduction coefficient of 0.7 in the AASHTO normative equation was recommended for predicting the shear strength of dry joints when produced with recycled coarse aggregates concrete.

Keywords:
Dry Joints; Recycled Aggregates Concrete; Push-Off.

8.1.1 INTRODUCTION

The concern with the environment and the scarcity of natural resources has driven, in recent years, research on reusable and sustainable materials. On a global scale, the construction industry has demonstrated a tremendous environmental impact due to the extraction of a large number of rocks necessary to obtain concrete, implying the destruction of natural environments and atmospheric pollution due to the generation of dust [1].

Among the solutions found to reduce this impact, the reuse of construction and demolition waste to produce aggregates that will be used to produce new concrete [2], known as recycled aggregate concrete (RAC), was highlighted.

The recycled aggregates derived from this waste present high heterogeneity due to the immense variation in materials present. One of those with the highest concentration is mortar.

The main properties influenced by the presence of mortar in the recycled aggregates are water absorption, specific mass, abrasion, and surface texture of the grains [3]. The high porosity of the mortar attributes to the recycled aggregate high rates of water absorption and reduction of its specific mass. Due to the irregular texture, the mortar also attributes a better surface texture to the grain and, consequently, a more significant physical wear.

Mortar adhered to recycled aggregates represents a weak link in concrete. The bond region between the natural aggregate and the adhered mortar corresponds to a low-strength region known as the transition zone, causing an increase in the water content on the aggregate surface, increasing the water/cement ratio (w/c) in that region. When recycled aggregates are used to produce new concrete, a second transition zone appears, now between the cementitious matrix and the recycled aggregate, attributing to this type of concrete a lower condition of mechanical strength [4,5].

Incorporating recycled aggregates into concrete reduces its mechanical strength and durability [6]. The percentage of substitution of natural aggregates for recycled ones is directly related to the decrease in the mechanical resistance of concrete. According to Chen et al. [7], the modulus of elasticity of recycled aggregate concrete can decrease by about 20% compared to ordinary concrete. Khatab et al. [8] showed that for a replacement rate of 50% of natural aggregates by recycled ones, there was a decrease of 12% in the compressive strength of concrete, reaching 23% strength reduction when the replacement content was 100%. Meddah et al. [9] verified that the splitting tensile strength of recycled concrete decreases about 9% compared to normal strength concrete. Naouaoui et al. [3] cite that recycled aggregates can increase the water absorption of concrete by up to 50%. Lavado et al. [10] showed that for concrete made from recycled aggregates, the results of the slump test were reduced by about 38% when compared to concrete made from natural aggregates. Feng et al. [11] showed that the Poisson ratio of concrete decreased by 10% when replacing natural aggregates with recycled ones. It was also verified that when fine aggregates were replaced by sea sand and when sea water was used in the mixture composition, the Poisson coefficient of recycled coarse aggregate concrete increased by 20%.

With the advent and growth in the use of RAC in structural elements, this paper discusses the use of recycled coarse aggregates in dry joints with shear keys, which allow the connection of prestressed segmental bridge staves. In this type of structure, the bridge superstructure is divided into segments, called staves, and in the region where these staves are connected, there are shear keys. These joints present concrete protuberances along the cross-section of the dowels, called shear keys, and their resistance to shear stresses is given by the mechanical locking of these keys (Figure 8.1.1).

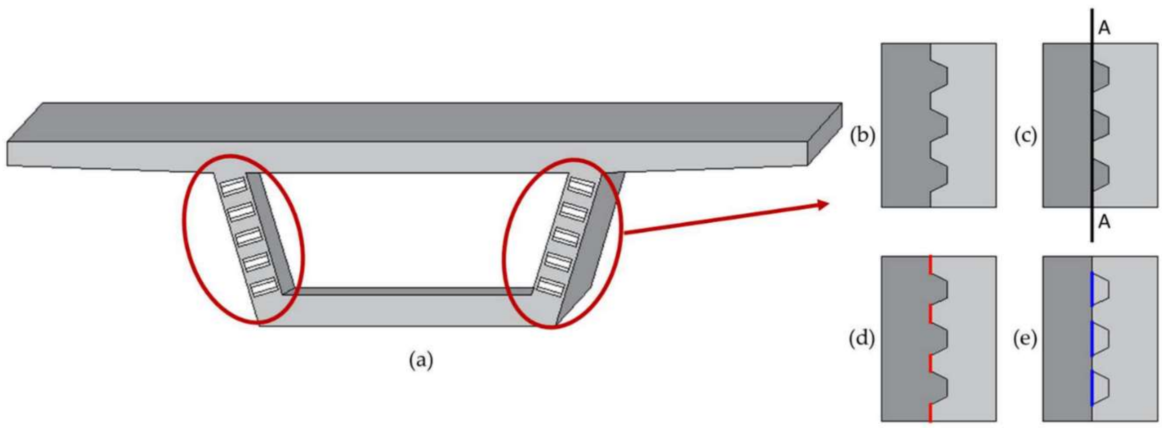

Figure 8.1.1 - (a) Representation of a segmental post-tensioned bridge arch, (b) detail of the region of the dry joint of shear key, (c) representation of the shear plane, (d) representation of the smooth region of the joint and (e) representation of the key region.

The sum of two strength portions gives the shear strength of dry joints: the portion due to the flat region of the joint (Figure 8.1.1c) and the shear keyed region (Figure 8.1.1d).

The flat region of the joint behaves similarly to two concrete interfaces sliding against each other, with no reinforcement crossing the shear plane (Figure 8.1.1b). The shear- friction theory proposed by P. Birkeland and H. Birkeland [12] establishes that the stress transfer mechanism between these two parts depends on the friction generated. The theory shows that the resistance portion of this region is directly related to the surface roughness because protuberances on the surface of the sliding interface generate mechanical locking that contributes to shear resistance. The coefficient of friction (μ) can be determined by calculating the ratio between the shear stress and confinement stress, as proposed by Buyukozturk et al. [13]. This parameter is used to quantify the frictional component of a system.

On the other hand, the keyed region corresponds to the behavior of a monolithic concrete piece, and its strength is directly related to the properties of the concrete used.

If the part is subjected to confinement action, both the flat region and the keyed region benefit from strength gains. The confinement contributes to a better mechanical interlock between the protuberances on the flat surface of the joint and provides the concrete with a state of confinement.

The behavior of concrete, when submitted to shear, depends on the strength of its aggregates in relation to the strength of the cement matrix. If the aggregates have lower strength than the cementitious matrix, the cracks tend to cut them [14,15,16,17]. The opposite occurs in concrete with aggregates having superior strength to the cementitious matrix, where cracks tend to bypass them, as shown in Figure 8.1.2.

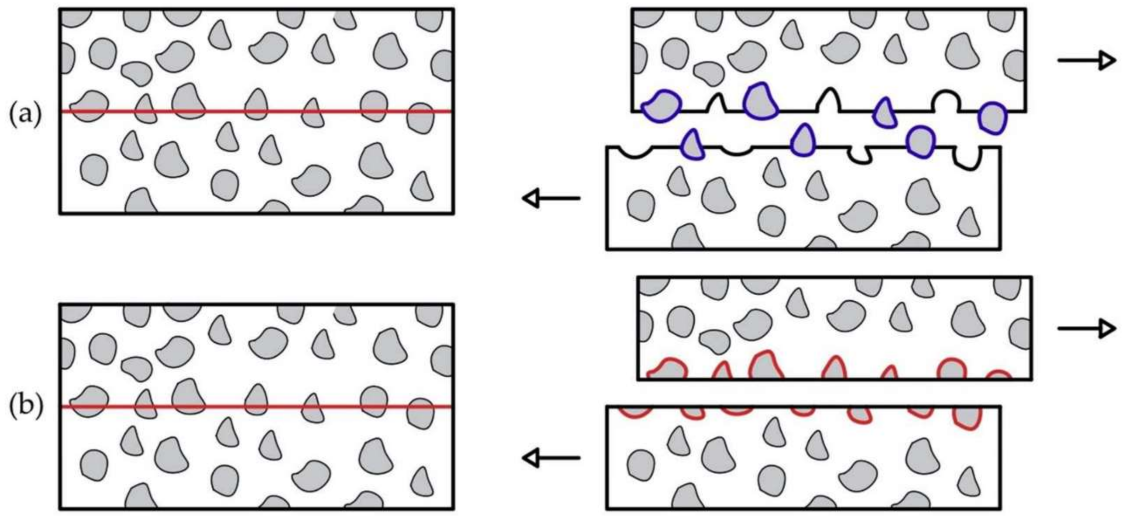

Figure 8.1.2 - Crack propagation in concrete with aggregates (a) more and (b) less resistant than the cementitious matrix.

When the cracks bypass the aggregates, an irregular and rough surface appears at the shear interface due to the exposed aggregates. This surface plays a mechanical interlocking mechanism between the aggregates, contributing to the shear strength of this concrete.

However, when the cracks cut the aggregates, surfaces with slight roughness appear at the shear interface, decreasing the interlocking effect of the aggregates and thus reducing the shear strength portion of this concrete.

Several kinds of research have been conducted in recent years on the mechanical behavior of dry joints of prestressed segmental bridges using conventional concrete. Ahmed and Aziz in 2019 [18] conducted state-of-the-art research on the topic and gathered those performed between 1959 and 2019. To date, no study using recycled aggregate concrete in dry joints has been carried out.

As a result of much research, equations for predicting the strength of these joints have been proposed.

Of the studies proposing equations, Buyukozturk et al. [13] verified the behavior of flat joints and single-keyed joints, whether they contain epoxy resin or not. The authors produced specimens for push-off rupture tests submitted to confining stresses of 0.69, 2.07, and 3.45 MPa. They concluded that the confining stress is a fundamental parameter for the strength of the joints, both flat and keyed, with the strength being higher as the confining stress increases, and the presence of epoxy resin is another factor that positively influences the strength of the joints. Rombach and Specker [19] studied dry joints' behavior by using a numerical simulation of finite elements. The authors proposed an equation for predicting the shear strength of dry joints, which had the keyed configuration as a variable. Turmo et al. [20] evaluated the shear strength of dry joints according to equations found in the literature and proposed to adopt the one that most closely matched the experimental results to the Eurocode 2 guidelines. The chosen equation was used by AASHTO [21] because it presented the lowest standard deviation in the relationship between experimental and predicted results. The authors proposed an equation for predicting the shear strength of dry joints with concrete of compressive strength less than 50 MPa. Alcade et al. [22] developed a finite element study for four different types of joints varying the confining stress in 1.0, 2.0, and 3.0 MPa. The authors concluded that the average shear stress decreases as the number of keys increases, but this behavior changes at high confining stresses. The authors comment that this behavior results from high confining stresses providing the joints with a more plastic behavior to the keys. Therefore, they can develop their maximum resistant capacity. The authors proposed an equation for predicting the shear strength of dry joints with concrete of 50 MPa and confining stresses of less than 3.0 MPa. Ahmed and Aziz [18] performed state-of-the-art research of dry joints. The authors commented on the significant variability of parameters that hinder a good correlation between experimental and predicted results for dry joint strength, such as the small database, structural differences, and geometric modeling of specimens. Through statistical analysis, the authors proposed equations for predicting the shear strength of dry joints.

The equations used for predicting dry joint strength are gathered in Table 8.1.1. The designations and notation used in the equations are shown in Table 8.1.2.

Table 8.1.1 - Main equations for predicting the shear strength of dry joints.

Author/Standard	Equation	
AASHTO (1999) [21]	$V_u = A_k\sqrt{f_c}\,(0.9961 + 0.2048\sigma_n) + 0.6A_{sm}\sigma_n$	(1)
ATEP (1996) [23]	$V_u = A_j\,(1.14\sigma_n + 0.0564f_{cd})$	(2)
EUROCODE 2 [24]	$V_u = A_j\,(0.5f_{ctd} + 0.9\sigma_n)$	(3)
Buyukozturk et al. (1990) [13]	$V_u = A_j\left(0.647\sqrt{f_c} + 1.36\sigma_n\right)$	(4)
Rombach and Specker (2002) [19]	$V_u = 0.65\sigma_n A_j + ff_{ck}A_k$	(5)
Turmo et al. (2006) [20]	$V_u = A_k 0.01\sqrt[3]{f_{ck}^{2}}\,(7\sigma_n + 33) + 0.6A_{sm}\sigma_n$	(6)
Alcade et al. (2013) [22]	$V_u = 7.118A_k\,(1 - 0.064N_k) + 2.436A_{sm}\sigma_n\,(1 + 0.127N_k)$	(7)
Ahmed and Aziz (2019) [18]	$V_u = 0.6\sigma_n A_{sm} + (1.06A_k + 2100\sigma_n)\sqrt{f_c}$	(8)

Table 8.1.2 - Notation used in the equations in Table 8.2.1.

Variable	Notation	Description
Design Parameters	V_u	Maximum shear force (kN)
	σ_n	Confining Stress (MPa)
	f_{ck}	Characteristic compressive strength of concrete (MPa)
	f_c	Concrete compressive strength (MPa)
	f_{cd}	Design concrete compressive strength (MPa)
	f_{ctd}	Concrete tensile strength (MPa)
Geometric characteristics	A_j	Total joint area (mm^2)
	A_k	Area relative to the joint keys (mm^2)
	A_{sm}	Area related to the flat part of the joint (mm^2)
	N_k	Number of keys
	f	The factor relating to the key's cutout equal to 0.14

All the proposed equations were formulated for conventional concrete; no specific equations exist in the literature for joints produced with concrete made from recycled coarse aggregates.

The fact that recycled coarse aggregates are less resistant than conventional ones influences the shear strength of the concrete produced with them. Fonteboa et al. [25] analyzed the shear behavior of concrete with recycled coarse aggregates with 50% replacement content. The results showed a reduction of about 20% in the shear strength of these types of concrete compared to conventional concrete. Xiao et al. [26] investigated the influence of the replacement content of natural coarse aggregates by recycled ones on the shear strength of concrete. The results showed that the substitution level significantly influenced the ultimate load of specimens with the same compressive strength as concrete, with a similar load for substitution levels below 30%. However, they observed a reduction in load for substitution levels of 30% to 50%. Rahal [27] performing push-off tests, concluding that for replacement contents of 20% and 50% of natural aggregates by recycled aggregates, a decrease in shear strength of 7% was obtained when the replacement rate increased to 100% and when the shear strength decreased by 28%. Liu et al. [4] studied three different types of recycled aggregate concrete and verified the influence of the type of recycled aggregate on the strength of concrete when produced by them. The experimental results showed a decrease of up to 26% in the shear strength of concrete when compared to concrete produced with natural aggregates. Trindade et al. [28] studied the influence of the percentage of replacement of natural aggregates by recycled ones with different levels of compressive strength of the original concrete. The results showed that increasing the replacement content of aggregates directly influenced the loss of shear strength of concrete, and this loss was more significant in concrete with recycled aggregates with lower compressive strengths of the original concrete. The results showed losses of 18%, 33%, and 38% in the shear strength of the concrete for the replacement levels of 30, 50, and 100%, respectively, in the recycled aggregate concrete with low strength of the original concrete. For recycled aggregate concrete with high strength of the original concrete, the researchers comment that there was no statistically significant difference. Trindade et al. [29] studied the influence of the addition of steel fibers in the shear behavior of recycled coarse aggregate concrete, having different strengths from the original concrete. The results showed that the concrete from the group of aggregates with low strength of the original concrete presented about a 33% loss in shear strength, while for those from the high strength group, the results were statistically equal. The addition of steel fiber in the recycled coarse aggregate concrete provided an increase in shear strength of about 23.8% for the concrete from the group of aggregates with low strength of the original concrete and about 17% for those from the high strength group.

Global industry is increasingly facing a future scenario of applications of unconventional materials in civil construction due to the growing demand and scarcity of natural resources, as well as the pollution caused by the obtaining of materials. The studies regarding concrete produced with recycled aggregates show that this material has characteristics and properties that resemble conventional concrete, although its main disadvantage is its reduced resistance. Therefore, further research is needed to expand the applicability of this material in the future.

Due to the lack of research on the use of recycled coarse aggregate concrete (RAC) in dry joints and aiming to provide support for structural elements, this paper studies the behavior of dry joints of prestressed segmented bridges when produced with RAC. Twenty-seven dry joint specimens were produced with RAC with 100% coarse aggregate content. The variables analyzed were the number of keys (flat, single-keyed, and three-keyed) and the magnitude of the confining stress (varying in 1.0, 2.0, and 3.0 MPa). The maximum normalized shear stress of the joints produced with concrete from recycled coarse aggregates was compared to those of Jiang et al. [30] due to the similarity of the specimens, the concrete strength, and the variables used in this research, produced using conventional concrete. The cracking load and the failure mode of the joints were also analyzed. Then, the maximum normalized shear stress of the results obtained in this research was compared with those of other researchers. Finally, the viability of using the proposed equations was verified for calculating the ultimate capacity of dry joints of conventional concrete when used in RAC dry joints.

8.1.2 Materials and Methods

The methodology of this work is presented in the flowchart of Figure 8.1.3.

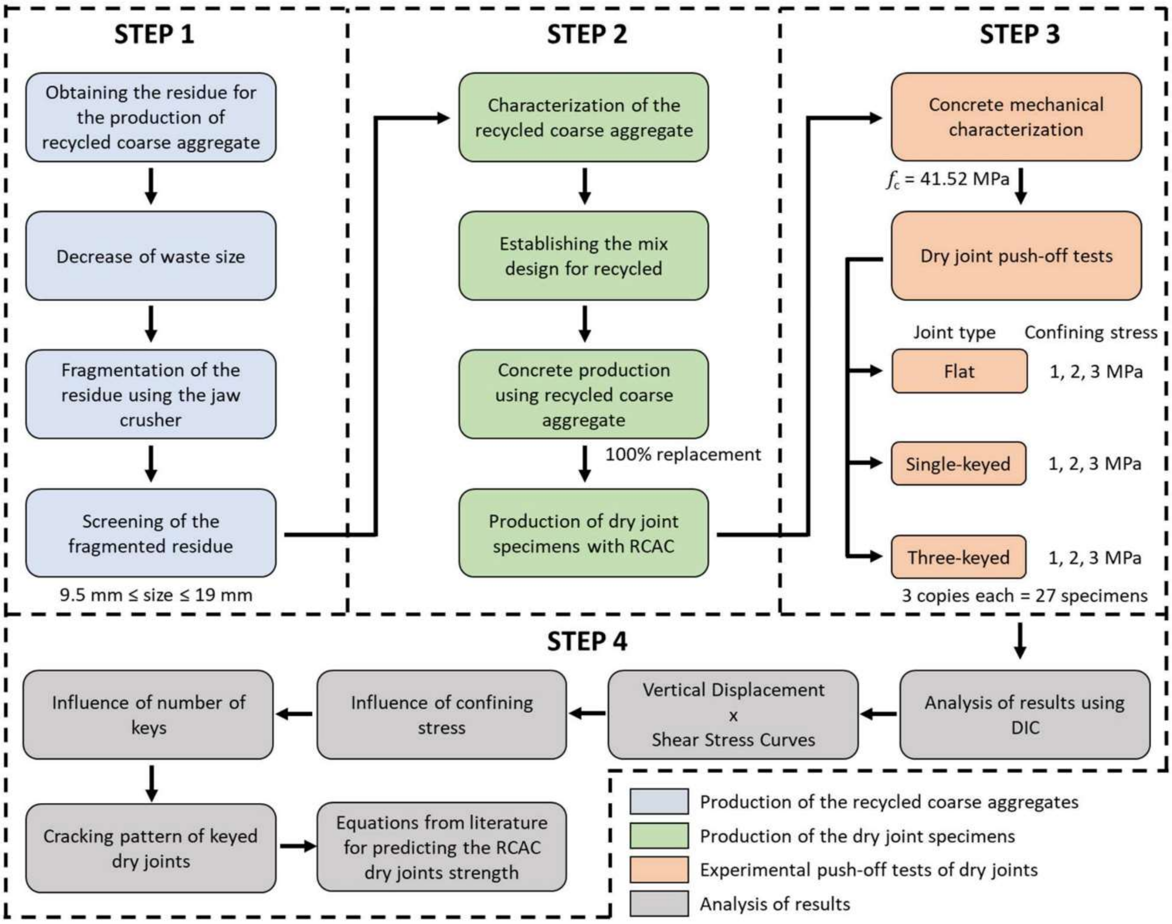

Figure 8.1.3 - Flowchart of the adopted methodology.

8.1.2.1 Materials

A Brazilian cement type CPII-E-32 [31] (Portland cement with the addition of granulated blast furnace slag and a minimum 28-day compressive strength of 32 MPa) was used as the main binder in the concrete production.

The conventional fine aggregate was natural quartz sand from the Paraíba do Sul River, in the city of Campos dos Goytacazes–RJ, with a specific mass equal to 2.63 g/cm3 [32] and a unit mass in the loose and dry state equal to 1.54 g/cm3 [32].

The recycled coarse aggregates were produced by crushing waste materials from specimens used in previous research, from which the concrete had a compressive strength of 50 to 70 MPa. Figure 8.1.4 shows the manufacturing process of the recycled coarse aggregates, and Table 8.1.3 shows information about the recycled coarse aggregates.

Figure 8.1.4 - Scheme for the production of recycled coarse aggregates; (a) specimens from previous tests with concrete having a compressive strength between 50 MPa and 70 MPa were collected; (b) the specimens were fragmented for size reduction and stored; (c) a jaw crusher was then used to reduce their size to the size of coarse aggregate for concrete; (d) the fragments were washed, sieved to a particle size between 19 and 9.5 mm and then stored in a dry place.

Table 8.1.3 - Physical characteristics of recycled coarse aggregates.

Specific Mass (g/cm^3) [33]	Water Absorption (%) [33]	Abrasion Micro-Deval (%) [34]	Adhered Mortar (%) (Adapted from [35])
2.31	5.55	13.97	40.0

Figure 8.1.5 shows the granulometry of the recycled coarse aggregates and the fine aggregates used in concrete.

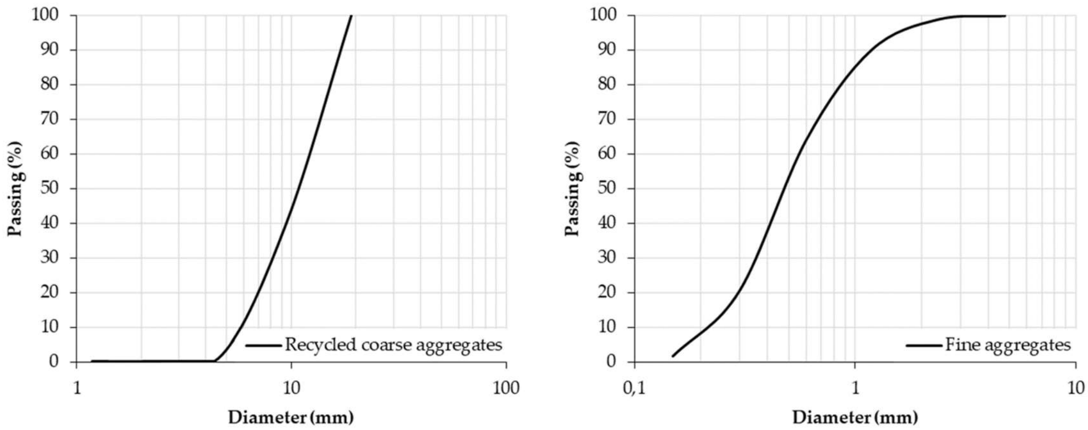

Figure 8.1.5 - Granulometry of aggregates.

8.1.2.2 Concrete Proportioning

The concrete dosage was performed to obtain a compressive strength of 30 MPa at 28 days. Table 8.1.4 shows the quantities of the materials in the dosage.

Table 8.1.4 - Concrete mixing ratios.

Material	Quantities/m^3
Portland Cement CP2-E-32	513.59 kg
Fine aggregate	735.85 kg
Recycled coarse aggregate	904 kg
Water	236.25 L
w/c	0.46

The compressive strength at 28 days was determined on cylindrical samples with a diameter of 100 mm and a height of 200 mm.

The concrete was produced with a 100% substitution content of conventional aggregates by recycled aggregates. Table 8.1.5 shows the properties of RAC used in producing the dry joint specimens.

Table 8.1.5 - Physics and mechanical characteristics of recycled coarse aggregate concrete.

RAC Properties	Values	Standard Deviation	Coefficient of Variation (%)
Compressive strength [36]	41.52 MPa	6.00 MPa	14.45
Tensile strength [37]	2.71 MPa	0.21 MPa	7.75
Modulus of Elasticity [38]	34.65 GPa	5.34 GPa	15.41
Density [39]	2450 kg/m^3	20 kg/m^3	0.82
Water absorption [39]	7.38%	0.63%	8.54

8.1.2.3 Details of Specimens

Push-off test specimens were produced similar to those used by other researchers [13,30,40,41,42,43,44] to study the shear behavior of dry joints with recycled coarse aggregate concrete.

The dimensions and configurations of the specimens used in the experiments of the flat, single-keyed, and three-keyed dry joints are shown in Figure 8.1.6.

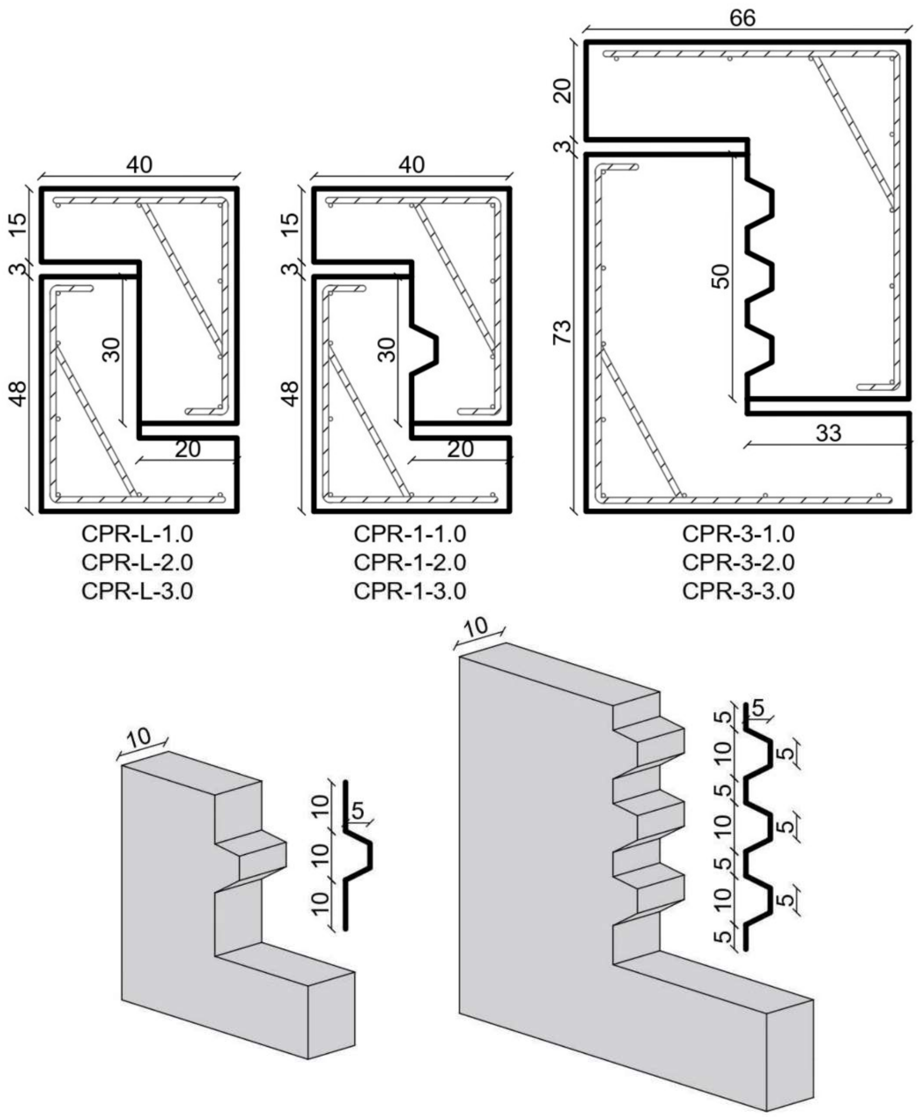

Figure 8.1.6 - Dimensions and geometry of the dry joint specimens (units in cm).

Twenty-seven dry joint specimens were produced, and the results were obtained using the average of three specimens. All specimens were 100 mm wide. Reinforcements with a diameter of 12 mm were used in the specimens to ensure that the failed occurs by shear-controlled failure in the keys. The flat and single-keyed dry joints specimens had a shear plane area of 30,000 mm2, and the three-keyed dry joints specimens had 50,000 mm2.

Table 8.1.6 shows information about the dry joint specimens. The following nomenclature was chosen: CPRX–J–T, where CPR means dry joint specimen with recycled coarse aggregates concrete; the X is the specimen number, varying from 1 to 3; the J is the joint type: (L) Flat, (1) single-keyed, and (3) three-keyed; and T is the applied confining stress (1.0, 2.0, or 3.0 MPa). For example, specimen CPR2-1-3.0 is the second specimen of the dry joint specimen with one key subjected to the 3.0 MPa confining stress.

Table 8.1.6 - Summary of the experimental program.

Specimen	Joint Type	Shear Area (mm^2)	Confining Stress (MPa)
CPR-L-1.0	Flat	30,000	1.0
CPR-L-2.0			2.0
CPR-L-3.0			3.0
CPR-1-1.0	Single-keyed	30,000	1.0
CPR-1-2.0			2.0
CPR-1-3.0			3.0
CPR-3-1.0	Three-keyed	50,000	1.0
CPR-3-2.0			2.0
CPR-3-3.0			3.0

8.1.2.4 Details of Specimens

The specimens were produced in wooden forms (Figure 8.1.7a). To produce the shear key specimens, the part that receives the key was produced first (Figure 8.1.7b). Then, the wooden parts were removed from the formwork in the shear plane, and the key part was cast using the previously part as a mold (Figure 8.1.7c). The flat joint specimens were produced similarly. The specimens are shown in Figure 8.1.8.

(a) (b) (c)

Figure 8.1.7 - Stages of casting the specimens: (a) wooden forms; (b) casting the part that receives the key; (c) concreting the key part.

Figure 8.1.8 - Dry joint specimens with recycled coarse aggregates concrete.

8.1.2.5 Setup and Instrumentation

For the push-off type rupture tests, a metallic gantry and a model 244.41 hydraulic actuator were used, coupled to a load cell with a capacity of 500 kN from MTS®. The tests were carried out with controlled deformation, with a speed of 1 mm/min, commanded by the hydraulic unit that recorded the applied load in real time, as shown in Figure 8.1.9.

Figure 8.1.9 - Hydraulic press for applying the load.

The specimens' confining stress (σn) was applied by a system of bars, nuts, and steel plates. The plates had dimensions of 200 × 300 × 20 mm and 200 × 500 × 20 mm. Applied compressive forces due to reaction forces were derived from the bars (F). Figure 8.1.10a presents the scheme for applying forces and generating the confining stress in the confinement system.

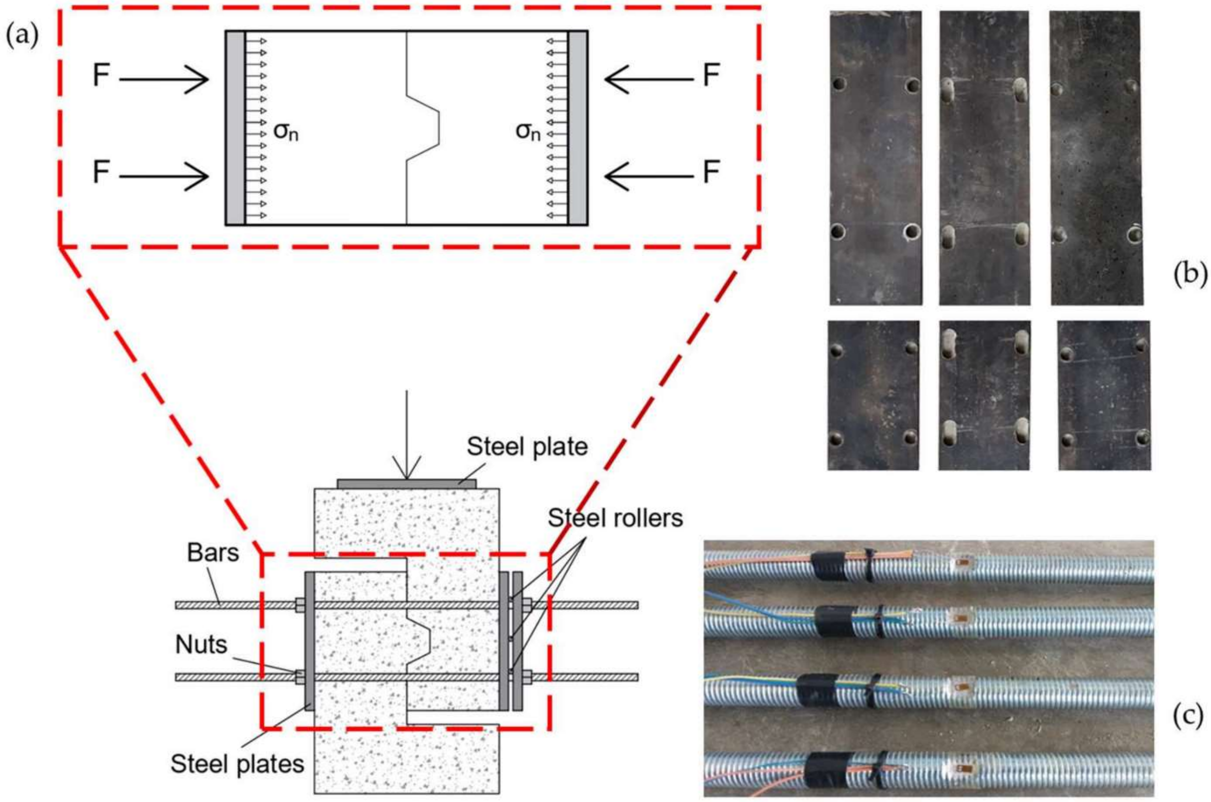

Figure 8.1.10 - (a) schematic of the confinement system, (b) metal plates used to apply the confinement stress, and (c) steel bars instrumented to generate the reaction force on the plates.

The reaction forces were generated due to the application of deformations in the steel bars. The rebars were instrumented with strain gauge model BX120-3AA (Figure 8.1.10c) and monitored in real-time as the nuts were tightened.

The plates were drilled for the passage of the bars to provide a uniform application of stresses in the specimens (Figure 8.1.10b). In addition, steel rollers were used between the glued plates on the side that slides vertically, enabling their vertical displacement.

Figure 8.1.11 shows the single-keyed dry joint specimen with installed the confining system.

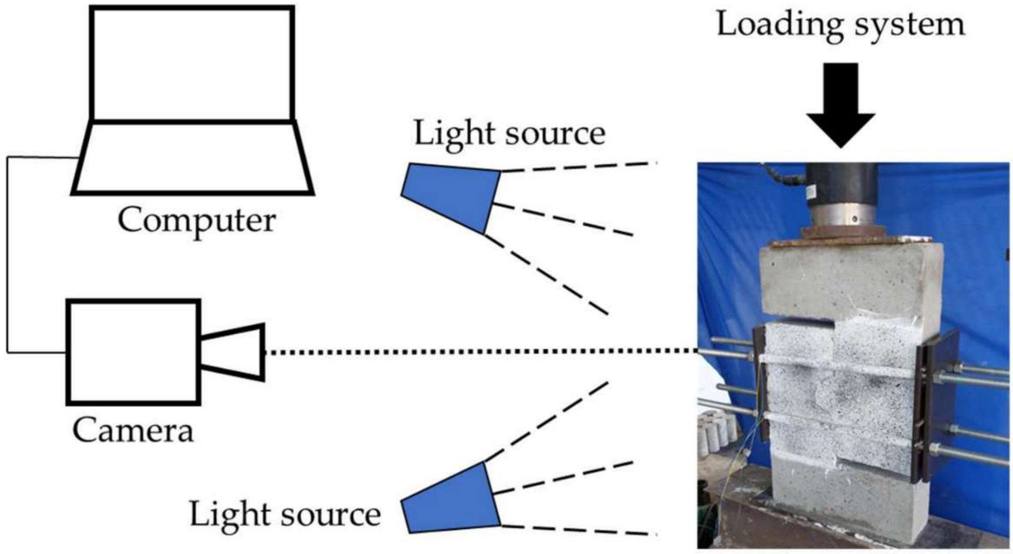

Figure 8.1.11 - Single-keyed specimen with installed the confining system and DIC setup.

The stresses applied were 1.0, 2.0, and 3.0 MPa. Table 8.1.7 shows the strains required in the bars for the reaction of the forces on the plates in specimens with shear areas of 30,000 mm2 and 50,000 mm2.

Table 8.1.7 - Deformations required in the threaded bars.

Confinement Stress (MPa)	Deformation in the Bar (με)	Reaction Force (kN)
1.0	114.71/191.18	7.50/12.5
2.0	229.41/382.35	15.0/25.0
3.0	344.12/573.53	22.5/37.5

8.1.3 Digital Image Correlation Technique

In this research, the installation of the test sample surface deformation measurement system by the image processing method (DIC) was performed by a Canon EOS REBEL T1i camera, configured with a maximum resolution of 2352 × 1568 pixels, placed on a tripod stand, 1000 mm from the object (FOV), which was attached. The setup included a Canon Lens Canon EF lens with a minimum focus distance of 0.023 m and a maximum focus distance of 0.35 m, which is illuminated by four LED lamps of 18 watts with a brightness of 1800 lux to control the brightness level of the sample surface plane to be consistent throughout the test.

To create the pattern on the monitored surface of the specimens, white paint was used to cover the entire region of interest to obtain an opaque base surface. Subsequently, a black spray was randomly sprayed over the base of the initial white paint. To capture each specimen's sequence of shots, the Windows application called digiCamControl was used. With this, it was possible to control the camera's shooting parameters; besides transferring images directly to the computer that allowed visualization of the resulting images displayed on the computer screen, the machine was configured for an acquisition frequency of 1 image every 2 s.

The images were obtained in a consistent way for all test samples, to prevent any interference that could be caused by external agents, such as lighting or capture angle. The camera was positioned 1 m away from the test samples, with a leveled horizontal orientation, and a blue background was placed behind the test sample. The focus of the camera was adjusted manually, and the environment was properly lit. A pre-capture was performed and analyzed, and the analysis software indicated if the quality of the captured image was compatible with that of the other tests by means of an analysis grid. If not, adjustments to the setup were made. The GOM Correlate Windows application [45] was used for Digital Image Correlation analysis. The analysis was based on the insertion of points on the mesh projected on the specimens and their respective displacements. With this, it was possible to calculate the deformations and displacements of these points concerning the applied load.

The GOM Correlate [45] software function "Distance" was used to analyze the sliding of both joint parts. The images were scaled based on the width of the test body, ensuring accurate measurements. Figure 8.1.12a shows the arrangement of points and distances in a single-keyed dry joint.

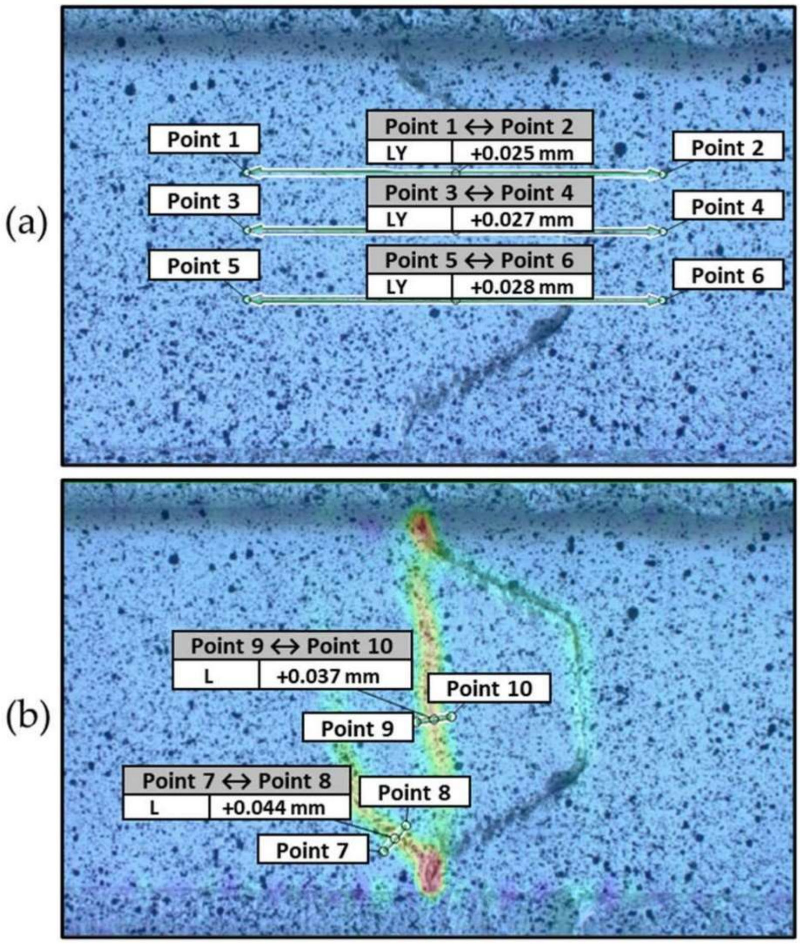

Figure 8.1.12 - Application of the GOM Correlate: (a) analysis of the vertical displacement of the specimen and (b) analysis of the crack opening in the shear key.

In recent years, crack analysis has been improved through new technologies and methods [46,47]. In this study, the cracking analysis was conducted by monitoring the deformation in the horizontal axis (εx) Through a mesh created in each figure in the GOM Correlate software, the strain history (εx) showed the displacement zones that triggered the appearance of the cracks. With this, it was possible to measure the opening of these cracks with the "Distance" tool of GOM Correlate [45]. Figure 8.1.12b shows the zones of high strain (εx) and the arrangement of virtual extensometers.

The utilization of this technique enabled the monitoring of deformations across the test specimen as the load increased, thereby enabling the visual examination of the stress and deformation fields of the material. Furthermore, the analysis of the data conducted using the software facilitated greater accuracy and optimization of the results. Moreover, the ease of assembling the testing setup and the simplicity with which the data were obtained gave this technique a considerable advantage in the research setting.

The results of the push-off tests were expressed in normalized shear stress versus sliding curves. The normalized shear stress was obtained by dividing the stress in the shear plane by the square root of the concrete compressive strength obtained in each specimen.

The curves were obtained by the average between the curves of the three samples of each specimen. It is observed that the maximum normalized stress in the average curves does not match the value of the average of the maximum normalized shear stress of the specimens because the curves of the samples presented different slopes for the maximum normalized stress.

8.1.4 Results and Discussion

8.1.4.1 Flat Dry Joints

Three flat dry joint specimens were subjected to confining stresses of 1.0, 2.0, and 3.0 MPa. Figure 8.1.13 shows the average normalized shear stress curves (τn) versus relative vertical displacement for the three confining stresses. An approximately linear increase can be seen up to the point where the joint surfaces start to slip. The slip increases gradually after the flat joint ruptures, and the load remains constant. The coefficients of friction (μ) of the flat joints with 1.0, 2.0, and 3.0 MPa of confining stress obtained through the Buyukozturk et al. [13] resulted in 0.566, 0.534, and 0.503, respectively, values close to those used by other researchers [20,30,41,42] for conventional concrete. No cracks were observed during the test, and the shear plane surface was not damaged; only a thin layer of dust was observed due to friction between both parts. The results showed that the confining stress contributed to the increased normalized shear stress of the flat RAC dry joints.

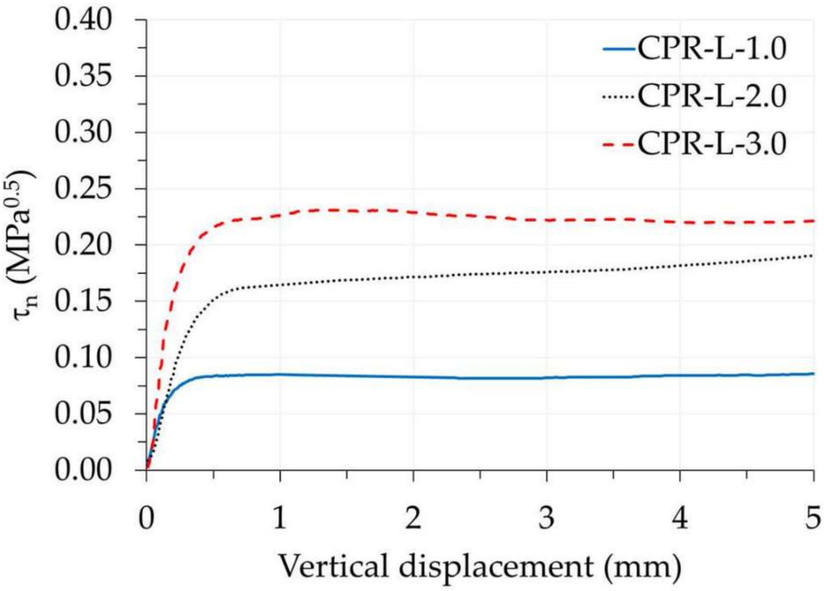

Figure 8.1.13 - Normalized shear stress versus relative vertical displacement curves for the flat RAC dry joint specimens.

8.1.4.2 Single-Keyed Dry Joints

Three single-keyed dry joints were tested at confining stresses of 1.0, 2.0, and 3.0 MPa. The results showed that increasing the confining stress increased the normalized shear stress of single-keyed RAC dry joints. The normalized shear stress versus relative vertical displacement curves is shown in Figure 8.1.14. It is observed that the normalized shear stress increases approximately linearly until reaching the strength limit of the key, and then high slip occurs in conjunction with the decrease in load.

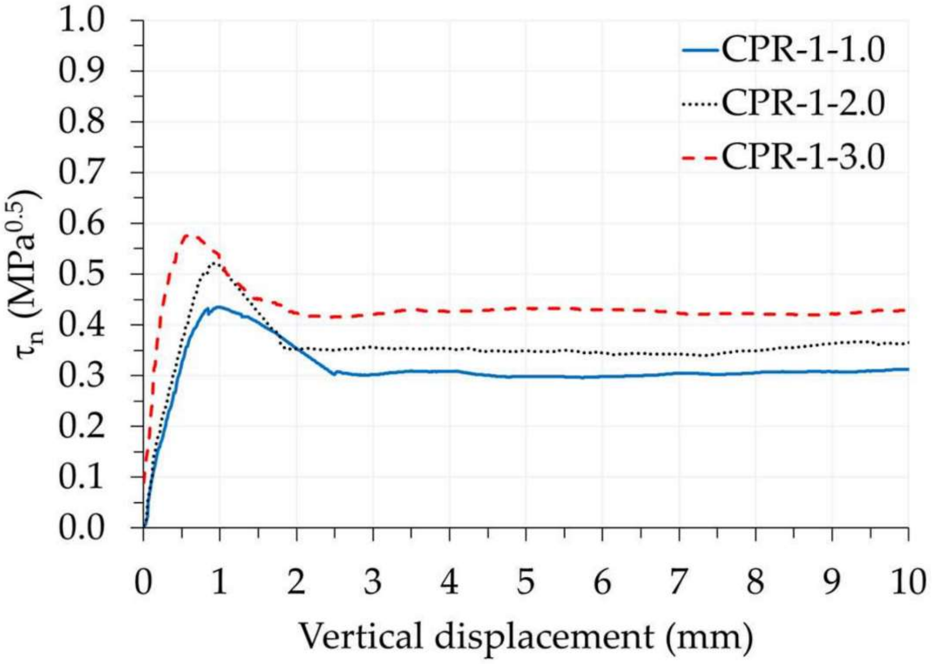

Figure 8.1.14 - Normalized shear stress versus relative vertical displacement curves for the single-keyed RAC dry joint specimens.

8.1.4.3 Three-Keyed Dry Joints

Three three-keyed dry joints were tested at confining stresses of 1.0, 2.0, and 3.0 MPa. Figure 8.1.15 shows the normalized shear stress versus relative vertical displacement curves; it is noticed an increase in the shear stress initially in a linear way; however, different from the curves of the single-keyed dry joints, when the load is close to the rupture, the curves tend to incline until reaching the rupture of the keys; this behavior shows higher ductility in the rupture of the three-keyed dry joints. This occurred due to the rupture in a sequence of the keys, where the first lower key is the first to rupture, followed sequentially by the others. This behavior has been seen by other researchers [22,30,40,42]. Again, it was observed that increasing the confining stress contributed positively to the increase in strength of three-keyed RAC dry joints.

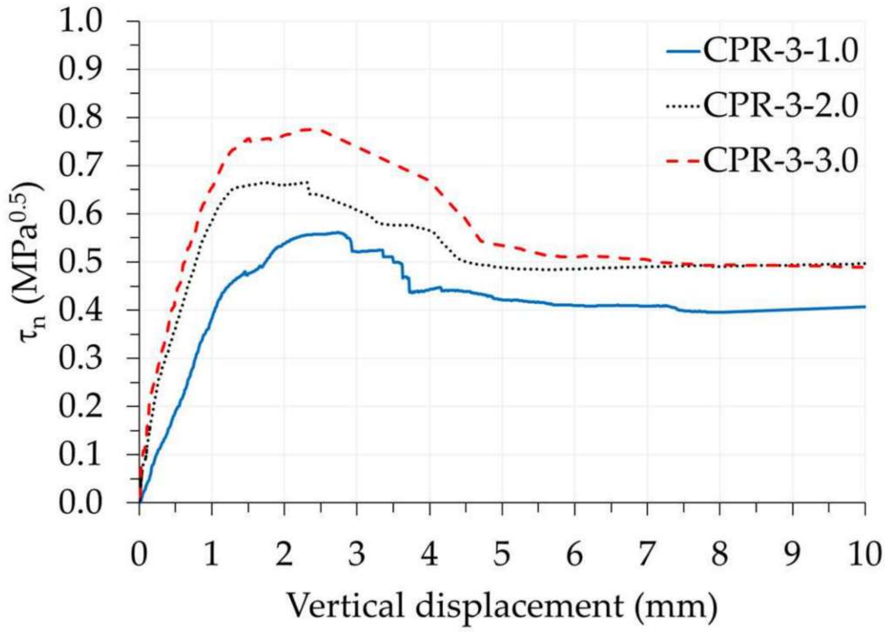

Figure 8.1.15 - Normalized shear stress versus relative vertical displacement curves for the three-keyed RAC dry joint specimens.

The failure load, maximum shear stress, normalized cracking shear stress, and maximum normalized shear stress at failure of the flat dry joints and single-keyed and three-keyed dry joints are presented in Table 8.1.8, along with the results of the maximum shear stress of Jiang et al. [30].

Table 8.1.8 - Summary of experimental results of the RAC dry joints and the results presented by Jiang et al. [30].

Specimens	Failure Load V_u (kN)	Maximum Shear Stress τ_u (MPa)	Normalized Cracking Shear Stress τ_{nf} ($MPa^{0.5}$)	Maximum Normalized τ_{un} ($MPa^{0.5}$)
CPR-L-1.0	16.98	0.57	-	0.09
CPR-L-2.0	32.01	1.07	-	0.17
CPR-L-3.0	45.31	1.51	-	0.23
CPR-1-1.0	86.18	2.87	0.20	0.45
CPR-1-2.0	104.89	3.50	0.28	0.52
CPR-1-3.0	115.11	3.84	0.35	0.60
CPR-3-1.0	180.34	3.61	0.45	0.56
CPR-3-2.0	228.89	4.58	0.62	0.68
CPR-3-3.0	256.60	5.13	0.72	0.80

Table 8.1.9 compares the experimental results of this research with those obtained by Jiang et al. [30].

Table 8.1.9 - Relationship between the experimental results of this research and those from Jiang et al. [30].

Joint	σ_n (MPa)	$\tau_{un}/\tau_{un,J}$
Flat	1	0.90
	2	0.94
Single-keyed	1	0.64
	2	0.59
Three-keyed	1	1.00
	2	0.93

The results showed that the dry joints of concrete with recycled coarse aggregates presented reduced shear strength values compared to conventional concrete (except the three-keyed joint submitted to confining stress of 1.0 MPa). This shows the brittle characteristic of this material to shear.

The lower resistance of RAC occurs because the recycled coarse aggregates have lower resistance than the conventional ones due to the percentage of adhered mortar. This characteristic contributes to the cracks to cut the recycled aggregates, reducing the mechanical interlock due to the reduction of roughness in the sliding surface, thus interfering with the shear strength of the joint [14].

The results obtained from experiments on smooth and three-keys RAC concrete joints showed values comparable to those of conventional concrete joints by Jiang et al. [30], while the one-key joints showed significantly lower values. This is likely due to the lower resistance of the RAC concrete compared to the conventional concrete, resulting in the one-key joints not reaching the full multiple resistance of the keys before breaking. However, the multiple keys joints of both types of concrete presented values of normalized shear stress that were similar in magnitude, which can be attributed to the progressive rupture effect of the keys.

8.1.4.4 Influence of the Confining Stress

Figure 8.1.16 shows the influence of the confining stress on the maximum normalized shear stress of dry joints with RAC and the results of Jiang et al. [30].

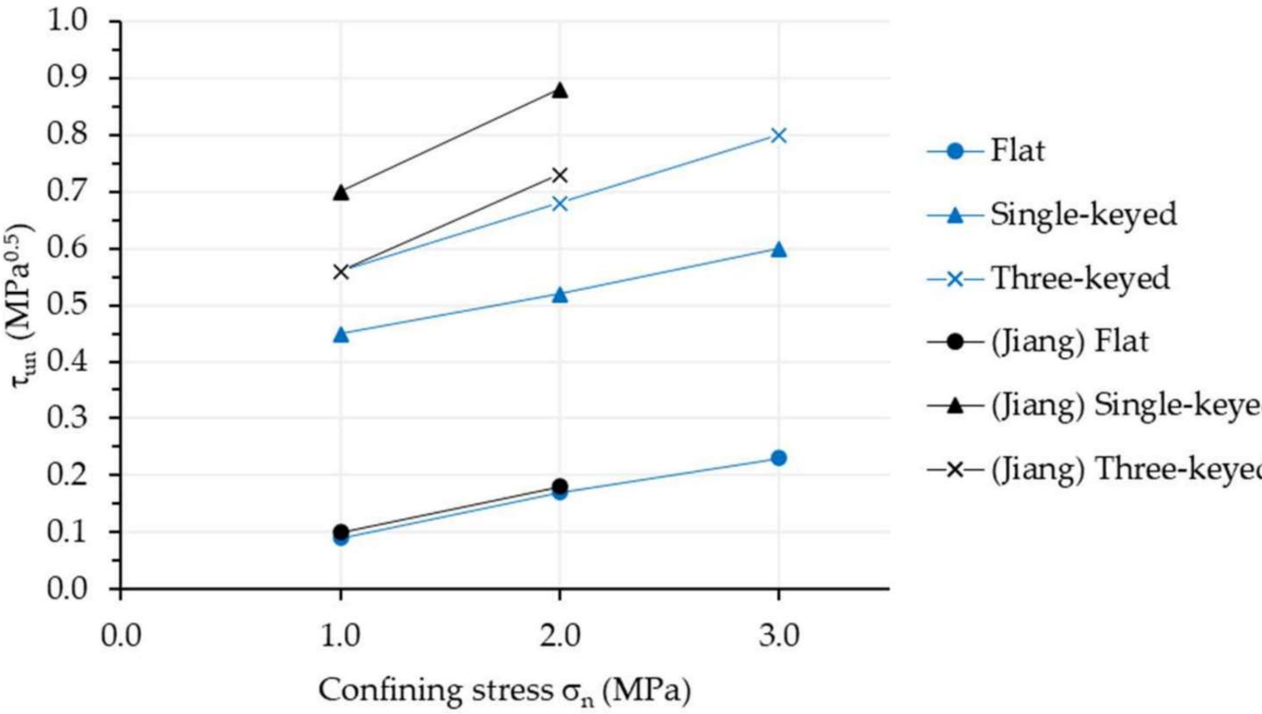

Figure 8.1.16 - Influence of confining stress on increasing the maximum normalized shear stress of the RAC dry joints and the results of Jiang et al. [30].

The results showed that maximum normalized shear stress increases as the confining stress increases for all dry joints with recycled coarse aggregate concrete, showing its importance as a resistant mechanism.

For flat joints, the strength gain when the confining stress increased from 1.0 to 2.0 MPa was 88.89%, and when it increased from 2.0 to 3.0 MPa, it was 35.29%.

For the joints with shear keys, the strength gain when the confining stress increased from 1.0 to 2.0 MPa was 15.56% for single-keyed joints and 21.43% for three-keyed joints. When the confining stress increased from 2.0 to 3.0 MPa, the strength gain was 15.38% for single-keyed joints and was 17.65% for three-keyed joints.

The experimental results of Jiang et al. [30] showed that the strength gain when the confining stress increased from 1.0 to 2.0 was 80% for flat joints, 25.71% for single-keyed joints, and 30.36% for three-keyed joints.

Comparing the flat joints, the increase in the confining stress was more effective in the strength gain of the dry joints produced with RAC. However, in joints with single- and three-keyed joints, the strength gain was more effective in joints produced with conventional concrete.

These results show that confinement in concrete with recycled coarse aggregates is less effective than in conventional concrete. As seen, the portion of resistance provided by the shear keyed is due to the monolithic region of concrete in the keyed that cuts the shear plane. Thus, this portion of resistance is directly related to the strength of the concrete used in the key. Therefore, the strength gain in concrete due to confinement is less effective in concrete with recycled coarse aggregates.

8.1.4.5 Influence of the Number of Keys

Figure 8.1.17 shows the influence of the number of keys on the maximum normalized shear stress for different confinement stresses in the dry joint with RAC.

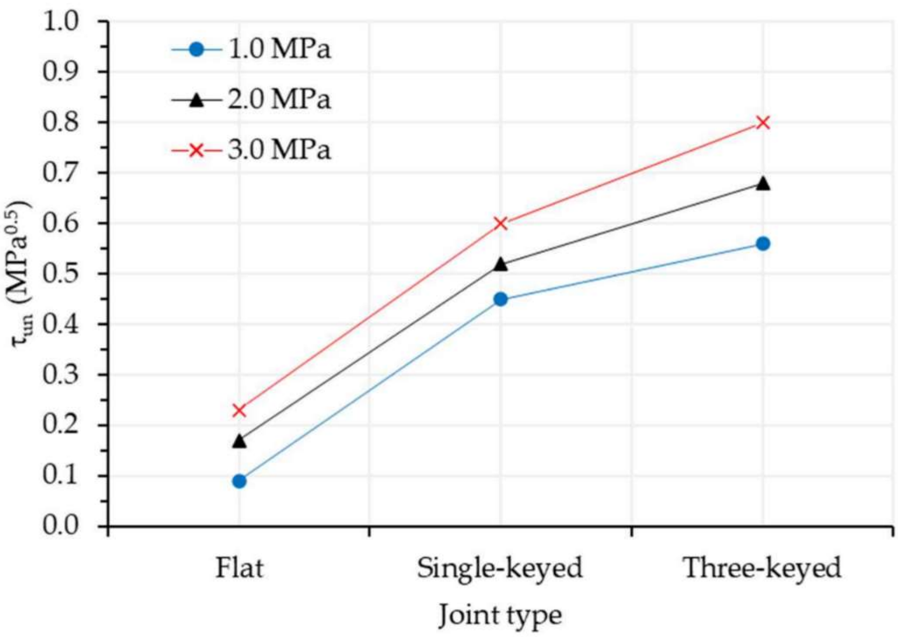

Figure 8.1.17 - Influence of the number of keys on the maximum normalized shear stress of the RAC dry joints.

It is observed that the maximum normalized shear stress increased when the number of keys was increased, and this gain was more effective when it was increased from none to single-keyed.

When the number of keys increased from none to one, the strength gain was 400%, 205.88%, and 160.87% for the confining stresses of 1.0, 2.0, and 3.0 MPa, respectively. When the number of keys increased from one to three, the strength gain was 24.44%, 30.77%, and 33.33% for the confining stresses of 1.0, 2.0, and 3.0 MPa, respectively.

This shows the typical behavior of multiple-keyed joints in not having a proportional gain in strength with the increasing number of keys due to the increase in imperfections and stress concentrations [22,30,40,42,47].

8.1.4.6 Cracking Pattern of Keyed Dry Joints Specimens

The single-keyed dry joints showed Jiang's type 2 cracking model [30]. In this model, an inclined crack at approximately 45° appears at the base of the shear key. As the load increases, several other small cracks appear in the shear plane at approximately 90°. Rupture occurs when all these little cracks cut through the entire shear key. Figure 8.1.18 shows the type 2 cracking model and the cracking kinetics of the specimen CPR1-1-1.0 with their load ratios with respect to the ultimate load (Vu).

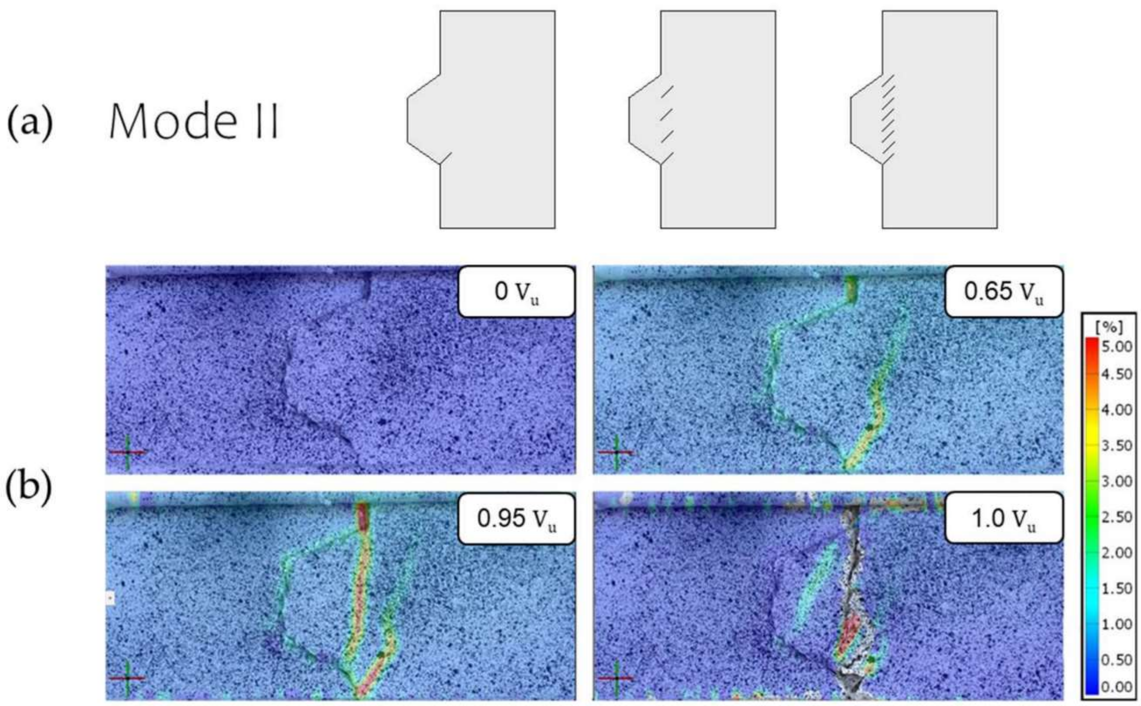

Figure 8.1.18 - (a) Crack model 2 of the single-keyed dry joints of Jiang et al. [30] and (b) crack pattern of the specimen CPR1-1-1.0.

In the three-keyed specimens, cracking occurred sequentially in the keys. The lower key was the first to crack and break, causing the other keys to break in sequence. Figure 8.1.19

shows the formation of cracks in the specimen CPR2-3-1.0, with their load proportions about the failure load (Vu) and those presented by Jiang et al. [30] for the three-keyed dry joints.

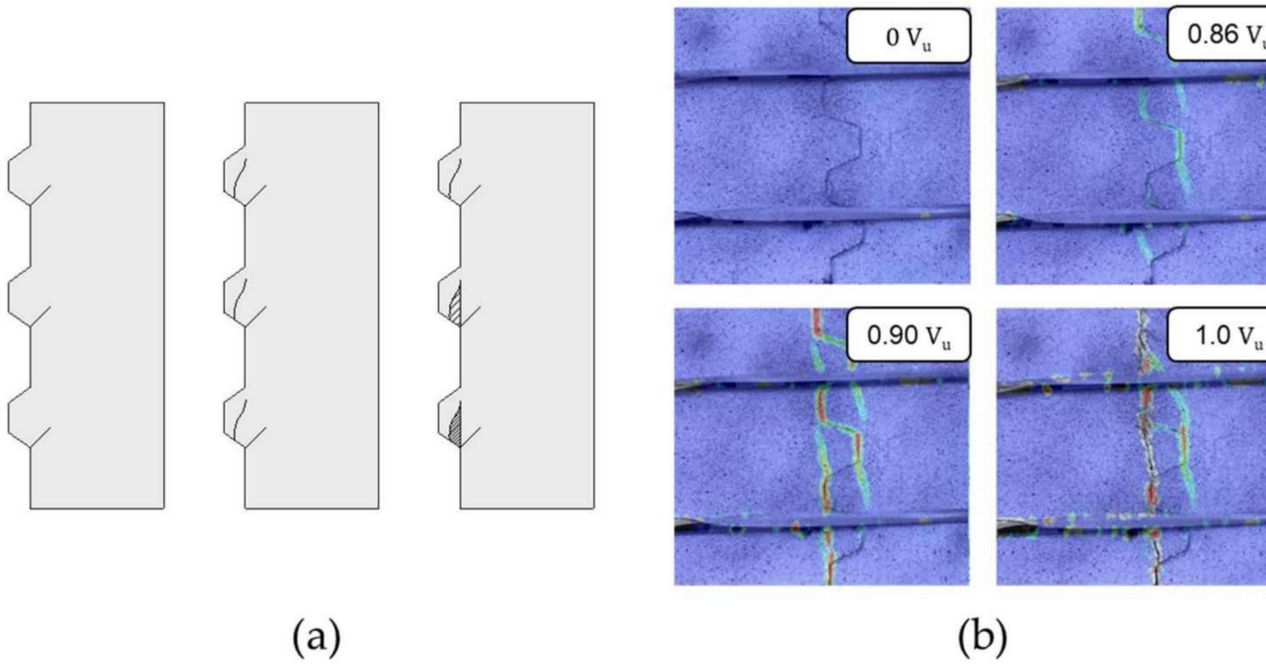

Figure 8.1.19 - (a) Crack model of the three-keyed dry joints of Jiang et al. [30] and (b) crack pattern of the specimen CPR2-3-1.0.

8.1.4.7 Comparison between the Results of This Research with Those of Other Researchers

Much research about the shear resistance of conventional or high strength dry concrete joints has been studied in recent years. Table 8.1.10 gathers information about the research.

Table 8.1.10 - Information about dry joints specimens from previous papers.

Paper	Joint Type	Concrete Strength Resistance (MPa)	Joint Width (mm)	Total Smooth Joint Ar (mm^2)
Buyukozturk [13]	Flat	47.37	76.2	5806.44
	Single-keyed	47.37	76.2	3992.9
Zhou [40]	Flat	52.2–52.8	250	50,000
	Single-keyed	37.1–56.2	250	25,000
	Three-keyed	30.2–63.7	250	50,000
Yang [41]	Single-keyed	60	100	10,000
Jiang [30]	Flat	40.49	100	20,000
	Single-keyed	41.51	100	10,000
	Three-keyed	41.82	100	20,000
Jiang [44]	Single-keyed	41.03	100	10,000
Liu [42]	Flat	123.9–125.59	150	45,000
	Single-keyed	123.9–125.59	150	30,000
	Three-keyed	123.6–124.66	150	30,000
Feng [43]	Single-keyed	64.21	100	10,000

Figure 8.1.20, Figure 8.1.21 and Figure 8.1.22 compare the maximum normalized shear stress versus confining stress obtained by other researchers and the experimental results of this research for flat, single-keyed, and three-keyed dry joints with recycled coarse aggregate concrete.

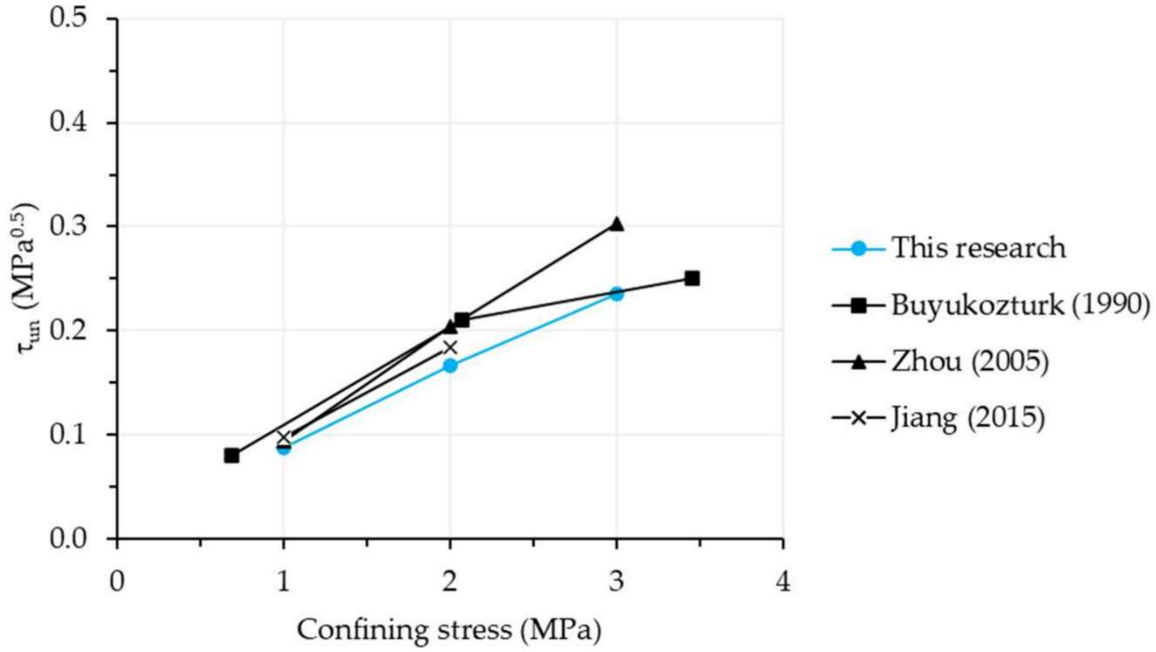

Figure 8.1.20 - Maximum normalized shear stress in flat dry joints obtained for specimens from ordinary (black lines) [13,30,40] and RAC (blue line).

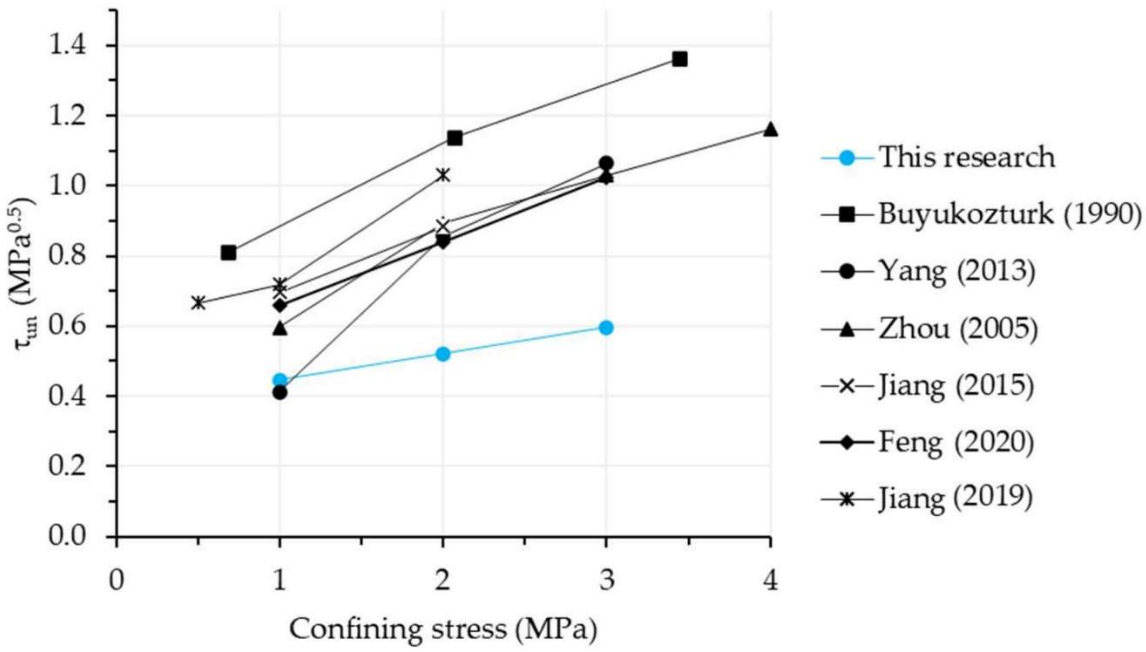

Figure 8.1.21 - Maximum normalized shear stress in single-keyed dry joints obtained for specimens from ordinary (black lines) [13,30,40,41,43,44] and RAC (blue line).

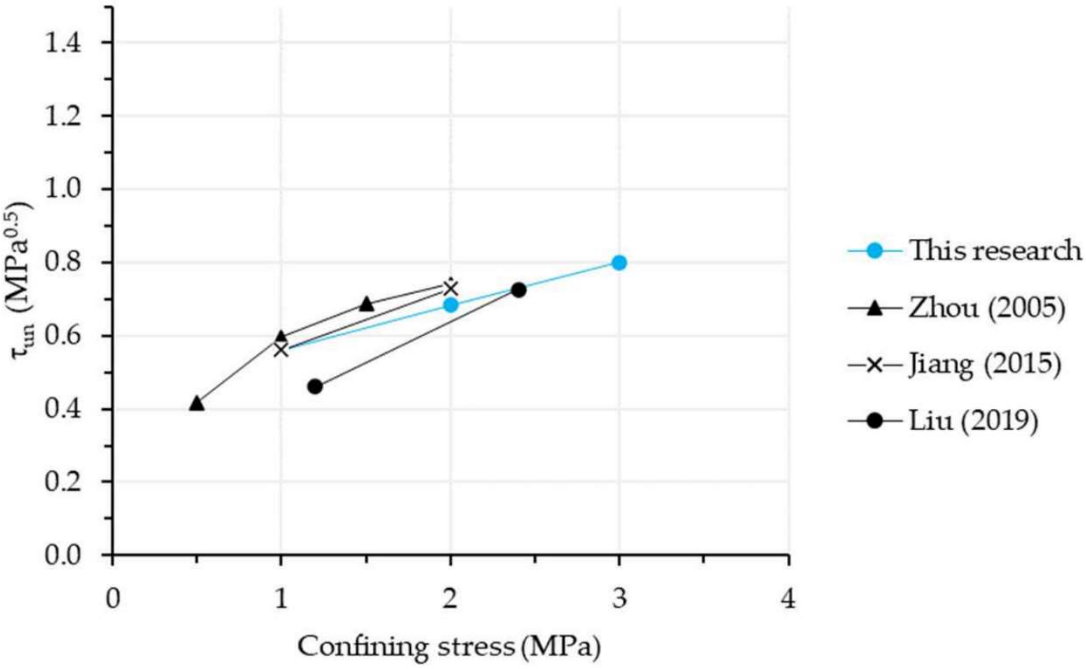

Figure 8.1.22 - Maximum normalized shear stress in three-keyed dry joints obtained for specimens from ordinary (black lines) [30,40,42] and RAC (blue line).

For flat joints, the results showed that dry joints of concrete with recycled coarse aggregates showed strengths close to those of conventional concrete. The shear plane area of smooth joints has been observed to vary between studies; however, Figure 8.1.20 reveals that this has had minimal effect on the comparison of results, as values have remained consistent between both types of concrete. This can be attributed to the similar friction coefficient of RAC and conventional concrete.

The results showed that the single-keyed dry joints with recycled coarse aggregate concrete presented the lowest maximum normalized shear stress values. The comparison of the results obtained from the key joints with those of the smooth joints, as seen in Figure 8.1.21, demonstrates a greater difference. This implies that the monolithic region of the key exhibits an increased contribution to the shear resistance of the joints, with the RAC concrete joints exhibiting the lowest values due to their lower resistance. In the three-keyed joints, the difference between the results was minor compared to the single-keyed joints; presenting even similar values, studies have found that in multi-key joints, the rupture sequence of the keys does not allow for the full resistance of all of the keys together, which results in values obtained from a break that are not equal to three times the values of single-key joints. This rupture sequence of the keys, however, does allow for RAC joints to reach values close to those of conventional concrete joints.

8.1.4.8 Equations for Predicting the Strength of RAC Dry Joints

Using Equations (1)–(8) for predicting the strength of RAC dry joints in terms of (τun), it can be seen in Figure 8.1.23 and Figure 8.1.24 that the most suitable equations for predicting single-keyed RAC dry joints were those of Turmo et al. [20], Rombach and Specker [19], and EUROCODE 2 [24]. The three-keyed RAC dry joints were Turmo et al. [20] and EUROCODE 2 [24].

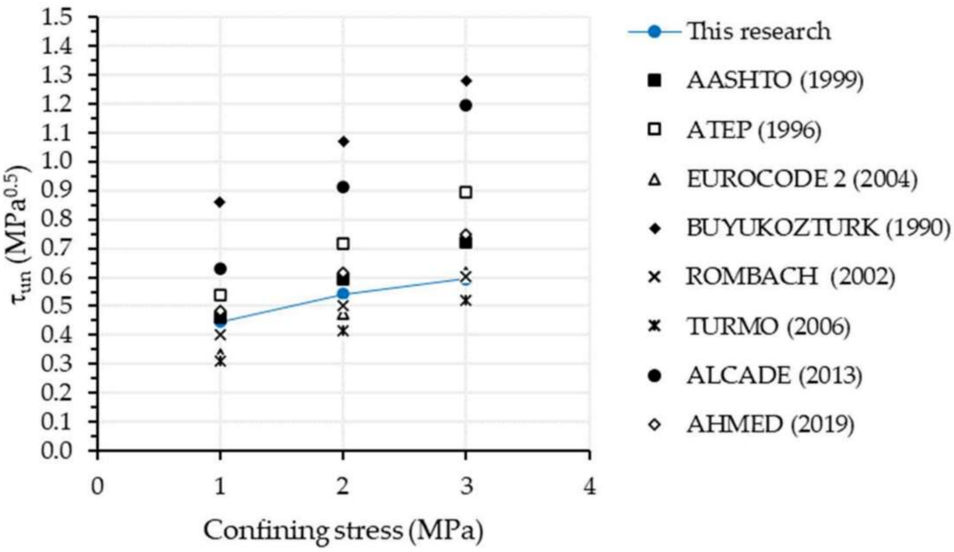

Figure 8.1.23 - Experimental results and prediction of maximum normalized shear stress of the single-keyed RAC dry joints using the equations in the literature [13,18,19,20,21,22,23,24].

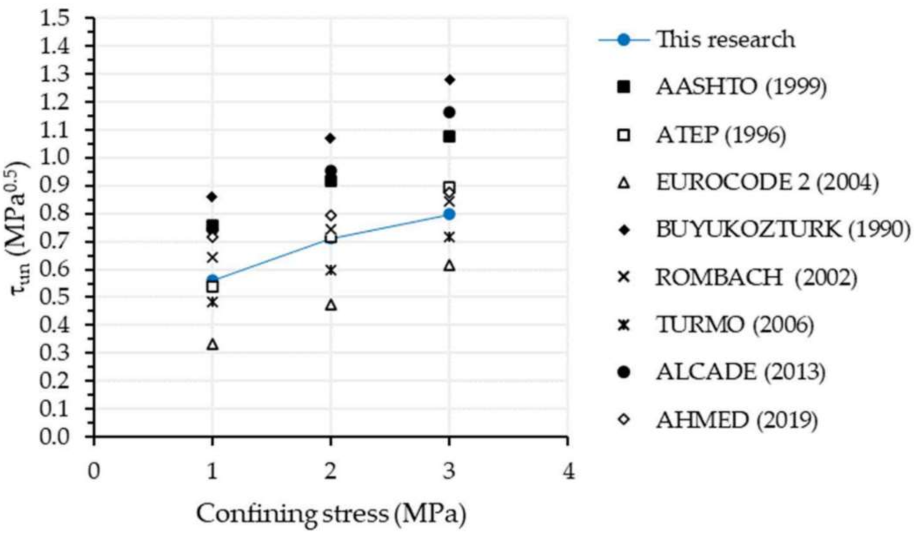

Figure 8.1.24 - Experimental results and prediction of maximum normalized shear stress of the three-keyed RAC dry joints using the equations in the literature [13,18,19,20,21,22,23,24].

The EUROCODE 2 equation has been formulated for calculating the shear resistance between concrete surfaces produced at different times. The coefficients proposed by the standard for indented interfaces (c = 0.50 and μ = 0.9) were adopted for predicting the resistance of dry joints. Nevertheless, the equation has been observed to present conservative values in contrast to the equations of Turmo et al. [20] and Rombach and Specker [19], which were specifically developed for calculating the resistance of dry joints.

Table 8.1.11 shows the relationship between the (τun) predicted by the equations in the literature and the experimental one.

Table 8.1.11 - Relationship between maximum normalized shear stress predicted by the literature equations and experimental results.

Specimens	AASHTO [1]	ATEP [2]	EUR [3]	BUYU [4]	ROMB [5]	TURM [6]	ALCA [7]	AHMD [8]
CPR-1-1.0	1.04	1.21	0.75	1.92	0.90	0.70	1.41	1.09
CPR-1-2.0	1.09	1.32	0.88	1.97	0.93	0.77	1.68	1.14
CPR-1-3.0	1.21	1.50	1.03	2.15	1.01	0.88	2.01	1.26
CPR-3-1.0	1.35	0.97	0.60	1.53	1.15	0.86	1.33	1.28
CPR-3-2.0	1.29	1.01	0.67	1.50	1.05	0.84	1.34	1.12
CPR-3-3.0	1.35	1.12	0.77	1.61	1.06	0.90	1.46	1.10

The normative equation of AASHTO [21] predicts with good approximation the strength of single-keyed RAC dry joint for low confining stresses; however, as the confining stress increases, the experimental results diverge from the prediction, as can be seen in Figure 8.1.25. The experimental results showed significantly different values for predicting RAC dry joints with three keys of the prediction of the normative equation.

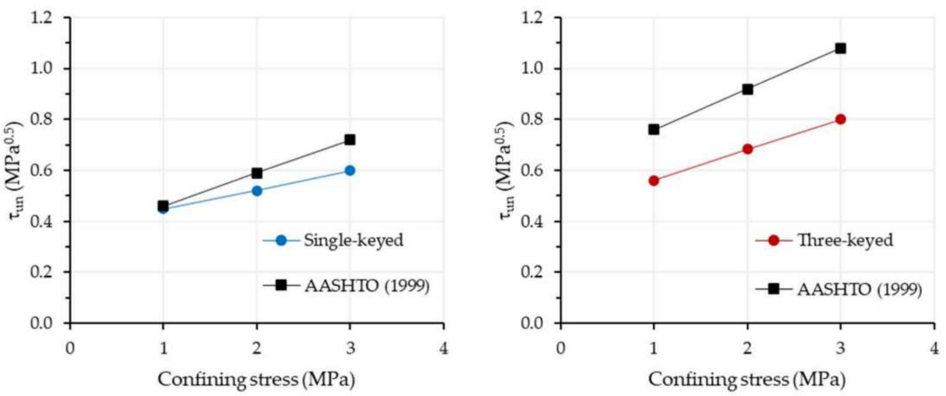

Figure 8.1.25 - Experimental results and prediction of maximum normalized shear stress by AASHTO [21].

Therefore, the authors recommend using a reduction coefficient of 0.7 for the equation of AASHTO in predicting the shear strength of recycled coarse aggregate concrete dry joints.

8.1.5 Conclusions

In this research, twenty-seven dry joint specimens produced with concrete from recycled coarse aggregates were subjected to push-off tests to study their shear strength. The variable parameters were the number of keys (flat, single-keyed, and three-keyed) and the magnitude of the confining stress (1.0, 2.0, and 3.0 MPa). The analysis of the results was performed using the digital image correlation method. It was possible to verify the relative vertical displacement between both parts of the joint and the cracking kinetics. Finally, the prediction of the literature equations for dry joints produced with recycled coarse aggregates concrete was verified. The results enabled the following conclusions:

- The dry joints produced with recycled coarse aggregates concrete showed similar behavior during the push-off test as those produced with conventional concrete. The failure of RAC joints was caused by the formation of a crack at the base of the shear keys, at an angle of approximately 45 degrees to the horizontal plane. With increasing load, additional cracks appeared in the shear plane of the keys, leading to the ultimate rupture when the cracks cut through the key. The cracking of single-keyed dry joint specimens with recycled coarse aggregates concrete followed model 2 as presented by Jiang et al. [30]. The cracking of the three-keyed dry joint specimens with recycled coarse aggregates concrete showed the cracking pattern in a sequence of the shear keys, as seen in previous work;
- The normalized shear strength of dry joints with recycled coarse aggregates concrete was lower when compared to the results of other researchers obtained with conventional concrete. The results of this study indicate that, although RAC concrete is less resistant than conventional concrete, its load versus vertical slip curves display similar trends. Furthermore, a reduction in the normalized shear stress was observed for smooth joints, with decreases of 10%, 18%, and 22% for the confining stresses of 1.0, 2.0, and 3.0 MPa, respectively. Single-key joints exhibited a greater reduction, with decreases of 38%, 49%, and 44%. The three-

keys joints showed the least difference between results, with reductions of 6% and 8% for the confining stresses of 1.0 and 2.0 MPa, respectively. This is likely due to the rupture effect in sequence of the keys, which does not permit the full strength of the keys in the joint;

- The confining stress proved an essential resistance mechanism for dry joints with recycled coarse aggregate concrete. When the confinement stress of the smooth joints was increased from 1.0 MPa to 2.0 MPa, the strength gain was 88.89%, and from 2.0 MPa to 3.0 MPa, it was 35.29%. For the joint with keys, when the confinement stress was increased from 1.0 MPa to 2.0 MPa, the strength gain was 15.56% for one key and 21.43% for three keys. Furthermore, when the confinement stress increased from 2.0 MPa to 3.0 MPa, the strength gain was 15.38% for one key and 17.65% for three keys;
- The number of keys influenced the resistance of the dry joints, and its increase was beneficial for the final resistance of the joint. When the number of keys increased from none to single-keyed, the strength gain was 400%, 205.88%, and 160.87% for the confining stresses of 1.0, 2.0, and 3.0 MPa, respectively. When the number of keys increased from single-keyed to three-keyed, the strength gain was 24.44%, 30.77%, and 33.33% for the confining stresses of 1.0, 2.0, and 3.0 MPa, respectively;
- Equations of the literature used to predict the maximum load on dry joints with recycled coarse aggregates concrete showed safe values. The results showed that for single-keyed RAC dry joints, the equations of Turmo et al. [20], Rombach and Specker [19], and EUROCODE 2 [24] provided conservative values, while for the three-keyed RAC dry joints were those of Turmo et al. [20] and EUROCODE 2 [24];
- The normative equation of AASHTO [21] satisfactorily predicted the strength of the single-keyed dry joint with recycled coarse aggregates concrete for the confining stress of 1.0 MPa; however, as the confining stress increased, the experimental results deviated from the forecast. For joints with three keys, the experimental results showed values far from the normative prediction;
- The authors recommend the consideration of a minimization coefficient in the AASHTO [21] normative equation in the value of 0.7 for the prediction of recycled coarse aggregates concrete dry joints.

In this study, the behavior of dry joints produced with recycled coarse aggregate concrete was found to be comparable to that of conventional concrete joints in terms of rupture and cracking mode. The application of this material in dry joints of prestressed segmental bridges was further reinforced through the use of a reduction coefficient in the AASHTO normative equation (0.7). Further studies are required, including an analysis of the bending effort exerted on dry joints due to moments in the bridge abutment, an evaluation of the mechanical behavior of RAC concrete dry joints with varying percentages of aggregate substitution, and an investigation into the behavior of the joints with increased shear keys.

8.1.6 Funding

This research was funded by Carlos Chagas Filho Foundation for Research Support of the State of Rio de Janeiro (FAPERJ).

8.1.7 discussion of Chapter 8.1

8.1.7.1 Key Findings

The experimental results indicated that RAC dry joint keys exhibit shear behavior that is comparable to, but slightly different from, that of traditional concrete joints. The differences in performance are primarily due to the inherent variability in the properties of recycled aggregates, such as differences in particle size distribution, strength, and durability. Despite these challenges, the study demonstrated that with appropriate design modifications, such as optimizing the mix design and joint geometry, RAC can be used effectively in structural applications. This finding is significant as it supports the use of recycled materials in construction, contributing to sustainability goals without sacrificing structural integrity.

8.1.7.2 Implications

The implications of these findings are particularly relevant in the context of sustainable construction. As the construction industry seeks to reduce its environmental footprint, the use of recycled materials like RAC becomes increasingly important. This study provides evidence that RAC can be a viable alternative to traditional concrete in certain structural applications, such as dry joints keys, provided that its unique properties are properly managed. The findings could encourage wider adoption of RAC in the industry, promoting the development of more sustainable construction practices. Additionally, the research highlights the need for updated design guidelines that account for the specific characteristics of recycled materials, ensuring their safe and effective use in structural applications.

8.1.7.3 Limitations

While the study offers promising results, there are some limitations that should be considered. The performance of RAC dry joint keys was evaluated under specific conditions, which may not encompass the full range of environmental and loading scenarios encountered in real-world applications. Additionally, the variability in the quality of recycled aggregates, depending on the source and processing methods, could affect the generalizability of the results. Further research is needed to explore the long-term performance of RAC in various conditions and to develop standardized methods for assessing the quality and suitability of recycled aggregates for structural use.

8.1.7.4 Future Work

Future research could focus on refining the mix design of RAC to further enhance its performance in structural applications. This could include exploring the use of additives or supplementary materials to improve the consistency and strength of RAC. Additionally, studies that investigate the long-term durability and performance of RAC in different environmental conditions, such as exposure to freeze-thaw cycles or corrosive environments, would provide valuable insights. Finally, expanding the research to include other structural applications of RAC, such as in beams, slabs, or load-bearing walls, could broaden the understanding of its potential in sustainable construction.

8.1.8 conclusion for Chapter 8.1

This chapter explored the shear behavior of recycled coarse aggregates concrete (RAC) dry joints keys, a topic of growing importance in the context of sustainable construction. The study found that while RAC dry joint keys can perform adequately, there are specific design considerations that must be taken into account to ensure their performance matches or exceeds that of traditional concrete joints. These findings contribute to the broader effort to incorporate sustainable materials into structural applications without compromising on safety or performance. The research highlights the potential of RAC as a viable material for structural applications, provided that its unique characteristics are properly accounted for in design.

The findings in this chapter highlight the potential for RAC to replace traditional materials in certain applications, provided that design modifications are made. Extending this exploration, the next chapter introduces a predictive model tailored to assess the strength of RAC in critical infrastructure applications.

8.1.9 references for chapter 8.1

[1] Cantero, B.; Bravo, M.; Brito, J.; Sáez del Bosque, I.F.; Medina, C. Mechanical Behaviour of Structural Concrete with Ground Recycled Concrete Cement and Mixed Recycled Aggregate. J. Clean. Prod. 2020, 275, 122913. [Google Scholar] [CrossRef].

[2] Pani, L.; Francesconi, L.; Rombi, J.; Mistretta, F.; Sassu, M.; Stochino, F. Effect of Parent Concrete on the Performance of Recycled Aggregate Concrete. Sustainability 2020, 12, 9399. [Google Scholar] [CrossRef].

[3] Naouaoui, K.; Bouyahyaoui, A.; Cherradi, T. Experimental Characterization of Recycled Aggregate Concrete. MATEC Web Conf. 2019, 303, 05004. [Google Scholar] [CrossRef] [Green Version].

[4] Liu, B.; Feng, C.; Deng, Z. Shear Behavior of Three Types of Recycled Aggregate Concrete. Constr. Build. Mater. 2019, 217, 557–572. [Google Scholar] [CrossRef].

[5] Patil, S.V.; Rao, K.B.; Nayak, G. Influence of Silica Fume on Mechanical Properties and Microhardness of Interfacial Transition Zone of Different Recycled Aggregate Concretes. Adv. Civ. Eng. Mater. 2021, 10, 412–426. [Google Scholar] [CrossRef].

[6] Silva, R.V.; Brito, J. Reinforced Recycled Aggregate Concrete Slabs: Structural Design Based on Eurocode 2. Eng. Struct. 2020, 204, 110047. [Google Scholar] [CrossRef].

[7] Chen, J.; Zhou, Y.; Yin, F. A Practical Equation for the Elastic Modulus of Recycled Aggregate Concrete. Buildings 2022, 12, 187. [Google Scholar] [CrossRef].

[8] Khatab, M.A.T.; Altmami, M. Correlation between Different Properties of Recycled Aggregate and Recycled Aggregate Concrete. AIP Conf. Proc. 2019, 2146, 020005. [Google Scholar] [CrossRef].

[9] Meddah, M.S.; Al-Harthy, A.; Ismail, M.A. Recycled Concrete Aggregates and Their Influences on Performances of Low and Normal Strength Concretes. Buildings 2020, 10, 167. [Google Scholar] [CrossRef].

[10] Lavado, J.; Bogas, J.; de Brito, J.; Hawreen, A. Fresh Properties of Recycled Aggregate Concrete. Constr. Build. Mater. 2020, 233, 117322. [Google Scholar] [CrossRef].

[11] Feng, W.; Tang, Y.; Yang, Y.; Cheng, Y.; Qiu, J.; Zhang, H.; Isleem, H.F.; Tayeh, B.A.; Namdar, A. Mechanical Behavior and Constitutive Model of Sustainable Concrete: Seawater and Sea-Sand Recycled Aggregate Concrete. Constr. Build. Mater. 2023, 364, 130010. [Google Scholar] [CrossRef].

[12] Birkeland, P.W.; Birkeland, H.W. Connections in Precast Concrete Construction. ACI J. Proc. 1966, 63, 345–368. [Google Scholar] [CrossRef].

[13] Buyukozturk, O.; Bakhoum, M.M.; Beattie, S.M. Shear Behavior of Joints in Precast Concrete Segmental Bridfes. J. Struct. Eng. 1990, 116, 3380–3401. [Google Scholar] [CrossRef].

[14] Xiao, J.; Sun, C.; Lange, D.A. Effect of Joint Interface Conditions on Shear Transfer Behavior of Recycled Aggregate Concrete. Constr. Build. Mater. 2016, 105, 343–355. [Google Scholar] [CrossRef].

[15] ACI 213R–03; Guide for Structural Lightweight-Aggregate Concrete. ACI Concrete Institute: Farmington Hills, MI, USA, 2014..

[16] Greene, G.; Graybeal, B. Lightweight Concrete: Mechanical Properties; Report No. Federal Highway Administration-HRT-13-062; McLean: Washington, DC, USA, 2013. [Google Scholar].

[17] Greene, G.; Graybeal, B. Lightweight Concrete: Shear Performance; Report No. Federal Highway Administration-HRT-15-022; McLean: Washington, DC, USA, 2015. [Google Scholar].

[18] Ahmed, G.H.; Aziz, O.Q. Shear Strength of Joints in Precast Posttensioned Segmental Bridges during 1959–2019, Review and Analysis. Structures 2019, 20, 527–542. [Google Scholar] [CrossRef].

[19] Rombach, G.; Specker, A. Design of Joints in Segmental Hollow Box Girder Bridges. In Proceedings of the 1st FIB Kongress, Osaka, Japan, 13–19 October 2002; pp. 1–6. [Google Scholar].

[20] Turmo, J.; Ramos, G.; Aparicio, A.C. Resistencia de Juntas Secas Conjugadas de Puentes de Dovelas Prefabricadas de Hormigón: Propuesta Para El Eurocódigo 2. Mater. Constr. 2006, 56, 45–52. [Google Scholar] [CrossRef].

[21] AASHTO. Guide Specifications for Design and Construction of Segmental Concrete Bridges; AASHTO GSCB: Washington, DC, USA, 1999. [Google Scholar].

[22] Alcalde, M.; Cifuentes, H.; Medina, F. Influencia Del Número de Llaves En La Resistencia a Cortante de Juntas Secas Postensadas. Mater. Constr. 2013, 63, 297–307. [Google Scholar] [CrossRef] [Green Version].

[23] ATEP Proyecto y Construcción de Puentes y Estructuras Con Pretensado Exterior. Col. Ing. Caminos, Canales y Puertos, Madrid. 1996. H.P.10-96 vol E-6. Available online: https://books.google.co.jp/books/about/Proyecto_y_construcci%C3%B3n_de_puentes_y_es.html?id=l_QDPgAACAAJ&redir_esc=y (accessed on 1 March 2023).

[24] EN 1992-1-1:2004; EUROCODE 2 Design of Concrete Structures—Part 1-1: General Rules and Rules for Buildings. European Commission: Brussels, Belgium, 2004.

[25] Fonteboa, G.; Martínez, F.; Carro, D.; Eiras, J. Cortante-Fricción de Los Hormigones Reciclados. Mater. Constr. 2010, 60, 53–67. [Google Scholar] [CrossRef] [Green Version].

[26] Xiao, J.; Xie, H.; Yang, Z. Shear Transfer across a Crack in Recycled Aggregate Concrete. Cem. Concr. Res. 2012, 42, 700–709. [Google Scholar] [CrossRef].

[27] Rahal, K. Shear Strength of Recycled Aggregates Concrete. Procedia Eng. 2017, 210, 105–108. [Google Scholar] [CrossRef].

[28] Trindade, J.; Garcia, S.; Fonseca, G. Experimental Study of Direct Shear in Concrete with Recycled Aggregate. ACI Struct. J. 2020, 17, 233–243. [Google Scholar].

[29] Trindade, J.; Garcia, S.L.; Torres, H. Shear Strength of Concrete with Recycled Aggregates Reinforced with Steel Fibers. ACI Mater. J. 2021, 118, 185–198. [Google Scholar] [CrossRef].

[30] Jiang, H.; Chen, L.; Ma, Z.J.; Feng, W. Shear Behavior of Dry Joints with Castellated Keys in Precast Concrete Segmental Bridges. J. Bridg. Eng. 2015, 20, 1–12. [Google Scholar] [CrossRef].

[31] ABNT NBR 11578:1991; Cimento Portland Composto. ABNT: São Paulo, Brazil, 1991.

[32] ABNT NBR NM 52; Agregado Miúdo—Determinação Da Massa Específica e Massa Específica Aparente. ABNT: São Paulo, Brazil, 2003.

[33] ABNT NBR NM 53; Agregado Graúdo—Determinação de Massa Específica, Massa Específica Aparente e Absorção de Água. ABNT: São Paulo, Brazil, 2002.

[34] EN 1097-1:2011; Ensayos Para Determinar Las Propriedades Mecánicas y Físicas de Los Áridos. Asociación Española de Normalización y Certificación: Madrid, Spain, 2011.

[35] Bazuco, R.S. Utilização de Agregados Reciclados de Concreto Para a Produção de Novos Concretos. Master's Thesis, Universidade Federal de Santa Catarina, Florianópolis, Brazil, 1999. [Google Scholar].

[36] ABNT NBR 5739; Concreto—Ensaio de Compressão de Corpos de Prova Cilíndricos. ABNT: São Paulo, Brazil, 2018.

[37] ABNT NBR 7222; Concreto e Argamassa—Determinação Da Resistência à Tração Por Compressão Diametral de Corpos de Prova Cilíndricos. ABNT: São Paulo, Brazil, 2011.

[38] ABNT NBR 8522; Concreto—Determinação Dos Módulos Estáticos de Elasticidade e de Deformação à Compressão. ABNT: São Paulo, Brazil, 2017.

[39] ABNT NBR 9778; Argamassa e Concreto Endurecidos—Determinação Da Absorção de Água, Índice de Vazios e Massa Específica. ABNT: São Paulo, Brazil, 2009.

[40] Zhou, X.; Mickleborough, N.; Li, Z. Shear Strength of Joints in Precast Concrete Segmental Bridges. ACI Struct. J. 2005, 102, 901–904. [Google Scholar].

[41] Yang, I.H.; Kim, K.C.; Kim, Y.J. Shear Strength of Dry Joints in Precast Concrete Modules. In Proceedings of the 13th East Asia-Pacific Conference on Structural Engineering and Construction, EASEC-13, Sapporo, Japan, 11–13 September 2013. [Google Scholar].

[42] Liu, T.; Wang, Z.; Guo, J.; Wang, J. Shear Strength of Dry Joints in Precast UHPC Segmental Bridges: Experimental and Theoretical Research. J. Bridg. Eng. 2019, 24, 04018100. [Google Scholar] [CrossRef].

[43] Feng, J.; Liang, W.; Jiang, H.; Huang, C.; Zhang, J. Shear Performance of Single-Keyed Dry Joints between Reactive Power Concrete and High Strength Concrete in Push-off Tests. Sci. Prog. 2020, 103, 1–27. [Google Scholar] [CrossRef].

[44] Jiang, H.; Feng, J.; Liu, A.; Liang, W.; Tan, Y.; Liang, H. Effect of Specimen Thickness and Coarse Aggregate Size on Shear Strength of Single-Keyed Dry Joints in Precast Concrete Segmental Bridges. Struct. Concr. 2019, 20, 955–970. [Google Scholar] [CrossRef].

[45] 3D Metrology GOM Correlate 2020; Precise Industrial: Rockwood, TN, USA, 2020.

[46] Tang, Y.; Huang, Z.; Chen, Z.; Chen, M.; Zhou, H.; Zhang, H.; Sun, J. Novel Visual Crack Width Measurement Based on Backbone Double-Scale Features for Improved Detection Automation. Eng. Struct. 2023, 274, 115158. [Google Scholar] [CrossRef].

[47] Que, Y.; Dai, Y.; Ji, X.; Kwan Leung, A.; Chen, Z.; Tang, Y.; Jiang, Z. Automatic Classification of Asphalt Pavement Cracks Using a Novel Integrated Generative Adversarial Networks and Improved VGG Model. Eng. Struct. 2023, 277, 115406. [Google Scholar] [CrossRef].

8.2 RECYCLED AGGREGATE CONCRETE IN BRIDGE DRY JOINTS: A NOVEL APPROACH FOR STRENGTH PREDICTION

This chapter is in publishment as an article in Engineering Sustainability.

PIEROTT, Rodrigo et al. Recycled Aggregate Concrete in Bridge Dry Joints: A Novel Approach for Strength Prediction. In: **Engineering Sustainability**.

Section 8.2 presents a novel approach for predicting the strength of recycled aggregate concrete in bridge dry joints. This chapter builds on the previous discussions of RAC's material properties by developing a robust predictive model that supports the integration of sustainable materials into large-scale infrastructure projects.

Abstract: This study delves into the application of Recycled Aggregate Concrete (RAC) in prestressed segmental bridges, with a focus on evaluating its mechanical properties in essential joint areas. Analyzing 27 dry joint specimens, it uncovers the comparative reduction in shear strength of RAC, especially in single-keyed joints, against traditional concrete. Incorporating machine learning techniques such as Linear Regression and Random Forest, the research successfully develops an innovative predictive model that accurately estimates RAC's load capacity in bridge constructions. This model, tailored to RAC's distinctive characteristics, signifies a leap forward in sustainable construction, marrying advanced data analytics with practical engineering to enhance RAC's effectiveness in pivotal structural roles.

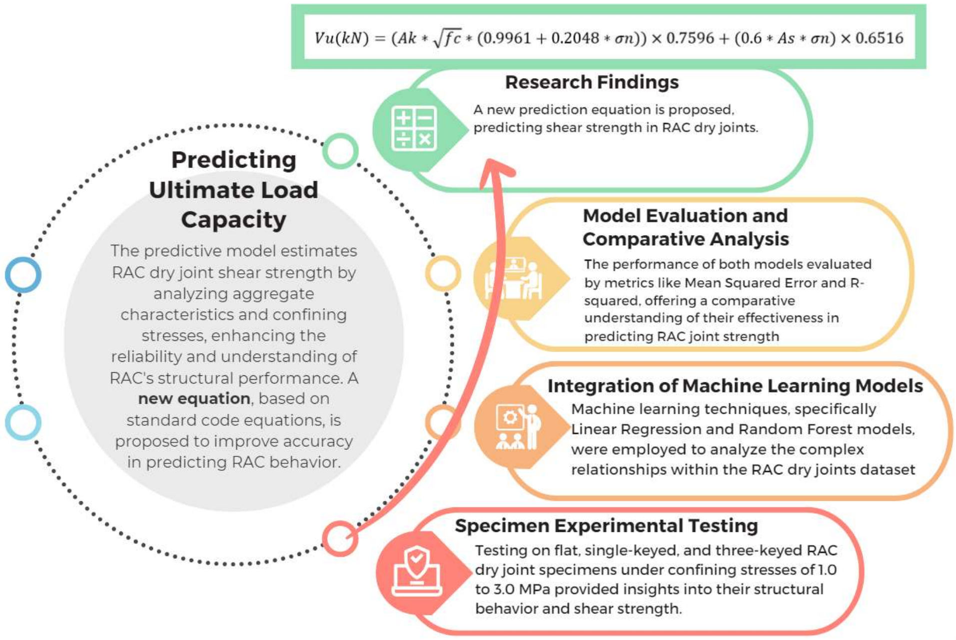

Keywords:
Dry Joints; Recycled Aggregates Concrete; Shear Strength; Machine Learning in Civil Engineering; Regression Modeling; Compressive Strength Prediction.

8.2.1 INTRODUCTION

The construction industry is undergoing significant changes, driven by the urgent need to protect the environment and manage resources more wisely. Traditionally, this industry has had a considerable environmental impact through activities like quarrying for concrete aggregates, which disrupts habitats and contribute to pollution. As highlighted by (Cantero et al., 2020), current research is increasingly focused on sustainable materials, with Recycled Aggregate Concrete (RAC) playing a central role (Pani et al., 2020)(Pani et al., 2020)(Pani et al., 2020)(Pani et al., 2020). RAC, which repurposes debris from construction and demolition, reduces the demand for new aggregates and minimizes waste.

However, RAC presents challenges due to the variability in recycled aggregates, particularly regarding their water absorption and mass, which are influenced by the mortar attached to the aggregates (NAOUAOUI et al., 2019)(NAOUAOUI et al., 2019)(NAOUAOUI et al., 2019)(NAOUAOUI et al., 2019). This variability leads to a weaker transition zone between the mortar and aggregates, resulting in a higher water-to-cement ratio and a subsequent decrease in the overall strength of the concrete (Chen et al., 2022; Khatab & Altmami, 2019)(Chen et al., 2022; Khatab & Altmami, 2019)(Chen et al., 2022; Khatab & Altmami, 2019)(Chen et al., 2022; Khatab & Altmami, 2019). These challenges are particularly pronounced in prestressed segmental bridges, where the mechanical prop-erties of RAC are critical, especially in the shear keys that connect the bridge segments.

Recent advancements have shown that innovative RAC mixtures, such as those using coarse recycled aggregates from electric arc furnace slags, can achieve similar compressive and tensile strengths to conventional concrete, making RAC a viable alternative for sustainable construction (Tamayo et al., 2019)(Tamayo et al., 2019)(Tamayo et al., 2019)(Tamayo et al., 2019). Moreover, treatment methods like carbonation or acetic acid immersion have been shown to enhance RAC's mechanical behavior, improving tensile and flexural strength (Kazmi et al., 2019)(Kazmi et al., 2019)(Kazmi et al., 2019)(Kazmi et al., 2019).

Durability is another crucial factor, especially under conditions like freeze-thaw and wet-dry cycles, which can significantly affect the longevity of structures like prestressed segmental bridges (Rangel et al., 2021)(Rangel et al., 2021)(Rangel et al., 2021)(Rangel et al., 2021). Despite these advancements, there is limited research on the performance of RAC in critical structural applications, particularly in the dry joints of prestressed segmental bridges, where shear strength is a primary concern.

While conventional predictive models for joint strength, such as those proposed by (Fonteboa et al., 2010) and (Xiao et al., 2012), have been developed for natural aggregate concrete, these models do not accurately reflect the behavior of RAC, which typically exhibits lower shear strength. This study aims to fill this gap by evaluating the performance of RAC in prestressed segmental bridge joints and developing a predictive model tailored to its unique properties.

Machine learning (ML) techniques, including Linear Regression and Random Forest, are employed to analyze the experimental data, providing a more accurate understanding of RAC's behavior in these critical applications. (Han et al., 2020) discuss an ensemble ML model for predicting the modulus of elasticity, showing higher accuracy than standalone models. Similarly, (Deng et al., 2018) use deep learning for compressive strength prediction, emphasizing efficiency and precision. (Zafar et al., 2020) highlight the effectiveness of the relevance vector machine (RVM) algorithm in predicting RAC strength.

This study employs ML to analyze experimental data, uncovering patterns that traditional statistics might miss. Linear Regression and Random Forest models are used to predict how factors like key area, smooth area, and confinement stress affect RAC's load capacity. The Random Forest model, in particular, excels at handling complex, nonlinear relationships, providing insights into the most critical factors for RAC strength and durability.

These findings contribute to developing a novel predictive model for RAC in prestressed segmental bridges. Shaped by empirical evidence and ML insights, this model offers a more accurate and reliable tool for designing and evaluating RAC in essential structural applications. The forthcoming sections will detail the new equation derived from this analysis, which is expected to significantly impact the field.

Previous studies, such as those by (Rahal, 2017) and (B. Liu et al., 2019a), consistently report decreased shear strength with increased recycled aggregate content. Trindade et al. (2020) further examine how steel fibers can mitigate this loss, though RAC still exhibits lower strength compared to conventional concrete.

This research explores RAC's use in prestressed segmented bridges, focusing on dry joints entirely made of RAC. By examining 27 specimens under varying conditions, this study contextualizes RAC's performance and advances the understanding of its application in structural engineering through the integration of advanced data analytics.

8.2.2 Materials

In the production of concrete for this study, Brazilian cement type CPII-E-32 was used as the primary binder. This cement, adhering to (ABNT NBR 11578:1991, 1991)(ABNT NBR 11578:1991, 1991) standards, is a Portland cement enriched with granulated blast furnace slag, boasting a minimum 28-day compressive strength of 32 MPa.

The concrete compressive strength tests were conducted in accordance with the (ABNT NBR 5739, 2018a) standard, which prescribes the use of cylindrical specimens due to their widespread acceptance in representing concrete behavior under compression.

The selection of fine aggregate was natural quartz sand, sourced from the Paraíba do Sul River in Campos dos Goytacazes, RJ. This sand was characterized by a specific mass of 2.63 g/cm³ and a unit mass of 1.54 g/cm³ in its loose and dry state, as specified by (ABNT NBR NM 52, 2003)(ABNT NBR NM 52, 2003).

For the coarse aggregates, a recycling approach was adopted. These were produced by crushing waste materials from specimens utilized in earlier research, where the original concrete exhibited a compressive strength ranging between 50 and 70 MPa. The process of manufacturing these recycled coarse aggregates is depicted in Figure 8.2.1, and detailed characteristics of these aggregates are provided in Table 8.2.1.

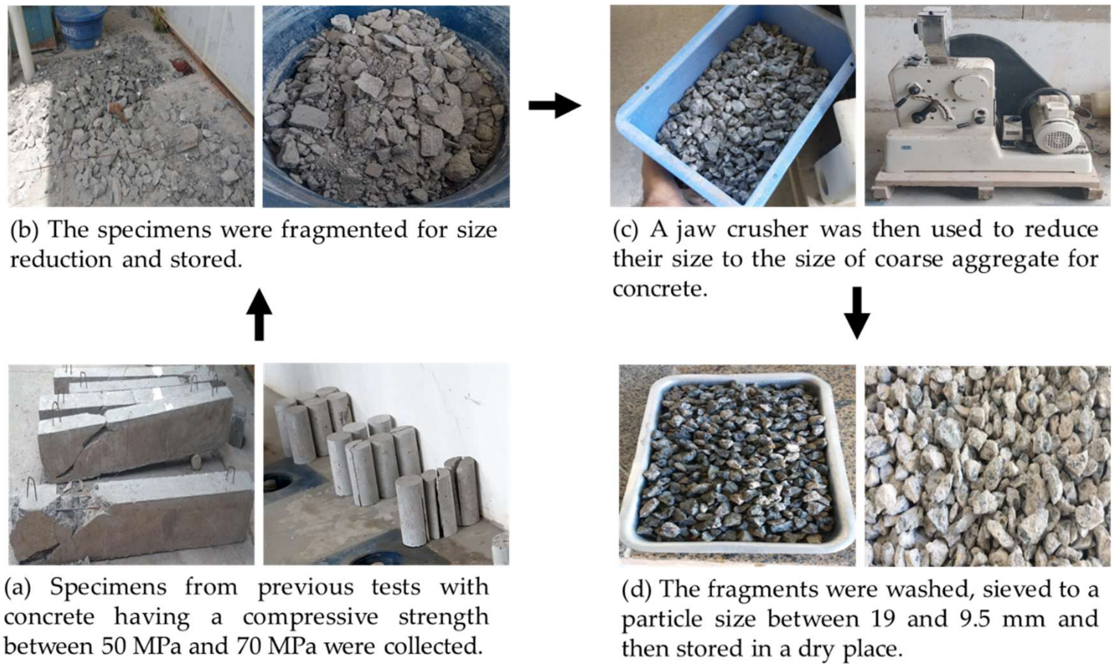

Figure 8.2.1 - Scheme for the production of recycled coarse aggregates (Sousa et al., 2023)(Sousa et al., 2023).

Table 8.2.1 - Physical characteristics of recycled coarse aggregates.

Specific mass (g/cm³) (ABNT NBR NM 53, 2002)(ABNT NBR NM 53, 2002)	**Water absorption (%)** (ABNT NBR NM 53, 2002)(ABNT NBR NM 53, 2002)	**Abrasion Micro-Deval (%)** (EN 1097-1:2011, 2011)(EN 1097-1:2011, 2011)	**Adhered mortar (%) (Adapted from** (Bazuco, 1999)(Bazuco, 1999)**)**
2.31	5.55	13.97	40.0

8.2.2.1 Concrete proportioning

The concrete mix was designed to achieve a target compressive strength of 30 MPa at 28 days. The specific material quantities used in the mix are detailed in Table 2.

Table 8.2.2 - Concrete mixing ratios.

Material	Quantities/m³
Portland Cement CP2-E-32	513.59 kg
Fine aggregate	735.85 kg
Recycled coarse aggregate	904 kg
Water	236.25 l
w/c	0.46

The 28-day compressive strength was measured using cylindrical samples, each with a diameter of 100 mm and height of 200 mm. For this study, the concrete was formulated with a complete replacement (100%) of coarse aggregates by recycled aggregates, while fine aggregates were not replaced. The recycled aggregates were prepared from construction and demolition waste, with the waste materials being approximately 5 to 6 years old. The properties of the recycled aggregate concrete (RAC) utilized in the production of the dry joint specimens are outlined in Table 8.2.3.

Table 8.2.3 - Physics and mechanical characteristics of recycled coarse aggregate concrete.

RAC Properties	Values	Standard Deviation	Coefficient of variation (%)
Compressive strength **(ABNT NBR 5739, 2018)(ABNT NBR 5739, 2018)**	41.52 MPa	6.00 MPa	14.45
Tensile strength **(ABNT NBR 7222, 2011)(ABNT NBR 7222, 2011)**	2.71 MPa	0.21 MPa	7.75
Modulus of Elasticity **(ABNT NBR 8522, 2017)(ABNT NBR 8522, 2017)**	34.65 GPa	5.34 GPa	15.41
Density **(ABNT NBR 9778, 2009)(ABNT NBR 9778, 2009)**	2450 kg/m³	20 kg/m³	0.82
Water absorption **(ABNT NBR 9778, 2009)(ABNT NBR 9778, 2009)**	7.38 %	0.63 %	8.54

8.2.2.2 Details of specimens

Push-off test specimens, designed to study the shear behavior of dry joints with recycled coarse aggregate concrete, were produced in a manner consistent with the approaches used by other researchers (Buyukozturk et al., 1990a; Feng et al., 2020a; Jiang et al., 2015a, 2019a; T. Liu et al., 2019a; Yang et al., 2013a; Zhou et al., 2005a)(Buyukozturk et al., 1990a; Feng et al., 2020a; Jiang et al., 2015a, 2019a; T. Liu et al., 2019a; Yang et al., 2013a; Zhou et al., 2005a). The dimensions and configurations for the flat, single-keyed, and three-keyed dry joint specimens utilized in our experiments are illustrated in Figure 8.2.2.

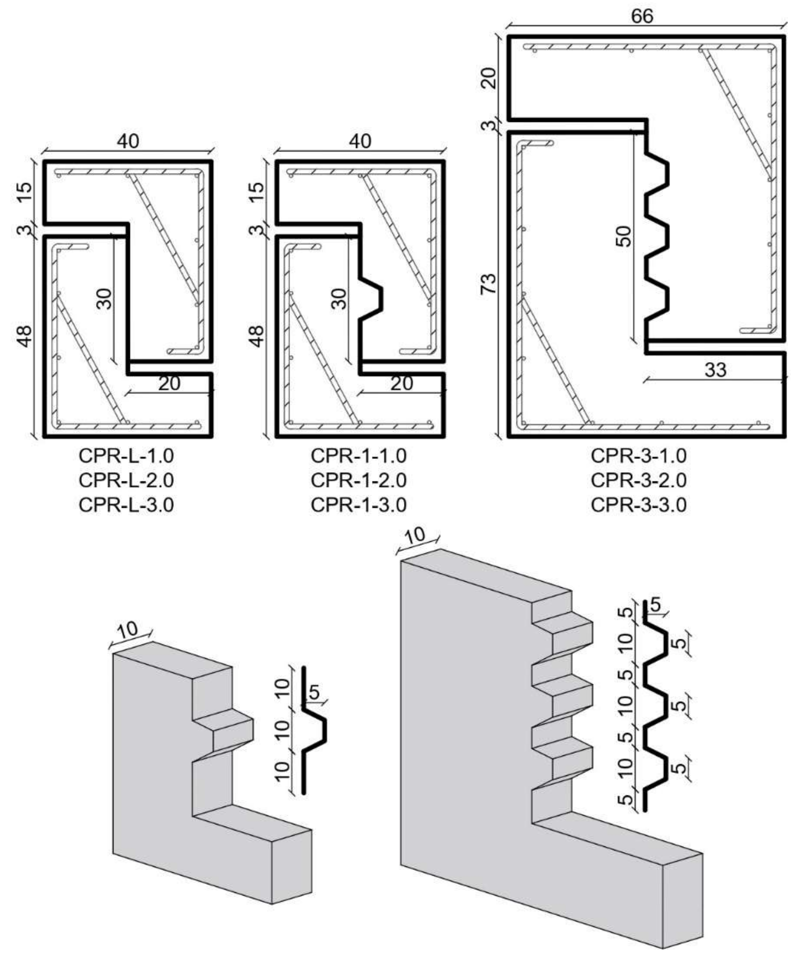

Figure 8.2.2 - Dimensions and geometry of the dry joint specimens (units in cm) (Sousa et al., 2023)

A total of twenty-seven dry joint specimens were fabricated, with the derived results being the average of three specimens for each type. Each specimen had a uniform width of 100 mm. To ensure shear-controlled failure in the keys, reinforcements with a 12 mm diameter were incorporated. The shear plane area of the flat and single-keyed dry joint specimens was 30000 mm², while for the three-keyed specimens, it was 50000 mm².

Details of the dry joint specimens are presented in Table 8.2.4. The adopted nomenclature for the specimens is 'CPR – J – T', where 'CPR' denotes a dry joint specimen made with recycled coarse aggregate concrete, 'J' indicates the joint type (L for Flat, 1 for single-keyed, 3 for three-keyed), and 'T' specifies the applied confining stress (1.0, 2.0, or 3.0 MPa). For instance, the specimen labeled 'CPR2-1-3.0' refers to the second flat joint specimen, single-keyed, subjected to a confining stress of 3.0 MPa. All specimens surfaces were ground using identical procedures to ensure uniformity in surface roughness, which was important for consistent shear testing.

Table 8.2.4 - Summary of the experimental program.

Specimen	Joint type	Shear area (mm^2)	Confining stress (MPa)
CPR-L-1.0	Flat	30000	1.0
CPR-L-2.0			2.0
CPR-L-3.0			3.0
CPR-1-1.0	Single-keyed	30000	1.0
CPR-1-2.0			2.0
CPR-1-3.0			3.0
CPR-3-1.0	Three-keyed	50000	1.0
CPR-3-2.0			2.0
CPR-3-3.0			3.0

8.2.3 Setup and instrumentation

The confining stress levels of 1.0, 2.0, and 3.0 MPa were selected based on their frequent use in studies addressing dry joints (Alcalde et al., 2013b; Jiang et al., 2015a, 2019a; Kassem et al., 2017; Shamass et al., 2015, 2017; Yang et al., 2013a; Zhou et al., 2005a). This confining stress simulates the pressure in the joints generated by the prestressing of the bridge segments.

The push-off rupture tests were conducted using a metallic gantry framework and a model 244.41 hydraulic actuator, linked to an MTS® load cell with a 500 kN capacity. These tests were performed under controlled deformation at a rate of 1 mm/min. The hydraulic unit not only controlled the deformation speed but also recorded the applied load in real-time.

The specimens' confining stress (n) was applied by a system of bars, nuts, and steel plates. The plates had dimensions of 200x300x20 mm and 200x500x20 mm. Applied compressive forces due to reaction forces derived from the bars (F). 2re 10.a presents the scheme for applying forces and generating the confining stress in the confinement system.

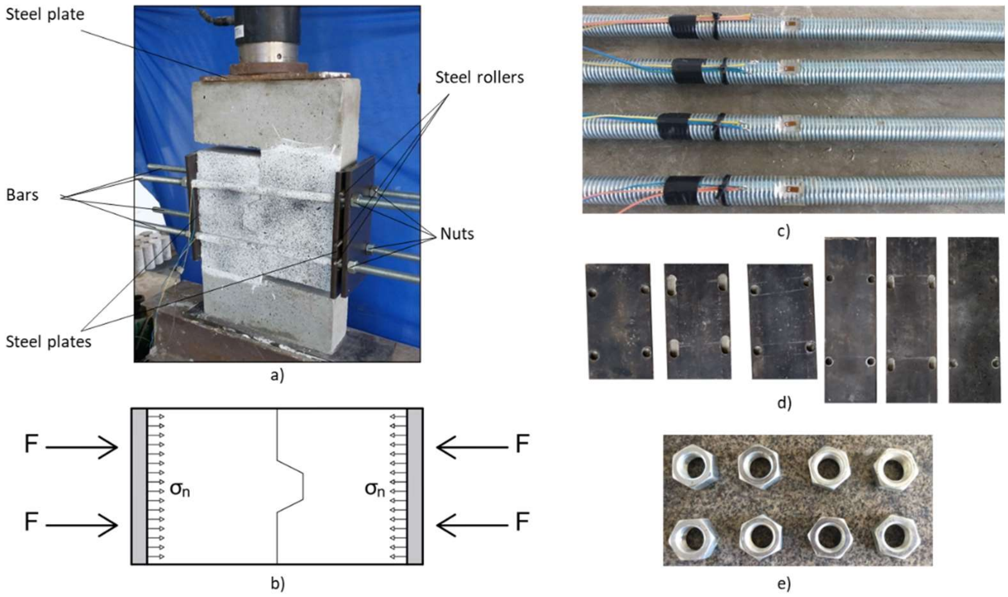

Figure 8.2.3 - a) schematic of the confinement system, b) schematic of the reaction forces, c) steel bars instrumented to generate the reaction force on the plates, d) metal plates used to apply the confinement stress and e) nuts used to deform the steel bars.

Reaction forces were induced by applying deformations to the steel reinforcement bars. These rebars were instrumented with BX120-3AA strain gauges (Figure 8.2.3.c) and monitored in real-time during the tightening of the nuts. To ensure a uniform distribution of stress across the specimens, the plates were drilled to allow the bars to pass through (Figure 8.2.3.b). Additionally, steel rollers were positioned between the adhered plates on the vertically sliding side to facilitate their vertical movement.

The end test criteria established was that the relative slip between the two parts of the specimen should reach 5 mm for smooth joints and 10 mm for keyed joints. This approach enabled the analysis of residual stress in the joint post-failure, which occurred at approximately 10% to 20% of the specified slip.

Applied stresses for the tests were set at 1.0, 2.0, and 3.0 MPa. Table 8.2.7 details the strains needed in the bars to induce the corresponding reaction forces on the plates, for specimens with shear areas of 30000 mm² and 50000 mm². Table 8.2.5 illustrates the required deformation in the threaded bars to achieve specific confining stress levels. The values were calculated based on the relationship between bar deformation and the applied reaction forces necessary to induce the desired confining stress across the shear plane of the specimens.

Table 8.2.5 - Summary of the experimental program.

Confinement stress (MPa)	Deformation in the bar (με)	Reaction force (kN)

1.0	114.71 / 191.18	7.50 / 12.5
2.0	229.41 / 382.35	15.0 / 25.0
3.0	344.12 / 573.53	22.5 / 37.5

The primary input parameters for this study included joint type (flat, single-keyed, three-keyed), applied con-fining stress (1.0, 2.0, 3.0 MPa), and specific concrete properties such as compressive strength and tensile strength. These parameters were selected based on their relevance to the shear performance of RAC in prestressed segmental bridges.

For testing purposes, the distinguishable parameters included the joint configuration and the level of confining stress applied during testing. These parameters were selected because they directly impact the shear strength and failure mode of the RAC joints. By systematically varying these parameters, the study aimed to isolate their effects on the overall structural performance of RAC.

The experimental setup was arranged as follows: Specimens were placed in a fixed position within a metallic frame designed to simulate in-situ conditions. A hydraulic actuator applied a controlled load to the top of the specimen, while confining stress was applied laterally using steel plates and bars. Strain gauges and displacement sensors were positioned at critical points to measure deformation and load response. Figure 8.2.4 provides a schematic representation of the test setup, highlighting the arrangement of these elements.

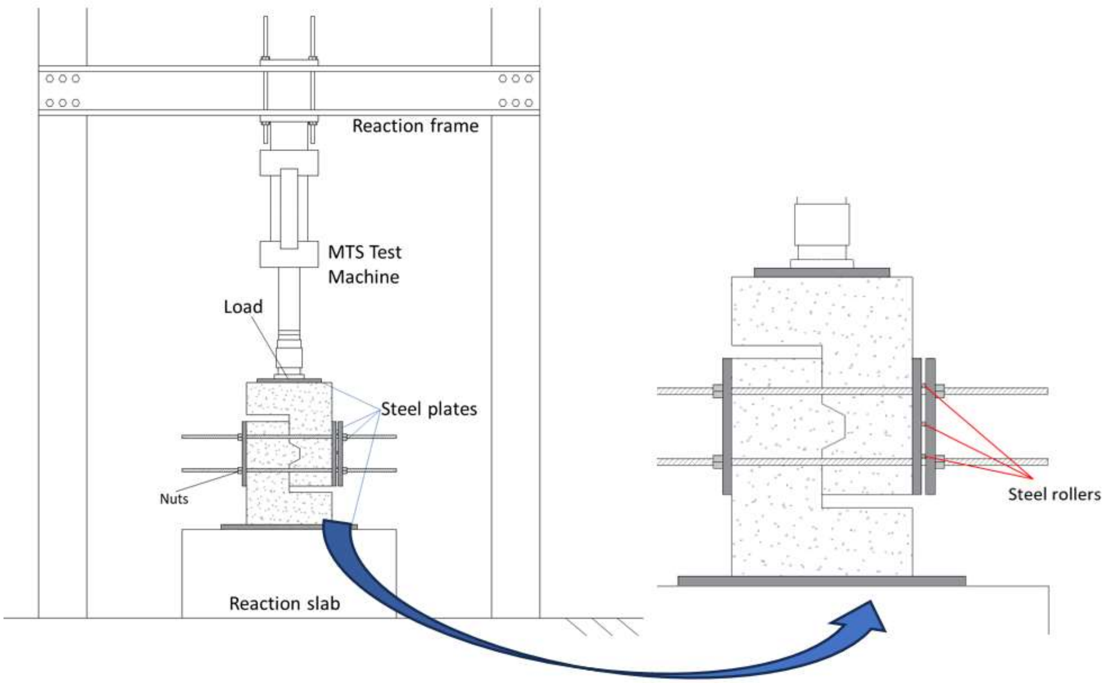

Figure 8.2.4 - Schematic Representation of Experimental Setup for Testing RAC Dry Joints.

The test was concluded upon reaching the failure load, defined as the point where a significant drop in load-bearing capacity was observed, indicating the onset of shear failure in the joint. The two sets of deformation and reaction force values presented in Table 8.2.5 correspond to the specimens with surface areas of 30,000 mm² and 50,000 mm², respectively

8.2.3.1 Machine learning analysis

In this study, a machine learning (ML) technique was employed to enhance the predictive accuracy of models estimating the shear strength of Recycled Aggregate Concrete (RAC) dry joints. The inherent variability in recycled materials presents challenges for traditional analytical methods, but ML excels in identifying patterns and relationships that might not be immediately apparent.

Several ML techniques were considered, with a focus on those capable of managing nonlinear relationships between input variables, such as joint type, confining stress, and concrete properties relating their impact on shear strength. The Random Forest algorithm was ultimately selected for its robustness and ability to handle complex data. As an ensemble learning method, Random Forest constructs multiple decision trees and combines their outputs to improve predictive performance and minimize overfitting.

In this study, the Random Forest algorithm was selected due to its capability to handle complex and nonlinear relationships within the dataset, making it particularly suitable for predicting shear strength in Recycled Aggregate Concrete (RAC) dry joints. The algorithm's ensemble nature, which combines the predictions of multiple decision trees, enhances accuracy and reduces the risk of overfitting, especially when dealing with the variability inherent in recycled materials.

The Random Forest model was trained using the experimental data collected from tests on RAC dry joints. The input variables included joint type (flat, single-keyed, three-keyed), applied confining stress (1.0, 2.0, and 3.0 MPa), and concrete properties (compressive strength, tensile strength, and modulus of elasticity). During the training phase, the model analyzed these inputs to understand their relationship with the observed shear strength outcomes.

The model's predictions were validated against the experimental results to assess its accuracy and robustness. This validation process involved comparing the predicted shear strengths with the actual measured values, demonstrating that the Random Forest model provided highly accurate predictions. Additionally, the algorithm identified the most influential factors affecting the shear strength of RAC dry joints, offering valuable insights into the behavior of these materials under different conditions.

By incorporating the Random Forest algorithm into the analysis, this study was able to capture the complex interactions among the various input variables, leading to more a precise predictions than traditional linear models could offer as presented at the results section.

8.2.3.2 Exploratory data analysis

The Exploratory Data Analysis (EDA) was a critical phase where the dataset was analyzed to uncover patterns and relationships within Recycled Aggregate Concrete (RAC) dry joints. The process began with data preprocessing, which involved cleaning and normalizing the data to ensure its quality for in-depth analysis. We then moved on to descriptive statistics, calculating measures like mean, standard deviation, and range to get a basic understanding of the data's tendencies and variability.

A key part of our EDA was correlation analysis, using Pearson correlation coefficients to explore the strength and direction of relationships between variables. This helped to identify which factors were most strongly associated with the shear strength of RAC dry joints. To visually interpret these relationships and distributions, we employed some graphical techniques, including histograms, box plots, scatter plots, and heatmaps. These visualizations were instrumental in revealing distribution patterns, outliers, and correlations in an intuitive manner.

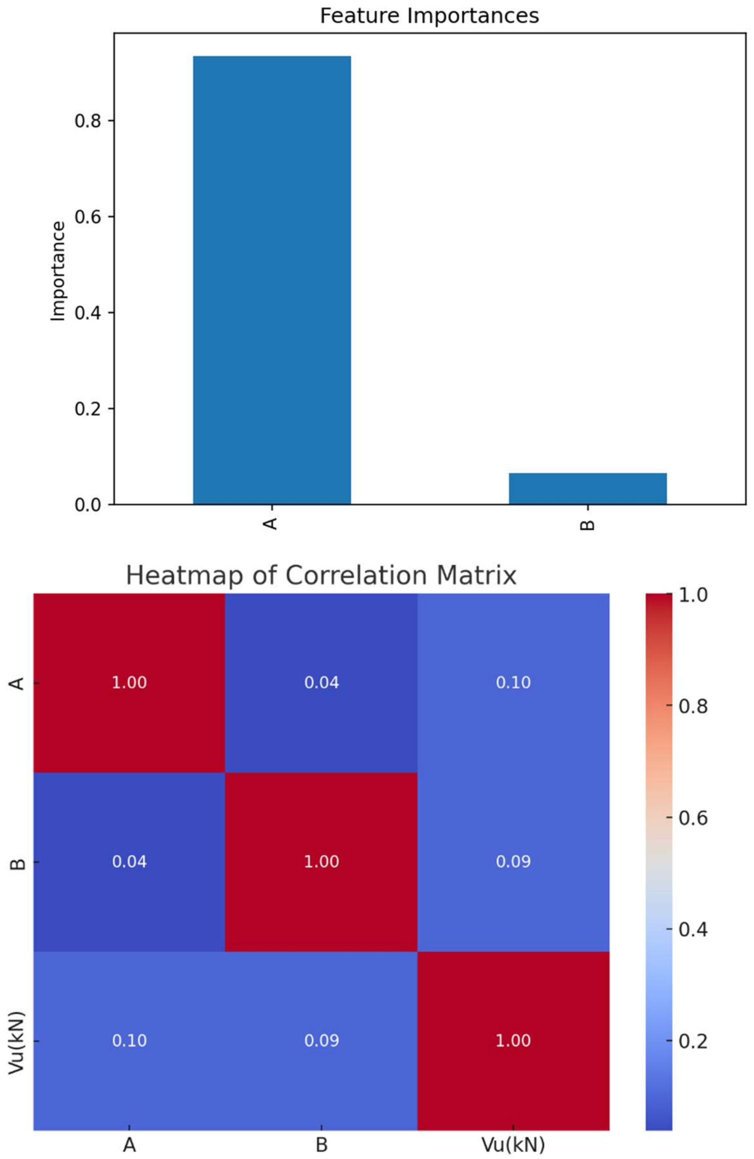

Figure 8.2.5 - (a) Importance analysis and (b) heatmap analysis.

Two main variables, A and B, were constructed to capture the combined effects of joint configuration and con-fining stress on shear strength. Although these variables are not entirely independent, their construction allows for the nuanced analysis of how these factors interact within the context of the experimental design. Making variables A and B not fully independent reflects the interactions between joint configuration and confining stress in RAC dry joints. Their interdependence allowed a more accurate modeling of how these factors influence shear strength, capturing the complex, interconnected behavior of the system. This approach leaded to more precise predictions.

Where Variable A is feature that multiplies the formula ($Ak * \sqrt{fc} * (0.9961 + 0.2048 * Confinement)$) and Variable B being the factor that multiplies ($0.6 * As * Confinement$) as will be presented in section 2.8.

The EDA provided valuable insights into the nature and behavior of RAC, guiding the development of the predictive models and highlighting areas for future research. It was an essential step in the present study, enabling a comprehensive understanding of the complex characteristics of RAC data gathered.

8.2.3.3 Development of a Modified Equation for Recycled Concrete Dry Joints

This section introduces the equations used for predicting dry joint strength, compiled in Table 8.2.1, alongside the relevant designations and notations, which are elucidated in Table 8.2.2. This sets the stage for a detailed discussion on the potential of RAC, driving the investigation towards filling the current knowledge gap with rigorous analysis and novel insights.

Table 8.2.6 provides a selection of principal equations from the literature for predicting the shear strength of dry joints. These equations represent a range of analytical and empirical approaches, reflecting diverse methodologies from fundamental mechanics to advanced data-informed models. Each entry in the table.

Table 8.2.6 - Key Equations for Predicting Shear Strength of Dry Joints.

Author/Standard	Equation	
(AASHTO, 1999a)(AASHTO, 1999a)	$V_u = A_k\sqrt{f_c}(0.9961 + 0.2048\sigma_n) + 0.6A_{sm}\sigma_n$	(1)
(ATEP, 1996a)(ATEP, 1996a)	$V_u = A_j(1.14\sigma_n + 0.0564f_{cd})$	(2)
(EUROCODE 2, 2004a)(EUROCODE 2, 2004a)	$V_u = A_j(0.5f_{ctd} + 0.9\sigma_n)$	(3)
(Buyukozturk et al., 1990b)(Buyukozturk et al., 1990b)	$V_u = A_j(0.647\sqrt{f_c} + 1.36\sigma_n)$	(4)
(Rombach & Specker, 2002a)(Rombach & Specker, 2002a)	$V_u = 0.65\sigma_n A_j + ff_{ck}A_k$	(5)
(Turmo et al., 2006a)(Turmo et al., 2006a)	$V_u = A_k 0.01\sqrt[3]{f_{ck}{}^2}(7\sigma_n + 33) + 0.6A_{sm}\sigma_n$	(6)
(Alcalde et al., 2013a)(Alcalde et al., 2013a)	$V_u = 7.118A_k(1 - 0.064N_k) + 2.436A_{sm}\sigma_n(1 + 0.127N_k)$	(7)
(Ahmed & Aziz, 2019)(Ahmed & Aziz, 2019)	$V_u = 0.6\sigma_n A_{sm} + (1.06A_k + 2100\sigma_n)\sqrt{f_c}$	(8)

Table 8.2.7 - Notation used in the equations in Table 8.2.1.

Variable	Notation	Description
Design Parameters	V_u	Maximum shear force (kN)
	σ_n	Confining Stress (MPa)
	f_{ck}	Characteristic compressive strength of concrete (MPa)
	f_c	Concrete compressive strength (MPa)
	f_{cd}	Design concrete compressive strength (MPa)
	f_{ctd}	Concrete tensile strength (MPa)
Geometric characteristics	A_j	Total joint area (mm²)
	A_k	Area relative to the joint keys (mm²)
	A_{sm}	Area related to the flat part of the joint (mm²)
	N_k	Number of keys
	f	The factor relating to the key′s cutout equal to 0.14

Notably, (AASHTO, 1999a) (AASHTO, 1999a), the most applied equation in this context tends to yield results that are higher than those observed in actual tests. This discrepancy highlights a significant risk in directly applying this equation to recycled concrete dry joints, as it may lead to an overestimation of shear strength and potentially compromise the safety and integrity of the structure. Therefore, caution and additional research are advised when considering these equations for recycled concrete applications.

To address this issue, we propose a new equation introducing a reduction factor to modify the (AASHTO, 1999b) (AASHTO, 1999b) equation. This adjustment aims to better align the equation's predictions with the specific characteristics and performance of recycled concrete in dry joint applications, ensuring a more accurate and safe assessment of shear strength.

To understand the data patterns, machine learning techniques were used. Two models, Linear Regression and Random Forest, were employed, each providing insights due to their inherent characteristics.

Linear Regression, a parametric approach, offered a direct relationship between the predictors and the response variable. Its simplicity allowed for the clear identification of the influence each predictor exerted on the ultimate load capacity. This was quantified through the regression coefficients, which directly indicated the expected change in load capacity with a unit change in the predictor variables.

On the other hand, the Random Forest model, a non-parametric ensemble technique, harnessed the power of multiple decision trees to capture non-linear relationships and interactions between variables that the linear model might miss. It provided a more nuanced understanding through its feature importance scores, which ranked the predictors based on their contribution to model accuracy.

The Random Forest model's superior R-squared value highlighted its effectiveness in modeling complex and potentially non-linear relationships within the dataset. The feature importance scores further emphasized the dominance of the variable A over B in determining the ultimate load capacity, a revelation that could guide more focused engineering practices.

Machine Learning Pseudoalgorithm

```
Data Preparation:
  Load data from CSV file into DataFrame
  Preprocess data: clean and normalize
  Create features 'A' and 'B'
  Define target variable 'y' as 'Vu(kN)'
  Set predictors 'X' as features 'A' and 'B'

Linear Regression Analysis:
  Initialize Linear Regression model
  Fit model with predictors 'X' and target 'y'
  Predict 'Vu(kN)' using fitted model
  Calculate model coefficients, MSE, RMSE, R2

Random Forest Regression Analysis:
  Initialize Random Forest Regressor with parameters
  Fit model with predictors 'X' and target 'y'
  Predict 'Vu(kN)' using fitted model
  Determine feature importances, MSE, RMSE, R2

Results Interpretation:
  Analyze coefficients from Linear Regression
  Evaluate feature importances from Random Forest
  Compare results of both models for accuracy and insights
```

These machine learning techniques, with their distinct yet complementary analytical capabilities, contributed significantly to the robust analysis of the dataset, uncovering data patterns that are crucial for accurate load capacity prediction in recycled concrete applications.

The data analysis was conducted on the properties of recycled concrete used for reinforced bridge structures. Descriptive statistics indicated a mean concrete resistance (fc) of 41.52 MPa, with key and smooth area averages of 20,000 mm². The dataset exhibited a standard deviation of 4.71 MPa in concrete resistance, suggesting moderate variability. The correlation matrix revealed a strong positive relationship (r = 0.982) between the variable A—defined as $Ak * \sqrt{fc} * (0.9961 + 0.2048 * \sigma n)$ and the ultimate load capacity Vu (kN), underpinning the variable's significance in load prediction.

Subsequently, machine learning techniques were applied to further elucidate the data patterns. The Random Forest model demonstrated a high feature importance score of 0.968 for variable A and a lower score of 0.032 for B—calculated as $0.6 * As * \sigma n$, highlighting the former's predictive power. The proposed model achieved high R-squared values of 0.979, indicating a robust fit to the observed data.

The machine learning analysis led to the refinement of the equation for predicting the ultimate load capacity. The revised equation, as derived from the regression model, was determined to be:

$$Vu(kN) = \left(Ak * \sqrt{fc} * (0.9961 + 0.2048 * \sigma n)\right) \times 0.7596 + (0.6 * As * \sigma n) \times 0.6516 \quad (Equation\ 1)$$

Where the reduction factors are defined, and the coefficients 0. 7596and 0. 6516 represent the factors by which each part of the equation should be multiplied. This equation, alongside the insights from the Random Forest model, offers an accurate method for estimating the load capacity of structures utilizing recycled concrete, considering their unique characteristics.

8.2.4 Results and Discussion

8.2.4.1 Shear strength of RAC dry joints

Three types of dry joint specimens—flat, single-keyed, and three-keyed—were evaluated under confining stress-es of 1.0, 2.0, and 3.0 MPa. For flat dry joints, a linear increase in normalized shear stress (τn) against relative vertical displacement was observed.

The failure patterns observed in the Recycled Aggregate Concrete (RAC) dry joints under varying confining stresses were analyzed to understand the structural behavior of different joint configurations. Figure 8.2.6 present the typical cracking and failure patterns observed in the joints for different ultimate loads.

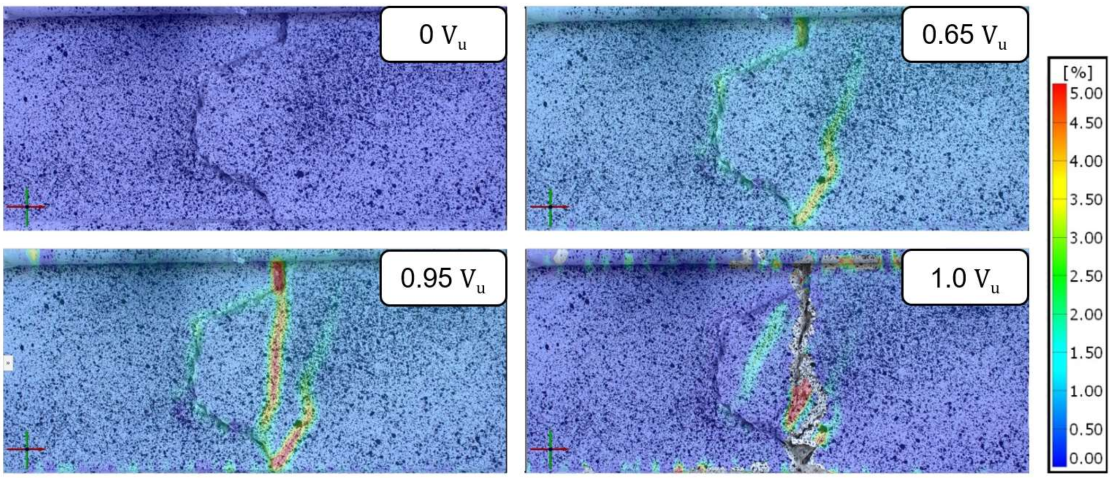

Figure 8.2.6 – (a) Importance analysis and (b) heatmap analysis.

Figure 8.2.6 presents the cracking patterns observed in Recycled Aggregate Concrete (RAC) dry joints at four different stages of ultimate shear: 0, 0.65, 0.95, and 1.0 of the ultimate shear capacity. These images illustrate the progression of crack development as the applied shear stress increases.

At 0 Vu (ultimate shear), the specimen shows no visible cracking, indicating the initial, unstrained state of the joint. At 0.65 of ultimate shear, initial cracks begin to form, primarily along the base of the key. These cracks indicate the onset of structural distress within the joint. At 0.95 of ultimate shear, the cracks become more pronounced and extensive, spreading through the joint and indicating significant stress concentration areas where the force attempts to shear the key off. The propagation of these cracks suggests an imminent failure. At 1.0 of ultimate shear (bottom-right), the cracks have fully developed to connect the entire key, leading to a complete failure of the joint. The pattern of cracking at this stage reflects the joint's maximum load-bearing capacity before collapse.

The behavior indicated no significant damage to the shear plane, just a thin layer of dust from friction. In single-keyed dry joints, increased confining stress resulted in higher normalized shear stress, with a pattern of linear increase until the key's strength limit, followed by significant slip and load decrease (Figure 8.2.7). The three-keyed joints exhibited a similar initial linear increase in stress, but with a noticeable incline near rupture, suggesting higher ductility due to sequential key ruptures. This behavior aligns with observations in previous research and confirms that higher confining stress improves joint strength across all types (Alcalde et al., 2013b; Jiang et al., 2015a; T. Liu et al., 2019a; Zhou et al., 2005a).

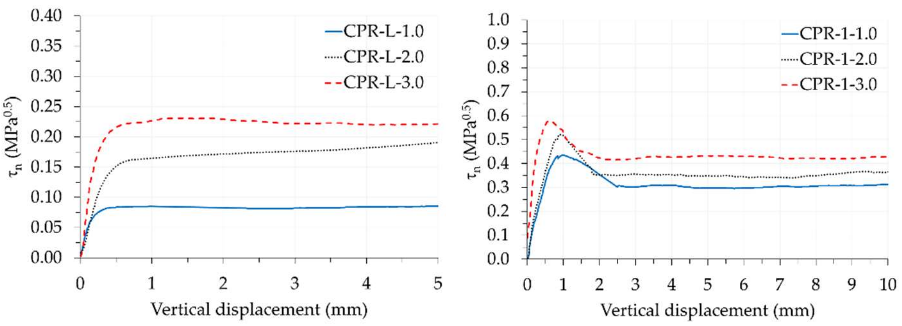

(a) (b)

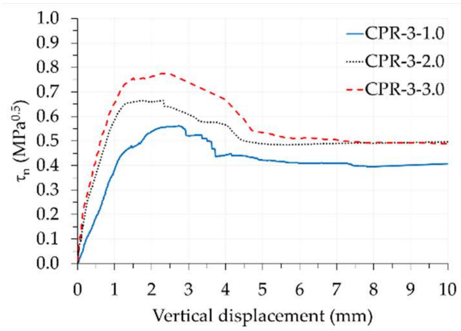

(c)

Figure 8.2.7 – Normalized shear stress versus relative vertical displacement curves for (a) flat, (b) single-keyed, (c) three-keyed RAC dry joint specimens.

The failure load, maximum shear stress, normalized cracking shear stress, and maximum normalized shear stress at failure of the flat dry joints, single-keyed and three-keyed dry joints are in Table 8.2.8.

Table 8.2.8 - Notation used in the equations in Table 8.2.1.

Specimens	Failure load V_u (kN)	Maximum shear stress τ_u (MPa)	Normalized cracking shear stress τ_{nf} (MPa$^{0.5}$)	Maximum normalized shear stress τ_{un} (MPa$^{0.5}$)	Standard deviation (MPa)
CPR-L-1.0	16.98	0.57	-	0.09	0.01
CPR-L-2.0	32.01	1.07	-	0.17	0.02
CPR-L-3.0	45.31	1.51	-	0.23	0.02
CPR-1-1.0	86.18	2.87	0.20	0.45	0.03
CPR-1-2.0	104.89	3.50	0.28	0.52	0.01
CPR-1-3.0	115.11	3.84	0.35	0.60	0.01
CPR-3-1.0	180.34	3.61	0.45	0.56	0.03
CPR-3-2.0	228.89	4.58	0.62	0.68	0.04
CPR-3-3.0	256.60	5.13	0.72	0.80	0.07

The results showed that the dry joints of concrete with recycled coarse aggregates presented reduced shear strength values compared to conventional concrete (except the three-keyed joint submitted to confining stress of 1.0 MPa). This shows the brittle characteristic of this material to shear.

The lower resistance of RAC occurs because the recycled coarse aggregates have lower resistance than the conventional ones due to the percentage of adhered mortar. This characteristic contributes to the cracks to cut the re-cycled aggregates, reducing the mechanical interlock due to the reduction of roughness in the sliding surface, thus interfering with the shear strength of the joint (Xiao et al., 2016)

8.2.4.2 Comparison between the results of this research with those of other researchers

Much research about the shear resistance of conventional or high strength dry concrete joints have been studied in recent years. Table 8.2.9 gathers information about them.

Table 8.2.9 - Dry joints specimens' data from previous works.

Paper	Joint type	Concrete strength resistance (MPa)	Joint width (mm)	Total smooth joint area (mm²)	Total monolithic joint area (mm²)	Total joint area (mm²)
(Buyukozturk et al., 1990b)(Buyukozturk et al., 1990b)	Flat	47.37	76.2	5806.44	-	5806.44
	Single-keyed	47.37	76.2	3992,9	7620	11612.9
(Zhou et al., 2005b)	Flat	52.2-52.8	250	50000	-	50000
	Single-keyed	37.1-56.2	250	25000	25000	50000
	Three-keyed	30.2-63.7	250	50000	75000	125000
(Yang et al., 2013b)	Single-keyed	60	100	10000	7000	17000
(Jiang et al., 2015b)	Flat	40.49	100	20000	-	20000
	Single-keyed	41.51	100	10000	10000	20000
	Three-keyed	41.82	100	20000	30000	50000
(Jiang et al., 2019b)	Single-keyed	41.03	100	10000	10000	20000
(T. Liu et al., 2019b)	Flat	123.9-125.59	150	45000	-	45000
	Single-keyed	123.9-125.59	150	30000	15000	45000
	Three-keyed	123.6-124.66	150	30000	45000	75000
(Feng et al., 2020b)	Single-keyed	64.21	100	10000	10000	20000
(Sousa et al., 2023)	Flat	41.52 (RAC)	100	30000	-	30000
	Single-keyed	41.52 (RAC)	100	20000	10000	30000
	Three-keyed	41.52 (RAC)	100	20000	30000	50000

Figure 8.2.8 compare the maximum normalized shear stress versus confining stress obtained by other researchers and the experimental results of this research for flat, single-keyed, e three-keyed dry joints with recycled coarse aggregates concrete.

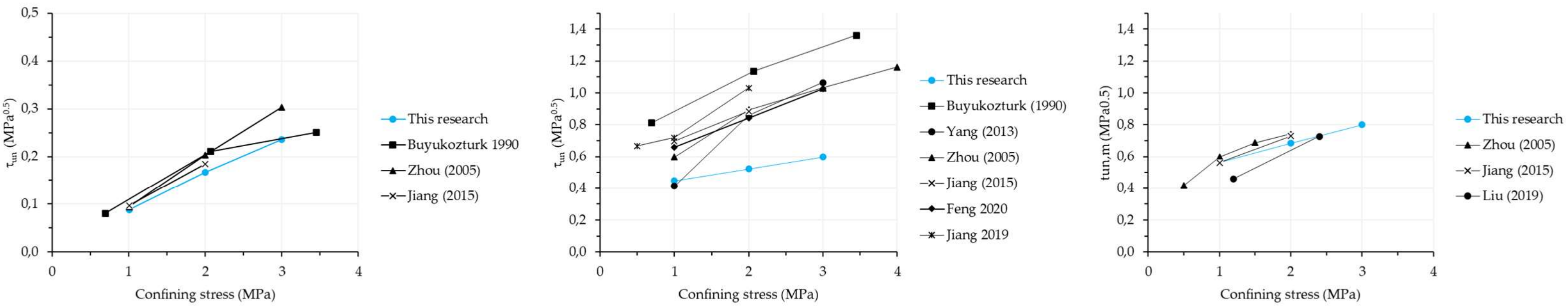

a) b) c)

Figure 8.2.8 – Maximum normalized shear stress in a) flat, b) single-keyed and c) three-keyed dry joints obtained for specimens from ordinary (black lines) and RAC (blue line).

Our results align with (Jiang et al., 2015a), who also observed reduced shear strength in RAC joints compared to conventional concrete. However, the ductility observed in three-keyed joints suggests a potential for RAC in specific applications, despite its lower strength.

For flat joints, the results showed that dry joints of concrete with recycled coarse aggregates showed strengths close to those of conventional concrete. The shear plane area of smooth joints has been observed to vary between studies; however, Figure 8.2.8 reveals that this has had minimal effect on the comparison of results, as values have remained consistent between both types of concrete.

The results showed that the single-keyed dry joints with recycled coarse aggregates concrete presented the lowest maximum normalized shear stress values. The comparison of the results obtained from the key joints with those of the smooth joints, as seen in Figure 8.2.9, demonstrates a greater difference. This implies that the monolithic region of the key exhibits an increased contribution to the shear resistance of the joints, with the RCA concrete joints exhibiting the lowest values due to its lower resistance. In the three-keyed joints, the difference between the results was minor compared to the single-keyed joints, presenting even similar values, studies have found that in multi-key joints, the rupture sequence of the keys does not allow for the full resistance of all of the keys together, which results in values obtained from a break that are not equal to three times the values of single-key joints. This rupture sequence of the keys, however, does allow for RCA joints to reach values close to those of conventional concrete joints.

8.2.4.3 Equations for predicting the strength of RAC dry joints

Utilizing Equations presented in Table 8.2.6 to predict the shear strength (τun) of Recycled Aggregate Concrete (RAC) dry joints does not align accurately with our study's findings. This misalignment underlines a significant gap between existing theoretical models and the empirical data collected, especially in the context of RAC dry joints. Our research indicates the need for a revised predictive approach that accurately reflects the unique characteristics and behavior of RAC in these applications.

Our study's comparative analysis involved findings from (Turmo et al., 2006b), (Rombach & Specker, 2002b), and the standards set in (EUROCODE 2, 2004b), with a specific focus on three-keyed RAC dry joints as reported by (Turmo et al., 2006b) and as outlined in (EUROCODE 2, 2004b). This comparison aimed to understand the discrepancies and align our findings within the broader context of existing literature and established codes.

Figure 8.2.9 illustrates the experimental results and the prediction of maximum normalized shear stress of single-keyed RAC dry joints using the equations from the literature. The (EUROCODE 2, 2004b) equation, formulated for calculating the shear resistance between concrete surfaces produced at different times, was observed to yield conservative values compared to the equations of (Turmo et al., 2006b) and (Rombach & Specker, 2002b), which were developed specifically for calculating the resistance of dry joints.

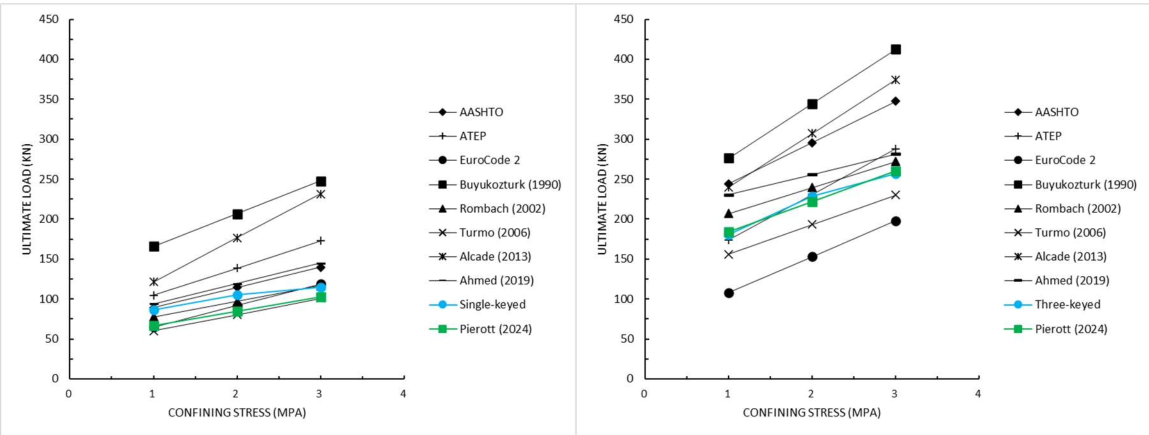

Figure 8.2.9 – Experimental results and prediction of maximum normalized shear stress of the single-keyed and three-keyed RAC dry joints using the equations in the literature and the proposed.

Table 8.2.11 details the relationship between the τun predicted by existing equations and our experimental results. The table demonstrates that the other proposed equations do not favor safety when applied to our data. For in-stance, the normative equation of (AASHTO, 1999b) approximates the strength of single-keyed RAC dry joints for low confining stresses. However, as the confining stress increases, the experimental results significantly diverge from the predictions, as evident in Figure 8.2.9. Particularly, the experimental values for predicting RAC dry joints with three keys differ markedly from the normative equation's prediction.

Table 8.2.9 - Relationship between maximum normalized shear stress predicted by the literature equations and experimental results.

Specimens	AASHTO 1	ATEP 2	EUR 3	BUYU 4	ROMB 5	TURM 6	ALCA 7	AHMD 8	Equation 1
CPR-1-1,0	1.04	1.21	0.75	1.92	0.90	0.70	1.41	1.09	0,77
CPR-1-2,0	1.09	1.32	0.88	1.97	0.93	0.77	1.68	1.14	0,81
CPR-1-3,0	1.21	1.50	1.03	2.15	1.01	0.88	2.01	1.26	0,89
CPR-3-1,0	1.35	0.97	0.60	1.53	1.15	0.86	1.33	1.28	1,02
CPR-3-2,0	1.29	1.01	0.67	1.50	1.05	0.84	1.34	1.12	0,97
CPR-3-3,0	1.35	1.12	0.77	1.61	1.06	0.90	1.46	1.10	1,01

1 (AASHTO, 1999c); 2 (ATEP, 1996b); 3 (EUROCODE 2, 2004a); 4 (Buyukozturk et al., 1990b); 5 (Rombach & Specker, 2002c); 6 (Turmo et al., 2006c); 7 (Alcalde et al., 2013c); 8 (Ahmed & Aziz, 2019).

To address these discrepancies and provide a more accurate representation of the observed phenomena, we developed Equation 1, as presented in section 2 and showcased in Table 8.2.11. This new equation aligns more closely with the experimental data, ensuring a safer and more reliable approach to predicting the strength of RAC dry joints.

As previously mentioned, the AASHTO equation was formulated for joints featuring only single key structures. It is inherent to the nature of the equation to extrapolate predictions to scenarios involving multiple keys.

Consequently, Equation 1 was developed to address these specific discrepancies and provide a more accurate representation of the observed phenomena as may be seen in Table 8.2.11.

The model was derived through a combination of empirical data analysis and machine learning techniques. The key steps involved identifying the most influential variables through feature importance analysis using Random Forest, followed by fitting a regression model to predict the ultimate shear strength. The final equation was vali-dated against experimental data.

8.2.5 Discussion

This study provides insights into the behavior of Recycled Aggregate Concrete (RAC) dry joints, particularly in the context of prestressed segmental bridges. The findings show that flat joints in RAC exhibit behavior comparable to conventional concrete, suggesting that RAC can be a viable alternative in certain applications. However, the single-keyed and three-keyed joints, while demonstrating reduced shear strength with increased recycled aggregate content, reveal distinctions. The improved ductility observed in the three-keyed joints suggests that certain design adaptations can mitigate some of the inherent brittleness associated with RAC, making it more suitable for specific structural applications where flexibility under load is advantageous.

One of the findings of this study is the identification and subsequent modification of existing predictive models for concrete shear strength, such as the ASHTO equation. The observed discrepancies between the experimental results and the predictions made by these conventional models highlighted the need for adjustments to better capture RAC’s unique properties. By incorporating a reduction factor into the equation, it can enhance the accuracy of shear strength predictions for RAC, thereby providing a tool for engineers and designers working with this material.

Moreover, the application of machine learning techniques, specifically Linear Regression and Random Forest provided a predictive modeling of RAC behavior. These methods allowed for a deeper analysis of the relationships between key variables and facilitated the development of a predictive model. The improved predictive accuracy achieved through these techniques sets the stage for further research into the broader applicability of these models.

These findings suggest that while RAC can be used in prestressed segmental bridges, design adjustments, such as increased confining stress or key modifications, may be necessary to compensate for its lower shear strength.

The results obtained suggest several pathways for future research. One limitation of this study is the focus on a specific range of confining stresses. Future research should explore a broader range of stresses and include long-term durability testing to fully assess RAC's potential in bridge construction. The refinement of the predictive models is also an ongoing process, and there is potential for further enhancement by incorporating additional variables and testing under different environmental conditions. Additionally, assessing the long-term performance of RAC, particularly in critical structural applications like prestressed segmental bridges, will be essential in validating its use and ensuring its durability and sustainability in the industry.

8.2.6 Conclusions

In this study, the use of Recycled Aggregate Concrete (RAC) in prestressed segmental bridges was investigated, with a focus on its mechanical properties, durability, and the challenges associated with predicting joint strength in RAC structures. The findings indicate that while RAC may offers significant environmental benefits and can achieve strengths comparable to conventional concrete in certain contexts, its variability presents challenges, particularly in single-keyed dry joints, where it exhibits lower shear strength. These challenges are especially pronounced in the critical joint areas of prestressed segmental bridges, where RAC's inconsistent mechanical properties can significantly affect performance. This research enhances the understanding of RAC's behavior in these specific structural applications and underscores the need for specialized design and analysis approaches.

The integration of machine learning techniques, especially the Random Forest model, was important in advancing the understanding of RAC for the proposed study. This approach provided insights into the complex data pat-terns, identifying key factors that influence the strength and durability of RAC in bridge applications. The development of a novel predictive equation for the load capacity of prestressed segmental bridges using RAC, represents an advancement in the equations proposed by the standard codes analyzed. The resulting model, which accounts for RAC's complex and varied properties, is expected to be a tool for researchers and practitioners in sustainable construction, enabling more precise and reliable design and evaluations.

This study contributes to the ongoing shift towards sustainable construction practices by demonstrating both the potential and the challenges of using RAC in demanding structural applications. It lays the groundwork for further research into the applicability and performance of RAC, particularly as the construction industry moves towards adopting more environmentally friendly materials.

8.2.7 DISCUSSION of Chapter 8.2

8.2.7.1 Key Findings

The novel predictive model developed in this chapter proved to be highly effective in estimating the strength of RAC in bridge dry joints. The model accurately accounted for the variability in RAC properties, offering a robust method for predicting performance in real-world applications. The findings suggest that RAC can perform comparably to traditional concrete when used in bridge dry joints, provided that appropriate design and material considerations are made. This predictive tool enables engineers to confidently use RAC in infrastructure projects, supporting both sustainability and structural integrity.

8.2.7.2 Implications

The implications of this research are significant for the future of sustainable infrastructure. The ability to accurately predict the strength of RAC in critical structural applications, such as bridge dry joints, opens the door for wider adoption of recycled materials in large-scale projects. This contributes to the reduction of construction waste and promotes the use of sustainable resources without compromising safety. The predictive model could serve as a valuable tool in both the design and maintenance phases of bridge construction, ensuring that structures built with RAC meet the necessary performance standards while supporting environmental goals.

8.2.7.3 Limitations

While the predictive model demonstrated strong accuracy in this study, its effectiveness is dependent on the quality and consistency of the input data. Variations in recycled aggregate sources, processing methods, and mix designs could impact the generalizability of the model across different projects. Additionally, the model's applicability may be limited to the specific conditions under which it was developed, such as particular types of bridges and environmental conditions. Future work should aim to validate the model under a broader range of scenarios to ensure its robustness and versatility.

8.2.7.4 Future Work

Future research should focus on expanding the predictive model to account for a wider range of RAC properties and environmental conditions. Incorporating additional variables, such as long-term durability factors, freeze-thaw cycles, and exposure to aggressive environments, would enhance the model’s utility in diverse applications. Field validation through real-world bridge projects would provide critical data to refine the model and confirm its reliability. Additionally, exploring the model's adaptability to other structural elements, beyond bridge dry joints, could further increase the adoption of RAC in sustainable infrastructure development.

8.2.8 CONCLUSION for Chapter 8.2

This chapter developed and applied a novel predictive model for assessing the strength of recycled aggregate concrete (RAC) in bridge dry joints. The research demonstrated that the predictive model was able to accurately forecast the performance of RAC dry joints, providing a reliable tool for engineers working with sustainable materials in bridge construction. The success of this approach highlights the potential for RAC to be used more widely in infrastructure projects, particularly where sustainability is a key concern. By offering accurate strength predictions, the model contributes to the confidence needed to incorporate recycled materials into critical structural applications like bridges. The successful application of predictive modeling in RAC provides a pathway for broader adoption of sustainable materials in structural design. Continuing with the theme of innovative materials, the final chapter examines the use of steel fibers in sand-lightweight concrete.

8.2.9 References for Chapter 8.2

AASHTO. (1999a). Guide Specifications for Design and Construction of Segmental Concrete Bridges.

AASHTO. (1999b). Guide Specifications for Design and Construction of Segmental Concrete Bridges.

AASHTO. (1999c). Guide Specifications for Design and Construction of Segmental Concrete Bridges.

ABNT NBR 5739. (2018a). Concreto — Ensaio de compressão de corpos de prova cilíndricos. Associação Brasileira de Normas Técnicas.

ABNT NBR 5739. (2018b). Concreto — Ensaio de compressão de corpos de prova cilíndricos. Associação Brasileira de Normas Técnicas.

ABNT NBR 7222. (2011). Concreto e argamassa — Determinação da resistência à tração por compressão diametral de corpos de prova cilíndricos. Associação Brasileira de Normas Técnicas. https://doi.org/01.080.10; 13.220.99

ABNT NBR 8522. (2017). Concreto - Determinação dos módulos estáticos de elasticidade e de deformação à compressão. Associação Brasileira de Normas Técnicas.

ABNT NBR 9778. (2009). Argamassa e concreto endurecidos - Determinação da absorção de água, índice de vazios e massa específica. Associação Brasileira de Normas Técnicas.

ABNT NBR 11578:1991. (1991). Cimento Portland composto. Associação Brasileira de Normas Técnicas.

ABNT NBR NM 52. (2003). Agregado miúdo - Determinação da massa específica e massa específica aparente. Associação Brasileira de Normas Técnicas.

ABNT NBR NM 53. (2002). Agregado graúdo – Determinação de massa específica , massa específica aparente e absorção de água. Associação Brasileira de Normas Técnicas.

Ahmed, G. H., & Aziz, O. Q. (2019). Shear strength of joints in precast posttensioned segmental bridges during 1959–2019, review and analysis. Structures, 20(May), 527–542. https://doi.org/10.1016/j.istruc.2019.06.007

Alcalde, M., Cifuentes, H., & Medina, F. (2013a). Influencia del número de llaves en la resistencia a cortante de juntas secas postensadas. Materiales de Construccion, 63(310), 297–307. https://doi.org/10.3989/mc.2013.07611

Alcalde, M., Cifuentes, H., & Medina, F. (2013b). Influencia del número de llaves en la resistencia a cortante de juntas secas postensadas. Materiales de Construccion, 63(310), 297–307. https://doi.org/10.3989/mc.2013.07611

Alcalde, M., Cifuentes, H., & Medina, F. (2013c). Influencia del número de llaves en la resistencia a cortante de juntas secas postensadas. Materiales de Construccion, 63(310), 297–307. https://doi.org/10.3989/mc.2013.07611

ATEP. (1996a). Proyecto y construcción de puentes y estructuras con pretensado exterior. Colegio de Ingenieros de Caminos, Canales y Puertos, H.P.10-96.

ATEP. (1996b). Proyecto y construcción de puentes y estructuras con pretensado exterior. Colegio de Ingenieros de Caminos, Canales y Puertos, H.P.10-96.

Bazuco, R. S. (1999). Utilização de agregados reciclados de concreto para a produção de novos concretos. Universidade Federal de Santa Catarina.

Buyukozturk, O., Bakhoum, M. M., & Beattie, S. M. (1990a). Shear behavior of joints in precast concrete segmental bridfes. Journal of Structural Engineering, 116(12), 3380–3401.

Buyukozturk, O., Bakhoum, M. M., & Beattie, S. M. (1990b). Shear behavior of joints in precast concrete segmental bridfes. Journal of Structural Engineering, 116(12), 3380–3401.

Cantero, B., Bravo, M., Brito, J., Sáez del Bosque, I. F., & Medina, C. (2020). Mechanical behaviour of structural concrete with ground recycled concrete cement and mixed recycled aggregate. Journal of Cleaner Production, 275. https://doi.org/10.1016/j.jclepro.2020.122913

Chen, J., Zhou, Y., & Yin, F. (2022). A Practical Equation for the Elastic Modulus of Recycled Aggregate Concrete. Buildings. https://doi.org/10.3390/%0Abuildings12020187

Deng, F., He, Y., Zhou, S., Yu, Y., Cheng, H., & Wu, X. (2018). Compressive strength prediction of recycled concrete based on deep learning. Construction and Building Materials. https://doi.org/10.1016/J.CONBUILDMAT.2018.04.169

EN 1097-1:2011. (2011). Ensayos para determinar las propriedades mecánicas y físicas de los áridos. Asociación Española de Normalización y Certificación.

EUROCODE 2. (2004a). Design of concrete structures - Part 1-1 : General rules and rules for buildings (Vol. 1).

EUROCODE 2. (2004b). Design of concrete structures - Part 1-1 : General rules and rules for buildings (Vol. 1).

Feng, J., Liang, W., Jiang, H., Huang, C., & Zhang, J. (2020a). Shear performance of single-keyed dry joints between reactive power concrete and high strength concrete in push-off tests. Science Progress, 103(2), 1–27. https://doi.org/10.1177/0036850420928643

Feng, J., Liang, W., Jiang, H., Huang, C., & Zhang, J. (2020b). Shear performance of single-keyed dry joints between reactive power concrete and high strength concrete in push-off tests. Science Progress, 103(2), 1–27. https://doi.org/10.1177/0036850420928643

Fonteboa, G., Martínez, F., Carro, D., & Eiras, J. (2010). Cortante-fricción de los hormigones reciclados. Materiales de Construccion, 60(299), 53–67. https://doi.org/10.3989/mc.2010.49708

Han, T., Siddique, A., Khayat, K., Huang, J., & Kumar, A. (2020). An ensemble machine learning approach for prediction and optimization of modulus of elasticity of recycled aggregate concrete. Construction and Building Materials, 244, 118271. https://doi.org/10.1016/j.conbuildmat.2020.118271

Jiang, H., Chen, L., Ma, Z. J., & Feng, W. (2015a). Shear behavior of dry joints with castellated keys in Precast concrete segmental bridges. Journal of Bridge Engineering, 20(2), 1–12. https://doi.org/https://doi.org/10.1061/(ASCE)BE.1943-5592. 0000649

Jiang, H., Chen, L., Ma, Z. J., & Feng, W. (2015b). Shear behavior of dry joints with castellated keys in Precast concrete segmental bridges. Journal of Bridge Engineering, 20(2), 1–12. https://doi.org/https://doi.org/10.1061/(ASCE)BE.1943-5592. 0000649

Jiang, H., Feng, J., Liu, A., Liang, W., Tan, Y., & Liang, H. (2019a). Effect of specimen thickness and coarse aggregate size on shear strength of single-keyed dry joints in precast concrete segmental bridges. Structural Concrete, 20(3), 955–970. https://doi.org/10.1002/suco.201800054

Jiang, H., Feng, J., Liu, A., Liang, W., Tan, Y., & Liang, H. (2019b). Effect of specimen thickness and coarse aggregate size on shear strength of single-keyed dry joints in precast concrete segmental bridges. Structural Concrete, 20(3), 955–970. https://doi.org/10.1002/suco.201800054

Kassem, M. A., El-Shafiey, T. F., Hussein, M., Afefy, H. M., & Hassan, A. (2017). Shear behaviour of SHCC dry joints in precast concrete construction. Journal of Bridge Engineering.

Kazmi, S., Munir, M., Wu, Y., Patnaikuni, I., Zhou, Y., & Xing, F. (2019). Influence of different treatment methods on the mechanical behavior of recycled aggregate concrete: A comparative study. Cement and Concrete Composites. https://doi.org/10.1016/j.cemconcomp.2019.103398

Khatab, M. A. T., & Altmami, M. (2019). Correlation between different properties of recycled aggregate and recycled aggregate concrete. AIP Conference Proceedings, 2146(August). https://doi.org/10.1063/1.5123692

Liu, B., Feng, C., & Deng, Z. (2019a). Shear behavior of three types of recycled aggregate concrete. Construction and Building Materials, 217, 557–572. https://doi.org/10.1016/j.conbuildmat.2019.05.079

Liu, B., Feng, C., & Deng, Z. (2019b). Shear behavior of three types of recycled aggregate concrete. Construction and Building Materials, 217, 557–572. https://doi.org/10.1016/j.conbuildmat.2019.05.079

Liu, T., Wang, Z., Guo, J., & Wang, J. (2019a). Shear Strength of Dry Joints in Precast UHPC Segmental Bridges: Experimental and Theoretical Research. Journal of Bridge Engineering, 24(1). https://doi.org/10.1061/(ASCE)BE.1943-5592.0001323

Liu, T., Wang, Z., Guo, J., & Wang, J. (2019b). Shear Strength of Dry Joints in Precast UHPC Segmental Bridges: Experimental and Theoretical Research. Journal of Bridge Engineering, 24(1). https://doi.org/10.1061/(ASCE)BE.1943-5592.0001323

NAOUAOUI, K., BOUYAHYAOUI, A., & CHERRADI, T. (2019). Experimental Characterization of Recycled Aggregate Concrete. MATEC Web of Conferences, 303(201 9), 05004. https://doi.org/10.1051/matecconf/201930305004

Pani, L., Francesconi, L., Rombi, J., Mistretta, F., Sassu, M., & Stochino, F. (2020). Effect of parent concrete on the performance of recycled aggregate concrete. Sustainability (Switzerland), 12(22), 1–17. https://doi.org/10.3390/su12229399

Rahal, K. (2017). Shear strength of recycled aggregates concrete. Procedia Engineering, 210(December), 105–108. https://doi.org/10.1016/j.proeng.2017.11.054

Rangel, C. S., Pepe, M., Amario, M., Menegatti, L. C., Martinelli, E., & Filho, R. T. T. (2021). Effects of Freeze-Thaw and Wet-Dry Cycles on Tension Stiffening Behavior of Reinforced RAC Elements. Applied Sciences. https://doi.org/10.3390/app112110063

Rombach, G., & Specker, A. (2002a). Design of joints in segmental hollow box girder bridges. Concrete Structures in the 21th Century, FIB Osaka, 1–6.

Rombach, G., & Specker, A. (2002b). Design of joints in segmental hollow box girder bridges. Concrete Structures in the 21th Century, FIB Osaka, 1–6.

Rombach, G., & Specker, A. (2002c). Design of joints in segmental hollow box girder bridges. Concrete Structures in the 21th Century, FIB Osaka, 1–6.

Shamass, R., Zhou, X., & Alfano, G. (2015). Finite-element analysis of shear-off failure of keyed dry joints in precast concrete segmental bridges. Journal of Bridge Engineering, 20(6), 1–12. https://doi.org/10.1061/(ASCE)BE.1943-5592.0000669

Shamass, R., Zhou, X., & Wu, Z. (2017). Numerical Analysis of Shear-Off Failure of Keyed Epoxied Joints in Precast Concrete Segmental Bridges. Journal of Bridge Engineering, 22(1), 04016108. https://doi.org/10.1061/(asce)be.1943-5592.0000971

Sousa, J. B., Garcia, S. L. G., & Pierott, R. M. R. (2023). Shear Behavior of Recycled Coarse Aggregates Concrete Dry Joints Keys Using Digital Image Correlation Technique. Infrastructures, 8(3). https://doi.org/10.3390/infrastructures8030060

Tamayo, P., Pacheco, J., Thomas, C., de Brito, J., & Rico, J. (2019). Mechanical and Durability Properties of Concrete with Coarse Recycled Aggregate Produced with Electric Arc Furnace Slag Concrete. Applied Sciences, 10, 216. https://doi.org/10.3390/app10010216

Trindade, J., Garcia, S., & Fonseca, G. (2020). Experimental study of direct shear in concrete with recycled aggregate. ACI Structural Journal.

Turmo, J., Ramos, G., & Aparicio, A. C. (2006a). Resistencia de juntas secas conjugadas de puentes de dovelas prefabricadas de hormigón: Propuesta para el Eurocódigo 2. Materiales de Construccion, 56(282), 45–52. https://doi.org/10.3989/mc.2006.v56.i282.26

Turmo, J., Ramos, G., & Aparicio, A. C. (2006b). Resistencia de juntas secas conjugadas de puentes de dovelas prefabricadas de hormigón: Propuesta para el Eurocódigo 2. Materiales de Construccion, 56(282), 45–52. https://doi.org/10.3989/mc.2006.v56.i282.26

Turmo, J., Ramos, G., & Aparicio, A. C. (2006c). Resistencia de juntas secas conjugadas de puentes de dovelas prefabricadas de hormigón: Propuesta para el Eurocódigo 2. Materiales de Construccion, 56(282), 45–52. https://doi.org/10.3989/mc.2006.v56.i282.26

Xiao, J., Sun, C., & Lange, D. A. (2016). Effect of joint interface conditions on shear transfer behavior of recycled aggregate concrete. Construction and Building Materials, 105, 343–355. https://doi.org/10.1016/j.conbuildmat.2015.12.015

Xiao, J., Xie, H., & Yang, Z. (2012). Shear transfer across a crack in recycled aggregate concrete. Cement and Concrete Research, 42(5), 700–709. https://doi.org/10.1016/j.cemconres.2012.02.006

Yang, I. H., Kim, K. C., & Kim, Y. J. (2013a). Shear strength of dry joints in precast concrete modules. The Thirteenth East Asia-Pacific Conference on Structural Engineering and Construction, EASEC-13.

Yang, I. H., Kim, K. C., & Kim, Y. J. (2013b). Shear strength of dry joints in precast concrete modules. The Thirteenth East Asia-Pacific Conference on Structural Engineering and Construction, EASEC-13.

Zafar, M. N., Saleem, M., Xia, J., & Saleem, M. A. (2020). Experimental Characterization of Prefabricated Bridge Deck Panels Prepared with Prestressed and Sustainable Ultra-High Performance Concrete. Applied Sciences. https://doi.org/10.3390/app10155132

Zhou, X., Mickleborough, N., & Li, Z. (2005a). Shear strength of joints in precast concrete segmental bridges. ACI Structural Journal, 102(6), 901–904.

Zhou, X., Mickleborough, N., & Li, Z. (2005b). Shear strength of joints in precast concrete segmental bridges. ACI Structural Journal, 102(6), 901–904.

9 CONCLUSIONS

This thesis has systematically explored the integration of predictive modeling techniques and empirical data into the structural design process, with the primary aim of enhancing the long-term performance of reinforced and prestressed concrete structures. The overarching goal was to address a gap in structural engineering: the limitations of traditional design methods that rely on static assumptions and deterministic models, which often fail to account for the dynamic factors affecting a structure's performance over time extremely complex nuances of the real-world case scenarios. This research has introduced methodologies that incorporate advanced optimization models and predictive tools, setting the stage for more resilient, adaptive, and efficient design practices in structural engineering.

The specific objectives outlined in this thesis have been thoroughly investigated, resulting in significant contributions to the field. First, the development of a mathematical optimization model for the design and detailing of reinforced concrete, as discussed in Chapter 4, marked an important shift from continuous to discrete optimization. This advancement allowed for the practical optimization of real-world reinforced concrete structures for the first time, opening new avenues for integrating machine learning techniques and data-driven solutions in structural design. The success of this model set the foundation for subsequent research, establishing a robust framework for addressing complex design challenges.

Chapter 5 furthered this exploration by delving into the issue of stress corrosion cracking (SCC) in prestressed concrete, a critical durability concern. The findings provided valuable insights into the environmental conditions that exacerbate SCC and underscored the need for improved design and maintenance strategies. This work was complemented by Chapter 6, which introduced predictive models for analyzing corrosion dynamics in chloride-rich environments. These models offered accurate forecasts of corrosion rates and progression, enabling more proactive maintenance and design decisions, particularly in environments prone to chloride-induced corrosion.

The focus then shifted to enhancing the structural performance of reinforced concrete columns through the use of welded steel mesh stirrups, as discussed in Chapter 7. The results demonstrated that this reinforcement strategy significantly improves the load-bearing capacity and ductility of concrete columns, making it a viable solution for enhancing structural resilience. This chapter’s findings contribute to the ongoing effort to develop more effective and economical reinforcement techniques.

Chapters 8 and 9 explored the potential of recycled aggregate concrete (RAC) in structural applications, with a particular focus on dry joint keys and bridge dry joints. The research demonstrated that RAC, when properly designed and utilized, can perform comparably to traditional concrete, supporting sustainability goals without compromising structural integrity. The development of a predictive model for RAC strength prediction in Chapter 9 was particularly noteworthy, as it provided a reliable tool for engineers working with sustainable materials in critical infrastructure projects.

Finally, Chapter 10 investigated the shear strength of sand-lightweight concrete deep beams reinforced with steel fibers, highlighting the potential of this innovative material combination in applications where both high strength and reduced weight are crucial. The findings support the broader use of steel fiber-reinforced lightweight concrete in modern construction, contributing to the ongoing transformation of the industry toward more efficient and sustainable practices.

9.1 MAIN CONTRIBUTIONS

The main contributions of this thesis, aimed at advancing structural engineering through the integration of predictive modeling and data-driven solutions, can be summarized as follows:

Advancement of Discrete Optimization Models: The thesis introduced a discrete optimization model that marked a departure from traditional continuous methods. This innovation enabled the practical optimization of real-world reinforced concrete structures, setting a new standard in structural design practices.

Integration of Predictive Models in Corrosion Analysis: By developing and applying predictive models for corrosion dynamics in chloride-rich environments, the thesis provided engineers with valuable tools for forecasting and mitigating corrosion-related damage in prestressed concrete structures.

Enhancement of Reinforcement Techniques: The research demonstrated the effectiveness of welded steel mesh stirrups in improving the structural performance of reinforced concrete columns, offering a practical solution for enhancing resilience, particularly in seismic regions.

Promotion of Sustainable Construction Materials: The thesis explored the use of recycled aggregate concrete in structural applications, validating its potential as a sustainable alternative to traditional concrete. The development of a predictive model for RAC strength prediction further supports its broader adoption in infrastructure projects.

Innovation in Lightweight Concrete Applications: The investigation of steel fiber-reinforced sand-lightweight concrete deep beams contributed to the understanding and application of innovative materials in structural design, particularly in contexts where weight reduction and high strength are critical.

9.2 LIMITATIONS AND FURTHER RESEARCH

While this thesis has made significant contributions to the field of structural engineering, certain limitations should be acknowledged, and avenues for further research should be explored:

Generalizability of Findings: The research, while comprehensive, was based on specific case studies and experimental setups, which may limit the generalizability of the findings across different structural types, materials, and environmental conditions.

Long-Term Performance Studies: Future research should focus on long-term studies to assess the durability and performance of the proposed materials and reinforcement techniques over extended periods, particularly in real-world applications.

Expansion of Predictive Models: There is potential to expand the predictive models developed in this thesis to include a broader range of variables and environmental conditions, enhancing their applicability and accuracy in diverse structural scenarios.

Integration of Emerging Technologies: Exploring the integration of emerging technologies, such as machine learning and advanced sensing, into the optimization and predictive modeling processes could lead to further innovations in structural engineering.

Policy and Industry Adoption: Future research could also focus on the development of guidelines and standards to support the adoption of these innovative techniques and materials in industry practice, ensuring their broader impact on the construction sector.

In conclusion, this thesis has addressed critical gaps in the field of structural engineering by introducing innovative optimization models, predictive tools, and sustainable materials. The advancements made in each specific objective contribute to a paradigm shift in how structures are designed, analyzed, and maintained, paving the way for more resilient, efficient, and sustainable built environments. Continued research and collaboration between academia, industry, and policymakers will be essential to further refine these innovations and ensure their successful implementation in practice.

9.3 FINAL CONCLUSION

All the research presented in this thesis culminates in the development of a comprehensive method that leverages finite data to significantly enhance structural design processes. By integrating random forest machine learning prediction methods, this work has proposed new, reliable equations applicable to various fields related to concrete structures. The innovative approach of using finite datasets and advanced predictive models not only addresses existing challenges in structural engineering but also sets a foundation for future research. This methodology opens up numerous opportunities for further exploration and application, providing a reliable framework for others in the field to build upon. The work presented here demonstrates the potential of combining empirical data with machine learning techniques to advance the science of structural design, ensuring that future developments in this area are grounded in robust, data-driven methods.

.

APPENDIX A – BIBLIOGRAPHIC PRODUCTION

This section presents additional research projects undertaken during my PhD period. While these studies may not be directly influenced by the central scientific question of this thesis, they undoubtedly contributed to the overall development of the work and enriched the research process.

APPENDIX B – SUSTAINABLE MATERIAL CHOICE FOR CONSTRUCTION PROJECTS: A LIFE CYCLE SUSTAINABILITY ASSESSMENT FRAMEWORK BASED ON BIM AND FUZZY-AHP

This chapter is published as an original research article in Building and Environment.
https://doi.org/10.1016/j.buildenv.2021.107805

FIGUEIREDO, Karoline; **PIEROTT, Rodrigo**; HAMMAD, Ahmed W.A.; HADDAD, Assed. Sustainable material choice for construction projects: A Life Cycle Sustainability Assessment framework based on BIM and Fuzzy-AHP. **Building and Environment**, v. 196, p. 107805, 2021.

ABSTRACT

Construction professionals and researchers are increasingly looking for sustainable solutions for buildings in a bid to reduce some of the negative impacts associated with the sector. A common misconception is to consider sustainability as only concerning environmental issues, without regard for the interaction between a triple bottom line framework that is comprised of social, economic, and environmental factors. Material choice is known to impact building sustainability directly since the use of certain materials can dramatically alter the footprint generated over the life cycle of the building. However, the construction industry is not yet equipped with approaches that simultaneously account for all three aspects of sustainability when it comes to deciding on materials to adopt. This paper proposes a decision-making framework for construction professionals and researchers involving the integration of Life Cycle Sustainability Assessment (LCSA), Multi-Criteria Decision Analysis (MCDA), and Building Information Modeling (BIM) to choose suitable materials for buildings. The framework is built based on a literature review of relevant papers to identify critical factors and challenges to implementing this integration. The Fuzzy Analytic Hierarchy Process was chosen

as the MCDA method within the proposed framework, given that the problem of material choice often contains subjectivity, uncertainty, and ambiguity, which is best solved with fuzzy logic. A residential building was adopted as a case study to validate the proposed framework, and LCSA is applied, covering the construction, operation, and end-of-life phases of the building.

Keywords:
Life Cycle Sustainability Assessment; Multi-Criteria Decision Analysis; Building Information Modeling; Sustainable buildings; Fuzzy Analytic Hierarchy Process.

9.4 INTRODUCTION

The construction industry is responsible for the significant consumption of natural resources, along with the generation of large amounts of waste [1]. In the last decade, researchers have attempted to study alternative materials, technologies, and design concepts that are less damaging to the environment. However, sustainability is not only concerned with environmental issues, as it involves an interaction between a triple bottom line framework comprised of social, economic, and environmental factors. In addition, several stakeholders are involved in a construction project, leading to the generation of various information from different parties and thus increasing uncertainty revolving around the decisions made [2]. Thus, there is a need for tools and technologies that facilitate a comprehensive analysis of a building and which cover all dimensionalities of sustainability.

Many decisions are made across the design, construction, and operation phases of a construction project. Such decisions can impact multiple aspects of a project. Hence, it is crucial to understand how such impacts reflect on several factors, including economic, environmental, and social ones. There are several examples in which a decision in the construction field impacts multiple criteria: the process to determine the best energy retrofit decision for a building, defining the impacts of different retrofit scenarios [3]; the equipment selection for construction projects [4]; and the definition of the construction system productivity [5]. One method to handle the simultaneous criteria that need to be evaluated before a decision is made is through multi-criteria decision analysis (MCDA), whereby concerns about various conflicting criteria can be formally incorporated into the decision-making process [6].

Of particular relevance in this study is the selection of suitable materials for building projects, which is a task that is linked to multiple criteria that require analysis and interpretation concurrently. Material selection in projects is traditionally based on satisfying technical requirements or economic limits, such as material strength and price, respectively, without considering the life cycle impact associated with the material [7]. In addition, almost 60% of the time is wasted in the early stages of designing construction projects on comparing different materials, resources, and construction methods [8]. To improve the selection of appropriate materials, this study proposes a framework that is based on Life Cycle Sustainability Assessment (LCSA) to evaluate the environmental, social, and economic impacts of building materials and make an appropriate choice. LCSA is the result of combining three main processes: i) Life Cycle Assessment (LCA), representing the environmental dimension [9]; ii) Social Life Cycle Assessment (S-LCA), representing the social dimension [10]; and iii) Life Cycle Costing (LCC), describing the economic dimension [11]. As such, LCSA can be represented in equation form as follows [2]:

$$\text{LCSA} = \text{LCA} + \text{S-LCA} + \text{LCC} \quad (1)$$

Application of LCSA within the construction industry is not without any challenges; a high degree of detail is required when considering an entire building as a functional equivalent of analysis within LCSA. The term 'functional equivalent' is introduced at the building level in contrast to the term 'functional unit' at the product level and includes all quantified functional requirements and technical requirements of the building used as a basis for comparison [12]. There are difficulties that exist in analyzing the building's life cycles due to the large number of data that needs to be considered [13,14].

When it comes to analyzing the environmental impacts of construction materials choices, the literature shows that the combination of LCA and MCDA is significantly beneficial, as it can simplify the basic understanding of multiple perspectives in impact assessment [15]. Several MCDA methods have been discussed previously, including AHP (Analytic Hierarchy Process) [16], TOPSIS (Technique for Order Preference by Similarity to an Ideal Solution) [17], PROMETHEE (Preference Ranking Organization Method for Enrichment Evaluations) [18], and DEMATEL (Decision Making Trial and Evaluation Laboratory) [19].

In this study, the MCDA method chosen is the Fuzzy Analytic Hierarchy Process (FAHP), a semiquantitative technique aimed to enrich its precedent, the Analytic Hierarchy Process (AHP) [20]. AHP uses a scale of numbers that shows how many times more important or dominant one item is over another item related to the criterion against which they are compared [20]. However, the method assumes that the users have complete information on the subject analyzed and that all respondents are equally qualified, which rarely is the case [21]. Coping with inaccuracies and ambiguities not addressed by the AHP method, fuzzy logic is integrated into the process. The FAHP substitutes the subjective scale of numbers used in AHP with fuzzy triangular numbers, permitting a pairwise comparison matrix to cope with criteria measurement. In recent years, researchers have applied fuzzy logic to explore and solve problems in construction projects, including type-2 fuzzy logic systems (IT2FLS) and fuzzy Decision-Making Trial and Evaluation Laboratory (DEMATEL) [22,23].

Finally, to facilitate the simulations and data collection required to generate elaborate results on impacts associated with material choices, Building Information Modeling (BIM) is utilized in this work. BIM can improve the application of LCSA for construction material choice, as it represents a repository of digital information that enables the management of all data in a project [24]. Although the LCSA, MCDA, and BIM methodologies are already widespread in the literature, few applications integrate these concepts into a decision-support framework for design decisions in the construction sector.

The novelty of this study is based on the presentation of a framework that applies Building LCSA during the project design phase using an MCDA and BIM to provide a choice on the most suitable and sustainable construction materials in a project. The framework is designed to be applied in the project design phase to ensure maximum control over material decisions and thus avoid further modifications in later stages of the project when the costs of implementing change are higher.

The remainder of the study is organized as follows: a literature review is presented in Section 2. Section 3 explains the research methods, applying the proposed framework on a residential building. The results and discussions of the study are presented in Section 4. Finally, concluding remarks are presented in Section 5.

9.5 LITERATURE REVIEW

A literature review of the proposed methodologies (LCSA, MCDA, and BIM) is presented in this section to highlight the use of such approaches in the construction literature. The review also focuses on methods deployed to support contractors and designers in the choice of materials for construction projects.

9.5.1 Life Cycle Sustainability Assessment

The Life Cycle Sustainability Assessment (LCSA) is an interdisciplinary framework that evaluates the impacts associated with products and processes from an environmental, social, and economic perspective simultaneously [25]. In this way, LCSA comprises three main aspects, including LCA, LCC, and S-LCA. In the literature, however, many questions about the full application of LCSA are still discussed [2] and many studies still implement only part of the evaluation. This is mainly because the three pillars of sustainability have different maturity levels, which hinders the broad implementation of LCSA.

The International Standards Organization (ISO), in the 1990s, published the most recognized standards of Environmental Life Cycle Assessment (E-LCA) methodology, usually referred to just as Life Cycle Assessment (LCA). According to ISO 14040, LCA is the compilation of inputs, outputs, and potential environmental impacts of a product system throughout its life cycle [26]. This approach has been widely applied in the construction sector as an essential tool to evaluate construction materials' environmental impacts in the different phases of the project life cycle [27]. LCA can be performed to analyze new buildings over their whole life cycle and can be implemented on existing buildings over their remaining life [28].

The LCA methodology is broken down into four main steps [29]: (i) Goal and Scope definition; (ii) Life Cycle Inventory (LCI) analysis; (iii) Life Cycle Impact Assessment (LCIA); and (iv) Interpretation. This four-phase LCA framework can also be applied to LCC and S-LCA [30]. The first step in LCA involves defining the main aspects of the study, including i). the Functional Equivalent, which describes the primary function fulfilled by a product system and indicates how much of this function is to be considered in the LCA study; ii) the System Boundary, which refers to how far the analysis will be done (i.e., cradle-to-grave, cradle-to-gate, gate-to-gate, gate-to-grave); iii) the study's assumptions and limitations; and iv) the choice of the impact categories to be used, such as global warming potential (GWP), acidification, and eutrophication.

The second phase of the methodology involves the compilation and quantification of inputs and outputs for the Functional Equivalent throughout the product's life cycle. The third step aims at understanding and evaluating the magnitude and significance of the potential environmental impacts. Lastly, the interpretation phase represents a technique for identifying and assessing all the information from the previous stages concerning the defined goal and scope.

In addition to LCA, several LCC and S-LCA approaches have been developed. LCC is defined as an assessment of all costs associated with a product's life cycle linked, as perceived by the supplier, manufacturer, or consumer [31]. LCC thus provides a way of specifying the estimated total incremental cost of developing, producing, using, and retiring a particular product [32]. The primary objective of LCC is to optimize the lifecycle economic costs of a project. When implemented in the construction sector, the LCC approach estimates the net present value of all relevant costs throughout the building's life cycle, including construction costs, maintenance, repair and replacement costs, energy costs, and residual values [33].

On the other hand, S-LCA refers to a systematic method that accounts for all impacts borne by society throughout the life cycle of a product [34]. Using the S-LCA approach, the practitioner deals with positive and negative effects on society [35]. Regarding the use of this approach in the construction sector, different social impacts can be examined, such as impacts on workers' safety, fair salary, and access to material resources [36].

When it comes to selecting construction materials, applications of the LCSA method are still under development, and there are some limitations in the process. Fauzi et al. [37] discussed several issues found in the literature on the LCSA application, and one aspect that deserves great emphasis is the difficulty of integrating the three approaches together (i.e., LCA, LCC, and S-LCA). In addition, not all the environmental and social indicators can be calculated as a function of the study's functional equivalent, which generates a significant drawback in result interpretation. There is also the issue of the lack of reliable economic and social impact databases that are still under development in comparison to a range of reliable environmental impacts' databases.

9.5.2 Multi-Criteria Decision Analysis

In construction, it is necessary to consider different views of the stakeholders involved to decide on specific aspects of a project, including quality, security, ethics, finance, and human resource aspects. Hence, multiple criteria are often embodied in a significant number of the decisions undertaken during the design stage of a project, and these have to be analyzed to ensure an optimum decision. A high number of methods in the scientific literature support strategic decision makings such as mathematical optimization [38], fuzzy set theory [39], and the analytic hierarchy process (AHP) [40]. The use of the MCDA method is encouraged to generate effective, sustainable solutions in construction [15]. However, implementing these techniques requires systematic tools and methods to be developed.

Regarding the construction materials choice, several MCDA methods are already applied in the literature. Nadoushani et al. [41] used the Delphi and AHP methods to identify the most sustainable façade system, among five different alternatives, to replace a real building's existing worn façade. The authors considered environmental, social, and economic criteria in the analysis. Akadiri et al. [42] proposed a model for selecting sustainable construction materials for single-family housing in the United Kingdom using Fuzzy AHP.

In this work, the Fuzzy Analytic Hierarchy Process (FAHP) method is used. The FAHP approach enriches its precedent, Analytic Hierarchy Process (AHP), combining it with fuzzy logic theory [20]. AHP is based on the Newtonian and Cartesian way of thinking, which consists of breaking down the problem into smaller parts as many times as necessary until a precise and scalable level is reached. AHP requires the use of experts, and one-to-one comparison judgments are applied among similar criteria, generating the priorities for classifying the alternatives [43]. To counter the AHP method's deficiency in its reliance on expert input [44], the Fuzzy AHP method is deployed, employing the fuzzy set theory concepts in hierarchical structure analysis using fuzzy numbers instead of real numbers.

9.5.3 Building Information Modeling

The concept of Building Information Modeling (BIM) revolutionized the way construction projects are conceived by developing virtual models with parameterized elements. It allows a constant update of the project in a dynamic fashion. Thus, the resulting model is a data-rich, intelligent, and parametric digital representation of the facility [45]. It provides professionals with the necessary information to perform useful analysis. BIM-based software enables professionals to reduce costs, detect design errors, and track building timelines.

The adoption rate of BIM has increased significantly in recent years. BIM is commonly adopted for enhancing decision-making by reducing the amount of work involved in evaluating various alternatives in the early design stages [46]. Furthermore, BIM is considered an effective tool to assist in building life cycle analysis [47]. Many studies in the literature discuss the advantages and challenges of integrating BIM and LCA. However, a more in-depth discussion covering the three dimensions of sustainability is necessary. Llatas et al. [2] conducted a systematic literature review regarding the integration of LCSA and BIM. This study showed that most papers found in the literature use BIM solely for assessing environmental impacts produced by buildings. Only six papers were related to environmental and economic impacts simultaneously, while none of the studies reviewed included the analysis of social impacts.

Obrecht et al. [47] performed a systematic literature review of studies relating to BIM as a tool to facilitate Building LCA application. They found that BIM is mainly used as a repository of information in LCA analysis; the BIM-based software is utilized to generate the materials take-off. The quantities are exported to other software to perform the LCA analysis. In this case, the BIM-LCA integration occurs manually. Conversely, there are studies that propose how the exchange process could be automated. However, this discussion contemplates only the environmental dimension of the life cycle analysis.

In this study, BIM is considered the primary tool for creating the inventory database used in the LCSA. Modeling the building using a BIM platform will allow the automatic generation of material quantities. This would also enable simulations to be carried out of the building, which can be useful for generating additional data for the LCSA analysis. BIM simulations are already enabled by tools developed in the market, such as Navisworks and Synchro [48].

9.6 MATERIALS AND METHODS

The environmental, social, and economic assessments involved in building construction are guided by a set of European standards entitled 'Sustainability of construction works — Sustainability assessment of buildings,' which were utilized. These standards are divided into four main parts: Part 1 - General framework [49], Part 2 - Framework for the assessment of environmental performance [28], Part 3 - Framework for the assessment of social performance [50], and Part 4 - Framework for the assessment of economic performance [51]. The four-phase LCA framework presented by ISO Standards can be applied to LCSA [52]. As such, the conceptual framework proposed in this research, which is given in **Figure 3.1**, is based on recommendations from ISO 14040 and 14044 standards on LCA [26,53]. ISO 15686-5, entitled 'Buildings and constructed assets - Service life planning - Part 5: Life-cycle costing', was used to guide the LCC application [54]. The UNEP 'Guidelines for Social Life Cycle Assessment of Products' was used as the basis for the application of S-LCA [55]. Finally, LCA, LCC, and S-LCA's harmonization was implemented into the proposed method according to what has already been discussed in the literature [2,37].

BIM is utilized to facilitate the material quantity take-off and as a simulation tool to calculate and understand the impacts of the building's whole life cycle [2]. The Fuzzy Analytic Hierarchy Process (FAHP) method is adopted as the MCDA method.

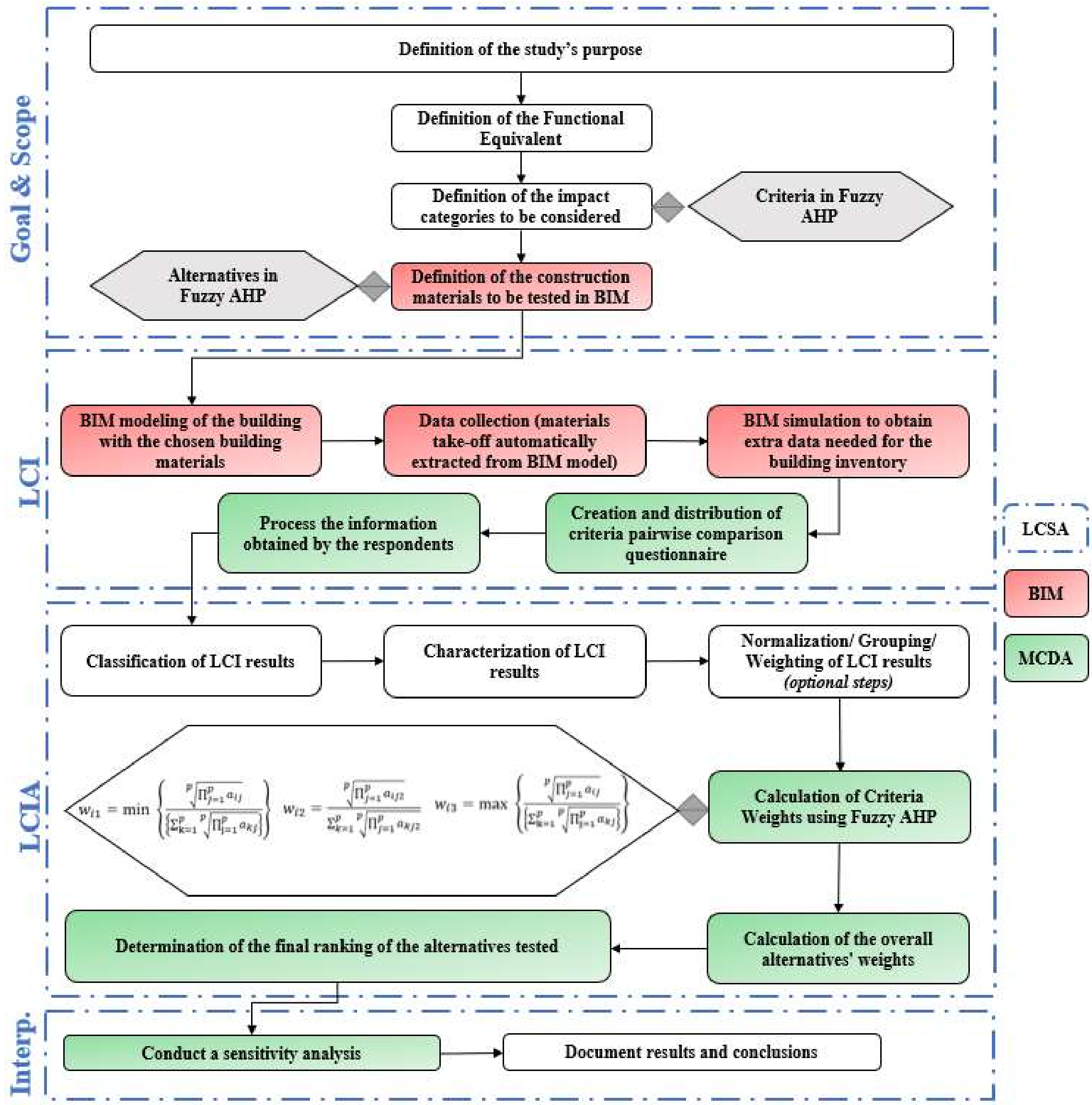

Figure 9.1 - Conceptual framework proposed in this work

The first stage of the framework in **Figure 3.1** involves defining all the features of the project. For LCSA, it is necessary to identify the goal and scope of the analysis clearly and accurately, including functional equivalent, system boundary, target audience, assumptions, and limitations of the study. A cradle-to-grave analysis is adopted in this study, where the following phases are considered: extraction of raw materials, transportation, fabrication, construction, operation, and demolition of the building. However, the study may also be restricted to only some stages of the building's life cycle depending on the goals of the decision-maker. The decision-maker can determine the study's system boundaries, considering the purpose of the analysis and its target audience [56]. The impact categories are to be chosen in line with the most relevant to the goals of the analysis. Construction materials are also clearly defined in this step. The impact categories from LCSA will be the criteria utilized in the decision-making process with MCDA, while the construction materials modeled in BIM will be the alternatives to be compared via MCDA.

It is necessary to choose the most appropriate MCDA method for the project, defining a multi-objective formulation that is the aim of the decision-maker to optimize. In this study, FAHP was proposed based on the constrained fuzzy arithmetic instead of the concept of standard fuzzy arithmetic. The constrained fuzzy arithmetic is a recent approach that has the advantage of eliminating the false increase of uncertainty of the overall fuzzy weights. In this study, it corresponds to a fuzzy extension of the geometric mean method, as it is the most applied approach in the literature [20].

The second step herein is to define the LCI and the three-dimensional (3-D) model developed in a BIM-based software. This step will be the primary tool to assist data collection and inventory creation. Utilizing BIM makes it possible to gather environmental, economic, and social data in the same model [57]. At this stage, all building data (i.e., construction materials and alternative construction methods) must be inserted into the BIM digital model to facilitate the analysis's continuity and data collection. Depending on the impact categories chosen for the study, it may be necessary to enrich the data collection with supplementary information. Therefore, it is suggested to use the BIM model to perform simulations and analyses that enable the determination of these additional data. Developments in BIM mean that professionals can make use of the interoperability between software so that there is no information loss during the process. Finally, regarding the application of FAHP, it is necessary to create a questionnaire tool to obtain professionals' opinions on their preferences among the impact categories tested, based on a pairwise comparison. The professionals' opinions must be collected at this stage so that the data can then be evaluated.

The third phase of the study necessitates evaluating the LCIA of the environmental, social, and economic pillars. At this analysis level, the LCIA methods assess the data collected during the LCI phase (i.e., ReCIPe [58], TRACI [59], CML [60], etc.). The classification and characterization steps are mandatory in LCIA, while normalization, grouping, and weighting are optional. In order to rank the alternatives, the MCDA method chosen is utilized. **Figure 3.2** shows how the analysis would be organized at this phase.

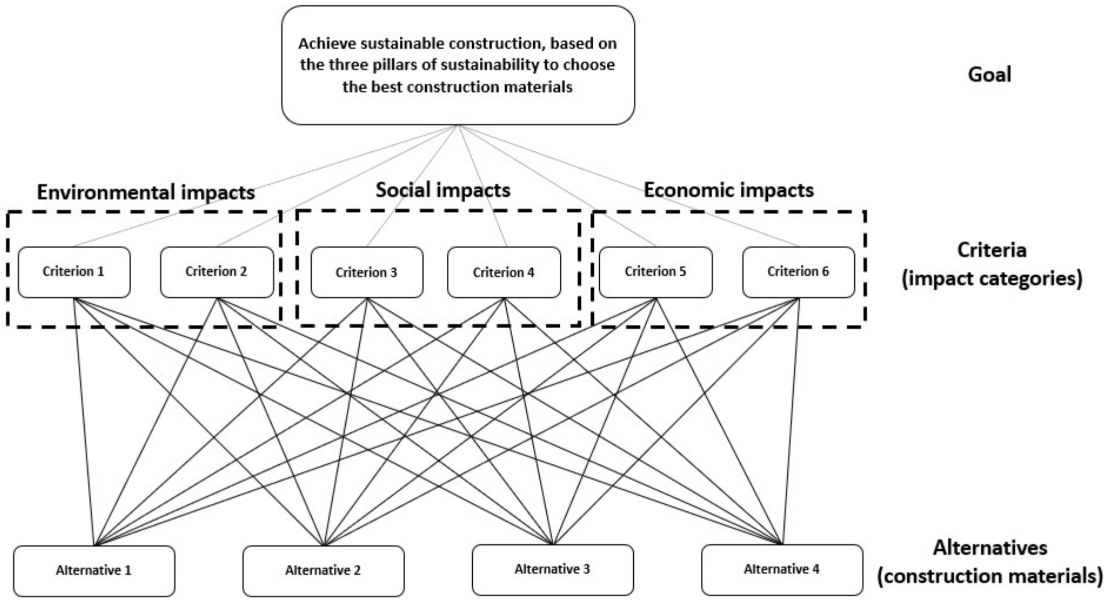

Figure 9.2 - Hierarchy used in the proposed framework

Depending on the project and the stakeholders involved, the ranking can be made in different ways since different impact categories can be prioritized in each case. For example, in a given project, environmental impacts may have a greater weight in comparison to the economic impacts for the target audience; this, however, may not be true for all projects. As such, the MCDA method is applied in this stage to calculate the criteria weights.

In FAHP, the process of pairwise comparison, similar to AHP, is conducted based on a questionnaire to determine how many times more important one object is over another. The respondents use a scale of integers from 1 (equally important) to 9 (extremely more important) in the questionnaire, as was proposed by Saaty in the crisp AHP method. The results are then transformed into triangular fuzzy numbers (TFN) to solve uncertainties in the response given. A TFN is a fuzzy number whose membership function is determined by three real numbers $c_1 \leq c_2 \leq c_3$ and it is commonly represented by $\tilde{c} = (c_1, c_2, c_3)$.

Let $\tilde{A} = \{\tilde{a}_{ij}\}_{i,j=1}^{p}$, $\tilde{a}_{ij} = (a_{ij}\ , a_{ij2}, a_{ij}\ )$ be the fuzzy pairwise comparison matrix for any $i, j \in \{1, \dots, p\}$, obtained after transforming the responses of the questionnaire distributed among professionals into TFNs. $\tilde{A}$ is a square matrix whose elements are TFNs defined in the range $[\frac{1}{9}, 9]$ and with the main diagonal equal to (1, 1, 1), since these elements represent the comparison of one object with itself, $\tilde{a}_{ii}$.

According to the fuzzy extension of the geometric mean method, the criteria weights are obtained by normalizing the geometric means of the rows of the pairwise comparison matrix

$\tilde{A}$. The problem found in this method, when the concept of standard fuzzy arithmetic is utilized, is that different values of the same variables enter the calculation simultaneously (for more details, see Krejcí et al. [61]), which means that the resulting TFNs do not represent the true ranges for fuzzy weights.

Therefore, when the standard fuzzy arithmetic is used, the calculation leads to a false increase in the model's uncertainty. This work proposes the use of constrained fuzzy arithmetic to calculate criteria weights. The fuzzy weight $\widetilde{w}$ of each criterion of the analysis is calculated based on the results of the pairwise comparison. For TFN, three different formulae are needed to calculate the lower, middle, and upper significant values. The criteria weights are determined by Eq. (2) - (4) [62], where $\widetilde{w}_i$ represents the fuzzy weight of criterion i and w_{i1}, w_{i2} and w_{i3} are real numbers, corresponding to the significant values of the triangular fuzzy number denoted as $\widetilde{w}_i = (w_{i1}, w_{i2}, w_{i3})$, $w_{i1} < w_{i2} < w_{i3}$.

$$w_{i1} = \min\left\{\frac{\sqrt[p]{\prod_{j=1}^{p} a_{ij}}}{\left\{\sum_{k=1}^{p} \sqrt[p]{\prod_{j=1}^{p} a_{kj}}\right\}};\ a_{rs} \in [a_{rs1}, a_{rs}\ ], \qquad r,s = 1,\dots,p, \qquad r < s\right\} \tag{2}$$

$$w_{i2} = \frac{\sqrt[p]{\prod_{j=1}^{p} a_{ij2}}}{\sum_{k=1}^{p} \sqrt[p]{\prod_{j=1}^{p} a_{kj2}}} \tag{3}$$

$$w_{i3} = \max\left\{\frac{\sqrt[p]{\prod_{j=1}^{p} a_{ij}}}{\left\{\sum_{k=1}^{p} \sqrt[p]{\prod_{j=1}^{p} a_{kj}}\right\}};\ a_{rs} \in [a_{rs}\ , a_{rs}\ ], \qquad r,s = 1,\dots,p, \qquad r < s\right\} \tag{4}$$

The defuzzification process is then carried out, in which a fuzzy set is mapped to a crisp set. An example of a defuzzification method widely used in the literature is the center of gravity (COG) method [63], in which the crisp set is obtained via the arithmetic mean of the elements of the fuzzy set. In this study, the authors propose the following formula:

$$COG(w_i) = \frac{\sum_{t=1}^{3} w_{it}}{3} \tag{5}$$

Defuzzified values are then normalized, and it is possible to evaluate the alternatives of construction materials, taking into account the ranking already created among the criteria and the results obtained from LCIA. The LCIA results should also be normalized, so that data from different impact categories can be compared on a common scale. The LCIA normalized values are considered as the weights of the alternative concerning each criterion, with u_i^k being the representation of the weight of the k-th alternative concerning criterion i. Then, the overall weight of alternative k will be calculated by Eq. (6), presented below:

$$u_k = \sum_{i=1}^{p} w_i \,. u_i^k \tag{6}$$

The last step herein is the interpretation phase, which corresponds to the MCDA method's application to assist the professionals in the decision-making process. The decision-maker must be able to select the optimum sustainable material for the project based on the three pillars of sustainability. In these terms, performing a Sensitivity Analysis (SA) is encouraged, as it allows the LCSA practitioner to compare all available alternatives that have been highlighted as suitable from the previous steps. Sensitivity analysis seeks to determine the effect of a given item's variation on the total impact assessed for that item. A sensitivity analysis is conducted to monitor the preference ranking's robustness among the alternatives tested in this work.

9.7 TOOLS TO VALIDATE THE PROPOSED FRAMEWORK

This part illustrates the practical application of the four phases of LCSA proposed in this study.

9.7.1 Goal and Scope

The scope of this study is to determine the best building materials among a pre-defined material list, considering environmental, economic, and social aspects. This work's functional equivalent consists of a 36-unit residential building composed of 10 stories (ground floor, eight floors, and a roof) constructed in Rio de Janeiro, Brazil. Each unit consists of two bedrooms, a sitting room, a kitchen, a bathroom, and a service area. The building service life considered in this work is 60 years. Finally, a gate-to-grave system boundary is used, comprising the following stages of the building life-cycle: construction, operation and maintenance (O&M), and end-of-life. For the end-of-life phase of the building, it was assumed that the building would be imploded, and the analysis would include the relevant material collection rates and landfilling rates. The same system boundary is adopted during the environmental, economic, and social analyses so that the harmonization of the three approaches occurs satisfactorily.

The environmental impact categories chosen for this study are widely discussed in the literature [64] and include Global Warming Potential (GWP), Acidification Potential (AP), and Eutrophication Potential (EP). GWP represents a measure of greenhouse gas emissions that may have adverse impacts on the ecosystem and human health. The acidification potential represents the ability to increase the concentration of H^+ in a molecule in the presence of water, which includes potential effects such as forest decline and deterioration of construction materials. The eutrophication potential measures excessively high levels of macronutrients, such as nitrogen and phosphorus, and can cause an undesirable change in species composition and high biomass production [65].

For the economic analysis, the impact category is the life-cycle cost associated with the building phases considered in the system boundary. During the O&M phase, in addition to the annual building maintenance and repair costs, it was decided to consider the annual energy cost for lighting and HVAC. Improving energy efficiency in buildings plays a crucial role in ensuring sustainable developments in the future, as it is known that energy resources are limited. Besides, construction material choice directly influences the energy efficiency and the sustainability of a building [66]. Lastly, for the social analysis, the stakeholder category adopted in this work refers to the workers. From this perspective, the impact category analyzed is fair salary, with Fair Wage Potential (FWP) adopted as the quantitative indicator.

To implement FAHP, each impact category is considered as a criterion. Since the evaluation criteria for building materials can have various connotations and meanings, there is no logical reason to treat them as if they are each of equal importance [15]. The dimensions and criteria chosen are presented in **Table 3.1**, where D_i refers to the dimension i, while C_j refers to the criterion j.

Table 0.1 - Dimensions and criteria to be considered in the analysis

Dimensions (D_i)	Criteria (C_j)	Units
(D_1) Environmental	(C_1) Global Warming Potential	kg CO_2 eq.
	(C_2) Acidification Potential	kg SO_2 eq.
	(C_3) Eutrophication Potential	kg N eq.
(D_2) Economic	(C_4) Life-cycle cost	Brazilian Real (R$)
(D_3) Social	(C_5) Fair Wage Potential	FWeq.

9.7.2 Life-Cycle Inventory

The building prototype for the case study was developed in Autodesk Revit®, a BIM-based software [67]. In this work, BIM is used as a tool to facilitate the material take-off process and the simulation needed to compare different building materials' behavior in terms of energy consumption. All materials to be used in the building must be defined in the BIM 3D model, with the definition of their physical and thermal properties. Therefore, the modeling was developed based on Level of Development (LOD) 400, in which the components are graphically represented as a specific object with detailing, fabrication, assembly, and installation information. The 3-D view and the plan view of the building are shown in **Figure 3.3**.

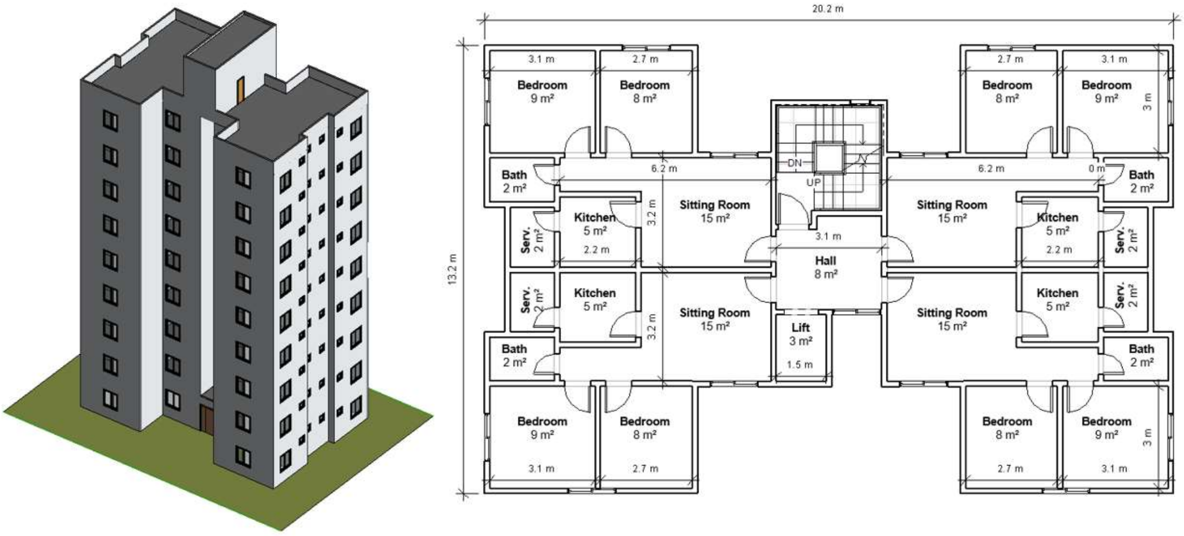

Figure 9.3 - Case study modeled in a BIM-based software

The materials for the different alternatives have been defined based on the experience of the professionals involved in this work, as shown in **Table 3.2**. Each alternative's material take-off was determined via four different BIM models, allowing an automatic quantitative data collection. Regarding the environmental analysis, the service life, in years, for each material, in addition to the transportation distance, in kilometers, from the manufacturer location to the building site by diesel truck, were defined.

An energy model was created for each alternative in the same BIM-based software used to model the structure regarding the economic analysis. An energy model in Autodesk Revit® is a particular form of geometry used by the energy simulation mechanism, capturing the building's main heat transfer paths. It is developed with Green Building XML schema (gbXML), a language designed to facilitate the transfer of building data stored in Building Information Models (BIM) to environmental analysis tools [68]. The assumptions made to create the energy models were the following: the building type is Multi-Family; the Sliver Space Tolerance is 0.3048m, and the building HVAC system is Split System with mechanical ventilation via cooling. The building's annual energy use was calculated, considering the energy for HVAC and lighting, as shown in **Table 3.3**.

Table 0.2 - Database concerning the four alternatives, where B.L. stands for 'Building Life.'

BIM Category	**Alternative 1**			
	Materials	**Material mass (kg)**	**Service Life (years)**	**Transportation distance (km)**
Ceilings	Acoustic ceiling system, fiberglass	4,390	50	72
	Suspended grid	1,827	50	72
	Paint, interior acrylic latex	318.6	7	24
Doors	Kiln-dried Ash hardwood lumber of 4"	5,810.31	50	38
	Wood stain, water-based	36.87	10	38
Slabs	Structural concrete, 4001-5000 psi	565,175	60 (B.L.)	17
	Steel	5,448	60 (B.L.)	17
Floors	Ceramic tile, unglazed	35,242	60	72
	Cement mortar	6,294	60	72
	Cement grout	780.6	60	72
Walls	Brick, 1/2" joint	929,061	150	17
	Lime mortar	161,037	60	72
	Grout fill: thickset mortar	260,827	60	72
	Reinforcing Steel	16,451	60	17
	Paint, exterior acrylic latex	1,052	10	24
Windows	Glazing, monolithic sheet, tempered	6,610	40	40
	Aluminium, (100x20x2) mm, 1,28 kg/m	1,002.45	60	63
	Paint, enamel, solvent-based	63.9	15	63
BIM Category	**Alternative 2**			
	Materials	**Material mass (kg)**	**Service Life (years)**	**Transportation distance (km)**
Ceilings	Ceiling tile, aluminium (3.37kg/m²)	5,498	70	63
	Suspended grid	1,827	50	63
	Powder coating, metal stock	636.3	50	1
Doors	Domestic softwood, US, AWC - EPD	2,333	30	38
	Polyurethane foam (PUR) rigid board	135.68	75	29

Table 3.2 - Database concerning the four alternatives, where B.L. stands for 'Building Life,' Continued.

Slabs	Glass Fibre Reinforced Concrete	567,321	60 (B.L.)	40
	Steel	81,409	60 (B.L.)	18
Floors	Terracotta tile	89,152	75	72
	Thickset mortar	13,280	60	72
	Cement grout, Latricrete - EPD	372,1	60	72
Walls	Concrete masonry unit (CMU), solid	1,217,571	100	72
	Mortar type N	71,158	60	72
	Paint, exterior acrylic latex	1,052	10	24
Windows	Glazing, double, insulated (air)	4,715	40	40
	Aluminium extrusion, anodized, AEC - EPD	3,318.6	60	63
	Paint, exterior metal coating, silicone-based	20.95	30	24
BIM Category	**Alternative 3**			
	Materials	**Material mass (kg)**	**Service Life (years)**	**Transportation distance (km)**
Ceilings	Acoustic ceiling tile - galvanized steel	7,962	75	43
	Suspended grid	1,827	50	43
Doors	Redwood decking, AWC - EPD	4,876	25	24
Slabs	Glass Fibre Reinforced Concrete	567,321	60 (B.L.)	40
	Fabricated steel reinforcement	81,409	60 (B.L.)	18
Floors	Tile backer board	16,270	40	72
Walls	Perlite filled clay block, Poroton	345,789	150	12
	Lime mortar (Mortar type K)	107,267	60	72
	Thickset mortar	260,941	60	72
	Fabricated steel reinforcement	16,458	60 (B.L.)	18
	Paint, exterior acrylic latex	1,052	10	24
Windows	Glazing, triple, insulated (air)	7,139	40	40
	Aluminium extrusion, anodized	3,318.6	60	63
	Paint, exterior metal coating, silicone-based	20.95	30	24
BIM Category	**Alternative 4**			
	Materials	**Material mass (kg)**	**Service Life (years)**	**Transportation distance (km)**
Ceilings	Ceiling tile, steel mesh	9,658	75	31
	Suspended grid	1,827	50	43
	Zinc coating (galvanized) for steel G60	298.6	60 (B.L.)	31
Doors	White oak lumber, 4 inches	190.5	50	38

Table 3.2 - Database concerning the four alternatives, where B.L. stands for 'Building Life,' Continued.

Slabs	Structural concrete, 4001-5000 psi	548,060	60 (B.L.)	24
	Steel	5,448	60 (B.L.)	17
Floors	Granite tile	60,178	50	21
	Cement mortar, Latricrete - EPD	7,143	60	72
	Cement grout, Latricrete - EPD	372.1	60	72
Walls	Perlite filled clay block, Poroton - EPD	345,789	150	12
	Lime mortar (Mortar type K)	107,267	60	72
	Thickset mortar	260,941	60	72
	Steel, concrete reinforcing steel	3,515	60 (B.L.)	17
	Paint, Brillux, Silicone facade paint - EPD	1,052	15	24
Windows	Electrochromic glass, Saint-Gobain, Sage Glass	8,386.3	50	40
	Aluminium extrusion, anodized, AEC - EPD	3,318.6	60	63
	Paint, exterior metal coating, silicone-based	20.95	30	24

Table 0.3 - Results of energy simulations in the BIM models

Alternatives	**Annual Energy Consumption for Lighting (kWh)**	**Annual Energy Consumption for HVAC (kWh)**
Alternative 1	21,591	81,225
Alternative 2	19,802	62,709
Alternative 3	20,234	71,739
Alternative 4	23,606	63,825

Data regarding the prices of materials, equipment, and construction services were used to analyze the economic impacts of the alternatives, and data about the construction workers in Rio de Janeiro, Brazil, were used to analyze the social implications. Depending on the materials and construction methods chosen for the building, different skills will be required to carry out the associated activities. The budget for materials and services and the number of professionals required for each alternative were determined based on the data found in SINAPI, which can be translated as ‘the Brazilian System of Costs and Indices Research of Civil Construction.’ SINAPI aims to produce monthly series of costs and indices for the Brazilian construction sector, along with a monthly series of average labor wages and average prices for materials, equipment, and construction services [69]. The data collected are summarized in **Table 3.4**.

Table 0.4 - Brazilian data regarding the resource requirement of workers in the construction sector

Category	Brazilian average wage *(Brazilian Real – R$)*	Professionals needed in each alternative			
		Construction phase			
		Alternative 01	Alternative 02	Alternative 03	Alternative 04
Bricklayer's mate	R$ 1,442.05	14	10	14	10
Bricklayer - level 1	R$ 1,507.78	0	3	0	0
Bricklayer - level 2	R$ 2,010.37	10	9	7	8
Bricklayer - level 3	R$ 2,372.24	2	0	4	5
Bricklayer - level 4	R$ 2,734.10	0	2	0	0
Master builder	R$ 3,091.89	1	1	1	1
Site engineer	R$ 9,483.29	1	1	1	1
		O&M phase			
Bricklayer/painter	R$ 1.846,12	2	2	2	2
		End-of-life phase			
Bricklayer's mate	R$ 1,442.05	2	2	2	2
Master builder	R$ 3,091.89	1	1	1	1

Finally, a questionnaire was distributed to the respondents to obtain their preferences among criteria, following what is proposed in the AHP method. The survey had been sent to 12 Brazilian engineers, but only 7 of them responded. All respondents had to have at least two years' experience in the LCA approach. Among them, four respondents work or have worked as site engineers, while three are sustainability engineers. The questionnaire required the engineers to conduct a pairwise comparison among the material sustainability criteria adopted in this study, as presented in **Figure 3.4**. The arithmetic mean of the responses from the seven professionals was calculated for each pairwise comparison. The final results are shown in **Table 3.5** and treated in the next stage of the proposed framework to transform crisp numbers into fuzzy ones.

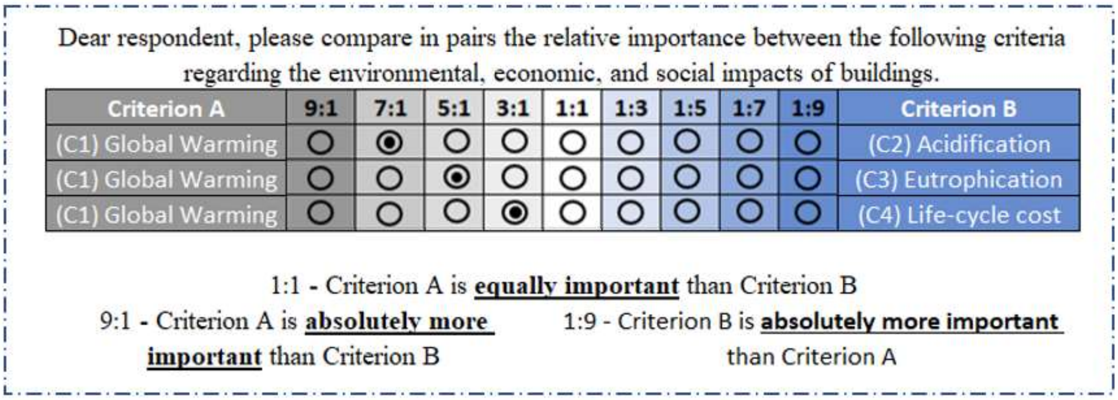

Figure 9.4 - Part of the questionnaire distributed to the engineers

Table 0.5 - Results of the pairwise comparison questionnaire based on crisp AHP.

	C_1	C_2	C_3	C_4	C_5
C_1	1	3	5	$^{1}/_{3}$	$^{1}/_{3}$
C_2	$^{1}/_{3}$	1	3	$^{1}/_{5}$	$^{1}/_{3}$
C_3	$^{1}/_{5}$	$^{1}/_{3}$	1	$^{1}/_{7}$	$^{1}/_{5}$
C_4	3	5	7	1	3
C_5	3	3	5	$^{1}/_{3}$	1

9.7.3 Life Cycle Impact Assessment

Life Cycle Impact Assessment is the third phase of the LCSA application. Different LCIA methodologies are available in the literature that represent different ways of evaluating the data collected during the LCI phase. The results of this phase are presented separately for each of the environmental, economic, and social impacts, as follows.

9.7.3.1 Environmental Impacts

TRACI 2.1 characterization scheme was adopted in this work to classify and characterize the environmental impacts [65]. Within the TRACI methodology, the impact categories are characterized at the midpoint level, drawing cause-effect chains to show the point at which each category is characterized. The Tally® application was used in this study to match each material in the 3-D BIM model in Autodesk Revit® with the GaBi database materials, allowing an automated exchange process [70]. The results for the four alternatives are presented in **Table 3.6**.

Table 0.6 - Environmental impacts for the alternatives evaluated in this study

	Impact Category	Construction phase	O&M phase	End-of-life phase	Total
Alt. 01	(C1) Global Warming (kg CO_2eq)	3,123	50,521	44,940	**98,584**
	(C2) Acidification (kg SO_2eq)	14.47	311.7	191.6	**517.77**
	(C3) Eutrophication (kg Neq)	1,178	17.23	10.49	**1,205.72**
Alt. 02	(C1) Global Warming (kg CO_2eq)	6,364	216,551	41,924	**264,839**
	(C2) Acidification (kg SO_2eq)	29.49	885.1	187.4	**1,101.99**
	(C3) Eutrophication (kg Neq)	2.40	41.82	9.99	**54.21**
Alt. 03	(C1) Global Warming (kg CO_2eq)	2,636	212,205	32,161	**247,002**
	(C2) Acidification (kg SO_2eq)	12.21	951	134.3	**1,097.51**
	(C3) Eutrophication (kg Neq)	0.99	45.35	7.49	**53.83**
Alt. 04	(C1) Global Warming (kg CO_2eq)	2,599	547,488	51,254	**601,341**
	(C2) Acidification (kg SO_2eq)	12.04	4,817	172	**5,001.04**
	(C3) Eutrophication (kg Neq)	0.98	112	11	**123.98**

9.7.3.2 Economic Impacts

For the economic analysis, the calculation was performed in Microsoft Excel. The prices and costs provided by SINAPI concerning the city of Rio de Janeiro, published on January 21, 2021, were imported to Microsoft Excel to determine the life-cycle cost for each alternative [69]. Regarding the annual expenses associated with the O&M phase, the net present value (NPV) formula was used in Excel, a metric to calculate the present value of a succession of future payments, deducting a capital cost rate. A rate of 3% was considered in the calculations.

The values presented in Table 3 regarding the annual consumption of energy in each alternative were multiplied by the tariff charged by the private company responsible for the electricity generation, distribution, and sale in Rio de Janeiro. The low voltage tariff for residential units that consume up to 300 kWh in January 2021 is 0.84183 [71]. It was considered that the annual consumption measured by BIM simulations would be the same throughout the building service life, that is, for 60 years. Regarding the annual maintenance and repair costs, an estimate was made considering the materials' service life for each alternative and the values presented in SINAPI. Elevator maintenance costs were not considered in the analysis, as the objective of this study is to focus on the choice of construction materials. The final results are shown in **Table 3.7**.

Table 0.7 - Life-cycle cost for the alternatives evaluated in this study, with the costs presented in Brazilian Real

Alternatives	Construction cost	Energy cost	Maintenance cost	End-of-life cost	Total life-cycle cost
Alt. 01	R$ 4,149,370.18	R$ 15,056,422.71	R$ 465,604.26	R$ 58,000.00	R$ 19,729,397.15
Alt. 02	R$ 4,225,102.32	R$ 12,082,950.40	R$ 614,177.41	R$ 58,000.00	R$ 16,980,230.13
Alt. 03	R$ 5,730,095.63	R$ 13,468,569.17	R$ 749,241.23	R$ 58,000.00	R$ 20,005,906.03
Alt. 04	R$ 5,426,852.74	R$ 12,803,436.88	R$ 619,001.18	R$ 58,000.00	R$ 18,907,290.80

9.7.3.3 Social Impacts

For the social analysis, the calculation was also performed in Microsoft Excel. The social impact category used the characterization model proposed by Neugebauer et al. [72] to transfer the qualitative midpoint impact category named 'Fair Wage' into a quantitative one. The inventory results of the actual average remuneration and the actual working time are multiplied with the regionalized inequality characterization factor. The Gini Coefficient related to Brazil, a measure of the deviation of income distribution among individuals or households within a country from a perfectly equal distribution, was adopted [73]. For this coefficient, a value of 0 represents absolute equality, and a value of 1 represents absolute inequality. Brazil occupies the 84ª position in the rankings, with a Gini Coefficient of 0.539.

Neugebauer et al. [72] proposed the following formula to characterize this impact category:

$$FWP_n = \frac{RW_n}{MLW_n} \times \frac{CWT_n}{RWT_n} \times \left(1 - IEF_n{}^2\right) \tag{7}$$

Where FWP_n indicates the Fair wage potential [expressed in FWeq.] representing process n within a product's life cycle taking place at a defined location; RW_n indicates the average monthly wages paid to the workers employed in process n; MLW_n is the minimum living monthly wages in the respective country or region; CWT_n represents the contracted working time per country or sector [hours/week]; RWT_n indicates the real working time [hours/week] of workers performing the process n; and IEF_n represents the inequality factor [expressed in percentages] of the country or region where process n is performed.

The MLW_n is the Brazilian minimum wage in January 2021, taken as R$ 1,100.00, while CWT_n equals 40 hours per week. RWT_n is equal to 49 hours for bricklayer's mates, 41 hours for site engineers, and 44 hours for the other categories. The Fair Wage Potential was calculated in Microsoft Excel, and the results are shown in **Table 3.8**.

Table 0.8 - Fair Wage Potential for the different workers' categories

Category	FWP_n (FWeq.)
Bricklayer's mate	0.7593
Bricklayer - Level 1	0.8841
Bricklayer - Level 2	1.1788
Bricklayer - Level 3	1.3910
Bricklayer - Level 4	1.6031
Master builder	1.8129
Site Engineer	5.9674
Bricklayer/Painter	1.0825

In order to assign this indicator to the functional equivalent, this work proposes to calculate a weighted average of these values, with the weights corresponding to the number of professionals in each category. With this, the fair wage potential for each alternative was obtained.

Finally, it is important to note that the FWP indicator is the only one to be maximized in this study; all others correspond to negative impacts and should be minimized. In order to facilitate the application of the MCDA method and the ranking of alternatives to be tested, the authors suggest that the inverse of FWP_n be used as the final indicator in the analysis. In this way, all the indicators used will be minimized. This calculation was performed, and the final results are presented in **Table 3.9**.

Table 0.9 - Social impacts for the alternatives evaluated in this study

Alternatives	Final results for social analysis
Alt. 01	0.858
Alt. 02	0.830
Alt. 03	0.884
Alt. 04	0.805

9.7.3.4 Weight Generation

The MCDA method is used to weigh the criteria established. The results obtained in the opinion questionnaire, presented in Table 5, need to be transformed into triangular fuzzy numbers. Among the several AHP fuzzification approaches to convert a crisp set to a fuzzy set, it was decided to apply the fuzzy extension of the geometric mean method based on constrained fuzzy arithmetic. Therefore, the pairwise comparison matrix elements were modeled by triangular fuzzy numbers, as shown in **Table 3.10**.

Table 0.10 - Fuzzy pairwise comparison matrix of the criteria

	C_1	C_2	C_3	C_4	C_5
C_1	(1,1,1)	(2,3,4)	(4,5,6)	$(\frac{1}{4},\frac{1}{3},\frac{1}{2})$	$(\frac{1}{4},\frac{1}{3},\frac{1}{2})$
C_2	$(\frac{1}{4},\frac{1}{3},\frac{1}{2})$	(1,1,1)	(2,3,4)	$(\frac{1}{6},\frac{1}{5},\frac{1}{4})$	$(\frac{1}{4},\frac{1}{3},\frac{1}{2})$
C_3	$(\frac{1}{6},\frac{1}{5},\frac{1}{4})$	$(\frac{1}{4},\frac{1}{3},\frac{1}{2})$	(1,1,1)	$(\frac{1}{8},\frac{1}{7},\frac{1}{6})$	$(\frac{1}{6},\frac{1}{5},\frac{1}{4})$
C_4	(2,3,4)	(4,5,6)	(6,7,8)	(1,1,1)	(2,3,4)
C_5	(2,3,4)	(2,3,4)	(4,5,6)	$(\frac{1}{4},\frac{1}{3},\frac{1}{2})$	(1,1,1)

With the pairwise comparison matrix constructed, criteria fuzzy weights can be obtained by Eq. (2) - (4). Then, the triangular fuzzy numbers were deffuzified using Eq. (5), and the nonfuzzy normalized weights were also calculated, as highlighted in **Table 3.11**. In order to facilitate the application of the formulas, the R Project for Statistical Computing was used, a free software environment for statistical computing and graphics [74].

Table 0.11 - Fuzzy and nonfuzzy criteria weights

Criteria	**Fuzzy Weights**	**Defuzzified Weights**	**Nonfuzzy Normalized Weights**
C_1	$\widetilde{w}_1 = (0.1216; 0.1616; 0.2184)$	$w_1 = 0.167$	$w_1 = 0.166$
C_2	$\widetilde{w}_2 = (0.0638; 0.0849; 0.1172)$	$w_2 = 0.089$	$w_2 = 0.088$
C_3	$\widetilde{w}_3 = (0.0337; 0.0417; 0.0544)$	$w_3 = 0.043$	$w_3 = 0.043$
C_4	$\widetilde{w}_4 = (0.3800; 0.4610; 0.5234)$	$w_4 = 0.455$	$w_4 = 0.451$
C_5	$\widetilde{w}_5 = (0.1876; 0.2508; 0.3218)$	$w_5 = 0.253$	$w_5 = 0.252$

With the weights of the criteria properly calculated, the process of evaluating the alternatives begins. The environmental, economic, and social LCIA results, referring to the four different material alternatives for the building, are normalized. The final normalized values will be considered as the weights of the alternative concerning each criterion. The normalization process results are presented in **Table 3.12**.

Table 0.12 - Alternative weights concerning the particular criteria

	A1	**A2**	**A3**	**A4**
C1	u_1^1 =0.081	$u_1^2 = 0.219$	$u_1^3 = 0.204$	$u_1^4 = 0.496$
C2	$u_2^1 = 0.067$	$u_2^2 = 0.143$	$u_2^3 = 0.142$	$u_2^4 = 0.648$
C3	$u_3^1 = 0.839$	$u_3^2 = 0.038$	$u_3^3 = 0.037$	$u_3^4 = 0.086$
C4	$u_4^1 = 0.261$	$u_4^2 = 0.225$	$u_4^3 = 0.265$	$u_4^4 = 0.250$
C5	$u_5^1 = 0.254$	$u_5^2 = 0.246$	$u_5^3 = 0.262$	$u_5^4 = 0.238$

With this, it is possible to create the final ranking of the alternatives utilizing Eq. (6) to calculate the alternatives' overall weights. As all the criteria chosen in this study indicate impact categories that should be minimized, the best alternative is the one with the lowest overall weight. The results are presented in **Table 3.13**.

Table 0.13 - Overall weights of the alternatives

Alternatives	**Overall weights**	**Ranking**
A1	$u_1 = 0.2372$	3rd
A2	$u_2 = 0.2137$	1st
A3	$u_3 = 0.2332$	2nd
A4	$u_4 = 0.3159$	4th

9.7.4 Interpretation

The consistency ratio (CR) of the criteria pairwise comparison matrix is 0.062; that is, CR is less than 0.1. Hence, the study is considered consistent and acceptable. The consistency ratio of a matrix can be determined by using Eq. (8), as follows:

$$CR = \frac{CI}{RI} \tag{8}$$

Where CI and RI are respectively the consistency index and the random index.

Alternative 2 is the most recommended for the analyzed building, corresponding to the alternative that achieves the best results concerning the sustainability criteria adopted. However, it is essential to note that the alternatives' overall ordering is strongly dependent on the criteria chosen. A sensitivity analysis is required to monitor the robustness of the preference ranking among the alternatives. The sensitivity analysis is carried out by gradual changes of the values of each criterion, whether global warming potential (C1), acidification potential (C2), eutrophication potential (C3), the life-cycle cost (C4), or fair wage potential (C5), and then observing the rank order due to such changes. In this way, the behavior of the ranking of alternatives could be monitored. Each criterion's weights were changed until reaching the null value, and then a new ranking was generated in each case. **Table 3.14** shows these results.

Table 0.14 - Sensitivity analysis results

	C_1 = null value		C_2 = null value	
Alternatives	Overall weights	Ranking	Overall weights	Ranking
A_1	$u_1 = 0.2237$	3rd	$u_1 = 0.2313$	3rd
A_2	$u_2 = 0.1774$	1st	$u_2 = 0.2011$	1st
A_3	$u_3 = 0.1994$	2nd	$u_3 = 0.2207$	2nd
A_4	$u_4 = 0.2336$	4th	$u_4 = 0.2589$	4th
	C_3 = null value		C_4 = null value	
Alternatives	Overall weights	Ranking	Overall weights	Ranking
A_1	$u_1 = 0.2011$	1st	$u_1 = 0.1195$	3rd
A_2	$u_2 = 0.2120$	2nd	$u_2 = 0.1124$	1st
A_3	$u_3 = 0.2316$	3rd	$u_3 = 0.1139$	2nd
A_4	$u_4 = 0.3122$	4th	$u_4 = 0.2032$	4th

	C_5 = null value	
Alternatives	Overall weights	Ranking
A_1	$u_1 = 0.1731$	3rd
A_2	$u_2 = 0.1517$	1st
A_3	$u_3 = 0.1673$	2nd
A_4	$u_4 = 0.2559$	4th

The changes made to criteria 1, 2, 4, and 5 did not differ in the final choice of alternative (that is, alternative 2 remained the most suitable, followed by alternatives 3, 1, and 4, respectively), which increases the credibility of the decision made in this study.

DISCUSSION

The approach presented in this study has great potential to contribute to selecting materials for the construction industry. Specifically, an emphasis needs to be placed on the possibility of considering environmental, economic, and social aspects simultaneously when choosing construction materials. This is extremely important to achieve more sustainable goals in a sector proven to be responsible for causing significant environmental and socio-economic impacts.

In order to use the BIM methodology as the primary tool in the data collection of the case study, quantitative indicators were chosen that could be related to the defined functional equivalent modeled in BIM. This, however, results in a limitation of the study, as there are only a few social indicators that can be related to the functional equivalent so far [37]. The social indicator was related only to an issue faced by workers; extension of the social indicators in the proposed framework is required in future works.

Even though the case study covered a large part of the analyzed building's life cycle, it is also essential that future works encompass the construction materials production phase, from the extraction of raw materials to the manufacturing processes. This has not yet been possible due to the absence of reliable databases, mainly on the social impacts related to these processes [2]. The creation of national and international databases is necessary and urgent so that the decision-making in the materials choices happens even more consciously.

The analysis of buildings' energy performance during the operation phase is a promising way to improve energy use. However, energy simulations performed in Autodesk Revit software may not provide accurate results, as the simulation may fail to capture some heat transfer paths from the building. To avoid this problem, a building of typical architecture was chosen in this paper's case study without using overhangs and side fins in the room divisions. The spaces' definition was made cautiously in Autodesk Revit before the modeling was transferred to the gbXML format.

The normalized LCIA results of the case study were placed on the graphs shown in Figure 3.5. Applying the integrated proposal among LCSA, BIM, and MCDA, Alternative 2 was the most sustainable option for the analyzed building. It can be seen that this alternative is the best choice, based on the two different criteria (i.e., C1 and C2). However, if the decision-makers had chosen to analyze the proposed building considering only criteria C3 and C4, Alternative 2 would have been considered the second option in the final ranking. Therefore, it is important to clearly define the impact categories by considering the objective of the analysis and the target audience. Ultimately, the use of fuzzy logic is strongly recommended as it helps deal with the subjectivity of choices made by decision-makers and, therefore, offers an avenue to handle a high degree of uncertainties.

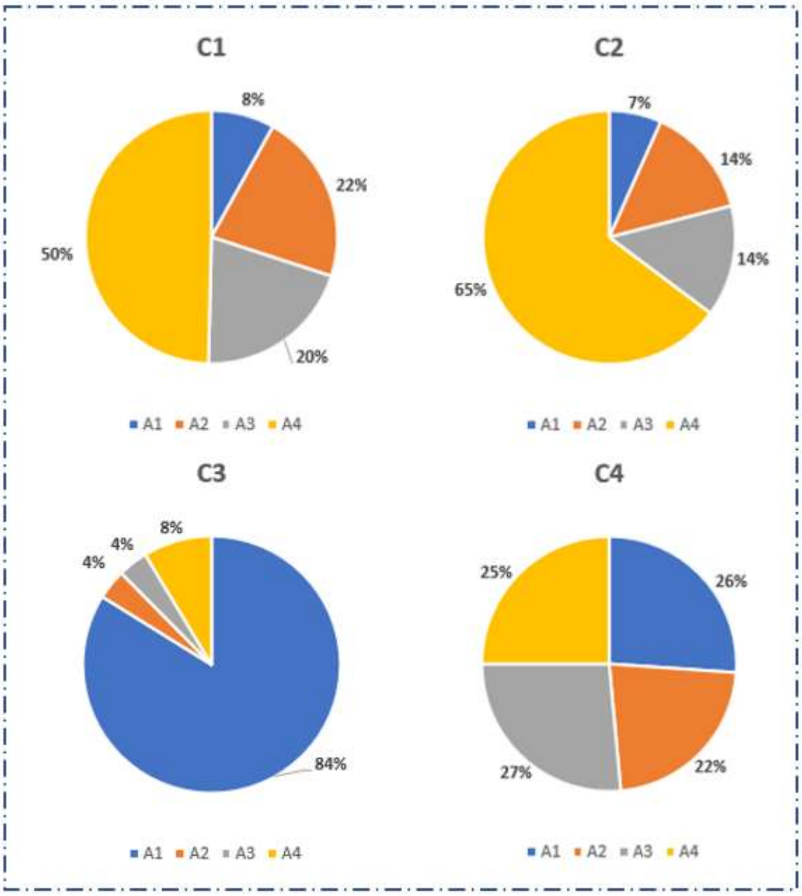

Figure 3.5 - Comparison of the four alternatives tested via LCSA

CONCLUSION

This work presents an innovative proposal for integrating LCSA, BIM, and MCDA to determine the most sustainable choice of materials for construction projects. Although a significant number of studies have adopted the previously listed approaches, none have yet implemented them simultaneously to improve the construction material choice. A case study of a residential building was evaluated to present the application of the developed framework. It is worth mentioning that this same framework can be easily applied in other construction projects with different impact categories by expanding the impacts database.

In the case study presented, four different material lists were tested for the same building to decide which alternative would be the most sustainable. Among the selected alternatives, a variation of up to 509.97% in global warming potential was found through the LCSA-BIM-MCDA integration. Also, a 16.11% variation in the energy cost for lighting and 22.80% variation in the energy cost for HVAC were detected. These variations can be even more significant when testing a greater number of material alternatives. The framework proposed allows construction professionals to quickly conduct a comparison between the alternatives.

In this work, the project was modeled for a proposed building, which brings certain limitations to the study compared to a real construction project, such as the impossibility of collecting data from the region's inhabitants and the need to make some assumptions on the construction methods used. Also, only one social impact category was assessed in the case study, which is a significant drawback of this work. These limitations must be considered in the interpretation phase, but this was deemed to be acceptable for this work since the purpose was to prove the framework's usability. There is also great difficulty in obtaining all the data related to the building, covering the environmental, economic, and social spheres. This study's future direction is to explore the use of the proposed framework in real buildings, identifying effective ways to weigh the various impacts and accurately measure the qualitative aspects.

9.8 REFERENCES

[1] R. Islam, T.H. Nazifa, A. Yuniarto, A.S.M. Shanawaz Uddin, S. Salmiati, S. Shahid, An empirical study of construction and demolition waste generation and implication of recycling, Waste Management. 95 (2019) 10–21. https://doi.org/10.1016/j.wasman.2019.05.049.

[2] C. Llatas, B. Soust-Verdaguer, A. Passer, Implementing Life Cycle Sustainability Assessment during design stages in Building Information Modelling: From systematic literature review to a methodological approach, Building and Environment. 182 (2020). https://doi.org/10.1016/j.buildenv.2020.107164.

[3] S. Torabi Moghadam, P. Lombardi, An interactive multi-criteria spatial decision support system for energy retrofitting of building stocks using CommuntiyVIZ to support urban energy

planning, Building and Environment. 163 (2019) 106233. https://doi.org/10.1016/j.buildenv.2019.106233.

[4] F. Zhang, Y. Ju, E.D.S. Gonzales, A. Wang, SNA-based multi-criteria evaluation of multiple construction equipment: A case study of loaders selection, Advanced Engineering Informatics. 44 (2020). https://doi.org/10.1016/j.aei.2020.101056.

[5] M. Shahpari, F.M. Saradj, M.S. Pishvaee, S. Piri, Assessing the productivity of prefabricated and in-situ construction systems using hybrid multi-criteria decision making method, Journal of Building Engineering. 27 (2020). https://doi.org/10.1016/j.jobe.2019.100979.

[6] A. Invidiata, M. Lavagna, E. Ghisi, Selecting design strategies using multi-criteria decision making to improve the sustainability of buildings, Building and Environment. 139 (2018) 58–68. https://doi.org/10.1016/j.buildenv.2018.04.041.

[7] A. Ijadi Maghsoodi, A. Ijadi Maghsoodi, P. Poursoltan, J. Antucheviciene, Z. Turskis, Dam construction material selection by implementing the integrated SWARA–CODAS approach with target-based attributes, Archives of Civil and Mechanical Engineering. 19 (2019) 1194–1210. https://doi.org/10.1016/j.acme.2019.06.010.

[8] M. Najjar, K. Figueiredo, M. Palumbo, A. Haddad, Integration of BIM and LCA: Evaluating the environmental impacts of building materials at an early stage of designing a typical office building, Journal of Building Engineering. 14 (2017) 115–126. https://doi.org/10.1016/j.jobe.2017.10.005.

[9] M.N. Nwodo, C.J. Anumba, A review of life cycle assessment of buildings using a systematic approach, Building and Environment. 162 (2019). https://doi.org/10.1016/j.buildenv.2019.106290.

[10] D.A. Ramos Huarachi, C.M. Piekarski, F.N. Puglieri, A.C. de Francisco, Past and future of Social Life Cycle Assessment: Historical evolution and research trends, Journal of Cleaner Production. 264 (2020). https://doi.org/10.1016/j.jclepro.2020.121506.

[11] I.M.C.S. Illankoon, W. Lu, Optimising choices of ‘building services’ for green building: Interdependence and life cycle costing, Building and Environment. 161 (2019). https://doi.org/10.1016/j.buildenv.2019.106247.

[12] C. Thibodeau, A. Bataille, M. Sié, Building rehabilitation life cycle assessment methodology–state of the art, Renewable and Sustainable Energy Reviews. 103 (2019) 408–422. https://doi.org/10.1016/j.rser.2018.12.037.

[13] M. Röck, A. Hollberg, G. Habert, A. Passer, LCA and BIM: Visualization of environmental potentials in building construction at early design stages, Building and Environment. 140 (2018) 153–161. https://doi.org/10.1016/j.buildenv.2018.05.006.

[14] M. Kamali, K. Hewage, A.S. Milani, Life cycle sustainability performance assessment framework for residential modular buildings: Aggregated sustainability indices, Building and Environment. 138 (2018) 21–41. https://doi.org/10.1016/j.buildenv.2018.04.019.

[15] G.M. Zanghelini, E. Cherubini, S.R. Soares, How Multi-Criteria Decision Analysis (MCDA) is aiding Life Cycle Assessment (LCA) in results interpretation, Journal of Cleaner Production. 172 (2018) 609–622. https://doi.org/10.1016/j.jclepro.2017.10.230.

[16] F. Leccese, G. Salvadori, M. Rocca, C. Buratti, E. Belloni, A method to assess lighting quality in educational rooms using analytic hierarchy process, Building and Environment. 168 (2020). https://doi.org/10.1016/j.buildenv.2019.106501.

[17] X. Ye, Y. Kang, Z. Yan, B. Chen, K. Zhong, Optimization study of return vent height for an impinging jet ventilation system with exhaust/return-split configuration by TOPSIS method, Building and Environment. 177 (2020). https://doi.org/10.1016/j.buildenv.2020.106858.

[18] Z. Morkunaite, V. Podvezko, E.K. Zavadskas, R. Bausys, Contractor selection for renovation of cultural heritage buildings by PROMETHEE method, Archives of Civil and Mechanical Engineering. 19 (2019) 1056–1071. https://doi.org/10.1016/j.acme.2019.05.008.

[19] M. Rostamnezhad, F. Nasirzadeh, Modeling social sustainability in construction projects by integrating system dynamics and fuzzy-DEMATEL method : a case study of highway project, Engineering, Construction and Architectural Management. 27 (2020) 1595–1618. https://doi.org/10.1108/ECAM-01-2018-0031.

[20] Y. Liu, C.M. Eckert, C. Earl, A review of fuzzy AHP methods for decision-making with subjective judgements, Expert Systems with Applications. 161 (2020). https://doi.org/10.1016/j.eswa.2020.113738.

[21] M. Ivanco, G. Hou, J. Michaeli, Sensitivity analysis method to address user disparities in the analytic hierarchy process, Expert Systems With Applications. 90 (2017) 111–126. https://doi.org/10.1016/j.eswa.2017.08.003.

[22] E. Harirchian, T. Lahmer, Developing a hierarchical type-2 fuzzy logic model to improve rapid evaluation of earthquake hazard safety of existing buildings, Structures. 28 (2020) 1384–1399. https://doi.org/10.1016/j.istruc.2020.09.048.

[23] E. Yadegaridehkordi, M. Hourmand, M. Nilashi, E. Alsolami, S. Samad, M. Mahmoud, A.A. Alarood, A. Zainol, H.D. Majeed, L. Shuib, Assessment of sustainability indicators for green building manufacturing using fuzzy multi-criteria decision making approach, Journal of Cleaner Production. 277 (2020). https://doi.org/10.1016/j.jclepro.2020.122905.

[24] T.O. Olawumi, D.W.M. Chan, Building information modelling and project information management framework for construction projects, Journal of Civil Engineering and Management. 25 (2019) 53–75. https://doi.org/doi.org/10.3846/jcem.2019.7841.

[25] N.C. Onat, M. Kucukvar, A. Halog, S. Cloutier, Systems thinking for life cycle sustainability assessment: A review of recent developments, applications, and future perspectives, Sustainability. 9 (2017) 1–25. https://doi.org/10.3390/su9050706.

[26] ISO, ISO 14040:2006 - Environmental management — Life cycle assessment — Principles and framework, 2006.

[27] M.R.M. Saade, G. Guest, B. Amor, Comparative whole building LCAs: How far are our expectations from the documented evidence?, Building and Environment. 167 (2020). https://doi.org/10.1016/j.buildenv.2019.106449.

[28] B. British Standards Institution, 15643-2: Sustainability of construction works - Assessment of buildings Part 2: Framework for the assessment of environmental performance, UK, 2011.

[29] ISO, ISO 14040:2006 - Environmental management — Life cycle assessment — Principles and framework, 2006.

[30] M.A. Gbededo, K. Liyanage, J.A. Garza-Reyes, Towards a Life Cycle Sustainability Analysis: A systematic review of approaches to sustainable manufacturing, Journal of Cleaner Production. 184 (2018) 1002–1015. https://doi.org/10.1016/j.jclepro.2018.02.310.

[31] O.S. Alshamrani, A. Alshibani, Automated decision support system for selecting the envelope and structural systems for educational facilities, Building and Environment. 181 (2020). https://doi.org/10.1016/j.buildenv.2020.106993.

[32] P. He, H. Feng, G. Hu, K. Hewage, G. Achari, C. Wang, R. Sadiq, Life cycle cost analysis for recycling high-tech minerals from waste mobile phones in China, Journal of Cleaner Production. 251 (2020). https://doi.org/10.1016/j.jclepro.2019.119498.

[33] R.S. Heralova, Life Cycle Costing as an Important Contribution to Feasibility Study in Construction Projects, in: Procedia Engineering, Elsevier Ltd, 2017: pp. 565–570. https://doi.org/10.1016/j.proeng.2017.08.031.

[34] M. Martín-Gamboa, A.C. Dias, L. Arroja, D. Iribarren, A protocol for the definition of supply chains in product social life cycle assessment: application to bioelectricity, Sustainable Energy and Fuels. 4 (2020) 5533–5542. https://doi.org/10.1039/d0se00919a.

[35] M.J. Goedkoop, D. Indrane, I.M. de Beer, Product Social Impact Assessment - Handbook 2018, Amersfoort, 2018.

[36] Y.H. Dong, S.T. Ng, A social life cycle assessment model for building construction in Hong Kong, International Journal of Life Cycle Assessment. 20 (2015) 1166–1180. https://doi.org/10.1007/s11367-015-0908-5.

[37] R.T. Fauzi, P. Lavoie, L. Sorelli, M.D. Heidari, B. Amor, Exploring the current challenges and opportunities of Life Cycle Sustainability Assessment, Sustainability. 11 (2019) 1–17. https://doi.org/10.3390/su11030636.

[38] T. Balezentis, X. Chen, A. Galnaityte, V. Namiotko, Optimizing crop mix with respect to economic and environmental constraints: An integrated MCDM approach, Science of the Total Environment. 705 (2020). https://doi.org/10.1016/j.scitotenv.2019.135896.

[39] M. Seddiki, K. Anouche, A. Bennadji, Integrated FAHP-FPROMETHEE for thermal insulation of masonry buildings, Facilities. 36 (2018) 195–211. https://doi.org/10.1108/F-05-2016-0057.

[40] S. Guzmán-Sánchez, D. Jato-Espino, I. Lombillo, J.M. Diaz-Sarachaga, Assessment of the contributions of different flat roof types to achieving sustainable development, Building and Environment. 141 (2018) 182–192. https://doi.org/10.1016/j.buildenv.2018.05.063.

[41] Z.S.M. Nadoushani, A. Akbarnezhad, J.F. Jornet, J. Xiao, Multi-criteria selection of façade systems based on sustainability criteria, Building and Environment. 121 (2017) 67–78. https://doi.org/10.1016/j.buildenv.2017.05.016.

[42] P.O. Akadiri, P.O. Olomolaiye, E.A. Chinyio, Multi-criteria evaluation model for the selection of sustainable materials for building projects, Automation in Construction. 30 (2013) 113–125. https://doi.org/10.1016/j.autcon.2012.10.004.

[43] M. Mathew, R.K. Chakrabortty, M.J. Ryan, A novel approach integrating AHP and TOPSIS under spherical fuzzy sets for advanced manufacturing system selection, Engineering Applications of Artificial Intelligence. 96 (2020). https://doi.org/10.1016/j.engappai.2020.103988.

[44] S. Ali, S.M. Lee, C.M. Jang, Determination of the most optimal on-shore wind farm site location using a GIS-MCDM methodology: Evaluating the case of South Korea, Energies. 10 (2017). https://doi.org/10.3390/en10122072.

[45] H. Gao, C. Koch, Y. Wu, Building information modelling based building energy modelling: A review, Applied Energy. 238 (2019) 320–343. https://doi.org/10.1016/j.apenergy.2019.01.032.

[46] L. Chen, W. Pan, BIM-aided variable fuzzy multi-criteria decision making of low-carbon building measures selection, Sustainable Cities and Society. 27 (2016) 222–232. https://doi.org/10.1016/j.scs.2016.04.008.

[47] T.P. Obrecht, M. Röck, E. Hoxha, A. Passer, BIM and LCA integration: A systematic literature review, Sustainability. 12 (2020). https://doi.org/10.3390/su12145534.

[48] H.X. Li, Z. Ma, H. Liu, J. Wang, M. Al-Hussein, A. Mills, Exploring and verifying BIM-based energy simulation for building operations, Engineering, Construction and Architectural Management. 27 (2020) 1679–1702. https://doi.org/10.1108/ECAM-06-2019-0314.

[49] B. British Standards Institution, 15643-1: Sustainability of construction works -Sustainability assessment of buildings - Part 1: General framework, UK, 2010. https://doi.org/10.2307/1403464.

[50] B. British Standards Institution, 15643-3: Sustainability of construction works - Assessment of buildings Part 3: Framework for the assessment of social performance, UK, 2012. https://doi.org/EN 15643-4.

[51] B. British Standards Institution, 15643-4: Sustainability of construction works - Assessment of buildings Part 4: Framework for the assessment of economic performance, UK, 2012.

[52] Y.H. Dong, S.T. Ng, A modeling framework to evaluate sustainability of building construction based on LCSA, International Journal of Life Cycle Assessment. 21 (2016) 555–568. https://doi.org/10.1007/s11367-016-1044-6.

[53] ISO, ISO 14044:2006 - Environmental management -- Life cycle assessment -- Requirements and guidelines, 2006.

[54] ISO, ISO 15686-5:2017 - Buildings and constructed assets - Service life planning - Part 5: Life-cycle costing, 2017.

[55] UNEP/SETAC, Guidelines for Social Life Cycle Assessment of products, 2009.

[56] B. British Standards Institution, 15643-2: Sustainability of construction works - Assessment of buildings Part 2: Framework for the assessment of environmental performance, UK, 2011.

[57] A. Khan, A.N. Ghadg, Building Information Modelling (BIM) Based Sustainability Analysis for a Construction Project, in: Proceedings of Sustainable Infrastructure Development & Management (SIDM) 2019, 2019. https://doi.org/10.2139/ssrn.3366799.

[58] S. Liu, S. Qian, Towards sustainability-oriented decision making: Model development and its validation via a comparative case study on building construction methods, Sustainable Development. 27 (2019) 860–872. https://doi.org/10.1002/sd.1946.

[59] H. Gardner, J. Garcia, V. Hasik, M. Olinzock, A. Banawi, M.M. Bilec, Materials life cycle assessment of a living building, Procedia CIRP. 80 (2019) 458–463. https://doi.org/10.1016/j.procir.2019.01.021.

[60] A. Abd Rashid, J. Idris, S. Yusoff, Environmental Impact Analysis on Residential Building in Malaysia Using Life Cycle Assessment, Sustainability. 9 (2017) 329. https://doi.org/10.3390/su9030329.

[61] J. Krejčí, O. Pavlačka, J. Talašová, A fuzzy extension of Analytic Hierarchy Process based on the constrained fuzzy arithmetic, Fuzzy Optimization and Decision Making. 16 (2017) 89–110. https://doi.org/10.1007/s10700-016-9241-0.

[62] J. Krejčí, O. Pavlačka, J. Talašová, A fuzzy extension of Analytic Hierarchy Process based on the constrained fuzzy arithmetic, Fuzzy Optimization and Decision Making. 16 (2017) 89–110. https://doi.org/10.1007/s10700-016-9241-0.

[63] I.Y. Subbotin, M.G. Voskoglou, A Triangular Fuzzy Model for Assessing Critical Thinking Skills, International Journal of Applications of Fuzzy Sets and Artificial Intelligence. 4 (2014) 173–186.

[64] E.K. Lee, X. Zhang, P.R. Adler, G.S. Kleppel, X.X. Romeiko, Spatially and temporally explicit life cycle global warming, eutrophication, and acidification impacts from corn production in the U.S. Midwest, Journal of Cleaner Production. 242 (2020). https://doi.org/10.1016/j.jclepro.2019.118465.

[65] J. Bare, D. Young, M. Hopton, Tool for the Reduction and Assessment of Chemical and other Environmental Impacts (TRACI), 2012.

[66] Z.S. Chen, L. Martínez, J.P. Chang, X.J. Wang, S.H. Xionge, K.S. Chin, Sustainable building material selection: A QFD- and ELECTRE III-embedded hybrid MCGDM approach with consensus building, Engineering Applications of Artificial Intelligence. 85 (2019) 783–807. https://doi.org/10.1016/j.engappai.2019.08.006.

[67] Autodesk Official Store, Revit | BIM Software , (n.d.). https://www.autodesk.com/products/revit/overview?us_oa=dotcom-us&us_si=52124493-b1b4-4097-ad45-fef0cb1c086a&us_pt=RVT&us_at=Overview (accessed February 21, 2021).

[68] About the Energy Model | Revit Products 2018 | Autodesk Knowledge Network, (n.d.). https://knowledge.autodesk.com/support/revit-products/learn-explore/caas/CloudHelp/cloudhelp/2018/ENU/Revit-Analyze/files/GUID-5D7C8522-4DC2-4618-AEC9-2555CB276B2D-htm.html (accessed March 10, 2020).

[69] IBGE, Sistema Nacional de Pesquisa de Custos e Índices da Construção Civil - SINAPI, (2020). https://www.ibge.gov.br/estatisticas/economicas/precos-e-custos/9270-sistema-nacional-de-pesquisa-de-custos-e-indices-da-construcao-civil.html?=&t=resultados (accessed February 4, 2021).

[70] R. Phillips, L. Troup, D. Fannon, M.J. Eckelman, Triple bottom line sustainability assessment of window-to-wall ratio in US office buildings, Building and Environment. 182 (2020). https://doi.org/10.1016/j.buildenv.2020.107057.

[71] Portal Light, Composição da Tarifa - Residências, (2021). http://www.light.com.br/para-residencias/Sua-Conta/composicao-da-tarifa.aspx (accessed January 9, 2021).

[72] S. Neugebauer, Y. Emara, C. Hellerström, M. Finkbeiner, Calculation of Fair wage potentials along products' life cycle – Introduction of a new midpoint impact category for social life cycle assessment, Journal of Cleaner Production. 143 (2017) 1221–1232. https://doi.org/10.1016/j.jclepro.2016.11.172.

[73] World Bank (2020), Human Development Reports - United Nations Development Programme, (n.d.). http://hdr.undp.org/en/indicators/67106 (accessed January 8, 2021).

[74] The R Foundation, R: The R Project for Statistical Computing, (n.d.). https://www.r-project.org/ (accessed February 22, 2021).

APPENDIX C – INTEGRATING DIGITAL TWIN AND BLOCKCHAIN FOR DYNAMIC BUILDING LIFE CYCLE SUSTAINABILITY ASSESSMENT

This chapter is submitted as an original research article.

https://doi.org/10.1016/j.jobe.2024.111018

FIGUEIREDO, Karoline; **PIEROTT, Rodrigo** et al. Integrating Digital Twin and Blockchain for Dynamic Building Life Cycle Sustainability Assessment.

Abstract: The Life Cycle Sustainability Assessment (LCSA) methodology represents a possible solution to meet the requirements of a sustainable built environment by adopting a lifecycle perspective and simultaneously accounting for all sustainability pillars. Nevertheless, the LCSA application is typically focused on the early design stages of a building and does not consider real-time information, representing a static LCSA approach. Therefore, based on the results derived from a systematic literature review on this subject, this paper proposes a comprehensive framework that demonstrates how the integration of LCSA with Digital Twin and Blockchain can enhance building sustainability. A platform based on Smart Contracts is presented to facilitate the integration of these technologies. A case study is also conducted to validate the framework's applicability and showcase its benefits in achieving sustainable outcomes in the built environment. This research contributes to improving dynamic impact assessments and achieving sustainability, thus fostering sustainable practices in construction projects.

Keywords:
BIM; Blockchain; Digital Twin; Dynamic Analysis; Life Cycle Sustainability Assessment; Sustainable Construction.

9.9 INTRODUCTION

Life Cycle Sustainability Assessment (LCSA) emerged as a thorough methodology based on the life cycle thinking approach. This approach takes into account the fact that all phases of a product's life cycle have an impact on the environment and have socio-economic repercussions. All these issues, in turn, need to be assessed in order to achieve sustainability [1]. The LCSA methodology is the result of combining three key processes: i) Life Cycle

Assessment (LCA), related to the environmental pillar of sustainability; ii) Life Cycle Costing (LCC), associated with the economic pillar; and iii) Social Life Cycle Assessment (S-LCA), linked to the social pillar.

In recent years, researchers have started emphasizing the importance of incorporating dynamic aspects into building sustainability assessments, which involves considering time-dependent factors and real-time impact scores to assess the impacts across different time horizons [2]. This topic still receives little attention in the literature, particularly when it comes to research that validates this concept in building case studies. Considering the specific application of LCA, thus assessing only environmental aspects, some efforts have already been presented in the literature with the aim of transforming this application into a dynamic LCA. This emerging field, Dynamic Life Cycle Assessment (DLCA), aims to provide a more comprehensive and accurate understanding of the environmental implications over time.

Yet, while the concept of DLCA holds significant potential for advancing the understanding of the dynamic nature of environmental impacts, there is a notable gap in the literature regarding the standardization of this application and the extrapolation to a dynamic LCSA, considering the three pillars of sustainability. In this context, tools and technology that facilitate the life-cycle data collection and real-time data visualization needed to produce in-depth conclusions during the building sustainability assessment seem pertinent.

Building Information Modeling (BIM) might be one of the most apparent solutions in this regard. BIM is a widely used methodology in the construction industry and refers to a working procedure based on a digital representation of the facility. Besides, BIM incorporates all stakeholders into the workflow and facilitates data access along the project's life cycle [3]. Therefore, a BIM model consists of a 3-D digital model containing both geometric and semantic data of building elements. However, the current state of BIM lacks semantic completeness in managing dynamic data and is considered incompatible with the Internet of Things (IoT) integration, a tough challenge currently discussed in the literature [4].

In order to deal with this issue, research has focused on synchronizing the cyber-physical bi-directional data flow between the digital model and the existing building, making use of the Digital Twin (DT) paradigm. Conceptually, a DT is a virtual representation of an object or system, serving as the real-time digital counterpart of the asset during its life cycle [5]. From the construction standpoint, several DT applications have been investigated under the BIM field, understanding a construction DT as a digital prototype with increased detail and precision and using the BIM model as the primary data source to develop the DT [4].

Unfortunately, this data aggregation throughout the facility's life cycle can generate a security risk due to the presence of multiple parties and sources. Traceability, confidentiality, and security issues may arise as obstacles while developing a construction DT. From this perspective, applying blockchain technology can provide a plausible avenue for dealing with these issues. Blockchain is nowadays the most prominent Distributed Ledger Technology (DLT) in the market [6]. DLT is a transaction system that runs on a distributed peer-to-peer (P2P) network and does not require a central authority to arbitrate such transactions [7]. In turn, a blockchain is a DLT that represents a database with interconnected blocks of data cryptographically protected against tampering [8], in which the data integrity is reached through the process of hashing [7]. Regarding the projects associated with the built environment, blockchain can offer a tamper-proof solution throughout the information supervision of built assets [9].

In this vein, one of the critical objectives of this research is to explore how the knowledge gained from the individual application of LCSA, DT, and blockchain can be harmonized into an integrative solution for dynamic building assessments. Despite significant advancements in each of these domains, there is still a critical need to bridge the gap between theory and practical implementation within the construction industry. Therefore, this study begins with a systematic literature review, presenting a comprehensive bibliometric analysis and defining the state-of-the-art of LCSA, DT and blockchain in construction. Particularly, this paper intends to answer the following research questions (RQ):

(RQ1) Is it feasible to extrapolate the discussion on Building LCSA, typically focused exclusively on the early design stages and not considering real-time information, via applying different levels of Digital Twins throughout the entire life cycle of the building and creating a dynamic approach?

(RQ2) How does integrating blockchain and Digital Twin contribute to enhancing the precision, reliability, and comprehensiveness of dynamic sustainability assessments in the built environment, particularly regarding ensuring data security and user privacy?

Based on the conclusions derived from the systematic review, an integrative framework is proposed to showcase how this integration can enhance sustainability in construction and advance research in this field. A proof of concept is then presented to validate the framework and showcase its applicability, highlighting the innovative potential of combining LCSA, DT, and blockchain within the construction industry. By analyzing the challenges encountered in the framework application, a platform based on Smart Contracts is also proposed to integrate the technologies, with a semantic architecture being illustrated.

9.10 RESEARCH METHODS

This study systematically explores LCSA, DT, and blockchain within the construction industry, aiming to culminate in an integrative framework. The research methods, illustrated in **Figure 9.1**, span three distinct phases: systematic literature review, framework development and proof of concept.

The study starts with a systematic literature review based on the PRISMA guidelines [10] to achieve the findings needed to answer the research questions posed herein. In this phase, a scientific evolution analysis is proposed based on a bibliometric and text data mining exploration to grasp the progression of the concepts over time. Then, a meticulous examination to delineate the current state-of-the-art in LCSA, DT, and blockchain within the construction industry is carried out, serving as the foundation for the subsequent phases.

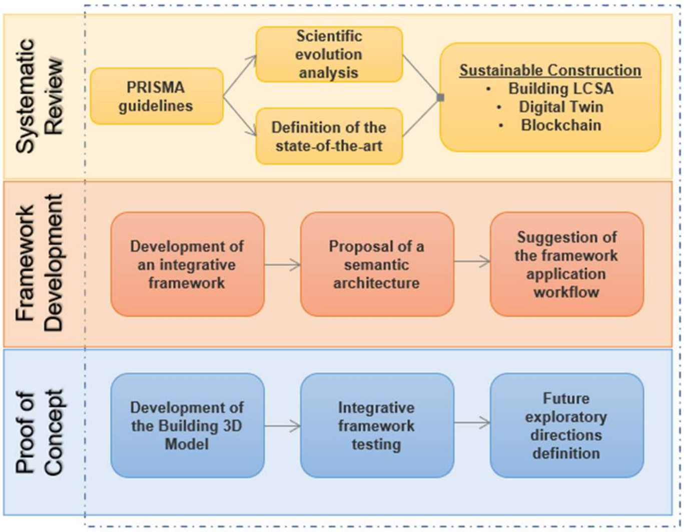

Figure 9.1 - Research methods proposed for this study

Scopus was chosen as the preferred search database. The study intends to provide quantitative and qualitative assessments of the research trends and key publications in the field, in addition to identifying existing gaps in the literature. Firstly, the search considered LCSA, DT, and blockchain being used together. After that, the study was conducted by searching for the chosen keywords related to each concept separately in article titles and abstracts. The keywords were combined with logical operators AND, OR, and NOT. The data was collected in September 2023. **Table 9.1** shows the different interactions carried out in this study.

The first key objective of the review was to evaluate current research trends and establish the status of LCSA, DT and blockchain within the context of sustainable construction. Therefore, all interactions presented in **Table 9.1** contained critical terms related to sustainability. Then, the documents were screened and filtered, considering the overall relevance of the papers. Relevance criteria involved the inclusion of journal articles and review articles while excluding books, book chapters, and conference papers. Furthermore, to maintain uniformity in language, the search was restricted to documents in English. **Figure 9.2** illustrates the steps of the systematic literature review conducted in this study based on the PRISMA guidelines.

Table 0.1 - Keywords used in each interaction of the literature review search

Interactions in *Scopus* and *Web of Science* databases	**Keywords used**
First interaction	("Building" OR “Construction”) AND ("LCSA" OR "Life Cycle Sustainability Assessment" OR "TBL" OR “Triple bottom line” OR (“Environmental” AND “Economic” AND “Social”)) AND ("Digital Twin" OR “data-driven simulation” OR “cyber-physical”) AND ("Blockchain" OR “Distributed Ledger Technology” OR “DLT”)
Second interaction	("Building" OR “Construction”) AND ("LCSA" OR "Life Cycle Sustainability Assessment" OR "TBL" OR “Triple bottom line” OR (“Environmental” AND “Economic” AND “Social”))
Third interaction	("Building" OR “Construction”) AND ("Digital Twin" OR “data-driven simulation” OR “cyber-physical”) AND (“Sustainable” OR “Sustainability”)
Fourth interaction	("Building" OR “Construction”) AND ("Blockchain" OR “Distributed Ledger Technology” OR “DLT”) AND (“Sustainable” OR “Sustainability”)

The first key objective of the review was to evaluate current research trends and establish the status of LCSA, DT and blockchain within the context of sustainable construction.

Therefore, all interactions presented in **Table 9.1** contained critical terms related to sustainability. Then, the documents were screened and filtered, considering the overall relevance of the papers. Relevance criteria involved the inclusion of journal articles and review articles while excluding books, book chapters, and conference papers. Furthermore, to maintain uniformity in language, the search was restricted to documents in English. **Figure 9.2** illustrates the steps of the systematic literature review conducted in this study based on the PRISMA guidelines.

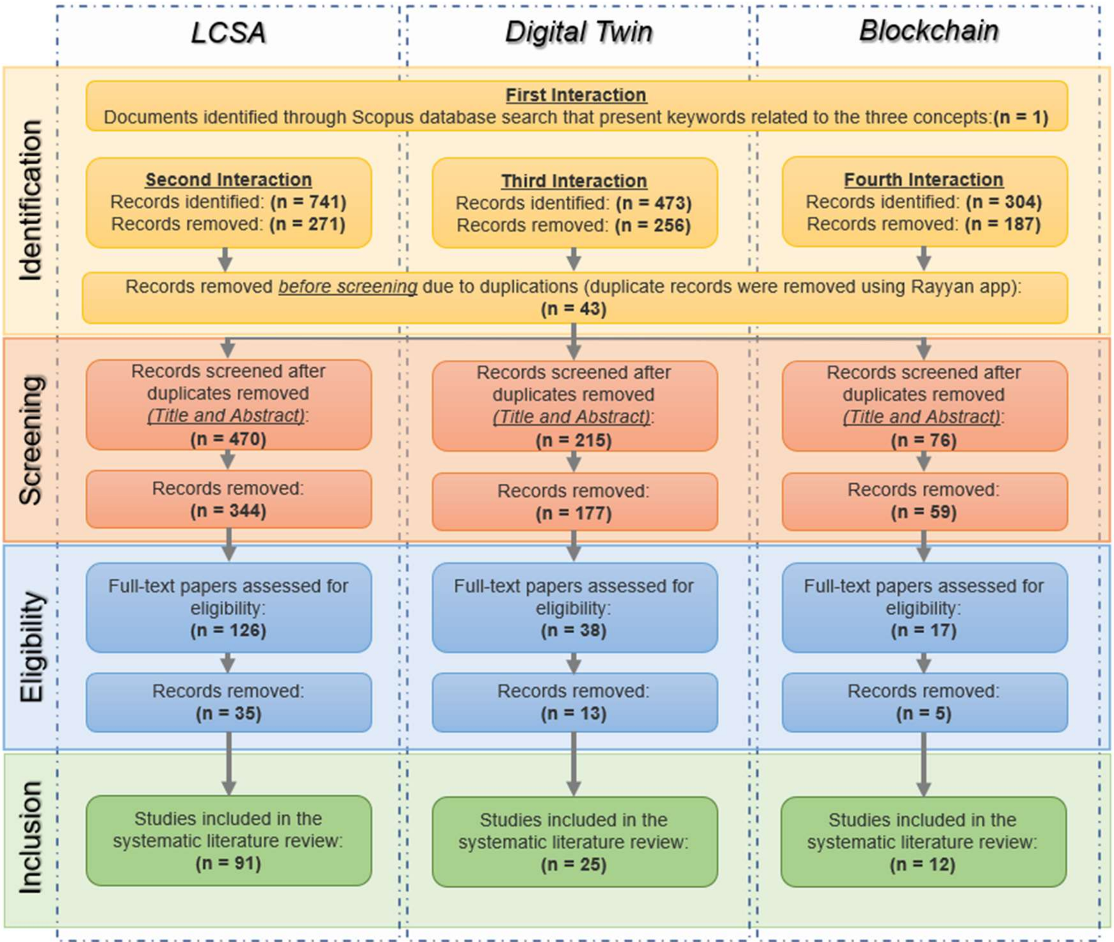

Figure 9.2 - PRISMA-based diagram for the systematic literature review conducted in this study

The culmination of the systematic review sets the stage for the second phase of the methodology proposed in this study, related to the framework development. In this phase, a comprehensive framework is proposed to seamlessly integrate LCSA, DT, and blockchain within the construction domain. In the context of this study, the integration proposed is a multifaceted endeavor. To ensure that this integration is both practical and comprehensive, the framework is designed to provide a structured and all-encompassing approach, allowing practitioners to consider every critical facet of these broad concepts.

The final phase is related to the Proof of Concept of the framework developed herein. This phase will start with creating a 3D model that emulates real-world construction scenarios, enabling practical testing of the framework. The main goal is to use rigorous testing to assess the framework's effectiveness, potential for enhancing sustainability, and adaptability to diverse scenarios. Ultimately, the discussion of this study's results intends to consider a forward-looking perspective, identifying areas for future exploration, refinement, and innovation. All these phases will be discussed in the following sections of this paper.

9.11 LITERATURE REVIEW

9.11.1 Scientific evolution analysis

A bibliometric analysis was conducted (i) separately on each approach (LCSA, DT, blockchain) and (ii) accumulatively via the use of these concepts together in the same study. The decision to search for studies that include at least one of the three approaches is due to the understanding that the advancements in each topic can be extrapolated and combined to achieve the objectives of this paper. The results of this analysis are used to show the current research stage on these concepts.

The papers filtered in the literature search were classified via a bibliometric analysis using text data mining and clustering. For this, the authors utilized specialized software, namely VOSViewer (version 1.6.18), developed by researchers from Leiden University in Sweden [11]. VOSviewer uses the VOS mapping technique to construct a bibliometric map, where VOS stands for Visualisation of Similarities [12]. The maps created based on the co-occurrence of terms among the papers found in the second, third, and fourth interactions, related to applying the methodologies with a sustainability focus, are shown respectively in **Figures 9.3, 9.4, and 9.5**. The distance between two keywords in these figures indicates their relatedness. The closer two terms are located, the stronger their relatedness.

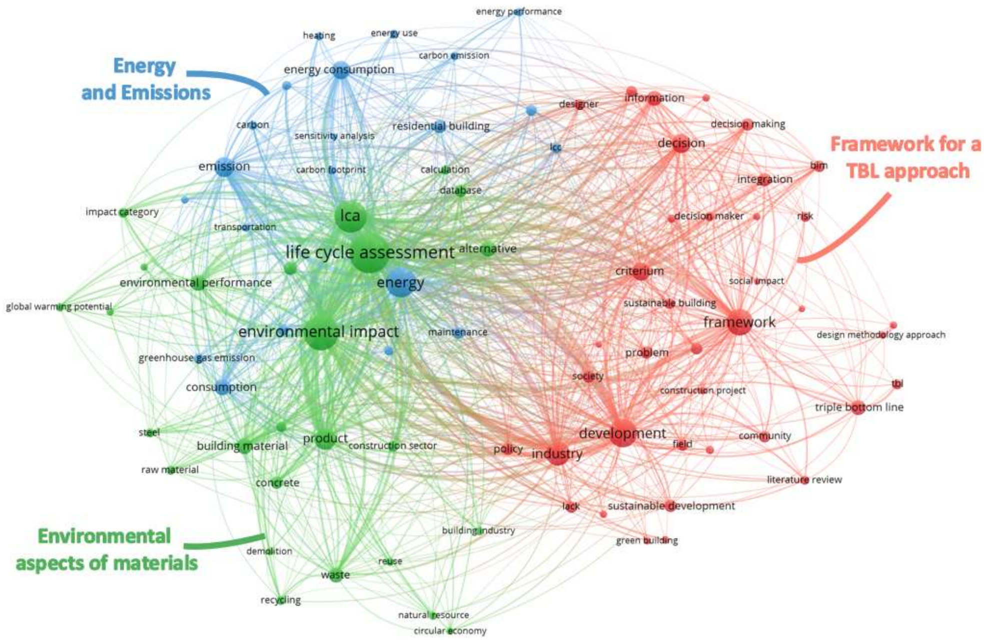

Figure 9.3 - A map based on the co-occurrence of terms in scientific papers related to Building LCSA, divided into three clusters.

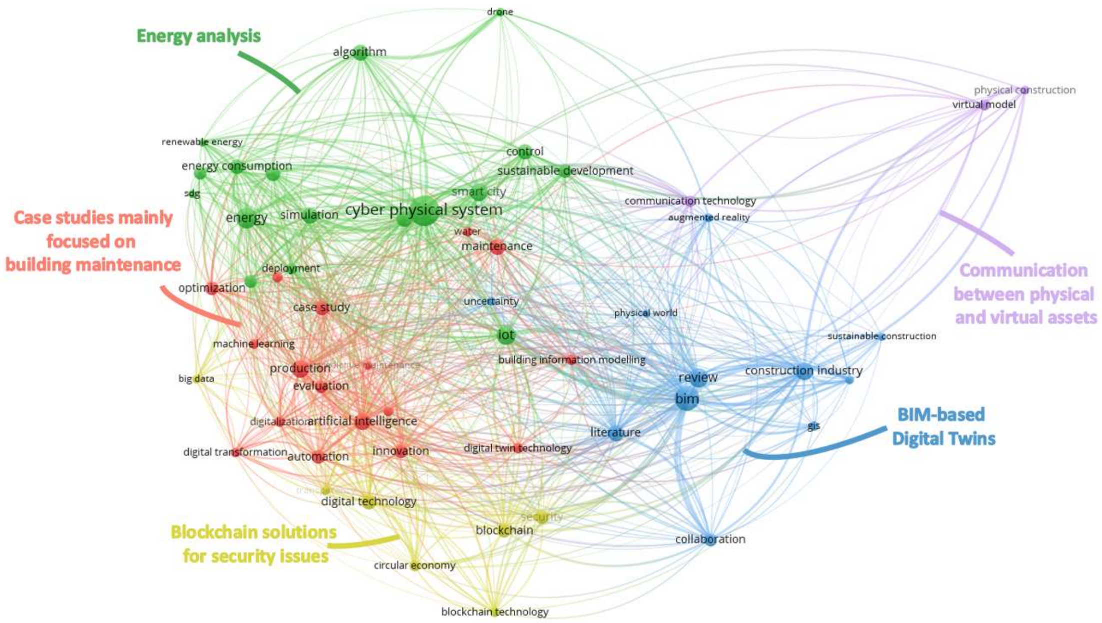

Figure 9.4 - A map based on the co-occurrence of terms in scientific papers related to Building Digital Twin, divided into five clusters.

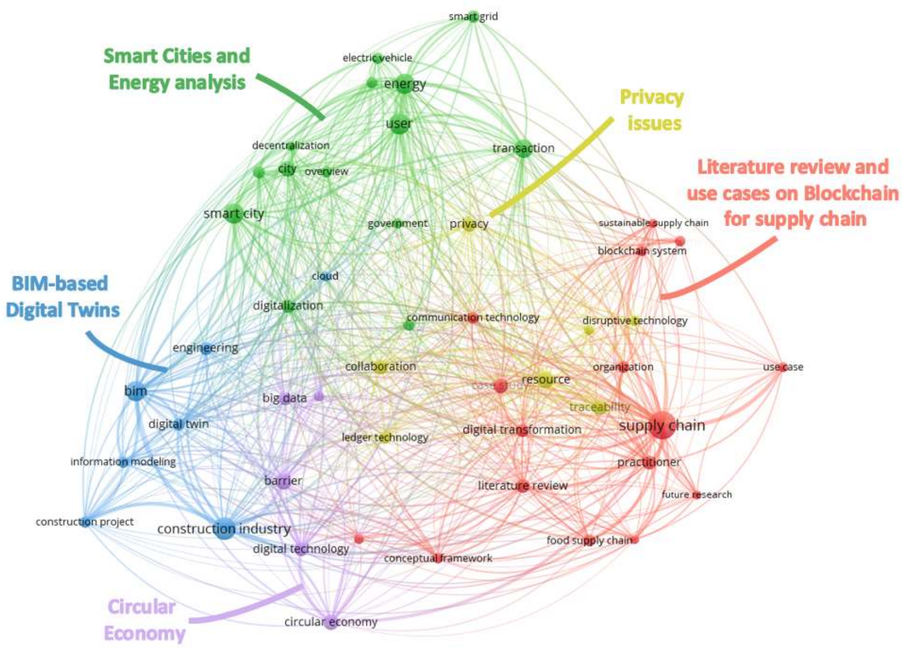

Figure 9.5 - A map based on the co-occurrence of terms in scientific papers related to Blockchain applied in the construction industry, divided into five clusters.

Although many articles mention the application of LCSA, it is essential to note that many of these publications tend to be limited in scope, predominantly addressing environmental assessments without fully encompassing all three pillars of sustainability, as indicated by the green cluster in **Figure 9.3**. Besides, several publications focus on energy analysis and carbon emission, as shown in the blue cluster. Finally, papers that delve deeper into a triple-bottom-line approach typically emerge from literature review searches or the development of conceptual frameworks. This approach aims to mitigate the ongoing challenges of harmonizing LCA, LCC, and S-LCA. This specific focus can be observed within the red cluster.

In turn, an evident correlation with the BIM methodology emerges regarding the use of DT in the construction industry. Many papers utilize a BIM-based DT model in their analyses, as evidenced in the blue cluster in **Figure 9.4**. Also, it was possible to derive two critical areas of DT application in the construction industry. On the one hand, numerous publications concentrate on applying DTs for energy analysis, showcasing their relevance to sustainability outcomes. On the other hand, another significant cluster underscores the adoption of DTs for building maintenance, emphasizing their role in optimizing facility operations. This application is closely linked to information and control systems, which are crucial for leveraging DTs to enhance the sustainability of physical facilities. Notably, some articles have begun to address this need by discussing the integration of BIM-based DTs with blockchain, highlighted in the yellow cluster.

Ultimately, **Figure 9.5** is related to the application of blockchain in the construction industry. Notably, many papers in this interaction also involve the application of BIM-based DTs, reaffirming the potential benefits of this integration in construction projects, as shown in blue. Besides, four more clusters were identified as the key research areas on using blockchain to advance sustainability: smart cities and energy analysis; supply chain, particularly in terms of transparency and traceability; circular economy; and the use of blockchain to solve privacy issues, acknowledging the importance of data security and user confidentiality.

9.11.2 Definition of the state-of-the-art of LCSA, Digital Twin, and Blockchain in construction

After conducting a scientific evolution analysis, the documents were filtered for further careful investigation. This step aimed to find the most relevant works to assist in developing an integrative framework. The most significant articles for each topic that have been reviewed are discussed in the following subsections.

9.11.2.1 Life Cycle Sustainability Assessment

The Life Cycle Sustainability Assessment (LCSA) is an interdisciplinary framework that simultaneously evaluates the impacts associated with products and processes from an environmental, social, and economic perspective [13]. The techniques that form the LCSA framework (i.e., LCA, LCC, and S-LCA) follow the same methodological structure based on the ISO 14040 standard. This methodological structure is divided into four stages: Goal and Scope definition, Life Cycle Inventory (LCI), Life Cycle Impact Assessment (LCIA), and Interpretation [14].

Although the three life-cycle methodologies have similarities, significant differences in each technique have been identified in the literature [15]. For instance, not all the economic and social indicators can be estimated as a function of the functional unit of the study, resulting in a significant drawback in the interpretation stage [16]. In this vein, numerous issues concerning the complete application of LCSA remain unanswered in the literature, and many studies continue to execute only a portion of the evaluation. This is primarily due to the varying maturity levels of the three sustainability pillars, which impedes the widespread adoption of LCSA.

Regarding the use of LCSA as a decision-making technique in the construction industry, researchers have applied this methodology mainly during the early stages of a building design

[15,17–19]. A recent study introduced an innovative LCSA model designed for integration into the design phase of new building projects and energy refurbishments for existing buildings [20]. The authors further developed a novel formulation and weighting method to derive a final LCSA index, facilitating a holistic assessment of design scenarios and considering the three pillars of sustainability. The study also innovatively integrates Machine Learning (ML) techniques into the optimization process, enhancing the efficiency of design assessments while upholding their precision.

Nevertheless, when considering using this methodology in different stages of the building's life cycle, a new challenge emerges related to the need for more temporal information in the assessments. Notably, the current LCSA methods take a stagnant approach that fails to consider dynamic factors during the building life cycle, such as material deterioration, varying energy consumption, and technology up-gradation, resulting in inaccurate sustainability assessments [21]. In this context, the data inventory can be considered the most sensitive and challenging step of an LCSA application since it leads to the creation of a model that should represent, as accurately as possible, all the exchanges between the distinct phases of a process [22]. So far, the need for more impact data sources adapted to the specific requirements of a building project has been seen in the literature [15]. Besides, it has been noted that impact assessments are typically based on data from historical series, which hinders the use of LCSA for rapid corrective actions on a project.

Therefore, it becomes necessary to consider a dynamic LCSA approach in which a dynamic life cycle inventory (D-LCI) is considered, along with time-dependent characterization factors, to assess the impacts by considering real-time impact scores for any time horizon [23]. This topic still receives little attention in the literature, particularly when it comes to research that validates this concept in building case studies. However, considering the specific application of LCA, thus assessing only environmental aspects, some efforts were already presented in the literature with the aim of transforming this application into a dynamic LCA.

For example, Ferrari et al. [24] proposed the integration of the life cycle inventory (LCI) stage with the Enterprise Resource Planning (ERP) system to overcome some limitations in LCA inventory data. The authors highlighted that many companies already have part of the primary inventory data in an ERP system, thus making it possible to dynamize LCA applications by exploiting the data collected by ERP. This idea was discussed with a focus on manufacturing companies and implemented in a case study related to the environmental monitoring needs of a ceramic tile manufacturer.

Recent works started to discuss a dynamic LCA approach in the construction domain but with specific and limited goals. Ramon et al. [25] analyzed the operational phase in building LCA assessments by employing a dynamic energy consumption and electricity mix approach and integrating future climate model data and dynamic energy simulations. In turn, Apostolopoulos et al. [26] evaluated a set of energy-efficient retrofit measures in a residential case study in Greece. In this study, carbon emissions, primary energy needs, and lifecycle costs were analyzed. The authors considered that a Dynamic-LCA approach was implemented due to the use of a specific building energy variable, incorporating time-dependent features in the context of temporal and spatial variations.

In a notable case study centered in Quebec, Canada, the authors investigated the increasing utilization of wood in non-residential buildings through LCA [27]. This study compared a conventional static LCA, which adopts fixed time horizons for assessing environmental impacts, with a dynamic approach using the DynCO2 tool. The findings underline the importance of considering both short-term and long-term consequences, as conventional static LCAs may provide incomplete insights, especially when dealing with elementary flows with varying values. Still, this study did not apply a dynamic life-cycle inventory. The analysis was considered dynamic due to the use of a dynamic characterization method during the LCIA phase.

Other recent publications presented different frameworks for a dynamic LCSA application but with limited advances in this field. Francis and Thomas [21] developed a methodological framework that allows practitioners to set desired values for material use, material replacement alternatives, energy mix, and water recycling percentage to evaluate the building impacts of the selected combination of values. It can be observed that the authors considered more environmental indicators as compared to economic and social ones. Besides, the framework continues to resemble the traditional LCSA application, allowing the comparison of several alternatives from manual changes in the system.

Another point that deserves attention is that although the number of lifecycle approaches is constantly growing in construction, the number of Environmental-LCA applications is still much more significant than LCC and S-LCA studies. Besides, previous thorough literature reviews have revealed that most investigations over the last 20 years focus on the impacts generated during the extraction and manufacturing stages of building materials and components, moderately or infrequently considering the other building life cycle stages specified in international standards (i.e., construction installation, use, maintenance, repair, demolition, processing, disposal, recycling, etc.) [28]. It reveals another research gap that needs to be solved in the literature.

In light of the above, it becomes evident that the foundational realm of LCA, which has evolved in tandem with D-LCA and LCSA [21], must undergo further expansion to accommodate the dynamic influences and intricate interrelationships among the three sustainability pillars. This evolution can undoubtedly contribute to the progression and maturation of research in this domain, fostering a more holistic understanding of sustainability in construction and the built environment.

9.11.2.2 Digital Twin (DT)

A DT represents a collection of realistic models that intend to simulate the physical asset's real-time attributes, conditions, and behavior throughout its existence [29]. Particularly, communication between virtual models and physical assets in bi-directional coordination allows for changes in one environment to be reflected in the other and vice versa. This idea has been employed in various sectors and businesses, including construction. Unlike BIM, which focuses on centralizing data and information and is typically used as a single digital shadow [30], a building DT can provide timely optimization suggestions by mirroring the building's lifecycle and current status [31]. In this context, DTs of constructed assets can present different complexity levels from design to handover, depending on the availability of data and the model's sophistication [32].

Several contributions of using DT in the construction sector are discussed in the literature, such as the real-time building's remote monitoring and management and the maintenance and planning estimation [33]. A building DT is considered a contextual model of an entire building, bringing together third-party data and resulting in a dynamic digital replica that can be used to solve a wide range of issues [34]. The benefits of using a building DT vary from real-time data visualization to continuous asset monitoring and the development of self-learning capabilities [35]. However, a closer look at the literature reveals some gaps and shortcomings. Although the DT concept already provides solutions to current problems in building projects, research on this subject continues mainly at a theoretical level. Several articles that apply a building DT in a case study upgraded existing modules of a BIM model to a DT system without considering real-time data, thus only partially realizing a building DT [31].

Besides, the literature shows that the use of virtual models as a platform for continuously tracking building components during the operation and maintenance phases is underutilized despite the opportunities for building monitoring and control [36]. Previous methods for integrating virtual models and physical construction have primarily focused on resource and activity monitoring during the construction stage, as well as documentation of the as-built.

State-of-the-art literature on DT proves that the proliferation of the concept associated with the built environment and the construction industry has not been primarily driven by the need to achieve sustainable outcomes in this sector, with limited applications regarding sustainability assessments based on a triple-bottom-line approach. Notably, a recent study with a hybrid approach involving literature review, expert interviews, and modeling techniques stated that the relationship between DT and sustainable success remains insufficiently studied in the literature regarding the building and construction sectors [37]. There are several barriers to implementing DT in this context, such as interoperability issues, difficulty in protecting intellectual property, data uncertainties, connectivity, and cultural inertia.

However, as the demand for sustainable practices grows, research has started to pivot in this direction. Several studies have begun to outline specific goals for employing BIM-based DTs to achieve sustainability within construction. For instance, some efforts have focused on maximizing the recycling and reuse of demolition waste [38], while others have explored the development of Zero Energy Districts [39]. These studies represent critical steps toward integrating DT technology with sustainability principles, aligning the construction industry with the broader sustainability agenda.

Nonetheless, it is observed that the application intended to improve the LCSA methodology via DT implementation is still briefly addressed in the literature. Tagliabue et al. [40] have discussed the application of a BIM-based DT for sustainability assessments. Still, their case study primarily pertained to the design and operational phases, with a particular focus on energy efficiency. As a result, it did not encompass all sustainability pillars or consider the full array of parameters associated with sustainable construction. This gap between DT and comprehensive LCSA integration in the context of the construction industry points to an avenue for further research and innovation.

9.11.2.3 Blockchain

Blockchain is an innovative information technology that ensures decentralization, auditability, security, and smart execution in a process. At its core, a blockchain comprises consecutively linked blocks, each containing a pointer to the previous block, a timestamp, and a collection of data [41], and this structure guarantees that any data tampering is easily identified [42]. Briefly, the blockchain process collects the broadcasts of transactions into blocks, which are then hashed and receive a timestamp [43]. Hash is the name used to identify a cryptographic function that encodes data to create a unique and fixed-length string in the chain [44].

Due to these cryptographic functions, it is practically impossible to carry out the opposite process and get the original data from an already-formed hash, which ensures data authenticity and security [43]. Furthermore, the timestamp created in this process provides reliable evidence that the data must have existed at that moment to get into that specific hash [45], thus further enhancing the security and auditability of the blockchain. In turn, blockchain excludes the need for a trusted third party to validate transactions due to its decentralization characteristic, resulting in a delegation of authority among network contributors that improves the service trust [46].

In the blockchain domain, smart contracts play a pivotal role. They are used as agreements between parties expressed in the form of computer code [47]. A smart contract can automatically self-execute processes based on satisfying preset conditions [48], in addition to determining the content, norms, rights, and obligations of each member of the chain [49]. When considering applying blockchain technology to projects associated with the built environment, smart contracts seem to be a possible solution to the slow, fragile, and expensive transactions observed in this context [50].

Unfortunately, it is noteworthy that the construction industry has historically lagged behind in adopting information technology within its processes [51]. Consequently, the application of blockchain technology in the construction sector remains predominantly a theoretical discussion. Despite its theoretical underpinnings, the potential for blockchain to revolutionize the construction industry by streamlining transactions and enhancing security cannot be underestimated. It is essential to recognize that the adoption of blockchain in the construction industry faces challenges related to technical expertise, interoperability, and cost [52]. However, as the technology matures and awareness grows, more practical applications are expected to emerge, fostering a profound transformation in the built environment.

9.11.3 Preliminary Integration Attempts Presented in the Literature

The systematic review of the literature revealed a scarcity of studies that effectively leverage DTs to enhance all three pillars of sustainability from a life-cycle perspective. Moreover, the practical application of blockchain technology in construction projects remains theoretical mainly, with limited case studies available within the construction industry. However, some preliminary integration attempts presented in the literature are worth analyzing.

Previous studies have emphasized the benefits of integrating BIM and blockchain [53–55]. While highly effective in managing project information, the BIM methodology lacks certain features such as confidentiality, traceability, provenance tracking, non-repudiation, and data ownership. In this vein, by integrating BIM and blockchain, various challenges inherent to the construction project lifecycle can be addressed [56]. For example, a blockchain platform can alleviate project delays resulting from BIM model discrepancies or stakeholder conflicts [57]. Nonetheless, several technical barriers are linked to this proposal, such as the necessity for greater computational power to add a BIM model to a blockchain [58].

Considering a BIM model as the primary data source for constructing a building DT, it becomes evident that integrating blockchain technology into DT is a logical next step. Several frameworks have been proposed to satisfactorily apply this integration, some focusing on project management [59] and others on manufacturing systems [60]. In the construction industry context, two prominent blockchain platforms available in the market, Ethereum and Hyperledger Fabric, can be harnessed for this purpose [61].

In turn, the integration of BIM and Environmental LCA has gained substantial traction in the literature, and different 'LCA Profiles' have emerged, establishing associations between LCA processes and construction materials or components, often represented as BIM objects [62]. BIM's role in this context is linked to an information aggregator and context provider, offering a rich dataset to support the LCA analysis. Therefore, LCA tools and plug-ins are pivotal in connecting the information sourced from BIM with the corresponding LCA processes within the databases [63]. Still, while promising, recent studies have shown that this integration has sometimes led to inaccurate results within the current designers' workflow [64,65]. This conclusion underscores the critical need for analysis tools that seamlessly align with the dynamic nature of a building project.

In a parallel vein, exploring synergies between LCSA and BIM-based DTs promises to revolutionize sustainability practices in the construction industry. As discussed in a recent study by Boje et al. [62], a fully monitored construction project could help track events in real time and provide inputs for a dynamic sustainability assessment, but this lies in the scope of a DT model and not a BIM model. Therefore, the authors introduced a streamlined LCSA of an office building with a limited scope to showcase the complementary roles of BIM and DT. However, it is essential to note that the utilization of BIM and DT in this case study was primarily restricted to environmental LCA during modules A1, A2, A3 (product stages), B6 (operational energy), and B7 (operational water). This limited application did not fully address the potential of LCSA-DT integration, leaving room for further exploration and development in this evolving field.

Regarding the use of blockchain, Zhao et al. [59] highlighted a significant challenge concerning the current levels of blockchain technology employed in the literature, which may not meet the requirements for DTs applied in construction management. Several drawbacks arise, such as high latency and performance loss due to the large amount of transaction data associated with a construction project. To address this, the authors proposed a framework to enhance collaboration and communication among project stakeholders, mainly when internet connections are unstable, focusing specifically on project management.

Moreover, integrating blockchain technology in life-cycle approaches can significantly enhance data reliability and trustworthiness, enabling better tracking of a building's life-cycle performance. For example, when combined with IoT sensors for automatically collecting data, blockchain can track a product and record its footprint along its entire value chain [66]. Additionally, all inventory data can be stored, processed, and validated on a blockchain platform [67], potentially improving the quality of LCSA inventories and enhancing the sustainability decision-making process for construction projects.

9.12 FRAMEWORK DEVELOPMENT

This section introduces the integrative framework presented in this work, as illustrated in **Figure 9.6**. The framework's primary focus lies in integrating a building DT with blockchain technology to enhance the application of the LCSA methodology in the construction industry, thereby advancing sustainability goals. The proposed framework emphasizes the dynamic nature of LCSA, to be conducted across different phases of a building's life cycle with real-time data derived from a digital building twin. It is also essential to recognize that the digital building model's complexity will evolve, adapting to the available data at different stages of the building's existence. By incorporating blockchain technology, the framework not only ensures the integrity, traceability, and transparency of data but also revolutionizes the collaboration and data exchange processes among diverse stakeholders.

Many researchers advocate for applying life cycle techniques during the building design stage, recognizing the significant influence of stakeholders in these early phases, which diminishes as the project approaches completion. However, this application is inherently hindered by the dearth of data available at the inception of the project life cycle. The workflow articulated in this study presents a dynamic approach, enabling LCSA to be executed throughout various building phases, supported by additional technologies. This innovative approach treats LCSA as an iterative process that evolves alongside the physical building. In this context, the LCSA results in the pre-construction phase play a pivotal role in enhancing design decisions. Subsequently, the digital model continuously evolves by assimilating real-time data, allowing for ongoing LCSAs that support the building's construction, renovation, and maintenance.

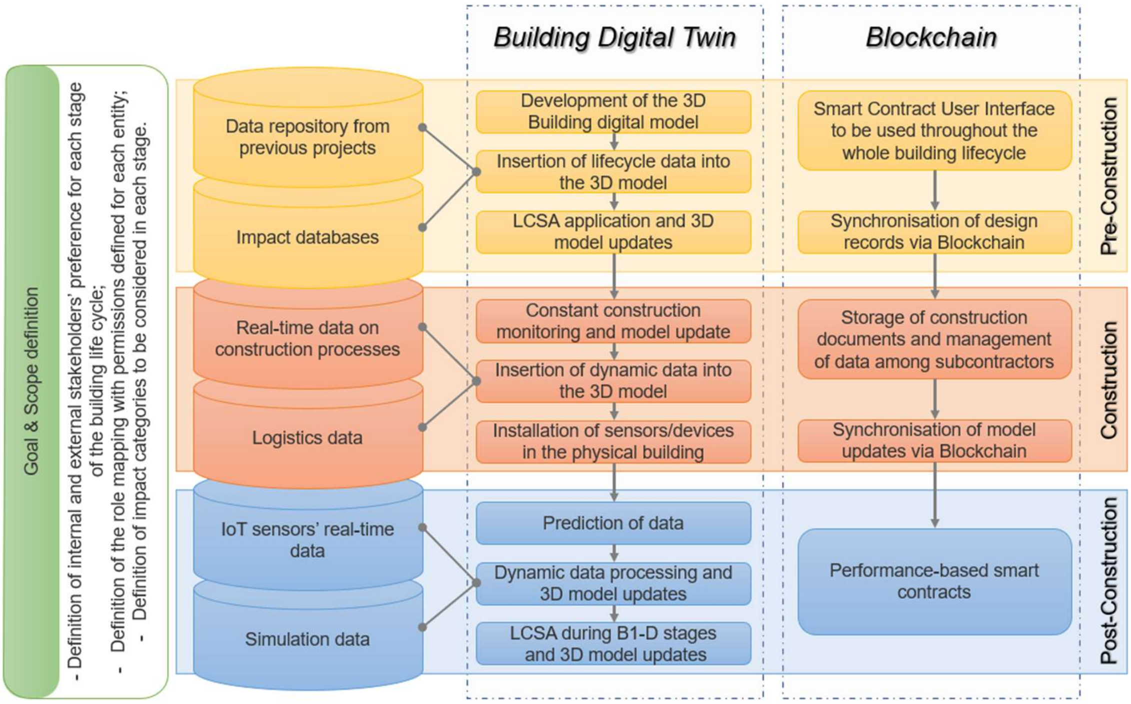

Figure 9.6 - The integration framework proposed in this study

In contrast to conventional LCSA with its fixed time horizon, the proposed framework proposes a dynamic LCSA approach adaptable to different stages of the building's life cycle. While retaining the fundamental methodological structure based on the ISO 14040 standard, it emphasizes the importance of clearly and accurately defining the goal and scope of LCSA at each building stage. This encompasses elements like functional unit, system boundary, target audience, assumptions, and limitations, ensuring that the selected impact categories align with the specific sustainability objectives of each building stage.

The digital model is established and constantly updated in the pre-construction phase as design decisions are made. This descriptive DT, driven by 3D-BIM models, incorporates detailed information about construction materials, aiding in the early-stage conceptualization and sustainable material choices. During construction, real-time data is collected and seamlessly integrated into the digital model, establishing a bidirectional connection between the digital and physical assets. This synchronization empowers the utilization of real-time data in LCSA, elevating the quality of decision-making and creating a construction data repository for future projects. Furthermore, it facilitates construction simulations, virtual job site planning, and safety planning, enhancing sustainability across all three pillars.

In the post-construction phase, the DT model receives updates encompassing static data from various sources, including impact databases and data repositories from prior projects. These updates are complemented by dynamic data IoT sensors. Integrating artificial intelligence (AI) and machine learning is also encouraged, driving building assessments to a level of autonomy and connectivity, significantly reducing human intervention while maintaining sustainability goals. The DT's role in decision-making spans various domains, from material selection to energy efficiency and thermal comfort.

The digital twin's role in decision-making is extensive, offering benefits in material selection, energy efficiency, and thermal comfort. While its application during pre-construction and construction stages remains an emerging topic, the framework envisions using digital twins as quality control tools in design, fabrication, and assembly processes, thus improving sustainability outcomes.

The framework also proposes using blockchain technology to record all design changes, addressing the long-standing challenge of absent chronological records in traditional building models. Blockchain synchronization promises transparency, security, and streamlined collaboration among diverse professionals in the construction project. Smart contracts within blockchain technology guarantee transaction security without imposing extensive knowledge or workflow alterations on stakeholders. This innovative approach delivers benefits across all stages of a building's life cycle, addressing concerns associated with inspection records and operations during fabrication.

By employing blockchain for digital fabrication drawing production, real-time data synchronization, and data record tracking, transparency and collaboration within the construction process are significantly enhanced. Furthermore, blockchain technology can establish efficient connections among professionals and offer innovative solutions to external stakeholders, culminating in heightened value creation.

Finally, the LCSA interpretation step should assist the stakeholders in the decision-making process related to each stage of the building life cycle. The decision-makers must be able to select the optimum sustainable choice for the building based on the three pillars of sustainability. In these terms, utilizing multi-criteria decision-making (MCDM) methods to facilitate the decision and performing a Sensitivity Analysis during interpretation is encouraged, as it allows the LCSA practitioner to compare all possibilities highlighted as suitable for the building during the previous LCSA steps.

9.12.1 Demonstration of the proposed framework for Proof of Concept

A case study is examined to validate the applicability of the proposed framework. It was considered a building of typical architecture in the southeast of Brazil to present a discussion representative of the Brazilian construction industry. The analyzed building is a 17-unit residential building composed of 6 stories (ground floor, four floors, and a roof) in Rio de Janeiro, Brazil. The baseline 3D model was modeled in Autodesk Revit 2023, with data integrated and extracted using Dynamo as the visual programming language. The whole process was developed on the Microsoft Windows 11 operating system, using an Intel core i7 processor at 2.3 GHz and 32GB of RAM.

This case study serves as a vital component in developing and validating the integrative framework. The primary objective of this case study is not to comprehensively apply the entire framework across all stages of a building's life cycle. Instead, the focus is on testing and validating specific aspects, primarily within the pre-construction phase, using available tools in the market. The rationale behind this approach is to understand the practical challenges, feasibility, and functionality of integrating LCSA, DT, and blockchain technologies within the critical context of a construction project. Focusing on the pre-construction phase, where significant sustainability decisions are made, materials and methods are selected, and the foundation for a building's life cycle is laid, this case study allows for a targeted assessment of the framework's effectiveness. Ultimately, it acknowledges that while the ultimate goal is to apply the framework across all stages of a building's life cycle, a phased approach to validation is crucial.

The process begins with developing a detailed 3D model using specialized Autodesk Revit software. This BIM model acts as the primary data source, creating the foundational DT while offering a comprehensive building representation. It includes physical attributes, materials, systems, and design elements. Subsequently, a BIM-based DT is crafted to provide a real-time virtual replica of the physical building. This DT serves as the dynamic element in the process, continuously engaging with the actual building throughout its lifecycle.

With the insertion of lifecycle data in the 3D building model, the first LCSA application occurs, following all recommendations proposed by ISO 14040 and 14044 standards. The

LCSA scope during the pre-construction stage is to determine the best building elements and methods among a pre-defined list, considering environmental, economic, and social impacts. In this study, the functional unit of the study corresponds to all architectural materials and assemblies for the whole building, including all materials required for manufacturing and use, such as sealants, adhesives, coatings, and finishing. Besides, the definition of the functional unit considers that it is related to a multi-family residential building with a service life of 60 years. In this work, a 1% cut-off factor by mass was considered to determine which materials to exclude from the assessment.

Furthermore, a cradle-to-grave system boundary is adopted in this study, in which the following stages are considered: extraction of raw materials, transportation, fabrication, construction, operation, and end of life. For the end-of-life phase, it is assumed that the building would be imploded, and the assessment would include the relevant material collection and landfilling rates. The same system boundary is adopted for environmental, economic, and social evaluations to guarantee that the harmonization of the three approaches occurs satisfactorily.

Ultimately, to enable seamless data transfer and to export the building model to different computational tools to perform various building analyses, it is suggested to make use of the Industry Foundation Classes (IFC) data model, a standardized and digital way to describe the built environment's data [68], providing software-agnostic data interoperability in the Architecture, Engineering, and Construction (AEC) industry [69]. Remarkably, in this case study, it is proposed that the final IFC models are exported to the ACCA software to use the *usBIM.blockchain* application, which allows practitioners to register any document uploaded to the platform on a public blockchain. The steps taken are represented in **Figure 9.7**.

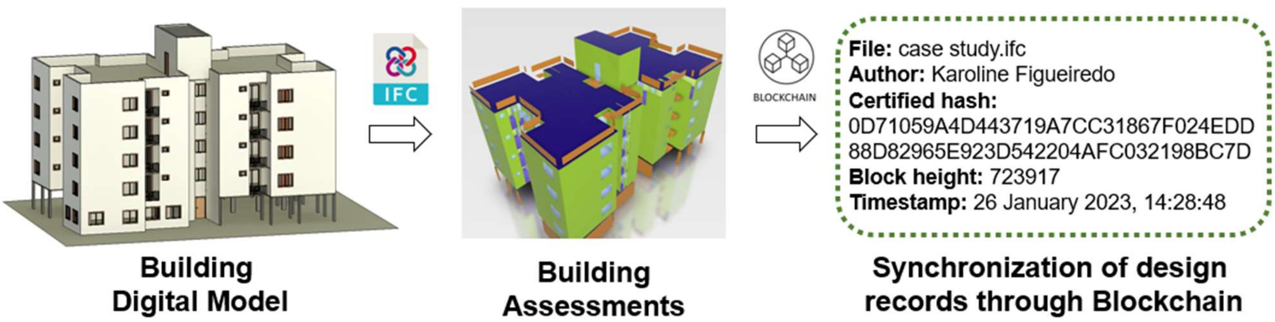

Figure 9.7 - First steps applied in the case study

On the one hand, some papers suggest exporting the Bill of Quantities (BoQ) from the BIM software to a specific tool related to life cycle approaches or using plug-ins and add-ons to conduct the LCSA calculation in the BIM tool [63]. On the other hand, some researchers encourage the inclusion of environmental, social, and economic data within the BIM model using different data sources [19]. This last approach is the most supported here since it represents the evolution of the building's digital model with the centralization of more data and information, thus allowing the growth of the building's digital shadow in BIM into a building's DT in the following stages of the building life cycle. Therefore, the modeling process of this case study incorporated an efficient data integration method. Building materials' properties and additional data were seamlessly integrated into Autodesk Revit using a custom Dynamo script. This approach augmented the existing dataset, enhancing the depth and accuracy of information associated with building elements.

In the context of the pre-construction stage, specific impact categories were meticulously selected to evaluate the building's sustainability from a holistic perspective. The Global Warming Potential (GWP), measured in kg CO_2 eq., was chosen as the environmental impact category, addressing the carbon footprint of the building materials and processes. The economic assessment focused on the building's life-cycle cost, encompassing aspects related to the cost-effectiveness of materials and construction methods. In parallel, the social assessment emphasized the well-being of workers and local communities, adopting the "Social Impact Rating" category. This rating category is considered a multifaceted approach, encompassing ethical labor practices, local sourcing, sustainable production methods, and community engagement—acknowledging the importance of social responsibility in construction projects.

An extensive inventory database was established in Microsoft Excel to support the data integration and augmentation process. This database was comprised of the most frequently employed construction materials and building systems within the Brazilian construction sector. It drew upon data derived from previous projects conducted by a construction company in the state of Rio de Janeiro. The database contained a comprehensive array of information, including properties of materials, cost data, and regional availability.

The gathering process was underpinned by the construction company's extensive experience in real-world projects, ensuring that the data reflected practical, on-the-ground considerations. Moreover, this wealth of data enabled the computation of final values to be inserted into the new parameters in Autodesk Revit, facilitating the quantification of environmental, economic, and social aspects within the building's life cycle. Utilizing this industry-derived data not only enhanced the accuracy of the assessments but also underscored the relevance of the study's findings to real-world construction practices. The summary of this process is provided in **Figure 9.8**, offering a succinct representation of the new parameters created in the 3D model and the database's content while maintaining the discussion's brevity.

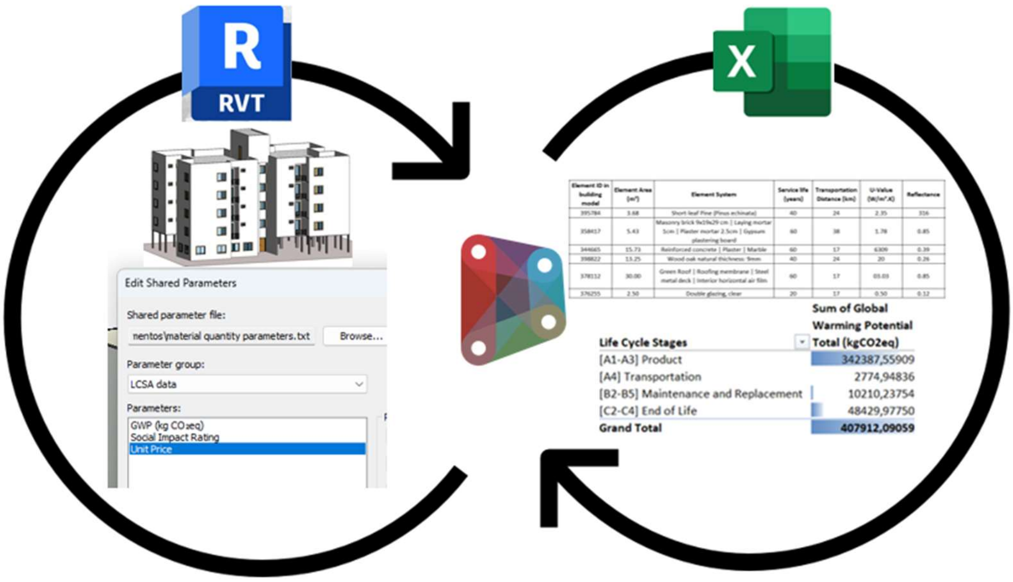

Figure 9.8 - The process of integrating the inventory database with the building model

It is important to highlight that the traditional architectural design process in BIM often involves manual exploration and iteration of design alternatives, which can be time-consuming and limit the exploration of diverse possibilities. This proposal encourages using visual programming languages, such as Dynamo, that offer a promising approach to automate and optimize this process by leveraging computational tools.

Therefore, in order to facilitate the analysis of various design iterations and their corresponding environmental, economic, and social impacts, a systematic approach was adopted. Firstly, Dynamo, a visual programming language, was employed to establish a connection between the inventory database stored in Excel sheets and the Revit environment. This integration allowed for the seamless transfer of vital material information from the database to the Revit model, enriching each building element with detailed data.

Secondly, a script was developed to update the baseline 3D model in Revit and generate alternative design options for key building elements. This script enabled the variation of parameters such as door types, window types, external wall configurations, and slab types, resulting in the creation of 24 distinct alternatives for the building construction. By systematically altering these elements, the script facilitated the exploration of diverse design possibilities, each with its unique set of environmental, economic, and social implications.

A snapshot of the Dynamo code utilized in this case study is presented in **Figure 9.9**, providing insight into the technical implementation of the data integration process. Furthermore, to streamline the analysis of each design iteration, a Python code was developed to collect data from the material takeoff of every solution. This Python script extracted essential data points from the Revit model and exported them to an Excel spreadsheet for further analysis. The script overview is detailed in **Figure 9.10**, outlining the key functions and procedures involved in the data collection process.

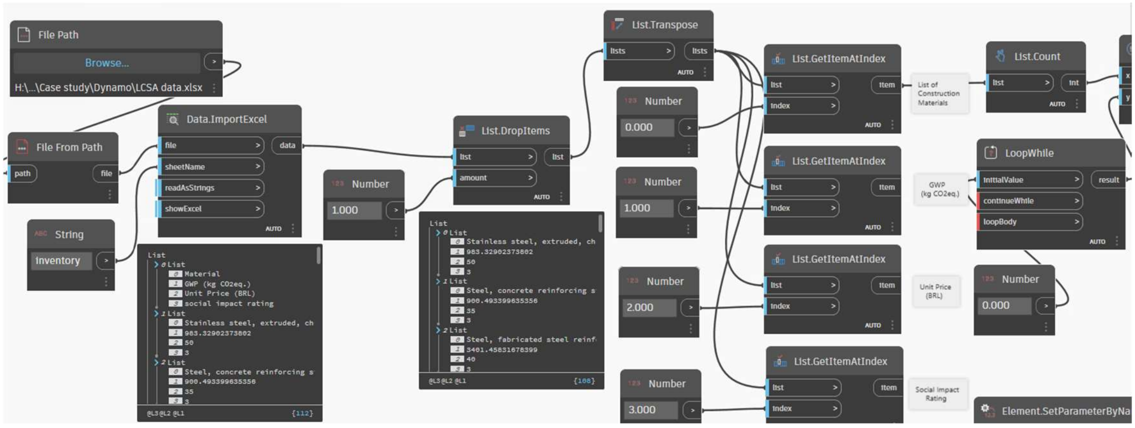

Figure 9.9 - Part of the Dynamo code used in this case study

```
Script Overview

BEGIN SCRIPT

  IMPORT necessary libraries for geometry, Revit API, and
    ↪ Excel manipulation

  DEFINE document as the active Revit document

  FUNCTION get_materials_of_elements(category):
      INITIALIZE elements as a collection of elements of the
        ↪ specified category
      INITIALIZE materials_per_element as an empty
        ↪ dictionary

      FOR each element in elements:
          GET the material ID of the element if available
          IF material ID exists:
              GET material from document using material ID
              IF material name is not in
                ↪ materials_per_element:
                  INITIALIZE a new list for this material
              APPEND element to the list for this material

      RETURN materials_per_element

  FUNCTION calculate_material_quantities(
    ↪ materials_per_category, category_name):
      INITIALIZE material_quantities as an empty dictionary

      FOR each material and its elements list:
          INITIALIZE total_quantity to 0.0
          CALCULATE total_quantity based on the
            ↪ category_name
          UPDATE material_quantities with the calculated
            ↪ total_quantity

      RETURN material_quantities

  FUNCTION export_material_quantities_to_excel(
    ↪ material_quantities, file_path):
      CREATE a DataFrame from material_quantities
      WRITE DataFrame to Excel file at specified file_path


  MAIN:
      DEFINE categories and corresponding names
      INITIALIZE all_material_quantities as an empty
        ↪ dictionary

      FOR each category and its name:
          GET materials using get_materials_of_elements
          CALCULATE quantities using
            ↪ calculate_material_quantities
          UPDATE all_material_quantities with calculated
            ↪ quantities

      EXPORT all_material_quantities to Excel

      SET OUTPUT as the Excel file path

END SCRIPT
```

Figure 9.10 – Script Overview

Subsequently, the exported data was subjected to rigorous evaluation and assessment to quantify the environmental, economic, and social impacts associated with each design alternative. **Figures 9.11 and 9.12** delineate the algorithms employed to export material quantities to Excel and determine the least environmental impact materials, respectively. These algorithms provided a structured framework for analyzing the collected data and deriving meaningful insights into the sustainability implications of various design choices.

Algorithm Export Material Quantities to Excel

```
Initialize Document from Revit's active UI document
Define Categories with BuiltInCategory enums and names
Initialize ExcelFilePaths as an empty list
for each Category in Categories do
    Set CurrentCategory to the key of the current item in Categories
    Set CategoryName to the value of the current item in Categories
    MaterialsPerElement ← GetMaterialsOfElements(CurrentCategory)
    MaterialQuantities ← CalculateMaterialQuantities(MaterialsPerElement, CategoryName)
    ExcelFilePath ← ExportMaterialQuantitiesToExcel(MaterialQuantities, 'address.xlsx', CategoryName)
    Append ExcelFilePath to ExcelFilePaths
end for
Output ← ExcelFilePaths
```

Figure 9.11- Algorithm to Export Material Quantities to Excel

By leveraging computational tools and scripting techniques, this approach facilitated a systematic exploration of design alternatives and their corresponding sustainability outcomes. Moreover, it underscored the importance of integrating data-driven decision-making processes within the architectural design workflow, paving the way for more informed and sustainable design practices in the construction industry.

```
Algorithm Determine the Least Environmental Impact Materials
Initialize Document from Revit's active UI document
Define Categories with BuiltInCategory enums and names
Initialize ExcelFilePaths as an empty list
Initialize MaterialImpacts as an empty dictionary
for each Category in Categories do
    Set CurrentCategory to the key of the current item in Categories
    Set CategoryName to the value of the current item in Categories
    MaterialsPerElement ← GetMaterialsOfElements(CurrentCategory)
    MaterialQuantities ← CalculateMaterialQuanti-
ties(MaterialsPerElement, CategoryName)
    ExcelFilePath ← ExportMaterialQuantitiesToExcel(MaterialQuantities,
'address.xlsx', CategoryName)
    Append ExcelFilePath to ExcelFilePaths
end for
Output ← ExcelFilePaths
# Now we process the Excel files to calculate environmental impacts
for each FilePath in ExcelFilePaths do
    Set Data ← ReadExcelFile(FilePath)
    for each Row in Data do
        Set Material ← Row['Material']
        Set Quantity ← Row['Quantity']
        Set Impact ← CalculateEnvironmentalImpact(Material, Quantity)
        if Material not in MaterialImpacts then
            MaterialImpacts[Material] ← Impact
        else
            MaterialImpacts[Material] ← MaterialImpacts[Material] + Im-
pact
        end if
    end for
end for
Set LeastImpactMaterial ← GetMaterialWithLeastIm-
pact(MaterialImpacts)
PresentMaterialChoices(LeastImpactMaterial)
function CalculateEnvironmentalImpact(Material, Quantity)
    # Define the environmental impact calculation logic
    return EnvironmentalImpact
end function
function GetMaterialWithLeastImpact(MaterialImpacts)
    # Logic to identify the material with the least environmental impact
    return MaterialWithLeastImpact
end function
function PresentMaterialChoices(Material)
    # Logic to present the material choices
end function
```

Figure 9.12 - Algorithm to Determine the Least Environmental Impact Materials

9.13 RESULTS AND DISCUSSION

This work intends to prove that integrating LCSA, DT, and blockchain creates a powerful Decision Support System (DSS) to be applied in the built environment. This DSS facilitates data-driven decision-making by providing stakeholders with real-time insights, allowing them to optimize design choices, material selections, and operational strategies throughout the building life cycle. Besides, this solution empowers stakeholders to make more informed and sustainable decisions, fostering a more efficient and environmentally conscious building industry. In order to thoroughly discuss the findings of this work, this section will be divided into three parts, as presented below.

9.13.1 Research Questions and Their Implications

From the investigation conducted, key findings emerge related to a dynamic approach to achieving sustainability in the construction industry. It is understood that this industry still lacks an integrated and systematized methodology for assessing the triple-bottom-line sustainability of building projects, considering the impacts generated from the extraction of raw materials to the building end-of-life phase and benefiting the decision-making process throughout the whole building lifecycle. In addition, there is still a need to develop more guidelines related to the social and economic impacts generated by construction so that the sustainability assessment encompasses the three pillars comprehensively. This is a significant research gap, directly affecting the achievement of more sustainable buildings.

In this context, the proposed framework adds to a growing corpus of research showing the steps to be taken to create an iterative and dynamic building sustainability assessment. This addresses RQ1 by offering a strategy to extrapolate the discussion on BIM-LCSA integration, usually focused exclusively on the early design stages of a building project. The workflow proposed in this study demonstrates the possibility of applying LCSA during different building phases with the aid of a building DT. From centralizing data and information in the same digital model and adopting a project management methodology focused on achieving sustainable goals, it will become much easier to carry out dynamic life cycle assessments at different stages of the building's life cycle.

It is proposed that the LCSA results in the pre-construction phase improve design decisions and that, later, the digital model continues to be fed with real-time data so that new LCSAs can be applied and assist in the construction, renovation, and maintenance of the building. It is also expected that practitioners consider the future of individual elements and components since their impacts can be calculated and analyzed by integrating LCSA and BIM-based DT. Deconstruction practices should be tested and compared to benefit decision-making during the building's end of life. These possibilities address RQ1 by proposing different levels of DTs throughout the entire building life cycle and creating a dynamic approach to improve building decisions.

In turn, one primary application that a BIM-based DT can play a significant role in is ensuring that the sustainability assessment of a building takes into account temporal information. As implemented in conventional LCSA, using fixed time horizons may limit the availability of crucial data, leading to less realistic sustainability assessments. Addressing RQ2, the proposed framework offers a dynamic LCSA approach that can be applied at various stages of the building's life cycle. By harnessing the power of DT and blockchain, sustainability assessments are enabled to continuously access and utilize real-time data without creating security and transparency issues. This seamless integration ensures that LCSAs remain current and adaptable, providing stakeholders with an up-to-date understanding of the building's environmental, economic, and social impacts throughout its entire life span.

Moreover, incorporating blockchain technology further enhances the credibility and transparency of data sources, fostering trust and reliability in the sustainability evaluation process. Blockchain's decentralized and immutable nature ensures the synchronization of design records across all stages of the building's life cycle, safeguarding data integrity and preventing discrepancies that may arise from multiple stakeholders' contributions. Consequently, this synergistic utilization of DT and blockchain empowers stakeholders to make informed decisions, optimize sustainability outcomes, and drive transformative change in the construction industry.

9.13.2 Case Study Results and Challenges

Demonstrating the proposed framework via a building case study provides the reader with greater insight into how the proposed development can be leveraged to support relevant queries for various stages of a building life cycle. This building case study was tested with a focus on the building design stage, providing an opportunity to validate the effectiveness of integrating different technologies to achieve sustainability in the construction industry. Moreover, this integrative approach lays the foundation for extending real-time sustainability evaluations to subsequent phases of the building's life cycle, offering the potential to enhance decision-making processes and sustainability outcomes throughout the entire building's lifespan.

The analysis of 24 different building design alternatives was conducted, starting with the baseline solution. The presentation of results was then organized according to the sustainability indicators evaluated, followed by an interpretation of the findings and their alignment with the proposed framework. All results were normalized to standardize the data and ensure that each criterion carries equal weight in this multi-criteria analysis. Besides, each alternative was represented by a unique combination of construction elements from a pre-selected list. For example, the baseline solution is considered the first combination, represented by "d1 w1 e1 s1," where "d1" refers to door type 1, "w1" refers to window type 1, "e1" refers to external wall type 1, and "s1" refers to slab type 1. The LCSA result summary related to the baseline 3D model is presented in **Table 9.2**, while the comparison among the different alternatives is visually shown in **Figure 9.13**.

Table 0.2 - Life Cycle Impact Assessment result summary

Sustainability Dimension	Impact categories	Total
Environmental	Global Warming Potential (kg CO_2eq)	716,327
Economic	Life-cycle cost (Brazilian Real - BRL)	18,952,789
Social	Social Impact Rating	3.784

Notably, it is essential to emphasize that while the social indicator is intended to be maximized in this study, other indicators reflect negative impacts and are aimed to be minimized. To facilitate a consistent comparison, the inverse of the social indicator was employed as the final indicator throughout the analysis. This approach guarantees the uniform minimization of all indicators considered in this study.

In this case study, the primary objective was not to determine the single most suitable solution for the building, as this would necessitate assigning specific weights to each criterion during the MCDM analysis [17]. The relative importance of these criteria varies based on project-specific factors and the preferences of stakeholders, aligning with the proposed integrative framework that stresses the significance of incorporating stakeholder preferences to achieve optimal and context-specific decisions.

Nonetheless, while the case study was focused on the building design stage, the authors recognize the importance of testing the framework during the operational phase of an actual building. As part of the ongoing research, the authors are actively collecting data from a physical building where a 3D-BIM model developed in the design stage will continue to be utilized throughout the building operational phase. By integrating real-time data collected from IoT sensors during the operational stage, it is aimed to validate the framework's performance over the entire building life cycle.

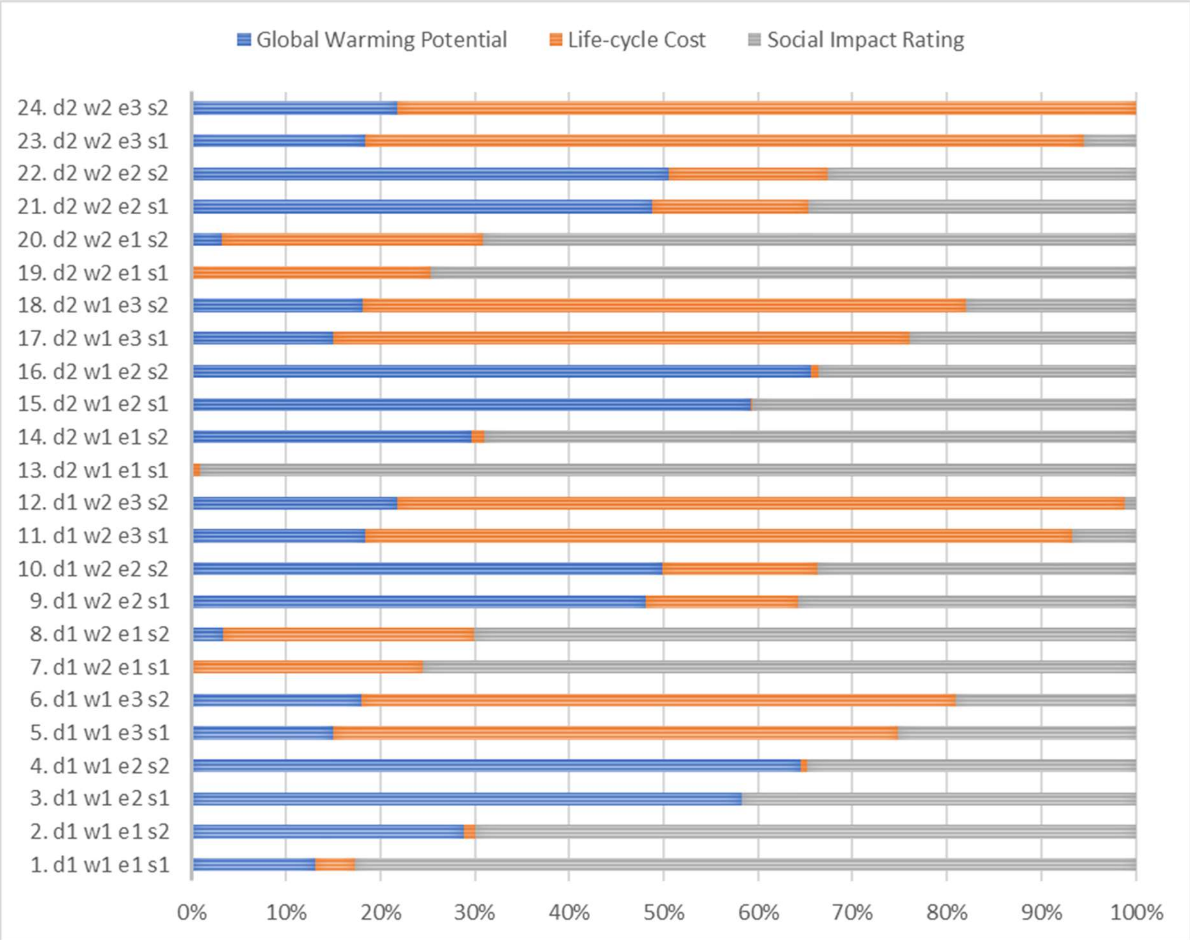

Figure 9.13 - Comparison of impact categories for 24 building design combinations

While exploring the feasibility of integrating different technologies in the construction industry, it is essential to acknowledge the challenges inherent in employing available market tools. One of the most significant issues is the interoperability challenge, where various devices and platforms often struggle to communicate effectively with one another, hindering the seamless flow of information and data. Additionally, these tools may not inherently support the diverse requirements of sustainability assessments in different building life cycle phases. Recognizing these obstacles, this paper underscores the necessity of developing a novel platform that can bridge the existing gaps, fostering a more integrated, efficient, and robust ecosystem for comprehensive sustainability assessments.

9.13.3 The Role of a Semantic Platform and Future Development

In order to facilitate the entire implementation of the integrative framework, it is suggested the creation of a platform for integrating the concepts, with a Smart Contract user interface to be used throughout the whole building life cycle. This platform aims to address interoperability concerns and ensure the effective utilization of digital twins, blockchain technology, and real-time data for enhancing sustainability across the building life cycle.

Figure 9.14 presents the semantic architecture for this platform. Three different layers are proposed here (i.e., the database layer, the logic layer, and the user interface) to allow the platform to be operable. The database layer consists of the 3-D building models and all data to be inserted and generated. Simulations should be carried out throughout the entire project lifecycle, either to benefit decision-making of which components and methods to use or to optimize the use of building systems during the operational building stage.

Sensors and devices should collect real-time data from the physical building. In contrast, the building model should be calibrated to accept data from numerous data streams, such as video devices, laser scanners, accelerometers, Radio Frequency Identification (RFID) devices, or displacement sensors [32]. In this way, up-to-date simulations can be performed based on real-time data, and all data generated must be recorded in the blockchain platform. The logic layer may be divided into building phases as the stakeholders and processes involved can differ. Ultimately, the user interface is based on Smart Contracts to protect all data exchange throughout the building life cycle and guarantee data reliability and traceability.

Besides, the team should choose a blockchain platform that aligns with the project requirements. In this decision, it is fundamental to consider factors such as scalability, data privacy, consensus mechanism, and smart contract capabilities. Then, designing and deploying smart contracts that define how the data will be stored, accessed, and managed becomes necessary. These smart contracts will dictate the logic governing interactions with the data.

In turn, the proposed framework also suggests that the practitioner define the role mapping with permissions for each entity at this stage. For example, a specific entity may need permission to modify any file (i.e., building 3D models, 2D drawings, documents, and reports) generated during the design stages. However, this entity may not need permission during fabrication and assembly. In this context, it is necessary to precisely define a role mapping with permissions defined for each entity, which will directly affect the logic layer of the proposed platform. It is illustrated in **Figure 9.15**.

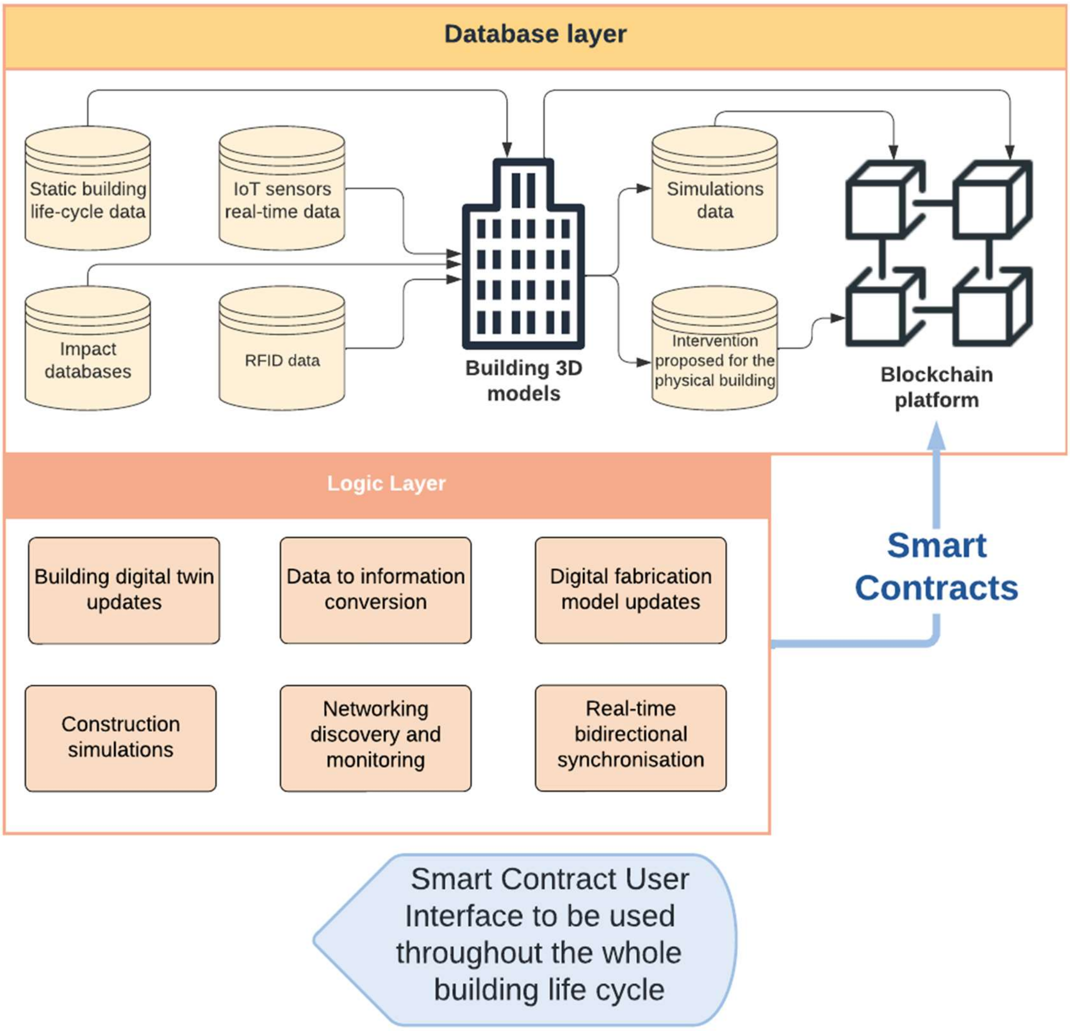

Figure 9.14 - Proposed semantic architecture for the integrated framework

	Pre-Construction												Construction												Post-Construction							
	Building 3D Model				2D Drawings				Documents and Reports				Building 3D Model				2D Drawings				Documents and Reports				Building 3D Model				Documents and Reports			
	C	R	U	D	C	R	U	D	C	R	U	D	C	R	U	D	C	R	U	D	C	R	U	D	C	R	U	D	C	R	U	D
Owner	✗	✓	✗	✗	✗	✓	✗	✗	✗	✓	✗	✗	✗	✓	✗	✗	✗	✓	✗	✗	✗	✓	✗	✗	✗	✓	✓	✗	✓	✓	✓	✓
Designer	✓	✓	✓	✓	✓	✓	✓	✓	✓	✓	✓	✓	✓	✓	✓	✗	✓	✓	✓	✗	✓	✓	✓	✗	✓	✓	✓	✗	✓	✓	✗	✗
Manufacturers	✗	✗	✗	✗	✗	✗	✗	✗	✗	✗	✗	✗	✗	✓	✓	✗	✓	✓	✓	✗	✓	✓	✓	✗	✗	✗	✗	✗	✗	✗	✗	✗
Engineer	✗	✓	✓	✓	✗	✓	✓	✗	✓	✓	✓	✓	✗	✓	✓	✗	✗	✓	✓	✗	✓	✓	✓	✓	✗	✓	✓	✗	✓	✓	✓	✓
Devices	✗	✗	✗	✗	✗	✗	✗	✗	✗	✗	✗	✗	✗	✗	✗	✗	✗	✗	✗	✗	✗	✗	✗	✗	✗	✓	✓	✗	✓	✓	✓	✗

Permissions: C = Create; R = Read; U = Update; D = Delete.

Figure 9.15 - Proposed role mapping with permissions defined for each entity

The semantic architecture for the integrative system is an innovative proposal to guide the following steps in this ongoing research. To enhance the accuracy of this architecture, future iterations of the framework will explore the integration of IoT sensors in a physical building to collect real-time data. Besides, this architecture will be developed with a focus on scalability and its potential for broader industry adoption. The main goal is that researchers and industry stakeholders can explore this platform in various building types and construction projects, ranging from small-scale developments to large infrastructure projects. Ultimately, identifying potential challenges and opportunities will facilitate widespread acceptance and integration.

9.14 CONCLUSION

This paper elaborated on viable ways to improve the LCSA application in buildings, focusing on a dynamic sustainability assessment. This need arose from the observation that relying on historical data in impact assessments is recurrent, ignoring the impact of time-related changes in building data. This simplification compromises the reliability of LCSA findings, introducing a potential bias and questioning the overall validity of sustainability assessments in the construction industry.

In this context, this paper presented a framework that integrates the LCSA methodology with DT and blockchain. On the one hand, the building DT model provides a real-time digital representation of the physical building throughout its life cycle. On the other hand, blockchain is introduced to address the critical aspects of data security, integrity, and transparent collaboration in sustainable construction practices. The integration proposed in this work, demonstrated in a building of typical architecture in the southeast of Brazil, is an earnest attempt to offer practical solutions to the challenges faced in embracing construction sustainability comprehensively.

Although research has illuminated the importance of combining different technologies to aid the application of LCSA to built assets, the integration of LCSA, DT, and blockchain in a building remains briefly addressed in the literature, as proved by the systematic review posed in this work. Combining these concepts can benefit the decision-making process of which materials and methods would be most suitable for a building, as well as the most appropriate decisions during construction and post-construction, considering the three pillars of sustainability.

The limitations of this work can be stated as follows: even though the integration of DT and blockchain in the dynamic LCSA process has shown promising results in the proposed building case study, it has laid the foundation for a dynamic LCSA approach exclusively within the building design stage. To advance the field, future research should focus on expanding the framework's capabilities and addressing any limitations encountered. Investigating innovative technologies, refining assessment methodologies, and exploring real-world applications will further solidify the proposed framework's potential for transformative change in sustainable building practices. Still, the discussion presented in this work set the stage for future research and implementation of dynamic LCSAs during buildings' pre-construction, construction, and post-construction phases. Ultimately, it is essential to highlight that the study presented in this paper is part of a larger research project on developing an application software to be used in real-world buildings.

9.15 REFERENCES

[1] S. Sala, F. Farioli, A. Zamagni, Life cycle sustainability assessment in the context of sustainability science progress (part 2), International Journal of Life Cycle Assessment. 18 (2013) 1686–1697. https://doi.org/10.1007/S11367-012-0509-5/TABLES/1.

[2] H. Amini Toosi, M. Lavagna, F. Leonforte, C. Del Pero, N. Aste, A novel LCSA-Machine learning based optimization model for sustainable building design-A case study of energy storage systems, Build Environ. 209 (2022) 108656. https://doi.org/10.1016/J.BUILDENV.2021.108656.

[3] S. Kubicki, A. Guerriero, L. Schwartz, E. Daher, B. Idris, Assessment of synchronous interactive devices for BIM project coordination: Prospective ergonomics approach, Autom Constr. 101 (2019) 160–178. https://doi.org/10.1016/J.AUTCON.2018.12.009.

[4] C. Boje, A. Guerriero, S. Kubicki, Y. Rezgui, Towards a semantic Construction Digital Twin: Directions for future research, Autom Constr. 114 (2020) 103179. https://doi.org/10.1016/J.AUTCON.2020.103179.

[5] Y.-H. Kuo, F. Pilati, T. Qu, G.Q. Huang, Digital twin-enabled smart industrial systems: recent developments and future perspectives, Int J Comput Integr Manuf. 34 (2021) 685–689. https://doi.org/10.1080/0951192X.2021.1959710.

[6] J. Li, M. Kassem, Applications of distributed ledger technology (DLT) and Blockchain-enabled smart contracts in construction, Autom Constr. 132 (2021) 103955. https://doi.org/10.1016/J.AUTCON.2021.103955.

[7] J.J. Hunhevicz, D.M. Hall, Do you need a blockchain in construction? Use case categories and decision framework for DLT design options, Advanced Engineering Informatics. 45 (2020) 101094. https://doi.org/10.1016/J.AEI.2020.101094.

[8] A.I. Sanka, M. Irfan, I. Huang, R.C.C. Cheung, A survey of breakthrough in blockchain technology: Adoptions, applications, challenges and future research, Comput Commun. 169 (2021) 179–201. https://doi.org/10.1016/j.comcom.2020.12.028.

[9] X. Li, L. Wu, R. Zhao, W. Lu, F. Xue, Two-layer Adaptive Blockchain-based Supervision model for off-site modular housing production, Comput Ind. 128 (2021). https://doi.org/10.1016/j.compind.2021.103437.

[10] M.J. Page, J.E. McKenzie, P.M. Bossuyt, I. Boutron, T.C. Hoffmann, C.D. Mulrow, L. Shamseer, J.M. Tetzlaff, E.A. Akl, S.E. Brennan, R. Chou, J. Glanville, J.M. Grimshaw, A. Hróbjartsson, M.M. Lalu, T. Li, E.W. Loder, E. Mayo-Wilson, S. McDonald, L.A. McGuinness, L.A. Stewart, J. Thomas, A.C. Tricco, V.A. Welch, P. Whiting, D. Moher, The PRISMA 2020 statement: an updated guideline for reporting systematic reviews, BMJ. 372 (2021). https://doi.org/10.1136/BMJ.N71.

[11] A.X. Naves, A REVIEW OF LIFE CYCLE COSTING IN THE CONSTRUCTION INDUSTRY AS A BOTTOM LINE FOR LIFE CYCLE SUSTAINABILITY ASSESSMENT, Universidade Federal Fluminense, 2015.

[12] N. Jan van Eck, L. Waltman, Software survey: VOSviewer, a computer program for bibliometric mapping, Scientometrics. 84 (2010) 523–538. https://doi.org/10.1007/s11192-009-0146-3.

[13] N.C. Onat, M. Kucukvar, A. Halog, S. Cloutier, Systems thinking for life cycle sustainability assessment: A review of recent developments, applications, and future perspectives, Sustainability. 9 (2017) 1–25. https://doi.org/10.3390/su9050706.

[14] ISO, ISO 14040:2006 - Environmental management — Life cycle assessment — Principles and framework, 2006.

[15] C. Llatas, B. Soust-Verdaguer, A. Passer, Implementing Life Cycle Sustainability Assessment during design stages in Building Information Modelling: From systematic literature review to a methodological approach, Build Environ. 182 (2020). https://doi.org/10.1016/j.buildenv.2020.107164.

[16] R.T. Fauzi, P. Lavoie, L. Sorelli, M.D. Heidari, B. Amor, Exploring the current challenges and opportunities of Life Cycle Sustainability Assessment, Sustainability. 11 (2019) 1–17. https://doi.org/10.3390/su11030636.

[17] K. Figueiredo, R. Pierott, A.W.A. Hammad, A. Haddad, Sustainable material choice for construction projects: A Life Cycle Sustainability Assessment framework based on BIM and Fuzzy-AHP, Build Environ. 196 (2021) 107805. https://doi.org/10.1016/J.BUILDENV.2021.107805.

[18] B. Soust-Verdaguer, J.A. Gutiérrez Moreno, C. Llatas, Utilization of an Automatic Tool for Building Material Selection by Integrating Life Cycle Sustainability Assessment in the Early Design Stages in BIM, Sustainability 2023, Vol. 15, Page 2274. 15 (2023) 2274. https://doi.org/10.3390/SU15032274.

[19] C. LLatas, B. Soust-Verdaguer, A. Hollberg, E. Palumbo, R. Quiñones, BIM-based LCSA application in early design stages using IFC, Autom Constr. 138 (2022) 104259. https://doi.org/10.1016/J.AUTCON.2022.104259.

[20] Y. Pigné, T.N. Gutiérrez, T. Gibon, T. Schaubroeck, E. Popovici, A.H. Shimako, E. Benetto, L. Tiruta-Barna, A tool to operationalize dynamic LCA, including time differentiation on the complete background database, International Journal of Life Cycle Assessment. 25 (2020) 267–279. https://doi.org/10.1007/s11367-019-01696-6.

[21] A. Francis, A. Thomas, A framework for dynamic life cycle sustainability assessment and policy analysis of built environment through a system dynamics approach, Sustain Cities Soc. 76 (2022) 103521. https://doi.org/10.1016/J.SCS.2021.103521.

[22] L. Patouillard, P. Collet, P. Lesage, P. Tirado Seco, C. Bulle, M. Margni, Prioritizing regionalization efforts in life cycle assessment through global sensitivity analysis: a sector meta-analysis based on ecoinvent v3, International Journal of Life Cycle Assessment. 24 (2019) 2238–2254. https://doi.org/10.1007/S11367-019-01635-5/FIGURES/5.

[23] A. Levasseur, P. Lesage, M. Margni, L. Deschěnes, R. Samson, Considering Time in LCA: Dynamic LCA and Its Application to Global Warming Impact Assessments, Environ Sci Technol. 44 (2010) 3169–3174. https://doi.org/10.1021/ES9030003.

[24] A.M. Ferrari, L. Volpi, D. Settembre-Blundo, F.E. García-Muiña, Dynamic life cycle assessment (LCA) integrating life cycle inventory (LCI) and Enterprise resource planning (ERP) in an industry 4.0 environment, J Clean Prod. 286 (2021) 125314. https://doi.org/10.1016/J.JCLEPRO.2020.125314.

[25] D. Ramon, K. Allacker, D. Trigaux, H. Wouters, N.P.M. van Lipzig, Dynamic modelling of operational energy use in a building LCA: A case study of a Belgian office building, Energy Build. 278 (2023) 112634. https://doi.org/10.1016/J.ENBUILD.2022.112634.

[26] V. Apostolopoulos, I. Mamounakis, A. Seitaridis, N. Tagkoulis, D.S. Kourkoumpas, P. Iliadis, K. Angelakoglou, N. Nikolopoulos, An integrated life cycle assessment and life cycle costing approach towards sustainable building renovation via a dynamic online tool, Appl Energy. 334 (2023) 120710. https://doi.org/10.1016/J.APENERGY.2023.120710.

[27] S. Cordier, P. Blanchet, F. Robichaud, B. Amor, Dynamic LCA of the increased use of wood in buildings and its consequences: Integration of CO2 sequestration and material

substitutions, Build Environ. 226 (2022) 109695. https://doi.org/10.1016/J.BUILDENV.2022.109695.

[28] V. Hasik, M. Ororbia, G.P. Warn, M.M. Bilec, Whole building life cycle environmental impacts and costs: A sensitivity study of design and service decisions, Build Environ. 163 (2019) 106316. https://doi.org/10.1016/J.BUILDENV.2019.106316.

[29] S. Haag, R. Anderl, Digital twin – Proof of concept, Manuf Lett. 15 (2018) 64–66. https://doi.org/10.1016/J.MFGLET.2018.02.006.

[30] S.M.E. Sepasgozar, Differentiating Digital Twin from Digital Shadow: Elucidating a Paradigm Shift to Expedite a Smart, Sustainable Built Environment, Buildings. 11 (2021) 151. https://doi.org/10.3390/buildings11040151.

[31] Y. Peng, M. Zhang, F. Yu, J. Xu, S. Gao, Digital Twin Hospital Buildings: An Exemplary Case Study through Continuous Lifecycle Integration, Advances in Civil Engineering. 2020 (2020). https://doi.org/10.1155/2020/8846667.

[32] H. Seaton, C. Savian, S. Sepasgozar, A. Sawhney, Digital twins from design to handover of constructed assets, London, 2022. https://www.rics.org/pt-br/wbef/home/reports-and-research/digital-twins-from-design-to-handover-of-constructed-assets/ (accessed June 8, 2022).

[33] Y. Celik, I. Petri, Y. Rezgui, Leveraging BIM and blockchain for digital twins, in: 2021 IEEE International Conference on Engineering, Technology and Innovation, ICE/ITMC 2021 - Proceedings, Institute of Electrical and Electronics Engineers Inc., 2021. https://doi.org/10.1109/ICE/ITMC52061.2021.9570246.

[34] C. Coupry, S. Noblecourt, P. Richard, D. Baudry, D. Bigaud, BIM-Based Digital Twin and XR Devices to Improve Maintenance Procedures in Smart Buildings: A Literature Review, Applied Sciences 2021, Vol. 11, Page 6810. 11 (2021) 6810. https://doi.org/10.3390/APP11156810.

[35] M. Ramos, P. Pereira, D.-G. Joe Opoku, S. Perera, R. Osei-Kyei, M. Rashidi, T. Famakinwa, K. Bamdad, Drivers for Digital Twin Adoption in the Construction Industry: A Systematic Literature Review, Buildings . 12 (2022) 113. https://doi.org/10.3390/BUILDINGS12020113.

[36] A. Akanmu, C.J. Anumba, Cyber-physical systems integration of building information models and the physical construction, Engineering, Construction and Architectural Management. 22 (2015) 516–535. https://doi.org/10.1108/ECAM-07-2014-0097/FULL/PDF.

[37] A.F. Kineber, A.K. Singh, A. Fazeli, S.R. Mohandes, C. Cheung, M. Arashpour, O. Ejohwomu, T. Zayed, Modelling the relationship between digital twins implementation barriers

and sustainability pillars: Insights from building and construction sector, Sustain Cities Soc. 99 (2023) 104930. https://doi.org/10.1016/J.SCS.2023.104930.

[38] K. Kang, S. Besklubova, Y. Dai, R.Y. Zhong, Building demolition waste management through smart BIM: A case study in Hong Kong, Waste Management. 143 (2022) 69–83. https://doi.org/10.1016/J.WASMAN.2022.02.027.

[39] S. Agostinelli, F. Cumo, M.M. Nezhad, G. Orsini, G. Piras, Renewable Energy System Controlled by Open-Source Tools and Digital Twin Model: Zero Energy Port Area in Italy, Energies (Basel). 15 (2022). https://doi.org/10.3390/EN15051817.

[40] L.C. Tagliabue, F.R. Cecconi, S. Maltese, S. Rinaldi, A.L.C. Ciribini, A. Flammini, Leveraging digital twin for sustainability assessment of an educational building, Sustainability (Switzerland). 13 (2021) 1–16. https://doi.org/10.3390/SU13020480.

[41] G. Estevam, L.M. Palma, L.R. Silva, J.E. Martina, M. Vigil, Accurate and decentralized timestamping using smart contracts on the Ethereum blockchain, Inf Process Manag. 58 (2021). https://doi.org/10.1016/j.ipm.2020.102471.

[42] S. Saxena, B. Bhushan, M.A. Ahad, Blockchain based solutions to secure IoT: Background, integration trends and a way forward, Journal of Network and Computer Applications. 181 (2021). https://doi.org/10.1016/j.jnca.2021.103050.

[43] V.L. Lemieux, Trusting records: is Blockchain technology the answer?, Records Management Journal. 26 (2016) 110–139. https://doi.org/10.1108/RMJ-12-2015-0042/FULL/PDF.

[44] V. Tsiatsis, S. Karnouskos, J. Höller, D. Boyle, C. Mulligan, Chapter 6 - Security, in: Internet of Things (Second Edition), Academic Press, 2019: pp. 127–142. https://doi.org/10.1016/B978-0-12-814435-0.00018-3.

[45] S. Nakamoto, Bitcoin: A Peer-to-Peer Electronic Cash System, (2008). https://git.dhimmel.com/bitcoin-whitepaper/ (accessed March 16, 2021).

[46] T. Hewa, M. Ylianttila, M. Liyanage, Survey on blockchain based smart contracts: Applications, opportunities and challenges, Journal of Network and Computer Applications. 177 (2021). https://doi.org/10.1016/j.jnca.2020.102857.

[47] L. Wu, W. Lu, F. Xue, X. Li, R. Zhao, M. Tang, Linking permissioned blockchain to Internet of Things (IoT)-BIM platform for off-site production management in modular construction, Comput Ind. 135 (2022) 103573. https://doi.org/10.1016/J.COMPIND.2021.103573.

[48] P. Kuhle, D. Arroyo, E. Schuster, Building A blockchain-based decentralized digital asset management system for commercial aircraft leasing, Comput Ind. 126 (2021) 103393. https://doi.org/10.1016/J.COMPIND.2020.103393.

[49] T.Y. Chen, H.F. Chang, Critical success factors and architecture of innovation services models in data industry, Expert Syst Appl. 213 (2023) 119014. https://doi.org/10.1016/J.ESWA.2022.119014.

[50] S. Chaveesuk, B. Khalid, W. Chaiyasoonthorn, Understanding Stakeholders Needs for Using Blockchain Based Smart Contracts in Construction Industry of Thailand: Extended TAM Framework, in: International Conference on Human System Interaction, HSI, IEEE Computer Society, 2020: pp. 137–141. https://doi.org/10.1109/HSI49210.2020.9142675.

[51] McKinsey & Company, Imagining construction's digital future | McKinsey, (2016). https://www.mckinsey.com/business-functions/operations/our-insights/imagining-constructions-digital-future# (accessed March 28, 2021).

[52] K. Figueiredo, A.W.A. Hammad, A. Haddad, V.W.Y. Tam, Assessing the usability of blockchain for sustainability: Extending key themes to the construction industry, J Clean Prod. 343 (2022) 131047. https://doi.org/10.1016/J.JCLEPRO.2022.131047.

[53] M. Das, X. Tao, J.C.P. Cheng, BIM security: A critical review and recommendations using encryption strategy and blockchain, Autom Constr. 126 (2021). https://doi.org/10.1016/j.autcon.2021.103682.

[54] X. Tao, Y. Liu, P.K.Y. Wong, K. Chen, M. Das, J.C.P. Cheng, Confidentiality-minded framework for blockchain-based BIM design collaboration, Autom Constr. 136 (2022) 104172. https://doi.org/10.1016/J.AUTCON.2022.104172.

[55] F. Elghaish, M.R. Hosseini, T. Kocaturk, M. Arashpour, M. Bararzadeh Ledari, Digitalised circular construction supply chain: An integrated BIM-Blockchain solution, Autom Constr. 148 (2023) 104746. https://doi.org/10.1016/J.AUTCON.2023.104746.

[56] N.O. Nawari, S. Ravindran, Blockchain and the built environment: Potentials and limitations, Journal of Building Engineering. 25 (2019). https://doi.org/10.1016/j.jobe.2019.100832.

[57] K.M. San, C.F. Choy, W.P. Fung, The Potentials and Impacts of Blockchain Technology in Construction Industry: A Literature Review, in: IOP Conf Ser Mater Sci Eng, 2019. https://doi.org/10.1088/1757-899X/495/1/012005.

[58] N.O. Nawari, Blockchain Technologies: Hyperledger Fabric in BIM Work Processes, in: Lecture Notes in Civil Engineering, Springer, 2021: pp. 813–823. https://doi.org/10.1007/978-3-030-51295-8_56.

[59] R. Zhao, Z. Chen, F. Xue, A blockchain 3.0 paradigm for digital twins in construction project management, Autom Constr. 145 (2023) 104645. https://doi.org/10.1016/J.AUTCON.2022.104645.

[60] W. Shen, T. Hu, C. Zhang, S. Ma, Secure sharing of big digital twin data for smart manufacturing based on blockchain, J Manuf Syst. 61 (2021) 338–350. https://doi.org/10.1016/J.JMSY.2021.09.014.

[61] R. Yang, R. Wakefield, S. Lyu, S. Jayasuriya, F. Han, X. Yi, X. Yang, G. Amarasinghe, S. Chen, Public and private blockchain in construction business process and information integration, Autom Constr. 118 (2020) 103276. https://doi.org/10.1016/J.AUTCON.2020.103276.

[62] C. Boje, Á.J. Hahn Menacho, A. Marvuglia, E. Benetto, S. Kubicki, T. Schaubroeck, T. Navarrete Gutiérrez, A framework using BIM and digital twins in facilitating LCSA for buildings, Journal of Building Engineering. 76 (2023) 107232. https://doi.org/10.1016/J.JOBE.2023.107232.

[63] M.V.A.P.M. Filho, B.B.F. da Costa, M. Najjar, K. V. Figueiredo, M.B. de Mendonça, A.N. Haddad, Sustainability Assessment of a Low-Income Building: A BIM-LCSA-FAHP-Based Analysis, Buildings 2022, Vol. 12, Page 181. 12 (2022) 181. https://doi.org/10.3390/BUILDINGS12020181.

[64] A. Hollberg, G. Genova, G. Habert, Evaluation of BIM-based LCA results for building design, Autom Constr. 109 (2020). https://doi.org/10.1016/j.autcon.2019.102972.

[65] B. Soust-Verdaguer, C. Llatas, A. García-Martínez, Critical review of bim-based LCA method to buildings, Energy Build. 136 (2017) 110–120. https://doi.org/10.1016/j.enbuild.2016.12.009.

[66] Y. Wang, M. Singgih, J. Wang, M. Rit, Making sense of blockchain technology: How will it transform supply chains?, Int J Prod Econ. 211 (2019) 221–236. https://doi.org/10.1016/J.IJPE.2019.02.002.

[67] M. Shou, T. Domenech, Integrating LCA and blockchain technology to promote circular fashion – A case study of leather handbags, J Clean Prod. 373 (2022) 133557. https://doi.org/10.1016/J.JCLEPRO.2022.133557.

[68] ISO, Industry Foundation Classes (IFC) for data sharing in the construction and facility management industries — Part 1: Data schema, 2018. https://www.iso.org/standard/70303.html (accessed February 8, 2022).

[69] L.J.N. Oostwegel, Š. Jaud, S. Muhič, K. Malovrh Rebec, Digitalization of culturally significant buildings: ensuring high-quality data exchanges in the heritage domain using

OpenBIM, Herit Sci. 10 (2022) 1–14. https://doi.org/10.1186/S40494-021-00640-Y/TABLES/3.

APPENDIX D – TOWARDS DYNAMIC LIFE CYCLE SUSTAINABILITY ASSESSMENTS: A REAL-WORLD CASE STUDY INTEGRATING DIGITAL TWIN AND BLOCKCHAIN

This chapter is submitted as an original research article.
https://doi.org/10.1016/j.jobe.2024.111018

FIGUEIREDO, Karoline; **PIEROTT, Rodrigo** et al. Towards Dynamic Life Cycle Sustainability Assessments: A Real-World Case Study Integrating Digital Twin and Blockchain.

Abstract: Sustainability in construction necessitates a triple-bottom-line approach, integrating environmental, economic, and social considerations throughout the project lifecycle. However, conventional sustainability assessments face challenges in data management and methodological standardization, in addition to being typically based on static data, compromising the reliability of findings. This paper introduces a novel framework integrating Life Cycle Sustainability Assessment (LCSA), Digital Twin, and blockchain. Developed using the Design Science Research methodology, a machine-learning-based software application is presented to facilitate dynamic sustainability assessments by leveraging real-time data from IoT sensors. This integration aims to enhance traditional sustainability assessments by harnessing the benefits of Digital Twin technology, such as real-time monitoring, predictive analysis, and scenario testing, to provide more accurate and timely insights into the sustainability performance of construction projects. Additionally, blockchain technology is utilized to ensure data integrity and transparency throughout the assessment process, addressing data security and trustworthiness concerns. A real-world case study comparing static and dynamic LCSA outcomes demonstrates the approach's efficacy. Comparative analysis reveals significant disparities in impact assessments, such as a 20.37% increase in non-renewable energy demand from static to dynamic LCSA after 12 months of real-time data collection. This approach provides critical insights into the temporal variability of sustainability impacts, underscoring the transformative potential of integrating real-time data into LCSA frameworks.

Keywords:
Blockchain; Digital Twin; Energy Performance Gap; Life Cycle Sustainability Assessment; Machine Learning.

9.16 INTRODUCTION

Sustainability, at its core, entails the creation of projects that strike a delicate balance between environmental, economic, and social considerations, with a commitment to meeting both present and future needs [1]. In the construction industry, this means prioritizing projects that consider the three pillars of sustainability and that are capable of adapting to changing conditions and meeting the needs of all stakeholders. In this vein, a triple-bottom-line (TBL) approach for construction projects is essential, where environmental, social, and economic factors are considered simultaneously to develop more sustainable built assets.

Besides, sustainability in the construction industry demands a holistic approach that considers the entire life cycle of buildings and infrastructure. Building upon the TBL framework, Life Cycle Sustainability Assessment (LCSA) emerges as a crucial tool. LCSA ensures a comprehensive examination of a built asset's impacts and benefits throughout its entire life cycle, aligning with the broader sustainability goals of considering the three sustainability dimensions together [2]. However, the integration of LCSA in construction presents several challenges, particularly in terms of data management and methodological standardization.

First, the sheer volume of data required for assessing functional and technical aspects throughout the life cycle poses a significant hurdle [3]. Moreover, the lack of standardized approaches in combining Life Cycle Assessment (LCA), Life Cycle Costing (LCC), and Social Life Cycle Assessment (S-LCA) methodologies, related to environmental, economic, and social dimensions, respectively, creates gaps in the effective application of LCSA to building projects [4] Ultimately, static data is often utilized in building impact assessments, making the impact of time-related changes on the data frequently overlooked [5]. This oversight jeopardizes the reliability of LCSA findings and compromises the overall validity of sustainability assessments in the construction industry.

To address these challenges, this paper introduces a machine learning-based framework application that plays a central role in dynamically enhancing LCSA. More specifically, the development of a robust and adaptive software solution is presented, integrating a Building Information Modeling-based Digital Twin (BIM-based DT) and blockchain technology into the LCSA framework. This integration aims to revolutionize sustainability assessments in construction by offering a strategic response to the complexities posed by data management, static data reliance, and methodological standardization challenges. By combining these cutting-edge technologies, this research aims to create a dynamic, real-time, and secure framework for sustainability assessments throughout the entire life cycle of buildings.

Particularly, this paper intends to discuss the rationale behind each component of the proposed integration. Firstly, the LCSA application ensures a holistic environmental, economic, and social evaluation. Secondly, the building DT model evolves from a Building Information Model (BIM) and provides a real-time digital representation of the physical building throughout its life cycle. Lastly, blockchain is introduced to address the critical aspects of data security, integrity, and transparent collaboration in the evolving landscape of sustainable construction practices. This integration is not only conceptual; it is an earnest attempt to offer practical solutions to the challenges the construction industry faces in embracing sustainability comprehensively.

This investigation is underpinned by several hypotheses, each addressing specific facets of this integrated approach. The primary hypothesis proposes that the amalgamation of BIM, DT, and blockchain in the LCSA process will substantially elevate the precision, comprehensiveness, and reliability of sustainability assessments within the construction industry. Recent literature indicates that the utilization of BIM furnishes crucial static information at the building level, contributing to more accurate environmental assessments [6–10]. Anticipating that the DT, complementing BIM, will provide a dynamic evaluation of impacts, this paper also hypothesizes the DT's potential to offer insights beyond traditional LCSA capabilities. Additionally, blockchain integration is expected to play a pivotal role in ensuring the security, transparency, and integrity of real-time data collected, addressing confidentiality concerns commonly disregarded in building LCSAs.

In totality, the integrated approach is hypothesized to enhance not only the assessment of environmental impacts but also the evaluation of economic and social aspects, culminating in a more holistic building LCSA. Therefore, the research question (RQ) guiding this study is as follows:

(RQ) What are the roles of BIM-based DT and blockchain in facilitating a dynamic and comprehensive LCSA, and how does their integrated use contribute to sustainability in the construction industry?

While LCSA offers a comprehensive framework for evaluating building life cycles, this paper focuses primarily on energy consumption due to its critical role in overall sustainability. This decision aligns with industry imperatives to address challenges such as the Energy Performance Gap (EPG) and the growing demand for energy-efficient buildings [11]. By prioritizing energy analysis within LCSA, this study aims to tackle multifaceted challenges, including discrepancies between predicted and actual energy performance [12]. This emphasis reflects industry recognition of energy's pivotal role in environmental, economic, and social sustainability outcomes, aiming to advance practical solutions for enhancing energy efficiency in the built environment.

This paper is organized as follows: Section 2 provides the literature review, offering essential contextual information to identify the research problem and motivation. Section 3 describes the methodology used in this research, outlining the approach and techniques employed. Section 4 presents the software development proposed in this work. A real-world case study is given in Section 5 to demonstrate the software's usability and validate this proposal. Section 6 showcases the main results obtained from the research and provides a comprehensive analysis and discussion of these findings. Finally, Section 7 presents the study's conclusion, summarizing the key findings, discussing their implications, and offering insights into potential future research directions.

9.17 LITERATURE REVIEW

This section proposes a comprehensive literature review, the synthesis of which is presented below. This review will enable the identification of existing gaps in the literature and lay the foundation for the proposed integration of concepts.

9.17.1 Life Cycle Sustainability Assessment

The LCSA methodology is an interdisciplinary framework that simultaneously evaluates the impacts associated with products and processes from an environmental, social, and economic perspective [13]. The techniques that form the LCSA framework (i.e., LCA, LCC, and S-LCA) follow the same methodological structure based on the ISO 14040 standard. This methodological structure is divided into four stages: Goal and Scope definition, Life Cycle Inventory (LCI), Life Cycle Impact Assessment (LCIA), and Interpretation [14].

Regarding the use of LCSA as a decision-making technique in the construction industry, researchers have applied this methodology mainly during the early stages of a building design [2,4,15,16]. A recent study introduced an innovative LCSA model designed for integration into the design phase of new building projects and energy refurbishments for existing buildings [17]. The authors further developed a novel formulation and weighting method to derive a final

LCSA index, facilitating a holistic assessment of design scenarios and considering the three pillars of sustainability. The study also innovatively integrates machine learning techniques into the optimization process, enhancing the efficiency of design assessments while upholding their precision.

Nevertheless, when considering using this methodology in different stages of the building's life cycle, a new challenge emerges related to the need for more temporal information in the assessments. Notably, the current LCSA methods take a stagnant approach that fails to consider dynamic factors during the building life cycle, such as material deterioration, varying energy consumption, and technology up-gradation, resulting in inaccurate sustainability assessments [18]. In this context, the data inventory can be considered the most sensitive and challenging step of an LCSA application since it leads to the creation of a model that should represent, as accurately as possible, all the exchanges between the distinct phases of a process [19]. So far, the need for more impact data sources adapted to the specific requirements of a building project has been seen in the literature [4]. Besides, it has been noted that impact assessments are typically based on data from historical series, which hinders the use of LCSA for rapid corrective actions on a project.

Other recent publications presented different frameworks for a dynamic LCSA application but with limited advances in this field. Francis and Thomas [18] developed a methodological framework that allows practitioners to set desired values for material use, material replacement alternatives, energy mix, and water recycling percentage to evaluate the building impacts of the selected combination of values. It can be observed that the authors considered more environmental indicators than economic and social ones. Besides, the framework continues to resemble the traditional LCSA application, allowing the comparison of several alternatives from manual changes in the system.

9.17.1.1 BIM-LCSA integration

Considering the specific application of LCA, thus assessing only environmental aspects, the integration with BIM has gained substantial traction in the literature. Different 'LCA Profiles' have emerged, establishing associations between LCA processes and construction materials or components, often represented as BIM objects [20]. BIM's role in this context is linked to an information aggregator and context provider, offering a rich dataset to support the LCA analysis. Therefore, LCA tools and plug-ins are pivotal in connecting the information sourced from BIM with the corresponding LCA processes within the databases [21]. Still, while promising, recent studies have shown that this integration has sometimes led to inaccurate results within the current designers' workflow [6,7]. This conclusion underscores the critical need for analysis tools that seamlessly align with the dynamic nature of a building project.

In turn, it is observed that the application intended to improve the LCSA methodology via BIM integration is still briefly addressed in the literature. For example, Boje et al. [20] discussed how BIM-based DT data can affect LCSA outcomes. However, the case study presented to validate the proposed framework was related to a simplified version of this integration with limited scope, argumentation, and data. Notably, the case study was focused on demonstrating the complementary roles between BIM and DT, being limited in scope to Environmental LCA.

9.17.2 Digital Twins in Construction

Unlike BIM, which focuses on centralizing data and information and is typically used as a single digital shadow [22], a building DT can provide timely optimization suggestions by mirroring the building's lifecycle and current status [23]. In this context, DTs of constructed assets can present different complexity levels from design to handover, depending on the availability of data and the model's sophistication [24].

A recent review paper [25] has highlighted that most methods for creating DTs are only effective for specific purposes and may not be suitable for other types of projects. Additionally, many of these applications begin by generating a 3D BIM model and then incorporating non-geometric information from sensors or devices in the physical world into the digital model. This additional data can include various parameters such as temperature, humidity, pressure, vibration frequency, flow rate, cost, energy consumption, and more. This data insertion guarantees the transformation of the model into a BIM-based DT representation.

For example, a recent publication presents a case study of a university building using IoT sensors integrated with the virtual BIM model with a focus on environmental aspects [26]. Throughout the process, the effectiveness and challenges of the proposed framework architecture were analyzed. However, to avoid difficulties in rendering the model for web-based viewers, the authors decided to reduce the size of the BIM model created using Autodesk Revit to 20 MB from over 500 MB. To achieve this, they performed BIM lightweight and removed all irrelevant elements of the building, such as members, floors, and redundant data. They retained only the spatial information necessary for environmental monitoring and manually deleted all unnecessary elements per the system requirements. Therefore, this DT model is not suitable for other types of analysis.

In turn, the literature shows that using virtual models as a platform for continuously tracking building components during the operation and maintenance phases is underutilized despite building monitoring and control opportunities. Previous methods for integrating virtual models and physical construction have primarily focused on resource and activity monitoring during the construction stage, as well as documentation of the as-built [27].

9.17.3 Blockchain in Construction

In the ever-evolving domain of data analysis and machine learning, the integrity and trustworthiness of data are fundamental. Traditional methods of securing data typically rely on centralized systems, which are susceptible to single points of failure and malicious alterations. Blockchain technology offers a solution to these challenges by providing a decentralized and immutable ledger system [28].

The advantages of using blockchain for this purpose are multifold. It provides immutability, ensuring that once the data is stored, it cannot be altered, which is crucial for maintaining records that may be subject to future scrutiny or auditing [29]. The decentralized nature of blockchain means that it does not rely on a central point of trust, making the data integrity mechanism robust against failures. Moreover, the transparency and trust provided by blockchain mean that all participants can verify the data independently, fostering a trustful environment [30].

When considering blockchain utilization in the construction sector, this technology is encouraged in all stages of the building life cycle. For example, professionals traditionally raised concerns about the absence of systematic records of inspection and operations during the fabrication stage [31]. Utilizing a digital fabrication drawing production with the synchronization of data records will enable higher transparency and better collaboration opportunities. Besides, using information from the factory, it is possible to develop a digital fabrication model in real-time, improving the digital building model and facilitating LCSA applications [5]. Ultimately, Blockchain can establish more efficient connections among different professionals and provide innovative solutions for the challenges faced by external stakeholders through a dynamic perspective on value creation [32].

9.18 METHODOLOGY

The methodology applied in this work is the Design Science Research (DSR) [33], structured according to Peffers et al. [34]. The methodology encompasses the following key phases: (1) problem identification and motivation, (2) definition of solution objectives, (3) artifact design and development, (4) demonstration, (5) evaluation, and (6) communication.

In previous attempts at implementing life cycle techniques in building projects, the authors encountered several limitations [2,21,35–37]. These challenges prompted a re-evaluation of the approach, leading to the exploration of innovative solutions in the literature and the market. The scrutiny revealed inherent complexities related to data management, methodological standardization, and an overreliance on static data. Importantly, it became apparent that a paradigm shift was needed to overcome these challenges and enhance the accuracy and reliability of sustainability assessments.

Furthermore, the significance of privacy and security concerns emerged, especially when dealing with real-time data collected from buildings. This concern gained prominence during attempts at LCSA applications where limitations were encountered. The privacy of occupants and the need for secure data management became central issues that conventional approaches struggled to address effectively.

In this vein, the integration of DT technology for real-time data collection and visualization, coupled with blockchain to ensure user privacy, emerged as a viable option. On the one hand, DT technology, evolving from the BIM methodology, was introduced as a dynamic solution capable of providing real-time data and a comprehensive representation of the building throughout its lifecycle. This evolution addresses limitations from previous LCSA attempts and introduces a more robust approach to building data representation. On the other hand, blockchain, known for its capabilities in ensuring data security, integrity, and transparent collaboration, emerged as a vital component in guaranteeing the confidentiality of sensitive information gathered from building occupants.

This conceptual atomization of the problem underscores the intricate challenges faced in sustainability assessments, each component representing a critical aspect that the integrated approach seeks to address. Therefore, a rigorous literature review was conducted to systematically address these challenges. This review focused on applying LCSA, DT, and blockchain concepts in the construction industry. The objective was to gain insights into the existing landscape, identify potential synergies, and understand the feasibility of integrating these concepts to enhance sustainability assessments in the construction domain. This research aims to contribute to a more robust and effective sustainability assessment framework in the construction industry by recognizing the interplay of challenges, solutions, and the need for an integrated approach.

Based on this, the identified problems in sustainability assessments in the construction industry necessitate a well-defined set of objectives for the proposed solution. The objectives of this study are twofold:

Objective 1: Enhance the precision, comprehensiveness, and reliability of sustainability assessments, focusing on addressing the dynamic aspects of building impacts and advancing the understanding of sustainability over time.

Objective 2: Address privacy and security concerns in real-time data collection in buildings.

Then, the artifact design and development step involves designing an integration process to be implemented in building projects. This solution will be demonstrated and validated through a real-world case study application. The subsequent steps involve evaluating challenges in implementing the proposed integrative framework, defining future exploratory directions, and addressing the research question posed. A visual representation of the methodology is presented in **Figure 10.1**.

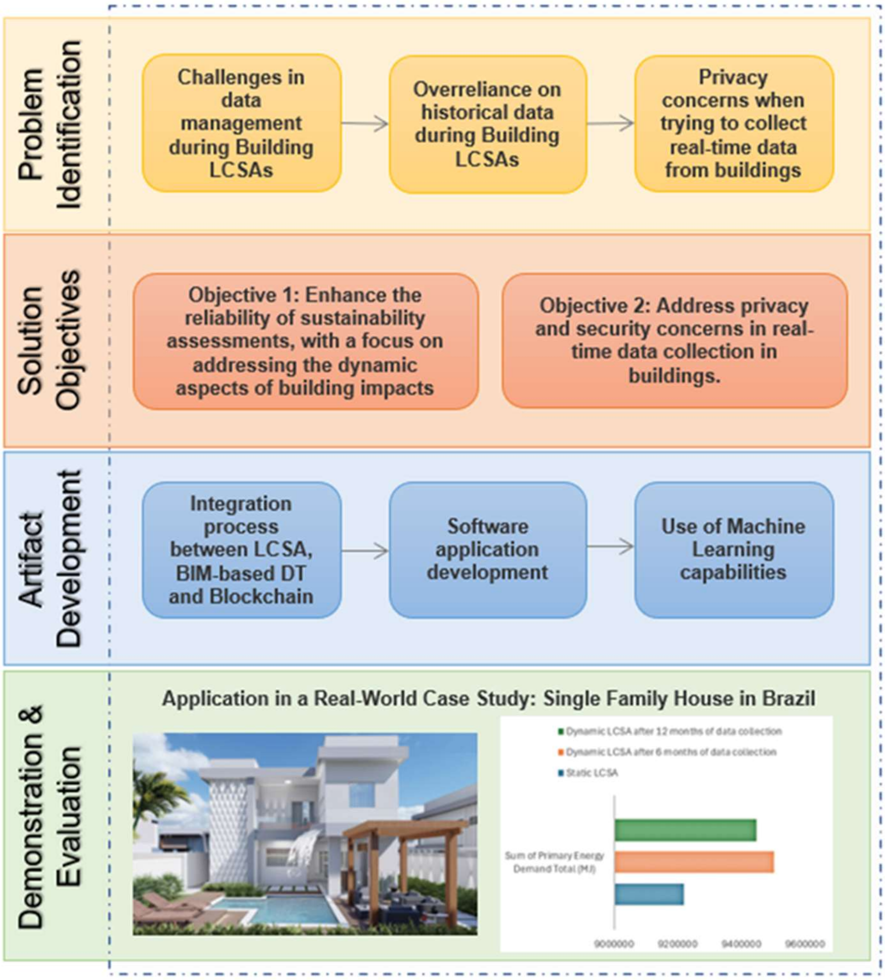

Figure 9.16 - Methodology proposed for this study

9.19 INTEGRATED FRAMEWORK

This section introduces the development of an integrated framework based on what has been discussed so far. In this study, a machine learning-based approach was developed to predict and analyze real-time energy consumption within the context of LCSA. The selection of the *RandomForestRegressor* was driven by its robustness in handling complex datasets and its ability to evolve predictions over time through an interactive user interface. The primary aim is to accurately predict unknown energy consumption values, indicated as -1 in the dataset, and to refine these predictions over time through a real-time user interface.

9.19.1 Data Collection and Preprocessing

The core of the software development lies in the collection and preprocessing of a dataset, denoted as $D = \{(x_1, y_1), (x_2, y_2), \ldots, (x_n, y_n)\}$, comprising n samples. This dataset encapsulates critical variables such as Temperature (T), Season (S), Occupants Ratio (O), Room Size (R), and Power Cost (Co) that are carefully chosen for their potential impact on energy consumption, energy cost and thermal comfort of occupants, which serves as the key impact categories in LCSA. The target variable, y, in our analysis, represents the Total Energy Consumption C. Knowing that, the target variables are get from dataset D, then it is extracted the feature matrix X and the target vector y. Also, the Energy Cost is calculated and stored in the model, considering the power distribution company's cost rating related to the period when the data was gathered.

The dataset is then divided into training and test sets, with the training set comprising $(1 - test\_size) \times n$ samples and the test set comprising $test\_size \times n$ samples. This split was important for validating the model's performance on unseen data. Finally, the RandomForestRegressor model was trained on the subset of the dataset with known energy consumption values from in-loco gathering data. The training process involved optimizing a set of hyperparameters $\theta = \{\theta_1, \theta_2, \ldots, \theta_k\}$, including 'n_estimators', 'max_depth', and 'min_samples_split'. The optimal hyperparameters θ^* were identified using 5-fold cross-validation, which facilitated the fine-tuning of the model to minimize loss.

A distinctive feature of this methodology is the incorporation of an interactive interface. This interface enables the system to update specific records of energy consumption collected from Internet of Things (IoT) sensors and devices, thereby enhancing the model's adaptability and accuracy over time, reaching a smart model. The algorithm dynamically incorporates IoT inputs into the model, re-predicting energy consumption values for records previously marked as unknown.

9.19.2 Digital Twin-Driven Model Evaluation

Post-training, the model's performance is rigorously evaluated using metrics such as Mean Squared Error (MSE), Root Mean Squared Error (RMSE), and Mean Absolute Error (MAE). These metrics not only assess the accuracy of the model but also provide essential insights into its error margins, critical for the reliability of energy consumption predictions.

Visualization techniques, encompassing scatter plots, feature importance charts, pair plots, and heatmaps, contribute to a holistic understanding of the model and the intricate relationships between diverse features. Notably, the data fueling these evaluations originates directly from strategically positioned IoT sensors within the physical building. These sensors seamlessly interface with a 3D building model, forming a robust DT. This integration ensures real-time representation and dynamic adaptation to the building's evolving conditions.

In this context, the developed algorithm represents a groundbreaking fusion of automated machine learning predictions with adaptability driven by data generated from IoT sensors. This integration not only serves as a cutting-edge tool for predicting energy consumption but also stands as an integral component within a broader LCSA framework. The building DT, through its dynamic connection with real-world data, reinforces the model's practicality and contributes significantly to the comprehensive evaluation of sustainability in building projects.

9.19.3 Blockchain-Ensured Data Integrity

Within the Python script developed for predicting energy consumption, blockchain technology is seamlessly integrated to fortify the integrity of the gathered data. The process involves creating a cryptographic hash of the file's contents, essentially forming a compact digital fingerprint. A Python library, PyChain, is utilized to simulate blockchain behavior, although the recommendation stands for considering a more advanced network. PyChain facilitates the creation of a new block containing the file's hash, appending it to the existing chain and securely linking it to the preceding one. This interconnection guarantees that any attempt to manipulate the data becomes readily detectable, as it necessitates altering the entire chain.

Integrating blockchain technology to protect the output of a machine learning model represents an innovative approach to ensuring data integrity. In this implementation, blockchain serves as a robust tool to create an immutable record of energy consumption and energy costs, enhancing the reliability and trustworthiness of the analysis. As the technology matures and becomes more accessible, the role of blockchain in securing and verifying data will likely expand, offering a new standard for data integrity.

In the context of integrating this idea with a building DT, it is important to highlight that the data collected pertains to the daily energy use of occupants, accounting for their presence or absence from home. This level of granularity is crucial for accurate predictions. Here, blockchain plays a pivotal role in guaranteeing the privacy of occupants. Blockchain safeguards sensitive information related to occupants' daily routines, usage patterns, and home occupancy times by ensuring an immutable data record. As the technology matures, blockchain's significance in securing and verifying data, particularly in scenarios involving personal privacy, is poised to become a cornerstone in data analytics and machine learning applications.

9.19.4 Pseudocode for the Integrated Framework

Figure 10.2 presents the pseudocode outlining the integrated framework for predicting real-time energy consumption, leveraging DT, and ensuring data integrity through blockchain technology. This pseudocode emphasizes key steps, including data preprocessing, model training, real-time adaptability through an interactive interface, evaluation, visualization, DT integration, and blockchain-enabled data integrity and privacy assurance.

Algorithm 1 Pseudocode for Energy Consumption Prediction

```
BEGIN
IMPORT libraries (sklearn, seaborn, hashlib, pychain)
Initialize PyChain ledger as blockchain
procedure DisplayDataFrame(df)
    Create a table from dataframe
end procedure
procedure CreateHash(data)
    Create a SHA-256 hash of the data
    return the hash
end procedure
procedure RecordToBlockchain(data_hash)
    Add the hash to the blockchain as a new block
end procedure
procedure PredictEnergyConsumption(df, model)
    Select rows where EnergyConsumption is -1 for prediction
    if rows exist then
        Predict energy consumption
        Round and update the predictions in the dataframe
        Recalculate and update EnergyCost
    end if
    return updated dataframe
end procedure
procedure Analyze(df, initial)
    Split data into known and unknown energy consumption
    Prepare training and test sets
    Configure and perform GridSearchCV with RandomForestRegressor
    if initial then
        return best estimator
    else
        Calculate Mean Squared Error
        Visualize predictions and data analysis
    end if
end procedure
procedure LoadAndAnalyze
    Load data from 'input.csv'
    Calculate initial EnergyCost
    Copy dataframe for predictions
    Get best model from ANALYZE
    Predict energy consumption and save to 'output.csv'
    Hash and record the contents of 'output.csv' to blockchain
    while unknown EnergyConsumption exists do
        Interactive update and analysis process
    end while
end procedure
MAIN
LoadAndAnalyze
END
```

Figure 9.17 - Pseudocode of the software application proposed in this study

9.20 CASE STUDY

A case study is examined to validate the practicality and efficacy of the proposed software application. The whole process was developed on the Microsoft Windows 11 operating system, using an Intel core i7 processor at 2.3 GHz and 32GB of RAM. It was considered an actual single-family house of typical architecture in the southeast region of Brazil to present a discussion representative of the Brazilian construction industry. The analyzed construction features a two-story design, with a ground floor and an upper floor, with a total built area of 230m². The project was developed in April 2020, and the baseline 3D model was modeled in Autodesk Revit 2021. The construction stage lasted from May 2020 to August 2021, situated in Campos dos Goytacazes - RJ, Brazil, 21°45'02.2" S 41°21'31.4" W. **Figure 10.3** displays some orthographic views of this project, along with a rendered image and the 3D model in Revit. The model was developed based on the Level of Development (LOD) 400, using graphical representation of components, with detailed information on fabrication, assembly and installation.

During the later design stage, a static LCSA was performed using the 3D BIM model, considering a building service life of 60 years. The analysis employed a cradle-to-grave system boundary, encompassing product manufacturing, transportation, construction, operation and maintenance (O&M), and end-of-life phases. For the end-of-life phase, assumed to involve implosion, the analysis factored in material collection and landfilling rates. This consistent system boundary was applied across environmental, economic, and social analyses for effective harmonization.

Figure 9.18 - The case study used in this study

The environmental impact categories chosen for this study are widely discussed in the literature and are related to building energy consumption. This consumption is divided into Primary Energy Demand (PED), Non-renewable Energy Demand (NED), and Renewable Energy Demand (RED). For the economic analysis, the impact category is the life-cycle cost associated with the energy usage for lighting and HVAC, considering all building phases within the system boundary of this study. Finally, the social analysis focuses on Indoor Air Quality (IAQ) as a crucial dimension of occupant well-being and satisfaction. A comprehensive checklist was developed to assess various factors influencing IAQ during the building's life cycle. This checklist encompasses ventilation systems, natural ventilation, material choices, maintenance practices, air filtration, humidity control, and compliance with standards.

This assessment, based on the static BIM model, provided insights into the environmental, economic, and social dimensions associated with the building life cycle. Having established the baseline with the static LCSA and after constructing this house, the Revit model was upgraded to Revit 2024, a more contemporary software version. This update was accompanied by a meticulous data integration and extraction process using Dynamo, a visual programming language recognized for its versatility and efficiency in architectural and construction contexts. The 3D model was augmented with additional as-built data to transform it into a comprehensive DT of the house. This integration and extraction were essential for ensuring the continued relevance and accuracy of the digital representation of the structure, enabling extensive analysis and assessment within the scope of the study.

The installation of sensors in the house was carried out with the owner's explicit consent. The sensors were installed to monitor various aspects of the house's environment, including temperature, humidity, and air quality, among others. However, it was made clear that the privacy of the occupant data must be fully guaranteed. This means that any data collected will be treated with the utmost confidentiality and will not be shared with any third party without the explicit consent of the occupant. Additionally, measures have been put in place to ensure that the data collected is only used for the intended purpose and is not misused in any way.

Leveraging this real-time data, the developed software played a pivotal role in estimating energy consumption, energy cost, and IAQ. The integration of machine learning algorithms, including the *RandomForestRegressor*, allowed for accurate predictions and adaptability based on the dynamic input from the installed IoT sensors. The Random Forest algorithm is a versatile machine learning model employed in our work to enhance the accuracy of predictions. Its significance comes from its collective method, which utilizes multiple decision trees to make predictions based on various subsets of the dataset, ensuring robustness against overfitting and improving prediction reliability.

In our framework, *RandomForestRegressor* is instrumental for interpreting the real-time data collected from IoT sensors, enabling the framework to adapt its predictions dynamically as new data is received. This continuous learning aspect is crucial for maintaining the precision of sustainability assessments and facilitating intelligent decision-making in the management of building systems. By leveraging the Random Forest model, we ensure that our framework remains sensitive to the evolving patterns and trends in the data, supporting a sustainable and responsive building environment and enhancing the ongoing dynamic method proposed.

This relationship between real-time data from the sensors and the framework's predictive capabilities not only facilitated precise estimations but also contributed to the overall dynamic adaptability and responsiveness of the model. Ultimately, using blockchain ensures occupant privacy as agreed with the owner. In this way, the proposed application can be utilized to maximize the utility of the collected data for improving the sustainability assessment framework within the broader context of the DT, blockchain, and LCSA integration.

9.21 RESULTS AND DISCUSSION

This section first presents the findings from the static LCSA based on a 3D BIM. It is followed by an analysis of the dynamic LCSA outcomes derived from the evolved DT, which provides insights into the transformative potential of real-time data integration from IoT sensors. A comparative analysis then illustrates the discrepancies and enhancements between the static and dynamic approaches. Finally, a discussion is presented about the roles of BIM-based DT and blockchain in fostering a dynamic and comprehensive LCSA, answering the research question posed in the Introduction section.

9.21.1 Static LCSA Findings

In order to carry out the static LCSA, an energy model was created using Autodesk Revit, which was derived from the house's 3D BIM model. This model, structured according to the Green Building XML schema (gbXML), encompasses the primary heat transfer pathways within the building. The gbXML schema is specifically designed to streamline the transfer of building data from BIM platforms to environmental analysis tools [2]. Utilizing this model, the annual energy consumption of the building was estimated, considering the energy used by both HVAC and lighting systems.

This work adopted the TRACI 2.1 characterization scheme to classify and understand environmental impacts. The TRACI methodology characterizes impact categories at the midpoint level by drawing cause-effect chains to identify the point at which each category is characterized [38]. In this study, the Tally® application was used to match each material in the 3D BIM model in Autodesk Revit with the GaBi database materials, allowing for an automated exchange process [39]. Besides, the estimated annual energy use calculated through the energy model was added to the Tally® application to consider this data in the environmental impact calculations.

The reference unit used in this study was the full collection of processes and materials required to construct a single-family house, which is quantified according to the given goal and scope of the assessment over the entire life of the building. For example, Figure 4 presents data obtained from Tally to analyze material mass and non-renewable energy demand across each life cycle stage. The total energy calculation encompasses all stages of the design options studied, including material manufacturing, transportation, maintenance, replacement, and eventual end-of-life considerations.

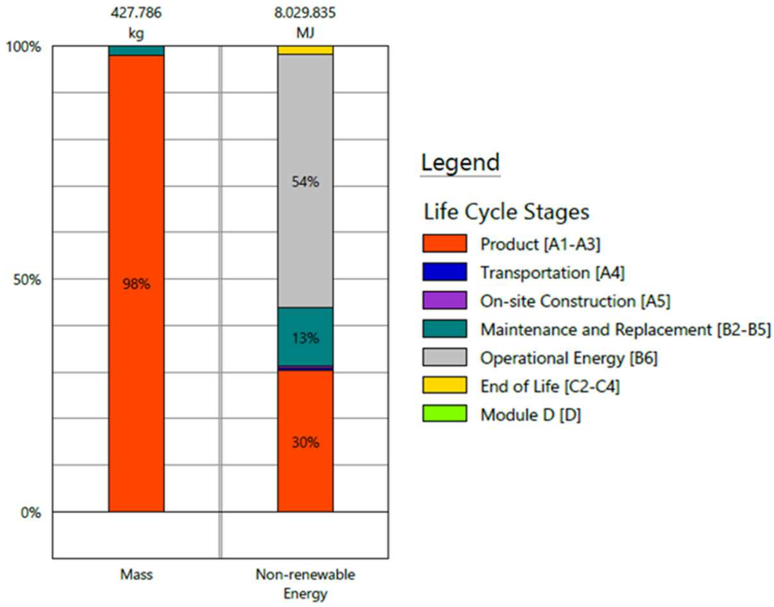

Figure 9.19 - Static data obtained during the design stage of the case study

9.21.2 Dynamic LCSA Outcomes

The dynamic LCSA, facilitated by advanced machine learning techniques integrating DT and blockchain technologies, revealed a significant shift in the building's energy consumption profile. The real-time data, sourced from IoT sensors installed in the house, provided insights into the actual energy usage, diverging from the initial predictions of the static LCSA. This dynamic approach offered an accurate reflection of the building's energy consumption, accounting for variables like occupant behavior, environmental conditions, and material performance over time.

The integration of the *RandomForestRegressor* algorithm within the software application played a critical role in dynamically predicting and adjusting the energy consumption values. The software's ability to iteratively learn and adapt to real-time data led to a more nuanced understanding of the building's energy dynamics, surpassing the static LCSA's capabilities. **Figure 10.5** presents a pair plot, a graphical matrix that illustrates the relationship between multiple variables in the dataset.

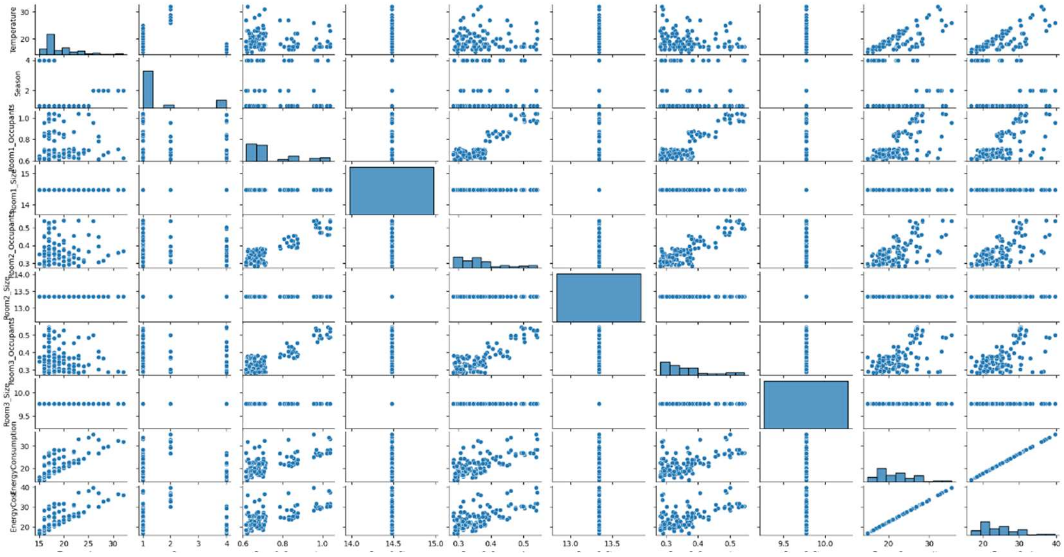

Figure 9.20 - Pair plot of building energy consumption dynamic data

On the diagonal, histograms reveal the distribution of each individual variable, providing insight into their individual characteristics, being the spread and central tendency. Off-diagonal scatter plots compare the interactions between pairs of variables, which in this case study, highlight the trends and potential outliers, which are the constant variables (Room Size). These visual relationships are crucial for identifying how variables influence each other and were essential to step in exploratory data analysis. The box plots adjacent to the histograms offer a view of each variable's distribution, median, and outliers. For this study, the occupancy ratio and temperature showed a strong correlation with the proposed model.

9.21.3 Comparative Analysis

The comparative analysis reveals fluctuations in the environmental impacts across different stages of the building's life cycle. Notably, the static LCSA performed during the design stage offers a baseline understanding of energy demands. However, as seen in the dynamic LCSAs conducted after 6 and 12 months, variations emerge due to real-time adaptations and changes in occupant behavior and energy consumption patterns.

The developed algorithm, utilizing automated machine learning predictions with IoT-driven adaptability, stands as a novel and flexible tool. Importantly, it is a foundational component in the broader LCSA framework, enriching the dynamic and comprehensive assessment of sustainability in building projects. In this context, the primary objective here was to rigorously compare the findings of the static LCSA based on the initial 3D BIM model with the outcomes of the dynamic LCSA utilizing the augmented DT.

As shown in **Figure 10.6**, the increments in all three types of Energy Demand suggest that the building undergoes alterations that impact its energy efficiency over time. This reinforces the significance of dynamic assessments, as they consider evolving conditions, ensuring a more accurate representation of the building's sustainability profile. Moreover, it is crucial to recognize that these disparities will likely amplify over time. The dynamic LCSA approach, facilitated by the BIM-based DT, allows for continuous updates based on the building's actual performance and usage patterns. This ongoing adaptability becomes increasingly pertinent as unforeseen alterations occur throughout the building's life cycle, which was not accounted for during the initial design stage.

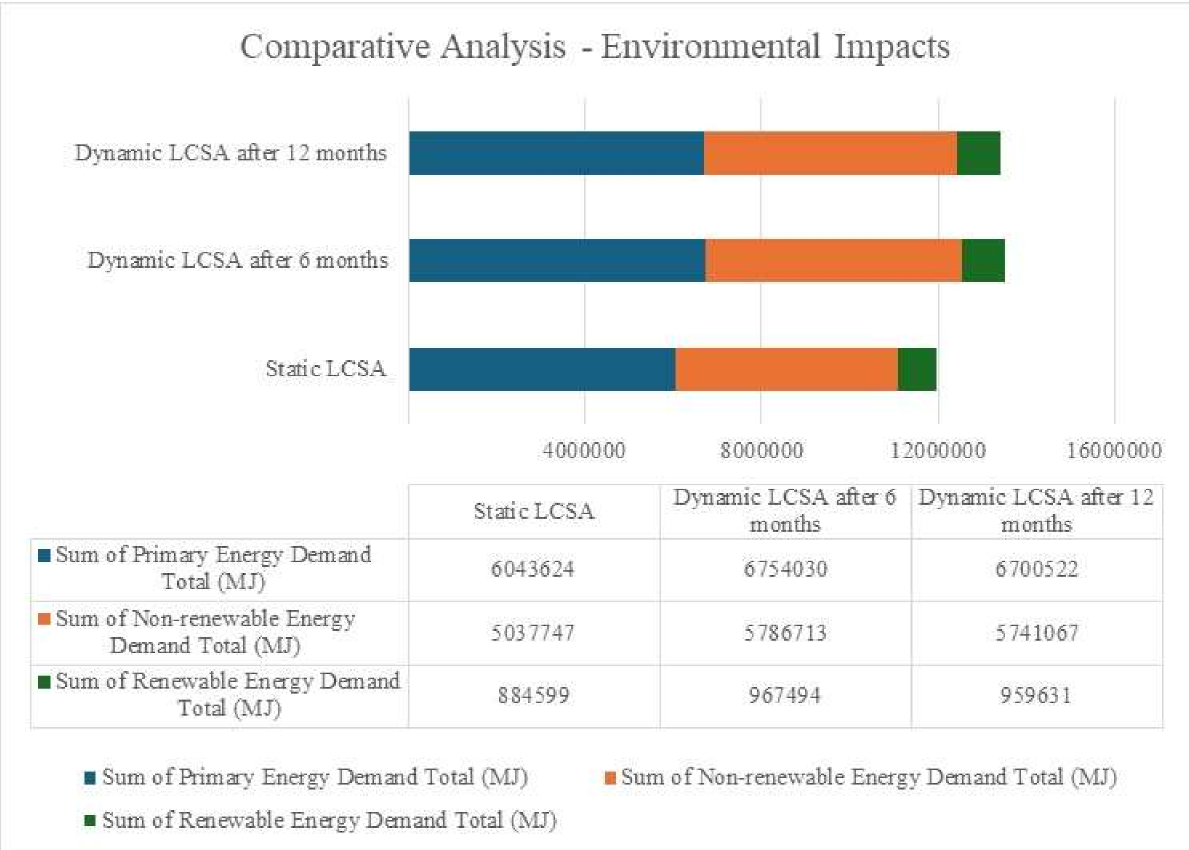

Figure 9.21 - Comparative Analysis between Static and Dynamic LCSAs

Ultimately, the software's ability to perform dynamic LCSAs not only captures the present state of sustainability impacts but also positions itself as a valuable tool for predicting and managing future sustainability considerations. As the building evolves, the software can continue to provide insights, offering a proactive approach to sustainable construction practices.

This aligns seamlessly with the primary goal of this study – to enhance the comprehensiveness and accuracy of sustainability assessments throughout the entire life cycle of buildings.

Although our discussion primarily focuses on environmental aspects, it is imperative to acknowledge the potential for incorporating economic and social factors within the same framework. While real-time data collection over 12 months allows for robust environmental analysis, observing tangible changes in economic and social factors may take longer. However, the inherent adaptability of this dynamic LCSA approach, facilitated by the BIM-based DT and blockchain, provides a foundation for incorporating economic and social considerations in future decision-making processes.

As the building's lifecycle progresses, ongoing updates based on actual performance and usage patterns enable stakeholders to monitor economic indicators, such as operational costs and return on investment, as well as social factors, including occupant satisfaction. Recognizing that these disparities are likely to amplify over time underscores the importance of adopting a holistic approach that considers the interconnectedness of environmental, economic, and social dimensions in sustainability assessments.

9.21.4 Insights on the Integration of DT and Blockchain into the LCSA framework

Applying LCSA in the construction industry is not without its obstacles, both in research and practice; managing a vast amount of data is necessary when considering all functional and technical requirements of a built asset throughout its life cycle [2]. In this vein, the integration of BIM-based DT and blockchain technologies within the LCSA framework signifies a paradigm shift in sustainable construction practices.

Particularly, a critical aspect of our study involves the data's origin from IoT sensors, intricately connected to a 3D building model as a building DT. This ensures that predictions are firmly rooted in real-time conditions. By anchoring LCSA in real-world data, the framework contributes to the dynamic and comprehensive evaluation of sustainability in building projects, furthering the objectives of this research. Besides, the software's focus on energy consumption, a pivotal impact category spanning environmental, economic, and social dimensions, contributes to the dynamic and comprehensive evaluation of sustainability in building projects. It is understood that, over time, the DT implementation will become even more vital, accommodating unforeseen changes throughout the building's life cycle that were not considered in the static LCSA during the design stage.

The developed algorithm, combining automated machine learning predictions with IoT-driven adaptability, represents a novel and flexible tool for predicting energy consumption. Importantly, this tool serves as a foundational component in the broader LCSA scheme, contributing to the dynamic and comprehensive assessment of sustainability in building projects. By focusing on energy consumption as a critical impact category, the software ensures that LCSA encompasses environmental, economic, and social dimensions, thus addressing the research question posed in this paper.

Ultimately, the integration of blockchain technology addresses critical aspects of data security, integrity, and transparent collaboration within the LCSA framework. Blockchain's immutability safeguards the integrity of the data collected from IoT sensors, ensuring that predictions and assessments are transmitted as trustworthy information. While blockchain introduces performance and scalability considerations, its role in securing and verifying real-time data, especially concerning privacy-sensitive information, is crucial. As blockchain technology matures, its potential to become a cornerstone in data analytics and machine learning applications, particularly in scenarios involving personal privacy, is evident.

9.22 CONCLUSION

This study aimed to address the challenges that hinder sustainability assessments in the construction industry. These challenges include the lack of standardized approaches, reliance on static data, and the significant amount of data required for life cycle assessments. Particularly, the use of static data can lead to a lack of consideration for changes over time, which can impact the reliability of LCSA findings. Therefore, this paper elaborated on integrating key concepts, namely DT and blockchain, to address the challenges the construction industry faces in embracing sustainability comprehensively.

Based on the Design Science Research methodology, the exploration proposed culminated in developing an advanced software application tailored for application in diverse building projects. This is a machine learning-based software application that integrates BIM-based DT and blockchain technology into the LCSA framework. LCSA provides a holistic evaluation of the environmental, economic, and social dimensions of buildings. The BIM-based DT model provides a real-time digital representation of the physical building throughout its life cycle. Finally, blockchain addresses critical aspects of data security, integrity, and user privacy, a cornerstone in sustainable construction practices. This integration aims to create a dynamic, real-time, and secure framework for sustainability assessments across the entire life cycle of buildings.

In turn, the comparative analysis between static and dynamic LCSAs conducted in this study aimed to showcase the transformative potential of the integrated technologies. By transitioning from a static to a dynamic approach, the research illustrated improvements, discrepancies, and nuanced insights gained. The outcomes of this comparative study contribute essential knowledge to sustainable construction practices, underscoring the effectiveness of the proposed framework in enhancing the comprehensiveness and accuracy of sustainability assessments in building projects.

Demonstrated through a real-world case study on a typical Brazilian structure, this integration represents a great effort to provide practical solutions to the challenges faced in construction sustainability. Notably, the sum of non-renewable and renewable energy demand increased by 20.37% and 19.70%, respectively, from the static LCSA to the dynamic LCSA calculated after 12 months of real-time data collection. These outcomes underscore the effectiveness of the proposed framework in enhancing the comprehensiveness and accuracy of sustainability assessments in building projects.

While acknowledging the promising results of integrating DT and blockchain to achieve a dynamic LCSA process, a number of limitations remain to be addressed. The specificity of the case study, while providing valuable insights and validating the proposed framework, necessitates caution in extrapolating the results universally. Future research should focus on diversifying case studies to fortify the robustness and applicability of the integrated approach across varied construction projects. This acknowledgment emphasizes the need for continuous exploration and refinement in pursuing sustainable construction practices.

Besides, while blockchain enhances data integrity, considerations must be acknowledged. Blockchain can introduce performance and scalability issues, primarily when implemented on a large scale. The added layer of complexity means that developers and users must understand how to interact with and maintain the blockchain. Additionally, as a relatively new technology, it may not always be the best solution and should be applied carefully, considering the specific use cases and requirements. Therefore, through rigorous exploration and analysis, future research aims to illuminate the transformative potential of these integrated technologies and their collective impact on sustainability practices in the construction sector.

9.23 REFERENCES

[1] H. Hummels, A. Argyrou, Planetary demands: Redefining sustainable development and sustainable entrepreneurship, J Clean Prod 278 (2021) 123804. https://doi.org/10.1016/J.JCLEPRO.2020.123804.

[2] K. Figueiredo, R. Pierott, A.W.A. Hammad, A. Haddad, Sustainable material choice for construction projects: A Life Cycle Sustainability Assessment framework based on BIM and Fuzzy-AHP, Build Environ 196 (2021) 107805. https://doi.org/10.1016/J.BUILDENV.2021.107805.

[3] H. Amini Toosi, M. Lavagna, F. Leonforte, C. Del Pero, N. Aste, A novel LCSA-Machine learning based optimization model for sustainable building design-A case study of energy storage systems, Build Environ 209 (2022) 108656. https://doi.org/10.1016/J.BUILDENV.2021.108656.

[4] C. Llatas, B. Soust-Verdaguer, A. Passer, Implementing Life Cycle Sustainability Assessment during design stages in Building Information Modelling: From systematic literature review to a methodological approach, Build Environ 182 (2020). https://doi.org/10.1016/j.buildenv.2020.107164.

[5] K. Figueiredo, A.W.A. Hammad, A. Haddad, Improving Sustainability in the Built Environment through a BIM-based Integration of Digital Twin and Blockchain, Cognitive Digital Twins for Smart Lifecycle Management of Built Environment and Infrastructure (2023) 101–122. https://doi.org/10.1201/9781003230199-6.

[6] A. Hollberg, G. Genova, G. Habert, Evaluation of BIM-based LCA results for building design, Autom Constr 109 (2020). https://doi.org/10.1016/j.autcon.2019.102972.

[7] B. Soust-Verdaguer, C. Llatas, A. García-Martínez, Critical review of bim-based LCA method to buildings, Energy Build 136 (2017) 110–120. https://doi.org/10.1016/j.enbuild.2016.12.009.

[8] K. Safari, H. AzariJafari, Challenges and opportunities for integrating BIM and LCA: Methodological choices and framework development, Sustain Cities Soc 67 (2021) 102728. https://doi.org/10.1016/J.SCS.2021.102728.

[9] M. Najjar, K. Figueiredo, M. Palumbo, A. Haddad, Integration of BIM and LCA: Evaluating the environmental impacts of building materials at an early stage of designing a typical office building, Journal of Building Engineering 14 (2017). https://doi.org/10.1016/j.jobe.2017.10.005.

[10] V.WY. Tam, Y. Zhou, C. Illankoon, K.N. Le, A critical review on BIM and LCA integration using the ISO 14040 framework, Build Environ 213 (2022) 108865. https://doi.org/10.1016/J.BUILDENV.2022.108865.

[11] P. De Wilde, The gap between predicted and measured energy performance of buildings: A framework for investigation, Autom Constr 41 (2014) 40–49. https://doi.org/10.1016/J.AUTCON.2014.02.009.

[12] D. Calì, T. Osterhage, R. Streblow, D. Müller, Energy performance gap in refurbished German dwellings: Lesson learned from a field test, Energy Build 127 (2016) 1146–1158. https://doi.org/10.1016/J.ENBUILD.2016.05.020.

[13] N.C. Onat, M. Kucukvar, A. Halog, S. Cloutier, Systems thinking for life cycle sustainability assessment: A review of recent developments, applications, and future perspectives, Sustainability 9 (2017) 1–25. https://doi.org/10.3390/su9050706.

[14] ISO, ISO 14040:2006 - Environmental management — Life cycle assessment — Principles and framework, 2006.

[15] B. Soust-Verdaguer, J.A. Gutiérrez Moreno, C. Llatas, Utilization of an Automatic Tool for Building Material Selection by Integrating Life Cycle Sustainability Assessment in the Early Design Stages in BIM, Sustainability 2023, Vol. 15, Page 2274 15 (2023) 2274. https://doi.org/10.3390/SU15032274.

[16] C. LLatas, B. Soust-Verdaguer, A. Hollberg, E. Palumbo, R. Quiñones, BIM-based LCSA application in early design stages using IFC, Autom Constr 138 (2022) 104259. https://doi.org/10.1016/J.AUTCON.2022.104259.

[17] Y. Pigné, T.N. Gutiérrez, T. Gibon, T. Schaubroeck, E. Popovici, A.H. Shimako, E. Benetto, L. Tiruta-Barna, A tool to operationalize dynamic LCA, including time differentiation on the complete background database, International Journal of Life Cycle Assessment 25 (2020) 267–279. https://doi.org/10.1007/s11367-019-01696-6.

[18] A. Francis, A. Thomas, A framework for dynamic life cycle sustainability assessment and policy analysis of built environment through a system dynamics approach, Sustain Cities Soc 76 (2022) 103521. https://doi.org/10.1016/J.SCS.2021.103521.

[19] L. Patouillard, P. Collet, P. Lesage, P. Tirado Seco, C. Bulle, M. Margni, Prioritizing regionalization efforts in life cycle assessment through global sensitivity analysis: a sector meta-analysis based on ecoinvent v3, International Journal of Life Cycle Assessment 24 (2019) 2238–2254. https://doi.org/10.1007/S11367-019-01635-5/FIGURES/5.

[20] C. Boje, Á.J. Hahn Menacho, A. Marvuglia, E. Benetto, S. Kubicki, T. Schaubroeck, T. Navarrete Gutiérrez, A framework using BIM and digital twins in facilitating LCSA for

buildings, Journal of Building Engineering 76 (2023) 107232. https://doi.org/10.1016/J.JOBE.2023.107232.

[21] M.V.A.P.M. Filho, B.B.F. da Costa, M. Najjar, K. V. Figueiredo, M.B. de Mendonça, A.N. Haddad, Sustainability Assessment of a Low-Income Building: A BIM-LCSA-FAHP-Based Analysis, Buildings 2022, Vol. 12, Page 181 12 (2022) 181. https://doi.org/10.3390/BUILDINGS12020181.

[22] S.M.E. Sepasgozar, Differentiating Digital Twin from Digital Shadow: Elucidating a Paradigm Shift to Expedite a Smart, Sustainable Built Environment, Buildings 11 (2021) 151. https://doi.org/10.3390/buildings11040151.

[23] Y. Peng, M. Zhang, F. Yu, J. Xu, S. Gao, Digital Twin Hospital Buildings: An Exemplary Case Study through Continuous Lifecycle Integration, Advances in Civil Engineering 2020 (2020). https://doi.org/10.1155/2020/8846667.

[24] H. Seaton, C. Savian, S. Sepasgozar, A. Sawhney, Digital twins from design to handover of constructed assets, London, 2022. https://www.rics.org/pt-br/wbef/home/reports-and-research/digital-twins-from-design-to-handover-of-constructed-assets/ (accessed June 8, 2022).

[25] F. Jiang, L. Ma, T. Broyd, K. Chen, Digital twin and its implementations in the civil engineering sector, Autom Constr 130 (2021) 103838. https://doi.org/10.1016/J.AUTCON.2021.103838.

[26] T.W. Kang, Y. Mo, A comprehensive digital twin framework for building environment monitoring with emphasis on real-time data connectivity and predictability, Developments in the Built Environment 17 (2024) 100309. https://doi.org/10.1016/J.DIBE.2023.100309.

[27] A. Akanmu, C.J. Anumba, Cyber-physical systems integration of building information models and the physical construction, Engineering, Construction and Architectural Management 22 (2015) 516–535. https://doi.org/10.1108/ECAM-07-2014-0097/FULL/PDF.

[28] K. Figueiredo, A.W.A. Hammad, A. Haddad, V.W.Y. Tam, Assessing the usability of blockchain for sustainability: Extending key themes to the construction industry, J Clean Prod 343 (2022) 131047. https://doi.org/10.1016/J.JCLEPRO.2022.131047.

[29] H. Hamledari, M. Fischer, Role of Blockchain-Enabled Smart Contracts in Automating Construction Progress Payments, Journal of Legal Affairs and Dispute Resolution in Engineering and Construction 13 (2021). https://doi.org/10.1061/(asce)la.1943-4170.0000442.

[30] C. Esposito, M. Ficco, B.B. Gupta, Blockchain-based authentication and authorization for smart city applications, Inf Process Manag 58 (2021) 102468. https://doi.org/10.1016/j.ipm.2020.102468.

[31] L. Wu, W. Lu, F. Xue, X. Li, R. Zhao, M. Tang, Linking permissioned blockchain to Internet of Things (IoT)-BIM platform for off-site production management in modular construction, Comput Ind 135 (2022) 103573. https://doi.org/10.1016/J.COMPIND.2021.103573.

[32] Y. Wan, Y. Gao, Y. Hu, Blockchain application and collaborative innovation in the manufacturing industry: Based on the perspective of social trust, Technol Forecast Soc Change 177 (2022) 121540. https://doi.org/10.1016/J.TECHFORE.2022.121540.

[33] J.O. De Sordi, Design Science Research Methodology: Theory Development from Artifacts, Palgrave Macmillan Cham, 2021. https://doi.org/10.1007/978-3-030-82156-2.

[34] K. Peffers, T. Tuunanen, M.A. Rothenberger, S. Chatterjee, A Design Science Research Methodology for Information Systems Research, Journal of Management Information Systems 24 (2014) 45–77. https://doi.org/10.2753/MIS0742-1222240302.

[35] K. Figueiredo, A.W.A. Hammad, A. Haddad, Sustainable Construction Achieved Through Life Cycle Assessment: Methodology, Limitations and the Way Forward, Elsevier Ltd., 2020. https://doi.org/10.1016/b978-0-12-803581-8.11360-8.

[36] M. Najjar, K. Figueiredo, A.W.A. Hammad, A. Haddad, Integrated optimization with building information modeling and life cycle assessment for generating energy efficient buildings, Appl Energy 250 (2019). https://doi.org/10.1016/j.apenergy.2019.05.101.

[37] K. Figueiredo, A.W. Hammad, V.W.Y. Tam, A.C.J. Evangelista, A. Haddad, Sustainable Construction Project Decision-Support tools: Integration of Life Cycle Sustainability Assessment and Multi- Criteria Decision Making, in: P. Rahnamayiezekavat, V. Tam, S. Saha (Eds.), 1st International Conference on International Conference on Construction Project Management and Construction Engineering (ICCPMCE-2018), Sydney, Australia, 2018: pp. 128–133.

[38] J. Bare, D. Young, M. Hopton, TRACI version 2.1 - User's Manual, 2012.

[39] KT Innovations, Tally® Revit Application, (n.d.). https://kierantimberlake.com/page/tally (accessed December 29, 2023).

APPENDIX E – SHEAR STRENGTH OF SAND-LIGHTWEIGHT CONCRETE DEEP BEAMSWITH STEEL FIBERS

This chapter is published as a Paper at ACI Structural Journal.
10.14359/51729347

GARCIA, Sergio; PEREIRA, Alonso; **PIEROTT, Rodrigo**. Shear Strength of Sand-Lightweight Concrete Deep Beams with Steel Fibers. In: **ACI Structural Journal.** No. 118-S40.

Chapter 8 explores the shear strength of sand-lightweight concrete deep beams reinforced with steel fibers. This chapter investigates how this combination can achieve both high strength and reduced weight, making it a promising solution for modern construction challenges that demand both performance and efficiency.

ABSTRACT

Buildings play Six deep beams without transversal reinforcement made of sand-lightweight concrete and six deep beams made of sand-lightweight concrete with 1.0% of steel fibers were tested and compared with conventional concrete deep beams with and without fibers. The shear-span to deep beam height (a/h) was 0.5, 0.8, and 1.0. The cross section heights were 400, 600, and 700 mm (15.7, 23.6, and 27.6 in.). The deep beams were tested to failure under a four-point bending test, using a hydraulic actuator with 500 kN (674 kip) capacity load cell. After testing, it was concluded that the shearstrength values were smaller in larger span deep beams. The presence of steel fibers increased the maximum strength and contributed quantify to the strength to diagonal cracking. The maximum shear load in steel fiber deep beams increased by approximately 16%. The size effect was more significant in sand-lightweight concrete deep beams. Besides, it was proposed a coefficient to validate the cracking strut-and-tie model (CSTM) to evaluate the applicability in deep beams of sand-lightweight concrete with and without steel fibers and the experimental maximum shear predictions are compared according to some codes for sand-lightweight concrete deep beams and by codes and some codes and researchers for sand lightweight concrete deep beams with steel fibers..

Keywords:
Deep Beams, Sand-Lightweight, Shear, Steel Fibers.

9.24 INTRODUCTION

Deep beams are structural elements employed in building fronts, transition beams, and water tank reservoirs, as well as in geotechnical structures, underground containment elements, underground or garage floor curtains, and piling crown blocks in offshore structures.

There are many advantages of using structural lightweight concrete (SLC). The cost of transporting precast elements made of lightweight materials that are less expensive than those made of standard conventional weight materials. Offshore structures also require that the elements be more buoyant and easier to tow. Other good properties of SLC are: cost/effectiveness (good cost and high durability ratio), good compressive and fire resistance, good acoustic and thermal control, among others. However, shear strength along a plane in lightweight concrete is lower than in ordinary concrete structures. This occurs because lightweight aggregates allow cracks to propagate easily through them instead of deviating the cracks around them, as it happens in low strength concretes. In lightweight concretes, cracking is associated with aggregate fragmentation since aggregate strength is comparable to matrix strength and the resulting "smooth-face crack" is less effective in shear stress transmission.1-4 Researches using lightweight concrete deep beams5-7 have concluded that the use of lightweight concrete leads to lower ultimate shear strengths when compared to normal weight concrete (NWC). Yang6 and Yang et al.8 noted that the influence of overall depth (h) on the propagation and distribution of cracks in lightweight concrete deep beams is similar to that of conventional concrete deep beams. Yang6 reported that the ratio of the first diagonal crack strength to the ultimate strength for lightweight concrete deep beams increased slightly with the increase the ratio of shear-span to beam height (a/h) and h, showing that a higher ratio appeared in all-lightweight concrete (ALWC) deep beams than in sand-lightweight concrete (SLWC) deep beams.

To overcome the disadvantages of lightweight concrete, the addition of fibers is an effective alternative solution. There is high stress concentration at the end of a crack, and no stress propagation is observed. When the stress reaches the matrix strength, the concrete ruptures abruptly. By adding fibers to the matrix, the material gains ductility and increases its stiffness. This happens because fibers are used as stress transfer bridges, increasing the element's strength, and avoiding rupture. Several studies9-12 on deep beams reinforced with fibers in NWC have been carried out. It was concluded that fibers' addition increases the maximum strength, and the rupture is more ductile.

Chen et al.13 stated that the rupture mechanism and the deep beam load capacity are governed essentially by shear. Therefore, the size effect becomes inevitable. According to the findings presented in Chen et al.,13 the size effect on deep concrete beams can be explained by the fragility of the material, and the energy release rate in cracked planes. By increasing h, the value of the shear span increases, therefore the energy-releasing zone along the crack length also increases. Also, it has been reported13 that the shear strength of reinforced concrete (RC) beams decreases as the beam depth increases. Conventional concrete deep beams14,15 with and without fiber addition have been analyzed regarding the size effect. Birrcher et al.14 concluded that the maximum diagonal crack width at a given percentage of the maximum applied load tended to increase as the overall depth of the member increased from 584 to 1067 mm (23 to 42 in.), but not from 1067 to 1905 mm (42 to 75 in.), reducing shear strength. Shuraim and El-Sayed15 stated that the shear stresses at failure appeared to decrease with the increase of beam depth indicating size effect. Chen et al.,13 who studied the behavior of SLWC and ALWC deep beams, showed that the size effect in low weight concrete (LWC) deep beams was more significant than in NWC deep beams. Furthermore, the effect of overall section depth on the ultimate shear stress was slightly greater in SLWC deep beams compared to ALWC deep beams.

On the presented subject and with the aim of study the size effect in deep beams with incorporations of fibers, sand-lightweight fiber concrete (SLWFC) deep beams were studied.

Considering the latest research regarding this subject, to add other elements not yet studied, lightweight concrete deep beams with the addition of steel fiber were studied. This paper presents the results of twelve deep beams, six of concrete with lightweight coarse aggregates, and six with lightweight coarse aggregates with insertion of 1% steel fibers. The size effect of these SLWC and SLWFC deep beams are compared with those of conventional concrete and fiber-reinforced conventional concrete deep beams.

9.25 RESEARCH SIGNIFICANCE

Even though lightweight concrete exhibits many advantages, especially weight reduction, it has a more fragile rupture and less shear strength than conventional concrete. The latter is due to the decrease in its aggregate interlocking effect. Therefore, the incorporation of steel fibers in deep beams without transversal reinforcement may increase the shear capacity and reducing fragility when the ultimate capacity is reached. It was also aimed to evaluate the size effect in SLWFC deep beams.

9.26 EXPERIMENTAL INVESTIGATION

9.26.1 Materials

Four batches of concrete were made to cast the beams. The concrete was in a metal formwork capable of shaping up to three deep beams at a time, with flexible molding for size and length. The concrete was compacted in the formwork with the aid of a needle-type immersion vibrator. A Brazilian type V portland cement (high early strength cement16) was used. The consistency of the concrete was obtained by the slump test17 and is equal to 45 mm (0.1 in.) for both concrete types (SLWC and SLWFC). For each concrete, six cylindrical specimens of dimensions 200 x 100 mm (7.8 x 3.9 in.) were produced: three for the compressive strength test18 and three for the diametral tensile strength test,19 and both tested at 28 days.

For the production of the concrete, it was used expanded clay as coarse aggregate, produced (known as expanded clay 1506) and quartz sand as fine aggregate from the RJ. Table 1 presents the properties of the used aggregates. Table 2 shows the composition of the concretes used in this research. Highrange water-reducing admixture was used, and its amount was calculated in relation to cement consumption. Table 3 shows the real specific mass, compressive strength (fcm), and diametral tensile strength (fct,sp) of the tested concretes.

Table 6.1 - Properties of materials.

Aggregate type		Maximum diameter (mm)	Real specific mass (g/m^3)	Fineness module (mm)
Coarse	Expanded clay	15.00	0.60	3.60
Fine	Sand	1.70	2.73	1.03

Table 6.2 - Composition of concretes.

Concrete type	*W/C*	Material consumption (kg/m^3)					
		W	C	LG	S	HRWRA	SF
Sand-lightweight	0.38	199.5	428.9	308.0	571.2	9.4	0
Sand-lightweight with fibers	0.38	199.5	428.9	306.5	559.2	15.0	78.5

Table 6.3 - Properties of SLWC and SLWFC.

Concrete type	Real specific mass (g/m^3)	f_{cm} (MPa)	$f_{ct,sp}$ (MPa)
Sand-lightweight	1720	30.1	2.6
Sand-lightweight with fibers	1880	33.5	4.0

The fibers used to produce the SLWFC were of metallic type with end anchor, with 33 mm (1.3 in.) in length, 0.55 mm (0.02 in.) in diameter, form factor of 60, 7850 kg/m3 of specific mass and 1100 MPa (160 ksi) of tensile strength. The amount of fiber added to concrete was 1.0% in volume, corresponding to 78.5 kg/m3.

After 24 hours of concreting, the deep beams were demoulding and covered with a damp blanket. The cylindrical specimens were submerged into water until the age of 28 days to ensure the concrete curing process.

9.26.2 Details of deep beams

In each group, three deep beams were considered with shear-span to overall height ratio a/h = 0.5—two with a/h = 1.0 and one with a/h = 0.8—and h of 400, 600, and 700 mm (15.7, 23.6, and 27.6 in.) as shown in Table 4.

The beam's nomenclature was divided into three parts. The first one refers to the concrete type: SLCB for sandlightweight concrete beams and SLFCB for sand-lightweight fiber concrete beams. The second part refers to the shearspan to overall height of a/h: 05 for a/h = 0.5; 08 for a/h = 0.8; and 10 for a/h = 1.0. The third part refers to the deep beam height: 4 for h = 400 mm (15.7 in.); 6 for h = 600 mm (23.6 in.); and 7 for h = 700 mm (27.6 in.).

Table 6.4 - Details of deep beams.

Nomenclature	Concrete type	f_{cm} (MPa)	a/h	h (mm)	a (mm)	d (mm)	L (
SLCB054	Sand-lightweight	30.1	0.5	400	200	361.6	8
SLCB056				600	300	557.1	1
SLCB057				700	350	657.1	1
SLCB104			1.0	400	400	359.1	1
SLCB106				600	600	554.0	1
SLCB087			0.8	700	560	654.0	1
SLFCB054	Sand-lightweight with fibers	33.5	0.5	400	200	361.6	8
SLFCB056				600	300	557.1	1
SLFCB057				700	305	657.1	1
SLFCB104			1.0	400	400	359.1	1
SLFCB106				600	600	554.0	1
SLFCB087			0.8	700	560	654.0	1

All the deep beams had the same width, bw = 150 mm (5.9 in.). The distance between the load application points was constant and equal to 200 mm (7.8 in.). The length (L) of each deep beam varied according to the shear-span to overall height ratio a/h and the h. Bars of 10.0, 12.5, and 16.0 mm (0.4, 0.5, and 0.6 in.) in diameter were distributed in two layers to compose the longitudinal tension reinforcement. Figure 1 shows the cross section details of the deep beams, including the longitudinal tension reinforcement arrangement.

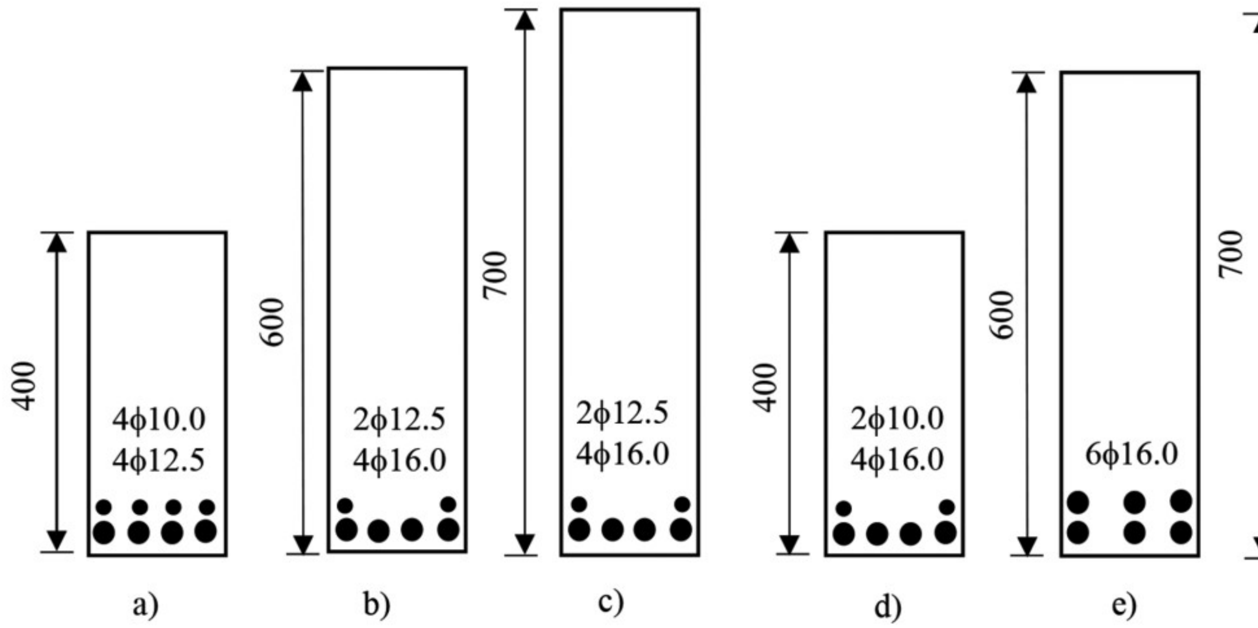

Figure 6.1 - Detail of longitudinal tension reinforcement of deep beams: (a) shear-span to overall height ratio a/h = 0.5, h = 400 m (15.7 in.); (b) a/h = 0.5, h = 600 mm (23.6 in.), (c) a/h = 0.5, h =

700 mm (27.6 in.), (d) a/h = 1.0, h = 400 mm (15.7 in.); (e) a/h = 1.0, h = 600 mm (23.6 in.); and (f) a/h = 0.8, h = 700 mm (27.6 in.).

The longitudinal tension reinforcement (ribbed bars) was continuous throughout the length of the beam and welded to its ends on carbon steel plates to provide the required anchorage (refer to Fig. 2). This technique ensured the cover and spacing between the bars throughout the length of the beam.

9.26.3 Instrumentation and testing procedures

The deep beams have undergone four-point bending tests, performed at a metallic structure frame-type with a hydraulic actuator model 244.41, which was coupled to a 500 kN (112 kip) capacity load cell. The system was controlled by the hydraulic unity that registered in real-time the applied loading at a 100 Hz acquirement frequency, and the tests were performed under displacement control at a speed of 0.3 mm/s.

Figure 6.2 - Detail of longitudinal tension reinforcement welded in carbon steel plate..

The deep beams were positioned under a metal frame, as shown in Fig. 3, and the loads were applied on a metal profile that transferred the load to the beam through two 100 x 150 x 20 mm (3.9 x 5.9 x 0.7 in.) metal plates, 200 mm (7.9 in.) apart. Figure 4 illustrates the test scheme and experimental instrumentation. The vertical displacement was monitored by a linear variable differential transformer (LVDT), located under the beam in the middle of the span length.

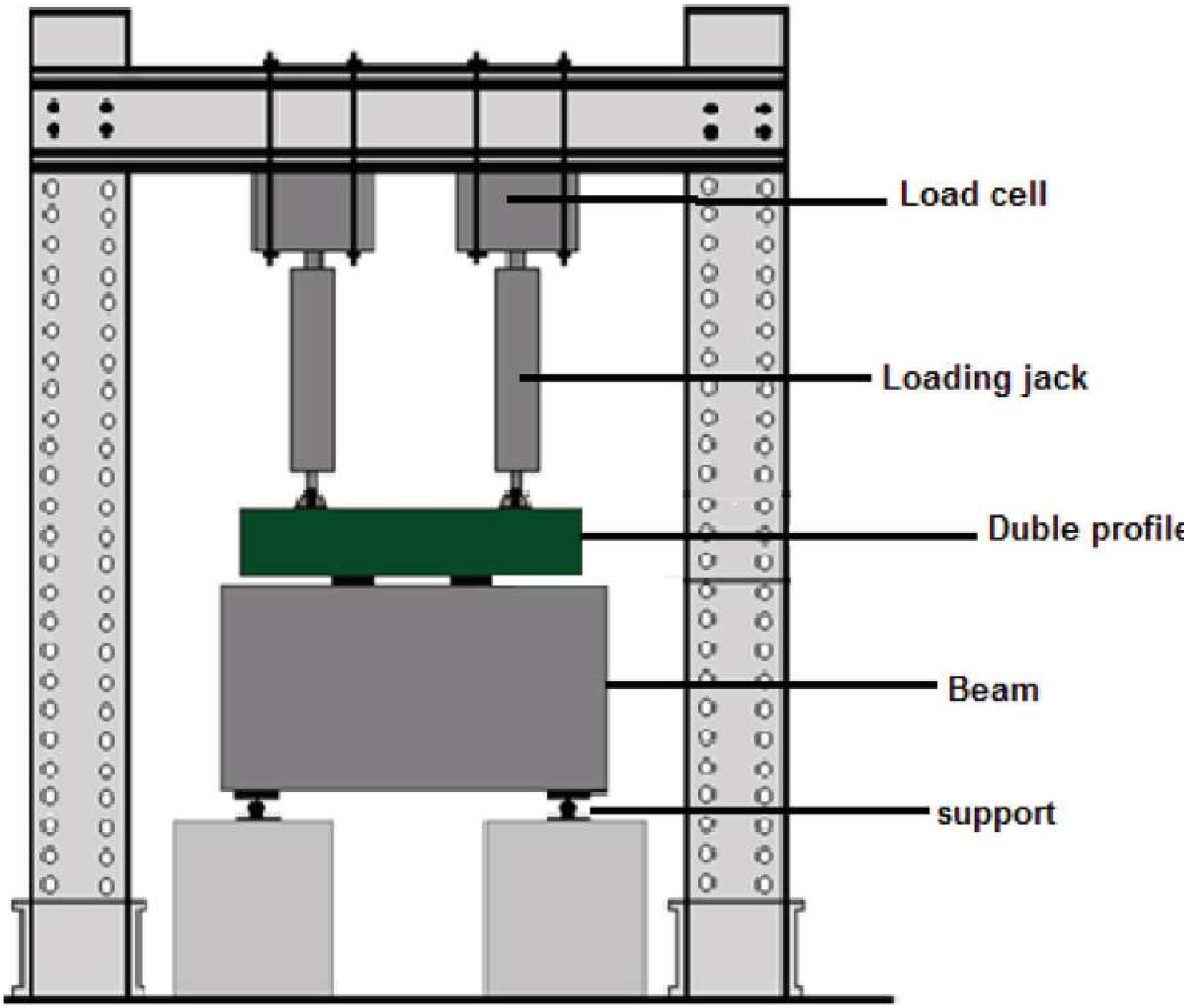

Figure 6.3 - Metal frame used in test.

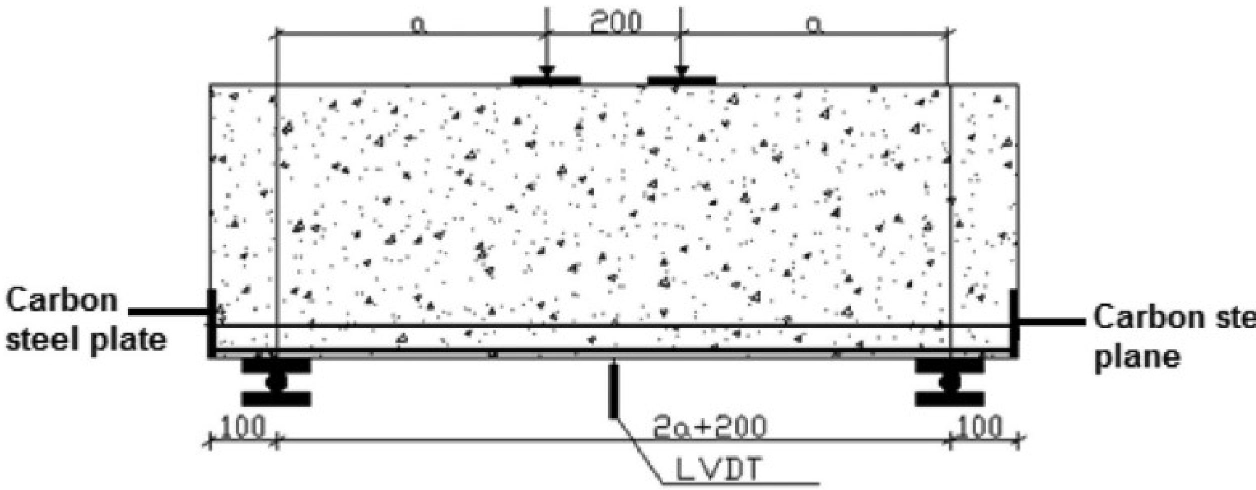

Figure 6.4 - Test scheme and instrumentation of deep beams.

Table 6.5 - Summary of experimental results.

Deep beams	Load (kN)		Shear strength (MPa)		Normalized shear ($MPa^{-0.5}$)	
	V_{cr}	V_{max}	τ_{cr}	τ_{max}	$\tau_{cr}/\sqrt{f_{cm}}$ (I)	$\tau_{max}/\sqrt{f_{cm}}$ (II)
SLCB054	140.5	257.8	2.59	4.75	0.45	0.83
SLCB056	175.3	386.8	2.10	4.63	0.36	0.76
SLCB057	199.5	441.0	2.02	4.47	0.34	0.74
SLCB104	99.3	244.0	1.84	4.53	0.30	0.74
SLCB106	101.6	311.5	1.22	3.75	0.21	0.63
SLCB087	100.0	354.3	1.02	3.61	0.17	0.60
SLFCB054	217.2	339.3	4.00	6.26	0.63	0.98
SLFCB056	228.6	486.1	2.74	5.82	0.44	0.93
SLFCB057	293.6	554.2	2.98	5.62	0.48	0.91
SLFCB104	131.2	282.2	2.44	5.24	0.38	0.81
SLFCB106	180.6	395.1	2.17	4.75	0.35	0.76
SLFCB087	248.5	450.5	2.53	4.59	0.41	0.74

9.27 EXPERIMENTAL RESULTS AND DISCUSSION

9.27.1 Relationship between load versus vertical displacement

Figures 5 and 6 show the load curves versus vertical displacement of the SLWC and the SLWFC deep beams with a shear-span to overall height ratio of a/h = 0.5 and a/h = 0.8 and 1.0, respectively.

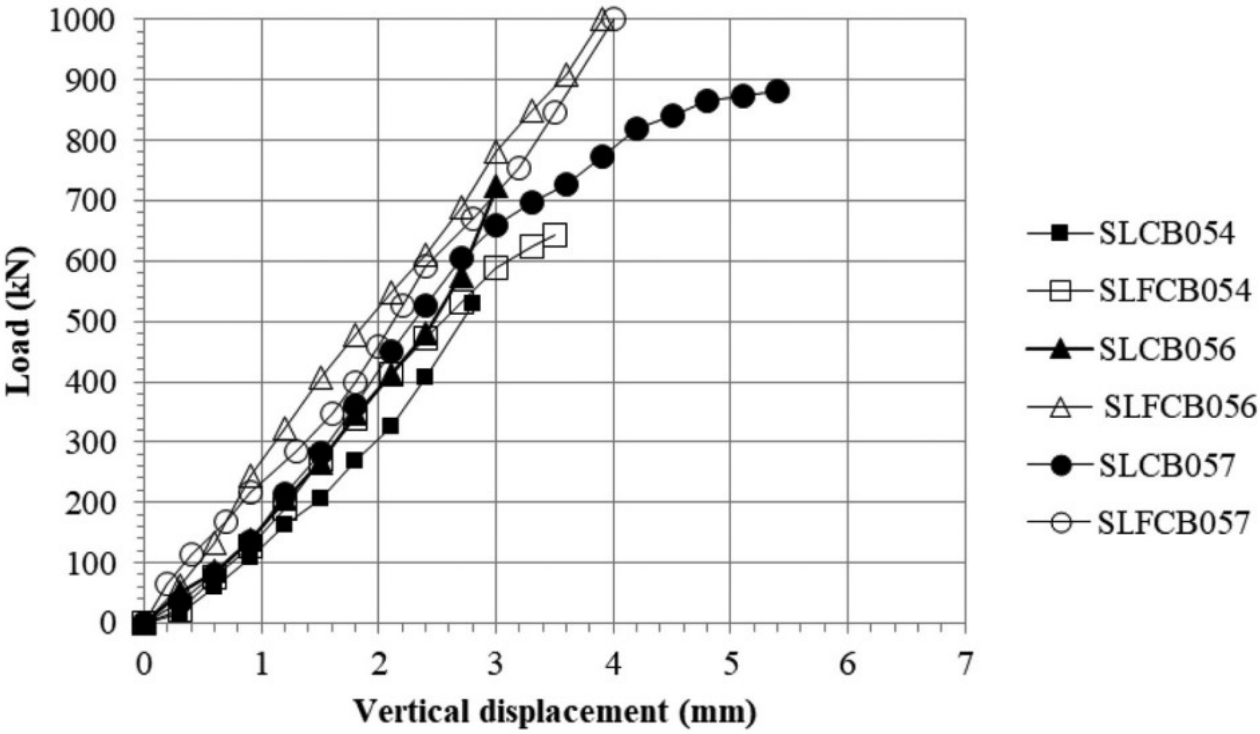

Figure 6.5 - Load versus vertical displacement curves of deep beams with shear-span to overall height ratio of a/h = 0.5.

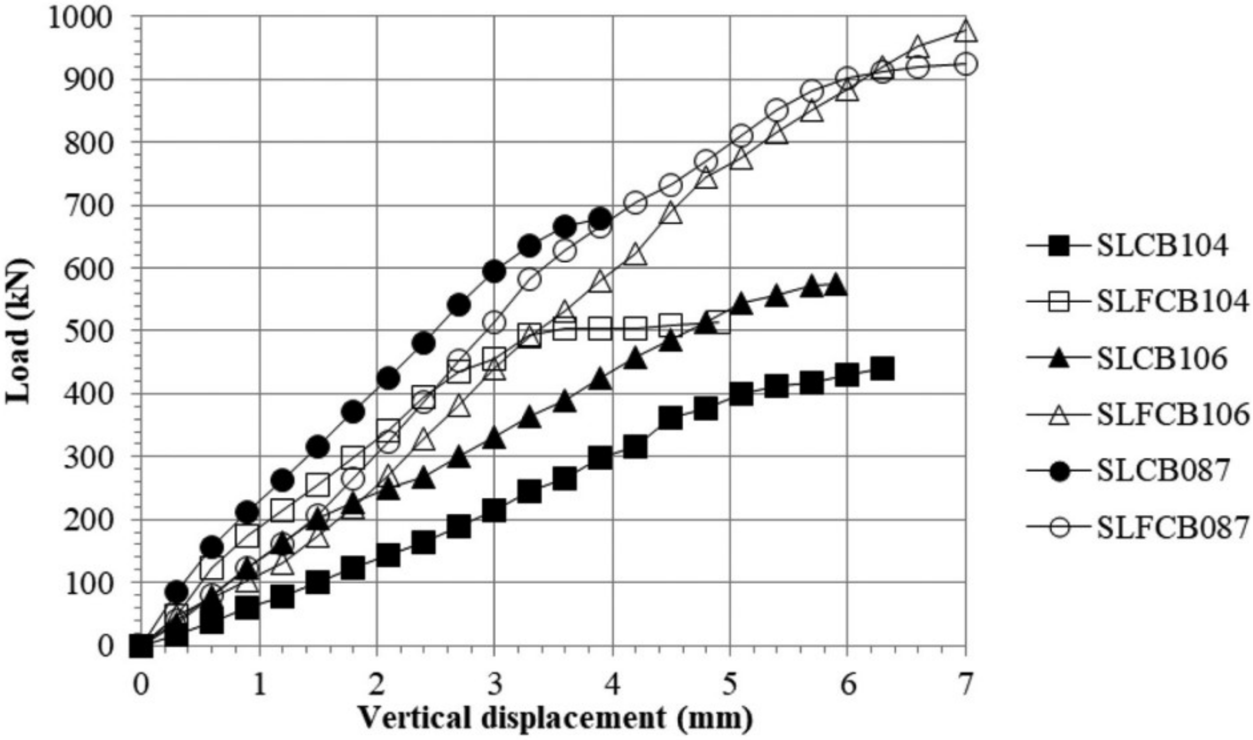

Figure 6.6 - Load versus vertical displacement curves of deep beams with shear-span to overall height ratio of a/h = 0.8 and 1.0.

For the same load levels, it can be seen that the SLWFC deep beams had less vertical displacements. Exceptionally the deep beams SLCB087 and SLFCB087 did not behave as expected. As previously confirmed by Narayan and Darwish,20 it can be seen that the insertion of 1.0% of steel fiber reduces the vertical displacements of the deep beams at all stress levels. This reduction occurs because steel fibers delay the appearance of cracks. Also, the fibers sew the microcracks, making their propagation more difficult and increasing the aggregate interlock.

It can also be observed that the deep beams with shearspan to overall height ratio of a/h = 0.8 and 1.0 presented greater vertical displacements than their corresponding ones of a/h = 0.5. This occurs because of the greater the shear span, the lower the stiffness.

9.27.2 Diagonal cracking shear and maximum normalized

Table 5 shows the diagonal cracking shear (τcr = Vcr/bwd) and maximum (τmax = Vmax/bwd) normalized by √fcm, as well as the difference between both quantities.

The strength to diagonal cracking for SLWC deep beams with a shear-span to overall height ratio of a/h = 0.5 was approximately 45.8 to 54% of the maximum shear, with an average value of 52.6%; for those with a shear-span to overall height ratio of a/h = 0.8 and 1.0, the values ranged from 59.4 to 71.6% of the maximum shear, with an average of 66.6%.

For SLWFC deep beams, the strength to diagonal cracking of the ones with a shear-span to overall height ratio of a/h = 0.5 ranged from 35.7 to 52.7% of the maximum shear, with an average value of 47.2%; while for those with a shear-span to overall height ratio of a/h = 0.8 and 1.0, the strength to diagonal cracking was between 44.6 to 53.9% of maximum shear, with an average value of 53.1%.

The deep beams with a shear-span to overall height ratio of a/h = 0.5 (SLFCB054, SLFCB056, and SLFCB057) with their SLWC replicas, it could be noticed an increase in diagonal cracking shear of 28.6, 18.2, and 29.2%, respectively. The deep beams with a shear-span to overall height ratio of a/h = 1.0 and 0.8 (SLFCB104, SLFCB106, and SLFCB087) exhibited an increase in diagonal cracking compared to their SLWC replicas equal to 21.1, 40.9, and 58.5%, respectively. The average increase value for the deep beams with a shearspan to overall height ratio of a/h = 0.5 was 25.3%, while for the ones with a shear-span to overall height ratio of a/h = 1.0 and 0.8, it was 60.2%.

The deep beams with a shear-span to overall height ratio of a/h = 0.5 (SLFCB054, SLFCB056, and SLFCB057), when compared to their SLWC replicas, showed an increase in the maximum shear load of 15.3, 18.3, and 18.7%, respectively. An increase in maximum shear was also found in deep beams with a shear-span to overall height ratio of a/h = 1.0 and 0.8 (SLFCB104, SLFCB106, and SLFCB087) in relation to their SLWC replicas, as values being 8.6, 17.8, and 18.9%, respectively. The average increase value for the deep beams with a shear-span to overall height ratio of a/h = 0.5 was 17.4%, while for the ones with a shear-span to overall height ratio of a/h = 0.8 and 1.0 was 15.1%. In comparison, Mansur and Ong21 obtained an increase in load capacity of 16.3% by inserting 1% of metallic fibers in the conventional concrete deep beam, with shear-span to overall height ratio a/h = 1.14.

It can be seen that the SLWC deep beams presented lower shear strength than their fiber-reinforced concrete replicas. Thus, the presence of sand-lightweight coarse aggregates in the cracking planes reduces stress transfer capability due to decreased aggregate interlocking action.

9.27.3 Rupture mode

The rupture planes in all tested beams were formed along the diagonal cracks that joined the load and reaction points. However, the rupture mode was different for each concrete type.

In general, the SLWC deep beams are ruptured by diagonal compression. After the formation of the first crack in one of the spans, the other cracks formed in a parallel manner to the first one and propagated towards the point of load and support, followed by the rupture in one of the cracks, generating a strut, followed by rupture on one side by shear (Fig. 7). The widths of the strut were measured after rupture and it was found that they measured approximately the same value as the width of the support plates and application loads—that is, 100 mm (3.9 in.). The SLWFC deep beams presented cracking or diagonal tensile rupture, where there was the formation of inclined cracks, and then, due to the effect of the fibers addiction, the openings were reduced (Fig. 7).

Figures 8(a) and (b) show the rupture type of the SLWC deep beams and SLWFC deep beams, respectively. Figures 8(c) and (d) show the formed strut and its width, having a smooth surface with expanded clay cutting.

9.27.4 Size effect on maximum shear capacity

To evaluate the size effect on the SLWC deep beams, the values of Log h versus Log τmáx/$\sqrt{}$fcm are plotted in Fig. 9 for the deep beams with a shear-span to overall height ratio of a/h = 0.5, 0.8, and 1.0. The angular coefficient of the trend lines is shown caption.

It turns out that the concrete type influences the slope of these curves. This indicates the action of the fibers on the size effect due to the reduction of crack openings by making the aggregate interlocking more effective, and thus reducing the size effect on the SLWFC deep beams.

It is also observed that the shear-span to overall height ratio a/h influences the inclination of these curves, being softer for the deep beams with a shear-span to overall height ratio of a/h = 0.5. This demonstrates that the size effect was more significant in the deep beams with a shear-span to overall height ratio of a/h = 0.8 and 1.0.

9.27.5 Chen et al.'s model

The model proposed by Chen et al.22 for calculating the ultimate shear capacity, based on the experimental phenomena of diagonal crack patterns and strain distribution of longitudinal bars in shear span were considered. Mattock et al.1 evaluated the behavior of the model for deep beams in determining the ultimate shear capacity from experimental data of concrete with normal density in deep beams without core reinforcement, with vertical web reinforcement, plus ones with horizontal and vertical web reinforcement. Considering the statistical parameters, this model was the one that best fit the samples' behavior compared with others evaluated.

In this work, the cracking strut-and-tie model (CSTM) was used to evaluate its applicability to SLWC and SLWFC deep beams. This CSTM divides the diagonal strut in two parts: one is not affected by the flexural-shear cracks (Fsi) and the other the effective compressive strength of the part below the critical shear crack is derived from the forces transferred by the aggregate interlock, web reinforcement, and dowel action of longitudinal bars on the critical shear crack surface (Fsc). These methods suggest the shear strength of deep beams by the failure of concrete struts as follows.

$$V_{max} = 0.8(F_{si} + F_{sc})\sin\theta \qquad (1)$$

$$F_{si} = \sigma_{ci} w_{si} b \qquad (2)$$

$$F_{sc} = \sigma_{cc} w_{sc} b \qquad (3)$$

where sci and scc are the effective compressive strength of the uncracked and cracked parts of the strut, respectively; wsi and wsc are the strut widths; b is the beam width; and θ is the angle between the strut axis and the longitudinal bars.

The results obtained when the CSTM method was applied to these types of concrete proved to be unsafe. Thus, a general reduction coefficient was applied to the values obtained by the CSTM to obtain a result closer to the experimental ones.

Statistical analysis with several values multiplied by the τCSTM/τexp value was performed aiming to obtain mean values closer to 1 and with lower standard deviation. Table 6 shows the mean τCSTM/τexp values closest to 1 obtained from applying the reduction coefficient (λ).

It was found that this method was effective in determining the ultimate shear capacity and predicting the size effect in SLWC deep beam, providing a $\lambda = 0.70$ and to SLWFC deep beams, a $\lambda = 0.80$.

In Fig. 10, the values of Log h versus Log $\tau max/\sqrt{fcm}$ are plotted from the deep beams tested in this study and those obtained using CSTM, applying the coefficients obtained earlier.

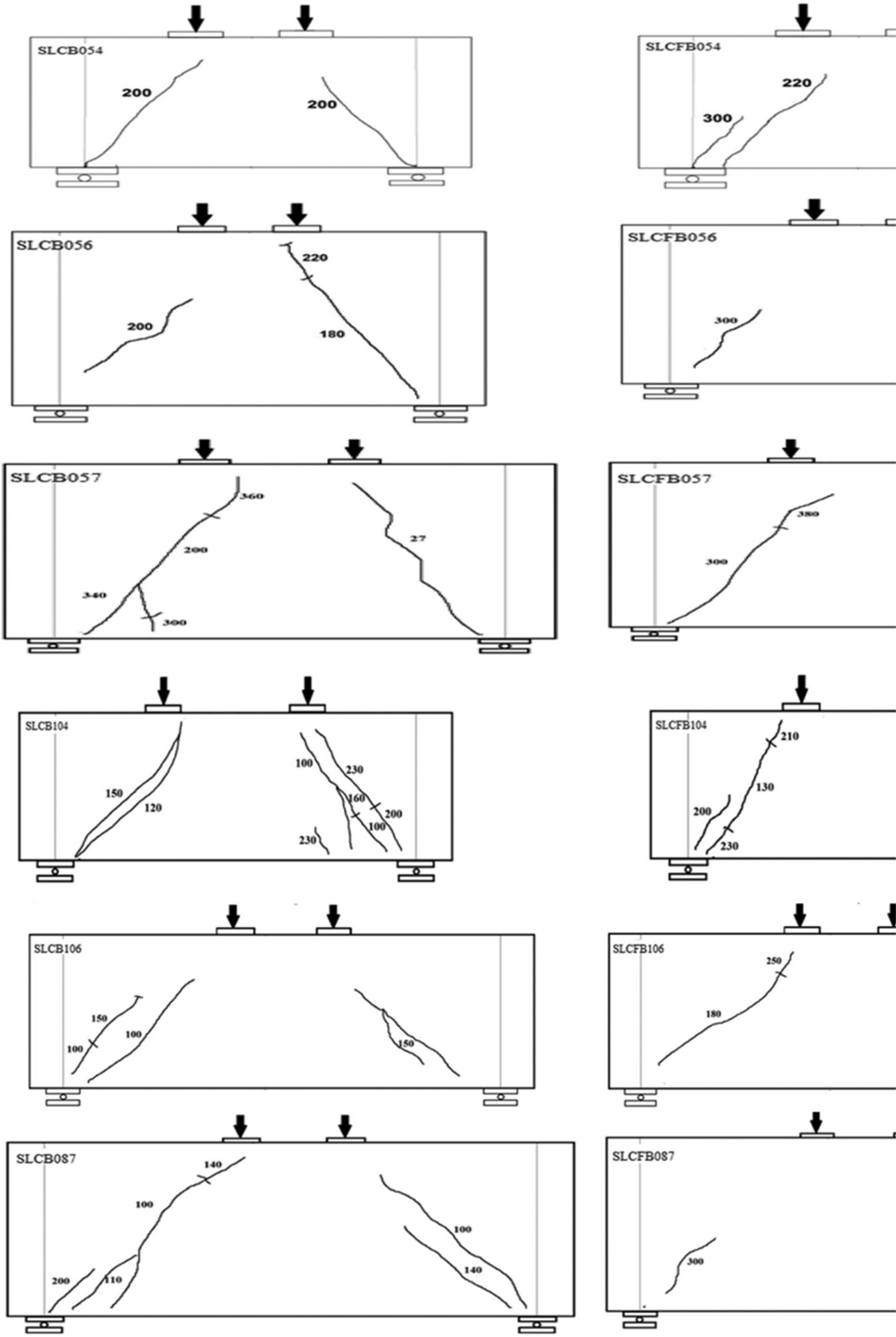
SLCB054
200
200
SLCFB054
220
300
SLCB056
220
200
180
SLCFB056
300
SLCB057
360
200
340
300
27
SLCFB057
380
300
SLCB104
100
230
150
120
160
200
100
230
SLCFB104
210
130
200
230
SLCB106
150
100
100
150
SLCFB106
250
180
SLCB087
140
100
100
200
110
140
SLCFB087
300

Figure 6.7 - Cracking pattern of tested deep beams.

Table 6.6 - Mean values and standard deviation of τCSTM/τexp applied to various values of λ.

Parameters	SLWC				
λ	0.75	0.70	0.65	0.60	0.90
Mean	1.11	1.03	0.96	0.88	1.105
Standard deviation	0.152	0.142	0.132	1.222	0.146

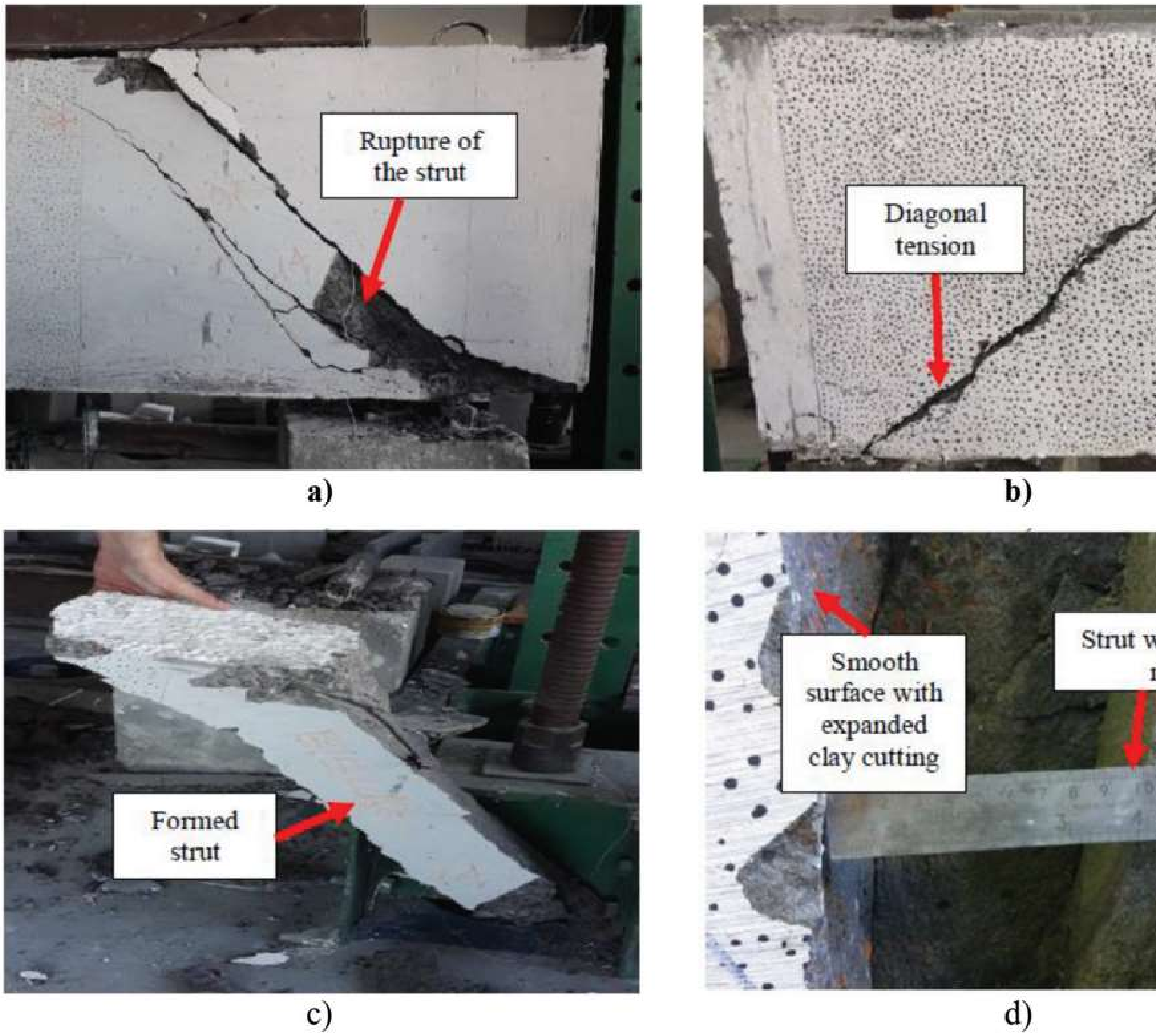

Figure 6.8 - Rupture mode of deep beams and strut: (a) SLWC; (b) SLWFC; (c) formed strut in SLWC; and (d) strut width equal to bearing plate and supports.

9.27.6 Influence of concrete type on maximum shear strength

Figures 11 and 12 plot the values of Log h versus Log τmax/√fcm, in SLWC deep beams with a shear-span to overall height ratio of a/h = 0.5 and a/h = 0.8 and 1.0, respectively. The angular coefficient of the trend line obtained from their experimental data appears.

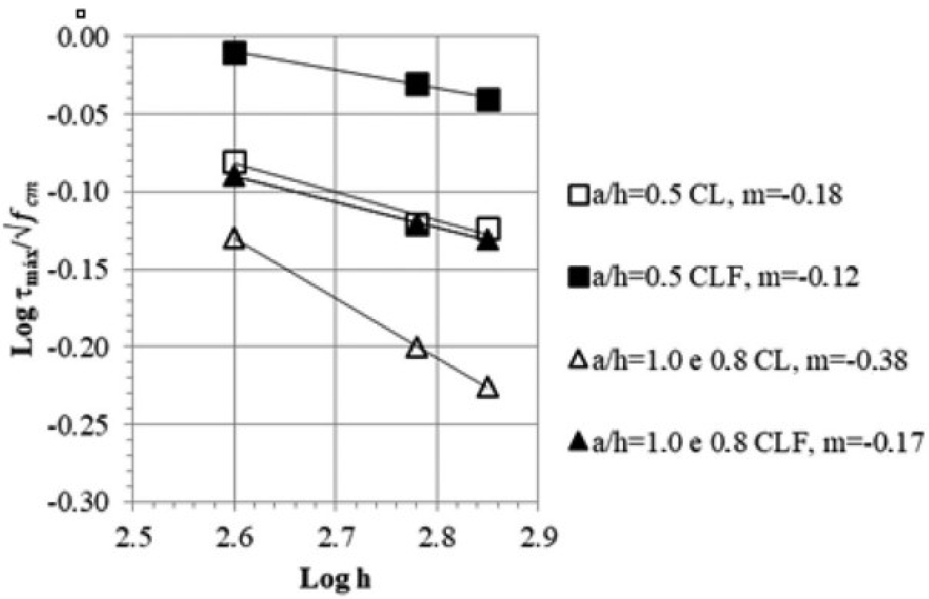

Figure 6.9 - Log. τmax/√fcm versus Log h of deep beams with shear-span to overall height ratio of a/h = 0.5, 0.8, and 1.0.

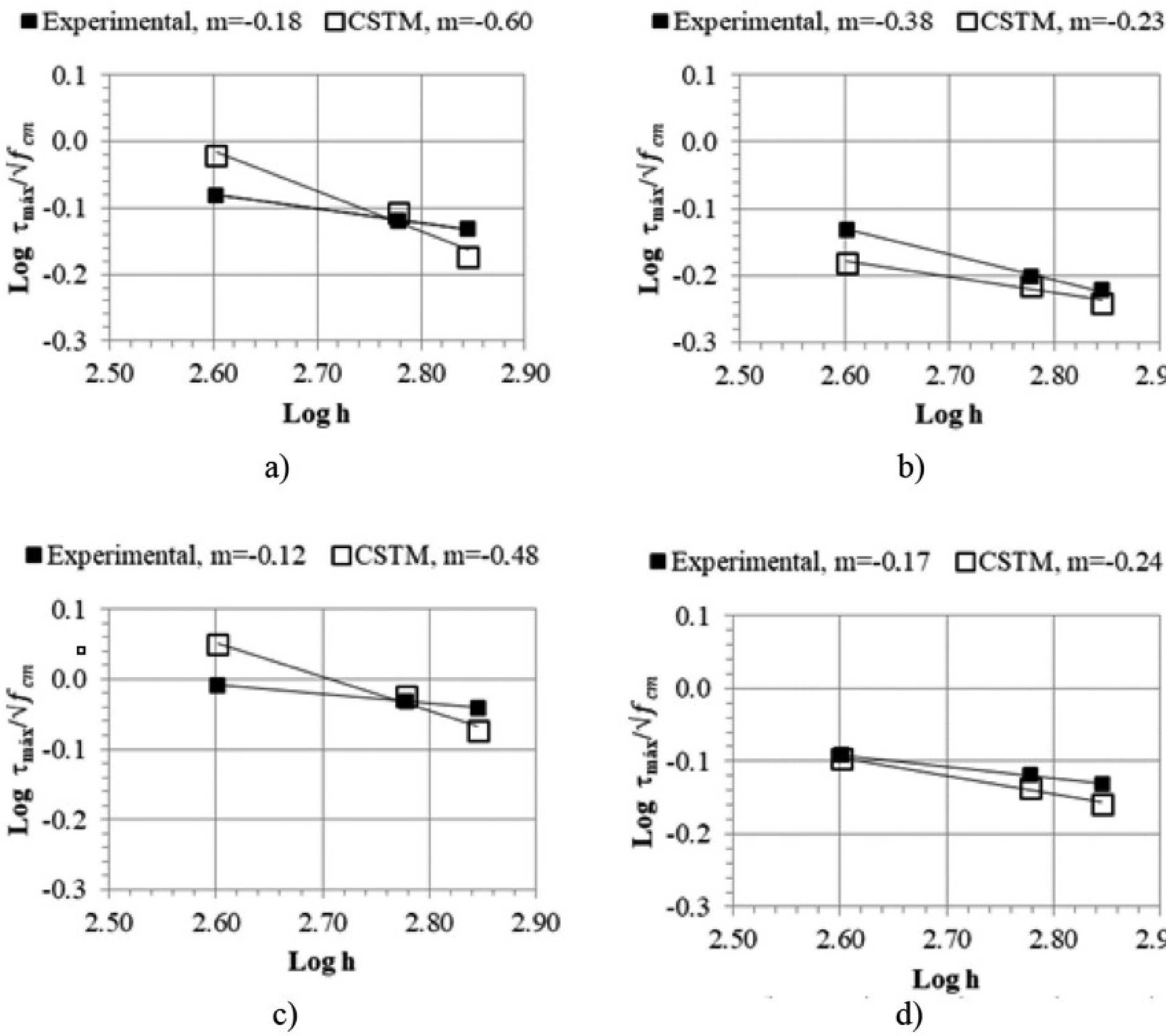

Figure 6.10 - Predicting size effect in SLWC deep beam: (a) with shear-span to overall height ratio of a/h = 0.5 and (b) a/h = 0.8 and 1.0, and SLWFC deep beam: (c) with a/h = 0.5 and (d) a/h = 0.8 and 1.0.

Conventional concrete deep beams showed higher maximum shear values when compared to sand-lightweight or all-lightweight concrete deep beams.

The deep beams studied by Shuraim and El-Sayed15 and Chen et al.13 showed that the size effect is more significant as concrete density decreases. However, the found slopes in SLWFC deep beams outfit the values for conventional concrete deep beams.

9.27.7 Comparison between experimental maximum shear and calculated by standards and equations

Table 7 presents the experimental maximum shear predictions calculated according to NBR 6118-14,23 code ACI 318-14,24 CSA A23.3-0425 for SLWC deep beams, and the coefficient γcs, which is the shear-span to overall height ratio between the value calculated by theoretical equations and experimental value. The codes suggest the shear strength of deep beams by the failure of concrete struts as follows, respectively

$$V_{\max} = 0.72\alpha_{v2}.f_c \qquad (4)$$

where αv2 = 1 – fck/250, fck is the characteristic compressive strength of concrete

$$V_{\max} = \phi\sqrt{f_c}\, b_w d \qquad (5)$$

where ϕ is a reduction coefficient

$$V_{\max} = 0.25\phi f_c b_w d \qquad (6)$$

where ϕc = 0.65.

Table 8 shows the experimental predictions for SLWFC deep beams calculated from the equations proposed by ACI 544-88,26 Li et al.,10 and Shahnewaz and Alam,27 and the coefficient γcs. The codes suggest the shear strength of deep beams by the failure of concrete struts as follows, respectively

$$V_{\max} = \frac{2}{3} f_t \left(\frac{d}{a}\right)^{\frac{1}{4}} b_w d \qquad (7)$$

where ft = 0.78 fc

Where ρ is the longitudinal reinforcement rate.

$$V_{\max} = \left[9.16 f_t^{\frac{2}{3}} \rho^{\frac{1}{3}} \left(\frac{d}{a}\right)\right] b_w d \qquad (8)$$

where Vf is the volume of fibers, and lf/df is the factor of the form of fibers.

$$V_{\max} = \left\{ \begin{array}{l} 0.2 + 0.34 f_c + 19\rho^{0.087} - 5.8\left(\frac{a}{d}\right)^{\frac{1}{2}} + 3.4 V_f^{\frac{1}{2}} - 800\left(\frac{l_f}{d_f}\right)^{-1.6} \\ -12\left[\left(\frac{a}{d}\right)V_f\right]^{0.05} - 197\left[\left(\frac{a}{d}\right)\left(\frac{l_f}{d_f}\right)\right]^{-1.4} + 105\left[V_f\left(\frac{l_f}{d_f}\right)\right]^{-2.12} \end{array} \right\} b_w d \qquad (9)$$

Table 6.7 - Summary of experimental and theoretical results for SLWC deep beams.

Deep beams	$V_{max,exp}$	Theoretical predictions			$\gamma_{cs}=V_{max,\ teó}/V_{ma}$	
		NBR 618-14[23] (I)	ACI 318-14[24] (II)	CSA A23.3-04[25] (III)	(I)	(II)
SLCB054	257.8	176.6	285.0	200.1	0.69	1.11
SLCB056	386.8	326.2	367.0	371.2	0.84	0.95
SLCB057	441.0	373.6	397.5	424.2	0.85	0.90
SLCB104	244.0	234.0	267.0	223.8	0.96	1.09
SLCB106	311.5	368.6	311.5	345.3	1.18	1.00
SLCB087	354.3	460.6	285	435.8	1.30	0.80

Table 6.8 - Summary of experimental and theoretical results for SLWFC deep beams.

Deep beams	$V_{max,exp}$	Theoretical predictions			$\gamma_{cs}=V_{max,\ teó}/V_{max,\ e}$	
		ACI 544-88[26] (I)	Li et al.[10] (II)	Shahnewaz and Alam[27] (III)	(I)	(II)
SLFCB054	339.3	177.5	585.1	298.2	0.52	1.72
SLFCB056	486.1	268.1	570.0	427.7	0.55	1.17
SLFCB057	554.2	308.3	507.8	469.6	0.56	0.92
SLFCB104	282.2	149.0	309.1	247.7	0.53	1.10
SLFCB106	395.1	225.1	296.7	350.6	0.57	0.75
SLFCB087	450.5	278.5	355.3	436.6	0.62	0.79

Figures 13 and 14 show the relationship between calculated and experimental shear values. The line at 45 degrees indicates a coefficient $\gamma cs = 1.0$.

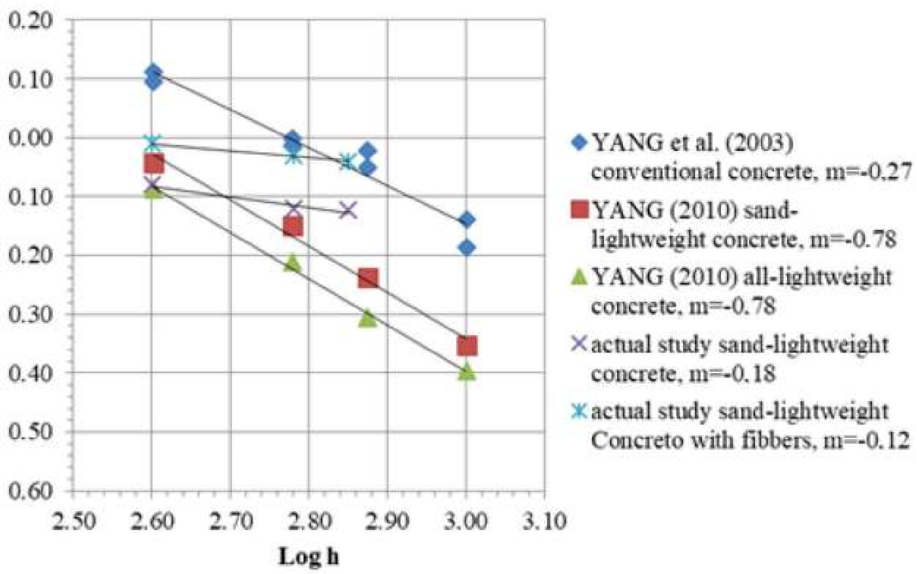

Figure 6.11 - Influence of height on normalized maximum shear strength of deep beams with shear-span to overall height ratio of a/h = 0.5.

For the SLWC deep beams, the predictions obtained by the considered codes were conservative for deep beams with a shear-span to overall height ratio of a/h = 0.5 because they presented a mean value of γcs below 1.0. The predictions were lower than the experimental loads for deep beams with a shear-span to overall height ratio of a/h = 0.8 and 1.0. However, the ACI 318-143 equation proved to be the most effective in predicting the ultimate loads for the deep beams with a shear-span to overall height ratio of a/h = 0.5, as they presented an average of γcs = 0.95. In contrast, the deep beams with a shear-span to overall height ratio of a/h = 0.8 and 1.0 γcs equal 1.0.

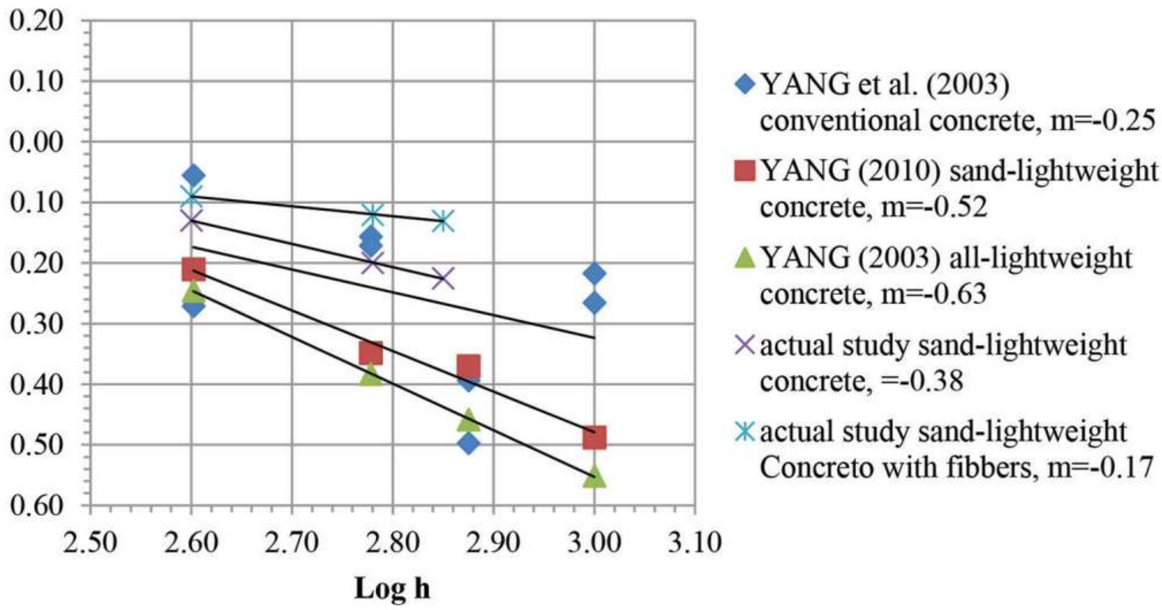

Figure 6.12 - Influence of height on normalized maximum shear strength of deep beams with shear-span to overall height ratio of a/h = 0.8 and 1.0.

For SLWFC deep beams, the code predictions of ACI 544-8826 and Li et al.10 were very conservative, generating a meager γcs value, which shows that the deep beams reached higher shear capacities than expected. Li et al.10 provided more accurate loading results than ACI 544-8826 for shear-span to overall height ratios of a/h = 0.8 and 1.0. Yet, some deep beams ruptured before the expected shear capacity, and others were below expectations. Nevertheless, Shahnewaz and Alam's model27 presented an average γcs value closer to 1.0, showing that it was the most efficient equation to predict the maximum shear.

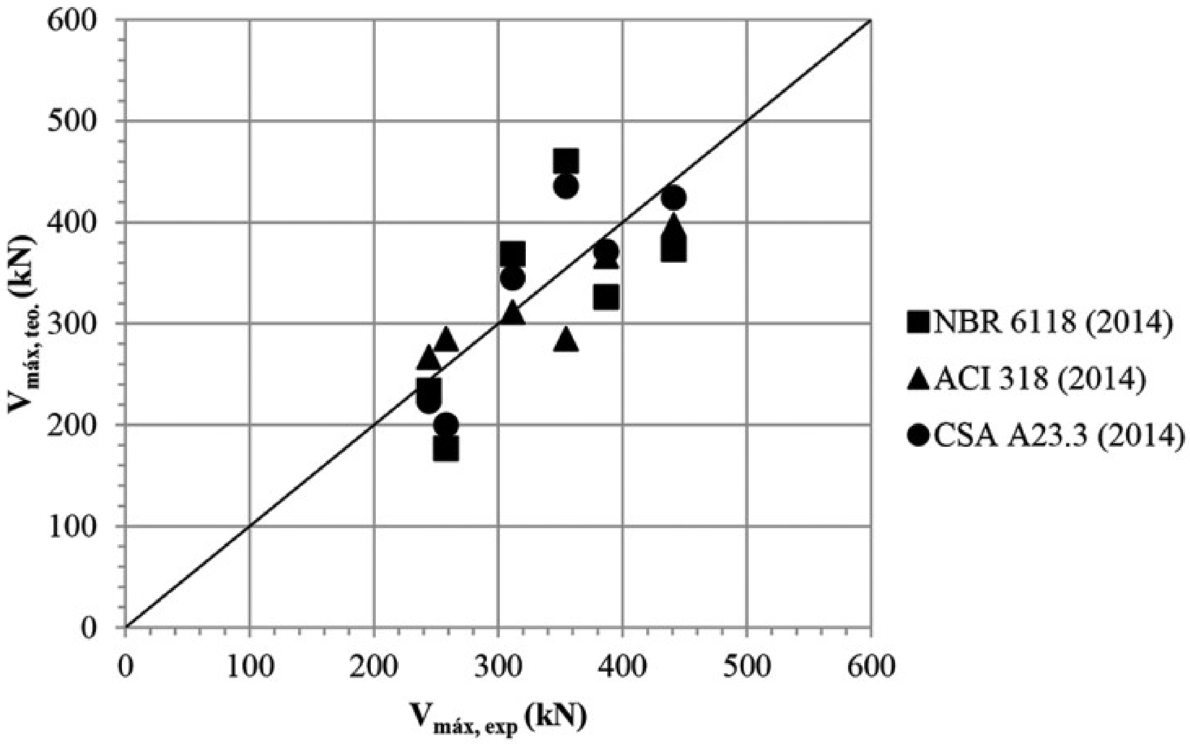

Figure 6.13 - Comparison between calculated and experimental maximum shear for SLWC deep beams.

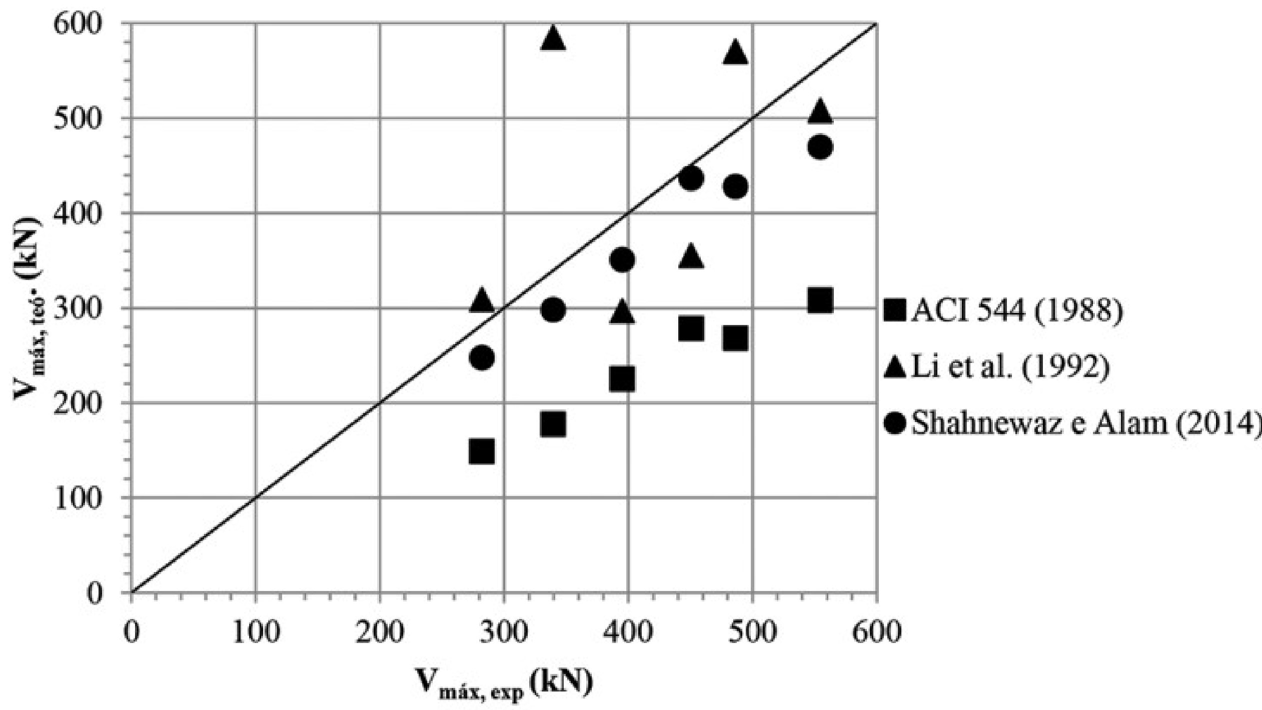

Figure 6.14 - Comparison between calculated and experimental maximum shear for SLWFC deep beams.

9.28 CONCLUSIONS

The following conclusions are drawn from the present study:

1. The values of maximum and diagonal cracking stresses of deep beams with shear-span to overall height ratios of $a/h = 0.8$ and 1.0 were lower when compared to their replicas with a shear-span to overall height ratio of $a/h = 0.5$. Thus, it was concluded that the shear strength mechanisms was lower in larger shear span deep beams;

2. The maximum shear in SLWFC deep beams was 17.4% for a shear-span to overall height ratio of $a/h = 0.5$ and 15.1% for a shear-span to overall height ratio of $a/h = 0.8$ and 1.0;

3. The fibers reduced crack opening and made aggregate interlocking more effective. Thus, there was attenuation in the slope of the Log h versus $\tau max/\sqrt{fcm}$ curves. It was concluded that the size effect was less significant in the SLWFC deep beams;

4. The size effect was more significant in SLWC deep beams in a shear-span to overall height ratio of $a/h = 0.8$ and 1.0 in comparison to deep beams in a shear-span to overall height ratio of $a/h = 0.5$;

5. SLWC and SLWFC deep beams had lower maximum shear strength than conventional concrete deep beams;

6. The analysis performed showed that the model proposed by Chen et al.22 is applicable to SLWC deep beam and SLWFC deep beam; The coefficients λ were 0.7 and 0.8, respectively;

7. The requirements of NBR 6118-1423 and CSA A23.3- 0425 were not effective in predicting the maximum shear of SLWC deep beams. The ACI 318-1424 equation proved to be the most effective, generating an average value of γcs closest to 1.0;

8. ACI 544-8826 and Li et al.10 were not accurate in predicting maximum shear in SLWFC deep beams. However, the equation proposed by Shahnewaz and Alam27 proved to be very effective with mean values of γcs closer to 1.0.

9.29 ACKNOWLEDGMENTS

This study was funded in part by the Coordination for the Improvement of Higher Education Personnel (CAPES) - Funding Code 001.

9.30 REFERENCES

1. Mattock, A. H.; Li, W. K.; and Wang, T. C., "Shear Transfer in Lightweight Reinforced Concrete," PCI Journal, Jan.-Feb. 1976, pp. 20-39.Boje, C., Guerriero, A., Kubicki, S. and Rezgui, Y. (2020), "Towards a semantic Construction Digital Twin: Directions for future research", Automation in Construction, Elsevier, Vol. 114, p. 103179.

2. Emiko, L.; Thamaraikkannan, V.; Huan, W. T.; and Thangayah, T., "Shear Transfer in Lightweight Concrete," Magazine of Concrete Research, V. 63, No. 6, 2011, pp. 393-00. doi: 10.1680/macr.9.00162

3. Sneed, L. H., Krc, K., and Wermager, S., "Interface Shear Transfer of Lightweight-Aggregate Concretes with Different Lightweight Aggregates," PCI Journal, March-Apr. 2016, pp. 38-55.

4. Floyd, R. W.; Hale, W. M.; and Bymaster, J. C., "Effect of Aggregate and Cementitious Material on Properties of Lightweight Self-Consolidating Concrete for Prestressed Members," Construction and Building Materials, V. 85, 2015, pp. 91-99. doi: 10.1016/j.conbuildmat.2015.03.084

5. Kong, F. K.. and Robins, P. J., "Web Reinforcement Effects on Lightweight Concrete Deep Beams," ACI Journal Proceedings, V. 68, No. 7, July 1971, pp. 514-520.

6. Yang, K. H., "Tests on Lightweight Concrete Deep Beams," ACI Structural Journal, V. 107, No. 6, Nov.-Dec. 2010, pp. 663-670.

7. Yang, K. H., and Ashour, A. F., "Aggregate Interlock in Lightweight Concrete Continuous Deep Beams," Engineering Structures, V. 33, No. 1, 2011, pp. 136-145. doi: 10.1016/j.engstruct.2010.09.026

8. Yang, K. H.; Chung, H. S.; Lee, E. T.; and Eun, H.-C., "Shear Characteristics of High-Strength Concrete Deep Beams Without Shear Reinforcements," Engineering Structures, V. 25, No. 10, 2003, pp. 1343-1352. doi: 10.1016/S0141-0296(03)00110-X

9. Sachan, A. K., and Kameswara Rao, C. V. S., "Behaviour of Fibre Reinforced Concrete Deep Beams," Cement and Concrete Composites, V. 12, No. 3, 1990, pp. 211-218. doi: 10.1016/0958-9465(90)90022-P

10. Li, V. C.; Ward, R.; and Hamza, A. M., "Steel and Synthetic Fibers as Shear Reinforcement," ACI Materials Journal, V. 89, No. 5, Sept.-Oct. 1992, pp. 499-08.

11. Visalakshia, B. S. S., and G., S. H., "Enhancement of Shear Strength of Deep Beams Using Hybrid Fibres and Suggesting an Alternative for Strut and Tie Model," Materials Today: Proceedings, V. 33, 2020, pp. 578-582. doi: 10.1016/j.matpr.2020.05.454

12. Moradi, M., and Esfahani, M. R., “Application of the Strut-and-Tie Method for Steel Fiber Reinforced Concrete Deep Beams,” Construction and Building Materials, V. 131, 2017, pp. 423-437. doi: 10.1016/j. conbuildmat.2016.11.042

13. Chen, H.; Yi, W. J.; and Ma, Z. J., “Shear Size Effect in Simply Supported RC Deep Beams,” Engineering Structures, V. 182, November 2018, 2019, pp. 268-78.

14. Birrcher, D. B.; Tuchscherer, R. G.; Huizinga, M.; and Bayrak, O., “Depth Effect in Deep Beams,” ACI Structural Journal, V. 111, No. 4, July-Aug. 2014, pp. 731-740. doi: 10.14359/51687002

15. Shuraim, A. B., and El-Sayed, A. K., “Experimental Verification of Strut and Tie Model for HSC Deep Beams Without Shear Reinforcement,” Engineering Structures, V. 117, 2016, pp. 71-85. doi: 10.1016/j. engstruct.2016.03.002

16. ABNT, “NBR 5733:1991 High Early Strength Portland Cement – Specification,” Rio de Janeiro, Brazilian Association of Technical Standards, 1991, 5 pp.

17. ABNT, “NBR NM 67:1998 Concrete – Slump Test for Determination of the Consistency,” Rio de Janeiro, Brazilian Association of Technical Standards, 1998, 8 pp.

18. ABNT, “ABNT NBR 5739 Concreto — Ensaio de compressão de corpos de prova cilíndricos,” 2018, 9 pp.

19. ABNT, “ABNT NBR 722 Argamassa e concreto - Determinação da resistência à tração por compressão diametral de corpos-de-prova cilíndricos,” 2011, 6 pp.

20. Narayanan, R., and Darwish, I. Y. S., “Fiber Concrete Deep Beams in Shear,” ACI Structural Journal, V. 85, No. 2, Mar.-Apr. 1988, pp. 141-149.

21. Mansur, M. A., and Ong, K. C. G., “Behavior of Reinforced Fiber Concrete Deep Beams in Shear,” ACI Structural Journal, V. 88, No. 1, Jan.-Feb. 1991, pp. 98-05.

22. Chen, H.; Yi, W.; and Hwang, H., “Cracking Strut-and-Tie Model for Shear Strength Evaluation of Reinforced Concrete Deep Beams,” Engineering Structures, V. 163, May 2018, pp. 396-408.

23. ABNT, “ABNT NBR 6118-Projeto de Estruturas de ConcretoProcedimentos,” 2014, 255 pp.

24. ACI Committee 318, “Building Code Requirements for Structural Concrete (ACI 318-14) and Commentary,” American Concrete Institute, Farmington Hills, MI, 2014, 520 pp.

25. CSA A23.3, “Design of Concrete Structures,” Mississauga, Ontario, Canadian Standards Association, 2004, 240 pp.

26. ACI Committee 544, "Design Considerations for Steel Fiber Reinforced Concrete (ACI 544.4R-88)," American Concrete Institute, Farmington Hills, MI, Reapproved 1999, 18 pp.

27. Shahnewaz, M., and Alam, M. S., "Improved Shear Equations for Steel Fiber-Reinforced Concrete Deep and Slender Beams," ACI Structural Journal, V. 111, No. 4, July-Aug. 2014, pp. 851-860. doi: 10.14359/51686736